Haukur Ingason · Ying Zhen Li
Anders Lönnermark

Tunnel Fire Dynamics

Springer

Tunnel Fire Dynamics

Haukur Ingason • Ying Zhen Li
Anders Lönnermark

Tunnel Fire Dynamics

Springer

Haukur Ingason
Fire Research
SP Technical Research Institute of Sweden
Borås
Sweden

Anders Lönnermark
Fire Research
SP Technical Research Institute of Sweden
Borås
Sweden

Ying Zhen Li
Fire Research
SP Technical Research Institute of Sweden
Borås
Sweden

ISBN 978-1-4939-2198-0 ISBN 978-1-4939-2199-7 (eBook)
DOI 10.1007/978-1-4939-2199-7
Springer New York Heidelberg Dordrecht London

Library of Congress Control Number: 2014954828

Preface

Fire safety engineering in tunnels is essential in order to obtain good safety for tunnel users. The knowledge about fire safety in tunnels has increased over the past few decades due to both new research and analysis of real accidents. The aim of this book is to give researchers, engineers, and authorities worldwide a good insight into the fire phenomena in tunnels and the physics behind it. Guidance in calculation of important parameters such as heat release rates, critical velocity, spread of smoke gases and heat, temperatures, heat fluxes, fire spread, and flame lengths is given as well as the theories behind them. A comprehensive overview of how fires in vehicles develop and how different physical parameters such as flammability, ventilation, and geometry influence them is presented. The focus is not on the design aspects of fire safety in tunnels, although some parts are described. It is more about understanding the dynamics and developments of fires in tunnels and other underground constructions.

The tunnels are becoming more and more complex and the need for performance based design increases. The authors have found the need for presenting and gathering the latest knowledge on fire research and experience from different testing. Therefore, the emphasis is on engineering relations and physics of fires. This will provide good and solid background information which the readers can on their own hand, use in its daily research and engineering work.

The knowledge presented here comes very much from research that the authors have been involved in, but also from other large-scale experiments and practical experience. The book can also serve as a base for a university education for those who are interested to understand the basics of tunnel fire safety engineering using correlations and formulas obtained within different fields.

The book is divided into numerous chapters where the focus ranges from direct physical phenomena to advanced calculation models. The catastrophic fires that have occurred in tunnels are put into context of the subject of this book, namely fire dynamics in tunnels. These fires have raised the level of awareness about the problem and through experimental and theoretical work by many researchers around the world the knowledge level on the fire physics has increased

considerably. This knowledge needs to find its way to the engineers working with the problems on daily basis and, therefore, it is our hope that the book will serve as a platform for practicing engineers, researchers, and students dealing with fire safety in tunnels.

Borås 2014-07-06

Haukur Ingason
Ying Zhen Li
Anders Lönnermark

Acknowledgement

We would like to thank Dr Margaret McNamee, Dr Francine Amon and Dr David Lange at SP Fire Research for their valuable comments. The research presented in this book would not have been possible without financial support from SP Tunnel and Underground Safety Center. We also want to thank other Swedish research colleagues for their contribution and financial support through research projects from the Swedish Fire Research Board (BRANDFORSK), the Swedish Research Council (FORMAS), the Swedish Civil Contingencies Agency (MSB), and the Swedish Transport Administration (Trafikverket). Finally, we would like to thank the technicians at SP Fire Research who so skilfully carried out all the high quality large-scale and model-scale experimental work together with us.

Contents

Chapter 1
Introduction

Abstract An introduction to the main differences between open fires, building fires and tunnel fires is given as the basis for better insight into the physics of fires in tunnels. An overview is given of what type of fires is to be expected in different types of tunnels and what consequences such fires may have. A short description of mitigation systems commonly used to increase the fire safety in tunnels is also given and their main features are put into the context of fire dynamics. Finally, the major fire incidents that have occurred are summarized and analysed in order to understand the main reasons for their different consequences.

1.1 Introduction

The main purpose of this book is to provide a sound understanding of fire dynamics in tunnels. The word "tunnels" is broadly used to mean road tunnels, rail tunnels, metro tunnels, mines or tunnels during construction. The book aims to improve knowledge on fire physics and thereby facilitate understanding of this physics for practicing engineers and researchers. It is important to state now that there is no large difference in the fire physics describing these types of tunnels, independent of their use or complexity. Parameters such as length and cross-sectional geometry are important, but the vehicles that burn inside these different tunnels and the mitigation systems that are applied as well as construction protection adopted are also important.

Fire dynamics usually relates to fire behaviour in ordinary sized compartments (rooms) or corridors. The knowledge of fire chemistry and fire dynamics is treated either with or without the direct interaction of the compartment and the ventilation conditions. Much of the fire research to date has been carried out either inside a normal-sized building compartment or in a building with a large volume (For example, fire laboratory) where one can assume no interaction of the environment with the fire plume (open fire). Some research has also been carried out on outdoor fires, where an external wind potentially has a strong effect.

H. Ingason et al., *Tunnel Fire Dynamics,* DOI 10.1007/978-1-4939-2199-7_1

Most of the fundamental research on fire dynamics in tunnels is focused on smoke spread in tunnels with low ceiling heights and on fire development in single burning vehicles. The requirement for the ventilation systems to prevent back-layering of smoke, that is, the critical velocity, is the single most investigated parameter in tunnel fire research [1]. Combining the knowledge on fire dynamics in buildings and that in tunnels is a challenge, as there are major differences that cannot readily by explained for both types of constructions. In many cases, this creates confusion that is difficult to resolve. One such example is the misconception or misunderstanding that is present concerning well-ventilated fires and under-ventilated fires in tunnels and buildings. The basic phenomena for these terms are explained in detail in Chap. 2 in this book.

The influence of ventilation on heat release rates (HRRs) in vehicle fires and how the smoke, toxic gases and heat spread in the tunnel is very important to understand. This is apparent owing to the occurrence of many disastrous tunnel fires in the past two decades. Thus, in order to determine an appropriate design fire for a fire safety system in a tunnel, some understanding on fire development in vehicle fires and how the fire interacts with its environment is required.

The research carried out in ordinary compartments or corridors, in large laboratory buildings and outdoor (open fires) is of great value and it is important that it be used as a platform in tunnel fire research. Therefore, it is crucial to have a good understanding on the main differences between these different types of fires.

1.2 Characteristics of Tunnel Fires

Tunnel fires differ in many aspects from open fires and building fires. Open fire is defined here as a fire without any interaction with its surrounding geometry or enclosure. This can be the case for a fire outside a building in a quiescent environment or inside a building that is sufficiently large that the fire is not directly affected by its presence. A fire outside a building that is exposed to strong external wind is not considered here.

According to this definition, there are at least two important ways in which tunnel fires differ from the open fires [2], that is, in terms of:

- The heat feedback from the surrounding environment
- The effect of natural ventilation on the fire

The heat feedback to the fuel surface in open fires is governed by the flame volume. In tunnel fires it is the same, except that additional parameters such as tunnel lining, cross-sectional area and ventilation also play an important role.

The oxygen needed for combustion is not always readily available in tunnels in the same way as in the open (where full access can always be assumed). The conditions may either develop to a well-ventilated fire (fuel-controlled) where unreacted air by-passes the burning vehicles, or under-ventilated fire (ventilation-controlled) giving rise to large amounts of toxic fume and products of incomplete combustion.

A fire that develops in a tunnel interacts with the ventilation airflow and generates complicated air flow patterns and turbulence in the vicinity of the fire. The heat generated by the fire warms up the surrounding air, and in the case of a slope inside the tunnel, buoyancy forces are created along the tunnel which could govern the movement of the air flow inside the tunnel. This may lead to drastic changes in the ventilation flow pattern for the whole tunnel system. If the resulting longitudinal flow velocity is not high enough, a reverse flow of hot gases in the ceiling will be created. This phenomenon is better known as back-layering. In order to prevent any type of back-layering, the longitudinal velocity inside the tunnel has to be higher than a critical value. Usually, this critical value is about 3–3.5 m/s for most tunnels. The main problem with natural ventilation in tunnels is that not only the tunnel geometry, the size and the location of the fire govern the flow of hot gases in the tunnel, but also winds and atmospheric conditions outside the portals may have a strong influence on the ventilation system.

The complexity in understanding what is happening inside a tunnel is difficult for the rescue personnel such as firefighters who have to deal with the situation while the fire is developing. The smoke can only be visual from portals, so the decision to attack the fire can only be based on which portal the smoke exits unless a closed-circuit television (CCTV) system exists. Effects of the fire on the natural ventilation inside the tunnel not only complicate firefighting procedures but also present extreme hazards by rapidly propagating toxic fumes and gases far away from the fire. Sudden changes in the air flow could easily occur due to pressure changes inside and outside the tunnel portals. This situation can only be controlled when mechanical systems are applied and the smoke management becomes much easier and a safer environment for evacuees and firefighters can be created in the case of a good ventilation design. In contrast, in building fires the firefighters can always observe the situation from a safe position outside the building. According to Ingason [2], tunnel fires differ from building compartment fires in at least three important ways, that is, in terms of:

- The effects of the *ventilation factor*
- The *flashover* conditions
- The *stratification* development

The maximum HRR in compartment fires is usually dictated by the ventilation factor. The ventilation factor is a parameter defined by the opening areas and height of the openings of the compartment, see Chap. 2 for detailed information. In tunnels the situation is entirely different. The size of the fire and its position within the tunnel, the slope of the tunnel in the vicinity of the fire, the cross-sectional area where the fire takes place, the total length of tunnel, the type of the tunnel lining material (concrete, blasted rock) and the meteorological conditions at the entrance and exit are the parameters that govern the natural ventilation within the tunnel system. This means that tunnels work more or less like communicating vessels. The results of this is that the excess air available for combustion is an order of magnitude higher than in compartment fires which are governed by the ventilation factor. Tunnels are also often equipped with mechanical ventilation which is sometimes termed forced

ventilation. The mechanical ventilation consists of supply/exhaust fans and/or jet fans in the ceiling. In Chap. 13, these ventilation systems are presented more thoroughly. The consequence of using mechanical ventilation is mainly seen in terms of the combustion efficiency, spread of heat and smoke as well as the HRR in tunnels. These ventilation conditions differ significantly from compartment fires which are usually naturally ventilated through windows or other openings. There are many buildings equipped with mechanical ventilation but the flow rate is relatively small as compared to the fire size, and usually when a fire becomes fully developed the windows break and the fire becomes dominated by the ventilation.

In very long tunnel tunnels with natural ventilation and nearly no slope, over several kilometres, it can be shown that the natural flow inside a tunnel and towards the fire source may be predicted by the ventilation factor at the portals (cross-sectional area times the square root of the height). This has not been experimentally verified but theoretical investigations by the authors show that this may be the case. This means that previous thinking about how natural ventilation is governed in very long tunnels with nearly no slope needs to be reconsidered. Generally, the smoke flow descends to the floor level after travelling a certain distance. Then the smoke flow could approximately be considered as being fully mixed, but still there exists indistinct layers, that is: a lower layer with incoming fresh air (partly vitiated) and an upper layer with outgoing combustion products.

Flashover is defined as the rapid transition to a state such that all the surfaces of the combustible materials within a compartment are involved in the combustion. Fires in compartments can easily grow to ‘flashover’ within a few minutes. Flashover is not expected to take place outside a confined space such as a compartment. The volume of the compartment is very important as is the composition of the materials found in the compartment together with the opening sizes. Tunnel fires, in that sense meaning fires in a long space with two large portal openings, are therefore not likely to grow to a conventional flashover. The main reason is due to large heat losses from the fire to the surrounding walls, lack of fuel in relation to the volume size and containment of hot fire gases. The flashover phenomenon is explained in details in Chap. 2.

Experiments and theoretical considerations show that flashover can easily occur in a train compartment or a truck cabin located inside a tunnel [3, 4], see Fig. 1.1. This type of flashover will not occur inside a tunnel space. In the same way, the risk of secondary deflagration due to under-ventilated fires is much lower in tunnels than in building compartment fires [2]. The main reason for this is the difference in the ventilation conditions as explained above and the geometry and heat losses to the surrounding tunnel walls. The amount of fuel load in relation to the tunnel volume also plays an important role.

Although flashover appears to be impossible in a tunnel fire, an under-ventilated fire in a tunnel is possible. This should be given special attention. In an under-ventilated fire, the consequences of the activation of a powerful ventilation system may be dramatic. The flame volume may suddenly increase in size and length, and the fire may easily spread forward due to the preheated vehicles downstream of the

Fig. 1.1 Initial stages of a "flashed over" situation in a metro train carriage. The flames start to plunge out from the broken windows and open doors. (photo Per Rohlén)

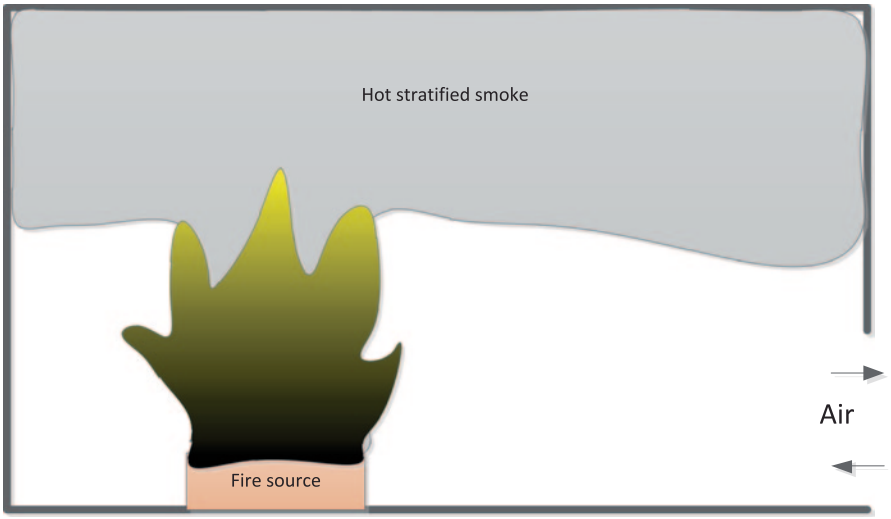

Fig. 1.2 The smoke stratification in the early stage of a compartment fire

fire, although this phenomenon cannot be defined as 'flashover' in the traditional sense of the word [2].

The stratification formation of the smoke layer differs from compartment fires. In the early stages of compartment fires, an upper quiescent buoyant smoke layer is formed with a cold smoke free layer below, see Fig. 1.2. Due to the confinement of the compartment, the smoke layer descends gradually to a level slightly lower than the upper edge of the door or windows. Therefore, at least in the early stage, the height of the openings governs the smoke layer height. However, this is not the case in a tunnel fire.

At a short distance from the point where the fire plume impinges on the tunnel ceiling, the smoke flow transits to a longitudinal flow on both sides in a tunnel

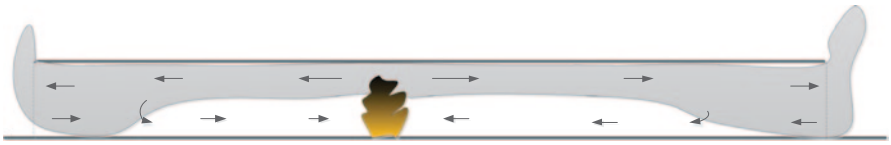

Fig. 1.3 The smoke stratification in a tunnel fire with low ventilation

with essentially no longitudinal ventilation and nearly no slope. Eventually such a layer will be become thicker and descend towards the tunnel floor, see Fig. 1.3. The distance from the fire when this may occur is dependent on the fire size, the tunnel type and the perimeter and height of the tunnel cross-section [2]. See Chap. 12 for further information concerning smoke stratification in tunnels.

If a longitudinal ventilation system is activated, this stratified layer will gradually disperse. At first on the upstream side of the fire, a smoke layer will still exist (back-layering). On the downstream side, the stratification of the smoke is gradually dispersed. This will be governed by the heat losses to the surrounding walls and by the turbulent mixing between the buoyant smoke layer and the opposite moving cold layer. The smoke stratification is important for those who have to escape from the tunnel. The characteristics of the smoke spread are highly dependent on the air velocity and location in the tunnel.

Despite the fact that the fire behaviour can be different depending on the envelope (tunnel, building or in the open) the measures to deal with it vary. Further, the fire load itself in a tunnel is very different from that in a building. The vehicles in tunnels are in most cases the only fuel that is available. In underground car parks, one may find some similarities, and much research has been conducted on car park fires which is very useful for tunnel fire research. In Chaps. 4 and 5, an overview of fire development in vehicles is given.

The mitigation methods (technical safety systems) to deal with tunnel fires vary. In the following section, a short overview of different mitigation methods is given. These systems are described in more details in different chapters in this book.

1.3 Mitigation Systems in Tunnels

A mitigation system is defined here as a technical system or a method to increase the safety during a fire. The systems that need some basic fire dynamic knowledge to design or handle are presented. These include the structural fire protection which relate to different boundary conditions such as the gas temperatures and heat fluxes, the ventilation systems, the evacuation systems which relates to different combustion products, visibility and tenability requirements in the smoke, and finally, detection and suppression systems.

The heat exposure as an input for calculation of the load bearing capacity is important. The main load is through heat flux from burning vehicles. The heat fluxes

vary depending on the tunnel geometry, ventilation in the tunnel and the type and shape of the fire load. Although the heat flux in kilowatts per square meter (kW/m^2) is should be used for describing the heat exposure onto a tunnel construction, it is seldom applied as input into models for calculating temperature rises inside the structure. Instead different types of time–temperature curves are given and the boundary conditions are given as a lumped heat flow constant. The time–temperature curves are usually standardized fire curves (ISO 834 [5], HC [6], RWS [7] etc.), see Chap. 8, Sect. 1, and can vary depending on the guidelines used. In tunnels, the time–temperature curves are usually more severe than those used in buildings. This difference has to do with the dynamics of the combustion process. In well-ventilated tunnels with relatively low ceiling height, the maximum gas temperatures can easily reach a level of 1350 °C, whereas in buildings this is usually in the range of 900–1100 °C. The main reason for this is the difference in the ventilation conditions and thereby the heat flux exposure. The understanding of heat fluxes and temperature development is of great importance and is explained in more detail in Chaps. 8 and 10.

The ventilation system is one of the most important safety features in tunnels. It makes it possible to control the smoke spread and thereby influence the outcome of a fire incident. The mechanical systems can be controlled automatically or by persons in a control center for a specific tunnel or tunnels. In the early history of ventilation design (late sixties), the systems mainly consisted of smoke extraction systems that is, the smoke was exhausted out of the tunnels. The terminology for these types of systems is “semi-transverse” or “fully transverse” systems. “Semi-transverse” means that they only exhaust the smoke whereas “fully transverse” both supply fresh air along the tunnel and exhaust the smoke. Today, these systems have been optimized in the design and are termed point extraction systems. The tunnels in the Alps regions, especially those which have bidirectional traffic, are often equipped with point extraction systems but such systems are also found in other parts of the world. The smoke is not only controlled by extracting the smoke but also by the longitudinal flow created inside the tunnel. Additional jet fans in the ceiling have also be applied to control the longitudinal flows. These systems and their functions are explained in details in Chap. 13. Transverse systems have been shifted to only using longitudinal ventilation by mounting jet fans in the ceiling. This is considerably easier to build and much less expensive. The conceptual idea in unidirectional tunnels is to create a smoke free area upstream of the fire site. The main design parameters are the HRR in MW of a design fire and the critical velocity needed to prevent back-layering inside the tunnel. In Chaps. 4 and 5, different HRRs and fire growth rates are given and in Chap. 6, different design fire concepts are presented. One of the main risks with ventilation systems is the possible enhancing of the fire development and increased risk for fire spread between vehicles. Fire spread in tunnels is presented comprehensively in Chap. 11. Fire spread as governed by the flame length is presented in Chap. 9 and as governed by the heat flux in Chap. 10.

The evacuation systems consist of escape routes at equal intervals inside the tunnels or rescue stations. This is usually arranged as a bypass between two parallel tunnel tubes or safe havens built specifically for evacuees. These distances varies

considerably and are usually determined through national laws, directives, standards or guidelines. It is also possible to perform an engineering analysis considering the effects of the fire on the tunnel users that need to evacuate the tunnel. This type of analysis requires a sound knowledge of fire physics and the dynamics of the smoke products, for example, smoke stratification as presented in Chap. 12, and heat development inside the tunnel. The more advanced methods can be combined with advance Computational Fluid Dynamic (CFD) calculations, as presented in Chap. 17.

Simpler one dimensional (1D) calculation can also be used for sensitivity analysis. The 1D models are presented in Chap. 7 (gas composition), Chap. 8 (gas temperatures) and Chap. 14 (visibility). Knowledge about gas composition is vital when performing this type of calculation. Further, the smoke densities and temperature distribution are important. The basic data about gas composition and production of smoke and gases in different types of fires are given in Chaps. 7, 8, 14 and 15 (tenability). By calculating the walking speed, which is dependent on the visibility, and the hazardous environment the evacuees are exposed to (toxic gases, temperatures), the evacuation time when (or not) they reach a safe region can be derived.

The detection systems are necessary to alert the tunnel users, fire services and the controller of the tunnel systems to an incident. Due to the variation in fire development and conditions in the tunnels, every fire is unique and can be difficult to discover. The main indicators from fires are convective heat, smoke particles, gas composition or radiation. Nowadays, digital analysis using surveillance cameras inside the tunnels are also used as a part of the alerting systems. Depending on the technology used and the fire scenarios, the response of the systems varies. The most common system is based on line detectors, where the convective heat from the fire indicates that there is a fire. Depending on the fire size, tunnel height and ventilation rate, the systems can vary in response time. Other systems detect the smoke particles travelling inside the tunnel which requires that the smoke is lifted by the convective flow (buoyancy) to the location of the detectors. Flame detectors are another type of system that observes the electromagnetic radiation from the flames. If the fires are hidden inside the vehicles, such detectors are not able to detect the fire. Systems based on gas composition are also available. The common factor with all these systems is the dependence on the physics of the fire which, therefore, requires a good basic knowledge on fire dynamics in tunnels when working with these systems. The detection technology is briefly described in Chap. 16, and the basics for the indicators for these systems are well covered through chapters such as 7, 8, 10, 12 and 14.

The suppression systems work actively to control or prevent further fire development in vehicles inside tunnels. The generic name for such systems today is fixed fire fighting systems (FFFS), which covers most type of water based systems. The dynamics of such systems are given by the interaction of water spray with the convective heat from the fire and the suppression of heat and combustion products at the fuel surfaces. The cooling mechanism and downward drag of smoke are parameters that require good basic understanding by engineers and researchers when designing such systems. The water spray systems create different sizes of droplets

and thereby interact with the fire in different way. Large droplets penetrate more easily towards the fuel surface, while small droplets evaporate more easily in the convective gas volume and thereby reduce the gas temperature effectively. This in turn affects the re-radiation to the fuel surface and further development of heat and smoke. An understanding of the energy balance at the fuel surface is vital and gives an indication of the effectiveness of the system. The basic knowledge of fire physics and the interaction of the water with the fire are described in detail in Chap. 16. Large-scale fire tests with FFFS are presented in Chap. 16, while large-scale and model scale tests where no FFFS are involved are presented in Chap. 3.

The model scale technique is an important instrument in order to obtain useful and reliable information concerning fire dynamics in tunnels. In Chap. 18, different types of scaling techniques are presented and outlined. The model scale technique is one of the most effective methods in gaining new knowledge and therefore it is important to present the theories behind it. Much of the knowledge presented in this book actually comes from model scale experiments carried out by the authors for different types of conditions in tunnels. Another knowledge base to obtain valuable information is real incidents occurred in tunnels. In the following section, analysis of numerous large fire incidents is given.

1.4 Incidents in Tunnel

In order to better understand the physics of tunnel fires, a collection of previous large tunnel fires are analysed. These fires have occurred in road tunnels, rail tunnels or metro tunnels. The main difference between the various incidents lies in the way these incidents occur and develop initially.

1.4.1 Fires in Road Tunnels

The road tunnel incidents presented here are typically related to the type of occurrence, that is, a collision between vehicles, collision between a vehicle and tunnel structure or single vehicle fire in an engine compartments, brakes or due to other technical mishaps. The behaviour of the drivers, either controlling the vehicle or as an evacuee, is a major factor in the outcome of these incidents. Fighting these fires as long as only a single vehicle is burning, and there is access to a ventilation system, is usually not a problem. The problem arises when multiple vehicles become involved and there are many evacuees involved in the incident.

The first impression when studying road vehicle fires is that the presence of heavy goods vehicle (HGV) fires dominates the consequences, both concerning the damage to the tunnel construction and in terms of the number of fatalities. Hazardous goods (bulk) transports have seldom been found to be involved in large incidents. One possible reason for this is the safety education given to the drivers

and the regular maintenance of the vehicles. The commodity transported by general HGVs has the same potential to cause havoc as hazardous goods transport with petrol or diesel in a tunnel fire. The fire tests in the Runehamar tunnel in 2003 [8] clearly exhibited this.

Although the largest contribution in tunnel fires is from HGV fires, the most frequent fires are single vehicle fires, such as passenger car fires. Buses and coaches are not frequently involved in tunnel fires, but there is definitely the potential for a large incident compared to a single HGV or passenger vehicle fire. The incitement to install extinguishing systems in this type of vehicles will reduce the risk in the future. The greatest problems arise when multiple vehicles become involved in the initial incident. The risk for fire spread becomes the largest threat.

The fire physics presented in this handbook will teach the reader that the tunnel ceiling height in combination with the ventilation conditions is the single most important parameter for further fire development once a fire has started. The initial type of fire load in the vehicles involved in the incident is also a contributing factor. The tunnel height is probably the most underestimated parameter in fire hazard in tunnels. The lower the tunnel height, the higher the risk for continuous fire spread, especially in queue situations or when large vehicles become involved. This is due to the long flame lengths and thereby the high incident heat fluxes created by these fires. The flame lengths, heat fluxes and risk for fire spread are presented in Chaps. 9, 10 and 11, respectively.

Table 1.1 contains a summary of large fire incidents involving HGV fires, where no direct fatalities have been documented. In Table 1.2, a summary of large fire incidents involving HGVs where fatalities are documented is presented. In many of these incidents, the passengers or drivers were killed in the accident itself, not necessarily because of the fire.

Lönnermark [12] made an analysis of fires involving HGVs and found that fires in tunnels involving only one burning HGV very seldom lead to fatalities, but as soon two or more HGVs are involved, the fire most often leads to fatalities. These conclusions are reflected in what can be interpreted from Tables 1.1 and 1.2.

Kim et al. [13] continued the analyses of different types of accidents and identified the basic parameters for why certain road tunnel fires developed to catastrophic fires while others did not. They concluded that all collision fires where HGVs were involved and the fire spread from the initial vehicles involved in the collision are extremely hazardous to road users and special measures should be taken to avoid them. Kim et al. also indicated that it is likely that the fire rescue service will be faced with a sudden increase of gas temperatures and come across a substantial number of evacuees which are injured, unconscious or even dead in such fires.

In Kim et al.'s study [13] it was found that the collision fires involving only passenger cars at the initial stage of the fires did not spread to the neighbouring vehicles. It was reported that the fires were easily extinguished by the driver or the fire brigade [14]. Although fire spread in fire accidents involving a single vehicle is not common, single fires can propagate to other vehicles when the initial fire originated from a HGV with a large fire load.

Table 1.1 Summary of fires in road tunnels involving HGVs, lorries or trucks, *not* leading to fatalities [9–11]

Year	Tunnel, length	Location	Cause of fire	Duration	Consequences for		
					People	Vehicles	Structure
1968	Moorfleet L = 243 m	Hamburg, Germany	Breaks jamming	1 h 30 min	None	1 HGV	Serious damage for 34 m
1976	B6 L = 430 m	Paris, France		1 h	12 slight injured (smoke)	1 HGV	Damage for 150 m
1983, 3 Feb.	Fréjus, L = 12,868 m	Modane, France–Italy	Gear box breaking	1 h 50 min	None	1 HGV	Serious damage, 200 m
1984	St. Gotthard, L = 16,322 m	Goe-schenen, Switzerland	Fire in engine	24 min	None	1 HGV	Serious damage for 150 m
1993	Fréjus L = 12,870 m	France/Italy	Engine fire	2 h	None	1 HGV	
1994, 5 July	St. Gotthard L = 16,322 m	Goe-schenen, Switzerland	Friction wheel	2 h	None	1 HGV (with trailer)	Serious damage to ceiling, pavement and equipment 50 m, tunnel closed for 2.5 days
1996, 18 Nov.	Channel tunnel L = 50,000 m	England–France	Suspected		30 injured by smoke	10 HGVs	Severe damage to the tunnel ceiling
1997, 31 Oct.	St. Gotthard L = 16,322 m	Switzerland	Fire in engine compartment	1 h 20 min	None	1 HGV	Serious damage 100 m
2000, 14 July	Seljestads-tunnel L = 1272 m	Norway	Engine compartment	45 min	6 injured	1 HGV 6 cars 1 MC	Severe damage
2002	Tauern L = 6400 m	Austria	Faulty engine			1 HGV	Severe damage
2004	Fréjus L = 12,870 m	France/Italy	Breaks caught fire	2.5 h	30 evacuated	1 HGV	
2006 20th Sep	Mastrafjord	Norway	Engine problems	0.5 h	None	1 HGV	

Table 1.1 (continued)

Year	Tunnel, length	Location	Cause of fire	Duration	Consequences for		
					People	Vehicles	Structure
2008 16th June	Södra Länken	Sweden	Engine problems	0.5 h	None	1 HGV	
2010 20th Jan.	Trojane L = 3000 m	Slovenia	Multiple collision involving 6 HGVs	< 1 h	5 injured	2 HGV	Damage to tunnel linings
2011 29th Mar.	Oslofjord L = 7230 m	Norway	Engine problem	< 1 h	4 injured	1 HGV	
2011 23rd June	Oslofjord L = 7230 m	Norway	Engine breakdown	< 1 h	12 injured	1 HGV	Damage to tunnel linings
2013	Gudvanga	Norway	Engine problems	1 h	70 injured	1 HGV	Damage to tunnel linings

Table 1.2 Summary of fires in tunnels involving HGVs, lorries or trucks, leading to fatalities [9–11]

Year	Tunnel, length	Location	Cause of fire	Duration	Consequences for		
					People	Vehicles	Structure
1978, 11 August	Velsen L = 770 m	Velsen, Netherlands	Front–back collision	1 h 20 min	Five dead Five injured	2 HGVs Four cars	Serious damage 30 m
1979, 11 July	Nihonzaka L = 2 045 m	Shizuoka, Japan	Front–back collision	4 days	Seven dead Two injured	127 HGVs, 46 cars	Serious damage 1100 m
1980, 17 April	Kajiwara L = 740 m	Japan	Collision with side wall and over-turning	1 h 20 min	One dead	Two trucks	Damage 280 m
1982, 7 April	Caldecott L = 1083 m	Oakland, USA	Front–back collision	2 h 40 min	Seven dead Two injured	3 HGV, one bus, four cars	Serious damage, 580 m
1987, 18 February	Gumefens L = 340 m	Bern, Switzerland	Mass collision on slippery road	2 h	Two dead	2 HGV one van	Slight damage
1993	Serra a Ripoli L = 442 m	Bologna, Italy	Vehicle out of control and collision	2 h 30 min	Four dead Four injured	4 HGV 11 cars	Serious damage to lining
1996, 18 March	Isola delle Femmine L = 150 m	Sicilia, Italy	Bus crashed into back of tanker		Five dead 34 injured	One tanker, one bus, 18 cars	Damage to lining and lighting
1999, 24 March	Mont Blanc L = 11,600 m	France–Italy	Not known	53 h	39 dead	23 HGVs, one small truck, nine cars, 1 MC	Severe damage (900 m), the tunnel closed for 3 years
1999, 29 May	Tauern L = 6400 m	Austria	Leakage of paints and varnishes	15 h	12 dead	16 HGVs 24 cars	Closed for 3 months
2001, 6 August	Gleinalm L = 8320 m	Austria	Front collision lorry-car		Five dead Four injured	1 HGV one car	
2001, 24 October	St. Gotthard L = 16,322	Switzerland	Collision	2 days	11 dead	13 HGVs 10 cars	Severe damage, 230 m, closed for 2 months
2003, 14 Apr	Baregg	Switzerland	Front–rear collision		One dead One injured		

Table 1.2 (continued)

Year	Tunnel, length	Location	Cause of fire	Duration	Consequences for		
					People	Vehicles	Structure
2005, 4 June	Fréjus L = 12,900 m	France/Italy	Engine fire		Two dead, 21 injured	4 HGV	10 km of equipment to be repaired
2006, 25 October	Eidsvoll L = 1200 m	Norway	Head collision, a car and a HGV loaded with hydraulic oil	1–2 h	Car driver died in accident, Two injured	HGV, Car	Two concrete element damaged, lighting, asphalt damaged
2006, 16 September	Viamala L = 700 m	Switzerland	A bus and two cars in a crash		Nine died, Five injured	Bus, two cars, fire spread to additional two cars	Damage to lining
2007, 23rd March	Burnley L = 3400 m	Australia	Rear–front collision HGV and cars	1 h	Three dead Two injured	Multi-vehicle pileup involving three trucks and four cars	FFFS, no damage
2007, 10th September	San Martino L = 4800 m	Italy	HGV crashed into wall		Two dead 10 injured	1 HGV	
2007, 12 October	Newhall L = 167 m	USA	Two HGVs collided	6–8 h	Three dead 10 injured	30 HGV one car	Severe damage
2009, 10th May	Follo L = 900 m	Norway	HGV collided with entrance wall	1.5 h	One dead	1 HGV	Severe damage, 60 tunnel concrete element replaced, 500 m technical installations
2014, 1st March	Yanhou	China	Two tankers		31 dead	42 vehicles destroyed	

Kim et al. [13] were able to show that fires in road tunnels can be divided into two main categories. One category is fire incidents which involve only one vehicle without any involvement or influence from other vehicles at ignition. The list of road tunnel incidents shows that these kinds of fires develop relatively slowly if there is no other special factor which may accelerate the progress, such as fuel leakage or explosion of cargo. They are initially small and show some sign of fire, such as smoke and flames, so neighbouring vehicles can see what is happening and prepare for the emergency within a reasonable time.

The other category is fire incidents which involve more than one vehicle at the start of the fire and occur as a result of traffic incidents such as a collision between vehicles or between a vehicle and the wall of the road tunnel. These kinds of fires are expected to occur suddenly without any previous signs so they have the potential to develop into a catastrophic fire. The first category was named "single fires" and the latter "collision fires". Among the 69 fires in road tunnels that were analysed, 48 (69.6%) were single fires and 21 (30. 4%) cases were collision fires.

Kim et al. [13] proposed that the two categories (single fire and collision fire) can be divided into subcategories depending on whether the fire has spread or not. The fire spread was defined as fires propagated to another vehicle which is not engaged in the initial fire. The definition proposed by Kim et al. [13] of each incident category were as follows:

- *Incident Category 1 (IC1)*: single fire that does not spread to other vehicles.
- *Incident Category 2 (IC2)*: single fire that propagates to neighbouring vehicles.
- *Incident Category 3 (IC3)*: collision fire that is limited to the vehicles which are involved in the collision.
- *Incident Category 4 (IC4)*: collision fire that spreads to other vehicles which are not involved in the collision.

The reason for focusing on the fire spread was that it was found to be one of the key factors determining the consequences of the tunnel fires studied. The spread of fire increased the intensity and size of the fire and hampered the operations of the fire brigade. Fire spread also involves more vehicles and road tunnel users in an emerging incident so it can potentially claim many casualties and economic losses. If a fire does not spread to neighbouring vehicles, the size or the intensity of the fire will be limited.

Forty three fires of Incident Category 1 (*IC1)* were included in this group. Of these, 25 fires occurred in HGVs, three fires in passenger cars, 14 in buses or coaches and one in a mobile crane. Among 48 single fires, fire spread was found in only five cases. Interestingly, all *IC2* fires originated from HGVs. These were either a petrol truck or lorries carrying a great quantity of combustible goods, for example, tyres in the Frejus tunnel fire of 2005, 9 t of margarine and 12 t of flour in the Mont Blanc road tunnel fire of 1999, 600 polystyrene boxes in the Suzaka tunnel fire of 1967, hazardous material in the Salang tunnel fire of 1982, and 11 t of carbon disulphate in the Holland tunnel fire of 1945. It is reported that most of

Table 1.3 Analysis on the previous fires in road tunnels [13]

Type (%)	Category	No. of fire (%)	Location of original fire	Casualties
Single fire[a] (69.6)	IC1	43 (62.3)	HGV: 25	Casualty: 11
			Bus or coach: 14	No casualty: 32
			Passenger car: 3	
			Mobile crane: 1	
	IC2	5 (7.3)	HGV 5	In all fires, casualties occurred
Collision fire (30.4)	IC3	7 (10.1)	Motorcycle + 2 cars:1	In five cases, casualties occurred
			Lorry + bus or car: 2	
			Car + wall: 2	
			Car + car or bus: 2	
	IC4	13 (18.8)	HGV(s) + cars: 5	In all fires, casualties occurred
			HGV + wall: 1HGV + HGV: 1	
			HGV + car (bus): 3	
			Not known: 3	
	Not known	1 (1.5)	Not known	Not known

[a] Incidents where only smoke is produced without flame are included into single fires

these five fires had unique factors which may have exacerbated the progress of the fire, that is, oil leakage (Mont Blanc road tunnel, 1999), inadequate operational procedures (Suzaka tunnel, 1967) and explosion (Salang tunnel, 1982 and Holland tunnel, 1945). All *IC2* fires claimed casualties and caused significant damage to the vehicles.

Seven fires in *IC3* are summarized in Table 1.3. Two cases were related to HGVs: HGV + bus and HGV + car but no cases with HGV + HGV. The other five cases were collisions between vehicles such as cars, buses and motorcycles and the wall of the road tunnel. Human fatalities occurred in five cases. It is not clear whether human losses were caused by the collision or the fire. However, the likelihood of death or injury in *IC3* fires is very high.

Among 21 collision fires, 13 fires in *IC4* are reported. In all 13 cases, more than one HGV was engaged in the collision incidents. All *IC4* fires started in HGVs or in the vehicles which collided with HGVs. Casualties occurred in all *IC4* fires either due to the fires or the collisions. Collisions between car(s) and bus(es) and subsequent fires were not reported at all.

The situation for the fire fighters becomes difficult to master, and access to the fire site depends very much on the technical equipment provided. The ventilation system is one example of such system, see Chap. 13. FFFS is also a technical system that can improve the conditions for fire fighters, although the final extinction needs to be carried out manually by the firefighters. The longer the tunnels the more difficult the fires will be to fight, unless there is access through escape routes.

1.4.2 Fires in Rail Tunnels

In rail tunnels, the fires are often related to technical failure in the rolling stock, either in locomotive machinery, the restaurant area, electrical system, ventilation system or arson. These fires are often observed by the passengers or staff, and can be dealt with directly. If the fire starts on the outside, it can be due to failure in hydraulic systems (leakage, spray etc.) or overheating of brakes. Such fires are more difficult to discover, and usually not possible to combat until full stop. After full stop these fires can develop fairly rapidly. In some cases, the cause of the fire is due to derailment/collision, but these types of fires are difficult to prevent due to the complexity of the incidents. Freight trains deserve special attention here, as there are very few crew members, but the potential for a fire of long duration is higher. Fighting fires in rolling stock is very difficult and places enormous pressure on the rescue services. The sites of rail accident can also be difficult to reach.

The potential for a huge incident with many fatalities is much higher in rail and metro tunnels or stations compared to road tunnels, simply because of the large number of passengers. The frequency, however, of serious fires in rolling stock is much lower than for road vehicles. The stringent fire requirements on interior and exterior solid materials in modern rolling stock and the type of potential fire risks can explain this difference. In road vehicles there are minimal fire resistance requirements, which are reflected in the consequences of road vehicle fires.

As mentioned previously, however, the potential for many fatalities in rolling stock fires is high, although the risk for fire spread is relatively low provided the initial fire in a given section of the train (inside a wagon), does not develop to a fully flashed over fire (fully developed). The fire development inside a carriage has the same governing physical parameters as a compartment fire. The fuel load, the ventilation conditions through openings such as doors or windows, and the size of the ignition source, are all important parameters for the fire development. The quality of the interior material and the windows are also very important. It is first after the fire becomes flashed over that there is a risk for continuous fire spread to neighbouring carriages. Such fires have occurred with disastrous outcome. In Tables 1.4 and 1.5, the Deagu fire 2003, the Kaprun fire 2001 and the Baku fire 1995 are all example of such fires.

Other types of rolling stock, such as freight trains, may also create hazardous situations, although they usually do not include numerous passengers. The potential for a significant and long duration fire is higher. Examples of such fires can be found in Table 1.4, for example, Summit 1984, Baltimore 2001 and Eurotunnel 1996 and 2008.

For freight trains carrying fuel tanks or HGVs, the main consequence is the damage to the tunnel structure, similar to that in case of a road tunnel fire. In passenger train fires, the main consequence is generally not the damage to the tunnel structure but the number of potential fatalities. Most fire incidents with passenger trains do

Table 1.4 A list of key fire incidents in rail tunnels [9, 14–17]

Year	Name Country Length	Initial fire location	Most possible cause or location of fire	Consequence
2008	Channel tunnel UK/France L = 51 km	Near the front of the train	One HGV	650 m damage
2000	Kitzsteinhorn Austria L = 3.3 km	Rear end of the train	Hydraulic oil leak age to electrical heater	155 dead
1999	Salerno Italy L = 9 km		Smoke bomb	Four dead Nine injured
1998	Guizhou Chaoyangba #2 China L = 0.8 km		Gas canister leak-age, explosion	Six dead 20 injured
1996	Channel tunnel UK/France L = 51 km		Suspected arson	34 injured Severe damage to structure
1991	Dayaoshan tunnel China L = 14.3 km		Cigarette	12 dead 20+ injured
1984	Summit tunnel UK L = 2.6 km		Derailment 13 fuel tanks	Shut for several months
1976	Baocheng China		Derailment, fuel tanks	75 dead 38 injured
1972	Hokoriku Japan		Restaurant fire	30 dead 690 injured
1971	Wranduk Yugoslavia L = 1.5 km		Engine fire	34 dead 120 injured
1921	Batignolles France L = 1 km		Collision	28 dead

not correspond to a large number of deaths. This could be due to the fact that railway tunnels are high and of large cross-sections where people could have some time to evacuate through the portals or cross-passages before the toxic smoke completely descends to inhalation level. The channel tunnel having a small cross-section but equipped with a service tunnel and many cross-passages is an exception. For tunnels not equipped with cross-passages and other active fire protection systems, the consequences can be expected to be more serious.

Another issue for railway tunnels is that the longitudinal ventilation initially developed and commonly used for smoke control in road tunnels has been widely adopted in railway tunnels. In particular during the evacuation stage of a fire incident, this ventilation scheme could make the situation worse in some cases.

Table 1.5 A list of key fire incidents in metro tunnels [9, 14–17]

Year	Name Country	Initial fire source	Most possible cause or location of fire	Consequence
2003	Jungangno metro	In train	Arson, Petrol	198 dead and 146 injured
	Daegu, South Korea			
1995	Baku metro	Rear of 4th car out of 5	Electrical fault	289 dead and 265 injured
	Azerbaijan			
1991	Moscow metro	Underneath of a carriage	Electrical fault	Seven dead and over 10 injured
	Russia			
1990	New York metro US	Inside the tunnel	Cable	Two dead and 200 injured
1987	King Cross station	Escalator in the Station	Cigarette	31 dead
	UK			
1979	San Francisco metro	Underneath of a carriage	Electrical fault	One dead and 58 injured
	US			
1972	Hokoriku tunnel	Carriage	Restaurant	30 dead and 690 injured
	Japan			
1903	Couronnes metro		Electrical fault	84 dead
	France			

1.4.3 Fires in Metro Tunnels

A summary of the key incidents in metro tunnels is presented in Table 1.5. It can be seen that in these fire incidents, electrical fault is the main cause. Further, compared to railway incidents, the consequence of these metro fire incidents is characterised by more deaths. Arson fires require special attention. Despite the small number of arson fires, the resulting consequence can be expected to be most serious. The reason for the catastrophic consequences in these metro tunnel fire incidents is mainly due to the small cross-section of the tunnel and the large number of passengers on board and in the station. Nowadays, metro systems are becoming more and more complicated and constructed at numerous levels down to significant depths. Accordingly, fire safety issues will require greater attention in the future.

1.5 Summary

Catastrophic fires that have occurred in different types of tunnels continue to remind engineers and authorities that this is an important safety field. The large infrastructure projects being undertaken requiring significant investments, demand concomitant safety solutions that are sound and reliable. Without proper knowledge about fire incidents and experiences learned from them, we will not be able to continue developing such solutions. Therefore, it is very important to analyse incidents that have occurred and try to systematize them in order to understand what the key parameters are for the outcome of these incidents. The analysis carried out by Kim et al. on road tunnel fires is a good example of such analysis and systematisation. By dividing the incidents in road tunnels into four incident categories they were able to identify the critical issues, for example, the fire spread to adjacent vehicles. As long as the fire stays in one vehicle, it remains manageable albeit difficult to deal with. In order to better understand these incidents, we need to analyse them from the point of view of fire dynamics and the interaction of the tunnel, vehicle, mitigation and humans. The following chapters give a deep insight into the fire physics of tunnels and thereby constitute a very good knowledge base for future tunnel engineers.

References

1. Ingason H Key Note Paper—State of the Art of Tunnel Fire Research. In: 9th International Symposium on Fire Safety Science, Karlsruhe, 21–26 September 2008
2. Ingason H (2012) Fire Dynamics in Tunnels. In: Beard AN, Carvel RO (eds) In The Handbook of Tunnel Fire Safety, 2nd Edtion ICE Publishing, London, pp 273–304
3. Lönnermark A, Lindström J, Li YZ, Claesson A, Kumm M, Ingason H (2012) Full-scale fire tests with a commuter train in a tunnel. SP Technical Research Institute of Sweden, Borås, Sweden
4. Li YZ, Ingason H, Lönnermark A Fire development in different scales of a train carriages. In: 11th International Symposium on Fire Safety Science, New Zealand, 2014
5. Fire-resistance tests—Elements of building construction—Part 1: General requirements (1999). First edn. International Organization for Standardization, ISO
6. Fire resistance tests—Part 2: Alternative and additional procedures (1999). First edn. European Committee for Standardization
7. Beproeving van het gedrag bij verhitting van twee isolatiematerialen ter bescherming van tunnels bij brand (1979). Instituut TNO voor Bouwmaterialen en Bouwconstructies, Delft, The Netherlands
8. Ingason H, Lönnermark A (2005) Heat Release Rates from Heavy Goods Vehicle Trailers in Tunnels. Fire Safety Journal 40:646–668
9. Lönnermark A (2005) On the Characteristics of Fires in Tunnels. Doctoral Thesis, Doctoral thesis, Department of Fire Safety Engineering, Lund University, Lund, Sweden
10. Carvel RO, Marlair G (2005) A history of tunnel fire experiments. In: Beard AN, Carvel RO (eds) The handbook of tunnel fire safety. Thomas Telford Publishing, London, pp 201–230
11. Fire and Smoke Control in Road Tunnels (1999), PIARC
12. Lönnermark A Goods on HGVs during Fires in Tunnels. In: 4th International Conference on Traffic and Safety in Road Tunnels, Hamburg, Germany, 25–27 April 2007. Pöyry

13. Kim HK, Lönnermark A, Ingason H (2010) Effective Firefighting Operations in Road Tunnels. SP Report 2010:10. SP Technical Research Institute of Sweden, Borås, Sweden
14. Carvel RO (2004) Fire Size in Tunnels. Thesis for the degree of Doctor of Philosophy, Thesis for the degree of Doctor of Philosophy, Heriot-Watt University, Edinburgh, Scotland
15. Bergmeister K, Francesconi S (2004) Causes and Frequency of Incidents in Tunnels
16. Fire Accidents in the World's Road Tunnels. (2006) http://home.no.net/lotsberg/artiklar/brann/en_tab.html
17. Beard AN, Carvel RO (2012) Handbook of tunnel fire safety—Second Edition. ICE Publishing

Chapter 2
Fuel and Ventilation Controlled Fires

Abstract The effect of ventilation on fire development is one of the most important phenomena to understand in tunnel fire safety engineering. Ventilation controls the combustion process and is usually the phenomenon that engineers find most difficult to comprehend. Tunnel fires are considerably different from compartment fires in the way flashover occurs and develops; misconceptions about the effects of ventilation in tunnel fires are clarified in this chapter. The difference between fuel-controlled fires and ventilation-controlled fires is shown and explained. This chapter lays out the basics for understanding the role of ventilation interactions with other combustion phenomena and in fire development. This chapter is based partly on theory, but also includes experimental data obtained by the authors.

Keywords Ventilation control · Fuel control · Oxygen · Combustion

2.1 Introduction

The basic knowledge about fire physics in tunnels is derived from research in compartment or corridor fires. Major theoretical and experimental work was carried out in the 1950s and 1960s followed up by numerical applications in the 1980s and 1990s. This work provided the knowledge base for understanding fire physics and development in tunnel fires and has been used as a basis for many theoretical breakthroughs. This progression, of course, is due to the limited amount of basic fire research that has focussed solely on tunnel fires [1]. In the following sections, the effects of ventilation that are based on knowledge from compartment fires and which have been applied to tunnel fires are identified and explained wherever possible.

2.2 Fire Development in Building Fires

Fire development in compartments or enclosures inside buildings is usually divided into periods or stages. In textbooks [2, 3], four distinct time periods of the complete fire development process in compartments are usually identified. The fire starts

H. Ingason et al., *Tunnel Fire Dynamics,* DOI 10.1007/978-1-4939-2199-7_2

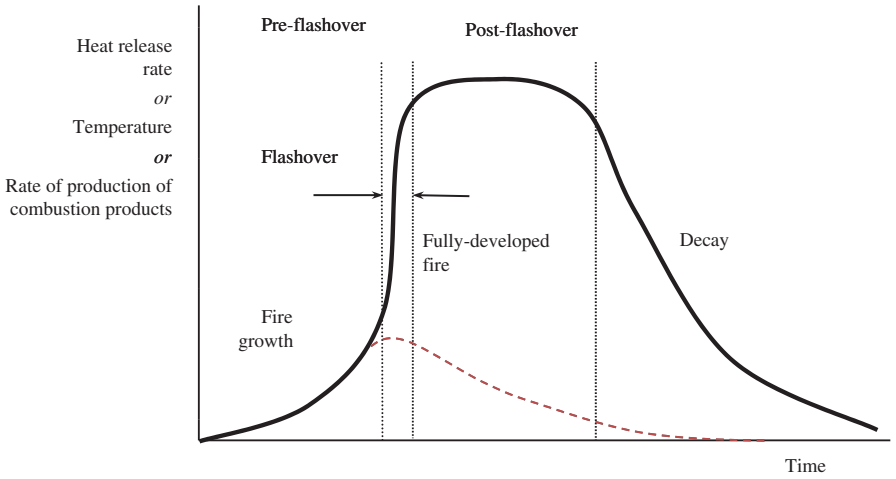

Fig. 2.1 Phases of a typical compartment fire [4]

with a *growth* period which either transitions to a rapid *flashover period* or, if that stage is not achieved, starts to decay and the fire ends. If flashover occurs, the fire becomes *fully developed* during the third period, with relatively constant conditions, before it starts to *decay* during the last period. This complete fire development is represented in Fig. 2.1 and is given as either heat release rate (HRR), temperature, or rate of combustion products as a function of time. Usually the growth period is defined as the *preflashover* stage, and the *post-flashover* stage includes the fully developed fire and the decay period. The fire development in tunnels cannot be described in the same way because the interactions with the enclosure differ considerably.

Traditionally, compartment fires are defined as either *fuel-controlled* or *ventilation-controlled*. In the growth period or the pre-flashover stage of a compartment fire there is sufficient oxygen available for combustion and the fire growth is entirely dependent on the flammability and configuration of the fuel. During this stage, the fire is defined as fuel-controlled. The fire after the growth period can either continue to develop up to and beyond a point at which interaction with the compartment boundaries becomes significant (flashover) or it can start to decay (dashed line in Fig. 2.1). There are two factors that determine the direction of the fire development: a lack of fuel will impede development; or the fire will become ventilation-controlled if there is enough fuel but the fire grows to a size dictated by the inflow of fresh air $(\dot{m}_a)$. The definition and mathematical expression of the difference between fuel- and ventilation-controlled fires will be given in Sect. 2.4.

Unfortunately, there are different interpretations and use of the terminology for fuel and ventilation control. This has resulted in a great confusion among the practicing engineers. A fuel-controlled fire, that is when there is enough oxygen to combust all the available fuel vapors in the enclosure, is also described as well

ventilated, over ventilated, oxygen rich or fuel lean. A ventilation-controlled fire, that is when there is not enough oxygen available to combust all the fuel available inside the enclosure, is sometimes described as under ventilated, fuel rich or oxygen starved [4]. This can cause confusion for the reader, but as authors use different words to describe the same physical phenomena it is unavoidable and difficult to deal with. Due to this confusion it is very important to understand the basic difference of these two combustion modes. The term fuel and ventilation control will be used in this chapter.

For compartment fires the transition period between fuel- and ventilation-controlled fire is usually defined as the 'flashover'. Flashover means that everything that can burn inside a compartment starts to burn during this stage. The situation is shown in Fig. 2.1 as a sudden increase in the HRR. This can also be described as a sudden increase in gas temperature, production of yields of gases such as carbon dioxide (CO_2) or other well defined production terms.

2.3 Fire Development in Tunnel Fires

Tunnel fires are generally fuel-controlled as there are seldom restrictions to air access. Tunnels usually have two or more portals and therefore act as communicating spaces if no mechanical ventilation is installed. The fire is supplied with air due to pressure differences between the fire gases and the atmosphere and possibly the pressure difference between portals. This is represented by the diagrams on the left side in Fig. 2.2 for fuel-controlled compartment fires and tunnel fires. However, in severe fires such as the Mont Blanc, Tauern, and the St. Gotthard fire disasters [5] with multiple large vehicles involved, the supply of air was not enough to sustain complete combustion. This will result in a sudden increase in the production of carbon monoxide (CO) and all the oxygen (O_2) that is transported to the fire source could be consumed. This may not be the case if only one vehicle is burning, but will definitely occur when more vehicles are involved. This situation is represented by the picture on the right side in Fig. 2.2 for ventilation-controlled tunnel and compartment fires.

The way the air is supplied to the fire source is a key issue for these types of large fires. If there is a supply of fresh air between burning vehicles the fire will continue to develop as long as there is enough oxygen available. If the fire is supplied with air from one direction as in longitudinal ventilated tunnels, it is possible to estimate how much air is needed to sustain complete combustion.

Figure 2.3 shows the possible fire development in large tunnel fires such as the Mont Blanc and the Tauern fires where many large vehicles were completely consumed in the fire. In such large fires there are five different zones assumed [4]:

- burnt out cooling zone
- glowing ember zone
- combustion zone

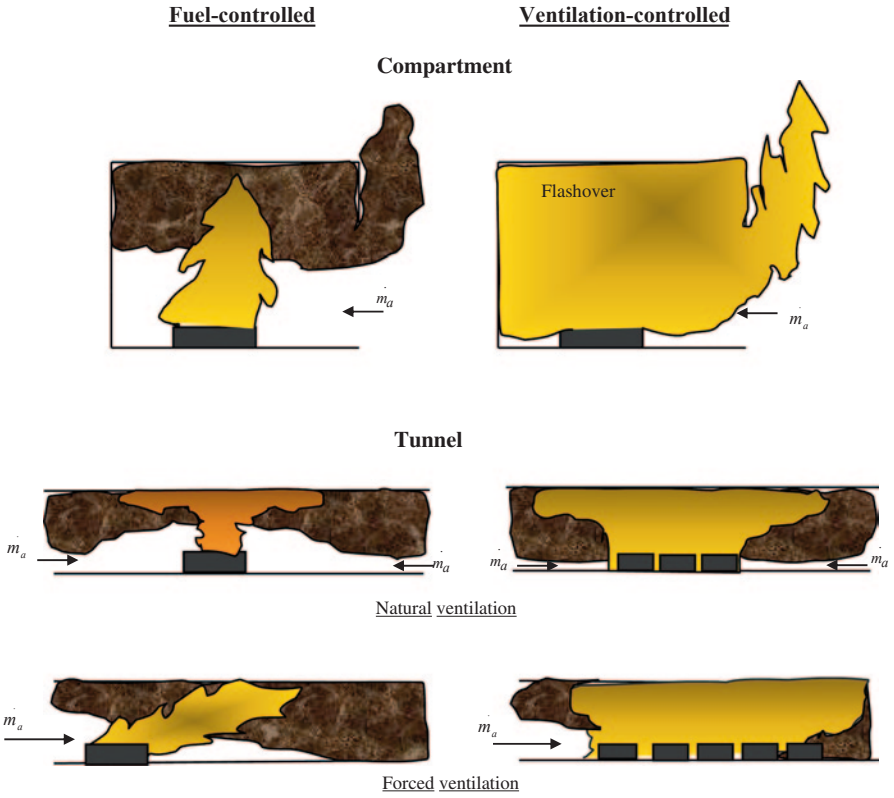

Fig. 2.2 Fuel-controlled (*left-side*) and ventilation-controlled fires in a compartment and a tunnel (*right-side*) with natural draught (*middle*) and forced ventilation (*lower*), respectively [4]. The *arrows* indicate the flow of fresh air

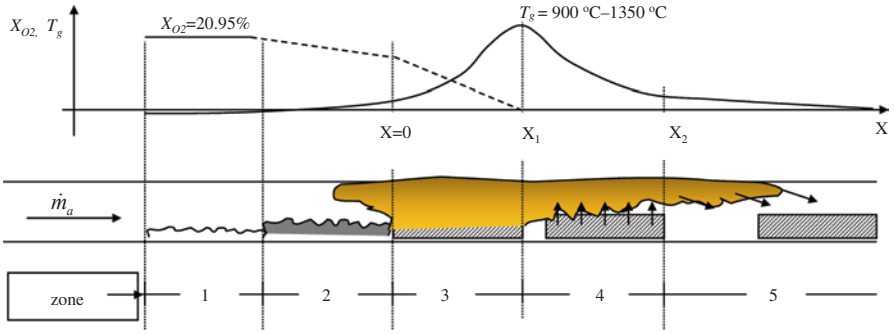

Fig. 2.3 Schematic representation of the burning process of a ventilation-controlled fire in a tunnel [4]

- excess fuel zone
- preheating zone

Figure 2.3 is based on the original work by de Ris [6]. Provided that there are enough large vehicles in the vicinity of the initial fire, these different zones move forwards in a dynamic manner. The most interesting zone is the 'combustion zone' involving the burning vehicles. The combustion zone starts at $x=0$ (see Fig. 2.3) and contains fully developed fires in numerous vehicles. Here, we assume that there is enough fuel-vapor and oxygen to support continuous combustion. Flames are observed throughout this zone. The gas temperature beyond $x=0$ increases rapidly until it reaches a peak value at $x=x_1$, that is just behind the combustion zone. At the same time, the oxygen supplied to the combustion zone is rapidly depleted. The explanation given by de Ris [6] on oxygen reduction was originally deduced for duct fires. De Ris' explanation fits very well to a tunnel situation with numerous large vehicles placed close together, and where the fire can spread easily. The 'excess fuel zone', where all oxygen has been consumed in the combustion zone, starts at $x=x_1$. Fuel vaporises from the vehicles throughout this zone, although no combustion takes place here due to lack of oxygen. This will occur up to a point along the tunnel where the gas temperature has decreased to the fuel pyrolysis temperature. This temperature (at the surface of the material) can be assumed to be higher than 300 °C for the majority of solid materials. Beyond this point, that is point $x=x_2$ in Fig. 2.3, no vaporisation of the vehicles occurs. At the same time the hot gas flows into a so-called 'preheating zone' and exchanges heat with the tunnel walls and preheats the vehicles that have not yet started to burn within this zone.

Model scale tests carried out by Hansen and Ingason [7] verifies very well this process in longitudinal tunnel flows with multiple objects burning. The oxygen on the downstream side is virtually zero, and the CO production starts to increase significantly. The increase of CO production is the best indicator of a ventilation-controlled situation. This is discussed in more detail in Sect. 2.6.

There is a third mode of combustion conditions related to ventilation in buildings and tunnels. This is a mode of inerting (sometime called vitiation or mixing of vitiated air) of the fire source. This mode may be very important for fires in tunnels with natural ventilation. If the base of the fire source is completely surrounded by air that has high content of inerting gases (vitiated air) such as CO_2 it may self-extinguish. The inerting air, which is a mixture of air and combustion products, has usually about 13 % oxygen when the fire will self-extinguish (That is, flammability limits are exceeded) [8]. This limit is to some extent temperature dependent [9]. Increasing temperature tends to lower the flammability limits and thereby the concentration when the fire self-extinguishes. The temperature dependence is discussed in further detail in Sect. 2.7.

There are mainly two situations where inerting may occur in tunnel fires. The first one is in very long tunnels (tens of kilometres) with natural ventilation and nearly no slope and where one can expect long back-layering distances. The backflow of mixed air toward the fire may be highly inerted due to mixing of combustion products that are transported backward from the fire with fresh air flowing from the entrance toward the fire, see Fig. 2.4.

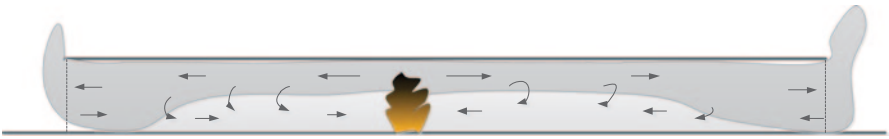

Fig. 2.4 Schematic representation of an inerted fire in a long tunnel. The *arrows* pointing toward the fire indicate inerted (vitiated) air flow

When this inerted air reaches the base of the fire it will affect the combustion efficiency. Depending on the degree of mixing and stratification of the airflow that reaches the fire source, different effects are observed. Currents with pure fresh air along the tunnel floor will usually supply the fire with sufficient oxygen to sustain combustion at the lower levels of the fire. At the upper/higher levels, some influences on the combustion efficiency may occur. Self-extinguishment due to inerted backflow is difficult to obtain in this situation, simply because the mixing of fresh air and combustion products is not efficient enough. The entire base of the fire has to be covered with inerted air of less than 13 % oxygen in order to obtain self-extinguishment.

Self-extinguishment in tunnels due to inerted air has been observed in experiments with a model scale tunnel but the experimental conditions were in these cases quite special [10, 11]. The fresh air was choked upstream of the fire by reducing the inlet area. As the fresh airflow was reduced, the degree of mixing upstream of the fire increased. At a certain critical area the fire self-extinguished due to the inerted air (< 13 % oxygen) created by the mixing of the backflow combustion products and inflowing fresh air.

When inerted air surrounds the fire source, and conditions reach the flammability limits, the fire will not produce much CO or smoke. The radiation levels decrease and some flames lifting from the fire source can be observed [10–12]. This has been observed in many fire tests by the authors. There is nothing which indicates that this would not occur in a similar situation in a tunnel fire, that is when the surrounding inerted air reaches the flammability limits, the flame volume, CO production, and soot production will decrease considerably.

The second condition where vitiation may occur is in a long tunnel with only one opening, such as a tunnel under construction or a mine tunnel. If no mechanical ventilation is present, or the ventilation is shut off after a fire, this could result in smoke and combustion gases redrawn back to the fire from either one or two directions, as it mixes with the fresh air coming in from the portal. This may result in self-extinguishment of the fire. This has not been reported from any real fires, but Lönnermark and Ingason [13], reported about this phenomena in model scale tests carried out using dead end tunnels with only one portal at a higher level than the dead end, where the fire source was located. The fire did not succeed to establish a circulating flow between the fire source and the portal, so the mixing backflow coming toward the fire source had less than 13 % oxygen when the fire self-extinguished. The combustion conditions were influenced prior to reaching the flammability limits and the HRR of the fire was reduced significantly compared to a fully ventilated fire.

2.4 Fuel or Ventilation Control in a Compartment Fire

In this section, the focus is on fully developed fires in a compartment. The parameters that govern whether the fire will go to flashover include the fire load, the dimensions of the compartment and the ventilation openings as well as the thermal properties of the surrounding walls. Flashover in a compartment has been explained as thermal instability caused by the energy generation rate increasing faster with temperature than the rate of aggregated energy losses [14]. Usually, this phenomenon occurs during a short period and results in a rapid increase of HRR, gas temperatures, and production of combustion products. After a flashover has occurred in a compartment, the rate of heat release will develop to produce temperatures of 900–1100 °C. The period after flashover is called the post-flashover stage or the fully-developed fire period, see Fig. 2.1. During this period, the HRR is assumed to be dictated by the oxygen flow through the openings and the fire is therefore defined as 'ventilation-controlled', see Figs. 2.2 and 2.5. The heat released depends upon the amount of air available within the compartment. The air mass flow rate through the opening, $\dot{m}_a$, can be expressed in general terms [15, 16] as:

$$\dot{m}_a = \delta \rho_a \sqrt{g} A_0 \sqrt{h_0} \tag{2.1}$$

where δ is a proportionality constant which is a weak function of temperature, ρ_a is the ambient density (kg/m^3), A_0 is the area of the opening (m^2) and h_0 is the height of the opening (m). The mass flow rate of the fresh air flowing into a compartment could be simply estimated using the classic enclosure fire theory.

If we consider Fig. 2.5, we can integrate the total mass flow rate entering the enclosure by the following equation:

$$\dot{m}_a = \int_0^{h_1} C_d \rho_a w u(z) dz \tag{2.2}$$

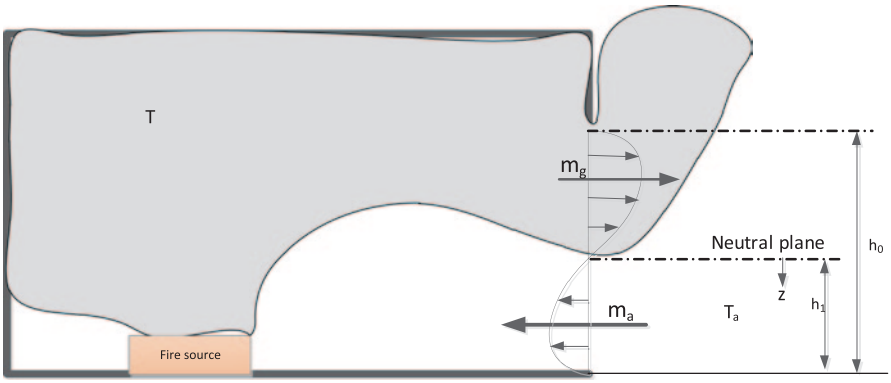

Fig. 2.5 Post-flashover in a compartment fire

where C_d is the flow coefficient, h_1 is the height from the neutral layer to the floor level and u(z) is the velocity as a function of height z, see Fig. 2.5. The *w* is the width of the opening (with the area A_0) which can be the door width. With aid of Bernoulli's equation we can obtain the following relationship for the horizontal velocity entering the enclosure:

$$u(z) = \sqrt{\frac{2g\Delta\rho}{\rho_a}}\sqrt{z} \tag{2.3}$$

where $\Delta\rho = \rho_a - \rho = \rho_a\left(1 - \frac{T_a}{T}\right)$. Introducing Eq. (2.3) into (2.2) yields the following equation:

$$\dot{m}_a = C_d \rho_a w \sqrt{\frac{2g\Delta\rho}{\rho_a}} \int_0^{h_1} \sqrt{z}\, dz \tag{2.4}$$

Integration of Eq. (2.4) yields the following equation:

$$\dot{m}_a = \frac{2}{3} C_d \rho_a w \sqrt{\frac{2g\Delta\rho}{\rho_a}} h_1^{3/2} \tag{2.5}$$

Karlsson and Quintiere [3] gives a correlation between h_1 and h_0:

$$h_1 = \frac{h_0}{1 + (\rho_a / \rho)^{1/3}} \tag{2.6}$$

Introducing Eq. (2.6) into Eq. (2.5) we yield the following relationship:

$$\dot{m}_a = \frac{2}{3} C_d \rho_a w h_0 \sqrt{2}\sqrt{g} \sqrt{\frac{\Delta\rho / \rho_a}{\left[1 + (\rho_a / \rho)^{1/3}\right]^3}} \sqrt{h_0} \tag{2.7}$$

Karlsson and Quintiere [3] have shown that the term $\sqrt{\frac{\Delta\rho / \rho_a}{\left[1 + (\rho_a / \rho)^{1/3}\right]^3}}$, which they define as *density factor*, can be approximated by a value of 0.214 in the case of fully developed fires in an enclosure, see Fig. 2.6.

Thus Eq. (2.7) can be simplified to:

$$\dot{m}_a = \frac{2}{3} 0.214 \sqrt{2} C_d \rho_a \sqrt{g} A_0 \sqrt{h_0} \tag{2.8}$$

where we use $wh_0 = A_0$. Eq. (2.8) can be rewritten and is identical to Eq. (2.1):

$$\dot{m}_a = \delta \rho_a \sqrt{g} A_0 \sqrt{h_0} \tag{2.9}$$

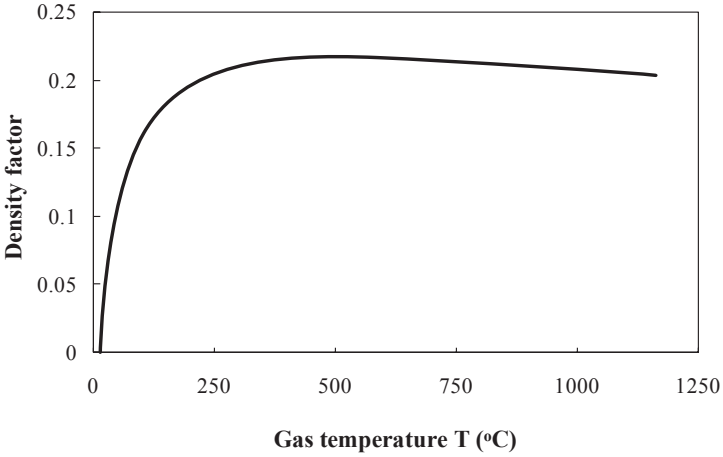

Fig. 2.6 The density factor as a function of the gas temperature inside the compartment

where $\delta = \frac{2}{3} C_d \sqrt{2} \sqrt{\frac{\Delta\rho / \rho_a}{\left[1 + (\rho_a / \rho)^{1/3}\right]^3}}$. This means that for a fully developed fire, δ is a weak function of the gas temperature. The value of δ has been estimated to be either 0.13 [16] or 0.14 [15], respectively, for postflashover fires. Assuming that C_d is equal to 0.7 and the density factor is 0.214, we obtain $\delta = 0.14$ using the equation for δ. The value of $\delta\rho_a\sqrt{g}$ in the preflashover case (fuel-controlled) is 0.3 (kg/s m$^{-5/2}$) and 0.5 (kg/s m$^{-5/2}$) in the postflashover (ventilation-controlled) case assuming the density, ρ_a, is equal to 1.22 kg/m^3 and g equal to 9.81 m/s^2. For the postflashover this can be written as:

$$\dot{m}_a = 0.5 A_0 \sqrt{h_0} \tag{2.10}$$

The term $A_0\sqrt{h_0}$ is better known as the 'ventilation factor' and originates from Bernoulli's equation applied to density flow through a single opening [2].

Assuming that each kg of oxygen used for combustion produces about 13.1×10^3 kJ [17, 18] and that the mass fraction of oxygen (Y_{O_2}) in air is 0.231 we can approximate the maximum HRR that is possible *inside* a compartment during the ventilation-controlled stage. If we use the values given earlier in combination with Eq. (2.1), that is $13.1 \times 10^3 \times 0.231 \times \dot{m}_a$ where $\dot{m}_a = \delta\rho_a\sqrt{g}A_0\sqrt{h_0}$, we obtain the maximum HRR, $\dot{Q}_{\max}$ (kW), within the compartment ($\delta\rho_a\sqrt{g} = 0.5$ kg/s m$^{-5/2}$) as [4]:

$$\dot{Q}_{\max} \approx 1500 A_0 \sqrt{h_0} \tag{2.11}$$

According to all text book literature, all the oxygen entering the compartment is assumed to be consumed within the compartment. This assumption has been challenged by Li et al. [19] as they pointed out that it is impossible to consume all

Fig. 2.7 A fully developed fire in a train coach (photo Tomas Karlsson)

the oxygen that enters the compartment inside the compartment itself. It was stated that the maximum HRR can be estimated based on full consumption of the oxygen flowing in through the openings multiplied by a correction factor, which depends on the heat absorbed by the fuel surfaces and the fuels available. The heat absorbed by the surfaces is proportional to the heat of combustion and inversely proportional to the heat of pyrolysis. In summary, Li et al. [19] concluded that although these types of fires are normally called ventilation-controlled fires, they are also closely related to the type and configuration of the fuels inside the compartment, that is they are in some way also fuel controlled because much of the combustion process occurs outside the openings in fully developed fires.

Ingason [20] explains this in a slightly different way, purely based on the earlier view that in a flashover situation all the oxygen is consumed inside the compartment. This includes the assumption that the rate at which air enters the compartment is insufficient to burn all the volatiles vaporising within the compartment and the excess volatiles will be carried through the opening with the outflowing combustion products (That is, all oxygen is consumed and unburned fuel will leave the compartment). This is normally accompanied by external flaming in the vicinity of the opening as shown in Fig. 2.7.

Ingason [20] reported that this phenomenon becomes important when one wishes to estimate the maximum HRR in a 'postflashover' steel body train coach located *inside* a tunnel. Equation (2.10) may underestimate the maximum HRR within the tunnel if excess volatiles are burned outside the train coach. Model scale tests (1:10) of a fully developed fire in a train coach showed that the maximum heat release when all windows were open was on average 72 % higher than the value obtained according to Eq. (2.11) [20]. This means that 42 % of the total fuel vaporised within

the coach (assuming that all the oxygen in the entrained air is consumed within the coach) is burned outside the openings.

Bullen and Thomas [21] have showed that the amount of excess fuel burning outside the openings is mainly dependent on the fuel surface area and the ventilation factor $A_0\sqrt{h_0}$. Thus, assuming that this factor is relatively constant for this type of geometry (a train coach) the maximum HRR according to Eq. (2.11) was proposed by Ingason [20] to be multiplied by a factor of 1.72. Ingason [20] proposed a more general expression of Eq. (2.11), where maximum HRR in a train coach after flashover such as the one shown in Fig. 2.7 can then be estimated according to the following equation:

$$Q_{\max} \approx \eta 1500 A_0 \sqrt{h_0} \tag{2.12}$$

where η is a correction factor which may be determined from experiments. Li et al. found that this correction factor can vary considerably. The correction factor ranged from 0.67 to 1.7 and was found to be around 1.27 in full scale tests carried out with a commuter train inside a tunnel [19]. The work of Li et al. [19] will be presented in more detail in Chap. 6.

Example 2.1
What is the HRR of the burning train coach shown in Fig. 2.7? The coach windows are 1.0 m wide and 1.0 m high and there are seven windows on each side. The door opening is 1 m wide and 2 m high. The total opening area times the square root of the opening heights is 15.4 $m^{5/2}$ $\left(\sum A_{0,window}\sqrt{h_{0,window}} + A_{0,door}\sqrt{h_{0,door}} = 15.4\ \mathrm{m}^{5/2}\right)$.

Solution: According to Eq. (2.11) the maximum HRR is equal to 23 MW. This means that if this coach were burning in a tunnel the total HRR inside the tunnel would be higher than 23 MW since fuel volatiles are burning outside the openings. This can be estimated by multiplying the value obtained using Eq. (2.12) by a constant of 1.7. Thus, the maximum HRR from the burning coach in Fig. 2.7 is estimated to be 40 MW. This estimated value could be conservative since the highest correction factor obtained from tests is used in the calculation.

2.5 Fuel or Ventilation Control in a Tunnel with Longitudinal Flow

Ingason [4] has developed a method to determine whether a tunnel fire is fuel or ventilation-controlled. According to the definition of fuel control (or well-ventilated), the oxygen or the oxidant is in unlimited supply and the rate of combustion is independent of the oxygen supply rate or mass flow rate of air. The HRR is then determined by the fuel supply rate or mass flow rate of the vaporised fuel. The combustion behavior is then similar to that of combustion in the open where access to air is unlimited. The combustion efficiency will be controlled by the local mixing of air and fuel.

A ventilation-controlled fire (or under-ventilated) is, in contrast, controlled by the oxygen supply and the rate of combustion or HRR becomes dependent on both

air and fuel supply rates. The efficiency of combustion depends on the fuel supply rate relative to the oxygen supply rate. When precisely the necessary amount of oxygen is available to enable complete combustion one says that the mixture is "stoichiometric". The stoichiometric coefficient, r, which gives the mass ratio of air to fuel required for stoichiometric combustion of fuel to produce CO_2 and H_2O, can be obtained using the following equation by Ingason [4]:

$$r = \frac{137.8\left(a + \frac{b}{4} - \frac{c}{2}\right)}{12a + b + 16c} \tag{2.13}$$

where the letter index comes from a generic fuel ($C_aH_bO_c$). In order to demonstrate the use of Eq. (2.13) let us consider an example.

Example 2.2
How much air is required to completely burn 1 kg of propene, C_3H_6?

Solution: Here $a = 3$, $b = 6$ and $c = 0$. With the aid of Eq. (2.13) we obtain the stoichiometric ratio, $r = 14.7$. This means that 14.7 kg of air are required to completely burn 1 kg of propene.

There are many different ways of characterising the relationship between air (oxygen) supply and the fuel supply. Tewarson [22] define the fuel-to-air equivalence ratio, ϕ, as.

$$\phi = \frac{r\dot{m}_f}{\dot{m}_a} \tag{2.14}$$

where $\dot{m}_a$ is the mass flow rate of air (oxygen) supply, $\dot{m}_f$ is the fuel mass loss rate (fuel supply, in kg/s) and r is the stoichiometric coefficient for complete combustion obtained by Eq. (2.13). Beyler [23] defines the equivalence ratio ϕ as the normalized fuel to air ratio, which is the same as given by Tewarson.

The fuel-to-air equivalence ratio, ϕ, can be used to determine whether a fire is fuel-controlled or not. In the case when the fuel-to-air equivalence ratio ϕ is less than one, $\phi < 1$, then the fire is assumed to be fuel controlled (well-ventilated). When the fuel-to-air equivalence ratio, ϕ, is equal to one $(\phi = 1)$, the combustion process is stoichiometric (complete combustion). In the case when the fuel-to-air equivalence ratio, ϕ, is larger than one, (That is, $\phi > 1$) then the fire is assumed to be ventilation-controlled (under-ventilated).

2.5.1 Fuel Control

When the fire is fuel-controlled $(\phi < 1)$, the HRR is directly proportional to the fuel mass loss rate, $\dot{m}_f$. The chemical HRR, $\dot{Q}$ (kW), which is directly proportional to the fuel mass loss rate, $\dot{m}_f$ (kg/s), can then be calculated using the following equation:

$$\dot{Q} = \dot{m}_f \chi \Delta H_c \tag{2.15}$$

where ΔH_c is the net heat of complete combustion (kJ/kg), that is in which the water produced is in the form of a vapour. In fires the combustion of fuel vapours is never complete, and thus the effective heat of combustion ($\Delta H_{c,eff} = \chi \Delta H_c$) is always less than the net heat of complete combustion (ΔH_c). Further, the combustion efficiency χ is the ratio of the effective heat of combustion to net heat of complete combustion, that is, $\chi = \Delta H_{c,eff} / \Delta H_c$ [24] (Tewarson [24] refers to the 'effective heat of combustion' as the 'chemical heat of combustion'). The fuel mass loss rate is sometimes expressed as the fuel mass loss rate per unit area of fuel (A_f), $\dot{m}''_f$, which means that $\dot{m}_f$ can be replaced by $\dot{m}''_f A_f$ in Eq. (2.16).

2.5.2 Ventilation Control

If the fuel-to-air mass ratio is larger than the stoichiometric value, $\phi > 1$, then the fire is defined as ventilation-controlled and the HRR, $\dot{Q}$, is directly proportional to the mass flow rate of air, $\dot{m}_a$, (That is, proportional to the oxygen supply) available for combustion. Sometimes, but not always, we can simplify this by saying that the oxygen concentration in the gases flowing out of the compartment or the tunnel portal is essentially zero. One notable exception is ventilation-controlled fires in large compartments with small openings (That is, no flashover). There are different methods to determine the HRR for the ventilation-control conditions. The simplest is the following equation, which assumes complete combustion and that all the supplied air, $\dot{m}_a$, is consumed:

$$\dot{Q} = \dot{m}_a \frac{\Delta H_c}{r} \tag{2.16}$$

where the ratio $\Delta H_c / r$ is nearly constant for most carbon based material [18]. The energy release per kg of air consumed is approximately 3000 kJ/kg. If all the oxygen were consumed, the energy released would correspond to 13×10^3 kJ/kg of oxygen consumed. This can be derived by dividing the ratio $\Delta H_c / r$ with 0.231 which is the mass fraction of oxygen in air. This number is well known from calorimeter measurements in fire laboratories [25] which use the average value of 13.1×10^3 kJ/kg when calculating the HRR based on gas measurement and mass flow rates of combustion gases in a hood system.

2.5.3 Determination of Combustion Mode

The combustion mode is important to know. There are different ways to obtain that. In order to make a simple estimation of the combustion mode, that is determine whether the fire is fuel-controlled, stoichiometric or ventilation-controlled in a tunnel, we can combine Eqs. (2.14) and (2.15), and assume $\chi = 1$, to give:

$$\phi = \frac{\dot{Q}}{3000\dot{m}_a} \tag{2.17}$$

Equation (2.17) assumes that not all the air is necessarily consumed. Depending on the value of ϕ the degree of combustion efficiency is determined. If we assume stoichiometric combustion, that is ϕ becomes equal to 1, then the mass flow rate to obtain a complete combustion is

$$\dot{m}_a = \frac{\dot{Q}}{3000} \tag{2.18}$$

This equation can also be written as:

$$\dot{Q} = 3000\dot{m}_a \tag{2.19}$$

where $\dot{Q}$ is now in kW. This equation is of interest to estimate the fire size in a train coach with airflow $\dot{m}_a$ through windows and door openings. It can also be used to estimate how large a fire can become in a tunnel with a longitudinal flow, assuming good ventilation conditions around the fire source. If we have a tunnel with a cross-sectional area A (m^2) and we have a longitudinal centreline air flow $u(m/s)$ at an ambient temperature of 293 K.

$$\dot{Q} = 3130uA \tag{2.20}$$

where $\dot{Q}$ is in kW and a flow coefficient C_d of 0.87 for a longitudinal flow in tunnel is assumed.

In some cases, it is of interest to know how much oxygen is left after the combustion assuming that all the fuels are consumed. The mass fraction of unreacted oxygen or air passing the fire can be estimated using the following equation [4]:

$$\beta = \frac{\dot{m}_a - \dfrac{\dot{Q}}{3000}}{\dot{m}_a} \tag{2.21}$$

Here, it is assumed that not all the air ($\dot{m}_a$) is consumed by the fire. The use of Eqs. (2.17) and (2.21) is illustrated by Example 2.3.

Example 2.3

Assume a fire is burning in a Heavy Goods Vehicle (HGV) in a tunnel which is 6 m high and 10 m wide and having longitudinal ventilation inside the tunnel with a centreline velocity of 2 m/s. The fire is estimated to reach a peak HRR of 150 MW. Is the fire ventilation-controlled or fuel-controlled when the fire becomes 150 MW? The air density within the tunnel is $\rho_a = 1.2$ kg/m^3. What is the largest fire that can exist in the tunnel before it becomes ventilation-controlled?

Solution: First we calculate the mass flow rate of air; $\dot{m}_a = 0.87 \times 1.2 \times 2 \times 6 \times 10 = 125$ kg/s, *where 0.87 is the flow contraction coefficient*

for tunnel flow. Equation (2.17) gives $\phi = 150000/(3000 \times 125) = 0.4$. *This value is less than 1 and therefore the fire is fuel-controlled* ($\phi < 1$). *This also means that unreacted air is passing the combustion zone. The mass fraction of unreacted air can be obtained with Eq. (2.21);* $\beta = (125 - (150\,000/(3000)))/125 = 0.6$. *This means that 60% of the available oxygen in the airflow remains unreacted and 40% has been consumed in the fire. Using Eq. (2.20) we find that the fire cannot be larger than* $3130 \times 2 \times 6 \times 10 = 375{,}000$ *kW (375 MW), unless it becomes ventilation-controlled. If we put 375,000 kW into Eq. (2.21) we get* $\beta = 0$ *which implies that all oxygen has been consumed in the fire.*

When the oxygen concentration at a given distance downstream of the fire in a forced ventilation flow is essentially zero, the fire gradually changes from fuel-controlled ($\phi < 1$) to ventilation-controlled fire ($\phi > 1$).

Ingason [4] proposed to use the ratio of mass flow of CO and CO_2 as an indicator of a ventilation-controlled fire. This can be expressed as the ratio $\dot{m}_{CO}/\dot{m}_{CO_2}$. When the values of the ratio begin to increase considerably, $\dot{m}_{CO}$ is the parameter that increases fastest, which indicates that there is not enough oxygen to combust all the available fuel. Tests in nontunnel environments showed that the ratio $\dot{m}_{CO}/\dot{m}_{CO_2}$ increases exponentially as the fire become ventilation-controlled for both diffusion flames of propane and propylene and wood crib fires [24]. Tewarson [26] investigated this thoroughly and presented a correlation between the ratio $\dot{m}_{CO}/\dot{m}_{CO_2}$. Tewarson [26] was able to show that wood crib fires become ventilation-controlled when the ratio $\dot{m}_{CO}/\dot{m}_{CO_2} > 0.036$ and gas diffusion flames become ventilation-controlled when this ratio is greater than 0.1. Ingason [4] proposed the following equation for $\dot{m}_{CO}/\dot{m}_{CO_2}$

$$\frac{\dot{m}_{CO}}{\dot{m}_{CO_2}} = \frac{M_{CO}X_{CO}}{M_{CO_2}X_{CO_2}} = 0.636\frac{X_{CO}}{X_{CO_2}} \tag{2.22}$$

as an indicator for combustion mode where X is the volume concentration (or mole fraction) and M is the molecular weight (M is 28 g/mol for CO and 44 g/mol for CO_2). Thus, the limits for ventilation control when using this equation are $X_{CO}/X_{CO_2} > 0.057$ for wood cribs and 0.157 for gas diffusion flames.

Hansen and Ingason [7, 27] performed fire tests in a 10 m long model-scale tunnel (1:15) where the longitudinal flow varied as well as the amount of fuel (number of wood pallet piles) used in the tests. The HRRs from the fire when four piles of scaled wood pallets were burned varied from 454 to 504 kW. For a single pile, the HRR was about 150 kW. The velocity in the tunnel was 0.3, 0.6, and 0.9 m/s, respectively and the cross-sectional area was 0.24 m^2. The maximum size of a fire that can exist, as calculated using Eq. (2.20): $3130 \times 0.6 \times 0.24 = 451$ kW before it becomes ventilation-controlled. This is very close to the HRR measured in the tests. This means that the fire, when spreading to all four of the wood pallet piles, should be ventilation-controlled and some increase in the CO production should be expected.

Therefore, analysis of not yet published information on gas concentrations from one test is included and discussed. Test number 11 of the test series in question was selected for the analysis. The peak HRR was measured to be 464 kW. In full scale

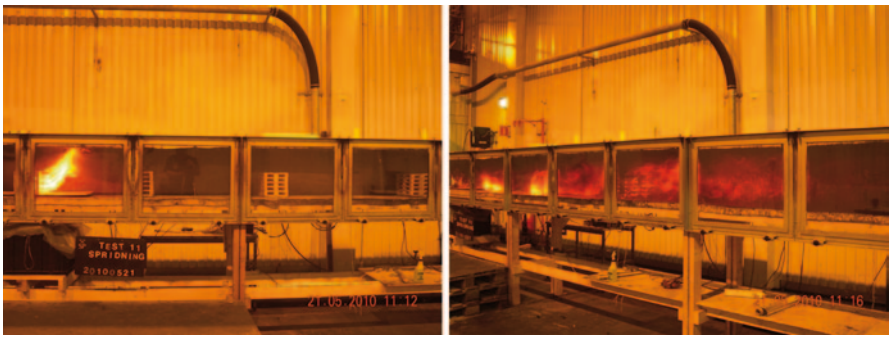

Fig. 2.8 Reduced scale tests using scaled wood pallets. This is test number 11, presented by Hansen and Ingason [7, 27]

this corresponds to HRR of 404 MW, which is a very large tunnel fire. This would correspond to two to four HGV vehicles burning at the same time. In Fig. 2.8 photos of the test setup are shown. The photo to the left shows test number 11 shortly after ignition of the first wood pallet pile. The longitudinal ventilation rate was 0.6 m/s, which corresponds to 2.32 m/s in full scale. The free-space distance between the first pile and the second one was 0.7 m, between the second and the third 0.9 m and between the third and the last one 1.1 m. Multiplying these lengths with the scale factor of 15 gives the full scale free space lengths 10.5, 13.5, and 16.5 m, respectively. In the photo to the right, we see that the fire has spread to all the wood pallet piles used in the test 11. The gas concentrations (O_2, CO_2, and CO) were measured on the downstream side 8.75 m from the entrance of the tunnel and approximately 2 m from the last pile. In Fig. 2.9, results of the gas concentration measurements at the ceiling height (0.9×H) are shown.

It is of interest to investigate the ratio X_{CO}/X_{CO_2} in order to determine if the fire is ventilation-controlled. From the graph in Fig. 2.9 (time equal to 423 s), we obtain a CO concentration of 2.0 %, a CO_2 concentration at the corresponding time of 19 % and the O_2 is only 0.5 % (essentially zero). This means that the ratio X_{CO}/X_{CO_2} is 2/19 = 0.105, which is higher than 0.056 given earlier for wood. In summary, we can say that this exercise with the test data indicates that Eqs. (2.17) to (2.22) are good indicators of the conditions in a tunnel with a longitudinal ventilation flow.

Although one should calculate the average values of O_2, CO_2, and CO based on numerous points over the tunnel cross-section, this was not possible as the only additional measuring point was the CO measuring point at half the tunnel height in the tests. The value of CO at the corresponding time was 2 %. The CO_2 instrument at the same position had only a measurement range from 0–10 %, and there was no O_2 measurement available at this height and length position. However, there was a thermocouple tree at the same position with five measuring points. These measurements show that there was very little variation in the temperature over the cross-section. Thus, one can conclude that the values shown in Fig. 2.9 are quite representative for the entire cross-section. Therefore, the theory that the condition for a ventilation-controlled fire is defined by $X_{CO}/X_{CO_2} > 0.056$ for wood is confirmed.

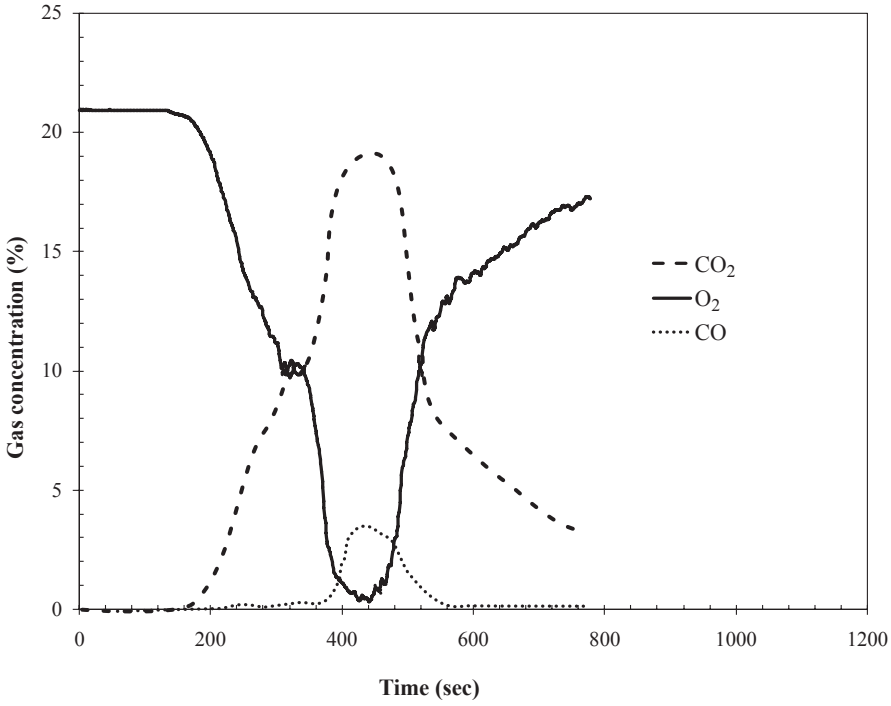

Fig. 2.9 The measured gas concentrations of O_2, CO_2, and CO 8.8 m from the entrance of tunnel for test number 11 in Hansen and Ingason [7, 27]

If there were additional wood pallet piles present in the tests, those piles would simply not ignite, at least not until the first piles have burned out. Due to the extremely high temperatures, these additional piles would continue to generate pyrolysis gases in accordance to the description given in Fig. 2.3.

This test really confirms how tunnel fires with longitudinal flow become ventilation-controlled. This is almost an extreme situation, and in order to obtain it one needs many large vehicles inside the tunnel and the fire must spread between them.

There is a misconception among engineers and scientists that when the oxygen concentration becomes lower than the flammability limits the fire will become ventilation-controlled or under-ventilated. That would mean that when the oxygen concentration is close to 13 %, the fire will not become larger and the size of the fire is governed by the air flow toward the fire. This is simply not true as has been shown earlier, both theoretically and experimentally. One may speculate that, in a case in which the second, third, or the fourth pile, or a vehicle in a real situation, is surrounded by oxygen concentrations lower than 13 %, the fire may self-extinguish or become ventilation-controlled. This explanation would not hold simply because the surrounding gas temperature is also a governing parameter for the combustion process. As in a combustion engine, a tunnel fire can burn until all the oxygen has been consumed as shown by test 11. This requires that the ventilation conditions and the surrounding gas temperature are suitable.

2.6 Effects of Vitiation on the Combustion Process

It is a well-known fact that a diffusion flame in an inerted environment will extinguish before consuming all the available oxygen from the surrounding atmosphere at ambient gas temperature or at least relatively low gas temperatures. It is also well known that if the surrounding gas temperature increases, the amount of oxygen that can be consumed will increase. This would establish a theorem that there is a correlation between the surrounding gas temperature and the level of oxygen at which the fire will self-extinguish. It is also known that as the conditions get closer to these limits, production of soot and CO decreases. This contradicts the idea of ventilation control, as one would expect an increase in the production of these parameters.

Beyler [28] has established a correlation between these critical conditions that depend on the surrounding gas temperature and the oxygen concentration. Beyler simply assumed that the critical adiabatic flame temperature governs the extinction of the fire. During adiabatic conditions, it is known that the energy released by combustion of the available oxygen in the surrounding air will raise the bulk gas temperature of the surrounding air by an amount equal to:

$$\dot{Q} = \dot{m}_a c_p (T_f - T) \tag{2.23}$$

where c_p is the average specific heat of gas over a given temperature range.

We can rearrange Eq. (2.16) as follows:

$$\dot{Q} = \dot{m}_a \frac{\Delta H_c}{r} = \dot{m}_a 3000 = Y_{O_2} \dot{m}_a 13100 \tag{2.24}$$

If we use the relationship $\dot{m}_{O_2} = \mathrm{Y}_{O_2} \dot{m}_a = X_{O_2} \frac{M_{O_2}}{M_a} \dot{m}_a$ where Y is mass fraction and M is mole mass (g/mol), and put it into Eq. (2.24) and combine it with Eq. (2.23) we obtain:

$$X_{O_2} = \frac{M_a}{M_{O_2}} \frac{c_p (T_f - T)}{13100} \tag{2.25}$$

If we assume the average c_p over the temperature range of interest (300–1700 K) is equal to 1.1 kJ/(kg K), and a critical adiabatic flame temperature of 1700 K as proposed by Beyler [28] for most hydrocarbon fuels, and use $M_a = 28.95$ g/mol, $M_{O_2} = 32$ g/mol, we will obtain a correlation using the relationship between the surrounding gas temperature and the oxygen concentration in % that indicates the oxygen level at which the fire would self-extinguish:

$$X_{O_2} = 0.0076(1427 - T) \tag{2.26}$$

Here T is given in °C. In Fig. 2.10, Eq. (2.26) is plotted as function of the temperate in °C.

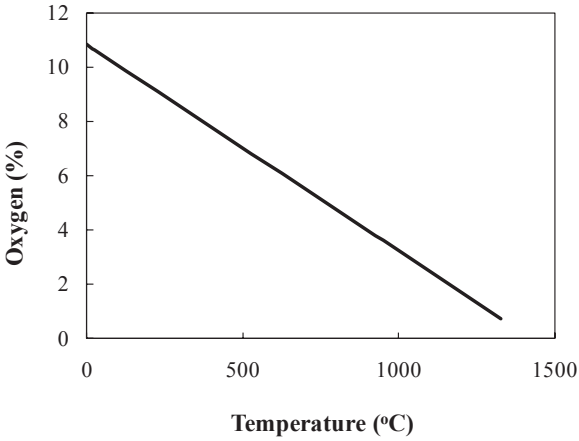

Fig. 2.10 The correlation between the critical oxygen volume concentration and the critical gas temperature according to Eq. (2.26)

This correlation can be used to estimate the effects of inerted air on fires in tunnels with longitudinal or natural ventilation. If we use the temperature measured in Hansen and Ingason [7, 27] on the downstream side of the fire, the highest temperatures measured in Test 11 were about 950 °C. This would mean that the lowest oxygen contents would be about 3.6 %, which is higher than those measured in the fire tests, that is, a value less than 1 %. The use of Eq. (2.26) is very valuable in order to better understand the fire physics in tunnels with longitudinal ventilation. In tunnels with natural ventilation and recirculating mixed or inerted air, the temperatures are lower in the combustion zone, and therefore one should expect higher levels of oxygen before it starts to affect the HRR. Most likely, there are also 3D local effects in this process, which is difficult to estimate and calculate in a one dimension process.

2.7 Summary

The chapter gives an overview of different effects of ventilation on the combustion process. It explains the differences between a fuel-controlled (well-ventilated) fire and a ventilation-controlled (under-ventilated) fire. A comparison between compartment fires and tunnel fires is given in order to explain the physical meaning of the terms fuel and ventilation control. A third condition was also introduced, namely the effects of inerting, which in some aspects can be classified as under-ventilated fire. This appears to be more important than earlier thought, as in naturally ventilated tunnels this may become an important phenomenon. The effects of the surrounding temperature on the vitiation or inerting effect of the mixing air are also shown.

References

1. Ingason H (2008) Key Note Paper - State of the Art of Tunnel Fire Research. In: 9th International Symposium on Fire Safety Science, Karlsruhe, 21–26 September 2008
2. Drysdale D (1999) An Introduction to Fire Dynamics. 2nd Edition edn. John Wiley & Sons
3. Karlsson B, Quintier JG (2000) Enclosure Fire Dynamics. CRC Press
4. Ingason H (2012) Fire Dynamics in Tunnels. In: Beard AN, Carvel RO (eds) In The Handbook of Tunnel Fire Safety, 2nd Edtion ICE Publishing, London, pp 273–304
5. Beard AN, Carvel RO (eds) (2005) The handbook of tunnel fire safety. Thomas Telford Publishing, London
6. de Ris J (1970) Duct Fires. Combustion and Science Technology 2:239–258
7. Hansen R, Ingason H (2010) Model scale fire experiments in a model tunnel with wooden pallets at varying distances. SiST 2010:08, Mälardalen University, Västerås
8. Beyler C (1995) Flammability limits of premixed and diffusion flames. In: SFPE Handbook of Fire Protection Engineering, 2nd Edition. pp 2-147–160
9. Quintiere JG, Rangwala AS (2003) A Theory for Flame Extinction based on Flame Temperature. Paper presented at the Fire and Materials Conference Papers
10. Ingason H (1995) Effects of Ventilation on Heat Release Rate of Pool Fires in a Model Tunnel. SP Swedish National Testing and Research Institute, Borås, Sweden
11. Ingason H, Nireus K, Werling P (1997) Fire Tests in a Blasted Rock Tunnel. FOA, Sweden
12. Morehart JH, Zukoski EE, Kubota T (1991) Characteristics of Large Diffusion Flames Burning in Vitiated Atmosphere. In: Third International Symposium on Fire Safety Science, Edinburgh, Scotland, 8-12 July 1991. IAFSS, pp 575–583
13. Lönnermark A, Hugosson J, Ingason H (2010) Fire incidents during contruction work of tunnels – Model-scale experiments. SP Report 2010:86. SP Technical Research Institute of Sweden
14. Thomas PH, Bullen ML, Quintiere JG, McCaffrey BJ (1980) Flashover and Instabilities in Fire Behavior. Combustion and Flame 38:159–171
15. Tewarson A (1984) Fully Developed Enclosure Fires of Wood Cribs. In: 20th Symp. (Int) on Combustion, Ann Arbor, MI, USA, 12-17 August 1984. The Combustion Institute, pp 1555–1566
16. Babrauskas V (1981) A closed-form approximation for post-flashover compartment fire temperatures. Fire Safety Journal Vol. 4 No. 1
17. Parker WJ (1984) Calculations of the Heat Release Rate by Oxygen Consumption for Various Applications. Journal of Fire Sciences 2 (September/October):380–395
18. Huggett C (1980) Estimation of Rate of Heat Release by Means of Oxygen Consumption Measurements. Fire and Materials 4 (2):61–65
19. Li YZ, Ingason H, Lönnermark A (2014) Fire development in different scales of a train carriages. In: 11th International Symposium on Fire Safety Science, New Zealand
20. Ingason H (2007) Model Scale Railcar Fire Tests. Fire Safety Journal 42 (4):271–282
21. Bullen ML, Thomas PH (1979) Comaprtment fires with non-cellulosic fuels,. In: 17th Symposium (Int) on Combustion, Pittsburgh, 1979. The Combustion Institute, pp 1139–1148
22. Tewarson A (2002) Generation of Heat and Chemical Compounds in Fires. In: DiNenno PJ, Drysdale D, Beyler CL et al. (eds) The 3rd edition of SFPE Handbook of Fire Protection Engineering. Third edition edn. National Fire Protection Association, Quincy, MA, USA, pp 3–82 – 83–161
23. Beyler CL (1985) Major Species Production by Solid Fuels in a Two Layer Compartment Fire Environment. In: Fire Safety Science - Proceedings of the First International Symposium, Gaithersburg, USA, 7–11 October 1985. IAFSS, pp 431–440
24. Tewarson A (1995) Generation of Heat and Chemical Compounds in Fires. In: DiNenno PJ, Beyler CL, Custer RLP et al. (eds) SFPE Handbook of Fire Protection Engineering. 2 edn. The National Fire Protection Association, USA

25. Janssens M, Parker WJ (1995) Oxygen Consumption Calorimetry. In: Babrauskas V, Grayson TJ (eds) Heat Release in Fires. E & FN Spon, London, UK, pp 31–59
26. Tewarson A (1988) Generation of Heat and Chemical Compounds in Fires. In: DiNenno PJ, Beyler CL, Custer RLP, Walton WD, Watts JM (eds) SFPE Handbook of Fire Protection Engineering. First Edition edn. NFPA, pp 1–179 – 171–199
27. Hansen R, Ingason H (2012) Heat release rates of multiple objects at varying distances. Fire Safety Journal 52:1–10
28. Beyler C (2002) Flammability limits of premixed and diffusion flames. In: In third Edition SFPE Handbook of Fire Protection Engineering. 3rd Edition edn., pp 2–173–172–187

Chapter 3
Tunnel Fire Tests

Abstract This chapter gives a detailed overview of numerous large-scale fire tests carried out in different types of tunnels. Some important model scale tunnel fire tests are also included. The information given, sets the level of knowledge from this type of tunnel fire testing. The reason for doing tests is to obtain new knowledge about different phenomena. Although the focus is on large-scale testing, the fundamental knowledge is obtained both from large-scale and intermediate size tunnel testing as well as laboratory testing (For example, scale models). The aim is usually to investigate some specific problems such as influence of different ventilation systems on smoke and temperature distribution along the tunnel, the fire development in different type of vehicles, and the effect of heat exposure on the integrity and strength of the tunnel construction.

Keywords Fire tests · Measurements · Heat release rate (HRR) · Temperature · Flame length · Large-scale · Model scale

3.1 Introduction

Large-scale testing is generally costly as they are time consuming and logistically complicated to perform. This is one of the main reasons why the number of large-scale tests in tunnels is limited. The information obtained is sometimes incomplete and the instrumentation is often insufficient. There is a need, however, to perform large-scale tests in order to obtain acceptable verification in realistic scale. The data obtained from such large-scale tunnel fire tests, provides the basis for the technical standards and guidelines used for tunnel design today [1, 2].

An overview and analysis of large-scale tests performed in road and railway tunnels is given here. The analysis presented in this chapter is largely based on an overview given by Ingason [3]. The overview includes some additional information obtained since the overview was first published in 2007. The analysis of the large-scale experiment focus on presenting the following parameters:

- Measured maximum or peak heat release rates (HRR)
- Fuel mass loss rate

H. Ingason et al., *Tunnel Fire Dynamics,* DOI 10.1007/978-1-4939-2199-7_3

- Measured peak gas temperatures
- Flame lengths

In the second part, an overview of some model scale tests is given. It contains short description of the tests, and includes the main conclusions drawn. The main references are also included, both for the large-scale and model scale tests.

3.2 Overview of Large-Scale Tunnel Experiments

The variety of the large-scale tests is in the fire source, both type and HRR, instrumentation, technical documentation, tunnel geometry and ventilation conditions. A summation of all scientifically orientated large-scale tunnel fire tests that have been carried out worldwide since the beginning of 1960s until 2014, is given in Table 3.1. This summary excludes all commercial or legal orientated (reconstruction) large-scale testing and large-scale tunnel tests with fire suppression systems. The tests with fire suppression systems will be described in Chap. 16. These systems today, are termed as Fixed Fire Fighting Systems (FFFS). The data on HRR, temperatures, and flame lengths are given wherever possible.

The number of scientifically aimed large-scale fire test programs have been carried out to date is slightly more than a dozen. Most of the tests program included less than 30 tests, except for the Memorial test series which included 98 tests. The focus has mainly been on the heat and smoke spread and how different ventilation systems influence the parameters listed earlier. Nearly half of the test series included FFFS tests (sprinkler), which, as mentioned earlier, will be presented in more details in Chap. 16, but in this chapter the focus is on the results from free burn tests.

The quality of large-scale tests carried out in the 1960s–1980s varied considerably. The key fire hazard parameter, the HRR, has not been quantified in these tests. The boundary conditions such as wind at portals, air temperatures, lining surface etc. were usually not the most favorable for validation of advanced computer models. They were performed to fill a wide gap of nonexiting knowledge about influence of the ventilation systems on tunnel fires rather than to fulfill the need for advanced theoretical studies or validation of Computation Fluid Dynamic (CFD) fire models.

The first series of large-scale tunnel fire test were performed in the 1960s and the 1970s in Europe. They were mainly directed to solve the fire problems of road tunnels in Europe. Grant et al. [4] considered these tests as ‘tantalizing snapshots’ primarily due to the inadequate HRR data. The documentation on fuel mass loss rates, combustion efficiency, ventilation flow rates and wind, and pressure conditions was not sufficient to fully validate the functional relationships derived theoretically or in laboratory scale tests at that time.

Among these well-known large-scale tunnel fire test series in the 1960s and the 1970s in Europe are the Ofenegg (1965, 24 m^2, 190 m)[1] [5] series, the Glasgow

[1] (test year, cross section, tunnel length).

Table 3.1 Scientifically aimed large-scale fire tests performed since the middle of 1960s [3]

Test program, country, year	No of tests	Fire source	Tunnel cross section (m^2)	Tunnel height (m)	Tunnel length (m)	Measurements	Range of peak HRR (MW)	Comments
Ofenegg, Switzeland, 1965	11	Gasoline pool (6.6, 47.5, 95 m^2)	23	6	190	T, CO,O2,v, visibility	11–80	Single track rail tunnel, dead end, sprinkler
Glasgow, 1970	5	Kerosine pool (1.44, 2.88, 5.76 m^2)	39.5	5.2	620	T, OD	2–8	Disused railway tunnel
Zwenberg, Austria, 1974–1975	30	Gasoline pool (6.8, 13.6 m^2), wood and rubber	20	3.9	390	T, CO,CO2, NOx, CH, O2, v, OD	8–21	Disused railway tunnel
P.W.R.I, Japan, 1980	16	Gasoline pool (4, 6 m2), passenger car, bus	57.3	~6.8	700	T, CO, CO_2, v, OD, radiation	Pool: 9–14[a] Cars and buses un-known	Special test tunnel, sprinkler
P.W.R.I, Japan, 1980	8	Gasoline pool (4 m2), bus	58	~6.8	3277	T, CO, CO_2, O_2, v, OD, radiation	Pool: 9 Bus un-known	In use road tunnel, sprinkler
TUB—VTT, Finland, 1985	2	Wood cribs (simulate subway coach and collision of two cars)	24–31	5	140	HRR, T, m, CO, CO_2, O_2, v, OD	1.8–8	Disused cavern system
EUREKA EU499, Norway, 1990–1992	21	Wood cribs, heptane pool, cars, metro car, rail cars, HGV trailer and mockup	25–35	4.8–5.5	2300	HRR, T,CO, m,CO_2,O_2,SO_2,CxHy, NO, visibility, soot, m,v	2–120	Disused transportation tunnel
Memorial, USA, 1993–1995	98	Fuel oil (4.5–45 m2)	36 and 60	4.4 and 7.9	853	HRR, T, CO,CO_2,v, visibility	10–100	Disused road tunnel, sprinkler
Shimizu No. 3, Japan, 2001	10	Gasoline pool (1, 4, 9 m^2), cars, bus	115	8.5	1120	T, v, OD, radiation	2–30[a]	New road tunnel, sprinkler tests

Table 3.1 (continued)

Test program, country, year	No of tests	Fire source	Tunnel cross section (m^2)	Tunnel height (m)	Tunnel length (m)	Measurements	Range of peak HRR (MW)	Comments
2nd Benelux tunnel, The Netherlands, 2002	14	n-heptane + toulene, car, van, HGV mock up	50	5.1	872	HRR, T, m, radiation, v, OD, visibility	3–26	New road tunnel, sprinklers
Runehamar tunnel, Norway 2003, 2013	4	Cellulose, plastic, furniture, wood pallets	32–47	4.7–5.1	1600	HR, T,PT, CO, CO_2,O_2,HCN, H2O, isocyanates, OD, radiation	70–203	Disused road tunnel
Brunsberg, Sweden, 2011	2	Metro car	44	6.9	276	HRR, T,PT, CO, CO_2,O_2, OD, radiation	77	Disused rail tunnel
San Pedro tunnel, 2012	1	HGV mockup	37	5.2	600	HRR, T,PT, CO, CO_2,O_2, OD, radiation	150	Test tunnel
Carleton laboratory facility, 2011	2	Train and subway car	55	5.5	37	HRR, T, CO, CO_2,O_2	32–55	Laboratory facility

HRR heat release rate, *m* mass loss rate, *T* temperature, *PT* plate thermometer, *CO* carbon monoxide, CO_2 carbon dioxide, *CH* hydrocarbon, *HCN* cyanide, H_2O water vapour, *v* velocity, *OD* optical density, visibility=cameras for smoke registration.

[a] The bus was determined to be equal to 20 MW convective and 30 MW total

series (1970, 40 m^2, 620 m) [6] and the Zwenberg series (1974–1975, 20 m^2, 370 m) [7, 6, 8]. Both the Ofenegg [9] and the Zwenberg [8] test series have been reported with commendable detail on the test data and the test setup. A less known large-scale test series was carried out in Japan in the late 1970s and beginning of the 1980s [10] (P.W.R.I- Public Works Research Institute). The documentation in English is somewhat limited. The tests were carried out in a large-scale test tunnel (1980, 57.3 m^2, 700 m) built by P.W.R.I and in a full-size road tunnel; Kakei Tunnel (1980, 58 m^2, 3277 m). This was the first time cars and buses were used in large-scale test series in tunnels. As was the case in other tests in Europe at that time, no HRR measurements were carried out. Some weight loss estimations were, however, carried out.

The tests carried out in the 1960s and the 1970s did, and still have, a major influence on the standards and guidelines used for fire safety in tunnels.

The use of the Oxygen (O_2) Consumption Calorimetry [11, 12] made it possible to more easily and accurately measure the HRR in tunnel fires. By measuring the oxygen concentration in the fire smoke it was possible to determine the HRR. This was the start to a new era in large-scale tunnel fire testing in the 1980s and 1990s. There were other gas-based methods introduced as well. For example Tewarson [13] introduced another gas analysis technique, the Carbon Dioxide (CO_2) generation for measurement of HRR. This method was not as widely used in fire laboratories as the Oxygen Consumption Calorimetry but both these techniques found their way into the tunnel fire testing.

A German (Technische Universität Braunschweig (TUB)) and Finnish (VTT) cooperation [14, 15] (1985, 24–31 m^2, 140 m) lead to the performance of two large-scale tests in a tunnel using wood cribs as fuel to simulate fire in a subway car (80 GJ), and in two passenger cars (11.7 GJ) colliding in a tunnel. The original idea was to utilize the oxygen consumption technique, but due to large uncertainties in the oxygen and flow measurements it was never completed [16]. The cooperation between TUB–VTT developed and widened later into the EUREKA project EU499 (FIRETUN) (1990–1992, 25–35 m^2, 2300 m) [15] in the early 1990s. The oxygen consumption calorimetry was used for the first time in the EUREKA EU499 project and made it possible to measure the HRR from large vehicles with a relatively good accuracy, although not nearly as good as in fire laboratories.

The EUREKA EU499 tests were performed in the beginning of 1990s. They became a milestone concerning new valuable information for tunnel engineers. This was especially valid for the great variety in the HRR data for vehicle types such as cars, train coaches, subway coaches, and articulated lorry with furnitures [17–19]. The tests have resulted in significant improvements of information regarding HRR levels for single vehicles in tunnels. The EUREKA EU499 tests contain the most comprehensive fire testing of rail- and metro vehicles ever performed. In the EUREKA EU499 tests, there was very little consideration given to the risk of fire spread between vehicles, mainly because prior to and at the time of the performance of the tests, there had not been that many serious large fire accidents involving multiple vehicles as turned out to be the case in the late 1990s and in the beginning of 2000. The great majority of road tunnel fires consist of fires in one or two vehicles whereas large catastrophic fires can involve multiple vehicles.

Another milestone in large-scale tunnel fire testing was obtained in the Memorial tunnel test series (1993–1995, 36–60 m^2, 853 m) [20] carried out between 1993 and 1995. The fire source consisted of low sulfur No 2 fuel oil pans (diesel) and not real vehicles. The aim was to use a well-defined fire source in order to compare the performance of the different ventilation systems. In order to investigate the influence of vehicles on the ventilation flow, silhouettes representing vehicles were placed at different locations. A comprehensive instrumentation was located in both the upstream and downstream directions of the fire. There is no doubt that, the Memorial tests demonstrated very well the performance and control of different types of ventilation systems. The tests also provide a very important source for validation of Computational Fluid Dynamics (CFD) models. The memorial test data is the best-documented fire test results ever made available (CD-ROM).

The test results were used as a basis for the design of the ventilation system in the Boston Central Artery Tunnel (BCAT) project and they have already had a great impact on the design of smoke control systems worldwide. The usefulness of longitudinal- and exhaust-ventilation was clearly shown as well as the positive performance of foam sprinkler systems. A confirmation of the correlation between HRR and 'critical velocity' was established for the first time in a large-scale test, especially the HRR independence of longitudinal velocity over 3 m/s. To date, these fire experiments are the most comprehensive and most expensive large-scale tests ever performed. There is no doubt that the EUREKA tests and the Memorial tests are the most well-known and well reputed large-scale fire test series to date. They have already been established as the 'large-scale fire tests' and provide a new base for standards and knowledge in tunnel fire safety.

Since the beginning of the 21st century there have been to date some mediocre fire test series performed in large-scale tunnels. Large-scale tests were performed in the No. 3 Shimizu Tunnel (2001, 115 m^2, 1120 m) on the New Tomei Expressway, using gasoline pan fires, cars and a bus [21]. These tests included natural and longitudinal ventilation as well as water sprinklers. The main focus was on heat and smoke spread in a large-cross section tunnel (three lanes). In the Second Benelux tunnel in the Netherlands (2002, 50 m^2, 872 m, large-scale tests with cars and Heavy Goods Vehicles (HGVs) mock-ups using wood pallets were performed in 2002 [22]. Tests with natural- and longitudinal-ventilation and water sprinkler systems were also performed here. These tests provide very important results on the effects of longitudinal ventilation on HRRs in HGVs and on car fires. A large-scale test series was carried out in the Runehamar tunnel (2003, 47 m^2, 1600 m) [23, 24]. Four tests using a mock-up of HGV fire loads were carried out. These tests provide an important information on fire development in different types of ordinary hazard goods and show that this type of goods can create fires which are similar in size as a gasoline tanker fire. The initial fire growth rate is although not as fast or comparable to that of a petrol tanker fire. The tests showed clearly that, the maximum gas temperature levels from ordinary hazardous goods could easily be similar to those from of a tank fire. The results from the Runehamar tests have already had implications on design fires in road tunnels and the furnace testing of tunnel elements. Two large-scale tests series have been performed involving rolling stocks, that is, in the Brunsberg tunnel

and Carleton laboratory. They show that the peak HRR is much higher than what has been used in design. The maximum in those tests ranged from 32 to 77 MWs.

There are numerous tests found in the literature that has been carried out in 'intermediate-sized' tunnels. The cross sections vary between 5 and 13 m^2, which can be compared to the cross sections of the large-scale tests series presented which varied between 25 and 115 m^2. Apte et al. [25] presented a detailed study of pool fires in a tunnel (1991, 13 m^2, 130 m) using longitudinal ventilation in a typical mine roadway. These experiments were used for validating a computational fluid dynamics (CFD) approach to modelling tunnel fires. They also show the effects of longitudinal ventilation on burning rate of pool fires. An extensive series of experiment were carried at the Safety Executive Laboratory (HSE) in Buxton, England (1992–1993, 5.4 m^2, 366 m) [26]. Both obstructed- and open-tunnel situations were considered in the HSE tests. The former included one-third scale models of a part of a HGV shuttle train from the Channel Tunnel and the latter used kerosene pools. In the second phase of the test program, even wood cribs were used. The HRRs were measured using the oxygen consumption calorimetry technique and mass loss rates combined with a value of combustion efficiency. The objective was to provide data for CFD simulation of interaction of longitudinal flow and a back-layering smoke flow. The results suggested that the value of the critical velocity tended to some near constant value with increasing HRR, and thus did not conform to the simple theory developed by Thomas [27]. This discovery was very important for the design of longitudinal ventilation systems, especially when this finding was verified in the Memorial tunnel test series. Ingason et al. (1995, 9 m^2, 100 m) [28] presented results from tests carried out in an intermediate sized tunnel tests. These tests were carried out using wood cribs, pool fires, and a passenger car. The aim of these tests was to establish a correlation between optical smoke density and gas concentrations [29] for use in CFD simulations. The CFD codes at that time were not able to predict with any good accuracy the optical smoke density but they could predict the concentrations of gas species. The experiments showed a good correspondence between the measured optical density (visibility) and the measured gas concentrations at different locations in the tunnel and accordingly that this was an accessible way to predict the smoke optical density or visibility.

There are many other tests performed in large-scale tunnels, the main purpose has either been commercial testing or testing of the ventilation systems of a specific tunnel before it is put into operation. The fire source can either consist of pan fires, wood crib fires or car fires. Examples of such tests can be found in [30, 31] and in the Handbook of Tunnel Safety [32].

Within the framework of the legal enquiry initiated after the catastrophic fire in the Mont Blanc tunnel in 1999, a series of large-scale tests were conducted in the same tunnel (2000, 50 m^2, 11,600) [33]. The objective was to investigate the consequence of the fire during the first half hour. The tests were carried out in two phases. Three tests with diesel pool fires of 8 MW, modifying the smoke control conditions for each test, were carried out in the first phase and in the second phase a test with a real HGV truck and a trailer similar to that which generated the fire 1999 but with a much smaller amount of transported goods. The longitudinal flow at the fire

location was about 1.5 m/s. In order to limit the peak HRR tyres had been removed and fuel tank was emptied. Only 400 kg of margarine were stored in the trailer. The total calorific value of the truck and the trailer with its goods was estimated to be 76 GJ. This value can be compared to the real value, which was estimated to be 500–600 GJ. The HGV was ignited by setting on fire successively three small pools filled with a diesel oil and alcohol mixture, respectively place in the HGV driver's cab, behind the cab and between the cab, and the trailer. During the first 40 min, the HRR of the HGV fire remained lower than that of the pool fire, about 6 MW. Then the HRR reached a level of 23 MW, which can be related to the extensive burning of the HGV trailer.

3.3 Large-Scale Tunnel Fire Tests

In the following more detailed information is given for each of the tests listed in Table 3.1. Most of the tests are without interaction of FFFS (deluge water spray systems or deluge sprinkler system). For these test, wherever possible, information of maximum HRRs ($\dot{Q}_{\max}$), fuel mass loss rate ($\dot{m}''_f$), ambient (T_0) and maximum ceiling temperatures (T_{max}), and maximum horizontal flame lengths (L_f) along the ceiling is given. The maximum horizontal flame lengths along the ceiling is based on the ceiling temperature measurements, assumed flame tip at 600 °C as proposed by Rew and Deaves [34]. In case of interaction with FFFS short information is given in this chapter, but more detailed information is given in Chap. 16.

3.3.1 Ofenegg 1965

The first large-scale tunnel fire test series to obtain scientific and engineering information was carried out in the Ofenegg tunnel in Switzerland, in1965 [5]. These tests were carried out in order to study the ventilation capacities (natural, longitudinal[2], semitransverse[3]) in the case of a fire, especially in case of a gasoline tank fire. The tests were expected to give information on the hazardous level for tunnel users, possibilities to rescue people and the impact on tunnel construction and installations. Also the influence of a FFFS (deluge sprinkler nozzles) was investigated. This type of information was urgently needed in Switzerland due to the large road tunnel projects carried out in the 1960s. The tunnel used for these experiments was a single track railway tunnel (23 m^2, 3.8 m wide and 6 m high), with wall located 190 m from the one portal and the ceiling was 6 m high with a rounded top. By closing the

[2] Longitudinal ventilation consists of fans blowing in outside air through the rear end duct system with an air quantity of 39 m^3/s, that is, a longitudinal velocity of 1.7 m/s.

[3] Semitransverse system have air inlets at low levels but either no extraction or extraction at only a few points, so that the air and vehicle exhaust gases flow along the tunnel, at a velocity which increases along the tunnel length. The fresh air supply equal to 0.25 m^3/s, m.

cross section the test tunnel became a dead end tunnel of 190 m in length. A total of 11 tests were performed using gasoline pool fires on a concrete trough with the edge placed 131.5 m from the open entrance. The other end (190 m) was bricked up. The sizes of the pools used were 6.6, 47.5 and 95 m^2, respectively, with the smallest representing the contents of the fuel tanks of two cars and the largest a substantial spill from a gasoline tanker. The width of the trough (fuel pan) was 3.8 m and the length of the trough varied; 1.7, 12.5 and 25 m, respectively.

The experiments showed that large quantities of smoke were generated in all the tests. The smoke front travelled along the tunnel at speeds of up to 11 m/s and the visibility deteriorated in most cases 10–20 s after the start of the fires. Generally, the greater the fuel quantity, the worse the conditions [35]. It was found that the heat evolution was a decisive factor for the possible escape of people. With a semi-transverse ventilation system supplying up to 15 m^3/s the burning rate was virtually unchanged compared to no ventilation. With a longitudinal ventilation system giving an air velocity along the tunnel of about 1.7 m/s, averaged over the cross-section of the tunnel, the burning rate of a 47.5 m^2 fire was about twice that for the 47.5 m^2 fire with no ventilation.

An estimation of the HRR was made by Ingason [3] and the results are presented in Table 3.2. The estimation, which is based on the measured fuel flow rates for each test [5] and an assumed combustion efficiency of 0.8 in the tunnel and a heat of combustion of 43.7 MJ/kg, show that the average HRR was 2.1 MW/m^2 for the 6.6 m^2 fuel, 0.95 MW/m^2 for the 47.5 m^2 fuel, and 0.35 MW/m^2 for the largest one (95 m^2). In the open the HRRs is in the order of 2.4 MW/m^2 (0.055 $kg/(m^2\ s)$ and ΔH_c =43.7 MJ/kg [36]). It is clear that the burning rate per square meter in these tests is highly influenced by the ventilation rate and the test setup. The poor accessibility of the oxygen to the fuel bed as the troughs (pans) used was nearly as wide (3.8 m) as the tunnel (4.2 m) is one of the reasons. In a wider tunnel the results may have been quite different. In the case where the longitudinal ventilation was used the burning rate increased dramatically, especially for the large fire (test no 7a, 47.5 m^2), since the oxygen was more effectively mixed with the fuel. Compared to gasoline fire in the open, the burning rate became slightly less per square meter when the fire was small (6.6 m^2). The maximum ceiling temperature obtained was 1325 °C and the average HRR was estimated to be 70 MW. With a natural-ventilation or semitransverse-ventilation the temperatures were slightly lower or about 1200 °C and the average HRR was between 33 and 39 MW. In general, we see that the maximum ceiling temperature varies between 450 and 1325 °C for average HRRs between 12 and 70 MW. Clearly, the temperatures are not only dependent on the level of the HRR but also by the ventilation conditions.

In Table 3.2, an estimation of the flame length, L_f, from the centre of the trough is given as well. The flame length is given both towards the portal where most of the air flow was directed and towards the end of the tunnel. It is calculated from the centre of the pool fire and it is based on linear interpolation of the peak gas temperatures measured in the 0.5 m below the ceiling and represent the 600 °C temperature front [34]. Here the size of the pool in combination with the ventilation conditions plays an important role whether the temperatures become high or low.

Table 3.2 Relevant data from the Ofenegg tunnel tests in 1965 [3]

Test no	A_f(m^2)	Type of ventilation	FFFS	Air supply ventilation (m^3/s)	T_0 (°C)	Velocity at portals at max conditions (2 min) (outflow/inflow)	$\dot{m}''_f$ lower-upper (kg/(m^2 s))	HRR lower-upper[a] (MW)	Average HRR (MW)	Average HRR per square meter fuel area (MW/m^2)	T_{max} (°C)	L_f towards portal (m)	L_f towards end (m)
1	6.6	Natural	No	0	16	2.2/1.5	0.062–0.074	14–17	16	2.4	710	18	0
2		Semitransverse	No	15	17.5	2.2/2.3	0.046–0.062	11–14	12	1.8	830	23	0
2a		Longitudinal	No	39	11	4.2/1.1	0.046–0.062	12–16	14	2.1	450	NA	NA
3		Natural	Yes	0	16	1.9/2.7	NA	NA			950	21	0
5	47.5	Natural	No	0	10	4.8/2.3	0.021–0.026	35–43	39	0.8	1200	66	11
6		Semitransverse	No	15	10	NA	0.019–0.021	32–35	33	0.7	1180	100	11
7a		Longitudinal	No	39	11.3	5.8/0.5 (out)	0.032–0.043	60–80	70	1.5	1325	74	7
7		Natural	Yes	0	11.3	–	NA	NA			995	58	11
9	95	Natural	No	0	4.6	4.6/3	0.010–0.011	33–37	35	0.4	1020	79	23
10		Semitransverse	No	6	9	5/2	0.009–0.010	30–33	32	0.3	850	82	23
11		Natural	Yes	0	11.2	4.1/2.8	NA	NA	NA		800	NA	NA

[a] $HRR = \eta \dot{m}''_f A_f \Delta H_c$ where η is the combustion efficiency, $\dot{m}''_f$ is the burning rate per square meter, A_f is the fuel area and ΔHc is the heat of combustion. We assume η = 0.8 in tests with natural and semitransverse ventilation and η = 0.9 in the tests with longitudinal ventilation. The heat of combustion ΔHc is assumed to be equal to 43.7 MJ/kg and the fuel density is assumed to be 740 kg/m^3 [36]. *NA* Not Available

In the tests with the 6.6 and 47.5 m^2 pool fires the temperature in the ceiling increased rapidly, and reached a maximum after about 2 min from the ignition. Shortly after reaching the maximum, the temperature dropped rapidly down and after about 10 min from ignition the temperature was in all cases without FFFS less than 200 °C. In the case with the largest pool fire (95 m^2) and no FFFS, the temperature was relatively constant at its high temperatures for about 8–10 min. The oxygen measurements indicated that all the oxygen was consumed. This indicates that the 95 m^2 pool fire was ventilation-controlled. That the fire was ventilation controlled could explain the large difference in HRR data per square meter and temperature data compared to the smaller pool fires.

These tests were very valuable for design of the tunnel ventilation systems at that time. Much effort was put into analyzing data in order to relate it to the conditions of evacuation. These tests had also, a major impact on the view of using FFFS in Europe. It was not found feasible to use FFFS in tunnels due to some adverse effects of the system. The FFFS were able to extinguish the fire, but the visibility was reduced in the vicinity of the fire and after the fire was extinguished in the gasoline, fuel vapour continued to evaporate. In the last test the critical concentration (20 min), that is fuel concentration in the vapor phase within the flammable limits was obtained and due to hot particles in the fire zone the vapor cloud ignited. The deflagration created resulted in a velocity of 30 m/s.

3.3.2 Glasgow 1970

The Building Research Establishment (BRE) (former Fire Research Station (FRS)) in the UK carried out in collaboration with the Glasgow fire brigade five experimental fires in a disused railway tunnel in Glasgow [35]. The purpose of the tests was originally not tunnel related. The tests were actually carried out to investigate smoke spread in an enclosed shopping mall. A disused railway tunnel was used because it was a reasonable approximation to certain features of such a building [35]. The disused railway tunnel was 620 m long, 7.6 m wide and 5.2 m high. Fires of one, two or four trays of kerosene were burnt. The trays were square with side length of 1.2 m, or area of 1.44 m^2 with a fuel load of 45-L kerosene. The estimated HRR in each tray was 2 MW [35], or 1.39 MW/m^2.

The experimental instrumentation was scattered inside the tunnel. The smoke layer height and the time of arrival of the smoke front were measured at 20 different locations with human observers using breathing apparatus. According to Heselden [35] there were some temperature and smoke obscuration measurements done, but no details are given. Observations from the tests show that smoke layer was actually quite flat (horizontal) during the tests. Heselden [35] describes thoroughly the smoke conditions within the tunnel after ignition;

“In all the tests the bulk of the smoke formed a coherent layer, which was initially 1–2 m thick depending on the size of the fire, and which gradually deepened as the test progressed, reaching 3–4 m deep for the largest fire 10 min after ignition.

The velocity of advance of the layer was in the region of 1–1.5 m/s, discounting the initial 1/2 minute when the burning rate was building up to an equilibrium value. In two tests the smoke nose was followed to the end of the tunnel, a distance of 414 m from the fire. The smoke layer was then quite well defined even though it would have been only some 5°C above the air beneath. It was found that, a layer or plug of smoke reaching to ground level often formed at the tunnel entrance probably due to the mixing and cooling produced by a cross wind; this plug tended to be drawn back into the tunnel with air current induced by the fire. The air below the main smoke layer was not perfectly clear. Although the bulk of the smoke formed a layer, some optically thinner smoke tended to build up in the clear layer below even before the ceiling smoke layer had reached the end of the tunnel. This may have been due to some mixing of smoke downwards at the smoke nose, which was more turbulent than the layer following it, or to mixing at obstructions (which were very few), or to wisps of smoke cooled by contact with the wall, clinging to the wall, and moving downwards where they were swept up by and mixed into the main air flow to the fire."

The Glasgow tests have not been widely referred to in the tunnel literature, most likely due to the scattered data obtained from these tests and the fact that the tests were not originally performed to improve tunnel fire safety. More detailed information about these tests can be found in reference [37].

3.3.3 The West Meon Tests in Early 1970s

The FRS was also involved in other large-scale tunnel testing in collaboration with local fire brigades. Heselden [35] reports briefly on the tests carried out in Hampshire in UK in early 1970s without giving any further references. These tests were carried out in connection with proposals for the channel tunnel, which opened for traffic in 1994. The FRS in collaboration with the Hampshire Fire Brigade and British Railways carried out an experimental fire in a disused railway tunnel near West Meon, Hampshire. The tunnel was 480 m long, 8 m wide and 6 m high and the cars to be burnt were placed 45 m from one of the tunnel portals. During the burning of one car a smoke layer up to 3 m thick formed under the roof but observers were able to remain near the fire without any ill effects except headaches afterwards. The flow of the smoky hot gas was controlled by the wind of about 2 m/s that was blowing through the tunnel.

3.3.4 Zwenberg 1975

A decade after the Ofenegg tunnel tests, a new test series was carried out in the Zwenberg tunnel in Austria 1975 [7]. The reason for these tests was similar as for the Ofenegg tests. Large road tunnel projects were planned in the early 1970s in Austria. The aim was to investigate the effects of different types of ventilation (longitudinal,

semitransverse and transverse ventilation[4] on the distribution of smoke (visibility), heat and toxic gases, and the effects of heat on the ceiling construction and the exhaust fans. The Ofenegg tests concentrated on studying the conditions during fire with more or less unchanged ventilation pattern, whereas the main objective of the Zwenberg tests was to investigate how changing the ventilation pattern could influence conditions inside the tunnel. For the operation of tunnel ventilation the following two major questions had to be answered [6]:

1. What quantities of fresh air shall be supplied in order to provide the best conditions in case of tunnel fire?
2. What influence has forced longitudinal ventilation on the conditions inside the tunnel?

Beyond that, the scope of the research project was to study the effects of a tunnel fire on evacuees. In order to do that, the gas temperatures, content of toxic gases and oxygen in the tunnel, the visibility in the smoke, and the fire duration was measured. The aim was also to find ways to improve the situation in the tunnel by using different types of tunnel ventilation. The focus was also on the effects of the fire on the tunnel structure and technical equipment within the tunnel.

The tests were carried out in an abandoned railway tunnel owned by the Austrian Railways. The tunnel was 390 m long with a cross section of 20 m^2 (traffic space) and a ventilation duct of 4 m^2. The tunnel gradient was 2.5 % from the south to the north portal. The tunnel height up to the ventilation duct was 3.8 m and the tunnel width was 4.4 m. Fully transverse ventilation system was installed in the test tunnel, designed for a supply of 30 m^3/s of fresh air and for the same quantity of exhaust air. An injection fan installed near the southern portal was designed to provide a longitudinal flow up to 7 m/s in the traffic space. Every 6 m alternately a fresh air opening and a polluted air opening were installed.

The fire source was located 108 m from the south portal. It consisted of 12 individual concrete trays in two rows with a total volume of 900 L liquid (gasoline, diesel) corresponding to a surface area of 20 m^2 where the internal measures of each tray was 1 m wide and 1.7 m long. Only four trays (beside each other) were used in the standards test (6.8 m^2) and six in the large tests (13.6 m^2). A total of 46 measuring points for temperature were mounted, 11 for air and gas velocities, 19 for gas sampling (O_2, CO_2, CO, CH and NOx) and seven for visibility observations. Total of 30 tests, see Table 3.3, were performed using gasoline pools of 3.4, 6.8, and 13.6 m^2, respectively. The majority of the tests, 23 ‘standard fire’ tests, were run using four trays with a fuel area of 6.8 m^2 and 200 L of fuel. This fire size was found to be sufficient to obtain useful data and avoid damages on the installation. In the tests with the ‘standard fire’ following parameters were varied:

1. Location of the fresh air supply (from below or above)
2. Quantity of polluted air to be exhausted

[4] Transverse ventilation system has both extraction and supply of air. Fully transverse ventilation have equal amount of exhaust and supply air.

Table 3.3 Relevant data from the Zwenberg tunnel fire tests in 1975 [3]

Test no.	Identification code of test[a]	Test conditions[a]	Fuel (litre, area, fuel type)	T_0 (°C)	$\dot{m}''_f$ (kg/(m^2 s))	Average HRR[b] (MW)	T_{max} (°C)	L_f towards north portal (m)	L_f towards south portal (m)
101	U-1-1-7-F	TOF	100, 3.4 m^2, gasoline	NA	0.064	8	NA	NA	NA
102	U-1-1-2.5-F	TOF	200, 6.8 m^2, gasoline	NA	0.051	12	NA	NA	NA
103	U-1-1-0-F	FTV		12	0.044	10	904	19	6
104	U-1-1/3–0-F			10	0.052	12	1240	14	60
105	X-1-0-0-F	EO		12	0.054	13	1320	11	12
106	0-1-1/3-0-F			8	0.049	12	1222	15	12
107	0–1-1–0-F	FTV		10	0.035	8	1080	17	10
203	U-1-1-0-A	FTV		8	0.041	10	856	21	6
204	U-1-1/3-0-A			10	0.041	10	1118	16	11
205	X-1-0-0-A	EO		10	0.051	12	1254	17	14
206	0-1-1/3-0-A			8	0.049	12	1318	20	20
207	0-1-1-0-A	FTV		10	0.033	8	1134	19	10
208	U-0-1-0-A	STV		12	0.035	8	822	23	7
209	U-1-1-2-A	FTV		14	0.048	13	663	15	0
210	U-1-1/3–2-A			12	0.045	12	563	5	0
211	U-1-1-2-F	FTV		12	0.044	12	670	16	0
212	X-0-0-2-A	PLV		14	0.044	12	623	12	0
213	X-0-0-4-A	PLV		12	0.045	12	312	10	0
214	X-0-0-0-A	EO		16	0.040	9	1000	23	0
215	0-1-1–2-F	FTV		12	0.044	12	612	10	0

Table 3.3 (continued)

Test no.	Identification code of test[a]	Test conditions[a]	Fuel (litre, area, fuel type)	T_0 (°C)	$\dot{m}''_f$ (kg/(m^2 s))	Average HRR[b] (MW)	T_{max} (°C)	L_f towards north portal (m)	L_f towards south portal (m)
216	0-0-1-0-A	STV		13	0.037	9	893	26	5
217	0-0-1/3–0-A	STV		11	0.032	8	1165	26	10
218	0-1-1/3–2-A			10	0.040	11	623	12	0
219	X-1-0-2-A	EEO		6	0.040	11	675	16	0
221	X-1-0-2-A	EO		8	0.028	7	723	4	0
220	X-1-0-0-A	EO	200, 6.8, diesel	8	0.041	10	643	13	0
301	X-1-0-0-A	EO	400, 13.6, gasoline	6	0.042	20	1332	59	12
302	0-1-1/3-0-A			6	0.035	17	1320	46	31
303	0-0-1/3-0-A			8	0.044	21	1330	60	21
2000	U-0-1-0-A	STV	Wood, rubber	NA	NA	NA	NA	NA	NA

NA not available

[a] *TF* test of facility (preliminary tests), *FTV* fully transverse ventilation, *EO* extraction only, *STV* semi transverse ventilation, *PLV* pure longitudinal ventilation, *EEV* enlarged extraction opening

[b] We assume in tests with natural and semitransverse ventilation and in the tests with longitudinal ventilation. The heat of combustion is assumed to be equal to 43.7 MJ/kg and the fuel density is assumed to be 740 kg/m^3 [36]

3. Quantity of air supply
4. Forced longitudinal ventilation in traffic space
5. Conditions in the traffic space (open or obstructed)

The selected combination of different test parameters can be obtained from the second column in Table 3.3.

As an example the identification code of test 210, that is, U—1–1/3–2– A is given according to the following system:

U	Location of fresh air supply
	U = from below
	O = from above
	X = no supply
1	Quantity of exhausted air
	1= nominal quantity 30 m^3/s
	1/3 = 10 m^3/s
1/3	Supplied quantity of fresh air
	1 = nominal quantity 30 m^3/s
	1/3 = one third of 30 = 10 m^3/s
2	Longitudinal flow in the traffic space (2 m/s)
A	Condition in the traffic space
	F free cross section
	A test models in the traffic space

The ventilation arrangement, the pool size, the length of the tunnel, and that no FFFS were used, are the main parameters that differ these tests from the Ofenegg tests. The average burning rate per square meter varied between 0.032 kg/(m^2 s) and 0.064 kg/(m^2 s) with an average value of 0.043 kg/(m^2 s), whereas in the Ofenegg tests it varied between 0.009 kg/(m^2 s) and 0.074 kg/(m^2 s). In the open a corresponding value for large pool fires is 0.055 kg/(m^2 s) [36], see Chap. 4. The burning rates in the Zwenberg and the Ofenegg tests are not based on any weighted results, it was calculated as the total fuel consumption divided by an estimated burning time. This will lead to conservative values since the burning rate varies with time, especially in the beginning of the test and during the period when the fire starts to decrease. In between these periods it should be relatively constant. As shown earlier the variation in the burning rates per square meter in these tests is much less than in the Ofenegg tests. The main reason is probably that the fire size was not nearly as large as in the Ofenegg tests and also that the tunnel was open in both ends and the total width of the pool (two trays beside each other ~2.5 m) was much less than the width of the tunnel (4.4 m).

Feizlmayr reports [3] that two classes of danger areas were used when analysing the results of the Zwenberg tests; class 1 areas with fatal effects and class 2 areas of potential danger. This type of classification was used in the Ofenegg tests as well. The criteria for class 2 used were the following; 80 °C temperature, 4.3 % CO_2 and 1000 ppm (0.1 %) of CO at heat level. The results of the Zwenberg tests showed that

the extension of the danger area and smoke area (visibility) could be influenced to a great extent by the system of ventilation. The fully transverse ventilation (FTV), when properly designed air flow supply (throttle), was found to offer the best conditions for getting the fire situation under control. With semitransverse ventilation (STV) with only fresh air supply the system gave only modest improvements of the conditions within the tunnel. It was recommended to throttle the fresh air supply in order to improve the conditions. New STV installations should be designed so that in case of fire a quick change over from fresh air supply to air extraction could be achieved. In tunnels with bi-directional traffic, it was found that the FTV or STV (if properly designed) would be more effective in case of fire than the longitudinal ventilation system due to possibility of smoke extraction. Based on the Zwenberg tests, it was strongly recommended that longitudinal ventilation should be shut down in case of fire with exception that meteorological conditions require other measure to prevent the longitudinal flow. In tunnels with uni-directional traffic it was found that longitudinal ventilation system could protect the people on the upstream side of the fire, assuming that the vehicles were not trapped on the downstream side of the fire. The recommendations given after the Zwenberg tests have been a guide for the design of ventilation systems world-wide.

3.3.5 P.W.R.I 1980

The Public Works Research Institute (P.W.R.I.) in Japan performed two series of large-scale tests [10]. The first test series were carried out in P.W.R.I's own full-scale test tunnel facility and the second test series was carried out on the Chugoku Highway in the Kakeitou Tunnel. The full-scale tunnel at P.W.R.I. site has a total length of 700 m, a cross sectional area of 57.3 m^2 ($H = 6.8$ m) and is equipped with ventilation system and FFFS. The Kakeitou tunnel has a total length of 3277 m, a cross sectional area of 58 m^2 ($H = 6.7$ m), and is equipped with ventilating and FFFS. The majority of the experiments were conducted in the full-scale tunnel at P.W.R.I. but also in the Kakeitou tunnel. The main purpose of using the long tunnel was to determine the environment for people evacuating from tunnels.

The fire source consisted of gasoline pool (gasoline) fires, passenger cars, and large-sized buses. Gasoline pool fires of 4 and 6 m^2 were used to generate a HRR equal to the fire for large-sized vehicle, large-sized buses, and passenger cars. The pool fires were applied in order to accomplish steady and repeatable fires, which may not be the case in tests using real motor vehicles. Several real motor vehicles were, although used for confirmation of the results. Four to six sets of gasoline fire pools (trays) were arranged for fires, each having four 0.25 m^2 (a total of 1 m^2 fuel surface area) fire trays in one set. Further, 18 L of gasoline was uniformly placed in each fire tray in order to maintain almost the same burning rate for about 10 min after ignition. In the tests with passenger cars, doors of the driver's seat were left half-opened, while other doors and windows were closed. Approximately, 10–20 L of gasoline were put in the fuel tank of the passenger cars. For large-sized buses, the entrance door, exit doors, and the window next to the driver's seat were fully

opened, and 50 L of light oil was put in the fuel tank. With respect to passenger cars and buses, pieces of cloth soaked in advance in a small amount of gasoline were placed on the rear seats and ignited. A comprehensive instrumentation was used in these test series. The gas temperatures (84 points in the Kakei tunnel), concentrations of smoke (78 points in the Kakei tunnel), gas velocities (5 points), concentrations of O^2, CO gases (1 and 3 points, respectively), radiation (1 point), and burning velocity (mass loss rate) were measured.

No HRR measurements were carried out in these tests. The fuel mass loss rate of the pool fires was measured as a reduction in the level of fuel. It is reported that at 1 m/s longitudinal velocity the mass fuel rate was 0.63 cm/min (0.078 kg/(m^2 s) assuming 740 kg/m^3 for gasoline) and 1.24 cm/min (0.153 kg/(m^2 s)) at 4 m/s. The authors refer to outside door test yielding 0.42 cm/min (0.052 kg/(m^2 s)). These burning rates can be compared to values given in Table 3.2 (Ofenegg) and Table 3.3 (Zwenberg). At low velocities the values are in the same order, whereas at high wind velocity it is about factor of two higher. On passenger cars the burning rate was reported to be 7.4 kg/min (0.15 kg/s) at 1 m/s and 10 kg/min (0.17 kg/s) at 4 m/s. Assuming an average heat of combustion of 30 MJ/kg this would correspond to 4.4 and 5 MW, respectively. The burning rate of the seats in the buses was reported to be 6.9 to 8.1 kg/min (0.11 kg/s and 0.14 kg/s).

The ventilation system was able to create a longitudinal flow up to 5 m/s. The FFFS facilities were set so that comparisons could be made between the presence and absence of FFFS under the same fire sources and the same longitudinal flow. Duration of FFFS was set at about 20 min. The area of FFFS was that area directly above the fire source. In some tests the FFFS was used downstream from the fire source in order to check the water cooling effect on hot air currents. The amount of water discharge was set at about 6 L/(min m^2) on road surface. In order to review the possibility of fire spread to following vehicles congested during the fire, an experimental case was carried out using cars which were arranged longitudinally and transversely.

The influence of the temperature due to the fire was found to be only limited to the nearby areas of the fire. In Table 3.4 a summary of all peak HRRs and ceiling temperatures is given. The data show clearly the effects of the longitudinal flow on the peak temperature in the ceiling. Higher velocity tends to lower the ceiling temperature due to dispersion of the hot air. It was not possible to extract any information about the flame lengths from the information available. An estimation of the free flame height for the pool fires used in this test series indicates that the flames were not impinging on the ceiling. The ceiling temperatures given in Table 3.4 confirm these calculations.

It is pointed out in the report [10] that it is extremely important to determine the behaviour of smoke and to control smoke when considering the evacuation possibilities during a tunnel fire. It was concluded that in the case of a 4 m^2 gasoline fire or a large-sized bus fire, the conditions for evacuation could be maintained near the road surface for about 10 min and over a distance of 300–400 m, if the longitudinal velocity was lower than 2 m/s. However, if the wind velocity increased, the smoke spread over to the entire section was such that any type of evacuation would become difficult.

Table 3.4 The test programme for the P.W.R.I. test series in Japan 1980 [3, 10]

Test no.	Test tunnel	Fire source (m^2, litre fuel)	u (m/s)	FFFS discharge time after ignition (min)	$\dot{Q}_{max}$ (MW)[a]	T_{max} (+5 m from centre) (no FFFS) (°C)
1	P.W.R.I. 700 m	4 m^2, 288 L	0.65	–	9.6	252
2	″	4, 288	5	–	9.6	41
3	″	4, 288	0.65	3	9.6	NAs
4	″	4, 288	5	3	9.6	NAs
5	″	6, 432	2	–	14.4	429
6	″	6, 432	2	0	14.4	NAs
7	″	Passenger car	1	–	NA	62
8	″	Passenger car	3	–	NA	NA
9	″	Passenger car	5	–	NA	NA
10	″	Passenger car	1	2.4	NA	NAs
11	″	Passenger car	3	2.4	NA	NAs
12	″	Passenger car	5	2.4	NA	NAs
13	″	Large-sized bus	5	–	NA	166
14	″	Large-sized bus	0.65	1.4	NA	NAs
15	″	Large-sized bus	2	10.5	NA	NAs
16	″	Large-sized bus	5	1.37	NA	NAs
17	Kakei 3277 m	4, 288	0	–	9.6	511
18	“	4, 288	2	–	9.6	199
19	“	4, 288	5	–	9.6	69
20	“	4, 288	0	3	9.6	NAs
21	“	4, 288	2	3.16	9.6	NAs
22	“	4, 288	5	3	9.6	NAs
23	“	Large-sized bus	0	–	NA	186
24	“	Large-sized bus	0	2.5	NA	–

NA not available, *NAs* not available temperature due to the FFFS.

[a] Based on estimation and not measurements. Due to the good ventilation condition we assume free burning conditions that is 2.4 MW/m^2 for gasoline (0.055 kg/(m^2 s) and 43.7 MJ/kg [36])

It was also found that the wind velocity in order to prevent back-layering was 2.5 m/s and that increasing the wind velocity would influence the fire so that the amount of heat and smoke would increase. It was found that the FFFS facilities of the present scale were not able to extinguish gasoline fire and roofed motor vehicles, but they were able to lower the nearby temperature and prevent fire spread to nearby motor vehicles. It was also shown that the FFFS may cause the smoke to descend and deteriorate the evacuation environment near the road surface, and therefore precautions should be taken concerning the method of operation sprinkling facilities.

3.3.6 TUB-VTT Tests 1986

As a part of German–Finnish cooperation on tunnel fires, the Technische Universität Braunschweig (TUB) in Germany and the Technical Research Centre of Finland (VTT) performed two large-scale tunnel fire test in 1985 in Lappeenranta in South Eastern part of Finland. This cooperation developed and widened later into EUREKA project EU499.

Two pilot tests were carried out in a tunnel in a limestone quarry 45 m below ground. The tunnel was 140 cm long, 6 m wide and 5 m high (30 m^2), and had natural calcite rock surfaces which were unprotected and without reinforcements. The first experiment was designed to simulate a fire in a subway car stalled in a tunnel. The second experiment simulated the case when one car in a queue of cars in a tunnel catches fire. Forced ventilation of fresh air at the rate of 7 m^3/s was used. This generated a longitudinal flow of 0.2–0.4 m/s over the cross section prior to ignition. At the maximum HRR an inflow of 0.3 m/s were measured in the lower part of the cross section and outflow of about 6 m/s in the upper part of the cross section at same location that is 19 m inside the exit portal. The fire load was made of wood cribs (moisture 17%) nailed together in a way that allowed an air space of 50% of the total volume. Temperatures of air, rock surface of the walls and the ceiling and temperatures of the steel, and concrete columns placed on the floor were recorded on several locations. Also, concentrations of O_2, CO_2 and CO, and air flow velocities were measured close to the exit of the tunnel. Fuel burning rate was determined by measuring the mass loss of wood on a weighing platform. The original idea was to utilize the oxygen consumption technique, but due to large uncertainties in O_2 and flow measurements it was never completed [16]. Smoke level and visibility were observed visually close to the exit.

In the first test (F1–1) the fire load of 7600 kg was distributed over an area of 3.2×48 m (spread as a layer on light concrete blocks 0.47 m above ground). After ignition at the upstream end of the fire load the wood cribs burned without flashover with a constant velocity of 0.66 mm/s for 21.5 h.

In the second test (F1–2) the fire load consisted of eight separated piles (cluster) of wood cribs, 1.6×1.6 m of area and 0.8 m of height each with a mass of 500 kg. The free space between the piles was 1.6 m and the lower end of the wood cribs was 0.5 m over the tunnel floor. Two adjacent piles were ignited simultaneously at the upstream end of the fire load. The fire growth rate was quite steep and reached a peak HRR of 8 MW after about 15 min into the test and then started to decay. The two wood piles burned out since it never spread to the adjacent wood piles. Therefore, a new ignition was done at the other end (downstream side) of the wood crib cluster. The fire growth rate was slower this time and reached a HRR of about 3 MW after about 20 min. The HRR was relatively constant at 3 MW (except one short peak at 4 MW) for about 45 min. The main difference between the first ignition and the second ignition is that the fire spreads downwind after the first ignition and upwind in the second ignition. The highest gas temperature in the ceiling after the first ignition was obtained after about 20 min into the test (F1–2); 679 °C and

in the second ignition it was 405 °C obtained after about 26 min from the second ignition.

The experience from the tests shows that a spalling of the rock was a major problem. During the both experiments (F1-1 and F1-2) 10–20 cm thick layers of rock scaled off the walls and the ceiling in regions close to the fire, causing problems for safety of people carrying out the experiments, and also destroying some of the gauges during fire. One of the main conclusions from these experiments was that the theoretical calculations based on existing room fire codes did not reliably predict occurrence of flashover.

3.3.7 EUREKA EU499 Tests 1990–1992

The EUREKA EU499 test program was performed in an abandoned tunnel named Repparfjord Tunnel in northern Norway. The tunnel was 2.3 km long with a gradient less than 1 %, running north south from the main portal to a vertical shaft of 90 m height (cross section of the shaft was 9 m^2). The cross section of the tunnel was horseshoe shaped to rectangular with a flattened roof. The tunnel is approximately 5.3–7.0 m wide with a maximum height in the centre between 4.8 and 5.5 m.

The test programme included 21 large-scale tests, which were carried out in 1990, 1991, and 1992. The majority of the tests were performed in year 1992 as can be observed in Table 3.5. The main objectives of the EUREKA EU499 test program were to investigate the fire behavior of different type of fuels including real road and rail vehicles. Also to seek the possibilities of escape and rescue, and fire extinguish to see the damage of tunnel structure. The fire behavior of trains and HGVs revealed by these tests has had major effects on many design studies of large tunnel projects today.

The main results of the EUREKA EU499 project relates to the unique data of measured HRR for real vehicles where the oxygen consumption calorimetry was applied for the first time in large-scale tunnel tests. It also contained well-defined fire sources such as wood cribs and heptane pool fires, which are very valuable for scientific analysis. The wood crib tests showed a tendency of increased fire growth rate with increased ventilation rate, whereas it was not as apparent for the peak HRR. Results showed that generally the temperature of vehicles with body structure, which can melt away, for example, the aluminum subway coach and the school bus (GFRP), could reach ceiling temperatures from 800 to 1060 °C and HRR of 29–43 MW (tests 7, 11, and 14). For trains with steel body structure the HRR was less than 19 MW, fire duration longer and the ceiling temperatures tended to be lower than 800 °C (tests 4, 5, 12, and 13). For the passenger car, the highest temperature was between 210 and 480 °C and the HRR was up to 6 MW (tests 3 and 20). The same tendency about the influence of the body type on the results is found for the plastic car and the steel body passenger car. The estimated flame lengths are given in Table 3.5 as towards the portal and towards the vertical shaft. It is based on

Table 3.5 Relevant data from the test program for the EUREKA EU499 test series [3]

Test no.	Date of test	Fire load	u (m/s)	E_{tot} (GJ)	$\dot{Q}_{max}$ (MW)	T_0 (°C)	T_{max} (0 m) (°C)	T_{max} (+10 m from the centre) (°C)	L_f Towards portal (m)	L_f Towards shaft (m)
1	7.12.1990	Wood cribs no 1	0.3	27.5	NA	~5	NA	500	NA	NA
2	24.07.1991	Wood cribs no 2	0.3	27.5	NA	~5	NA	265	NA	NA
3	8.8.1991	Private car (steel body)	0.3	6	NA	~5	210	127	NA	NA
4	19.8.1991	Metro car F3 (steel)	0.3	33	NA	4.5	480	630	NA	~17
5	29.8.1991	Half rail car F5 (steel)	0.3	15.4	NA	1.7	NA	430	NA	NA
6	4.9.1991	Half rail car F6 (steel)	0.3	12.1	NA	4	NA	NA	NA	NA
7	23.8.1992	School bus (GFRP)	0.3	40.8	29	3	800	690	0	~17
8	28.8.1992	Wood cribs no 3	0.3	17.2	9.5	~8	NA	480	NA	NA
9	30.8.1992	Wood cribs no 4	3–4	17.9	11[a]	8.2	NA	440	NA	NA
10	31.8.1992	Wood cribs no 5	6–8	18	12[a]	10.4	NA	290	NA	NA
11	13.9.1992	1.5 rail cars F2Al+F7 (Aluminium +steel)	6–8/3–4	57.5	43	3.3	980	950	0	~20
12	25.9.1992	Rail car F2St (steel)	0.5	62.5	19	4.7	650	830	0	~20
13	7.10.1992	Rail car F1 (steel)	0.5	76.9	13	2.2	450	720	0	~20
14	14.10.1992	Metro car F4 (Aluminium)	0.5	41.4	35	1.6	810	1060	~11	~22

Table 3.5 (continued)

Test no.	Date of test	Fire load	u (m/s)	E_{tot} (GJ)	$\dot{Q}_{max}$ (MW)	T_0 (°C)	T_{max} (0 m) (°C)	T_{max} (+10 m from the centre) (°C)	L_f Towards portal (m)	L_f Towards shaft (m)
15	23.10.1992	Mixed load simulating truck load	0.5	63.3	17	~0	NA	400	NA	NA
16	27.10.1992	1 m^2 heptane pool no 1	0.6–1.0	18.2	3.5[b]	~0	NA	540	–[c]	–
17	28.10.1992	1 m^2 heptane pool no 2	1.5–2.0	27.3	3.5[b]	~0	340	400	–	–
18	29.10.1992	3 m^2 heptane pool no 3	1.5–2.0	21.2	7[b]	~0	NA	NA	–	–
19	29.10.1992	3 m^2 heptane pool no 4	2.0–2.5	54.5	7[b]	~0	NA	NA	–	–
20	4.11.1992	Private car (plastic)	0.5	7	6	0	480	250	NA	NA
21	12.11.1992	Heavy Goods Vehicle (HGV) with furnitures	6–8/3–4	87.4	128	~0	925	970	~19	38

[a] Fuel mass loss rate times where = 17 MJ/kg for wood

[b] Measured average burning rate 78 g/m^2 s multiplied with = 44.6 MJ/kg and 1 m^2

[c] minus (−) sign indicate that there were no horizontal flame lengths, L_f, registred by the thermocouples

600 °C flame tip obtained from maximum temperature graphs as a function of the distance from the centre of the fire given by Ekkehard [38].

The EUREKA EU499 tests show the importance of the glazed windows on the fire growth in the steel body trains. The fire growth rate is apparently governed by the sequence and timing of the window cracking. This can be shown by analyzing the temperature development inside the train compartments. The type of interior material (former or new design) appears not to be as eminent for the fire growth as expected. The type of body and the quality of the windows appears to be more important than the type of interior materials. For a heavy goods load (furniture's), which is not contained by any steel or aluminum body, the corresponding data were about 1000 °C and a HRR of 120–128 MW. The propagation speed of smoke front was constant along the tunnel, implying that the behavior smoke propagation was similar to the movement of gravity currents.

3.3.8 Memorial Tunnel Tests 1993–1995

The Memorial Tunnel Fire Ventilation Test Program (MTFVTP) consisted of a series of large-scale fire tests carried out in an abandoned road tunnel. Various tunnel ventilation systems and configurations of such systems were operated to evaluate their respective smoke and temperature management capabilities. The Memorial Tunnel test program was performed in a two-lane, 853 m long and 8.8 m wide road tunnel built in 1953, taken out of traffic 1987 and was a part of the West Virginia Turnpike. The tunnel has a 3.2 % upgrade from south to north portal. The tunnel was originally designed with a transverse ventilation system, consisting of a supply fan chamber at the south portal and an exhaust fan chamber at the north portal. An overhead air duct, formed by a concrete ceiling 4.3 m above the roadway, was split into supply and exhaust section by a vertical concrete dividing wall. In some of the tests, the horizontal ceiling was removed in order to put in place 24 reversible jet fans in-group of three equally spaced, over the tunnel. The cross section changed from rectangular shape with cross sectional area of 36.2 m^2 to more of a horseshoe shape with an height of 7.8 m and a cross sectional area of 60.4 m^2. These fans had a 56 kW motor and an outlet velocity of 34.2 m/s and a volume flow of 43 m^3/s. They were designed to withstand air temperatures of about 300 °C.

The test programme consisted of 98 tests where the type of ventilation, fuel size and FFFS were changed. The ventilation systems was modified and run with the following system configurations:

- Full Transverse Ventilation (FTV)
- Partial Transverse Ventilation (PTV)
- PTV with Single Point Extraction
- PTV with Oversized Exhaust Ports
- Point Supply and Point Exhaust Operation
- Natural Ventilation
- Longitudinal Ventilation with Jet Fans

Table 3.6 Relevant data from the Memorial Tests program with different type of ventilation system. In the case of the mechanical ventilation the peak temperature and flame lengths are obtained after the start of the ventilation [3]

Test Id.	Type of ventilation	u (m/s)	T_0 (°C)	H (m)	Nominal $\dot{Q}_{max}$ (MW)	T_{max} (°C)	L_f toward north portal (m)	L_f toward south portal (m)
101CR	Full Tranverse		21	4,4	10	574	–	–
103	Full Tranverse		19	4.4	20	1361	10	10
113A	Full Transverse		20	4.4	50	1354	37	0
217A	Partial Tranverse (PTV)		13	4.4	50	1350	45	6
238A	PTV-Two Zone		23	4.4	50	1224	21	13
239	PTV-Two Zone		21	4.4	100	1298	54	15
312A	PTV-Single Point Extraction		13	4.4	50	1301	42	7
318A	Point Supply and Point Extraction		11	4.4	50	1125	22	20
401A	PTV-Oversized Exhaust Ports		21	4.4	50	1082	21	12
605	Longitudinal	2.2	6	7.9	10	180	–	–
607	Longitudinal	2.1	6	7.9	20	366	–	–
624B	Longitudinal	2.3	14	7.9	50	720	–	21
625B	Longitudinal	2.2	15	7.9	100	1067	–	85
501	Natural ventilation		13	7.9	20	492	–	–
502	Natural ventilation		10	7.9	50	923	27	–

minus (−) sign indicate that there were no horizontal flame lengths, L_f, registred by the thermocouples

The tunnel was equipped with instrumentation and recording equipment for data acquisition. Sensors measuring air velocity, temperature, carbon monoxide (CO), carbon dioxide (CO_2), and total hydrocarbon content (THC) were installed at 12 cross sections along the tunnel. In total there were approximately 1400 measuring points, each point was recorded once every second during the test (the test time ranged from about 20 to 45 min). Smoke generation and movement and the resulting effect on visibility was assessed using seven remote-controlled television cameras with associated recording equipment.

It is not possible to present all the tests data from the Memorial Tunnel tests due to the large amount of tests performed (in total 98 tests). An extract of data for T_0, $T_{max,}$ and L_f is given in Table 3.6. The data is collected after the mechanical ventilation system has been started. For the full transverse ventilation, longitudinal ventilation, and the natural ventilation tests, test results with nominal HRRs of 10, 20, 50, and 100 MW were given. For partial transverse ventilation systems only 50

Table 3.7 Relevant data from the Memorial Test program. The table shows data from tests with mechanical ventilation where the data is taken prior to the start of the mechanical ventilation (that is, during the preburn time) [3]

Test Id.	T_0 (°C)	H (m)	Nominal $\dot{Q}_{max}$ (MW)	T_{max} (°C)	L_f toward north portal (m)	L_f toward south portal (m)
101CR	21	4.4	10	281	–	–
103	19	4.4	20	1053	8	7
217A	13	4.4	50	1169	8	9
239	21	4.4	100	1210	41	17
606A	6	7.9	10	152	–	–
618A	11	7.9	20	378	–	–
624B	10	7.9	50	829	10	7
615B	8	7.9	100	957	27	9

minus (−) sign indicate that there were no horizontal flame lengths, L_f, registred by the thermocouples

and 100 MW (if available) tests are presented. For comparison, data from tests with mechanical ventilation where the data is taken during the preburn time (the period prior to the start of the mechanical ventilation when there was a natural ventilation), is presented in Table 3.7.

Ventilation system effectiveness in managing smoke and temperature movement was tested in advance for the calculated fire sizes (nominal): 10, 20, 50, and 100 MW. The corresponding fuel surface area is 4.5 m^2, 9 m^2, 22.2 m^2 and 44.4 m^2, respectively, meaning an average HRR of 2.25 MW/m^2. The fire source consisted of low-sulfur No 2 fuel oil (diesel fuel with lowered sulfur content) in different pools. In addition to varying the fire size, systematic variations were made in airflow quantity, longitudinal air velocity near the fire, and fan response time for each ventilation system. Tests were also conducted to assess the impact of longitudinal air velocities on the effectiveness of a foam suppression system. Various smoke management strategies and combinations of strategies were employed, including extraction, transport, control direction of movement, and dilution to achieve the goals of offsetting buoyancy and external atmospheric condition and to prevent backlayering (critical velocity).

The main findings from the Memorial tests are according to the test report [20]:

- The Memorial Tunnel fire ventilation tests have shown that, longitudinal airflow near a fire is equally important as extraction rate for temperature and smoke management. Therefore, specifying a ventilation rate for temperature and smoke management, solely on its extraction capabilities, is insufficient. Further, any criteria established for emergency ventilation should include the impact of tunnel physical characteristics and tunnel ventilation system.
- Longitudinal ventilation using jet fans was shown to be capable of managing smoke and heat resulting from heat releases up to 100 MW. The required longitudinal air velocity to prevent back-layering in the Memorial Tunnel was approximately 3 m/s for a 100 MW fire.

- Jet fans positioned downstream of, and close to, the fire were subjected to temperatures high enough to cause failure. Accordingly, this condition needs to be considered in the system design and selection of emergency operational modes.
- Full transverse ventilation systems can be installed in single-zone or multi-zone configurations and can be operated in a balanced or unbalanced mode. Single-zone, balanced (equal flow rates for supply and exhaust air) full transverse systems indicated very limited smoke and temperature management capability. Multiple-zone full transverse systems have the inherent capability to manage smoke and temperature by creating longitudinal airflow.
- Partial transverse ventilation systems can be installed in single-zone or multi-zone configurations and can be operated in supply or exhaust mode. Single-zone partial transverse systems capable of only supplying air (no possible reversal of fans to exhaust air) were relatively ineffective in smoke or temperature management. Single-zone partial transverse systems which can be operated in the exhaust mode provided a degree of smoke and temperature management.
- Longitudinal airflow is a significant factor in the management of smoke and heat generated in a fire. Ventilation systems which effectively combine extraction and longitudinal airflow can significantly limit the spread of smoke and heat.
- Single point extraction (SPE) is a ventilation system configuration capable of extracting large volumes of smoke from a specific location through large, controlled openings in a ceiling exhaust duct, thus preventing extensive migration of smoke.
- Oversized exhaust ports (OEP) are a modification to transverse type systems which provides smoke extraction capability in the immediate location of a fire. Significant improvement in temperature and smoke conditions were obtained using OEPs relative to the basic transverse ventilation system using conventional size exhaust ports. The OEP enhancement is also applicable to tunnels with bi-directional traffic.
- Natural ventilation resulted in extensive spread of heat and smoke upgrade of the fire. However, the effects of natural buoyancy are dependent on the fire size and the physical characteristics of the tunnel.
- The restriction to visibility caused by smoke occurs more quickly than does a temperature high enough to be debilitating. Carbon monoxide (CO) levels near the roadway never exceeded the guidelines established for the Test Program.
- The effectiveness of the foam suppression system was not diminished by operation in strong longitudinal airflow.
- Adequate quantities of oxygen to support combustion were available from the tunnel air. The possible increase in fire intensity resulting from the initiation of ventilation did not outweigh the benefits.

3.3.9 Shimizu No. 3 2001

In year 2001, ten fire tests were conducted in the three-lane No. 3 Shimizu tunnel on the New Toumei expressway in Japan [39]. The tunnel was 1119 m long with a slope of 2% down from west to east. The cross-sectional area was 115 m^2 and the

width and the height was 16.5 m and 8.5 m, respectively. The cross section was shaped as a semicircle. The reason for performing these tests was to investigate the fire behavior in tunnels with large cross section regarding combustion rate, formation of smoke layer, interaction of longitudinal flow on the smoke distribution and behavior of FFFS on the smoke layer, and risk for fire spread. Comparison with the P.W.R.I tests (2-lane tunnel) was one of the main arguments for performing these tests. Numerous studies have been published from these tests focusing on different subjects concerning convective HRR and numerical simulations [40], smoke decent [41], plume fires in large tunnel cross section [42], and bus fire [43].

The fire source consisted of gasoline pools with an area of 1, 4, and 9 m^2. In the 1 m^2 pool fire, no forced ventilation was used. In the 4 m^2 pool fire case, tests were carried out both with and without forced ventilation. The forced ventilation consisted of longitudinal ventilation of 2 and 5 m/s from west to east portal. In the 9 m^2 case, longitudinal ventilation of 2 m/s was used. When no forced ventilation was used the west portal was blocked. One test with three passenger cars and a longitudinal velocity of 5 m/s was carried out as well as a single large bus with a longitudinal flow of 2 m/s. Jet fans installed in the west portal created the longitudinal flow in the tunnel. Measurements were made at a number of points throughout the tunnel. Temperature (91 points) was measured by type K thermocouples, optical smoke density (57 points) was measured by optical penetration type absorption density meters, heat radiation was measured by a radiation meter located on the floor 30 m west of the fire, and longitudinal air velocity was measured by means of a vane anemometer (measurable range 0.3–15 m/s) located 100 m east of the fire [40].

In Table 3.8, a summary of the information obtained from references [39–43] is given. There was no information about the ambient temperature, T_0, but only the temperature differences. There was no information on the discharge time of the FFFS available. There was not enough information available to obtain any horizontal flame length. Most likely there were no horizontal flames along the ceiling in these tests, which can be shown by using free burning flame height equations, see example, [44].

The information obtained from these tests is by no means unique. One exception is the test with the large bus and the fact that these tests were performed in a tunnel with a very large cross section. Since the fires used were relatively small it is difficult to see any dramatic effects of the size of the cross section on temperatures or smoke distribution.

3.3.10 2nd Benelux Tests 2002

Fourteen large-scale tests were carried out in the Second Benelux Tunnel in the Netherlands in 2002. The tests were designed to assess the tenability conditions for escaping motorists in case tunnel fire and to assess the efficiency of detection system, ventilation system, and FFFS for numerous type of fire sources. These were pool fires, passenger cars, a van, and mock-ups with truckloads. Temperatures, ra-

Table 3.8 Relevant data from test program and data for the No 3. Shimizu Tunnel tests in 2001 [3]

Test no.	Test id.	Fire source (m^2)	u (m/s)	T_0 (°C)	FFFS discharge time from ignition (min)	$\dot{Q}_{max}$ (MW)[a]	ΔT_{max} (°C)
1	1G-0	1	0	NA	NA	2.4	110
2	4G-0	4	0	NA	NA	9.6	577
3	4G-2	4	2	NA	NA	9.6	144
4	4G-5	4	5	NA	NA	9.6	58
5	4G-0	4	0	NA	NA	9.6	NA
6	4G-2	4	2	NA	NA	9.6	NA
7	4G-5	4	5	NA	NA	9.6	NA
8	9G-2	9	2	NA	NA	21.6	300
9		3 passenger cars	5	NA	NA	NA	NA
10		Single large bus	2	NA	NA	30[b]	283

NA not available

[a] Due to the good ventilation condition we assume free burning conditions that is 2.4 MW/m^2 for gasoline (0.055 kg/(m^2 s) 43.7 MJ/kg [36])

[b] This is estimated from the convective HRR of 20 MW derived by Kunikane et al. [43] because a FFFS was activated when the convective HRR was 16.5 MW. We assume that 67 % of the HRR is convective and thereby we can estimate the HRR = 20/0.67 = 30 MW

diation levels, and optical densities in the tunnel were measured, as well as smoke velocities and HRRs.

The tests were carried out in a sink tunnel outside Rotterdam. In Table 3.9 results from these tests are given. The tunnel has a rectangular cross section with a height of 5.1 m and a width of 9.8 m and a length of about 900 m. The tunnel has a maximum slope of 4.4 % and was equipped with longitudinal ventilation. A total of six jet fans were installed at the upstream portal of the tunnel in order to create air velocities up to 6 m/s. The test site was located at 265 m from the downstream portal. The test program included four pool fire tests with ventilation rates between 0 and 6 m/s. The pool fires consisted of a mixture of n-heptane/toluene. The pool fire source consisted of two and four fuel pans, respectively, where each pan measured 1.8 m long and 1 m wide and the fuel level was 0.5 m above the road surface. The total fuel surface was 3.6 m^2 in tests 1 and 2 and 7.2 m^2 in tests 3 and 4.

The effects of ventilation were tested in tests 5–10 using cars and covered truckloads. Passenger cars (tests 5, 6, and 7) and covered truckloads (tests 8, 9, and 10) were tested under different ventilation conditions. Each truckload consisted of 800 kg wooden pallets (total of 36 €-pallets, 4 piles with 9 pallets in each pile), with four tires placed on the top. The fire load was mounted in a mock-up of a truck with a cover of tarpaulin where the rear end was open. The total length of the mock-up was 4.5 m, the width was 2.4 m and the height was 2.5 m. The longitudinal ventilation was varied between 0 and 6 m/s. In tests 12–14, different FFFS were tested for

Table 3.9 Relevant data from the test program for the 2nd Benelux Tunnel tests [3]

Test nr.	Fire source	Type of ventilation	FFFS discharge time from ignition (min)	E_{tot} (GJ)	u (m/s)	T_0 (°C)	$\dot{Q}_{max}$ (MW)	T_{max} (°C)	L_f downstream (m)	L_f upstream (m)
1	n-heptane/toluene 3.6 m^2	No LTV[a]	No FFFS	NA	~1.5	~13	4.1	218	–	–
2	n-heptane/toluene 3.6 m^2	LTV	″	NA	4	~15	3.5	220	–	-
3a	n-heptane/toluene 7.2 m^2	No LTV	″	NA	1.9	~12	11.5	470	–	–
3b	n-heptane/toluene 7.2 m^2	LTV	″	NA	5	~12	11.5	250	–	–
4	n-heptane/toluene 7.2 m^2	LTV	″	NA	6	~11	11.4	210	–	–
5	Passenger car	No LTV	″	NA	~1.0	10	NA	230	–	–
6	Passenger car	No LTV	″	NA	~1.5	10	4.9	210	–	–
7	Passenger car	LTV	″	NA	6	10	4.8	110	–	–
8	Truck load, 36 wood pallets, four tyres	No LTV	″	~10	~1.5	10	13.2	400	–	–
9	Truck load, 36 wood pallets, four tyres	LTV	″	~10	5.3	10	19.5	290	–	–
10	Truck load, 36 wood pallets, four tyres	LTV	″	~10	5	10	16.2	300	–	–
11	Van	No LTV	FFFS activated at 14 min	NA	~1.0	10	7.4 (at 14 min)	300 (at 14 min)	–	–
12	Truck load—aluminium cover, 36 pallets four tyres	LTV	FFFS activated at 4 min	NA	3	11	6.2 (at 4 min)	270 (at 4 min)	–	–
13	Truck load—aluminium cover, 36 pallets—four tyres	LTV	FFFS activated at 10 min	NA	3	12	13.4 (at 10 min)	~500 (at 10 min)	–	–
14	Truck load—aluminium cover, 72 pallets—six tyres	LTV	FFFS activated at 21 min	19	~2.5	10	26 (at 12 min)	~600	10	–

Minus (−) sign indicate that there were no horizontal flame lengths, L_f, registred by the thermocouples

[a] LTV means longitudinal ventilation

different ventilation rates. In test 11, a van loaded with 800 kg of wooden pallets (36 pallets) and three tires on the top was tested. In tests 12 to 14, a covered truckload was tested with the same fire load as in tests 5–10, using aluminum covering. In test 14 no covering was used and the fire load was doubled to 1600 kg of wooden pallets.

In all the tests, except for the fuel pans, the fire sources were mounted on a weighing platform in order to measure the HRR. The HRR for the pans was obtained from the mass loss rate of the supply fuel tank. The centreline temperatures were measured at five different heights at distance of 10, 20, and 50 m upstream the fire and at 10, 20, 50, and 200 m downstream the fire. The radiation heat flux from the fire was measured with cooled heat flux meters at eye-level at distance of 5, 10, and 20 m from the fire centre. Ventilation velocities were measured at three positions upstream of the fire with hot wire anemometers and at three positions downstream the tunnel using bi-directional probes.

The effects of longitudinal ventilation (LTV) rate on the fire growth rate and peak HRRs of truck loads is an important knowledge that has been used by researcher world-wide. In test 8 the peak HRR was 13.2 MW (without ventilation), 19.5 MW in test 9 with 5.3 m/s ventilation and 16.2 MW in test 10 with 5 m/s. The tests with the 36 wood pallet fire load shows that, the fire growth rate with ventilation was approximately 4–6 times faster than the fire growth rate without ventilation and the peak HRR 1.5 and 1.2 times higher, respectively. The fire growth rate in the test with 72 pallets (26 MW) was about 1.9 times faster than the 36 wood pallet fire load with no ventilation (test 8).

One of the conclusions from these tests was that the back-layering of smoke was prevented by 3 m/s for all cases. This conclusion complies well with other investigations presented in this chapter. For a small truck fire, deadly conditions due to radiation exposure could be obtained within 10 m from the truck but not at 50 m downwind the fire. The visibility was reduced within few minutes at distances 100–200 m downwind the fire. The escape routes were obscured due to the smoke. An open deluge system reduced the temperature considerably. The risk for fire spread between adjacent vehicles was therefore not deemed to be high. Smoke temperatures downwind did not obtain fatal levels and the steam production was insignificant. Visibility was however reduced such that escape routes would become difficult to observe.

The performance of FFFS was tested in four fire tests with simulated truck loads, tests 11–14. The FFFS was designed with a water discharge density of 12 mm/min. The FFFS reduced gas temperatures significantly and the risk of fire spread was also reduced. The temperature downstream did not attain the lethal tenability and steam production was insignificant. However, the visibilities in these tests were reduced so that escape routes were difficult to detect. Further information about these FFFS tests of the 2nd Benelux tunnel tests are given in Chap. 16.

3.3.11 Runehamar 2003

Large-scale tunnel tests were carried out with HGV-trailer cargos in the Runehamar tunnel in Norway [45]. The tests were carried out by SP Fire Research in Sweden in cooperation with TNO in the Netherlands and SINTEF-NBL in Norway. The tunnel is a two-way-asphalted road tunnel that was taken out of use and is 1600 m long, 6 m high and 9 m wide, with a slope varying between 0.5–1 %. The tunnel was a blasted rock-tunnel with a cross section varying between 47 and 50 m^2. The test section was smaller than the tunnel itself. The area where the fire load was placed was 32 m^2.

In total, four tests were performed with fire in a HGV-trailer mock-up. In Table 3.10, results from these tests are given. The specific commodities used consisted of four different materials, each representing a category of material typically found in the cargo of a HGV-trailer. These commodities were: standardized wood pallets, plastic pallets made of polyethylene (PE), a standardized test commodity consisting of polystyrene cups (PS) in compartmented cardboard cartons and polyurethane mattresses (PUR). In total four tests were performed. In three tests, mixtures of the various cellulosic and plastic materials were used, and in one test a commodity consisting of furniture and fixtures was used. A polyester tarpaulin covered the cargo in each test. The HGV trailer mock-up was 10.45 m long, 2.9 m wide and 4.5 m high with the trailer floor at 1.1 m above the road surface.

In Test 1 the fire load consisted of 11 tonnes of wooden and plastic pallets. At a distance of 15 m from the downstream side (rear end of the trailer-mockup) there was a target consisting of one pallet row of the same test commodity as used in test. In Test 2, the fire load consisted of 6.9 tonnes of wooden pallets and mattresses (include a target at 15 m). In Test 3, the fire load consisted of 8.5 tonnes of furniture on wooden pallets including the target at 15 m. In this test the fire load had 10 tyres (800 kg) positioned around the frame at the locations where they would be on a real HGV trailer. In Test 4 the fire load consisted of 2.8 tonnes of plastic cups in cardboard boxes on wooden pallets (no target used in this test). In each test the amount (mass ratio) of plastic materials was estimated to be about 18–19 %.

In each test, two fans positioned near the tunnel portal were used to generate a longitudinal airflow, this was about 3 m/s (centreline) at the start of each test but reduced to about 2.4−2.5 m/s once the fires became fully involved. At the location of the fire experiments which was approximately 1 km into the tunnel, a 75 m length of the tunnel was lined with fire protective panels, this reduced the cross-sectional area of the tunnel to 32 m^2 in the vicinity of the fire. The tunnel height at the fire location was 4.7 m. The objectives of the test series were to investigate: (a) fire development in HGV cargo loads, (b) the influence of longitudinal ventilation on fire HRR and growth rate, (c) production of toxic gases, (d) fire spread between vehicles, (e) fire-fighting possibilities and (f) temperature development at the tunnel ceiling and along the tunnel.

Peak HRRs in the range of 67–202 MW and peak gas temperatures in the range of 1250–1350 °C were measured using nonhazardous cargoes. Prior to these tests

Table 3.10 Relevant data from the test program for the Runehamar tests [3].

Test nr.	Fire source	Target	E_{tot} (GJ)	U (m/s)	T_0 (°C)	$\dot{Q}_{max}$ (MW)	T_{max} (°C)	L_f down-stream (m)
1	360 wood pallets measuring 1200 × 800 × 150 mm, 20 wood pallets measuring 1200 × 1000 × 150 mm and 74 PE plastic pallets measuring 1200 × 800 × 150 mm—122 m^2 polyester tarpaulin	32 wood pallets and 6 PE pallets	242	2.4–3	12	202	1365	93
2	216 wood pallets and 240 PUR mattresses measuring 1200 × 800 × 150 mm—122 m^2 polyester tarpaulin	20 wood pallets and 20 PUR mattresses	141	2.4–3	11	157	1282	85
3	Furniture and fixtures (tightly packed plastic and wood cabinet doors, upholstered PUR arm rests, upholstered sofas, stuffed animals, potted plant (plastic), toy house of wood, plastic toys). 10 large rubber tyres (800 kg)—122 m^2 polyester tarpaulin	Upholstred sofa and arm rest on pallets	131	2.4–3	9.5	119	1281	61
4	600 corrugated paper cartons with interiors (600 mm × 400 mm × 500 mm; L × W × H) and 15% of total mass of unexpanded polystyrene (PS) cups (18,000 cups) and 40 wood pallets (1200 × 1000 × 150 mm)—10 m^2 polyester tarpaulin	No target	62	2.4–3	11	67	1305	37

this high temperature level had only been observed in tests with liquid fires in tunnels. These tests show that ordinary trailer loads can generate the same level of HRR and ceiling temperatures as a tanker fire. The fire development in all the tests was very fast, despite a relatively small ignition source. The peak HRRs were reached between 8 and 18 min after ignition. The linear fire growth rates were 20.1 MW/min for Test1, 26.3 MW/min for Test 2, 16.4 MW/min for Test 3 and 16.9 MW/min for Test 4.

Calculation of time to incapacitation 458 m from the fire was found to be about 6 min from the time of arrival of the smoke gases using wood and plastic pallets and about 2 min using PUR mattresses. A "pulsing" phenomenon was observed in Test 1 and 2. These tests also indicate that the fire fighters may experience serious problems when trying to fight this type of fire, even with the use of longitudinal ventilation of 2.4–3 m/s.

3.3.12 METRO Tests 2011

Two full scale tests were performed with a commuter train carriages in an abandoned tunnel [46,47]. The tests were a part of the research project METRO, which is an interdisciplinary collaborative research project between universities, research institutes, tunnel infrastructure owners, and fire departments in Sweden [48]. The tests were performed in the Brunsberg tunnel which is a 276 m long tunnel located in western Sweden. The cross section of the tunnel varied but the average ceiling height was 6.9 m and average width at the ground level was 6.4 m. In total the cross section was in average 44 m^2.

Two commuter train carriages used were of the type X1 and had been in operation a long period by the Stockholm Public Transport (SL) who donated the carriages for the tests. The X1 carriage was approximately 24 m long. There was a driver's compartment at one end and the length of the passenger compartment was 21.7 m. The width of the inside of the carriage was 3 m and the height along the centreline was 2.32 m. The height at the wall was 2.06 m. The horizontal part of the ceiling was approximately 1.1 m wide.

The fire was initiated inside the carriages using 1 L of petrol on a corner seat in order to simulate arson. The scenario for these two tests aimed to simulate an arsonist that ignited a seat in a corner. An empty milk container (paper with an inner plastic lining) was filled with 1 L of petrol. The ignition was achieved by placing the small ignition sources at different locations which ignited the spilled petrol from the empty milk container. When pulling a string attached to the milk container, it tumbled over and the petrol flowed out on the seat and floor and ignited by the burning fibre boards. The fire was then allowed to develop and spread to the luggage and other combustible material in the wagon. At the time of ignition the three doors on one side (below referred to as door 1, door 2, and door 3, counted from the front of the train) were open.

The train was in original shape and material (test 2), but the same type of carriage (X1) was used in both tests. The carriage used in the second test (test 3) was refur-

Table 3.11 Relevant data from the test program for the METRO tests

Test nr.	Fire source	E_{tot} (GJ)	u (m/s)	T_0 (°C)	$\dot{Q}_{max}$ (MW)	T_{max} (°C)
2	X1 original	64	2–2.5	10	76.7	1081
3	X1 refurbished	71	2–2.5	10	77.4	1118

bished to be similar to a modern C20 wagon (used in the Stockholm metro). The seats were refitted using X10 seats (relatively similar to C20 seats) and the walls and ceiling were covered by aluminium. The old walls and ceiling materials were retained behind the aluminium lining.

The data acquisition was comprehensive. Gas temperatures at numerous positions, HRR, gas concentrations, and smoke inside the carriage and the tunnel, as well as radiant fluxes, and gas velocities, were measured. The air velocity was measured 50 m upstream of the wagon, 3.45 m from the ground. Inside the carriage, temperature was measured at many positions, both as single thermocouples near the carriage ceiling and in thermocouple trees. Furthermore, CO, CO_2, and O_2 were sampled and analyzed in one position at three heights. The smoke density was also measured with a laser and photo cell system at three heights. In total there were 67 sensors or sampling points inside the carriage. At measuring station 50 m from the fire there were a total of 26 sensors or samplings points (temperature, velocity, optical density, CO, CO_2, O_2).

The necessary air flow was obtained using a mobile fan of type Mobile Ventilation Unit MGV- L125/100FD. The created air velocity in the tunnel was before the ignition 2–2.5 m/s.

The influence of the transitional fire load in mass transport systems carried on by passengers was one of the most important parameters to evaluate. To obtain a good estimation of what passengers in the Stockholm metro and commuter trains carry with them on the trains, a field study was carried out by Mälardalen University [49]. The field study showed that 87 % of all passengers in the commuter trains carried bags with them on the train and 82 % in the metro. The luggage that was used in the full scale test corresponds to an assumption that approximately 81 % of the passengers carried luggage and a loading of one passenger per seat available (98 seats) in the carriage. In total, 79 pieces of luggage were used with an average mass of 4.44 kg. This corresponds to a total transitional (extra) fire load of 351 kg. The different types of bags were filled with clothes and paper (reports and brochures). If an average energy content of 20 MJ/kg is assumed the extra fire load corresponds to 7.2 GJ.

Both tests were initiated inside the carriage and developed to fully flashover fires. The time to flashover was significantly different between the two cases. In the test with the original seats and linings the maximum HRR was 76.7 MW and occurred 12.7 min after ignition. The maximum HRR in the case where more modern seats and aluminium lining were used occurred after 117.9 min and was 77.4 MW. The results from the tests are given in Table 3.11. No flame lengths were reported from the tests.

Table 3.12 Relevant data from the test program for the Carleton University laboratory

Test nr.	Fire source	E_{tot} (GJ)	u (m/s)	T_0 (°C)	$\dot{Q}_{max}$ (MW)
1	Intercity train	50	2.4	10	32
2	Subway coach	23	2.4	10	52.5

3.3.13 Carleton University Laboratory Train Tests 2011

Hadjisophocleous et al. [50] described two large-scale tests to determine the fire development and HRR of intercity railcar and a subway car. Both cars were provided by the Korean Railroad Research Institute. The tests were carried in a test facility at Carleton University located 50 km west of Ottawa. The tunnel is 10 m wide, 5.5 m high and 37.5 m long and is equipped with a mechanical exhaust system that consists of three fans capable of exhausting a total of 132 m^3/s of air. This flow corresponds to a longitudinal flow of 2.4 m/s if one assumes a cross section of 55 m^2. The air flow is introduced into the tunnel through a door which only covered a small portion of the tunnel cross section at the lower part. Due to the short length of the tunnel model, the distribution of the flow in the tunnel model may be very different with the realistic scenarios. The exhaust fan system is designed to draw smoke from the tunnel through a large fan chamber which is equipped with the instrumentation for measuring the HRR using oxygen consumption calorimetry. The method requires measurements of the mass flow rate, CO_2, CO, and O2 concentrations of the exhaust gases.

Table 3.12 gives the relevant test data results. The intercity railcar has a length of 23 m, a width of 3 m, and a height of 3.7 m. The total weight of the railcar is 38 tons. The estimated fire load for the railcar was 50 GJ. The subway car had a length of 19.7 m, a width of 3.15 m and a height of 3.45 m. The estimated fire load of the subway car was about 50 % of the intercity railcar or just over 23 GJ.

In the test with intercity railcar, the fire starts to grow after about 1.7 min from ignition and by 5 min it reaches 10 MW. From there it grows slowly to 15 MW as more windows break. After the breakage of all windows, the HRR reaches the maximum value of 32 MW 18 min after ignition.

In the test of the subway car the fire takes more time to intensify than the intercity railcar fire; however once it starts to grow it does so very quickly. The maximum HRR of 52.5 MW was reached in about 9 min after ignition. In the test it took only 140 s for the fire to grow from 1 MW to 52.5 MW, which is an extremely rapid fire growth rate. According to Hadjisophocleous et. al. [50] this rapid fire growth is a result of the fact that four doors were open from the start of the fire so adequate ventilation was there to sustain such growth. This rapid fire development fits well to the description of a sudden flashover for the entire subway at about the same time frame.

The duration of the subway car fire was shorter than the intercity railcar fire due to the higher HRR and lower fuel load. Ceiling temperatures or flame lengths were not reported from the tests.

3.3.14 Singapore Tests 2011

In 2011, the Efectis Nederland BV on assignment of the Land Transport Authority (LTA) of Singapore carried out six large-scale tests FFFS tests in the TST tunnel facility in Spain [51,52]. One test was carried out with no interaction of the FFFS. This test is of interest to report in this chapter, the FFFS tests are presented in Chap. 16. The test consisted of simulated HGV consisting of 228 pallets with 48 plastic pallets (20%) and 180 wooden pallets (80%) were used in all fire tests. An air velocity of approximately 3 m/s was applied. The maximum HRR in this test was obtained after 14 min. The maximum HRR was 150 MW. Prior to this peak value, which probably was obtained after some pallets falling down, it was steady at a level of about 100 MW. The total integrated heat energy was 99.2 GJ.

3.3.15 Runehamar Test 2013

In 2013 SP Fire Research performed five large-scale water spray tests in the Runehamar tunnel on the assignment of the Swedish Transport Administration [53]. One test was also carried without interaction of the FFFS. The other five tests are reported on in Chap. 16. The Runehamar tunnel is situated about 5 km from Åndalsnes in Norway. It is a two-way asphalted road tunnel that was taken out of use in the late 1980 s. It is approximately 1600 m long, 6 m high and 9 m wide with a cross section of about 47 m^2. The fire source comprised of 420 wooden pallets placed in the center of the tunnel, 600 m from the west portal. A target consisting of a pile of 21 wood pallets was positioned 5 m from the rear end of the fuel mock-up. This type of test fuel mock-up is often used to simulate the pay load of a Heavy Goods Vehicle (HGV) trailer. The target is used to evaluate the risk for fire spread. The moisture content in the wood pallets varied between 15–20%. Each wood pallet weighed about 24 kg and was 0.143 m thick. The total length of the fuel load was just over 8.0 m. The total height of the fuel load was about 3 m. In total, the fuel load weighed just over ten tons. This means that the potential energy content is approximately 180 GJ. The target consists of 21 pallets, giving an additional energy of approximately 9 GJ (in total 189 GJ). The fuel mock-up was shielded with steel sheets both in front, back, and on the top. The fire developed up to 79 MW after 38 min. The velocity in the tunnel was about 3 m/s. The maximum ceiling temperature was 1366 °C.

3.4 Model Scale Fire Tests

In the following a summary of some important model scale tests are given. The level of accuracy on the data is not as extensive as for the large-scale tests.

3.4.1 The TNO Tests

A series of small-scale tests was performed by TNO in an 8 m long, 2 m high, and 2 m wide model tunnel [54]. In these tests very high gas temperatures were measured and the Rijkswaterstaat Tunnel Curve (the RWS Curve) in the Netherlands is based on these tests.

3.4.2 Automatic Water Spray System Tests

A total of 28 tests, including three free-burn tests, were carried out in a 1:15 scale model tunnel [55]. The main aim was to analyze the possibility of using an automatic water spray system instead of a deluge system in a tunnel fire. The fire spread between wood cribs with a free distance of 1.05 m (15.75 m in full scale) was also tested. Further, the effect of ventilation velocities and water flow rates on the activation of nozzles, HRR, fire growth rate, gas temperature, heat radiation, and fire spread was systematically investigated.

The tunnel itself was 10 m long, 0.6 m wide, and 0.4 m high, as shown in Fig. 2. Average longitudinal velocities of 0.52, 1.03, 1.54, and 2.07 m/s, obtained by adjusting a frequency regulator, were used in the test series. The corresponding large-scale velocities were 2, 4, 6, and 8 m/s, respectively.

The fire load consisted of wood cribs (pine). The weight of a wood crib is about 4.4 kg. The free distance between each horizontal stick was 0.033 m and the total fuel surface area of a wood crib was estimated to be 1.37 m^2. The estimated HRR for the main fuel load was about 200 MW in full scale.

3.4.3 Longitudinal Ventilation Tests

A total of 12 tests were carried out in a 1:23 scale model tunnel with longitudinal ventilation [56]. The fire load was simulated with the aid of wood cribs, corresponding to a scaled-down HGV (Heavy Goods Vehicle) fire load, and the fire spread between two or three wood cribs with a free distance of 0.65 m (about 15 m in full scale) was tested. The tunnel itself was 10 m long, 0.4 m wide, and two heights of 0.3 m and 0.2 m was used respectively. The parameters tested were: the number of wood cribs, type of wood cribs, the longitudinal ventilation rate and the ceiling height. The fire spread between wood cribs, with a free distance corresponding to 15 m in full scale, was also tested. The effects of different ventilation rates on the fire growth rate, fire spread, flame length, gas temperatures, and back-layering, were investigated.

3.4.4 Point Extraction Ventilation Tests

A total of 12 tests were carried out in a 1:23 scale model tunnel with point extraction ventilation [57]. The fire load was simulated using wood cribs. The parameters tested were the longitudinal ventilation rate, the arrangement of the exhaust openings, and the exhaust capacity. Moreover, the fire spread between wood cribs with a free distance of 0.65 m (about 15 m in full scale) was tested. The point extraction ventilation system was tested under different fire conditions together with either forced longitudinal ventilation or natural ventilation. The tunnel itself was 10 m long, 0.4 m wide, and 0.2 m high. The study focuses on smoke control using single and two point extraction systems. Further, the maximum HRR, fire growth rate, maximum excess temperature beneath the ceiling, flame length, and heat flux were analyzed using relationships obtained from theoretical considerations.

3.4.5 Tunnel Cross-Section Tests

A total of 42 tests were performed in model tunnels with longitudinal ventilation to study the effect of the height and width of a tunnel on the mass loss rate, HRR, and gas temperatures [58]. The tunnel was 10 m long with a scale of 1:20. The widths used were 0.3, 0.45, and 0.6 m and the height was varied between 0.25 and 0.4 m. Two different types of fuels were used: pools of heptane and wood cribs. The wood cribs were of three different types. Two were wood cribs with two different porosities and the other one had the laterally placed short pieces of wood replaced by pieces of polyethene. The velocities tested in the model tunnels were in a range of 0.22–1.12 m/s.

3.5 Summary

A dozen of large-scale fire test programs have been carried out to date. The main focus has been on the heat and smoke spread and how different ventilation systems influence these parameters. Nearly half of the test series included FFFS testing. The quality of large-scale tests carried out in the 1960s–1980s varies considerably and in all these tests there is a lack of the key fire hazard parameter; the HRR. In the analysis carried out here new estimated HRRs are given. There is no doubt that the EUREKA EU499 tests and the Memorial tests are the most well-known and well reputed large-scale fire test series to date. They have already been established as the ‘large-scale fire tests’ and provide a new base for standards and knowledge in tunnel fire safety. The use of oxygen consumption calorimetry has increased the quality in the HRR results and made it possible to measure HRRs from vehicles.

The analysis of liquid fires presented here show that the variation in the results is considerable and it is difficult to assume one value for each type of liquid fuel. Parameters that influence the burning rate for each fuel type are the pan geometry, the fuel depth, the ventilation conditions and the reciprocal tunnel, and the fuel pan geometry. Further, in the case when the tunnel cross-section is large and the width of the tunnel is larger than the width of the fuel pan, as was the case in the Ofenegg tests [9], the influence of the longitudinal ventilation on the burning rate appears to be small.

References

1. NFPA 502 (2004) Standard for Road Tunnels, Bridges, and other Limited Access Highways. 2004 edn. National Fire Protection Association
2. Fire and Smoke Control in Road Tunnels (1999), PIARC
3. Ingason H (2006) Fire Testing in Road and Railway Tunnels. In: Apted V (ed) Flammability testing of materials used in construction, transport and mining. Woodhead Publishing, pp 231–274
4. Grant GB, Jagger SF, Lea CJ (1998) Fires in tunnels. Phil Trans R Soc Lond 356:2873–2906
5. Haerter A Fire Tests in the Ofenegg-Tunnel in 1965. In: Ivarson E (ed) International Conference on Fires in Tunnels, SP REPORT 1994:54, Borås, Sweden, 10–11 October 1994. SP Sweden National Testing and Research Institute, pp 195–214
6. Feizlmayr A Research in Austria on tunnel fire, Paper J2, BHRA. In: 2nd Int Symp on Aerodynamics and Ventilation of Vehicle Tunnels, Cambrigde, UK, 1976. pp 19–40
7. Pucher K Fire Tests in the Zwenberg Tunnel (Austria). In: Ivarson E (ed) International Conference on Fires in Tunnels, Borås, Sweden, 1994. SP Swedish National Testing and Research Institute, pp 187–194
8. ILF (1976) Brandversuche in einem Tunnel. Ingenieurgemeinschaft Lässer-Feizlmayr; Bundesministerium f. Bauten u. Technik, Strassenforschung
9. Schlussbericht der Versuche im Ofenegg Tunnel von 17.5 - 31.5 1965 (1965). Kommission für Sicherheitsmassnahmen in Strassentunneln
10. State of the Road Tunnel Equipment in Japan – Ventilation, Lighting, Safety Equipment (1993). Public Works Research Institute, Japan
11. Huggett C (1980) Estimation of Rate of Heat Release by Means of Oxygen Consumption Measurements. Fire and Materials 4 (2):61–65
12. Parker WJ (1984) Calculations of the Heat Release Rate by Oxygen Consumption for Various Applications. Journal of Fire Sciences 2 (September/October):380–395
13. Tewarson A (1982) Experimental Evaluation of Flammability Parameters of Polymeric Materials. In: Lewin M, Atlas SM, Pearce EM (eds) Flame Retardant Polymeric Materials. Plenum Press, New York, pp 97–153
14. Keski-Rahkonen O Tunnel Fire Tests in Finland. In: Proceedings of the International Conference on Fires in Tunnels, Borås, 10–11 October 1994, 1994. Swedish National Testing and Research Institute, pp 222–237
15. Fires in Transport Tunnels: Report on Full-Scale Tests (1995). edited by Studiensgesellschaft Stahlanwendung e. V., Düsseldorf, Germany
16. Mikkola E (2004) Email correspondance to the author at 10 of September
17. Ingason H Heat Release Rate Measurements in Tunnel Fires. In: Ivarson E (ed) International Conference on Fires in Tunnels, Borås, Sweden, October 10–11, 1994 1994. SP Swedish National Testing and Research Institute, pp 86–103

18. Grant GB, Drysdale D Estimating Heat Release Rates from Large-scale Tunnel Fires. In: Fire Safety Science – Proceedings of the Fifth International Symposium, Melbourne, 1995, pp 1213–1224
19. Steinert C Smoke and Heat Production in Tunnel Fires. In: The International Conference on Fires in Tunnels, Borås, Sweden, 10–11 October 1994. SP Swedish National Testing and Research Institute, pp 123–137
20. Memorial Tunnel Fire Ventilation Test Program – Test Report (1995). Massachusetts Highway Department and Federal Highway Administration
21. Takekuni K Disaster Prevention of Road Tunnel and Characteristics of the Evacuation Environment during Fires in Large-scale Tunnels in Japan. In: 4th Joint Workshop COB/JTA 2Joint Meeting JTA/Cob Open Work Shop 2001 in Netherlands, 2001. pp 35–43
22. Lemaire A, van de Leur PHE, Kenyon YM (2002) Safety Proef: TNO Metingen Beneluxtunnel – Meetrapport. TNO
23. Ingason H, Lönnermark A Large-scale Fire Tests in the Runehamar tunnel – Heat Release Rate (HRR). In: Ingason H (ed) International Symposium on Catastrophic Tunnel Fires (CTF), Borås, Sweden, 20–21 November 2003. SP Swedish National Testing and Research Institute, pp SP Report 2004:2005, p. 2081–2092
24. Lönnermark A, Ingason H Large-scale Fire Tests in the Runehamar Tunnel – Gas Temperature and Radiation. In: Ingason H (ed) International Symposium on Catastrophic Tunnel Fires (CTF), Borås, Sweden, 20–21 November 2003. SP Swedish National Testing and Research Institute, pp SP Report 2004:2005, p. 2093–2103
25. Apte VB, Green AR, Kent JH Pool Fire Plume Flow in a Large-Scale Wind Tunnel. In: Cox G, Langford B (eds) Proceedings of the Third International Symposium on Fire Safety Science, Edinburgh, Scotland, 8–12 July 1991. Elsevier Applied Science, pp 425–434
26. Bettis RJ, Jagger SF, Lea CJ, Jones IP, Lennon S, Guilbert PW The Use of Physical and Mathematical Modelling to Assess the Hazards of Tunnel Fires. In: Cockram I (ed) 8th International Symposium on Aerodynamics and Ventilation of Vehicle Tunnels, Liverpool, 1994. Mech Eng Public Lim, pp 439–469
27. Thomas PH (1970) Movement of Smoke in Horizontal Corridors against an Air Flow. Inst. Fire Engrs Q
28. Ingason H, Nireus K, Werling P (1997) Fire Tests in a Blasted Rock Tunnel. FOA, Sweden
29. Ingason H, Persson B Prediction of Optical Density using CFD. In: Curtat M (ed) Fire Safety Science – Proceedings of the 6th International Symposium, Poitiers, 1999. pp 817–828
30. Perard M, Brousse B Full size tests beforeopening two French tunnels. In: Cockram I (ed) 8th Int Symp on Areodynamics and Ventilation of Vehicle Tunnels, Liverpool, UK, 1994. pp. 383–408
31. Casale E, Brousse B, Weatherill A, Marlier E Full Scale Fire Tests Performed in the Mont Blanc Tunnel – Evaluation of the Efficiency of the Fully Automatic Ventilation Responses. In: Fourth International Conference on Fires in Tunnels, Basel, Switzerland, 2–4 December 2002. pp 313–325
32. Beard AN, Carvel RO (2012) Handbook of tunnel fire safety – Second Edition. ICE Publishing
33. Brousse B, Voeltzel A, Botlan YL, Ruffin E (2002) Mont Blanc tunnel ventilation and fire tests. Tunnel Management International Vol. 5, Nr 1:13–22
34. Rew C, Deaves D Fire spread and flame length in ventilated tunnels – a model used in Channel tunnel assessments. In: Proceedings of the International Conference on Tunnel Fires and Escape from Tunnels, Lyon, France, 5–7 May 1999. Independent Technical Conferences Ltd, pp 397–406
35. Heselden A Studies of fire and smoke behavior relevant to tunnels. In: 2nd Int Symp on Aerodynamics and Ventilation of Vehicle Tunnels, Cambridge, UK, 23–25 March 1976. Paper J1, BHRA Fluid Engineering, pp J1–1– J1–18
36. Babrauskas V (1995) Burning rates. In: DiNenno PJ, Beyler CL, Custer RLP et al. (eds) In SFPE Handbook of Fire Protection Engineering, vol 2nd Edition. The Natioanl Fire Protection Association, USA, pp 3.1–3.15

37. Heselden A, Hinkley PL (1970) Smoke travel in shopping malls. Experiments in cooperation with Glasgow Fire Brigade. Parts 1 and 2. Fire Research Station
38. Ekkehard R Propagation and Development of Temperatures from Test with Railway and Road Vehicles. In: International Conference on Fires in Tunnels, Borås 10–11 of October, 1994. Swedish National Testing and Research Institute, pp 51–62
39. Shimoda A Evaluation of Evacuation Environment during Fires in Large-Scale Tunnels. In: 5th Joint Workshop COB/JTA, Japan, 2002. pp 117–125
40. Kunikane Y, Kawabata N, Takekuni K, Shimoda A Heat Release Rate Induced by Gasoline Pool Fire in a Large-Cross-Section Tunnel. In: 4th Int. Conf. Tunnel Fires, Basel, Switzerland, 2–4 December 2002. Tunnel Management International, pp 387–396
41. Kawabata N, Kunikane, Y., Yamamoto, N., Takekuni, K., and Shimoda, A. Numerical Simulation of Smoke Descent in a Tunnel Fire Accident. In: 4th Int. Conf. Tunnel Fires, Basel, Switzerland, 2002. pp 357–366
42. Kunikane Y, Kawabata N, Okubo K, Shimoda A Behaviour of Fire Plume in a Large Cross Sectional Tunnel. In: 11th Int. Symp. on AVVT, Luzern, Switzerland, 2003. pp 78–93
43. Kunikane Y, Kawabata N, Ishikawa T, Takekuni K, Shimoda A Thermal Fumes and Smoke Induced by Bus Fire Accident in Large Cross Sectional Tunnel. In: The fifth JSME-KSME Fluids Engineering Conference, Nagoya, Japan, 17–21 November 2002
44. Heskestad G (2002) Fire Plumes, Flame Height, and Air Entrainment. In: DiNenno PJ (ed) The SFPE Handbook of Fire Protection Engineering. Third edition edn. National Fire Protection Association, Quincy, Massachusetts, USA, pp 2–1–2–17
45. Ingason H, Lönnermark A, Li YZ (2011) Runehamar Tunnel Fire Tests. SP Technical Research Institute, SP Report 2011:55, Borås, Sweden
46. Lönnermark A, Lindström J, Li YZ, Claesson A, Kumm M, Ingason H (2012) Full-scale fire tests with a commuter train in a tunnel. SP Report 2012:05. SP Technical Research Institute of Sweden, Borås, Sweden
47. Lönnermark A, Lindström J, Li YZ, Ingason H, Kumm M Large-scale Commuter Train Tests – Results from the METRO Project. In: Proceedings from the Fifth International Symposium on Tunnel Safety and Security (ISTSS 2012), New York, USA, 14–16 March 2012. SP Technical Research Institute of Sweden, pp 447–456
48. Ingason H, Kumm M, Nilsson D, Lönnermark A, Claesson A, Li YZ, Fridolf K, Åkerstedt R, Nyman H, Dittmer T, Forsén R, Janzon B, Meyer G, Bryntse A, Carlberg T, Newlove-Eriksson L, Palm A (2012) The METRO project – Final Report 2010:08. Mälardalen University, Västerås
49. Kumm M (2010) Carried Fire Load in Mass Transport Systems – a study of occurrence, allocation and fire behavior of bags and luggage in metro and commuter trains in Stockholm. Mälardalen University, Västerås, Sweden
50. Hadjisophocleous G, Lee DH, Park WH Full-scale Experiments for Heat Release Rate Measurements of Railcar Fires. In: International Symposium on Tunnel Safety and Security (ISTSS), New York, 2012. SP Technical Research Institute of Sweden, pp 457–466
51. Cheong MK, Cheong WO, Leong KW, Lemaire AD, LM N (2013) Heat Release Rates of Heavy Goods Vehicle Fire in Tunnels with Fire Suppression System. Fire Technology. doi:10.1007/s10694-013-0367-0
52. Cheong MK, Cheong WO, Leong KW, Lemaire AD, Noordijk LM, Tarada F Heat release rates of heavy goods vehicle fires in tunnels. In: In: 15th International Symposium on Aerodynamics, Ventilation & Fire in Tunnels, Barcelona, Spain, 2013. BHR Group, pp 779–788
53. Ingason H, Appel G, Li YZ, Lundström U, Becker C Large-scale fire tests with a Fixed Fire Fighting System (FFFS). In: ISTSS 6th International Symposium on Tunnel Safety and Security, Marseille, 2014
54. Rapport betreffende de beproeving van het gedrag van twee isolatiematerialen ter bescherming van tunnels tegen brand (1980). Instituut TNO voor Bouwmaterialen en Bouwconstructies, Delft, The Netherlands

55. Li YZ, Ingason H (2013) Model scale tunnel fire tests with automatic sprinkler. Fire Safety Journal 61:298–313
56. Ingason H, Li YZ (2010) Model scale tunnel fire tests with longitudinal ventilation. Fire Safety Journal 45:371–384
57. Ingason H, Li YZ (2011) Model scale tunnel fire tests with point extraction ventilation. Journal of Fire Protection Engineering 21 (1):5–36
58. Lönnermark A, Ingason H (2007) The Effect of Cross-sectional Area and Air Velocity on the Conditions in a Tunnel during a Fire. SP Report 2007:05. SP Technical Research Institute of Sweden, Borås, Sweden

Chapter 4
Heat Release Rates in Tunnels

Abstract An overview of heat release rates (HRRs) for different vehicles driving through tunnels is presented. The focus is on understanding fire development and the influences of tunnel conditions on the HRR. The HRR describes the fire development in the form of energy release given in megawatts (MW) over a given time period. The chapter presents the basic theory of burning of fuels and summarizes the HRR for different types of vehicles, solid materials, and liquids. Influences of different physical parameters such as tunnel construction or ventilation on the HRR are addressed. The HRR is also given as a value per square metre of exposed fuel surface area.

Keywords Heat release rate (HRR) · Vehicles · Ventilation · Fuel · Burning rate · Surface area

4.1 Introduction

The tunnel length and the traffic density are usually the key design parameters when setting the level of safety in road tunnels. In more advanced engineering design of the fire protection systems, the HRR of the vehicles using the tunnel becomes an important input. In rail tunnels, engineering analysis is based on risk analysis and creation of a design fire for a given train. The HRR depends on factors such as the ignition source and vehicle type, their geometry and size, material type, the geometry of the tunnel, and the ventilation conditions. Furthermore, separations between vehicles are very important in relation to fire spread. The geometric configuration and proximity of fuels within a fuel package are also expected to significantly affect fire spread. For fire testing, fuel packages can be both real vehicles and mock-ups with arranged fuels such as pool fires or piled wood pallets.

Experience from large tunnel fires shows that the HRR is the most important parameter for describing the development and consequences of a fire. The HRR physically correlates to the mass burning rate of fuel and to the production of heat, smoke, and gases. In the engineering design of ventilation and evacuation systems, as well as the structural strength of a tunnel, the HRR is a key parameter. The design parameters usually involve tabulated peak HRR values in MW [1, 2]. In Chap. 6, design fires and curves are discussed in more detail.

H. Ingason et al., *Tunnel Fire Dynamics,* DOI 10.1007/978-1-4939-2199-7_4

In order to obtain an overview of the relevance of these tabulated design data, a summary of all available HRRs for vehicles and other type of fuels used in tunnels is needed. Results from experimental tests may vary considerably, even if the setup is similar. This is because not all factors can be exactly controlled. Using HRR results from different fire tests therefore, requires caution and wariness.

Compilations of HRR results for tunnel fires have been presented by the authors and others. This includes the overview given by Ingason [3] of HRRs of different vehicles until 2001 and the work in 2005 where Lönnermark and Ingason [4, 5] presented a compressed summary of peak HRRs and corresponding ceiling temperatures from large-scale tunnel fire tests. In 2006, Ingason [6] compiled and described most of the large-scale test data found in the literature, including HRR and gas temperatures; and, in the 2008 edition of the society of fire protection engineers (SFPE) Handbook of Fire Protection Engineering, Babrauskas published HRR curves from various transport vehicles and components [7]. The latest work is in the Handbook of Tunnel Fire Safety [8], the chapter on Heat Release Rates in Tunnel Fires: A Summary, authored by Ingason and Lönnermark in 2012 [9]. These summary works are largely reflected here and have been updated by the latest research.

The HRR during tunnel tests can be determined by different measuring techniques. The most common way is by using oxygen consumption calorimetry. The HRR can also be determined by measuring the weight loss of the fuel, the convective flow, or by using carbon dioxide generation calorimetry. The accuracy of these methods strongly depends on the measuring technique and the number and type of probes used. The calculation method also plays an important role but not as important as the technique used to determine the HRR.

Experience has shown that the total accuracy of HRR measurements in tunnel fires varies [10–12].The measurement error is on the order of 15–25 % in large-scale testing whereas in fire laboratories it is in the order of 7–11 %[13]. Ingason et al. [14] estimated the maximum error in their measurements in the EUREKA EU 499 testseries (FIRETUN) [15, 16] to be approximately 25 % (relative errors conservatively added), whereas in the Runehamar tests Ingason and Lönnermark [17] estimated the error to be 14.9 % (combined expanded relative standard uncertainty with a 95 % confidence interval [13]).This shows that the HRR measurements in tunnels yield relatively high uncertainty in the measured values.

In Chap. 3, the maximum or peak HRR values were presented for each large-scale test program, but in the following sections measured HRR are given for each type of vehicle or fuel, both as table values and in graphs.

4.2 Measured HRR in Different Vehicles

4.2.1 Road Vehicles

In Table 4.1, a summary of HRR measurements of passenger cars and other road vehicles is given [9]. For each test, an estimate of total calorific content, the measured peak-HRR and time to peak-HRR is given. In Table 4.1, the passenger cars have

Table 4.1 Large-scale experimental data on passenger cars [9]

Type of vehicle, model year, test nr, u=longitudinal ventilation m/s	Tunnel(T))/ Calorimeter C)	Tunnel cross-section (m^2)	Calorific content[b](GJ)	Peak HRR(MW)	Time to peak HRR (min)	Reference
Single passenger cars						
Ford Taunus 1.6, late 70's, test 1, NV	C		4	1.5	12	[19]
Datsun 160 J Sedan, late 70's, test 2, NV	C		4	1.8	10	
Datsun 180 B Sedan,late 70's, test 3, NV	C		4	2	14	
Fiat 127, late 70's, u=0.1 m/s	T	8	NA	3.6	12	[21]
Renault espaceJ11-II, 1988, test 20, u=0.5 m/s	T	30	7	6	8	[12]
CitroënBX,1986, NV[c]	C		5	4.3	15	[22]
Austin Maestro, 1982[c]	C		4	8.5	16	
Opel Kadett, 1990, test 6, u=1.5 m/s	T	50	NA	4.9	11	[23]
Opel Kadett, 1990, test 7, u=6 m/s	T	50	NA	4.8	38	
Renault 5,80's, test 3, NV	C		2.1	3.5	10	[24]
Renault 18, 80's, test 4, NV	C		3.1	2.1	29	
Small Car[a], 1995, test 8, NV	C		4.1	4.1	26	
Large car[a], 1995,test 7, NV	C		6.7	8.3	25	
Trabant, test 1, NV	C		3.1	3.7	11	[20]
Austin, test 2, NV	C		3.2	1.7	27	
Citroen, test 3, NV	C		8	4.6	17	
Citroen Jumper Van, test 11, u=1.6 m/s, sprinkler activated after 13.6 min	T	50	NA	7.6	NA	[23]
BRE test nr 7, NV	C		NA	4.8	45	[25]
BRE test nr 8, NV	C		NA	3.8	54	

Table 4.1 (continued)

Type of vehicle, model year, test nr, u=longitudinal ventilation m/s	Tunnel(T))/ Calorimeter C)	Tunnel cross-section (m^2)	Calorific content[b](GJ)	Peak HRR(MW)	Time to peak HRR (min)	Reference
Two passenger cars						
Citroen BX+Peugeot 305, 80's, test 6, NV	C		8.5	1.7	NA	[24]
Small car[a]+Large car[a], test 9, NV	C		7.9	7.5	13	
Large car[a]+Small car[a], test 10, NV	C		8.4	8.3	NA	
BMW+Renault 5, 80's, test 5, NV	C		NA	10	NA	
Polo+Trabant, test 6, NV	C		5.4	5.6	29	[20]
Peugeot+Trabant, test 5, NV	C		5.6	6.2	40	
Citroen+Trabant, test 7, NV	C		7.7	7.1	20	
Jetta+Ascona, test 8, NV	C		10	8.4	55	
BRE test nr 11 (stacked), NV	C		NA	8.5	12	[25]
Three passenger cars						
Golf+Trabant+Fiesta, test 4, NV	C		NA	8.9	33	[20]
BRE test nr 1, NV	C		NA	16	21	[25]
BREtest nr 2, NV	C		NA	7	55	
BREtest nr 3, NV	C		NA	11	10	

NA Not Available, *NV* Natural Ventilation

[a] Small Car (*SC*) includes the following cars: Peugeot 106, Renault Twingo-Clio, Citroen Saxo, Ford Fiesta, Opel Corsa, Fiat Punto, and WW Polo. Large Car (*LC*) includes the following cars: Peugeot 406, Renault Laguna, Citroen Xantia, Ford Mondeo, Opel Vectra, Fiat Tempra, and WW Passat

[b] Either based on integration of the HRR curve or estimation of fuel mass and heat of combustion. The error is estimated to be less than 25 %

[c] Cars burned in an approximate mockup of a Channel Tunnel shuttle wagon with a calorimeter hood/duct at each end

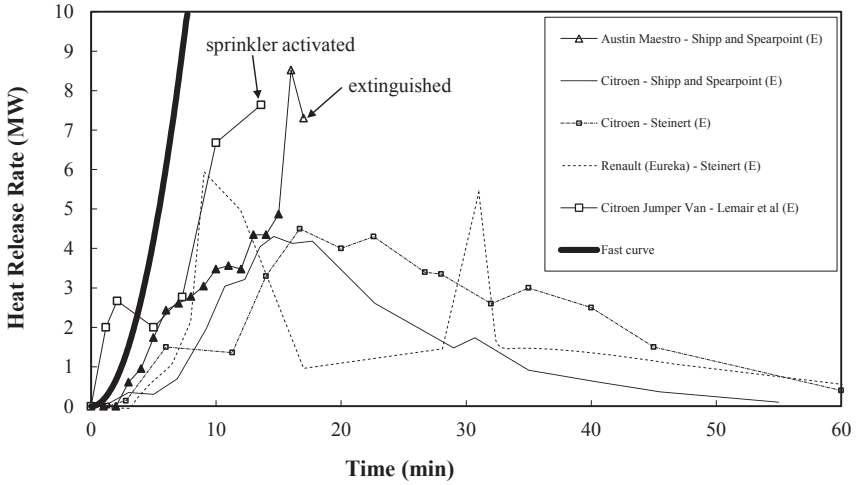

Fig. 4.1 Experimentally determined HRRs for single vehicle fires (passenger cars) [9]. Most of the data are extracted (*E*) from graphs found in the literature. If measured data are given it is indicated with (*M*). The references and more information are given in Table 4.1

either been burned under a calorimeter hood (C) or inside a tunnel (T), whereas all the large vehicles have been burned in tunnels.

4.2.1.1 Passenger Cars

HRRs in passenger cars are the most frequently obtained data found in the literature. Table 4.1 is essentially identical to the one given by Ingason and Lönnermark [9].

In Figs. 4.1 and 4.2 selected graphs of measured HRRs from single passenger cars are given. Most of these data are extracted from graphs given in each reference. For comparison, the t-squared fast fire growth curve [18] is also presented. In the following text, a short discussion of these tests is given.

HRRs from three full-scale laboratory tests using typical passenger cars (steel body) manufactured in the late 1970s (Car1, Car2, Car3) were presented by Mangs and Keski–Rahkonen [19]. The experiments were performed indoors using an oxygen calorimetry hood. Ignition was either inside the passenger cabin using a 0.09 m^2 heptane tray under the left front seat in test one or beneath the engine with an open 0.09 m^2 heptane tray yielding about 160 kW. The peak HRR ranged from 1.5–2 MW and the time to peak HRR varied from 10–14 min.

HRR of a plastic passenger car from a test in the EUREKA 499 test series [15, 16] was presented by Steinert [12]. The car used was a Renault Espace J11-II (1988) and was ignited in a transistor in the console in order to simulate a fire in the cable system. The peak HRR was 6 MW after 8 min.

HRRs of different types of passenger cars in a carpark, all with different types of car bodies (plastic and steel) have also been presented by Steinert [20]. The peak

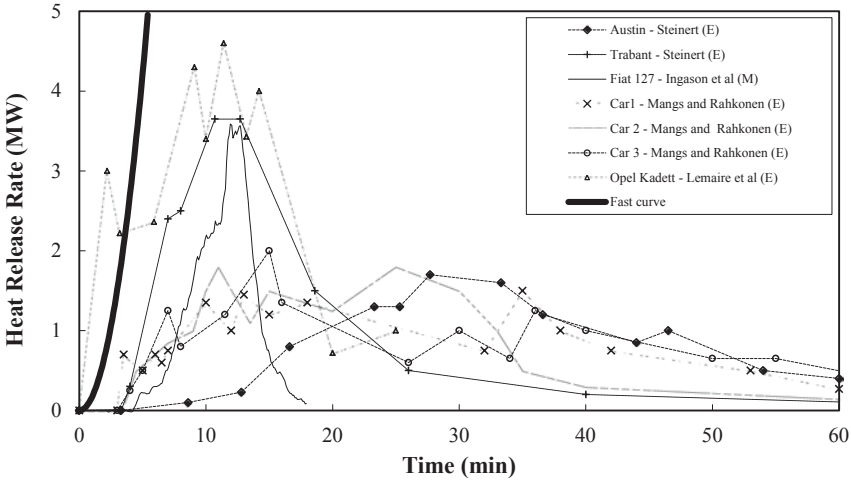

Fig. 4.2 Experimentally determined HRRs for single vehicle fires (passenger cars) [9]. Most of the data are extracted (*E*) from graphs found in the literature. If measured data are given it is indicated with (*M*). The references and more information are given in Table 4.1

HRR for single burning vehicles varied between 1.7–4.6 MW, acheived within the time frame of 11–27 min. A total of ten tests were performed in a carpark where the aim was to measure the HRR and quantify the risk for fire spread. The first three tests were carried out with single vehicles whereas the other six tests consisted of combinations of two and three passenger cars which were placed beside the ignited vehicle. The cars were ignited by dripping flammable liquid on the front seat with the front seat side window open. The peak HRR in the tests with two cars or three cars, presented by Steinert [20], varied between 5.6–8.9 MW and was achieved within the time frame of 20–55 min.

The HRRs for a 1982 Austin Maestro and a 1986 Citroën BX reported by Shipp and Spearpoint [22] are given in Fig. 4.1. The CitroënBX was ignited in the engine compartment with a small petrol pool fire of 5 kW. The Austin Maestro was ignited in the driver seat with a small wood crib of 10 kW. The test was carried out by using a calorimeter hood at each end of a canopy which was 8.7 m long and 3.5 m wide. The test setup was intended to represent a Channel Tunnel shuttle wagon. The peak HRR measured for the Citroën and the Austin Maestro was 4.3 and 8.5 MW, achieved after 15 and 16 min, respectively.

HRR measurements were presented by Lemair [23] for two Opel Kadetts (1990) performed with two different ventilation rates; 0 and 6 m/s, respectively. The fuel tank was filled with 25–30 l of petrol and the results are presented in Fig. 4.2. The peak HRR measured with no ventilation was 4.7 MW after 11.5 min, and with 6 m/s ventilation it was obtained in two steps: the first maximum was about 3 MW after 13 min, and the second one about 4.6 MW after 37 min. The high ventilation rate made it difficult for the fire to spread within the cabin in the opposite direction to

the ventilation flow. A test with a Citroen Jumper van was carried out during a test with a deluge sprinkler system in the tunnel ceiling. The sprinkler system was activated after about 13.6 min, see Fig. 4.1. Ingason et al. [21] presented HRR measurements for a Fiat 127 which was ignited in the engine compartment with an electrical device. The peak HRR was 3.6 MW after 12 min. The fire was extinguished by firefighters 13 min into the test, see Fig. 4.2.

Ten HRR measurements from passenger vehicle fires in a simulated carpark were presented by Joyeux [24]. Tests with one car and with two cars were carried out beneath a 10 MW calorimeter. Mazda, Renault, BMW, Citröen BX, and Peugeot, manufactured in the 1980s and 1990s, were used in the tests. The location of the ignition source was varied. In the first seven tests, the first car was ignited with a small petrol tray under the left front seat. In the other tests, the first car was ignited by a petrol tray placed under the car at gear box level. As can be seen in Table 4.1, the HRRs for single car fires (small and large passenger cars) varied from 1.5 to about 9 MW, but the majority of the tests show HRR values less than 5 MW. In the cases when two cars were involved the peak HRR varies between 3.5 and 10 MW.

Tests with passenger cars in a car park environment were presented by Shipp et al. [25]. Both single cars (BRE test nr. 7–8) and multiple cars (BRE test nr. 1–3) that were located side by side or stacked on each other were burned. The aim was to examine the time to reach a fully developed fire. The HRR of a fire starting in the passenger compartment or in the engine compartment of one of the vehicles was measured. The risk for fire spread from car to car was also documented. The results are only available in Table 4.1 and are indicated as BRE where BRE stands for British Research Establishment. The peak HRR for the two single vehicle tests was 3.8 and 4.8 MW after 54 and 45 min, respectively. With multiple vehicles it varied from 7–16 MW, occurring within a time frame of 10–55 min.

As the information on HRR in passenger cars is quite broad, it is possible to summarize it in a graph. In Fig. 4.3, a summary of the peak HRR data found for passenger cars is plotted as function of the time to peak HRR. It shows that the peak HRR for single vehicle fires (passenger cars) can vary from 1.5–8 MW, where most are lower than 5 MW. There are numerous test results available for two- and three-vehicle fires (passenger cars), although most of them are carried out in car parks and not tunnels. The variation in HRR for two-vehicle fires is 5.6–10 MW, and for three-vehicle fires it varies from 7–16 MW. The vast majority of tests show peak HHRs less than 10 MW, but one should bear in mind that these tests are mostly carried out in car parks, where very little longitudinal ventilation exists. Increased longitudinal ventilation may increase the fire spread between multiple vehicles, and thereby increase the peak HRR slightly.

The time to peak HRR varies between 8 and 55 min for single cars. In many of these tests, the peak occurs very late, depending on how the windows broke and which ventilation conditions were dominant. As indicated in Fig. 4.3 there is no clear correlation between the peak HRR and the time to achieve the peak HRR.

In over 80 % of the cases for single cars, the peak occurs within 8–30 min and for 60 % of the cases the peak occurs within 8–20 min. For two and three cars this

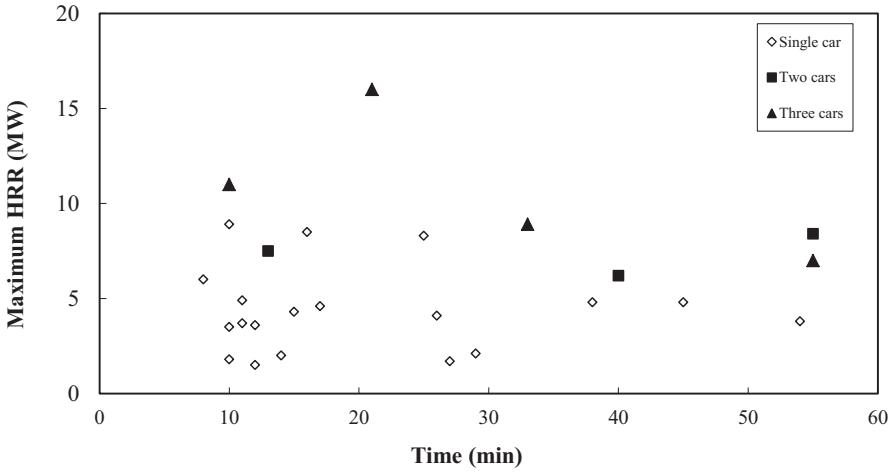

Fig. 4.3 Summary of time to reach peak HRR versus peak HRR for single, two- and three-vehicle fires (passenger cars)

time is more evenly distributed over the entire time spectra. In 95 % of the cases the HRR is less than 10 MW.

The experiments carried out by Joyeux [24, 26] indicated an increase in peak HRR for modern cars at the same time as the total energy content (GJ) was increasing. Ingason [3] analyzed the data and observed a tendency that peak HRR increased linearly with total calorific value (GJ) of the passenger cars involved. An analysis of all data available at that time showed that the average increase was about 0.7 MW/GJ. Lönnermark [27] did similar analysis for passenger cars and found out that the linear relationship between the peak HRR and the total energy content was 0.868 MW/GJ with a correlation coefficient R equal to 0.840.

4.2.1.2 Buses

There are not many large-scale tests with buses available. Only three tests which are relevant to this chapter are found in the literature. Details of these tests are provided in Table 4.2.

Ingason et al. [14] and Steinert [12] presented a measured HRR for a 12-m long Volvo school bus built in the 1960s made of fiberglass (EUREKA Bus, test 7). In the analysis of the HRR data, Steinert [12] used more coarse measurement points than Ingason et al. [14]. In Fig. 4.4 calculated values for the HRR of the test are given.

The peak HRR was measured to be 29 MW by Ingason et al. and 34 MW by Steinert. The total calorific content was estimated to be 41 GJ by Ingason et al. and 44 GJ by Steinert. The estimated time to peak HRR was 8 and 14 min, respectively.

In 2008, Axelsson et al. [28] carried out a large-scale experiment with a modern coach (Volvo manufactured in early 2000 with 49 seats). The test was conducted un-

Table 4.2 Large-scale experimental data on buses [9]

Type of vehicle, model year, test nr, *u*=longitudinal ventilation m/s	Tunnel (T)/Calorimeter (C)/Weightloss (W)	Tunnel cross-section (m^2)	Calorific content[d](GJ)	Peak HRR(MW)	Time to peak HRR (min)	Reference
Buses						
A 25–35 year old 12 m long Volvo school bus with 40 seats, EUREKA 499, test 7[a], u=0.3 m/s	T	30	41	29	8	[14]
A 25–35 year old 12 m long Volvo school bus with 40 seats, EUREKA 499, test 7[a], *u*=0.3 m/s	T	30	44	34	14	[12]
SP laboratory test with a modern tourist bus (Volvo), NV	C		NA	25[b)]	NA	[28]
A bus test in the Shimizu Tunnel, *u*=3–4 m/s	T	115	NA	30[c)]	7	[29]

NA Not Available, *NV* Natural Ventilation

[a] The test number sequence in the EUREKA 499 project is given in reference [30] and Table 3.5

[b] This value is based on estimation made by the authors of the report [28]

[c] This is estimated from the convective HRR of 20 MW derived by Kunikane et al [29] because a sprinkler system was activated when the convective HRR was 16.5 MW. We assume that 67% of the HRR is convective and thereby we can estimate the HRR=20/0.67=30 MW

[d] Based on integration of the HRR curve

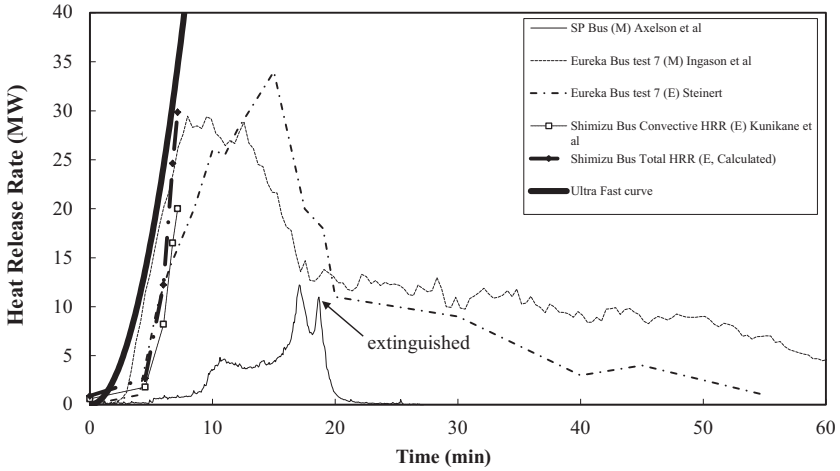

Fig. 4.4 HRRs for buses. More information about each test is given in Table 4.2 [9]. Most of the data are extracted (E) from graphs found in the literature. If measured data are given it is indicated with (M).

der a large hood calorimeter (nominal 10 MW capacity) inside a fire laboratory. The measured HRR is shown in Fig. 4.4. A t-squared ultrafast fire growth curve [18] is included for comparison. It is reported that the initial fire development was relatively slow. The fire was ignited with a 100 kW gas burner in the luggage compartment at the back of the bus and below the passenger compartment. The fire spread from the luggage compartment into the passenger compartment through the side windows. The fire started to grow significantly when three side windows in the passenger compartment had broken about 15–16 min after ignition. There are three peaks in the HRR curve given in Fig. 4.4. The first peak occurred after about 11 min, when the fire broke out on the side of the luggage compartment. The fire then spread into the passenger compartment through the windows between15–17 min after ignition. The situation in the fire laboratory became intolerable soon after that and the fire was extinguished manually at approximately 18.5 min after ignition (the last peak of the curve). There were problems with a leakage of heat and smoke as the hood collector did not have enough capacity during this period. The final HRR was probably higher than the measured peak shown in Fig. 4.4. The authors of the report estimated that the peak HRR could have been as high as 25 MW had the bus continued to burn.

The third test presented here was conducted in the Shimizu Tunnel in Japan. Part of the test was to examine the use of a sprinkler system [29], or a fixed firefighting system (FFFS), in road tunnels. The HRR was not measured but Kunikane et al. [29] estimated the convective peak HRR based on temperature measurements and the mass flow rate prior to the activation of the water spray system to be 16.5 MW. Kunikane et al. estimated that the peak convective HRR would have been approximately 20 MW if the FFFS had not been activated. Ingason [9] estimated the peak

HRR to be 30 MW by assuming that 67% of the total HRR is convective. Two HRR curves have been plotted in Fig. 4.4, one by extracting the information from Kunikane et al. [29] based on the convective HRR, and one showing the total HRR based on the assumption that 67% of the total HRR is convective.

4.2.1.3 Heavy Goods Vehicles

Most heavy goods vehicles (HGV) tests that have been carried out in tunnels use a mock-up simulating the cargo of a HGV trailer. Only those tests that are found in the literature and can be regarded as a free burning test, that is, without any interaction of a FFFS, such as sprinkler systems, are considered in this section. The peak HRR, fuel load and time to reach peak HRR are given in Table 4.3 and the HRRs are plotted in Fig. 4.5 and 4.6.

The first tests known as a HGV test was performed in 1992 in the EUREKA 499 test programme in Repparfjord in Norway [15]. A simulated HGV-trailer load (mock-up) was used, consisting of densely packed wood cribs supplemented by rubber tyres and plastic materials on the top (64 GJ). In this test, a natural ventilation rate of 0.7 m/s was obtained. The second test performed, also as a part of the EUREKA 499 test programme, was a fully equipped HGV truck and trailer loaded with mixed furniture (87 GJ) with varying longitudinal velocity during the test: 5–6 and 2–3 m/s. The peak HRR obtained was 23 MW after 15 min for the mock-up and 128 MW after 18 min for the real HGV.

A HGV test series was performed in the Mont Blanc tunnel in 2000 [31], with a HGV (truck and a trailer) similar to that which generated the fire in 1999 but with a much smaller amount of transported goods (35 instead of 76 GJ) [32, 31]. The fire load in the trailer consisted of 400 kg of margarine. The peak HRR of 23 MW was obtained after 47.5 min.

Another test series using HGV mock-ups was performed in the Second Benelux tunnel [23] in the Netherlands in 2001.Standardized wood pallets were arranged in two different configurations (approximately 10 and 20 GJ) with different longitudinal velocities: natural ventilation (~0.5 m/s), 4–5, and 5 m/s. The peak HRRs obtained were 13, 19, and 16 MW, respectively. The corresponding times were 16, 8, and 8 min.

A free burn test series was carried out in the Runehamar tunnel [17] in 2003. Four large-scale tests, each with a mockup of a HGV-trailer, which consisted of a steel rack system loaded with mixed commodities. The first test consisted of wood pallets and polyethylene pallets (Test T1), then wood pallets and polyurethane mattresses (Test T2), followed by furniture and fixtures with ten truck rubber tyres (Test T3), and finally paper cartons and polystyrene cups (Test T4).The commodity was covered with a polyester tarpaulin in each test and ignited on the upstream, front end, of the trailer. Initial longitudinal ventilation rates within the tunnel were in the range of 2.8–3.2 m/s. Peak HRRs measured were in the range of 66–202 MW. The peak HRRs were obtained between 7.1 and 18.4 min from ignition in the various tests.

Table 4.3 Large-scale experimental data on HGVs [9]

Type of vehicle, model year, test nr, u = longitudinal ventilation m/s	Tunnel (T)/Calorimeter (C)/Weight (W)	Tunnel cross-section (m^2)	Calorific content[d](GJ)	Peak HRR(MW)	Time to peak (min)	Reference
A simulated trailer load with total 11010 kg wood (82%[a]) and plastic pallets (18%), Runehamar test series, T1, u=3 m/s	T	32	240	202	18	[17]
A simulated trailer load with total 6930 kg wood pallets(82%[a]) and PUR mattresses (18%), Runehamar test series, T2, u=3 m/s	T	32	129	157	14	[17]
A Leyland DAF 310ATi—HGV trailer with 2 t of furniture, EUREKA 499, test 21, u=3–6 m/s	T	30	87	128	18	[36]
A simulated trailer with 8550 kg furniture, fixtures and rubber tyres, Runehamar test series, T3, u=3 m/s	T	32	152	119	10	[17]
A simulated trailer mockup with 2850 kg corrugated paper cartons filled with plastic cups (19%[a]), Runehamar test series, T4, u=3 m/s	T	32	67	67	14	[17]
A simulated trailer load with 72 wood pallets, Second Benelux tests, Test 14, u=1–2 m/s	T	50	19	26	12	[23]
A simulated trailer load with 36 wood pallets, Second Benelux tests, Test 8, 9 and 10, u=1.5, 5.3 and 5 m/s, respectively	T	50	10	13, 19 and 16	16, 8 and 8	[23]
A Simulated Truck Load (STL), EUREKA 499,test 15, u=0.7 m/s	T	30	63	17	15	[10]
Mont Blanc HGV mock up test	T	50	35	23	47.5	[31, 32]
A 3.49 t pickup truck loaded with 890 kg wood pallets; ignition in cargo, NV	W		26[b]	24[c)]	6.6	[37]

Table 4.3 (continued)

Type of vehicle, model year, test nr, u = longitudinal ventilation m/s	Tunnel (T)/Calorimeter (C)/Weight (W)	Tunnel cross-section (m^2)	Calorific content[d](GJ)	Peak HRR(MW)	Time to peak (min)	Reference
A 3.49 t pickup truck loaded with 890 kg wood pallets; ignition in cargo, NV	W		26[b]	21[c]	14.5	[37]
A 3.49 t pickup truck loaded with 452 kg plastic barrels; ignition of the seat, NV	W		25[d]	47[e]	43.8	[37]
Singapore—A test mock up consisting of wood and plastic pallets in a FFFS test	T	37.4		155	14	[33]
441 wood pallets in FFFS tests Runehamar	T	47	189	79	38	[35]

NA Not Available, *NV* Natural Ventilation

[a] Mass ratio of the total weight

[b] Estimated from the information given in the reference

[c] Given in the reference based on load cell measurements

[d] Either based on integration of the HRR curve or estimation of fuel mass and heat of combustion. The accuracy of these values may vary depending on the method and available information. The error is estimated to be less than 25%

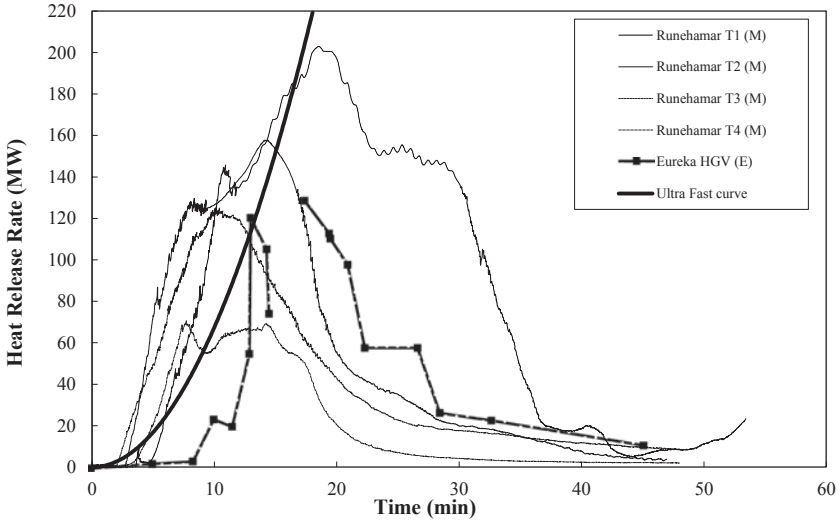

Fig. 4.5 The HRR for the HGV trailer mock-up tests presented in Table 4.3 [9]. (The EUREKA HGV test number 21 was for a real HGV, including the cab) [9].Most of the data are extracted (*E*) from graphs found in the literature. If measured data are given it is indicated with (*M*)

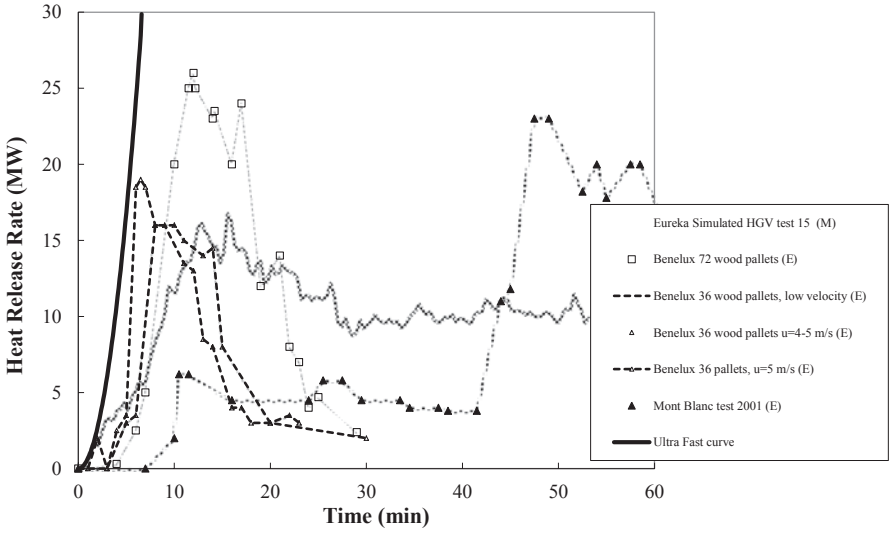

Fig. 4.6 The HRR for the HGV trailer mock-up tests presented in Table 4.3 [9].Most of the data are extracted (E) from graphs found in the literature. If measured data are given it is indicated with (M).

Since 2003, numerous large-scale tests with focus on testing FFFS have been performed. Most of them do not include a free burn test, and they are presented in more detail in Chap. 16. There are at least two test series that included at least one free burn test, namely a test in the Singapore programme with wood pallets and plastic pallets [33, 34]. Also, in 2013 fire tests with 441 wood pallets (420 main fire load and 21 in a target (a pile of wood pallet used to investigate plausible fire spread) were performed in the Runehamar tunnel [35].

The variation in the peak HRRs for HGVs are from 13–202 MW. The Runehamar test results in 2003 varied from 67–202 MW. One should bear in mind that nearly all the HGV tests (except the 120 MW EUREKA test that included a furniture load and a truck cabin where the fire was ignited inside) were carried out as a piled commodity on an elevated platform, with a minimum of containment of the fire load. In most cases a plastic tarpaulin covered the piled commodity and burned very fast without spreading the fire. The ignition source was also placed inside the commodity, usually on the upstream side. Initially the tarpaulin delayed the fire spread mainly due to wind protection, but as soon as it burned off, the wind affected the fire spread by deflecting the flames. The deflection of the flames throughout the cargo is the most important parameter for fast fire growth rates in this type of test mock-up. Any type of wind protection delayed the fire growth considerably. This is discussed in more detail in the fire growth rate Chap. 5.

These are all factors that may affect the initial fire growth rate in comparison to a fire in a real HGV. The peak HRR values, however, depend more on the amount of exposed fuel surface area (the way it is piled) and the ventilation conditions in close proximity to the fuel load (shielding effects, containment, etc.). This means that the way the commodity is piled or stored is an important factor to consider. If the cargo is relatively open it is possible to calculate the peak HRR based on exposed fuel surface area.

If the cargo is enclosed within a steel container or other time delaying material the fire development may be different compared to the values presented here. The effect of the tunnel geometry (especially the tunnel height) is also an important issue as the fire load interacts with its physical environment when it is burning.

In Fig. 4.7 a plot of the HRR versus time to reach a peak value is shown for all available experiments with HGV fire loads. It shows that the time to reach peak HRR is between 8–18 min and the peak HRR varies between 13–202 MWs.

Lönnermark [27] analyzed the correlation between the peak HRR and the total energy content of HGVs. There was a scatter in the data and there were differences in test conditions, but he concluded that there is a clear relationship between the peak HRR and the energy content using 0.866 MW/GJ ($R=0.910$).Later, Kashef et al. [38] examined the tests data from 2nd Benelux tunnel, EUREKA 499 tests and from the Runehamar tests, and showed that the peak HRR correlates with the released total energy for well ventilated fire using 0.9 MW/GJ. Although the existence of this good correlation, one should be careful in using them. There is no physical evidence for this correlation except that higher the total energy content is larger volume of combustible material is expected. The larger the volume or weight of material is in place, often the larger the exposed fuel surface area is. However,

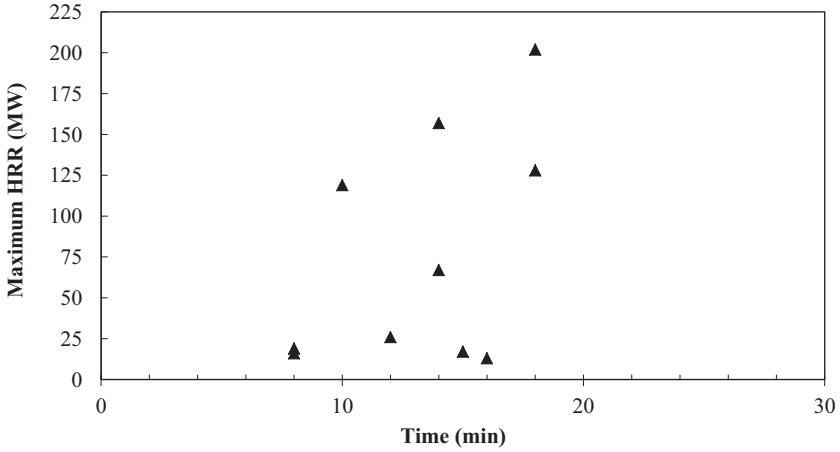

Fig. 4.7 Summary of time to reach peak HRR versus peak HRR for HGV fire loads

this does not always have to be true. It is more related to how the goods are stored, rather than how much volume or weight is in place. Larger exposed surface areas, for the same weight or volume of material, increase the peak HRR.

4.2.1.4 Tanker Fires

A full scale tanker test in a tunnel has never been reported. All the values found in the literature or in standards are based on estimates. These estimates show HRR values varying between 10–400 MW. These values are dependent on the initial type of accident, leakage flow, the way the gasoline or diesel is contained etc. The tank material (aluminium or steel) has a major effect on the result as well as the position of the vehicle (turn over, crash, etc.) in relation to the initial fire. Although there are no large-scale results reported on HRR tests using gasoline or diesel tankers found in the literature, there are numerous tests that have been carried out using pool fires, see Sect. 4.2.1.5.

The fire size of burning road gasoline tankers in tunnels reported in the literature are usually based on a possible spillage size and no concern is given to the road tanker itself containing a volume of liquid inside a tank. Heselden [39] assumed a gasoline fire to produce about 2 MW/m^2 (pool fire) and following Heselden proposal, Liew et al. [40] assumed a spillage area from a leaking tanker to be 50 m^2 thus producing a 100 MW fire.

Very few road gasoline tanker accidents in tunnels leading to fire have occurred in the world. The road tanker accident in the Caldecott tunnel in the USA in 1982, where a gasoline trailer collided and overturned, is the best source available today [41, 42]. Larson et al. [41] carried out a thorough analysis of the gasoline tanker accident in the Caldecott tunnel (USA 1982) showing that about 33 300 L gasoline

was burned within 40 min. Hence the average burning rate would be 14 L/s which yield about 430 MW fire assuming complete combustion. However, in tunnels complete combustion is usually not achieved for such large fires without a high velocity longitudinal ventilation system. An estimate given by Ingason indicates that the Caldecott tanker fire HRR was probably less than 300 MW [43]. The knowledge about the effects of ventilation on combustion efficiency in such large fires is not clearly known.

Ingason [43] describes how the HRR from a road gasoline tanker accident was estimated with aid of small-scale testing together with a theoretical calculation and analysis of an actual road tanker accident such as the Caldecott tanker fire. For the case studied, the initial spillage fire HRR caused by a collision can be in the range of 10–300 MW. This range includes small spillage fires created by small leaks where the entire spill burns up before it reaches the drainage system to large spillage fires creating a bulk tank fire where the tank is engulfed in flames. In the case of an aluminum road tanker, the initial spillage fire can eventually lead to a bulk tank fire since, the top of the tanks may open up. The unwetted walls will gradually disappear because aluminum parts will soften and fall into the tank and because parts will melt. The burning rate per square metre fuel surface could become more than five times higher than ordinary pool fires since, the gasoline bulk starts to boil after some time. Depending on the combustion efficiency the aluminum bulk tank fire HRR can be in the range of 200–300 MW and for the case studied the fire duration can be in the range of 50–60 min. Good agreement is found between the theoretically calculated burning rates and experimentally determined values for a bulk tank fire using model scale experiments [43]. As pool fires usually constitute the basis for estimation of tanker fire size, a more thorough analysis of such fires is given in Sect. 4.2.2.5.

4.2.1.5 Pool Fires (Liquid)

Babrauskas [44] presented numerous data on liquid pool fires that can be compared to the tests carried out in tunnels. Babrauskas [44] has also used the following equation, which was originally given by Zabetakis and Burgess [45] to calculate the HRR for pool fires:

$$\dot{q}'' = \dot{m}''_{\infty}(1 - e^{-k\beta D})\,\chi \Delta H_c \cdot A_f \tag{4.1}$$

where $\dot{m}''_{\infty}$ is the highest value for mass burning rate (kg/(m^2 s)) obtained from tabulated data for each fuel in Babrauskas [44] (in Table 3–1.13), D is the pool diameter (m), ΔH_c is the effective heat of combustion (MJ/kg), χ is the combustion efficiency, A_f is the pool area (m^2) and $k\beta$ is the product of the extinction–absorption coefficient of the flame k (1/m) and the mean bean-beam-length corrector β. The product $k\beta$ has the dimension (m^{-1}).Values for petroleum products from Table 3–1.13 in Babrauskas [44] are reproduced in Table 4.4, in order to be used later in tables and examples.

Table 4.4 Empirical constants for use in Eq. (4.1). Values reproduced for petroleum products from Table 3–1.13 in Babrauskas [44]

Material	Density (kg/m^3)	Heat of gasification L_g (KJ/kg)	Heat of combustion ΔH_c (MJ/kg)	Mass burning rate $\dot{m}''_\infty$ (kg/(m^2 s))	Empirical constant in Eq. (4.1) $k\beta$ (m^{-1})
Benzine	740	–	44.7	0.048	3.6
Gasoline	740	330	43.7	0.055	2.1
Kerosene	820	670	43.2	0.039	3.5
Jp-4	760		43.5	0.051	3.6
Jp-5	810	700	43.0	0.054	1.6
Transformer oil	760	–	46.4	0.039	0.7
Fuel oil	940–1000	–	39.7	0.035	1.7
Crude oil	830–880	–	42.5–42.7	0.022–0.045	2.8

Example 4.1 What is the HRR from a gasoline pan fire that is 1.5 m in diameter?

Solution: Use Eq. (4.1) and select corresponding values from Table 4.4. For gasoline $\dot{m}''_\infty = 0.055$ *kg/(m*^{2} *s),* $k\beta = 2.1$ *m*$^{-1}$, $\Delta H_{c,eff} = 43.7$ *MJ/kg (assuming* $\chi = 1$*) and the area is* $\pi x\ 1.5^2/4 = 0.56$ *m*^{2}*. The total HRR is* $0.055 \times (1 - e^{-2.1 \times 1.5}) \times 43.7 \times 0.56 = 1.3$ *MW or per fuel surface area* $\dot{q}'' = 1.3/0.56 = 2.3$ *MW/m*^{2}*.*

The HRR for different pool fire tests conducted in tunnels is presented in Table 4.5. The majority of the tests have been carried out using circular or square pans with relatively deep fuel depth, both with or without a water bed under the fuel. It is assumed that the depth of the fuel was more than 80 mm, and the minus sign (−) is given in cases where the fuel depth is uncertain or not reported. Tests with a fuel depth less than 80 mm are also presented in Table 4.5.

For comparison, values using Eq. (4.1) are given in Table 4.5. If no information is available for the fuel it does not appear in Table 4.5 and if the area A is not known, A is set equal to 1.0 m^2.

In the Ofenegg tests in 1965 [46] the influences of the ventilation conditions and the tunnel and fuel pan geometry on the burning rate were clearly demonstrated. The tunnel was only 190 m, with one portal (dead end tunnel). The distance from the portal to the nearest edge of the pans was 130 m. Three different types of ventilation conditions were possible to obtain in the test tunnel: natural ventilation, semi-transverse, and longitudinal ventilation.

In the case of natural ventilation one could expect that this is similar to an enclosure fire, that is, one opening at the portal. Estimation of the HRR using Eq. (4.1) yields a HRR of 84.5 MW. This is much higher than obtained in the natural ventilation tests for larger pans with A=47.5 and 95 m^2, or 35–39 MW (see Table 4.5). Even for the semi-transverse ventilation case the HRR was in the same range. The only explanation is the effect of inerting (vitiation) on the HRR, through mixing of combustion products with the incoming fresh air.

Table 4.5 Summary of pool fire tests in tunnels and laboratories

Fuel type	Test place/ ventilation (see Chap. 3 for more details about each test)	Fuel depth (mm)	Fuel area (m^2)	HRR (MW)	HRR per square metre fuel (MW/m^2)	Eq (4.1) HRR per square metre fuel (MW/m^2)
Gasoline	Ofenegg (test 1)—natural	–	6.6	16	2.4	2.4
	Offenegg (test 2)—semi-transverse	–	6.6	12	1.8	
	Offenegg (test 2a)-longitudinal	–	6.6	12	1.8	
	Offenegg (test 7a)—longitudinal	–	47.5	70	1.5	
	Offenegg (test 5)—natural	–	47.5	39	0.8	
	Offenegg (test 6)—semi-transvers	–	47.5	38	0.7	
	Offenegg (test 9)—natural	–	95	35	0.4	
	Offenegg (test 10)—semi-transverse	–	95	32	0.3	
	Zwenberg (test 101)	–	3.4	8	2.4	
	Zwenberg (test 210)	–	6.4	12	1.9	
	Zwenberg (test 301)	–	13.6	20	1.5	
	PWRI (test 1)	–	4.0	9.6	2.4	
	SP	50	2	5.8	2.9	2.4
	SP	7	2	4.5	1.6	
	SP	2–3	6	5	0.8	
Diesel	Zwenberg (test 220)	–	6.40	10	1.6	
	SP	–	2.8	3.5	1.3	1.6
	SP	20	1.2	1.8	1.5	
	SP	1–2	–	–	0.25–0.3	
Kerosene	SP	70	0.4	0.7	1.7	1.7
	Glasgow	–	–	–	1.4	
Heptane	EUREKA (test 16)	–	1.0	3.5	3.5	
	EUREKA (test 18)	–	3.0	7.0	2.3	

Table 4.5 (continued)

Fuel type	Test place/ ventilation (see Chap. 3 for more details about each test)	Fuel depth (mm)	Fuel area (m^2)	HRR (MW)	HRR per square metre fuel (MW/m^2)	Eq (4.1) HRR per square metre fuel (MW/m^2)
	SP	70	0.4	1.14	2.7	2.6
n-60 % heptane/40 % toluene	2nd Benelux (test 1)	–	3.6	4.10	1.1	
	2nd Benelux (test 2)	–	3.6	3.50	1.0	
	2nd Benelux (test 2)	–	7.2	11.5	1.6	
Low-sulfur No 2 fuel oil (diesel)	Memorial	–	4.5	10	2.2	
	Memorial	–	9.0	20	2.2	
	Memorial	–	22.2	50	2.3	
	Memorial	–	44.2	100	2.3	
JP-5	SP	5	2.8	4.8	1.7	
	SP	2.5	2.8	3.1	1.1	
	SP	1	2.8	1.1	0.4	

In the first test with natural ventilation, the average burning rate was 0.059 kg/(m^2 s) for a 6.6 m^2 fuel pan, that is, 2.4 MW/m^2. In the tests with semi-transverse and longitudinal ventilation and a 6.6 m^2 pan, the HRR per unit fuel area was reduced to 1.8 MW/m^2. In the tests with the 47.5 m^2 fuel pan the burning rate for natural and semi-transverse ventilation was 0.8 and 0.7 MW/m^2, respectively, whereas in the test with longitudinal ventilation the HRR is 1.5 MW/m^2. In the 95 m^2 pan the HRR per unit fuel area was only 0.3–0.4 MW/m^2 which corresponds to 83 % of the HRR per unit fuel area in the open.

It is evident that the HRR per unit fuel area and thereby the total HRR in these tests is highly influenced by ventilation and the test setup. The poor accessibility of oxygen to the fuel bed is the main reason [6] together with the fact that the Ofenegg tunnel was a ‘dead end’ tunnel. In the case when no mechanical ventilation was applied, the only air supply came from the portal on one side of the fire and therefore,one can expect effects of vitiation in the same way as described in Chap. 2, Sect. 2.6.

In the Zwenberg tests in Austria in 1974–1975 [47], the results were much more consistent with expectations in tunnel fires. The main reason is that the tunnel had two portals, which makes a huge difference in the way the air is supplied to the fire. Only mechanical ventilation was available (longitudinal, semi-transverse, and transverse ventilation). The average burning rate per square metre fuel area of gasoline for all the tests was 0.043 kg/(m^2 s) with a standard deviation of 0.0075 kg/(m^2 s). This corresponds to a HRR per unit fuel area of 1.9 MW/m^2, and standard

deviation of 0.3 MW/m^2. The average reduction in the burning rate was about 22 % of the HRR per fuel surface in the open.

Some tests with smaller fuel depths have been carried out by SP Technical Research Institute of Sweden (SP), but have not been reported earlier. In Table 4.5, tests with fuel depths less than10 mm, and tests with larger fuel depths are given. Most of them were conducted in a pan but the SP gasoline test of 2–3 mm consisted of continuous outflowing of 22 L/min of gasoline on a sloped concrete surface. The JP-5 tests with a small fuel depth were carried out on a water bed. It is clear from the results given in Table 4.5 that the fuel thickness is an important parameter to consider. The HRR per fuel surface area can be reduced by 70–80 % of the large fuel depth value if the fuel is only a few millimeters deep. A fuel on an asphalt road surface can be expected to be not more than a few millimeters thick. This has to be taken into account when considering the HRR from different pool fires on road surfaces.

In the cases where the ventilation did not have a large influence on the results, the calculated values in Table 4.5 show a very good correspondence with the values obtained from experiments with different types of pool fires.

Tests have been performed to study the influence of a layer of railway macadam on the HRR of a burning liquid spill [48]. The test shows that the presence of the macadam has a significant decreasing effect on the burning rate for the two fuels tested: heptane and diesel. The influence increases with the distance from the fuel surface to the upper layer of the macadam. This is discussed in more detail in Chap. 11 on fire spread.

4.2.1.6 Construction Vehicles

Vehicles used in the construction of tunnels are also presented here. Hansen and Ingason [49] presented large-scale tests of vehicles common in the mining industry. The tests were carried out in an underground mine in Sweden in 2011. The aim of the full-scale fire experiments was to determine the HRR because information was unavailable in the literature. This information is vital for fire safety engineers working in underground mines and tunnel construction sites. Two full-scale fire tests were carried out, one with a wheel loader and one with a drilling rig. Each of these vehicles had been in service for several years. The HRR results from the two vehicles tested are shown in Fig. 4.8.

The wheel loader was a Toro 501 DL and was diesel powered. The wheel loader was used for hauling iron ore between the production areas to a vertical shaft, where the iron ore was unloaded. The vehicle was 10.3 m long, 2.8 m wide and almost 3 m high. The total weight was 36 t. The fuel load consisted primarily of the four tyres. The tyre specification of 26.5 × 25 L5S implies a tyre with a section width of 26.5 in. (~ 0.66 m), a rim diameter of 25 in. (0.625 m) and with smooth extra deep tread. The total fire load of the wheel loader combustible components was estimated to be 76.2 GJ. The tyres of the wheel loader were filled with water (instead of air) due to the risk of tyre explosion during normal operation.

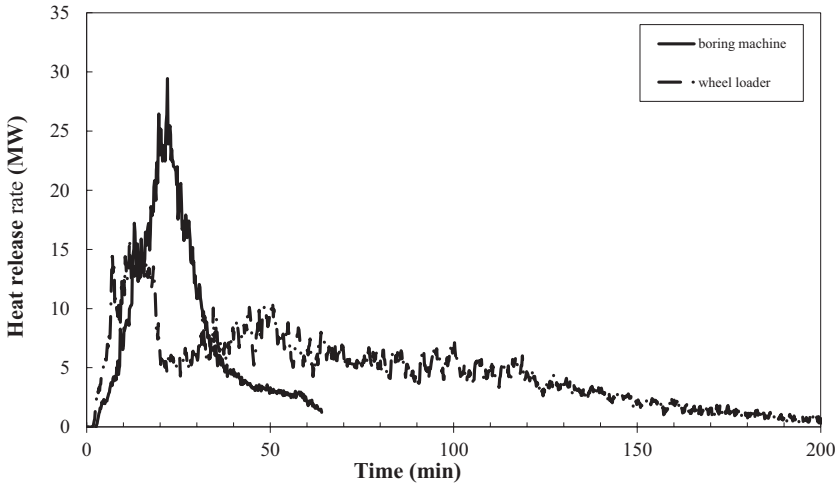

Fig. 4.8 A plot of HRR for a front wheel loader and a drilling machine [49]

The drilling rig was an Atlas Copco Rocket Boomer 322, which is an electrically driven vehicle commonly used in underground mines. The drilling rig was also equipped with a diesel powered engine which is used when moving the drilling rig from one site to another. The total length with boom was 12.4 m. The width was 2.2 m and the total height was about 3 m. The total weight was 18.4 t. The fuel load of the drilling rig consisted primarily of four tyres, the hydraulic oil and the hydraulic hoses. The tyre specification of 13.00 × 20 PR 18 implies a tyre with a section width of 13 in. (0.325 m) and a rim diameter of 20 in. (0.5 m).The combustible components were estimated to be 45.8 GJ.

In both tests, the ignition source consisted of a circular tray (1.1 m) that was placed under the fuel tank of each vehicle and located close to at least one tyre. The trays were filled with diesel fuel in order to simulate a pool fire caused by leaking diesel from the tank.

4.2.1.7 Rubber Tyres

As rubber tyres of large road or construction vehicles give an important contribution to the HRR, it is of interest to present some HRR results on rubber tyres.

Ingason and Hammarström [50] reported on a fire test with a front wheel loader rubber tyre under a large laboratory calorimeter. The test was carried out by igniting a pan with gravel and diesel placed under the tyre. The rubber tyre was a Good Year with the specification of 26.5R25 Tubeless. The total diameter of the tyre was 1.75 m and the total width (tread) was 0.67 m. The tread is the part of the tyre which

comes in contact with the road surface. The total external and exposed surface area of the rubber tyre was estimated to be about 8 m^2. The total weight, including the wheel rim, was 723 kg. A peak HRR of 3 MW after 90 min was recorded. It was also concluded that 86% of the total heat energy had been released 2.5 h after ignition.

In 1993, the BRE in the UK [51] conducted two large-scale tests on tyres under a large calorimeter at the Fire Research Station's Cardington Laboratory. In the first test, the tyres were stacked horizontally and in the second, vertically. In each test, a stack of eight tyres was burned and numerous measurements were made, among them the HRR. The tyres used were ordinary passenger car tyres without a steel rim. The vertical stacking (eight tyres high) produced a far more severe fire than the horizontally stacked tyres. The peak HRR was 1300 kW for the vertical stack and 500 kW for the horizontal stack. The reason for the difference was faster fire spread and better flow of air to the center of the tyres when stacked vertically compared to the horizontal stacking. In the horizontal case parts of the tyres that burned initially were burned out when the fire was terminated.

The Fire Laboratory of SINTEF in Norway presented in 1995 heat release data from two tests (A and B) with rubber tyres used for HGVs [52]. A pair of dual load bearing wheels was tested under a laboratory calorimeter. The ignition was simulated by heating the wheel rims. An insulated pipe was welded to the wheel rims and heated by a gas fire passing through the pipe. The metal wheel rim was heated to a temperature that ignited the rubber tyres. This procedure was continued for about 30 min prior to ignition. The size of the tyres varied, but in test A the tyre specification was 285/80 R22.5 and in Test B the tyre specification was 315/80 R22.5. This means that in test A the tyre was 285 mm wide with a 228 mm (0.8×285) high vertical surface and the rim diameter was 22.5 in. (575 mm). The exposed rubber area was estimated to be 4.2 m^2 for test A and 4.8 m^2 for test B (dual tyres) [50]. The measured maximum HRR for test A was 878 kW and for test B 964 kW. The time to attain the maximum HRR was 29 and 27 min, respectively, from ignition. The fire duration was about 60 min in both cases.

In 2005, Lönnermark and Blomqvist [53] carried out tests using ordinary passenger car rubber tyres and the peak HRR was recorded. The aim of the tests was to assess the emissions to air and water from a fire in tyres. Each test involved 32 passenger car tyres without a wheel rim. Two different storage setups were used: heaped and piled. Both setups represent common ways to store used tyres. The heap storage was more spread out. It had a base of 3×3 tyres, with the tyres stacked in a certain pattern above. The pile configuration consisted of a base with 2×2 tyres stacked on each other in a straight vertical pile. This means that there were eight tyres in each stack, that is, a total of 32 tyres. In both setups the tyres were placed on a steel pan, 2×2 m, under a large calorimeter. The tyres varied somewhat in size, but tyres that were as similar as possible were used. The maximum HRRs from the tests were as follows: heap storage—3.7, 3.6 and 3.7 MW; pile storage—3.6 MW. The maximum HRR in the pile storage test occurred 19 min after ignition.

4.2.2 Railway Rolling Stock

The literature describes very few measurements of HRR for rail and metro vehicles (rolling stock). The majority of the tests available are from the EUREKA 499 test series [15], but in recent years more test data have been published [54, 55]. In Table 4.6, a summary of available tests is given. For more information about each large-scale test, read Chap. 3.

The test results presented in Table 4.6 are based on tests with single coaches. The peak HRR is found to be in the range of 7–77 MW and the time to reach the peak HRR varies from 5–80 min. If the fire were to spread between the train coaches, the total HRR and the time to peak HRR would be much higher than the values given here although one cannot simply add the HRR for each coach to obtain an estimate of the total HRR because the first coach would not necessarily reach the peak HRR at the same time as the later ones. The EUREKA 499 tests show that there are many parameters that will affect the fire development in a train coach. These include the body type (steel, aluminum, etc.), the quality of the glazed windows, the size and geometry of the openings, the amount and type of combustible interior material and its initial moisture content, the construction of wagon joints, the air velocity within the tunnel and the geometry of the tunnel cross-section. These are all parameters which need to be considered in the design process of a rail or metro tunnel. A very important factor for the development of the fire is the quality and mounting of the windows. As long as the windows do not break or fall out (and there are no other large openings), the fire will develop slowly. On the other hand, if the windows break the fire can spread and intensify very quickly. In Fig. 4.9 time-resolved HRR curves are given for some of the tests presented in Table 4.6. For comparison, the t-squared ultrafast fire growth curve [18] is also included.

4.3 Parameters Influencing the HRR

The HRR can be affected by many parameters. This can be due to heat feedback from the tunnel construction, the ventilation conditions inside the tunnel and the geometry of the fuel. In the following text, a summary of these effects are presented.

4.3.1 Heat Feedback

When a vehicle fire occurs in a tunnel it communicates with its surrounding surface boundaries, hot smoky gases, and the surrounding flames through electromagnetic waves (radiation, see Chap. 10). The consequence will be a transient temperature increase of the tunnel structure surfaces. Depending on the type of lining or surface (rock, concrete, boards, etc.), the surface temperature will increase at different rates. The initial temperature of the surrounding surface can be very low, on the order of

Table 4.6 Large-scale experimental data on rolling stock [9]

Type of vehicle, test series, test nr, u = longitudinal ventilation m/s	Calorific content(GJ)	Peak HRR(MW)	Time to peak HRR (min)	Reference
Rail				
A joined railway car; two half cars, one of aluminium and one of steel, EUREKA 499, test 11, u=6–8/3–4 m/s	55	43	53	[12]
German IntercityExpress railway car (ICE), EUREKA 499, test 12, u=0.5 m/s	63	19	80	[14]
German Intercity passenger railway car (IC), EUREKA 499, test 13, u=0.5 m/s	77	13	25	[14]
British Rail 415, passenger railway car[a]	NA	16	NA	[56]
British Rail Sprinter, passenger railway car, fire retardant upholstered seatings[a]	NA	7	NA	[56]
Intercity train car (u=2.4 m/s) 37 m long tunnel Carleton laboratory facility	50	32	18	[55]
Metro				
German subway car, EUREKA 499, u=0.5 m/s	41	35	5	[14]
METRO test 2 (u=2–2.5 m/s)	64	76.7	12.7	[54]
METRO test 3 (u=2–2.5 m/s)	71	77.4	117.9	[54]
Subway car (u=2.4 m/s)37 m long enclosure Carleton laboratory facility	23	52.5	9	[55]

[a] The test report is confidential and no information is available on test setup, test procedure, measurement techniques, ventilation, etc.

5–10 ℃ for rock or concrete tunnels. In the vicinity of the fire, the flames radiate back toward the fuel surface, as well as outward to the surrounding surfaces and hot smoky gases. Depending on the ventilation conditions, a hot smoke layer is created above or downstream of the fire. This hot smoke layer interacts through radiation with the fuel source as well as the tunnel surfaces through convection and radiation. The outward radiated heat from the burning vehicle is partly reflected back from the tunnel surfaces and is partly absorbed, which will increase the surface temperature. Locally, above the fire, there is also a higher degree of exchange of convective heat to the tunnel surfaces. Gradually, the surrounding tunnel surfaces are heated up and the temperature rises continuously. At some point the surrounding surface become an important source of external radiation toward the burning fuel surface, especially in very large fires. This does not necessarily mean that the incident radiation toward

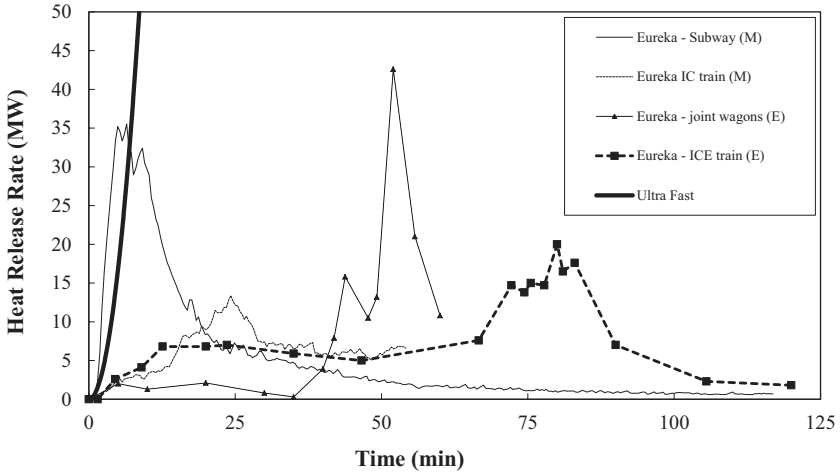

Fig. 4.9 The HRR for rail vehicle tests presented in Table 4.6 [9].Most of the data are extracted (*E*) from graphs found in the literature. If measured data are given it is indicated with (*M*)

the fuel surface is increasing continuously. The ceiling surface is usually covered by flames or black smoke, and therefore, a limited exchange of radiation with the fuel surface is obtained, and thereby the effects on the burning rate are indirect. The radiation from the ceiling surface is absorbed by the hot smoke gases and the flame volume, however, the side walls may have more direct interaction with the fuel surface. The extension of this interaction is dominated by view factors and the shielding effects within the fuel.

The HRR per square metre of a given fuel surface is given by the heat balance equation:

$$\dot{q}'' = (\dot{q}_f'' + \dot{q}_g'' + \dot{q}_w'' - \dot{q}_{rr}'')\frac{\Delta H_{c,eff}}{L_g} \tag{4.2}$$

where $\dot{q}''$ is the HRR per unit surface area (kW/m^2) of the fuel or vehicle, $\dot{q}_f''$ is the radiation from the flame volume toward the surface (kW/m^2), $\dot{q}_g''$ is the radiation from the hot smoke gases in the vicinity of the fire (kW/m^2), $\dot{q}_w''$ is the radiation from the surrounding walls and ceiling (kW/m^2) and $\dot{q}_{rr}''$ is the reradiation from the fuel surface (kW/m^2). In Fig. 4.10, the parameters in Eq. (4.2) are shown in a side perspective. $\dot{q}_g''$ can be written as $F_e\varepsilon_g\sigma T_g^4$ where T_g is the characteristic temperature of the smoke layer and $\dot{q}_w'' = F_w\varepsilon_w\sigma T_w^4$ where T_w the surface temperature of the surrounding tunnel structure (K). The view factor F can vary as well as the emissivity ε for the gas (index g) and the surface (index w). σ is the Stefan–Boltzmann constant 5.67×10^{-11} kW/(K^4 m^2).

The importance of each temperature term can vary spatially. In most cases it is dominated by T_g, but sometimes by T_w, especially if the side walls become warm. The surface temperature rise of the walls is time dependent, and varies for different

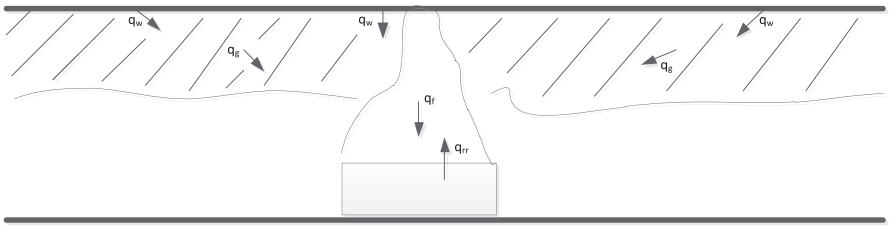

Fig. 4.10 An illustration of the terms used in Eq. (4.2)

materials. For example if a rock tunnel wall is suddenly exposed to 1000 °C, it will take about 6 min for the surface temperature to reach 80 % of the exposed gas temperature, and 20 min to reach 90 %. The corresponding numbers for concrete are 2 and 7 min, respectively, and 0.2 and 0.6 min for tunnels insulated with silicate boards. This means that the interaction of the wall temperatures to influence the mass burning rate of the fuel is not important in the early stages of the fire.

The flame volume above the fuel surface transfers radiation and convection $\dot{q}''_f$ to the burning surface. The flame volume and the gas temperature of the hot smoke above the fire becomes the dominating external source of radiation toward the fuel surface. The interactions with the fuel surface are governed by the 3D shape of the flame and gas volumes and its temperatures. The temperature in the zones above most open diffusion flames are often in the range of 800–900 °C rather than the 1200–1360 °C temperature range measured in tunnel fires. As radiation is absorbed by the flame volume and black smoke, the dominating radiation incident on the fuel surface is usually governed by conditions closer to the fuel surface. At the same time, $\dot{q}''_{rr}$ is the reradiation loss (note the minus sign) at the fuel surface. It can be written as $\dot{q}''_{rr} = \varepsilon\sigma T_s^4$ where L_g is the surface temperature of the fuel (here we assume ignition temperature) in Kelvin. In most cases, the view factor needs to be considered, but sometimes a value of one can be assumed in order to make a rough estimate.

In Eq. (4.2), $\Delta H_{c,eff}$ is the heat of combustion (kJ/kg) and L_g is the heat of gasification of the burning material (kJ/kg).

The $\dot{q}''_f$ varies from 22–77 kW/m^2 for large-scale flame heat fluxes [57]. For example assuming an 800 °C gas temperature corresponds to 75 kW/m^2, which correlate well the higher value of 77 kW/m^2. Babrauskas [58] show that for wood the heat flux can vary considerably depending on the exposure time. A value of $\dot{q}''_f = 25$ kW/m^2 seems reasonable for wood. Here it assumed that the flame volume behaves as an open fire, that is, the flame volume is in the vertical direction and does not deflect horizontally.

Example 4.2 What is $\dot{q}''$ for wood pallets assuming that $\dot{q}''_f = 25$ kW/m^2, $T_g = 100$ °C and $T_w = 10$ °C? Assume that F and ε are equal to one.

Solution: The following tabulated data [57] can be assumed for wood: $L_g = 1.8 \times 10^{3\,kJ/kg}$ *and* $\Delta H_{c,eff} = 13 \times 10^{3\,kJ/kg}$. *In the case when the pallets are burning with* $T_s = T_{ign}$ *(an ignition temperature of 300 °C for wood is a reasonable lower value for piloted ignition [58]),* $\dot{q}''_{rr} = 5.67 \times 10^{-11} \times (300 + 273)^4 = 6$ *kW/m*^{2}, $\dot{q}''_g = 5.67 \times 10^{-11} \times (100 + 273)^4 = 1.1$ *kW/m*^{2}, *and* $\dot{q}''_w = 5.67 \times 10^{-11} \times (10 + 273)^4 = 0.4$ *kW/m*^{2}. *The HRR*

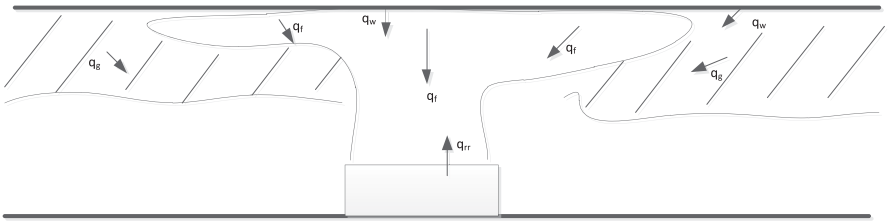

Fig. 4.11 Illustration of a large tunnel fire in which the flame deflects horizontally at the ceiling

per unit fuel surface area will be $\dot{q}'' = (25 + 1.1 + 0.4 - 6) \times 13/1.8 = 148$ *kW/m*^{2} *in accordance to Eq. (4.2). Tewarson [57] reported that* $\dot{q}''_{rr}$ *is equal to 10 kW/m*^{2} *for Douglas fir (wood). Using Tewarson's* $\dot{q}''_{rr}$ *value would lower the* $\dot{q}''$ *to 119 kW/m*^{2}.

This example shows that the increase in $\dot{q}''$ due to the gas or wall temperature is marginal in relation to many other parameters, especially the flame radiation $\dot{q}''_f$ and the ratio of $\Delta H_{c,\,eff}/L_g$ for fires in the early stages.

For a large fire scenario the flame volume will deflect at the ceiling and enhance the radiation from the deflected flame volume toward the fuel surface, see Fig. 4.11. The gas temperature will also be much higher. As mentioned earlier, the hot smoke and gases also radiate to the fuel surface. Simultaneously, the interaction of radiation is hampered by absorption and scattering in the flame volume and the hot smoke between the surfaces. The total heat balance and exchange are difficult to determine exactly, but Eq. (4.2) shows the most important parameters that are active in the process. The $\dot{q}''$ will most likely increase but at the same time there will be an attenuation of the radiation from the smoke (excluding the ceiling flame volume) and the tunnel walls. It is not certain that the $\dot{q}''$ will increase substantially even if the fire size increases as more fuel becomes involved and the large vertical flame volume and smoke could significantly hinder the radiation from the ceiling flame.

Although Eq. (4.2) is a simple relation, it shows the influence of the ceiling smoke layer and tunnel walls on the burning rate of the fuels burning inside a tunnel. This influence is perhaps not as large as one would expect, at least not during the important fire growth period that usually occurs within 10–20 min. There are other governing parameters, such as material properties, ventilation type and conditions, fuel geometry and tunnel height (deflection of flames) that are important. Also, one should bear in mind that this example assumes a line of sight between the fuel surface and the smoke layer surrounded by the tunnel surfaces, but in reality most fuels are geometrically complex. Most of the burning fuel surfaces do not have line of sight with the smoke layer and tunnel structure, but are hidden inside the fuel bed, or in vehicles. Also, note that the characteristic gas temperature further away is lower. The values of $\dot{q}''$ using Eq. (4.2) in the above analysis are probably conservative. In summary, the dominating parameter is the flame radiation and where radiation from gases and walls plays a less important role initially, but will contribute later in the fire development, although not nearly as much as the flame radiation. More information about the calculation of heat flux can be found in Chap. 10.

4.3.2 Effects of Tunnel Geometry

The effect of tunnel geometry on the HRR is an interesting research field. Carvel et al. [59] compared the increase of HRR due to tunnel geometry to similar situations in ambient outdoor conditions. A number of different experimental test series published in the literature were studied. The work included experiments involving liquid pools, wood cribs, and cars. The authors came to the conclusion that the width of the tunnel has a significant influence on the HRR from a fire in a tunnel. The results were explained by the surrounding wall and hot gas radiation to the pool surface, the temperature inside the tunnel, and the flow pattern near the fire. The analysis indicated that the height of the tunnel did not significantly affect the HRR enhancement.

Lönnermark and Ingason [60, 61] investigated the effect of geometry on the HRR using model scale tests and found that the dependency of the mass loss rate (MLR) and the HRR on the tunnel dimensions differ, especially for pool fires. Tests in a model-scale tunnel (scale 1:20) were performed to study the effect of the height and width of a tunnel on the MLR and the HRR. The tunnel was 10 m long. The widths used were 0.3, 0.45, and 0.6 m and the height was varied between 0.25 and 0.4 m. Two different types of fuels were used: pools of heptane and wood cribs. From the results it is clear that the dependency of the MLR and the HRR on the tunnel dimensions are different from each other, especially for pool fires. The results also indicate that the influence of tunnel dimensions is not only a radiation effect, as often assumed, but is probably a combination of radiation from surfaces and hot gases, influence of air flow patterns, the shape and position of the flame and combustion zone, and temperature distribution. The analysis shows that as several factors and processes are interacting, it is important to know the starting conditions to be able to predict the effect of a change in a specific parameter. In these tests the tunnel height was found to be the most important parameter influencing the enhanced HRR.

4.3.3 Effects of Ventilation on Peak HRR

The effect of longitudinal ventilation on the fire development of HGV fires has been of great interest among researchers and engineers for a long time. The use of critical velocity in the design of ventilation systems is one of the main reasons. When blowing high velocity air onto a fire, one should ask what the consequences on the HRR are. The interaction between the ventilation flow and the HRR has been thoroughly investigated by Carvel et al. [62–64]. In this chapter we will focus on the effects of ventilation on the peak HRR. In Chap. 5, the focus will be on fire growth.

The work carried out by Carvel's team at the Herriot–Watt University in Edinburgh was probabilistic in nature. The basis was that a Bayesian probabilistic approach was used to refine estimates made by a panel of experts and was combined with data from experimental fire tests in tunnels. The drawback of their work was

that their conclusions were based on rather limited experimental data and not on any physical experimental justifications. Fortunately, there has been new and more systematic research conducted in later studies with more consistent data [65–68].

In Carvel's studies it is stated that the size of HGV fires will be greatly increased by forced longitudinal ventilation. At a ventilation flow of 3 m/s such a fire will probably be four or five times larger than if natural ventilation was used. At 10 m/s the fire will probably be ten times larger. In their studies they used both wood crib tests, ordinary solid fuels, and vehicles. Neither the test results presented here nor estimates of HRR increases in vehicle fires show such a high increase as indicated by Carvel et al. The data on HRR per unit fuel surface area for vehicles presented earlier in this chapter cannot support the claim of a factor 4 to 10 increase for HGVs. These HRR values cannot physically be much larger than those obtained by Ingason and Li [66]. That is, the increase in peak HRR from ambient conditions is on the order of 1.4–1.55 for the ventilation rates tested (1.6–4.3 m/s in large scale) or by Lönnermark and Ingason [65] who showed that the increase in the peak HRR was in the range of 1.3–1.7 times the value measured outside the tunnel under ambient conditions. The only possible explanation for why Carvel et al. exhibited such a high increase in the peak HRR is due to the way the fuel was compared. Fuel that was ventilation controlled during ambient or natural ventilated conditions has probably been used in the comparison. If a fuel has a low porosity factor P, see definition in Sect. 4.3.4, the increase as presented by Carvel et al. can be easily obtained, which has been shown in Harmathy's work[69]. Harmathy had concluded that the heat released by the oxidation of the char plays an important role in the process of pyrolysis and thereby affects the HRR. Noncharring fuels (synthetic polymers) do not exhibit this influence on the HRR. This explains the increase in HRR due to ventilation obtained by Ingason and Li [66] who used charring material (wood cribs) in their model scale tests. This is crucial for our understanding of the effects of the ventilation rate on HRRs in tunnel fires.

The effects of ventilation on pool fires vary in the literature. Some show very little change in the mass burning rate and others show large effects. The trend in the experiments found in the literature is that these effects are larger for smaller pool fires as they are dominated by convective heat transfer from the flame volume, whereas larger pools are dominated by radiation heat flux from the flames. Therefore, the larger pool fires are less affected by the velocity.

Carvel et al. reported that the enhancing effect of ventilation for small pool fires is much less significant than that for HGV fires, while it increased by 50 % for large pool fires.

Ingason [70, 71] performed pool fire tests in a model-scale tunnel, using heptane, methanol, and xylene as fuels. For heptane, the maximum increase of the burning rate due to the tunnel was by a factor of 3.3 (0.13 kg/(m^2 s)) (u = 1 m/s) compared to 0.04 kg/(m^2 s) (free burn). Saito et al. [72] showed that the MLR for liquid fires increased in a tunnel compared to free burning conditions. The tests were performed with pool fires of methanol (0.1, 0.15, 0.2, and 0.25 m in diameter) and heptane (0.15 m in diameter). For the two smallest pools the effect of the tunnel (with an air velocity 0.08 m/s) on the MLR of methanol was only a few percent, while for the 0.25 m diameter pool the MLR in the tunnel was increased by a factor of 2.7

compared to freeburning conditions. For heptane, the tunnel (with an air velocity of 0.43 m/s) increased the MLR by approximately a factor of 4. For both fuels, the MLR was significantly decreased with increasing air velocity. This illustrates the importance of not only the ventilation and the tunnel cross-section but also the effects of the heat feedback from the flames, hot gases, and tunnel structure on the MLR.

Lönnermark and Ingason [61] performed a test series in a model-scale tunnel (1:20) and studied the effect of the width and the height of a tunnel on the MLR and HRR. They showed that the dependence of the MLR and the HRR on the tunnel dimensions are different from each other and that the effect of the height and the width of the tunnel on the MLR and HRR depends on the starting conditions. Here ventilation is an important factor.

Takeda and Akita studied the effects of tunnel conditions on fires and have also showed that the MLR and HRR are related to the ventilation factor [73]. They showed that the enhancement of the burning rate was associated with the dynamic balance between the rate of air supply and fuel gas supply.

Since, HGVs play such an important role for the outcome of fires in road tunnels [74], understanding the effect of the tunnel itself and of the air velocity inside the tunnel is important. One of the main problems when studying the effect of ventilation using different test series is that the conditions (tunnel dimension, starting ventilation conditions, etc.) vary between the test series. It is important to realise that several parameters affect the shape of the heat release curve, for example, the type of fuel used to represent the scenario, the air velocity inside the tunnel, and the tunnel geometry.

4.3.4 Fuel-Controlled Fires

According to Croce and Xin's experimental study of wood crib fires [75], the porosity of a wood crib is very important to determine if the wood crib is fuel controlled (well-ventilated) or ventilation controlled (under-ventilated). The porosity of a wood crib, P, is defined as:

$$P = \frac{A_v}{A_s} s^{1/2} b^{1/2} \tag{4.3}$$

where A_v is the total cross-sectional area of vertical crib shafts (m^2), A_s is the exposed surface area of the wood crib (m^2), s is the surface-to-surface spacing between adjacent sticks in a layer (m), and b is the stick thickness(with the same width and height) (m).

The porosity of a wood crib with the length L, the width l, and with a square cross-section of the sticks with the side b (see Fig. 4.12) can be defined as [60]:

$$P = \frac{A_v}{A_s} s_H^{1/2} b^{1/2} \tag{4.4}$$

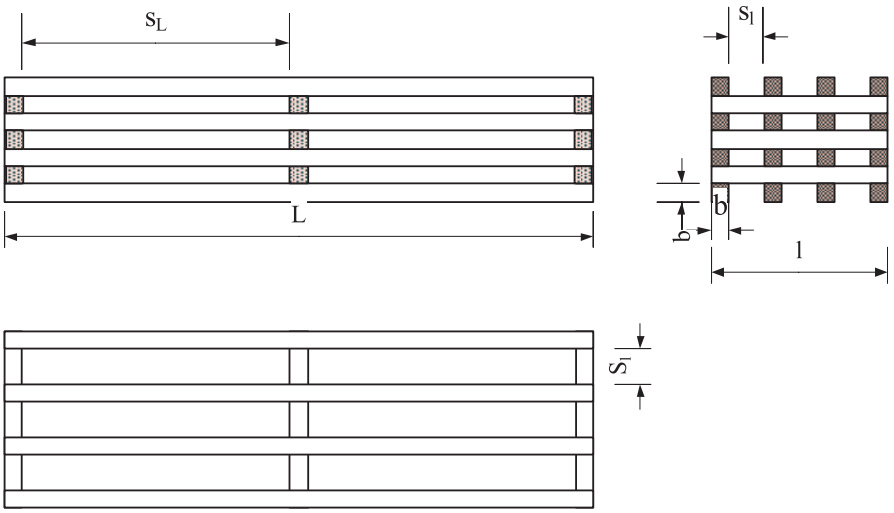

Fig. 4.12 Drawing of a wood crib and definition of different lengths [60]

where A_v is the total cross-sectional area of the vertical crib shafts

$$A_v = (L - n_l b)(l - n_L b) \tag{4.5}$$

and A_s is the total exposed surface area of the crib (based on the assumption that bottom and the top layers are with long sticks)

$$A_s = 4b(n_l N_l l + n_L N_L L) + 2b^2(n_l N_l + n_L N_L - n_l n_L N_L) - B \tag{4.6}$$

In the equation n_l, n_L, N_l, and N_L are the number of sticks in a layer with short sticks, the number of sticks in a layer with long sticks, the number of layers with short sticks, and the number of layers with long sticks, respectively. The parameter B is included to represent the area of the bottom of the wood crib that is not exposed. In the calculation of the porosity according to Eq. (4.4), the parameter s_H is included. This parameter corresponds to the hydraulic diameter of the rectangular space defined by the parameters $s_l = \left(\frac{l - n_L b}{n_L - 1}\right)$, $s_L = \left(\frac{L - n_l b}{n_l - 1}\right)$, and $s_H = \frac{2 s_l s_L}{s_l + s_L}$.

Equation (4.3) is used to calculate the porosity factor P (m) for square wood cribs used in research and Eq. (4.4) for long wood cribs in tunnel fire research.

The HRR increases rapidly with increasing porosity but this dependency weakens when the porosity is greater than 0.7 mm. In principal, this means that the HRR becomes a constant value as the cribs become more scattered.

For a solid fuel such as wood, the HRR is dependent on the net heat gained on the surfaces of the solid. This means that the total surface area is a very important parameter for combustion of solid fuels as the fire size becomes a multiplicand of the HRR per unit fuel surface area. Figure 4.13 shows the HRR per unit fuel surface

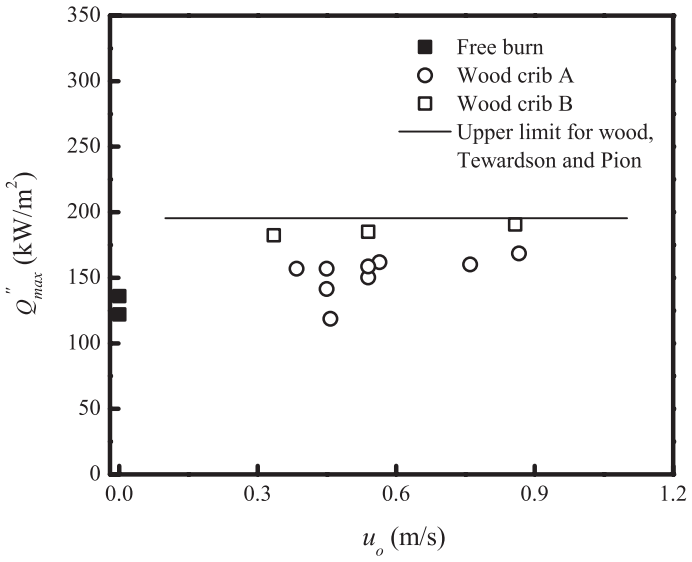

Fig. 4.13 The peak HRR per unit fuel surface area as a function of ventilation velocity [66]

area plotted against the ventilation velocity. It shows that the HRR per unit fuel surface area is a weak function of the ventilation velocity at best. The reason is that the fire is fuel-controlled[66]. An upper limit of the fuel MLR per unit fuel surface area presented by Tewarsonand Pion [76] for wood (Douglas fir) is 0.013 kg/(m^2 s), which correlates well with the experimental data given by Ingason and Li [66]. Based on data from model tunnel fire tests and from free burning tests(a test carried out without any boundary influences) they found that the fuel MLR per unit fuel surface area in a tunnel fire test is in a range of 1.4–1.55 times the value measured in a free burning test. If the value given by Tewarson and Pion is converted to HRR per fuel surface area of the wood cribs tested the $\dot{q}''$ corresponds to about 200 kW/m^2. This is shown as horizontal solid line in Fig. 4.13.

4.3.5 Ventilation-Controlled Fires

Ingason and Li [68] carried out model scale tests which could explain the region where a fire changes from fuel controlled to ventilation controlled. In the model scale tests conducted, the porosity P of the wood crib was chosen as 1.24 mm (>>0.7 mm)to minimize the effect of porosity on the HRR. This means that the wood crib should not show any type of ventilation control tendency during the tests.

The effect of the tunnel geometry and fire source was not investigated systematically in the study although data from two series of tests in model tunnels of different aspect ratios were used. The focus was on the analysis of the relationship between the HRR and ventilation velocity in the vicinity of the wood crib fuel.

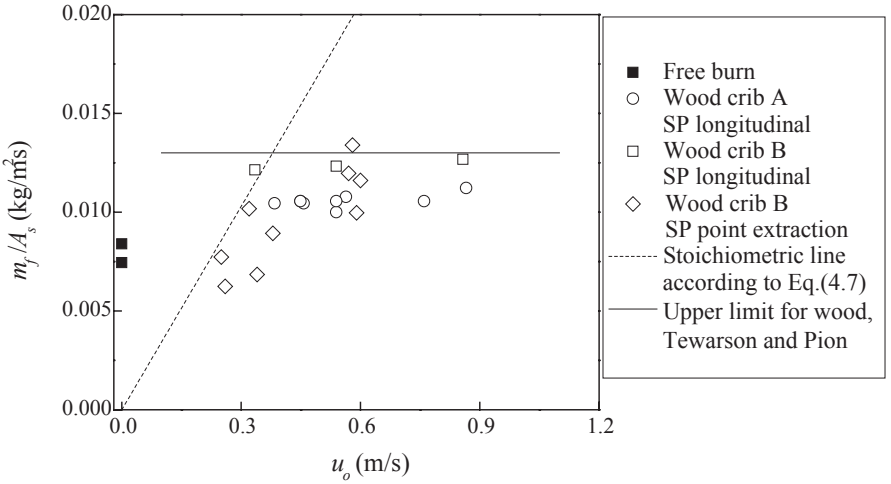

Fig. 4.14 The maximum fuel MLR per unit fuel surface area as a function of the ventilation velocity (single wood crib) [68]

Figure 4.14shows the fuel mass loss rate per unit area fuel surface against the ventilation velocity across the fire source. The stoichiometric fuel mass loss rate per unit fuel surface area is also given in Fig. 4.14. According to the principles of oxygen consumption, the stoichiometric fuel mass loss rate per fuel surface area, $\dot{m}_{f,stoi}$ (kg/(m^2 s)), can be expressed as:

$$\frac{\dot{m}_{f,stoi}}{A_s} = \frac{\dot{Q}}{\chi \Delta H_c A_s} = 0.24 \frac{A}{A_s} u_o \tag{4.7}$$

where A is the tunnel cross-sectional area (m^2), A_s is the fuel surface area(m^2) and u_o is the tunnel longitudinal velocity (m/s).

It is shown in Fig. 4.14 that for a longitudinal ventilation velocity less than 0.35 m/s the fuel MLR per unit fuel surface area increases with the ventilation velocity and follows the stoichiometric line. This indicates that the fire under these conditions is ventilation controlled. However, when the ventilation velocity rises above 0.35 m/s (1.6 m/s in large-scale) the fire is no longer sensitive to the ventilation velocity. This indicates that the fire becomes fuel-controlled. The upper limit of the fuel MLR per unit fuel surface area was about 0.013 kg/(m^2 s).It is also shown in Fig. 4.14 that within a range of 0.35–0.9 m/s, the fuel MLR per unit fuel surface area tends to be a weak function of velocity. However, it can be expected that the fuel MLR per unit fuel surface area will begin to decrease when the ventilation velocity is greater than a certain value due to the cooling effect of the ventilation. Comparing the data in tunnel fire tests and that in a free burning test shows that the ratio of fuel MLR per unit fuel surface area in a tunnel fire to that in a free burning test is about 1.5 in the constant region (fuel controlled), and that it can be less than 1 if the tunnel is ventilation controlled or influenced by vitiation as described in Chap. 2.

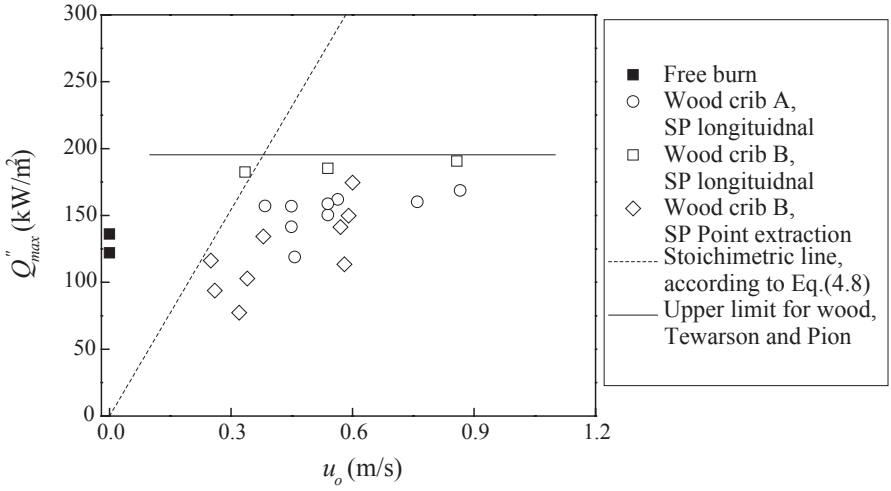

Fig. 4.15 The peak HRR per unit fuel surface area vs. ventilation velocity [68]

The above analysis is based on the fuel MLR of a single wood crib. In some tests, several wood cribs were burnt together and the total HRR was measured using the oxygen calorimetry technique rather than measuring the MLR.

Figure 4.15 shows the peak HRR per unit fuel surface area as a function of the ventilation velocity. The stoichiometric HRR per fuel surface area is plotted as a sloped solid line. For a fire with several wood cribs, the total fuel surface area was used. According to the principles of oxygen consumption, the stoichiometric HRR per fuel surface area, $\dot{Q}''_{stoi}$ (kW/m^2), can be expressed as:

$$\dot{Q}''_{stoi} = \frac{\dot{Q}}{A_s} = 3600 \frac{A}{A_s} u_o \tag{4.8}$$

The same trend is shown in Fig. 4.15 as in Fig. 4.14, although the data does not correlate as well. The reason is that in a test with several wood cribs, all surfaces of these wood cribs did not burn simultaneously. When the peak HRR occurred, part of the first wood crib had already started to decay. As a consequence, the peak HRR divided by the total fuel surface area is slightly lower for the case with several wood cribs compared to a single crib.

4.4 HRR per Exposed Fuel Surface Area

Ingason [6] has emphasized the importance of using and reporting HRR data given as MW/m^2 or kW/m^2 exposed fuel surface, or $\dot{q}''$. The main reason is the enormous variation in HRR data for each type of vehicle that uses transport tunnels or other underground spaces. By estimating the exposed fuel area of a vehicle it is possible

Table 4.7 The HRR parameters for different materials in Eq. (4.2) [57]

Type of material	$\dot{q}''_{rr}$ (kW/m^2)	L_g (kJ/g)	$\Delta H_{c,eff}$ (kJ/g)	$\dot{q}''_f$ (kW/m^2)	$\dot{q}''$ (kW/m^2)	HRP
Hexane	0.63	0.55	42.2	37	2791	77
Heptane	0.98	0.6	41	37	2461	68
Kerosene	1	0.85	40.3	29	1316	47
Polyethylene	15	2	38.4	61	883	19
Polystyrene	11.5	1.6	27	75	1072	17
Polyurethane (flexible)	17.5	1.95	17.8	70	479	9
Polyurethane (rigid)	18	3.25	16.4	51	167	5
PVC	10	1.7	5.7	50	134	3
Corrugated paper	10	2.2	13.2	25	90	6
Wood	10	1.8	13	25	108	7

to get a very good estimate of the peak HRR. Exposed fuel surface is defined here as the area where combustion/pyrolysis can possibly occur, that is, a fuel surface that is exposed to high incident heat radiation with enough oxygen to maintain combustion. For a box, the exposed fuel surface area is the sum of the outer surfaces, and not what is inside the box, whereas a seat can burn on all sides. A pile of wood pallets can burn on the surfaces that are exposed to air but when the pile falls down, the exposed surface area may increase rapidly and the peak HRR increases correspondingly.

Information can also be obtained by doing fire tests of only small portions of the cargo or the vehicle. This was done prior to the Runehamar tests in 2003 where, based on information from preliminary laboratory tests, the peak HRRs could be predicted with acceptable accuracy for three of the test commodities [11]. A summary of this data is given in references [6] and [9].

The ratio $\Delta H_{c,\,eff}/L_g$ has been given the name "Heat Release Parameter" (HRP) by Tewarson [57]. In order to explore the importance of the different parameters in Eq. (4.2) we can look at the range of values given by Tewarson[57], see Table 4.7.

Table 4.7 clearly shows the importance of the HRP to predict values of $\dot{q}''$ for different materials. The other parameters are also important, especially the total flame heat flux $\dot{q}''_f$ and the reradiation $\dot{q}''_{rr}$ which is related to the ignition temperature.

The values presented in Table 4.7 appear to have some correlation to the values presented by Ingason [6]. As is shown in Table 4.8 in Sect. 4.4.2, for different solid materials, $\dot{q}''$ ranges from 70 kW/m^2 for wood cribs to 500 kW/m^2 for furniture having a mixture of polyurethane foam, wood and plastics. For liquid fires the $\dot{q}''$ are in the same range as found in Table 4.7, see Sect. 4.4.1. The values of calculated HRR per fuel surface area for wood provided by Tewarson correspond well to those found in Table 4.8 for wood pallets, where $\dot{q}''$ was found to vary between 110 and 160 kW/m^2, see Sect. 4.4.2.

Table 4.8 Summary of HRR per fuel surface area for solid materials applied in large-scale tunnel fire tests [6, 9]

Type of fuel	Test series	Estimated fuel surface area (m^2)	HRR per square metre fuel surface area at maximum (MW/m^2)
Wood cribs	EUREKA (test 8, 9, and 10)	140	0.07–0.09
Wood pallets	2nd Benelux (tests 8, 9, 10, and 14)	120 (36 pallets) 240 (72 pallets)	0.11–0.16
82 % wood pallets and 18 % PE pallets	Runehamar (test 1)	1200	0.17
82 % wood pallets and 18 % PUR matrasses	Runehamar (test 2)	630	0.25
81 % wood pallets and cartons and 19 % plastic cups	Runehamar (test 4)	160	0.44
HGV-furniture	Runehamar (test 3)	240	0.5
HGV-furniture	EUREKA (test 21)	300	0.4
Runehamar 2013	Runehamar 2013	1470	0.06
Singapore 2012 80 % wood pallets and 20 % PE pallets	Singapore 2012	910	0.17
Rubber tyres	Diverse		0.11–0.21

4.4.1 Liquids

In Table 4.5, a summary of HRRs of all liquid pool fire tests and other relevant tests was shown, comparisons to Eq. (4.1) were also included. The comparison shows a good correspondence wherever the effects of ventilation were not dominant.

In Table 4.7, $\dot{q}''$ values for heptane and kerosene are presented. The values are 2.46 MW/m^2 for heptane and 1.32 MW/m^2 for kerosene, respectively. These values correspond well to fires reported or calculated using Eq. (4.2) having an area of about 0.4 m^2.

The variation in test results is considerable and it is difficult to assume one value for each type of liquid fuel. Parameters that influence the burning rate for each fuel type are the fuel pan geometry, the fuel depth, the ventilation conditions, and the tunnel geometry. In cases where the tunnel cross-section is large and the width of the pan is much smaller than the width of the tunnel, the influence of longitudinal ventilation on the burning rate appears to be small. If the fuel bed has about the same width as the tunnel the fire size is reduced. These effects increase as the length of the pan increases.

4.4.2 Solid Materials

In many of the large-scale tests presented in Chap. 3, solid materials such as pallets, cartons, or wood cribs have been used. It is of interest to compare the peak HRR per unit fuel surface area in order to see if these values are comparable between the tests series. This type of information could be used when estimating the peak HRR from HGV trailers with a tarpaulin as cargo coverage. In Table 4.8 a summary of the HRR per unit fuel surface area is given for tests that included solid materials based on the data presented in this chapter and in Chap. 3.

Tests that included solid wood cribs or pallets are found in the TUB-VTT tests, the EUREKA test series, and the 2nd Benelux tests. In the Runehamar tests wood pallets (about 82 % of the total mass) were integrated with other types of solid materials such as plastics (18 % of the total mass), cartons and,furniture and fixtures.

In the 2nd Benelux tests with wood pallets the HRR per unit fuel surface area varied between 0.11–0.16 MW/m^2 with an average value of 0.13 MW/m^2.This value tended to increase with increased ventilation rate. The fuel itself was not densely packed and thus could be regarded as fuel surface controlled. For wood cribs the opposite fire condition would be crib porosity controlled or ventilation controlled. In the EUREKA tests using a simulated truck load the wood sticks were so densely packed that the fire became crib porosity controlled (ventilation controlled) under normal conditions. This means that the peak HRR became lower than if it was fuel surface controlled. In the simulated truck load fire test, the HRR per unit fuel surface area was estimated to be in the order 0.04 MW/m^2. In the wood crib tests in the EUREKA test series the HRR varied between 0.07–0.09 MW/m^2 depending on the longitudinal velocity. It was not possible to establish with any certainty whether the wood cribs were fuel surface or crib porosity controlled. In the Runehamar tests in 2013, 441 pallets were used with a peak HRR of 79 MW in one of the tests, which was a free burn test, that is, no water spray was used. The fuel surface area of the pallets was estimated to be 3.3 m^2 and the peak HRR per unit fuel surface area was 0.06 MW/m^2, which is slightly less than the results from other tests. In the Singapore tests in 2012, 80 % of the fuel was wood pallets and 20 % was polyethylene pallets. The HRR per unit fuel surface was then 0.17 MW/m^2, assuming the surface area of the pallets to be 3.3 m^2. This is exactly the same value as obtained in the Runehamar test number 1 in 2003.

In the HGV test in the EUREKA 499 test series using furniture the HRR per unit fuel surface area was estimated to be approximately 0.4 MW/m^2. The total fuel surface of the furniture commodity was estimated to be about 300 m^2 and the peak HRR was120 MW.

The HRR per unit fuel surface area in the Runehamar tests was estimated to be about 0.17 MW/m^2 for test 1 with wood and plastic pallets, 0.25 MW/m^2 for test 2 with wood pallets and mattresses, 0.5 MW/m^2 for test 3 with furniture and fixtures and 0.44 MW/m^2 for test 4 with plastic cups in cartons.

In the large-scale tests presented here, the peak HRR for solid materials ranges from 0.07 to about 0.5 MW/m^2. An interesting observation is that the furniture tests

in the EUREKA 499 and Runehamar test series appear to be in the same order of magnitude. The reason is that both tests were performed under good ventilation conditions and that the fuel surface area was similar. The fuel surface area was estimated to be roughly 300 m^2 in the EUREKA 499 test and about 240 m^2 in the Runehamar test 2003. With this type of information it would be easy to estimate the peak HRR for a given type of fuel in a HGV fire.

For rubber tyres it is possible to estimate the HRR based on information given earlier in this chapter. Rough estimation indicates that the peak HRR for rubber tyres per exposed surface area is in the range of 0.11–0.21 MW/m^2. This information can be used to estimate the peak HRR for a certain size of a rubber tyre. One should also keep in mind that there is an important difference between the SINTEF test and the other tests, namely the presence of the rim in the SINTEF tests and the way the passenger car tyres were piled up, which may influence the estimation of the exposed fuel surface area. If the SINTEF tests are removed then the range of HRRs for rubber tyres per exposed external area is 0.11–0.15 MW/m^2.

Ingason and Hammarström [50] estimated the area when the tyre reached the first clear peak HRR to be 5.9 m^2. They argued that if they subtract the contribution from the diesel fire which was about 1.1 MW, they would have approximately 1.3 MW from the tyre. This means that the HRR per unit fuel surface area at this time was 0.20 MW/m^2. This is in line with the results obtained from other studies mentioned earlier. In this test, after the first HRR peak, the fire intensity decreased and the next abrupt increase occurred after about 70 min, when both sides of the tyre were fully involved in the fire and gases were coming from the inside of the tyre. The total exposed exterior fuel surface area of the tyre was about 8 m^2, meaning that the HRR per unit fuel surface area was about 0.25 MW/m^2.

4.4.3 Vehicle Fires

Vehicle fires can be either fuel controlled or ventilation controlled, depending on the fuels and openings available. According to Li et al's work [77], for a ventilation controlled vehicle fire, the openings available, including both the initial openings and those created during the fire, dictate the level of the peak HRR. The peak HRR in these tests can be estimated based on full consumption of the oxygen flowing in through the openings multiplied by a correction factor, which depends on the heat absorbed by the fuel surfaces and the fuels available. The heat absorbed by the surfaces is directly proportional to the heat of combustion and inversely proportional to the heat of pyrolysis. In addition, the fraction of the fuel surfaces exposed to the fire also has a strong influence on the peak HRR. In contrast, for a fuel-controlled vehicle fire, the peak HRR can be simply estimated by superposition.

In the following text a summary of the peak HRRs for different types of vehicles is given for the large-scale tests presented here. The data is presented in Table 4.8 as HRR per unit fuel surface area. It is only possible to present the cases where the fire was probably not ventilation controlled at peak conditions. In many of the vehicle

fires the enclosure structure of the vehicle (body) was burned off (For example, bodies made of aluminium, plastic, composite materials, etc.) allowing oxygen to become entrained in the fire plume. In some cases the enclosure was kept intact but the windows were large enough to preserve a fuel-controlled fire. However, in some of the tests the opening area of the windows controlled the HRR. In tests 12 and 13 with train wagons in the EUREKA 499 test series the fire developed very slowly due to the windows. The fire became ventilation-controlled and spread along the train wagon (steel body) at the same speed as the windows cracked due to the heat. In these tests the information on the fuel surface area is impossible to estimate, therefore, they have been excluded from the table.

Fully developed fires in passenger cars with steel bodies can be regarded as fuel surface controlled fires due to the large window area in comparison with the fuel surface area and the window height. This is not a generic condition as many modern cars have windows that do not necessarily break when a fire starts inside the car. The ventilation factor [78] for medium sized passenger cars is estimated to be in the range of 1.2–1.8, which is considerably higher than the limits for fuel-controlled enclosure fires (0.29) with wood cribs [78]. The peak HRR for single passenger cars (small and large) vary from 1.5–8 MW, but the majority of the tests show peak HRR values less than 5 MW [5]. When two cars are involved in the fire the peak HRR varies between 3.5 and 10 MW. The time to reach peak HRR varies between 10 and 55 min. The fuel surface area of the interior of a medium sized passenger car can be estimated to be in the range of 12–18 m^2. This includes the floor and ceiling area, instrument panel area, door area and the seat area (double sided).This would mean that the HRR per unit fuel surface area of a passenger car with a peak HRR of 5 MW can vary between 0.3–0.4 MW/m^2. The only test in a tunnel available is test no 20 in the EUREKA 499 test program. The car was a Renault Espace J11 with a plastic body. This car developed a peak HRR of 6 MW and the fuel surface area was estimated to be about 17 m^2, not including the ceiling.

Other vehicles with fuel-controlled fires were the tests 7, 11, 14, and 20 in the EUREKA 499 program, see Chap. 3, Sect. 3.3.7. In these tests, the main contribution is from the floor material and the seats. In tests carried out for different clients at SP Fire Research in Borås Sweden it was seen that fires in seats reach a peak HRR per unit fuel surface area of between 0.2 and 0.5 MW/m^2. This includes both bus seats and train seats. In Table 4.9, one can see that the total HRR per unit fuel surface area is in line with these values. It ranges between 0.20–0.38 MW/m^2. In a train there are numerous different materials in the interior of a coach or wagon. This material can be anything from textile, rubber, foam padding, PVC, cork, etc. What is interesting here is that the HRR per unit fuel surface area in fuel-controlled fires in different vehicles falls into a rather narrow range between 0.2 and 0.4 MW/m^2. This is also in line with the HRR per unit fuel surface area for the solid materials presented in Table 4.7. The HRR per unit fuel surface area of the individual materials have a greater variation, both lower and much higher, but it appears that the total effect of the mixed materials is not that broad.

Table 4.9 The summary of HRR per unit fuel surface area of vehicles with fuel-controlled fires [6, 9]

Type of fuel	Test series	Estimated fuel surface area (m^2)	HRR per square metre at maximum MW/m^2
Medium sized passenger cars	Assuming a 5 MW fire in the car	12–18	0.3–0.4
Passenger car plastic	Test 20 in EUREKA	17 (no ceiling)	0.35
Buss	Test 7 in EUREKA	80	0.36
Train	Test 11 in EUREKA	145	0.30
Subway coach	Test 14 in EUREKA	130	0.27
METRO tests	Test 2 and 3	230	0.33
Carleton laboratory facility	Intercity train	150	0.2
Carleton laboratory facility	Subway coach	130	0.38

4.5 Summary

Ingason [6] collected HRR data from all the large-scale tests available in the literature and normalized the peak HRR to the exposed fuel surface area. The fuel surface area was defined as the freely exposed area where release of gasified or vaporized fuel can occur. The reason for normalizing test data to the exposed fuel surface area was that this makes it convenient to compare the peak HRRs between different types of fuels and for different fire conditions. The results may be used to help estimate the peak HRR in different types of vehicles and with other solid and liquid fuels. Based on this work, the HRR data were divided into three different groups according to fuel type: liquid pool fires, ordinary solid materials such as wood pallets and wood cribs, and road and rail/metro vehicles.

It is important to understand how the reported HRRs were measured or calculated in order to make valid comparisons. Multiple car fire tests are mainly conducted in low ceiling car parks with nearly no longitudinal ventilation. The ignition source and location is a major factor for the time to reach the peak HRR for buses, as well as the body material of the bus (glass fibre, steel, aluminium, etc.). The type of cargo containment (tarpaulin, aluminium, steel, etc.) is very important for HGV fires, as well as the combustible material and the ventilation conditions. The ignition source and location is also an important factor on the time to reach a peak HRR for HGV fires. Any type of interaction with a water based spray system must also be considered as it significantly interacts with the combustible material and the environment.

It was concluded, based on the experimental tests considered so far, that the peak HRR per unit fuel surface area in a fuel-controlled fire for different vehicles is approximately between 0.2 and 0.4 MW/m^2 [6]; although, when HGV trailer mock-ups are included, this becomes about 0.2–0.5 MW/m^2. This is also in line with the

HRR per unit fuel surface area for solid materials. The HRR per unit fuel surface area for each individual material exhibits a greater variation, but it appears that the total effect of the mixed material leads to a narrow range of HRR values. This observation is very important to consider when establishing design fires for tunnels. It is essential to realize, however, that this is an initial finding; it is based upon tests in which the ventilation velocities have ranged from about 0.5 to about 6 m/s. In a real-world situation the ventilation velocity may be higher than 6 m/s (For example, there may be a natural wind). As a general rule, the total HRR for a single vehicle or item/fuel package in a tunnel fire depends on many factors. Further, the total HRR depends upon the potentiality for spread from one item to another. That is, the proximity of items (For example, vehicles) is of crucial importance. Therefore, it is very important to perform more large-scale tunnel fire tests using real vehicles to test these initial observations. Most of the existing vehicle fire data are for outdated vehicles, and therefore, a new large-scale tunnel test series with modern road and rail/metro vehicles is a pressing scientific need.

The other parameter of interest is the time to reach a peak HRR value. The data in Table 4.1 show that there is a great variety in the time to reach peak HRR. This time varies between 10 and 55 min.

The large-scale tests show that in a real tanker fire accident, where it is realistic to expect that the gasoline spreads over the entire tunnel width, one can expect the HRR per unit fuel surface area to be in the range of 0.35–2.6 MW/m^2 depending on the ventilation conditions and spread of the fuel over the road surface. In well-ventilated conditions with pan fuel depth that is larger than 70 mm and where the pan width is smaller than the tunnel width the HRR is expected to be about 2.4–2.6 MW/m^2 for gasoline. The effects of the fuel depth on the burning rate have not been considered here but in a real accident the burning rate could be reduced due to the cooling effect of the road surface.

References

1. Fire and Smoke Control in Road Tunnels (1999), PIARC
2. NFPA 502 (2004) Standard for Road Tunnels, Bridges, and other Limited Access Highways. 2004 edn. National Fire Protection Association
3. Ingason H An Overview of Vehicle Fires in Tunnels. In: Vardy A (ed) Fourth International Conference on Safety in Road and Rail Tunnels, Madrid, Spain, 2–6 April, 2001. pp. 425–434
4. Lönnermark A, Ingason H (2005) Gas Temperatures in Heavy Goods Vehicle Fires in Tunnels. Fire Safety Journal 40:506–527
5. Ingason H, Lönnermark A Recent Achievements Regarding Measuring of Time-heat and Time-temperature Development in Tunnels. In: 1st International Symposium on Safe & Reliable Tunnels, Prague, Czech Republic, 4–6 February 2004. pp 87–96
6. Ingason H (2006) Fire Testing in Road and Railway Tunnels. In: Apted V (ed) Flammability testing of materials used in construction, transport and mining. Woodhead Publishing, pp 231–274

7. Babrauskas V (2008) Heat Release Rates. In: DiNenno PJ, Drysdale D, Beyler CL et al. (eds) The SFPE Handbook of Fire Protection Engineering. Fourth Edition edn. National Fire Protection Association, Quincy, MA, USA, pp 3–1–3–59
8. Beard AN, Carvel RO (2012) Handbook of tunnel fire safety—Second Edition. ICE Publishing
9. Ingason H, Lönnermark A (2012) Heat Release Rates in Tunnel Fires: A Summary. In: Beard A, Carvel R (eds) In The Handbook of Tunnel Fire Safety, 2nd edition. ICE Publishing, London
10. Ingason H Heat Release Rate Measurements in Tunnel Fires. In: Ivarson E (ed) International Conference on Fires in Tunnels, Borås, Sweden, October 10–11, 1994 1994. SP Swedish National Testing and Research Institute, pp 86–103
11. Ingason H, Lönnermark A Large-scale Fire Tests in the Runehamar tunn—Heat Release Rate (HRR). In: Ingason H (ed) International Symposium on Catastrophic Tunnel Fires (CTF), Borås, Sweden, 20–21 November 2003. SP Swedish National Testing and Research Institute, pp SP Report 2004:2005, p. 2081–2092
12. Steinert C Smoke and Heat Production in Tunnel Fires. In: The International Conference on Fires in Tunnels, Borås, Sweden, 10–11 October 1994. SP Swedish National Testing and Research Institute, pp 123–137
13. Axelsson J, Andersson P, Lönnermark A, van Hees P, Wetterlund I (2001) Uncertainties in Measuring Heat and Smoke Release Rates in the Room/Corner Test and the SBI. SP Swedish National Testing and Research Institute, Borås, Sweden
14. Ingason H, Gustavsson S, Dahlberg M (1994) Heat Release Rate Measurements in Tunnel Fires. SP Swedish National Testing and Research Institute, Borås, Sweden
15. Fires in Transport Tunnels: Report on Full-Scale Tests (1995). edited by Studiensgesellschaft Stahlanwendung e. V., Düsseldorf, Germany
16. Proceedings of the International Conference on Fires in Tunnels (SP Report 1994:54). SP Swedish National Testing and Research Institute Borås, Sweden
17. Ingason H, Lönnermark A (2005) Heat Release Rates from Heavy Goods Vehicle Trailers in Tunnels. Fire Safety Journal 40:646–668
18. Karlsson B, Quintier JG (2000) Enclosure Fire Dynamics. CRC Press,
19. Mangs J, Keski-Rahkonen O (1994) Characterization of the Fire Behavior of a Burning Passenger Car. Part II: Parametrization of Measured Rate of Heat Release Curves. Fire Safety Journal 23:37–49
20. Steinert C (2000) Experimentelle Untersuchhungen zum Abbrand-und Feuerubersprungsverhalten von Personenkraftwagen. vfdb-Zeitschrift, Forschung, Technik und Management im Brandschutz 4:163–172
21. Ingason H, Nireus K, Werling P (1997) Fire Tests in a Blasted Rock Tunnel. FOA, Sweden
22. Shipp M, Spearpoint M (1995) Measurements of the Severity of Fires Involving Private Motor Vehicles. Fire and Materials Vol. 19:143–151
23. Lemaire A, van de Leur PHE, Kenyon YM (2002) Safety Proef: TNO Metingen Beneluxtunnel—Meetrapport. TNO
24. Joyeux D (1997) Development of Design Rules for Steel Structures Subjected to Natural Fires in Closed Car Parks. Centre Technique Industriel de la Construction Métallique, Saint-Rémy-lès-Chevreuse, France
25. Shipp M, Fraser-Mitchell J, Chitty R, Cullinan R, Crowder D, Clark P (2009) Fire Spread in Car Parks. Fire Safety Engineering (June):14–18
26. Joyeux D (1997) Natural Fires in Closed Car Parks—Car Fire Tests, INC-96/294d-DJ/NB.
27. Lönnermark A (2005) On the Characteristics of Fires in Tunnels. Doctoral Thesis, Doctoral thesis, Department of Fire Safety Engineering, Lund University, Lund, Sweden
28. Axelsson J, Försth M, Hammarström R, Johansson P (2008) Bus Fire Safety. SP Technical Research Institute of Sweden, Borås, Sweden
29. Kunikane Y, Kawabata N, Ishikawa T, Takekuni K, Shimoda A Thermal Fumes and Smoke Induced by Bus Fire Accident in Large Cross Sectional Tunnel. In: The fifth JSME-KSME Fluids Engineering Conference, Nagoya, Japan, 17–21 November 2002.

30. Haack A Introduction to the Eureka-EU 499 Firetun Project. In: Proceedings of the International Conference on Fires in Tunnels, SP Report 1994:54, Borås, Sweden, 1994
31. Brousse B, Perard M, Voeltzel A, Botlan YL Ventilation and fire tests in the Mont Blanc Tunnel to better understand the catastrophic fire of March 24th, 1999. In: Third international conference on Tunnel Fires and Escape from tunnels, Washington DC, USA, 9–11 October 2001. pp 211–222
32. Brousse B, Voeltzel A, Botlan YL, Ruffin E (2002) Mont Blanc tunnel ventilation and fire tests. Tunnel Management International Vol. 5, Nr 1:13–22
33. MK C, WO C, KW L, AD L, LM N, F T Heat release rates of heavy goods vehicle fires in tunnels. In: In: 15th International Symposium on Aerodynamics, Ventilation & Fire in Tunnels, Barcelona, Spain, 2013. BHR Group, pp 779–788
34. Cheong MK, Cheong WO, Leong KW, Lemaire AD, LM N (2013) Heat Release Rates of Heavy Goods Vehicle Fire in Tunnels with Fire Suppression System. Fire Technology. doi:10.1007/s10694-013-0367-0
35. Ingason H, Appel G, Li YZ, Lundström U, Becker C Large scale fire tests with a Fixed Fire Fighting System (FFFS). In: ISTSS 6th International Symposium on Tunnel Safety and Security, Marseille, 2014
36. Grant GB, Drysdale D Estimating Heat Release Rates from Large-scale Tunnel Fires. In: Fire Safety Science—Proceedings of the Fifth International Symposium, Melbourne, 1995. pp 1213–1224
37. Chuang Y-J, Tang C-H, Chen P-H, Lin C-Y (2005–2006) Experimental investigation of burning scenario of loaded 3.49-ton pickup trucks. Journal of Applied Fire Science 14 (1):pp 27–46
38. A. Kashef, J. Viegas, A. Mos, N H Proposed idealized design fire curves for road tunnels. In: 14th International Symposium on Aerodynamics and Ventilation of Tunnels, Dundee, Scotland 11–13 May, 2011
39. Heselden A Studies of fire and smoke behavior relevant to tunnels. In: 2nd Int Symp on Aerodynamics and Ventilation of Vehicle Tunnels, Cambridge, UK, 23–25 March 1976. Paper J1, BHRA Fluid Engineering, pp J1–1–J1–18
40. Liew S, Deaves D Safety Assessment of Dangerous Goods Transport in a Road Tunnel. In: Safety in Road and Rail Tunnels, First International Conference, Basel, Switzerland, 23rd–25th November 1992. pp 227–237
41. Larson DW, Reese RT, Wilmot EL The Caldecott Tunnel Fire Thermal Environments, Regulatory Considerations and Probabilities. Sandia National Laboratories
42. Caldecott Tunnel Near Oakland California, April 7, 1982 (Highway Accident Report Report No. 3665A.). Highway Accident Report Report No. 3665A. National Transportation Safety Board Washington D. C
43. Ingason H Small Scale Test of a Road Tanker Fire. In: Ivarson E (ed) International Conference on Fires in Tunnels, Borås, Sweden, October 10–11 1994. SP Swedish National Testing and Research Institute, pp. 238–248
44. Babrauskas V (2002) Heat Release Rates. In: DiNenno PJ, Drysdale D, Beyler CL et al. (eds) The SFPE Handbook of Fire Protection Engineering. Third edition edn. National Fire Protection Association, Quincy, MA, USA, pp 3–1–3–37
45. Zabetakis MG, Burgess DS (1961) Research on the hazards associated with the production and handling of liquid hydrogen. US Bureau of Mines, Pittsburgh, PA
46. Schlussbericht der Versuche im Ofenegg Tunnel von 17.5–31.5 1965 (1965). Kommission für Sicherheitsmassnahmen in Strassentunneln
47. ILF (1976) Brandversuche in einem Tunnel. Ingenieurgemeinschaft Lässer-Feizlmayr; Bundesministerium f. Bauten u. Technik, Strassenforschung
48. Lönnermark A, Kristensson P, Helltegen M, Bobert M Fire suppression and structure protection for cargo train tunnels: Macadam and HotFoam. In: Lönnermark A, Ingason H (eds) 3rd International Symposium on Safety and Security in Tunnels (ISTSS 2008), Stockholm, Sweden, 12–14 March 2008. SP Technical Research Institute of Sweden, pp 217–228

49. Hansen R, Ingason H (2013) Heat release rate measurements of burning mining vehicles in an underground mine. Fire Safety Journal 61 12–25
50. Ingason H, Hammarström R (2010) Fire test with a front wheel loader rubber tire. SP Technical Research Institute of Sweden, SP Report 2010:64
51. Shipp MP, Guy PS (1993) Fire Behaviour of Rubber Tyres. Fire Research Station report TCR 65/93
52. Hansen PA (1995) Fires in Tyres—Heat Release Rate and Response of Vehicles. SINTEF—Norwegian Fire Research Laboratory
53. Lönnermark A, Blomqvist P (2005) Emissions from Tyre Fires. SP Swedish National Testing and Research Institute, Borås, Sweden
54. Lönnermark A, Lindström J, Li YZ, Claesson A, Kumm M, Ingason H (2012) Full-scale fire tests with a commuter train in a tunnel. SP Technical Research Institute of Sweden, Borås, Sweden
55. Hadjisophocleous G, Lee DH, Park WH Full-scale Experiments for Heat Release Rate Measurements of Railcar Fires. In: International Symposium on Tunnel Safety and Security (ISTSS), New York, 2012. SP Technical Research Institute of Sweden, pp 457–466
56. Barber C, Gardiner A, Law M Structural Fire Design of the Øresund Tunnel. In: Ivarson E (ed) Proceedings of the International Conference on Fires in Tunnels, Borås, Sweden, 10–11 October 1994. SP Swedish National Testing and Research Institute, pp 313–332
57. Tewarson A (2002) Generation of Heat and Chemical Compounds in Fires. In: DiNenno PJ, Drysdale D, Beyler CL et al. (eds) The 3rd edition of SFPE Handbook of Fire Protection Engineering. Third edition edn. National Fire Protection Association, Quincy, MA, USA, pp 3–82–83–161
58. Babrauskas V Ignition of Wood—A Review of the State of the Art. In: Interflam 2001, Edinburgh, Scotland, 17–19 September 2001. Interscience Communications Ltd., pp 71–88
59. Carvel RO, Beard AN, Jowitt PW How Much do Tunnels Enhance the Heat Release Rate of Fires? In: Proc. 4th Int. Conf on Safety in Road and Rail Tunnels, Madrid, Spain, 2–6 April 2001. pp 457–466
60. Lönnermark A, Ingason H (2007) The Effect of Cross-sectional Area and Air Velocity on the Conditions in a Tunnel during a Fire. SP Report 2007:05. SP Technical Research Institute of Sweden, Borås, Sweden
61. Lönnermark A, Ingason H The Influence of Tunnel Dimensions on Fire Size. In: Proceedings of the 11th International Fire Science & Engineering Conference (Interflam 2007), London, UK, 3–5 September 2007. Interscience Communications, pp 1327–1338
62. Carvel RO, Beard AN, Jowitt PW, Drysdale DD (2001) Variation of Heat Release Rate with Forced Longitudinal Ventilation for Vehicle Fires in Tunnels. Fire Safety Journal 36 (6):569–596
63. Carvel RO, Beard AN, Jowitt PW (2001) The Influence of Longitudinal Ventilation Systems on Fires in Tunnels. Tunnelling and Underground Space Technology 16:3–21
64. Carvel RO, Beard AN, Jowitt PW The Influence of Longitudinal Ventilation and Tunnel Size on HGV Fires in Tunnel. In: 10th International Fire Science & Engineering Conference (Interflam 2004), Edinburgh, Scotland, 5–7 July 2004. Interscience Communications, pp 815–820
65. Lönnermark A, Ingason H The Effect of Air Velocity on Heat Release Rate and Fire Development during Fires in Tunnels. In: 9th International Symposium on Fire Safety Science, Karlsruhe, Germany, 21–26 September 2008. IAFSS, pp 701–712
66. Ingason H, Li YZ (2010) Model scale tunnel fire tests with longitudinal ventilation. Fire Safety Journal 45:371–384
67. Ingason H, Lönnermark A Effects of longitudinal ventilation on fire growth and maximum heat release rate. In: Lönnermark A, Ingason H (eds) Proceedings from the Fourth International Symposium on Tunnel Safety and Security, Frankfurt am Main, Germany, 17–19 March 2010. SP Technical research Instute of Sweden, pp 395–406
68. Ingason H, Li YZ (2011) Model scale tunnel fire tests with point extraction ventilation. Journal of Fire Protection Engineering 21 (1):5–36

69. Harmathy TZ (1978) Experimental Study on the Effect of Ventilation on the Burning of Piles of Solid Fuels. Combustion and Flame Vol. 31:p. 259–264
70. Ingason H (1995) Fire Experiments in a Model Tunnel using Pool Fires—Experimental Data. SP Swedish National Testing and Research Institute, Borås, Sweden
71. Ingason H (1995) Effects of Ventilation on Heat Release Rate of Pool Fires in a Model Tunnel. SP Swedish National Testing and Research Institute, Borås, Sweden
72. Saito N, Yamada T, Sekizawa A, Yanai E, Watanabe Y, Miyazaki S Experimental Study on Fire Behavior in a Wind Tunnel with a Reduced Scale Model. In: Vardy AE (ed) Second International Conference on Safety in Road and Rail Tunnels, Granada, Spain, 3–6 April 1995. University of Dundee and Independent Technical Conferences Ltd., pp 303–310
73. Takeda H, Akita K Critical Phenomenon in Compartment Fires with Liquid Fuels. In: Eighteenth Symposium (International) on Combustion, Waterloo, Canada, 17–22 August 1980. The Combustion Institute, pp 519–527
74. Lönnermark A Goods on HGVs during Fires in Tunnels. In: 4th International Conference on Traffic and Safety in Road Tunnels, Hamburg, Germany, 25–27 April 2007. Pöyry
75. Croce PA, Xin Y (2005) Scale modeling of quasi-steady wood crib fires in enclosures. Fire Safety Journal Vol. 40:245–266
76. Tewarson A, Pion RF (1976) Flammability of plastics. I. Burning intensity.. Combustion and Flame 26:85–103
77. Li YZ, Ingason H, Lönnermark A Fire development in different scales of a train carriages. In: 11th International Symposium on Fire Safety Science, New Zealand, 2014.
78. Drysdale D (1992) An Introduction to Fire Dynamics. John Wiley & Sons.;

Chapter 5
Fire Growth Rates in Tunnels

Abstract An overview of fire growth rates (FGR) for different vehicles travelling through tunnels is presented. The emphasis is on understanding the governing physics of fire growth rates. This includes ignition sources, geometry and type of the fuel, and the effects of the longitudinal ventilation flow. The FGR related parameters are decisive for tunnel fire safety. It dictates how fast the fire in different materials develops and influences the situation inside a tunnel in very different ways. The chapter gives a good understanding of the main mechanism behind the FGR of different types of vehicles and different solid materials. The effects of windbreaks on the FGR are explored.

Keywords Fire growth rate (FGR) · Heat release rate (HRR) · Flame spread · Ventilation · Windbreak

5.1 Introduction

The large numbers of catastrophic fires that have occurred in Europe and other places in the world have put focus on the fire development, especially the initial fire growth. Although, many of these fires developed to huge fires, the first 10 or 15 min of the fire were crucial for those who had to escape from the fire. A common component in all these fires has been the significance of the vehicle type, position in relation to portals and other vehicles, the ignition source, and the effects of the ventilation on FGR. The type and weight of load being carried by HGV vehicles played an important role in determining the severity of the fire. In most of the catastrophic road tunnel fires, the fire spread from a single heavy goods vehicle (HGV) to a neighboring vehicle of similar size, or alternatively due to collision between one or more HGV vehicles, see Chap. 1 and reference [1].

The size and type of ignition source is very important for the potential growth of the fire, from a small fire to a fully developed fire. The variety in ignition sources are tremendous, everything from electrical circuit failure, arson, overheated brakes, hot engine surfaces igniting leaking fuels up to large ignition sources (pool fires) due to collisions between vehicles or with tunnel construction. The period from a physical ignition to a notable growth of the fire, creating

H. Ingason et al., *Tunnel Fire Dynamics,* DOI 10.1007/978-1-4939-2199-7_5

smoke and heat influencing the tunnel users, is called the incipient period. It can vary from tens of seconds to tens of minutes, or more. The requirement for continuation of the fire growth lays in the geometry of the fuel, the combustible material adjacent to the ignition source, and the type of accelerators. The conditions for continuous fire growth depend on how large flames can be initially developed, and thereby the heat flux from those flames toward adjacent combustible materials. The ventilation plays an important role in this process. It mainly affects how these initial flames are tilted and consequently, how the fire spreads from there. High ventilation rates actually can prevent continuous fire spread; example of such an ignition delay is on the running vehicles which come to a stop. The flames may suddenly burst out after the stop, and the fire starts to develop rapidly. It is difficult to predict a potential fire growth from the incipient period to the continuous FGR period, where the heat release rate (HRR) continue to increase rapidly, and will lead to a fully developed fire if not intervened. In large-scale testing of fires, the incipient time is seldom simulated or tested, mainly because it is difficult to reproduce and also difficult to control. Therefore, the ignition sources are usually much larger than anticipated in the development of realistic fires that are not created by large ignition sources.

The HGVs consist of, or carry, highly flammable materials, and the fire spreads very rapidly with aid of the longitudinal ventilation inside the tunnel. The tunnel ceiling height also has a major effect on the outcome. In most of the Alp tunnel fires with numerous HGV vehicles involved, occurred in tunnels with relatively low ceiling height, in the range of 4–5 m. Together with the longitudinal flow, this combination becomes devastating for the FGR. The type of cover of the cargo is also a parameter that is of great importance and usually not mentioned in this context of FGR. Experiments carried out by the authors have shown that the blockage to the cargo can influence the FGR by a factor of two or more. This is extremely important to understand as the FGR is a key parameter for the fire safety design of tunnels, especially for the evacuation of the people in the tunnel during a fire.

Although the ventilation velocity may result in an increase of the HRR and the FGR, the forced longitudinal ventilation is important and necessary to prevent the smoke back flow in most tunnel fires. It constitutes the basis for the design of critical velocity and therefore gets such high focus among tunnel engineers.

Despite the fact that the effect of longitudinal ventilation on the FGR in HGV fires is an important issue, it has not been treated and explained by any solid physical theory before. Li and Ingason [2] presented a basic theory to express the relationship between the FGR and the governing parameters. This theory is presented in Sect. 5.2 and 5.3, and examples of how to use the equations are given. At first, the definition of the FGR in a tunnel fire needs to be presented. In most of the tunnel fire tests carried out, a linear increase in the HRR can be found in the main growth period, that is, in a range of about 20–80 % of the maximum HRR in the test. Therefore, the FGR discussed in this chapter is defined as the difference between 80 % of the maximum HRR and 20 % of the maximum HRR divided by the corresponding time difference.

The common understanding among engineers and researchers is that the fire growth rate increases considerably with the ventilation velocity in a tunnel fire. The question is only what parameters dominate and really control how fast a fire grows from its initial conditions. Those who have treated this phenomenon earlier have focused on the effects of ventilation and tunnel geometry on the FGR. For example, Carvel et al. [3–5] investigated the interaction of the ventilation flow with the FGR in a tunnel fire using a Bayesian probabilistic approach. This is the same method as used for maximum HRR, which has been discussed in Chap. 4. The basis for the conclusions is based on refined estimates made by a panel of experts and data from experimental fire tests in tunnels. Initially their conclusions were based on rather limited experimental data, but have been updated later [6, 7]. They found that the FGR could increase by a factor of five for 3 m/s and by factor of ten for 10 m/s, compared to the case with natural ventilation. It was also seen that the enhancing effects of ventilation for small pool fires is much less significant than that for HGV's (it may be reduced by 40 %), while that for large pool fires tended to increase by 50 %. For car fires, the enhancement of the ventilation rate on the heat release would not be significantly different relative to a car in a naturally ventilated tunnel. The FGR for car fires with natural ventilation would not be significantly influenced by forced ventilation rates of 1.5 m/s.

Lönnermark and Ingason [8] showed from model scale experiments that, the effect of the velocity on the increase factor on the fire development depends on the tunnel dimensions and the conditions inside the tunnel. The height and the width of the tunnel influence the results. However, how much the fire growth results are affected by the dimensions also seems to depend on how the FGR is calculated, that is what time periods or intervals are used. The effect of initial conditions of the fuel and the tunnel flow is also illustrated by the HRR ratio between the lowest velocity and the cases with higher velocity. For the case with the lowest velocity of 0.22 m/s (corresponding to a velocity of 1 m/s in real scale), the fire develops more slowly and reaches a lower maximum value compared to the cases with higher velocities. Almost all cases with the velocity of 0.22 m/s became somewhat under ventilated at the time of the highest mass loss rate or peak HRR. This is important to keep in mind since this can also be the case for real tunnels. This can significantly affect the effect of the velocity on the increase factors, and thereby the interpretation of the results.

Not only are the local ventilation conditions important, but also other factors as for example geometry of the tunnel, type of fuel, and the position and extension of the flame. This has been discussed in previous papers on the effect of the tunnel dimensions on the burning characteristics [9, 10]. Also the geometry of fuel, here represented by the porosity (see Chap. 4, Sect. 4.3.4), is important. The wood crib with the lower porosity was more affected by the velocity than was the wood crib with the higher porosity. It is also interesting to note that the increase factor, both for the peak HRR and for the FGR, seems to reach a constant value or at least increase more slowly when reaching above a certain velocity [8]. The tests were performed in a model scale tunnel, and one should be aware of that, not all parameters, for example radiation, scale perfectly when transforming the results into real scale.

However, experience from previous test series in model scale has shown that this kind of test series can be very valuable for studying different phenomena, processes, and parameter variations.

Li and Ingason [2] stated that the FGR in a ventilated tunnel fire should be related to the flame spread over the fuel surface. Theories on flame spread over a solid surface, especially over a vertical combustible wall, follow a very simple correlation. The forced air flow (convection) over a surface enhances the flame spread at a low ventilation velocity and gradually shows cooling effect on the flame spread at a high ventilation velocity. How the convective flow affects the spread is not clearly known [11]. Thomas [12] proposed an approximate formula applicable to wild fires, wood cribs, and urban conflagration which can be expressed as follows:

$$V\rho_f = C_k(1+u_o) \tag{5.1}$$

where V is the flame spread rate (m/s), ρ_f is the fuel density (kg/m^3), u_o is the wind velocity (m/s), C_k is a coefficient with a value of 0.07 for wildland fires and 0.05 for wood cribs.

In a tunnel fire, the longitudinal ventilation plays a key role in the flame spread, thus it is much different from an open fire or a room fire. Moreover, the relationship between the FGR and the flame spread over the fuel surface in a ventilated tunnel fire is not clearly known. The geometry of the fuel does play an important role. In order to obtain the effects on the FGR due to longitudinal ventilation, the fuel has to extend in the direction of the flame spread. If the fuel bed is short or cubical in shape, the effects of the ventilation are not expected to be as evident as if the fuel were geometrically elongated in the direction of the ventilation and thereby the flame spread. Therefore, for fire loads such as HGV trailers or long vehicles, the effects of the ventilation become more definite. If the fuel load is cubical in shape or extends more in the perpendicular direction of the longitudinal ventilation, the opposite effects may be expected, that is, increase ventilation rate may slow down the FGR. These effects have not been experimentally verified in longitudinal ventilation flows, but hypothetically they should be expected.

In the following, the work by Li and Ingason on influence of ventilation flow on FGR in tunnel fires with wind aided fire spread is presented. The work resulted in theoretical relationship between the flame spread rate and the FGR in a ventilated flow. A large amount of data relevant to the FGR from model and full scale tunnel fire tests was collected and applied to a detailed analysis of the FGR [2].

5.2 Theory of Fire Growth Rate

A schematic diagram of flame spread over a solid surface exposed to horizontal wind is shown in Fig. 5.1. The temperature in each control volume close to the pyrolysis zone increases gradually due to heat feedback from the flame and the hot gases until it reaches the ignition value where it starts to burn.

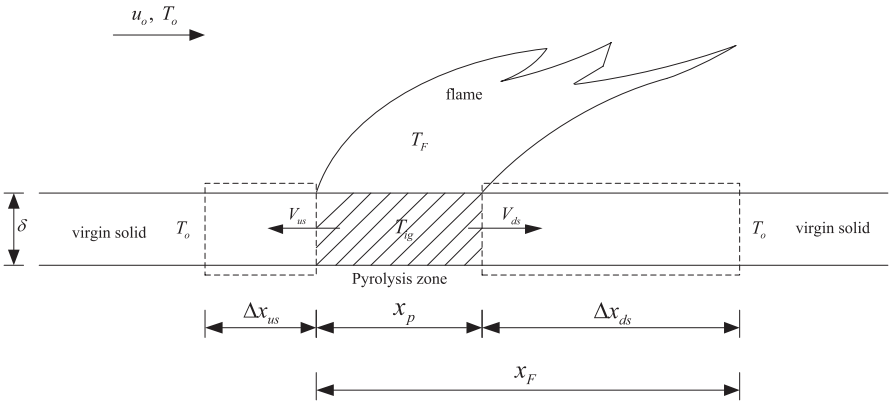

Fig. 5.1 A schematic diagram of flame spread over an elongated solid surface

The energy equations for the control volumes upstream and downstream can be expressed as [13]:

$$\rho_f c_f \delta (T_{ig} - T_o) V = \dot{q}'' \Delta x \tag{5.2}$$

where

$$\delta \approx \sqrt{\frac{k_f t}{\rho_f c_f}}, t = \frac{\Delta x}{V}$$

It can be transformed into:

$$V = \frac{\dot{q}''^2 \Delta x}{(k\rho c)_f (T_{ig} - T_o)^2} \tag{5.3}$$

In the above equations, c is the heat capacity (kJ/(kg K)), δ is the characteristic depth (m), T_{ig} is the ignition temperature (K), T_o is the initial temperature (K), $\dot{q}''$ is the heat flux per unit area (kW/m^2), t is the time (s), Δx is the distance from the pyrolysis region to the initial temperature region (m), and k is the thermal conductivity (kJ/(m s K)). Subscript f indicates fuel.

Therefore, the flame spread rate is intimately related to the heat flux and the distance Δx (m). Equation (5.3) represents a theoretical consideration in order to understand the governing relationships. At this stage, it should not be used for quantitative estimation of flame spread in tunnel fires.

5.2.1 Opposed Flow Spread (Upstream)

In a tunnel fire, the type of flame spread upstream of the fire source is the opposed flow spread. The forward flame heat flux upstream of the fire can be characterized as conduction in the gas phase which suggests [13]:

$$\dot{q}'' = k_a \frac{T_f - T_o}{\Delta x} \tag{5.4}$$

where subscript *a* indicates air.

Since the forward conduction in the gas phase dominates the heat transfer, the conduction must be balanced with convection which suggests:

$$\rho_a c_a u_o \frac{\partial T}{\partial x} \approx k_a \frac{\partial^2 T}{\partial x^2} \tag{5.5}$$

This suggests:

$$\Delta x \approx \frac{k_a}{\rho_a c_a u_o} \tag{5.6}$$

Combining all these equations we obtain:

$$V_{us} = \frac{(k\rho c)_a (T_F - T_o)^2}{(k\rho c)_f (T_{ig} - T_o)^2} u_o \propto \frac{1}{(k\rho c)_f} u_o \tag{5.7}$$

where subscript *F* indicates flame and *us* indicates upstream.

This means, the flame spread rate upstream of the fire linearly increases with the ventilation velocity. Equation (5.7) represents a theoretical consideration in order to understand the governing relationships. At this stage, it should not be used for quantitative estimation of flame spread in tunnel fires.

5.2.2 Wind-Aided Spread (Downstream)

In a tunnel fire, the flame spread downstream of the fire source is the type of wind-aided spread over a surface that extends in the direction of the air flow. The same equation as Eq. (5.3) can be obtained in such cases, but with different interpretation of the heat flux from the flame and the distance Δx.

The heat conduction through a thermally-thick fuel, that is, heat transfer to the fuel surface by heat convection and radiation are the dominant modes for the wind-aided spread downstream. Therefore, the heat flux from the flame downstream of the fire can be expressed as:

$$\dot{q}'' = \dot{q}_c'' + \dot{q}_r'' \tag{5.8}$$

where subscripts c and r indicate convective and radiative respectively. The radiative heat flux downstream could be reasoned to depend on the flame temperature which is intimately related to ambient oxygen concentration, given that the effect of the view factor due to different ventilation could be ignored. The convective heat flux in a turbulent flow can be expressed as follows:

$$\dot{q}_c'' = \frac{k}{l} N_u \Delta T \propto \mathrm{Re}^{0.8} \propto u_o^{0.8} \tag{5.9}$$

Therefore, the heat transfer from the flame downstream should be enhanced.

The fire plume and thereby the flame volume is deflected in a ventilated flow. This suggests the distance Δx increases with the ventilation velocity. Note that this distance is related to the pyrolysis length that cannot be explicitly predicted.

According to the above analysis, it is known that the flame spread rate downstream of the fire increases with the ventilation velocity, which could be expressed:

$$V_{ds} \propto u_o \tag{5.10}$$

However, how the flame spread rate downstream of the fire varies with the ventilation velocity is not clearly understood.

The flame spread in a tunnel fire, V, is a combination of flame spread upstream, V_{us}, and flame spread downstream, V_{ds}. Clearly, it is seen that in a tunnel fire both the flame spreads upstream and downstream increases with the ventilation velocity. Based on Thomas work and the above analysis, it can be assumed that the flame spread rate in a tunnel fire is proportional to the ventilation velocity.

Note that the flame spread rate is directly related to the properties of the fuel, that is, inversely proportional to the thermal inertia $k\rho c$ [5]. In addition, the surface orientation, air composition, atmospheric pressure, and ignition temperature also have influence on the flame spread. The air composition and atmospheric pressure will not be discussed here since they are normally ambient in our case. In addition, since the pilot ignition temperature for most of the commonly used solid fuels is in a range of 300–400 °C. The effect of the surface orientation of the fuel, which is difficult to estimate for a tunnel fire due to the complexity of the fuel configuration, will be implicitly considered with aid of empirical constants.

Therefore, the flame spread in a longitudinally ventilated tunnel fire can be approximately expressed as follows:

$$V \propto \frac{1}{(k\rho c)_f} u_o \tag{5.11}$$

It should be pointed out here that there is some evidence of the decrease effect under high ventilation conditions,that is, blow-off effect, since the cooling effect starts to dominate the combustion process under these conditions. However, it was not observed within the range of the tunnel fire tests that we have carried out and therefore it is not included here. It can be explained by the fact that the existing ventilation velocity in a tunnel fire is relatively low. Other parameters that can influence these effects are the way the fuel or the vehicles are constructed. As explained earlier, if the fuel surfaces are short in the direction of the ventilation flow, the effects can be opposite, that is, the FGR reduces as the flames are forced to the outside of the fuel instead of spreading upwards due to buoyancy effects under low ventilation conditions.

5.2.3 Relationship Between FGR and Flame Spread Rate

The HRR can be expressed as:

$$\dot{Q}(t) = \chi \dot{m}''_f \Delta H_c A(t) \tag{5.12}$$

where $\dot{Q}$ is the HRR (kW), $\dot{m}_f''$ is the fuel burning rate per unit area (kg/(m$^2 \cdot$s), χ is the combustion efficiency, ΔH_c is the net heat of complete combustion (kJ/kg), *A(t)* is the burning fuel surface area (m^2).

The mass loss rate per unit area is directly related to properties of the fuel, and heat transfer among the flame, hot gases, fuel, and the tunnel walls. Ideal values were found by Tewarson and Pion [14] based on the assumption that all heat losses were reduced to zero or exactly compensated by an imposed heat flux equal to the total heat losses from the fire source. Ingason and Li [15] compared the maximum mass loss rates per unit area from tunnel fire tests to the ideal value of Douglas fir and found that there is a good agreement between them. Therefore, the mass loss rate per unit area can be assumed to be a constant for a quasi-steady combustion process in a tunnel fire and the HRR can be directly related to the burning area for a specific fuel type.

In a large tunnel fire, the longitudinal flame spread dominates the fire development. Therefore, it is assumed that the fire is burnt over the whole cross section of the fuel, and then spreads longitudinally. In other words, the flame spread in a large tunnel fire is assumed to be one-dimensional flame spread in the longitudinal direction. Equation (5.12) can then be transformed into:

$$\frac{dQ}{dt} = w_p \dot{m}_f'' \chi \Delta H_c V \tag{5.13}$$

where w_p is the wet perimeter of the fuel (m),that is, the contact perimeter between fuel and gas in a cross section.

Thus the FGR in a large tunnel fire can be expressed in the following form:

$$\frac{dQ}{dt} \propto \frac{\dot{m}_f'' \chi \Delta H_c}{(k\rho c)_f} w_p u_o \tag{5.14}$$

Equation (5.14) shows that the properties of fuel play an important role for the FGR in a ventilated flow.

5.2.4 Fuels Consisting of Several Parts

If the fuel consists of several parts or layers with different materials, for example a combination of wood, plastic, and mattress, the HRR can be expressed as:

$$Q(t) = \sum_{i=1}^{N} \dot{m}_{f,i}'' \chi_i \Delta H_{c,i} A_i(t) \tag{5.15}$$

The FGR can be expressed as:

$$\frac{dQ(t)}{dt} = \sum_{i=1}^{N} \chi_i \dot{m}_{f,i}'' \Delta H_{c,i} w_{p,i} V_i(t) \tag{5.16}$$

Equation (5.16) can be transformed into:

$$\frac{dQ(t)}{dt} \propto u_o \sum_{i=1}^{N} \frac{\phi_i \chi_i \dot{m}_{f,i}'' \Delta H_{c,i}}{(k\rho c)_{f,i}} w_{p,i} \tag{5.17}$$

where $\varnothing_i$ is a correlation coefficient between flame spread velocity of the ith fuel and the ventilation velocity, and i indicates the index number of the fuel parts (maximum value = N).

A material property of the ith fuel, $C_{f,i}$, is defined here:

$$C_{f,i} = \frac{\dot{m}''_{f,i}\Delta H_{c,i}}{(k\rho c)_{f,i}} \tag{5.18}$$

For simplicity, it is assumed that the correlation coefficients $\varnothing_i$ for all the parts are the same, and the combustion efficiency is a constant. Then the FGR can be simplified into:

$$\frac{dQ(t)}{dt} \propto u_o \sum_{i=1}^{N} C_{f,i} w_{p,i} \tag{5.19}$$

These results can be applied to the fire scenario in a ventilated flow. For a tunnel fire, the special geometry of tunnel and the vehicle do have influence on the FGR, which thus needs to be analyzed in detail.

Several dimensionless parameters need to be defined here:

Dimensionless time:

$$t_o^* = t\sqrt{g / H} \tag{5.20}$$

Dimensionless HRR:

$$Q^* = \frac{Q}{\rho_o c_p T_o g^{1/2} H^{5/2}} \tag{5.21}$$

Dimensionless ventilation velocity:

$$u_o^* = \frac{u_o}{\sqrt{gH}} \tag{5.22}$$

Then the dimensionless FGR, dQ^* / dt^*, can be transformed into:

$$\frac{dQ^*}{dt^*} \propto \frac{u_o^*}{H^{3/2}} \sum_{i=1}^{N} C_{f,i} w_{p,i} \tag{5.23}$$

If the fuel only consists of one material, Eq. (5.23) can be transformed into:

$$\frac{dQ^*}{dt^*} \propto \frac{w_p u_o^*}{H^{3/2}} \tag{5.24}$$

5.3 Correlations for Fire Growth Rate

In Chap. 3 there is an extensive presentation of experiments that have been carried out in tunnels. The data gathered from these tests will be used to verify the results of theoretical analysis. The first step is to obtain better information about the typical

Table 5.1 Properties of fuels used in these tests [2]

Material	Burning rate per unit area, $\dot{m}''_f$ (kg/(m^2·s))	Heat of combustion ΔH_c (MJ/kg)	Thermal inertia kρc (kJ^2/(m^4·s·K^2))	Material property C_f	Relevant tests
Wood	0.013	16.7	0.15	1447	Runehamar tests Benelux tests Model scale tests
PE plastic	0.026	40.0	0.46	2441	Runehamar (T1)
PUR mattresses	0.032	25.0	0.04	20,000	Runehamar (T2)
Furniture	0.020	25.0	0.15	3333	Runehamar (T3)
Polystyrene	0.035	41.9	0.58	2531	Runehamar (T4)

fuel types used in these tests. Li and Ingason [2] presented such analysis. The properties of the fuels used are summarized in Table 5.1.

Data relevant to the FGR from the above tunnel fire tests were applied to the analysis. The FGRs were calculated based on the data in a range of about 20–80 % of the maximum HRR in these tests. Consequently, the FGR is assumed to be linear in this range. The linear trend can be easily seen by observing the measured data.

5.3.1 Comparison with Model Scale Tests

Figure 5.2 shows how the data from Li and Ingason [2] of the FGRs vary with the ventilation velocity in model scale tunnel fire tests with longitudinal ventilation. Clearly, it confirms the prediction of linearly increasing FGR with the ventilation velocity. It is also shown that the FGR is nearly three times larger than that in a free burn test, when the ventilation velocity equals 0.9 m/s, corresponding to 4.3 m/s in full scale. This means that the ventilation velocity plays a very important role in the fire development. The FGR in a tunnel fire tests is close to that in a free burn test when the ventilation velocity is equal to 0.3 m/s. As the FGR is one of the most important design parameters for tunnel safety, these results are considered as important.

Figure 5.3 shows the dimensionless FGRs in model scale tunnel fire tests. Clearly, it shows that the proposed line correlates with the tests data well. One data from the extraction ventilation tests at a dimensionless FGR of about 0.6 kW/s deviates from the proposed line significantly. The reason may be that the ventilation velocity across the fire source is estimated based on the ventilation system rather than by direct measurement in the point extraction ventilation tests. This means that larger error may be produced in these tests compared to others.

The proposed line in Fig. 5.3 can be expressed as follows:

$$\frac{dQ^*}{dt^*} = 1.1\times10^{-6}\frac{u_o^*}{H^{3/2}}\sum_{i=1}^{N} C_{f,i}w_{p,i} \tag{5.25}$$

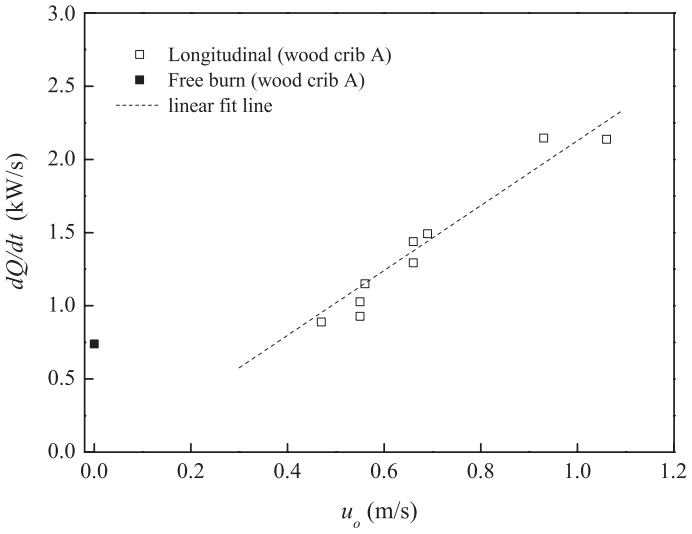

Fig. 5.2 The FGR as a function of the ventilation velocity in model scale [2]

A correlation coefficient of 0.9165 was found for the above equation. The correlation proves well the earlier assumption that the longitudinal flame spread dominates the flame spread in a tunnel fire.

For practical use, an expression of the FGR, dQ/dt, should be more useful than the dimensionless FGR, dQ^*/dt. Therefore Eq. (5.25) is written in another form:

$$\frac{dQ}{dt} = 1.2 \times 10^{-3} u_o \sum_{i=1}^{N} C_{f,i} w_{p,i} \tag{5.26}$$

For wood fires, the FGR in a ventilated tunnel can be approximately expressed as:

$$\frac{dQ}{dt} = 1.8 w_p u_o \tag{5.27}$$

5.3.2 Comparison with Full Scale Tests

Data from Runehamar tunnel fire tests [16–18] and 2nd Benelux tunnel fire tests [19] were used here to verify Eq. (5.25), and further to verify the method of predicting the FGR for fuels consisting of several parts.

Figure 5.4 shows the comparison of the FGRs in Runehamar tunnel fire tests and 2nd Benelux tunnel fire tests with the model scale tests. According to Eq. (5.18), each material corresponds to one material property $C_{f,i}$. The wet perimeter of the ith fuel $w_{p,i}$ is estimated by the contact perimeter in one cross section between the ith fuel and the air flow.

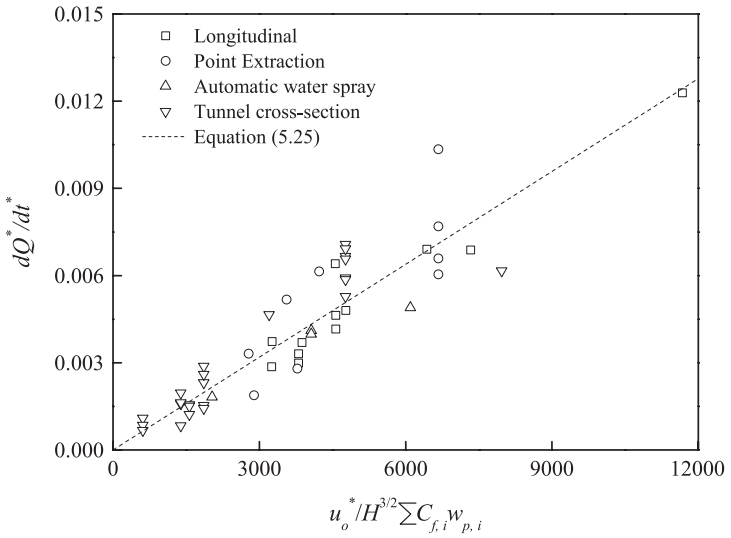

Fig. 5.3 The dimensionless FGR in model scale tests [2]

In Runehamar Test 1 (T1), the fuel consisted of wood pallets and plastic pallets. In Test 2, the fuel consisted of wood pallets and PUR mattresses made of polyurethane foam. In Test 3, the fuel mainly consisted of furniture. In Test 4, the fuel consisted of plastic cups in cardboard boxes on wood pallets. Since the outside cardboards were burned out after a while, it is difficult to estimate the wet parameter of the fuel in this test and also the material property of the fuel. A weighted average was used to estimate the material property here. The fuels used in the 2nd Benelux tests T8, T10, and T14 are all wood pallets.

The results in Fig. 5.4 show that the data from Runehamar tunnel fire tests and 2nd Benelux tunnel fire tests comply well with the data from model scale tests and Eq. (5.25). This indicates that the FGR can be scaled appropriately in model scale tests even with a scaling ratio of about 1:20. Further, it shows that Eq. (5.25) is applicable to predict the FGR for different types of fuels, even for fuels consisting of several parts.

Example 5.1 Estimate the FGR for a 10 m trailer loaded with furniture and PUR mattress in a 6 m high tunnel. The total exposed fuel surface area of 150 m^2 consists of 80 % furniture and 20 % PUR mattress. The fuel load is assumed to be uniformly distributed in the trailer. The velocity in the vicinity of the truck in the tunnel is 2 m/s. How much will the FGR increase if the velocity is 3 m/s instead?

Solution: Find values of the material property $C_{f,i}$ in Table 5.1, that is, 3333 for furniture and 20,000 for PUR mattress. The total wet perimeter of the fuel is 150/10 = 15 m, including 12 m for furniture and 3 m for PUR mattress. Now we can use Eq. (5.26) to estimate the FGR:

$$\frac{dQ}{dt} = 1.2\times10^{-3}\times2\times(3333\times12+20000\times3) = 240\ \text{kW/s} = 14.4\ \text{MW/min}.$$

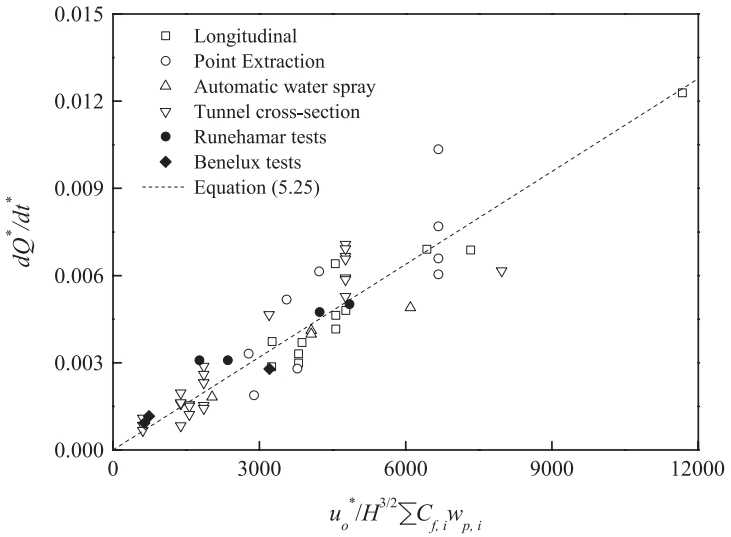

Fig. 5.4 Comparison of data from full scale tests with the model scale tests [2]

If the longitudinal ventilation rate was 3 m/s instead the FGR would have been 21.6 MW/min.

It can be seen that the PUR mattress contributes much on the fire output despite the small portion.

5.4 The Effects of Windbreaks on Fire Growth Rates

The theory of fire growth rates in tunnel fires presented above is suitable for fuels exposed to wind. In case that the fuels are not directly exposed to wind, the FGR could be expected to be lower, and thus the estimated FGR based on the proposed equations is also lower. Therefore, the proposed method tends to be conservative.

In a realistic vehicle fire, the fuels are complicated in structure and cannot be predetermined in most cases, for example fuel load and configurations for a HGV trailer. Solid rear doors on the HGV trailers block air movement into the fuel array. This will considerably slow down the rate of fire spread within the fuel load of the trailer. Most HGVs have rear doors and steel walls upfront and, further, the driver's cab itself presents a degree of obstruction to the flow of air through the fuels. The rest of the cargo area that could be covered with thin polyethylene tarpaulins burns easily. Despite this fact, data from previous full scale tests trying to simulate realistic HGVs fires can be used as a reference.

During the Runehamar large-scale tests in 2003 [17] (see Chap. 3, Sect. 3.3.11), the FGR was observed to be extremely high. It varied from 264 kW/s (15.8 MW/min) to 433 kW/s (26 MW/min) depending on the fuel load [16]. These values are

slightly different from the values originally calculated by Ingason and Lönnermark [17], who used slightly different time period to calculate the FGR. The highest FGR was obtained with a fuel load consisting of wood pallets and PUR mattresses, or 26 MW/min (Test 2). At the time of the performance of the Runehamar tests in 2003, the knowledge about effects of windbreaks or physical blockages of the fuel was not that well known. In the Runehamar tests, a polyethylene tarpaulin covered the entire volume with a fuel load (upfront ends, rear ends, sides, and ceiling) and relatively soon after ignition the tarpaulin burned away on the upstream side of the fuel and the horizontal wind aided fire spread inside the fuel stack was able to develop. This, of course, influenced the fire spread within the fuel drastically. If a windbreak in form of a board or steel sheet would have been mounted at the ends of the fuel load, especially the upstream end, a wake of circulating air would have been created inside the fuel load and the inside wind velocity would have been reduced considerably. This would have direct impact on the FGR.

In the testing of a water mist system in 2007, Mawhinney and Trellers [20] reported that the ventilation velocity had a large effect on the FGR which consisted of piled wood pallets. Addition of upstream panels to block wind penetration into the fuel array, which consisted of piles of wood pallets, had a significant reduction in HRR of the fires. The tests revealed how large an effect of the design of the HGV itself may have on the fire development. Today, most of the large-scale tests carried out with FFFS systems use windbreakers on both upstream and downstream side, see Chap. 16.

Large-scale tests carried out in 2013 by SP with FFFS [21], a comparison was carried out with and without windbreaker consisting of a thin steel sheets on the ends and top of the fuel. The longitudinal velocity inside the tunnel was 3 m/s. In Fig. 5.5, the effects of windbreak on the FGR is shown. The fire load, as explained in Chap. 16, Sect. 16.3.9, consisted of a potential 100 MW fire. The fuel consisted of 420 wood pallets with a total length of 8.4 m and width of 2.4 m. In test 5, the vertical steel sheets on the ends were removed. In test 6 the steel sheets were at place. In test 5 the FFFS was activated after about 7.3 min (23 MW) into the test and test 6, which is a free burn test, is plotted up to 23 MWs. The linear FGR for test 5 is about 5.5 MW/min and for test 6 it is 2.3 MW/min. This indicates a decrease of 58 % in FGR after the placement of the windbreakers. In order to illustrate these effects an example is presented.

Example 5.2 Assuming a HGV load with 420 wood pallets is burning with and without a windbreak. What would the resulting wind velocity be inside the fuel load behind the windbreak? Assume that the longitudinal velocity in the tunnel without a windbreak is 3 m/s. The FGRs are 2.3 MW/min with a windbreak and 5.5 MW/min without a windbreak.

Solution: As the wet perimeter w_p *in both cases is the same, the longitudinal velocity can be derived from Eq. (5.27). Since the relationship between the FGR and the longitudinal air velocity* u_o *is linear, we obtain:* $u_{0,windbreak} = 2.3/5.5 \times 3 = 1.25$ *m/s.*

The velocity obtained in example 5.2 is a reasonable value to be expected behind the windbreak. This relationship between the velocities has not been experimentally

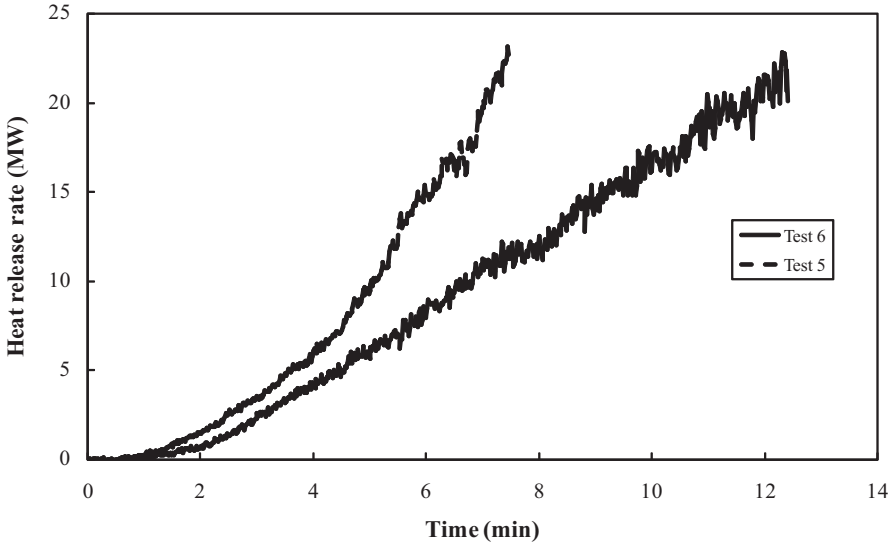

Fig. 5.5 Comparison of a large-scale test with (*test 6*) and without (*test 5*) windbreaker in a fire load consisting of 420 wood pallets [21]

verified, but shows the importance of the existence of a windbreak. A further research into this field is of great importance as most vehicles have windbreaks in one way or another.

5.5 Summary

A simple theoretical model of the FGR in a ventilated tunnel fire was presented. The relationship between the flame spread rate and the FGR in a ventilated flow was analyzed theoretically. A large amount of data relevant to the FGR from model and full scale tunnel fire tests was collected and applied to a detailed analysis of the effect of ventilation and fuels on the fire growth rate.

The longitudinal flame spread dominates the flame spread in a tunnel fire. The linear fire growth rates observed in large testing is related to the wind aided fire spreads inside the fuel stack. This process is clearly linear after reaching a given threshold value. The thermal inert, heat of combustion, the wet perimeter, and the mass burning rate per unit area of the fuel play important roles in the fire growth rate. A robust equation, that is, Eq. (5.25) or (5.26), that fits all the data of the FGR from model and full scale tunnel fire tests very well was proposed. Further, the proposed equation is applicable to predict the fire growth rate for different types of fuels, even for fuels consisting of several parts. However, additional tests results with ventilation velocities over 8 m/s in full-scale should be valuable to identify the transition conditions under which the cooling effect start to dominate.

The method presented in this chapter should be applicable to other ventilated fires, such as vehicle fires in the open under strong wind, in which the longitudinal fire spread also dominates the combustion process. This method of predicting the fire growth rate can also be applied to some other scenarios, such as rack storage fires, in which the dominating term is probably the vertical fire spread in an introduced vertical flow due to depletion of oxygen and buoyancy of the flame and hot gases.

The effects of windbreak were presented. These effects and the relation to the longitudinal wind velocity need to be further explored. The windbreaker exists in real vehicles and therefore it is of great importance to quantify these effects and put it into the context of the fire spread equations presented in this chapter.

References

1. Kim HK, Lönnermark A, Ingason H (2010) Effective Firefighting Operations in Road Tunnels. SP Report 2010:10. SP Technical Research Institute of Sweden, Borås, Sweden
2. Li YZ, Ingason H The Fire Growth Rate in a Ventilated Tunnel Fire. In: Tenth International Symposium on Fire Safety Science (IAFSS), Maryland, USA, 2011. pp 347–358
3. Carvel RO, Beard AN, Jowitt PW The Effect of Forced Longitudinal Ventilation on a HGV Fire in a Tunnel. In: Proceedings of the International Conference on Tunnel Fires and Escape from Tunnels, Lyon, France, 5–7 May 1999. pp 191–199
4. Carvel RO, Beard AN, Jowitt PW (2001) The Influence of Longitudinal Ventilation Systems on Fires in Tunnels. Tunnelling and Underground Space Technology 16:3–21
5. Carvel RO, Beard AN, Jowitt PW, Drysdale DD (2001) Variation of Heat Release Rate with Forced Longitudinal Ventilation for Vehicle Fires in Tunnels. Fire Safety Journal 36 (6):569–596
6. Carvel RO, Beard AN, Jowitt PW The Influence of Longitudinal Ventilation on Fire Size in Tunnel: Update. In: Vardy AE (ed) Fifth International Conference on safety in Road and Rail Tunnels, Marseille, France, 6–10 October 2003. University of Dundee and Tunnel Management International, pp 431–440
7. Carvel RO, Beard AN, Jowitt PW (2005) Fire Spread Between Vehicles in Tunnels: Effects of Tunnel Size, Longitudinal Ventilation and Vehicle Spacing. Fire Technology 41:271–304
8. Lönnermark A, Ingason H The Effect of Air Velocity on Heat Release Rate and Fire Development during Fires in Tunnels. In: 9th International Symposium on Fire Safety Science, Karlsruhe, Germany, 21–26 September 2008. IAFSS, pp 701–712
9. Lönnermark A, Ingason H The Influence of Tunnel Dimensions on Fire Size. In: Proceedings of the 11th International Fire Science & Engineering Conference (Interflam 2007), London, UK, 3–5 September 2007. Interscience Communications, pp 1327–1338
10. Lönnermark A, Ingason H The Influence of Tunnel Cross Section on Temperatures and Fire Development. In: Lönnermark A, Ingason H (eds) 3rd International Symposium on Safety and Security in Tunnels (ISTSS 2008), Stockholm, Sweden, 12–14 March 2008. SP Technical Research Institute of Sweden, pp 149–161
11. Drysdale D (1999) An Introduction to Fire Dynamics. 2nd Edition edn. John Wiley & Sons,
12. Thomas PH (1971) Rates of Spread for some Wind-Driven Fires. Forestry, XLIV:p. 2
13. Quintiere JG (2002) Surface Flame Spread. In: (ed.) DPJ (ed) The SFPE Handbook of Fire Protection Engineering (2nd ed). National Fire Protection Association, Quincy, MA, pp 246–257
14. Tewarson A, Pion RF (1976) Flammability of plastics. I. Burning intensity.. Combustion and Flame 26:85–103

15. Ingason H, Li YZ (2010) Model scale tunnel fire tests with longitudinal ventilation. Fire Safety Journal 45:371–384
16. Ingason H, Lönnermark A, Li YZ (2011) Runehamar Tunnel Fire Tests. SP Technical Research Institute, SP Report 2011:55
17. Ingason H, Lönnermark A (2005) Heat Release Rates from Heavy Goods Vehicle Trailers in Tunnels. Fire Safety Journal 40:646–668
18. Lönnermark A, Ingason H (2005) Gas Temperatures in Heavy Goods Vehicle Fires in Tunnels. Fire Safety Journal 40:506–527
19. Lemaire T, Kenyon Y (2006) Large Scale Fire Tests in the Second Benelux Tunnel. Fire Technology 42:329–350
20. Mawhinney JR, Trelles J COMPUTATIONAL FLUID DYNAMICS MODELLING OF WATER MIST SYSTEMS ON LARGE HGV FIRES IN TUNNELS. In: Presented at the Journée d'Etude Technique: Brouillard d'Eau – Quoi de Neuf?, at Pôle Européen de Sécurité CNPP – . Vernon, France, November 22, 2007
21. Ingason H, Appel G, Li YZ, Lundström U, Becker C Large scale fire tests with a Fixed Fire Fighting System (FFFS). In: ISTSS 6th International Symposium on Tunnel Safety and Security, Marseille, 2014, pp. 83–92

Chapter 6
Design Fire Curves

Abstract An overview of design fires in tunnels is given. Design fires are obtained from guidelines or standards, or exclusively for a specific tunnel project. They can be represented as a single constant design value or as a time dependent fire curve, either given in form of heat release rates (HRRs), temperatures or combustion products. Various ways exists to represent a design fire curve for tunnels. These can include different growth rates or combinations of growth rates with constant levels of design maximum values coupled to a decay period. The different type of design fire curves are put into the context of fire development in vehicles and tunnel fire dynamics. Mathematical representations of design fire curves are presented and discussed. An example of a new concept for creating a design fire curve is presented.

Keywords Heat release rate (HRR) · Design fire curve · Time-temperature curve · Fire growth rate (FGR) · Decay period · Fire products

6.1 Introduction

Mitigation systems are installed in tunnels to improve the safety of tunnel users and to prevent damages to the construction. The systems installed vary in type and costs. A design fire is needed when these mitigation systems are engineered for a specific tunnel project. The design fires represent the load to what the mitigation system should be functional during the incident. The design fire is most commonly represented as a single value of a maximum heat release rate (HRR) in megawatt (MW), a time-dependent HRR or as a time–temperature curve. The curves can also, but not as common, consist of time-dependent release of fire products such as smoke, CO or CO_2. A common definition given here for these types of curves is a "design fire curve".

The design fire curve can either represent a worst case scenario or a plausible fire scenario for a given tunnel. The values used for design fires can either be obtained for a specific project, or from guidelines or standards available for each tunnel type. Examples of guidelines for road tunnels are the report of World Road Association (PIARC) committee on Road Tunnels devoted to Fire and Smoke Control [1] and the National Fire Protection Association standard for road tunnels, NFPA 502 [2].

H. Ingason et al., *Tunnel Fire Dynamics,* DOI 10.1007/978-1-4939-2199-7_6

Other examples are national guidelines such as the French guidelines for road tunnels [3] or the RABT [4] in Germany.

For rolling stocks (train, subway, metro or tram) the guidelines only define time–temperature curves but not HRR as a single design value or as a function of time [5]. The focus is, therefore, on requirements on the fire resistance of the materials used in rolling stocks. The aim is to prevent the fire to develop or at least retard its growth and spread [6]. Example of such standard is the EN 45545–2:2013 which defines a classification system that specifies requirements for fire behaviour of materials and products used in trains. The classification system has been prepared by Technical Committee CEN/TC 256 "Railway applications" on behalf of the European Commission, based on the requirements of the EU Directive 2008/57/EC. Another well-known standard for design of fixed guideway transit and passenger rail systems (rolling stock) is NFPA 130 [7].

A common view about design fires in building environment is found in the work of ISO TC92 SC4, that is, the International Organisation of Standardization, Technical Committee 92, Sub Committee 4 on Fire Safety Engineering, which describes a methodology for selection of design fire scenarios and design fires that are credible but conservative for use in deterministic fire safety engineering analyses of any built environment including buildings, structures or transportation vehicles [8]. The selection of design fire scenarios is tailored to the fire safety design objectives, and accounts for the likelihood and consequences of potential scenarios.

Maevski [9] proclaimed that a design fire scenario for road tunnels represents a particular combination of events associated with factors such as type, size, location of ignition source, external environmental conditions and human intervention. The type of fuel and the fuel load density, as well as the fuel arrangement have to be defined. Maevski [9] specified, in detail, the periods that a design fire curve should include: (a) incipient phase—characterized by the initiating source, such as a smoldering or flaming one, (b) fire growth phase—period of propagation spread, potentially leading to flashover or full fuel involvement, (c) fully developed phase—nominally steady ventilation or fuel-controlled burning, (d) decay phase—period of declining fire severity and (e) extinction phase—point at which no more heat energy is being released.

Design fire curves are used for the design of the tunnel ventilation and egress systems. In case of use of fixed firefighting systems (FFFS), the effect of the FFFS needs to be introduced into the design fire curve. There are no such design fire curves available to date in guidelines, but new research efforts on FFFS will hopefully lead to development of such design curves. The designer is obligated to make a number of assumptions to ensure that the design will be able to save lives and retain the structural integrity of the tunnel under most of the foreseeable fire scenarios. To develop a design fire curve, or a tenability curve as defined by Maevski, the project must include a fire heat release curve, a design tenability curve, a design evacuation (egress) curve and a design systems response curve as a function of time. A tenability curve indicates all time steps and resulting impacts on casualties and tunnel structure. This allows for predicting how long the environment will be tenable in the tunnel, and aids to decide what needs to be done to achieve the safety goals.

Design fires are described in terms of variables used for quantitative analysis. These variables typically include the HRR of the fire, yield of toxic species and soot as functions of time [9].

The most common way to create a design fire curve is to combine the maximum HRR with different types of fire growth rates (FGR) [10, 11, 5] and decay rates. In case of using constant maximum HRR design values in tunnels, the design fire curves tend to include long periods with constant peak HRR value. From a physical point of view, these curves may appear unrealistic but they do provide the designer with a useful tool to test their design. The way these curves are represented mathematically is important for the applicability of these curves in the design process and, indirectly to the results of the fire safety analysis [12].

Regardless of what the design fire curves represent and how they are used, there is a great variety in the way they are mathematically expressed. In reality, the design fire curves represent an idealization of a real fire that might occur. The design fire curves used for tunnels include different types of fire growth rates, for example, linear growth ($\propto t$), quadratic growth ($\propto t^2$) or exponential ($\propto (1-e^{-t})\cdot e^{-t}$)). These growth functions can be combined with a maximum HRR value ($\dot{Q}_{max}$) and a decay function ($\propto t$ or e^{-t}) [12]. In building fire safety design, usually the growth rate alone ($\propto t^2$) is considered when growing fires are the unique fire scenario to be dealt with, whereas in tunnels the entire fire curve is considered.

Using different types of growth and decay rates combined with maximum HRR profiles as peak values or plateau periods means that the curve has to be represented mathematically for different time periods. The use of discontinuous equations means that the design curve is mathematically difficult to apply in the design process. A more convenient way would be to describe the design fire curve with a single mathematical expression. This would make the design process more simple, flexible and reliable [12]. In the following, different ways to represent a design fire are presented.

6.2 Design Fire Methods

6.2.1 Constant Values for Design Fires

The design values found in different guidelines or standards for road tunnels vary considerably depending on type of the vehicle. In Table 6.1, some constant design fire values for smoke control systems are given in MW. The design values are based on experimental data and consensus among members of technical committees working with these documents. The values represent well what has been found from experimental data. The HGV values vary most but that is also the case in the experimental data (13–202 MW). The variation in values for tanker fires can be explained by the fact that no experiments with tanker fires have been performed.

Design fire values were proposed by the UPTUN research project [13, 14]. It was used as input to other work packages within the project. The proposal is presented in

Table 6.1 Examples of design fires in MWs for road tunnels

Vehicle type	PIARC [1]	French [11]	Germany [4]	NFPA 502 [2]
Passenger car	2.5–5	2.5–5	5–10	5
Multiple passenger cars	8	8	5–10	15
Van	15	15		
Bus	20	20	20–30	30
HGV/lorry	20–30	30	20–30	150
Tanker	100	200	50–100	300

Table 6.2 Fire scenario recommendation, UPTUN WP2 proposal [14, 15]

		HRR (MW)	Road, examples vehicles	Rail, examples vehicles	Metro, examples vehicles	At the fire boundary
		5	1–2 cars			ISO 834
Risk for life	Risk for construction	10	Small van, 2–3 cars, ++	Electric locomotive	Low combustible passengers carriage	ISO 834
		20	Big van, public bus, multiple vehicles		Normal combustible passengers carriage	ISO 834
		30	Bus, empty HGV	Passengers carriage	Two carriages	ISO 834
		50	Combustibles load on truck	Open freight wagons with lorries	Multiple carriages (more than two)	ISO 834
		70	HGV load with combustibles (approx. 4 tonne)			HC
		100	HGV (average)			HC
		150	Loaded with easy comb. HGV (approx. 10 tons)			RWS
		200 or higher	Limited by oxygen, petrol tanker, multiple HGVs	Limited by oxygen		RWS

Table 6.2 and is based on information obtained from test data such as that given in Chaps. 3–5. It covers road, rail and metro tunnels. The UPTUN proposal suggests distinguishing between:

a. Fire scenarios where tunnel users, rescue teams and installed equipment necessary to provide safe evacuation and rescue operations (human safety) are at risk, and

Table 6.3 Design fire values in MWs used in different tunnel projects

Vehicle type	Used design values in different tunnel projects	Deutsche Bahn AG [5]
Locomotive	7, 12, 20, 25, 30	20
Rail car	2, 5, 10, 15, 25, 35, 40, 80	25
Metro	8, 15, 30	
Freight car	8, 52	8 (closed wagons), 52 (open wagons)

b. protection of the tunnel boundary to avoid structural collapse, unwanted fire and smoke spread by ventilation ducts or fire doors (fire resistance).

For (a) human safety, fire scenarios in terms of HRR were recommended, while for (b) fire resistance, time–temperature curves were recommended. This approach follows how fire safety is regulated in the building regulations and allows the application of some commonly accepted methods for the classification of fire resistance. In general, the UPTUN recommended several fire scenarios to be used for risk analysis of tunnel fire safety. Small fires may cause other problems that are not for larger fires. In risk analysis, it is significant to know how all possible scenarios contribute to the overall hazard. For (a) human safety, all proposed scenarios from 5 MW up to the actual design fire are recommended to be considered in risk analysis.

The following fire growth rate ($\alpha_{g,L}$), where L means linear, was recommended by the UPTUN:

- Peak HRR of fire $\leq$ 30 MW, $=> \alpha_{g,L} = 10$ MW/min
- Peak HRR of fire > 30 MW, $=> \alpha_{g,L} = 20$ MW/min

It was proposed that the duration of the fire to be determined by the amount of available combustible material (E_{tot}), where 100 % fuel consumption (80 % combustion efficiency) was assumed. The amount of fuel should be evaluated for each study and depend on the type of vehicles, load and traffic pattern. In particular, stationary traffic can have a large influence on the amount and availability of combustible material. For (b) fire resistance, only three curves were recommended, ISO 834 [16], the Hydrocarbon Curve (HC) [17] and the RWS-curve [18]. The same method to determine the duration applies for type a) scenarios [15].

There are no guidelines or standards available for rolling stocks given concrete design values in MWs. Designers work with time–temperature curves, smoke production in m^3/s or energy content in GJ [5], but often design fires in MWs are engineered for individual project. In Table 6.3, a summary of design values used in different tunnel projects are given. These values are not referred to as they are based on discussion with tunnel designers and from different presentations given at conferences. The purpose of presenting them here is to show the variety in the values used for design of the ventilation and egress systems. Values obtained by the Deutsche Bahn AG [5] are given for comparison in Table 6.3. Further, in Chap. 4, it has been shown that the experimental maximum HRR values for rolling stocks varies between 7 to 77 MW, where most of them were lower than 50 MW, which corresponds well to the range of values found in Table 6.3.

6.2.2 Time Dependent Methods for Design Fires

Time dependent design fire curves can be divided into three main types: linear curves, quadratic curves and exponential curves. In each case, this description can refer both to the growth and decay periods and can be combined in different ways. Three notable examples are described in more detail below [12] and in Table 6.4.

Linear Curve–Linear growth and decay with constant maximum period: The French tunnel recommendations [11] for fire ventilation assume a time dependency of HRR with a linear growth from zero to time t_{max}, a constant maximum HRR value to the time t_D, which is the time when the HRR starts to decay, and finally a linear decrease from the maximum HRR value to zero to the time t_d, which is the total duration time.

Quadratic Curve–Quadratic growth and exponential decay with constant maximum period: Ingason [10] proposed a time-dependent design fire curve for different types of vehicle with a quadratic growth from zero to time t_{max}, a constant maximum HRR value to the time t_D and finally an exponential decrease from the maximum HRR value to zero at infinity. If $t_D \le t_{\max}$, then no constant maximum HRR period is obtained. A new value of maximum HRR is calculated, see Table 6.4, and $t_{max} = t_D$.

Exponential Curve–Exponential growth and decay period: Ingason [19, 20] proposed a method to estimate the HRR given as a single exponential function of time instead of as three functions for different time interval. Ingason's work is based on the original work by Numajiri and Furukawa [21] and it is only applicable to fuel-controlled fires and fires with a small or negligible constant peak HRR period. The design parameters are the maximum HRR ($\dot{Q}_{max}$), the total calorific value (E_{tot}) and the parameter (n), which is an arbitrary chosen parameter with no physical meaning. Based on these parameters, t_{max} and t_d can be calculated, see Table 6.4. Other parameters are r and k, which are calculated based on the input parameters $\dot{Q}_{max}$ and E_{tot}. A further presentation of this equation is given in more detail later, see Eq. (6.1).

The mathematical expressions for these curves are summarized in Table 6.4. The index max refer to the maximum or peak values, the index D refer to the time when the decay period starts, the index d refer to the total fire duration, g refer to the growth period, L refer to a linear period, q refer to a quadratic period and *tot* refer to the total. The time is in seconds and the HRR is in kW (kJ/s). χ is the combustion efficiency and β_d is the ratio between the integrated energy at time t_d, (E_{tot,t_d}), and the total energy released (E_{tot}) and can be arbitrarily chosen. E_{tot,t_d} is always less or equal to the total calorific value E_{tot} and if they equal then $\beta_d = 1$ according to the definition.

In Table 6.5, data on the French design curves are given as an example of linear curves. The linear fire growth rate ($\alpha_{g,L}$) and linear decay rate ($\alpha_{D,L}$) have been calculated based on the given data given in Table 6.5. Note that the E_{tot} values in Table 6.5 have been partly recalculated. In order to obtain the same time specifications for t_{max}, t_D and t_d as given in references [13, 11] the value of E_{tot} had to be slightly changed when using the equations in Table 6.4 [12]. The original E_{tot} values in reference [11] are given in brackets. Also, note that $\dot{Q}_{max}$ is given in MW and

Table 6.4 Summary of mathematical description of different methods to describe a complete design curve for tunnel [12]

Curve identity method	HRR (kW) as a function of time t (s)	Time interval (s)	Time to maximum HRR t_{max} (s)	Time to decay, t_D (s), and/or fire duration, t_d (s)	Other conditions
Linear curve Linear growth and decay	$\dot{Q}(t) = \alpha_{g,L} t$	$0 \le t_{\max}$	$t_{\max} = \dfrac{\dot{Q}_{\max}}{\alpha_{g,L}}$	$t_D = \dfrac{2E_{tot}}{\dot{Q}_{\max}} + t_{\max} - t_d$	
	$\dot{Q}(t) = \alpha_{g,L} t_{\max} = \dot{Q}_{\max}$	$t_{\max} < t < t_D$		$\alpha_{D,L} = \dfrac{\dot{Q}_{\max}}{(t_d - t_D)}$	
	$\dot{Q}(t) = \dot{Q}_{\max} - \alpha_{D,L}(t - t_D)$	$t_D < t < t_d$			
Quadratic curve Quadratic growth and exponential decay	$\dot{Q}(t) = \alpha_{g,q} t^2$	$0 \le t_{\max}$	$t_{\max} = \sqrt{\dfrac{\dot{Q}_{\max}}{\alpha_{g,q}}}$	$t_D = \dfrac{E_{tot}}{\dot{Q}_{\max}} + \dfrac{2}{3} t_{\max} - \dfrac{1}{\alpha_{D,q}}$	If $t_D \le t_{\max}$ no constant period, then $\dot{Q}_{\max} \approx \chi \alpha_{D,q} E_{tot} \left(1 - \dfrac{\alpha_{D,q}^{3/2}}{6} \sqrt{\dfrac{\chi E_{tot}}{\alpha_{g,q}}}\right)^2$ $t_{\max} = \sqrt{\dfrac{\dot{Q}_{\max}}{\alpha_{g,q}}} = t_D$
	$\dot{Q}(t) = \alpha_{g,q} t_{\max}^2 = \dot{Q}_{\max}$	$t_{\max} < t < t_D$			
	$\dot{Q}(t) = \dot{Q}_{\max} e^{-\alpha_{D,q}(t - t_D)}$	$t \ge t_D$			
Exponential curve Exponential growth and decay	$\dot{Q}(t) = \dot{Q}_{\max} \cdot n \cdot r \cdot (1 - e^{-k \cdot t})^{n-1} \cdot e^{-k \cdot t}$	$t \ge 0$	$t_{\max} = \dfrac{\ln(n)}{k}$	$t_d = -\dfrac{1}{k} \cdot \ln(1 - \beta_d^{\frac{1}{n}})$ $\beta_d = E_{tot,t_d} / E_{tot}$	$n \approx 0.74294 e^{(2.9 \dot{Q}_{\max} t_{\max} / E_{tot})}$ $r = (1 - \dfrac{1}{n})^{1-n}$ $k = \dfrac{\dot{Q}_{\max}}{E_{tot}} \cdot r$

Note $\dot{Q}_{max}$ (kW), E_{tot} (kJ), $\alpha_{g,L}$ (kW/s), $\alpha_{D,L}$(kW/s), $\alpha_{g,q}$ (kW/s^2), $\alpha_{g,D}$ (s^{-1}), t (s), t_D (s), t_d (s) and t_{max} (s)

Table 6.5 Complementary data on design fire curves for road tunnels based on French regulations [13, 11]. These values are input parameters for the linear curve in Table 6.4

Type of vehicle	E_{tot} [a] (GJ)	Q_{max} (MW)	t_{max} (min)	t_D (min)	t_d (min)	$\alpha_{g,L}$ (kW/s)	$\alpha_{D,L}$ (kW/s)
2–3 cars, tunnel height ≤ 2.7 m	17 (15)	8	5	25	45	26.7	6.7
1 van, tunnel height ≤ 3.5 m	38 (40)	15	5	35	55	50.0	12.5
1 HGV[b], tunnel height > 3.5 m, no so-called 'hazardous goods'	144 (150)	30	10	70	100	50.0	16.7
1 HGV with high calorific potential[c], tunnel height > 3.5 m, no so-called 'hazardous goods'	450	100	10	70	90	166.7	83.3
One tanker, clearance height > 3.5 m, hazardous goods	960 (1000)	200	10	70	100	333.3	111.7

[a] E_{tot} modified values (original values given in bracket)
[b] *HGV* heavy goods vehicles
[c] Defined in reference [13]

Table 6.6 Proposed design values for creation of design fires for traffic tunnels by Ingason [10]. These values are input parameters for the quadratic curve in Table 6.4

Type of vehicle	Q_{max}(MW)	$\alpha_{g,q}$ (kW/s^2)	$\alpha_{D,q}$ (s^{-1})
Car	4	0.01	0.001
Bus	30	0.1	0.0007
Truck[a]	15–130	–	–
Train[b]	15	0.01	0.001
Subway car[c]	35	0.3	0.001

[a] The fire load of a truck may vary greatly
[b] Steel body
[c] Aluminium construction

E_{tot} in GJ in Table 6.5, whereas one should use kW and kJ in the equations given in Table 6.4. The time values (t_{max}, t_D and t_d) in Table 6.5 are given in minutes whereas seconds should be applied for the equations given in Table 6.4.

In Table 6.6, proposed design fires using quadratic curves is presented for traffic tunnels [10]. It was assumed that the design parameters for the quadratic curve should be considered as guidelines for the designers, and that they may need to be adjusted when more experimental data become available. No allowance was made for the possible spread of fire between different vehicles, nor for the possible effects of vitiation on HRR development.

Example 6.1 Plot three different design fire curves using the equations in Table 6.4 for linear, quadratic and exponential curves. Assume a metro wagon that ignite and burns for 60 min. The maximum HRR is 30 MW($\dot{Q}_{max}$ = 30 000 kW) and the total

calorific value is 60 GJ (E_{tot} = 60,000,000 kJ). The time to reach a maximum value for linear and quadratic curves is estimated to be 13 min, followed by a constant period up to time t_D, that is, the time when it starts to decay. For the exponential curve there exists no constant period, so t_{max} is set to 18 min, which is reasonable value in order to obtain the same fire growth as the other two curves. The $\alpha_{D,q}$ for the quadratic equation is set to 0,001 s^{-1}, in accordance to Table 6.6 for a metro wagon.

Solution: The input for the different curves is as follows:

Linear curve:

$$t_d = 60 \text{ min}, \ \alpha_{g,L} = \dot{Q}_{\max} / t_{\max} = 30000 / 780 = 38.5 \text{ kW/s},$$

$$t_D = \frac{2E_{tot}}{\dot{Q}_{\max}} + t_{\max} - t_d = 2 \times \frac{60000000}{30000} + 13 \times 60 - 60 \times 60 = 1200 \ s = 20 \text{ min},$$

$\alpha_{D,L} = \dfrac{\dot{Q}_{\max}}{(t_d - t_D)} = \dfrac{30000}{(60-20)\times 60} = 12.5$ kW/s. *Thus the linear curves to be plotted can be expressed as follows:*

$$\dot{Q}(t) = 38.5 \cdot t, \ 0 \le 780 \ s$$

$$\dot{Q}(t) = 30000, \ 780 \ s < t < 1200 \ s$$

$$\dot{Q}(t) = 30000 \cdot e^{-12.5(t-1200)}, \ t \ge 1200 \ s$$

Quadratic curve:

$$\alpha_{g,q} = \frac{\dot{Q}_{\max}}{t_{\max}^2} = \frac{30000}{(780)^2} = 0.049 \ \text{kW/s}^2$$

$$t_D = \frac{E_{tot}}{\dot{Q}_{\max}} + \frac{2}{3} t_{\max} - \frac{1}{\alpha_{D,q}} = \frac{60000000}{30000} + \frac{2}{3} 780 - \frac{1}{0.001} = 1520 \ s = 25 \text{ min}$$

and $\alpha_{D,q} = 0.001 \ s^{-1}$*, which was given earlier. Thus the quadratic curves to be plotted are as follows:*

$$\dot{Q}(t) = 0.049 t^2, \ t \le 780 \ s$$

$$\dot{Q}(t) = 30000, \ 780 \ s < t < 1520 \ s$$

$$\dot{Q}(t) = 30000 \cdot e^{-0.001(t-1520)}, \ t \ge 1520 \ s$$

Exponential curve:

$$n \approx 0.74294 \cdot e^{(2.9 Q_{\max} t_{\max} / E_{tot})} = 0.74294 \cdot e^{(2.9 \times 30000 \times 18 \times 60 / 60000000)} = 3.6,$$

$$r = (1 - \frac{1}{n})^{1-n} = (1 - \frac{1}{3.6})^{(1-3.6)} = 2.33$$

$$k = \dot{Q}_{\max} r / E_{tot} = 30000 \times 2.33 / 60000000 = 0.0012$$

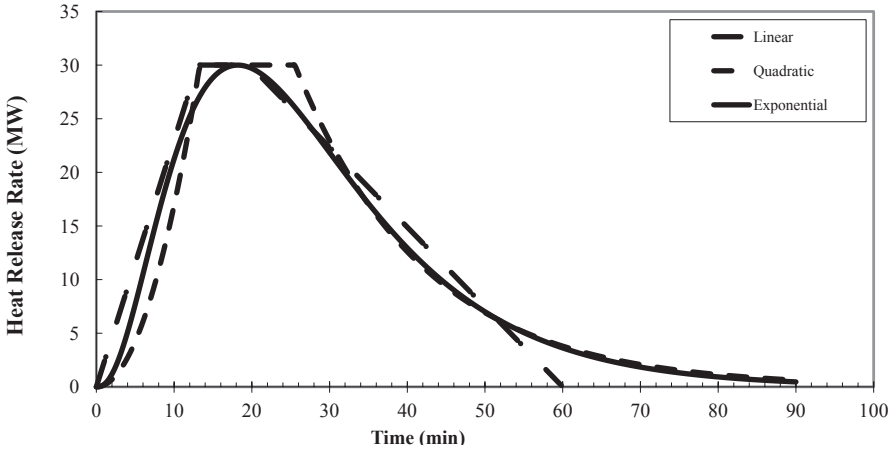

Fig. 6.1 Comparison of three different mathematical representation of a design fire curves from Table 6.4 and Example 6.1

The exponential curve can now be expressed in the following:

$$\dot{Q}(t) = 30000 \times 3.6 \times 2.33 \times (1 - e^{-0.0012t})^{(3.6-1)} \times e^{-0.0012t}, \; t \geq 0.$$

Now it is possible to plot three different design fire curves. In Fig. 6.1*, the results are shown for these three curves*.

The main advantage of working with the exponential curve as compared to the other two is that it is represented by one single mathematical equation and it is continuous for the entire time period. It also tends to follow better experimental data compared to the discontinuous formulations of the linear and quadratic equations. As it is only represented by one equation for the HRR, it is easy to sum up if multiple objects are considered when constructing a new design fire. Further advantage is that, it is very easy to describe a long incipient time by varying the n factor.

6.3 Exponential Design Fire Curve Method with Superposition

Hansen and Ingason [22, 23] applied the exponential curve concept presented in Table 6.4 for sum up of multiple objects in order to create a single curve. The design parameters were the maximum HRR ($\dot{Q}_{\max,i}$) for the individual object *i*, the total energy content $E_{tot,\,i}$ and the retard index (n_i), which is an arbitrarily chosen parameter with no physical meaning. Methods were explored to estimate the time to ignition of secondary objects, using physical models for fire spread. A critical heat flux as ignition criteria was compared to a method using critical ignition temperature. The time to ignition of secondary objects made it possible to estimate the value of n_i.

The time to the maximum HRR ($t_{max,\,i}$) and the fire duration ($t_{d,\,i}$) could also be calculated. The model also includes parameters such as the amplitude coefficient (r_i) and the time width coefficient (k_i), which are calculated based on the input parameters the maximum HRR and the total energy content value for each object.

The method uses the following equation when calculating the sum of all individual HRR from each component taking part in the fire development [22]:

$$\dot{Q} = \sum_i \dot{Q}_{\max,i} \cdot n_i \cdot r_i \cdot (1 - e^{-k_i \cdot t})^{n_i - 1} \cdot e^{-k_i \cdot t} \tag{6.1}$$

where

$$r_i = \left(1 - \frac{1}{n_i}\right)^{1-n_i}, k_i = \frac{\dot{Q}_{\max,i}}{E_{tot,i}} \cdot r_i, t_{\max,i} = \frac{\ln(n_i)}{k_i}$$

The above equation is enough for construction of a design fire, however, it needs an iterative calculation. Instead of using the equation for $t_{max,\,i}$, the retard index, n, could be approximately estimated using the following equation:

$$n_i \approx 0.74294 \cdot e^{(2.9 \dot{Q}_{\max,i} t_{\max,i} / E_{tot,i})} \tag{6.2}$$

Note that Eq. (6.2) is only an appxoimate solution of parameter n. The value of n should always be checked. For large values of n, large errors could be introduced. In such cases, only Eq. (6.1) should be used. The design fire curve method using Eq. (6.1) has been employed to make design fires for metro and tram carriages [24]. The results are presented in Sect. 6.3.3 and 6.3.4, respectively.

In the following, a short presentation of a method proposed by Li and Ingason [24] for calculation of the design parameters $\dot{Q}_{\max,i}$ and $E_{tot,\,i}$ is presented.

6.3.1 Determination of Design Fire Scenarios

The determination of fire scenarios has a great influence on the design fire. The related key parameters include ignition source, fuels available and geometry of the vehicle. Creation of a design fire is always a cost-effective problem, depending on the targeted safety level for the specific vehicle or tunnel.

In some scenarios, the fire could not become fully developed and the maximum HRR could be very low. For example, a 150 kW gas burner placed beside a seat consisted of fire retardant materials in a train carriage could be ignited but not burn after the gas burner is removed. However, in case of a large ignition source, for example an arson fire, the fuels in the carriage could probably be ignited immediately and the fire could spread to the neighboring fuels after a short time. This fire spread from the ignition source to neighboring fuels is defined as the critical fire spread for carriage fires [25]. After the critical fire spread occurred, the fire normally is able to spread easily along the carriage [25]. For conservative reasons in engineering applications, it can be assumed in most cases that the fire finally becomes fully developed, especially in case of lack of information.

6.3.2 Maximum Heat Release Rate

Full scale fire tests are the best way to obtain valuable information about maximum HRR. Available information on measured HRR from all the major large scale fire test series with vehicles can be found in Chaps. 3, 4 and 5. In Chap. 4, the summary of available experimental data shows that the peak HRR for single vehicle fires (passenger cars) can vary from 1.5 to 8 MW, where most were lower than 5 MW. The variation in HRR for two-vehicle fires was 5.6 to 10 MW, and for three-vehicle fires it varies from 7 to 16 MW. In 95 % of the cases the HRR is less than 10 MW. It was also stated that there are not many bus fire tests performed and therefore the uncertainty for the bus fire data is high. The peak HRR was found to be in the order of 25 to 30 MW. For HGVs (heavy goods vehicles) it was found that the highest measured maximum HRRs were obtained for the HGV trailers (single) with a solid combustible such as wood and plastic pallets. The peak HRR was in the range of 13 to 202 MW, whereas when projected on exposed fuel area it varied within a much smaller range, or 0.2–0.5 MW/m^2. The maximum HRR per unit fuel surface area for other types of vehicles varied in a narrower range, or between 0.2 and 0.4 MW/m^2. Measurements of maximum HRRs for rail and metro vehicles show that the peak HRR was in the range of 7 to 77 MW and for exposed fuel area varies between 0.2–0.4 MW/m^2.

However, in engineering applications, the fire scenarios and the fuels differ from one to another. Therefore, the full scale test data only acts as good references. Instead, theoretical models could be a good option to estimate the maximum HRR in such cases. Li et al. [25, 26] investigated the correlations between different scales of metro carriage fire tests in the framework of the METRO project [27], and proposed a simple model to estimate the maximum HRR for a fully developed metro carriage fire, and which has been proved to be able to correlate all the test data in different scales very well. The maximum HRR in a carriage fire is mainly related to the type and configuration of the fuels, the effective heat of combustion and the heat of pyrolysis. The maximum HRR for a fully developed carriage fire, $\dot{Q}_{\max}$ (MW), can be expressed as:

$$\dot{Q}_{\max} = \sum_i \min\left(1.85\dot{m}_a \sum_i \frac{\chi_{r,i}\Delta H_{c,i}}{L_{g,i}}, \dot{m}''_{f,\max,i} A_{f,i}\Delta H_{c,i}\right) \tag{6.3}$$

where the fraction of heat absorbed by the ith surface, $\chi_{r,i}$, in the above equation is defined as:

$$\chi_{r,i} = \chi_r \frac{A_i}{A_t} \tag{6.4}$$

and the maximum possible mass flow rate through openings:

$$\dot{m}_a = 0.5\sum_i A_{o,i} H_{o,i}^{1/2} \tag{6.5}$$

where $A_{o,i}$ and $H_{o,i}$ are the area (m^2) and the height (m) of ith opening respectively. X_r is the fraction of heat absorbed by the fuel surfaces in the total energy released inside the carriage, which has been found to be 0.23 in these scenarios. $X_{r,i}$ is the fraction of heat absorbed by the ith fuel surfaces A_i, $\Delta H_{c,i}$ is the heat of combustion (MJ/kg), L_g is the heat of pyrolysis (MJ/kg), A_i is the ith surface area and A_t is the total surface areas exposed to the internal flame and it is the sum of individual surface area A_i. The total surface area includes all fuel surfaces including interior wall surfaces. The physical meaning of the fraction $X_{r,i}$ is the heat from the combustion flame inside the carriage which is absorbed by the ith fuel surface. The fraction of heat absorbed by the ith fuel surfaces could be zero at some location where no fuel is left, for example a wall fully covered by insulating materials.

Note that although Eq. (6.3) was proposed for carriage fires, it in reality is a general equation for estimating the HRRs in tunnel fires, with the exception of ventilation controlled tunnel fires where the tunnel ventilation controls the fire size (This can be checked easily, see Chap. 2). Based on the term on the right hand side of Eq. (6.3), the HRR per unit fuel area (HRRPUA) can be defined as:

$$HRRPUA = \sum_i \dot{m}''_{f,\max,i} \Delta H_{c,i} \tag{6.6}$$

In estimation of the maximum HRR for one specific fuel, the exposed heat flux generally needs to be predetermined. Note that, in fully developed carriage fires, the maximum gas temperature normally in a range of 800 to 1000 °C, corresponding to a maximum radiation heat flux of around 75 to 150 kW/m^2. Li et al. [24] assumed that the value of 75 kW/m^2 could be used as an average effective value for all the exposed fuel surfaces, which also partly due to that data corresponding to this heat flux can be easily obtained from cone calorimeter tests. In case of lack of information, the values of HRRPUA for different fuel types proposed in Tables 4.5, 4.7, 4.8 and 4.9 in Chap. 4 could be used.

The availability of doors and windows is a key parameter for design fires of vehicles. The windows could break up while exposed to high heat intensity. Windows breakage due to fires has been studied by many researchers [28–31]. These studies suggest that the failure of the glazing doors and windows depends on many factors including glazing material (including different types of glass and polymer materials and different construction or treatments such as lamination and tempering/toughening), glazing thickness and surface area, glass defects (particularly micro cracks that are influenced by edge treatment) and edge frame material. The failure of a modern tempered glass used in a train carriage could be expected to occur for a gas temperature over 600 °C, or a heat flux over 40 kW/m^2. In design fires for carriages, the windows and doors could be assumed to fail after being exposed to high temperatures while lacking of information.

Example 6.2 Estimate the maximum HRR in a fully developed metro carriage fire, assuming that enough fuels are available inside the carriage (the fire is not fuel controlled). There are six doors (H=2 m, W=1 m) and 20 windows (H=1 m, W=1 m).

Table 6.7 Parameters for estimation of the maximum HRR

Fuels compositions	Fraction A_i/A_t (%)	ΔH_c	L_g
		MJ/kg	MJ/kg
Plywood	21	12.8	0.95
Laminate	57	7.6	2.01
Seat PUR	11	25.3	1.22
Luggage	11	21.4	1. 63

The parameters for the fuels are listed in Table 6.7. The fraction A_i/A_t is the percentage of the surface area for one fuel type in the total fuel surface areas.

Solution: Using Eq. (6.5) gives the total mass flow rate: $\dot{m}_a = 18.5$ *kg/s. Then use Eq. (6.3) to estimate the maximum HRR. Note that we have assumed that enough fuels are available inside the carriage and the fire is not fuel controlled. We directly use the left term in the parenthesis.* $\dot{Q}_{\max} = 1.85 \times 18.5 \times 0.23 \times (0.21 \times 12.8/0.95 + 0.57 \times 7.6/2.01 + 0.11 \times 25.3/1.22 + 0.11 \times 21.4/1.63) = 68.5$ *MW.*

Note that we made an assumption that enough fuels are available. In reality, if the fuel burning rates are known, Eq. (6.3) can be directly used without this assumption by using the right hand term in the parenthesis.

6.3.3 Time to Maximum Heat Release Rate

The time to maximum or peak HRR indicates how fast the fire grows up. The time to maximum HRR differs significantly from one scenario to another. It can be expected to be sensitive to the type, location and size of the ignition source and fuels, and the geometry of the vehicle.

The time to maximum HRR could be determined from the full scale test data. In Chap. 4, the summary of available experimental data shows that for single vehicle fires (passenger cars), the time to peak HRR varies between 8 and 55 min for single cars. In over 80 % of the cases for single cars, the maximum time to peak HRR occurs within 8–30 min and for 60 % of the cases it occurs within 8–20 min.

For bus fires, the time to reach peak HRR was less than 10 min. However, it should be kept in mind that the uncertainty of the bus fire data is high as mentioned earlier.

For the HGV tests it was found that the time to reach peak HRR was in the range of 8–18 min. The fire duration was less than 1 h for all the HGV trailer tests presented. The FGR after reaching 5 MW was nearly linear during all the tests carried out in the Runehamar tunnel 2003 and it varied between 16.4 and 26.3 MW/min [32]. In Chap. 5, it was shown that this is related to the wind aided fire spread inside the fuel stack. This process is clearly linear after reaching a given threshold HRR value.

For rail and metro carriages, measurements of HRRs show that the maximum HRR was in the range of 7–77 MW and the time to reach the peak HRR varied from

5 to 80 min. In the full scale metro carriage tests in Brunsberg tunnel [33] carried out by SP Fire Research, the time to maximum HRR was approximately 13 min in test 2, and 118 min in test 3 (see Chap. 3, Sect. 3.3.12). The reason for this difference was in the type of linings on wall and ceiling that was changed between the tests. In Test 2 the lining were combustible, whereas in Tests 3, the linings were covered with aluminium sheet which, after some time lost it capability to protect the old material behind. The ignition source, which was the same in both tests, corresponded to an arson fire, which supports the rapid increase in the growth period in Test 2 with combustible linings on the wall and ceiling. Li et al. argued that the t_{max} could be chosen as 15 min for such type of train carriage fires, to be on the safe side. Li et al.'s work presented in reference [25, 26] shows that the fires in the Brunsberg tunnel tests in the METRO project behaved as travelling fires after the critical fire spread occurred. In other words, the fire travelled along the carriage at a quite constant speed. This indicates a linear fire growth rate. The flame spread rate along the carriage is around 1.5 to 2 m/min. This information can be used for estimation of time to maximum HRR in the design fire. Due to the similarity in the geometry between a bus carriage and a metro carriage, the mechanism of fire spread along the carriage should be the same, and the results found by Li et al. could also be applied to bus carriage fires.

6.3.4 Energy Content

The total energy content of the fuels determines the duration of a fire, and is also correlated with the maximum HRR, as the integral of the HRR curve with respect to time should equal the total energy content. Accurate estimation of the energy content can be easily made after summarizing the fuels available, as the heat of combustion for a given fuel can be regarded as constant.

6.3.5 Reconstruction of a Large Scale Test

Li and Ingason [24] have reconstructed the fire curve in the METRO test 3 [33] summing up the HRR of individual objects. Based on the data obtained from the METRO test 3, the maximum HRR is 77 MW and the time to maximum HRR is around 118 min. From the fuel load, the energy content is estimated to be 60 GJ. The design fire for the METRO test 3 can therefore be constructed using the Eqs. (6.1) and (6.2). The result is shown in Fig. 6.2. Note that the average time to maximum HRR of 121 min is used rather than the exact time of 118 min to maximum HRR for better correlation. It can be seen that the estimated fire curve correlates very well with the measured fire curve. The maximum HRR could also be estimated using Eq. (6.3) and similar results are obtained.

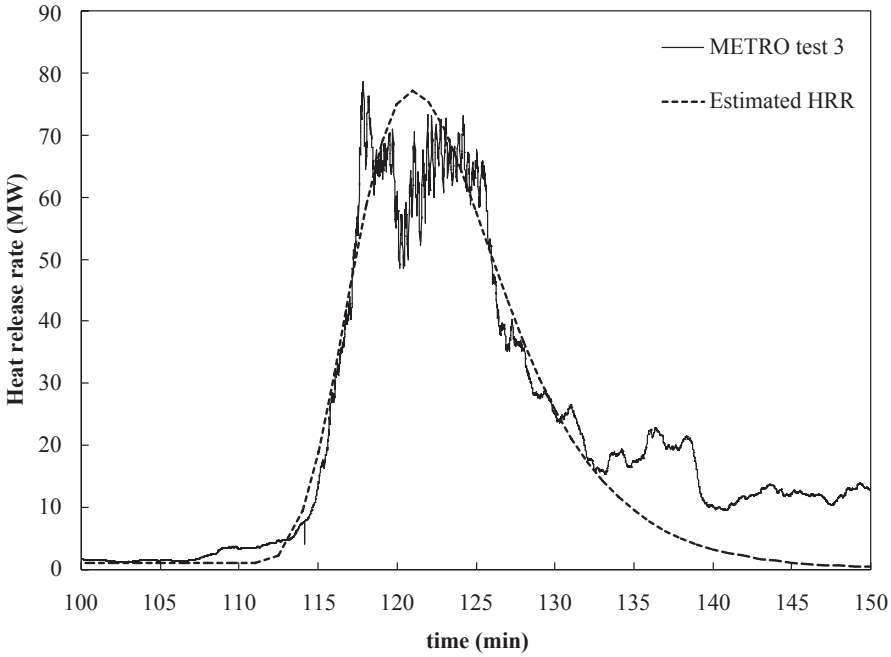

Fig. 6.2 Reconstruction of the METRO Test 3 using the exponential curve method [24]

6.3.6 Design Fire for a Tram Carriage

Li and Ingason [24] presented a construction of a design fire curve using Eq. (6.1) for a modern tram carriage. The tram carriage consisted of six sections with each having a length of 6 m. A tram involves quite limited fuel load and thus the fire usually become fuel-controlled. Equations (6.3)–(6.5) were used for estimation of the maximum HRR for each section of the tram carriage. The key parameters used for individual tram sections are listed in Table 6.8. For each section, the maximum HRR was estimated to be 12 MW and the energy content estimated to be 5 GJ. The difference in time to maximum between neighbouring sections depends on the spread speed. Li et al.'s work [25] shows that for the travelling fires in a carriage, the flame spread rate along the carriage is around 1.5 to 2 m/min. This knowledge was used in the analysis and a 2 m/min was selected as a conservative value. Therefore, the difference in time to maximum HRR between two neighbouring sections was estimated to be 3 min. The key parameter left to determine is the time to maximum HRR for the first section. This time was estimated to be around 10 min to assure that the HRR approximately reaches the maximum HRR at around 15 min.

Figure 6.3 shows the design fire for the tram constructed using Eq. (6.1). The total maximum HRR is 28 MW at 20.3 min. At the beginning of the fire, a HRR of 1 MW was also added as the output from the ignition source and limited fuels nearby. Clearly, it shows that after around 15 min the design fire reaches a plateau, that

Table 6.8 A summary of key parameters for individual sections in a tram [24]

Section no.	Energy content, E (GJ)	Maximum HRR, Q_{max} (MW)	Time to maximum HRR, t_{max} (min)
1	5	12	10
2	5	12	13
3	5	12	16
4	5	12	19
5	5	12	22
6	5	12	25
Sum	30	28	20.3

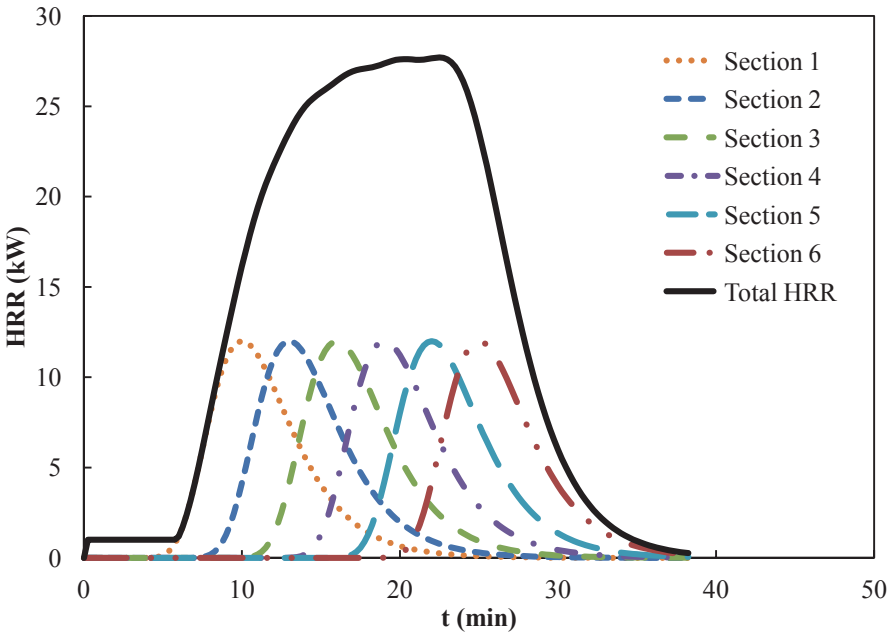

Fig. 6.3 The design fire for a tram using the summation method [24]

is, the HRR reaches 25 MW and keeps at this level for around 10 min. This indicates that an extended carriage length has limited influence on the design fire, that is, the maximum HRR for a longer carriage is approximately the same. We can also compare the design fire obtained to the standard t square curve (t^2) and it can be found that the design fire approximately follows the fast curve before the plateau. Note that the choice of the time to maximum HRR for the first section only affects the time to total HRR, but does not affect the total HRR and the shape of the design fire.

It should be kept in mind that the design fires proposed above are only suitable for the given carriages in the design scenarios defined above, rather than for all

vehicles of the same type and all scenarios. For other carriages and other scenarios, the method proposed can be used to construct their own design fires, depending on the information obtained and some reasonable assumptions.

6.3.7 Design Fire for a Road Vehicle

Similar methods can be used for construction of a HGV trailer fire or other types of vehicles. All important components that contribute to the fire development need to be considered. The main components are the number of tyres, the fuel tanks, interior material inside cabin, electrical cables, liquids, hoses, trailer cover materials, cargo, etc. For most vehicles, it is necessary to determine what the exposed fuel surfaces are and then obtain HRRPUA, for example from Tables 4.5, 4.7, 4.8 and 4.9. In order to calculate E_{tot} values for total mass and combustion efficiency ΔH_{eff} are necessary. In the following, an example is given in order to clarify the calculation process.

Example 6.3 A HGV truck with a trailer stops due to engine problems. The trailer does not carry any cargo but there are six tyres on the trailer. Assume a fire starts at time 12:04, with an ignition in the engine compartment. The $\dot{Q}_{\max,engine}$ is 2 MW, $E_{tot,engine}$ is 0.5 GJ and the time to reach $\dot{Q}_{\max}$ is $t_{\max,engine} = 5$ min. The fire spreads to the two tyres at the front of the truck. The ignition occurs simultaneously in both tyres. For each tire $\dot{Q}_{\max,tyre} = 1$ MW and $E_{tot,tyre} = 1$ GJ and the $t_{\max,tyre} = 15$ min. At the same time as the fire spread to the front tyres, it also spread to the driver cabin. The driver cabin has a fuel surface area of 25 m^2, and the HRRPUA for the cabin is 0.35 MW/m^2. The total amount of combustible material is 250 kg and the average heat of combustion is $\Delta H_{c,eff} = 25$ MJ/kg in the driver cabin. The best estimate is that $\dot{Q}_{\max,cabin}$ will occur $t_{\max,cabin} = 13$ min, that is at 12:17. The fire continues to spread and eventually will warm up the diesel tank behind the driver cabin. The fuel hoses will be destroyed and fuel starts to pour on the road surface. The pool area that is created on the road surface will be 4 m^2 and HRRPUA of the diesel is 1.7 MW/m^2. The $t_{\max,pool}$ is deemed to occur at 15 min. The total amount of diesel is 100 L. The density of diesel is 790 kg/m^3 and the heat of combustion is $\Delta H_{c,eff} = 40$ MJ/kg. At the same time, the fire spread to the tyres at the back of the truck and start to burn at the same time for both tyres. $\dot{Q}_{\max,tyre} = 1$ MW and $E_{tot,tyre} = 1$ GJ for each tyre and the $\dot{Q}_{\max,tyre}$ for both tyres occurs at $t_{\max,tyre} = 25$ min. Finally, the fire spread to all the tyres at the back of the trailer, in total six tyres. Each tyre have $\dot{Q}_{\max,tyre} = 1$ MW and $E_{tot,tyre} = 1$ GJ and $t_{\max,tyre}$ is estimated to occur at 35 min, and all six tyres burn at the same time. Create a design fire curve for the fire scenario described.

Solution: The procedure is done in an excel sheet, and then summed up in accordance to Eq. (6.1). A summary of the key parameters is given in Table 6.9. In Fig. 6.4, the HRR for each component/object is shown and the total HRR. Following values have been calculated by use of Eqs. (6.1) and (6.2):

Table 6.9 A summary of key parameters for individual parts

Object	$\dot{Q}_{\max}$ (MW)	E_{tot} (GJ)	$t_{\max}$ (min)	n_i	r_i	k_i
Engine	2	0.5	5	24.1	2.66	0.0106
2x tyre front-truck	2	2	15	10.1	2.58	0.0026
Cabin	8.75	6.26	13	17.6	2.64	0.0037
Diesel pool	6.8	3.2	15	298.5	2.71	0.0062
2x tyres back- truck	2	2	25	57.6	2.69	0.0027
6x tyres trailer	6	6	35	328	2.71	0.0027

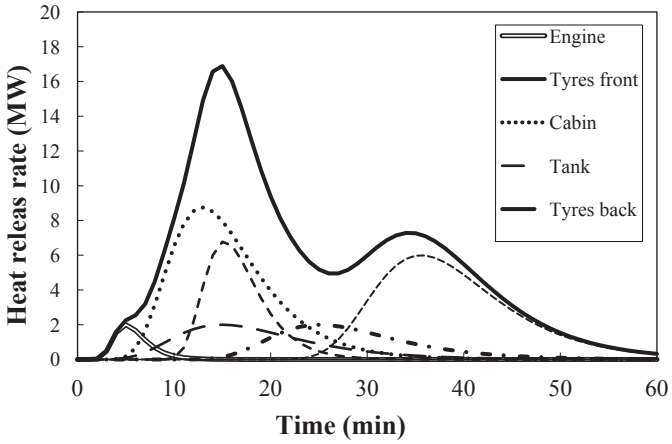

Fig. 6.4 The design fire curve for Example 6.3, with a HGV truck and an empty trailer

$E_{tot,cabin} = 250\ \text{kg} \times 25\ \text{MJ/kg} = 6250\ \text{MJ} = 6.25\ \text{GJ}$ and $E_{tot,pool} = 0.1\text{m}^3 \times 790\text{kg/m}^3 \times 40\ \text{MJ/kg} = 3200\ \text{MJ} = 3.2\ \text{GJ}$. The parameter n_i is calculated by Eq. (6.2).

6.4 New Concept for Design Curves

A new concept for design fires in tunnels was presented by Ingason and Li [34]. The concept is based on a simple engineering approach accounting for important geometrical and physical variables of the tunnel and the fuel. The engineering equations originate from the calculation of critical conditions inside the tunnel such as visibility, velocity and maximum ceiling temperature. The concept leads to a range of minimum design fires given in megawatts (MW) for a specific tunnel.

Important geometrical parameters that were identified include tunnel height and tunnel width. The fuel geometry, height above the road surface and projected area of the fuel, are also important. For evacuation, the visibility is the first parameter to become critical. Other important parameters relating to ventilation and construction include the critical velocity and maximum temperature beneath the ceiling. In order

to identify the limits for the range of design fires, it was decided to use the following critical conditions:

1. Visibility in the tunnel (see Chap. 14). It is possible to identify a HRR for a given critical visibility, assuming that tunnel users cannot find their way out or the escape path is too long and therefore they will be exposed to a toxic environment for a long time.
2. Critical velocity (see Chap. 13). The critical velocity is defined as the minimum longitudinal ventilation velocity to prevent reverse flow of smoke from a fire (back-layering) in the tunnel. There exists correlations which show that above a certain longitudinal velocity, the critical velocity will not change, independent of the HRR [35]. This approach has been used to find a minimum HRR related to a critical velocity.
3. Maximum ceiling temperature (see Chap. 8). Above a certain HRR from a single vehicle burning, the maximum temperature beneath the ceiling will not change [36]. In the present study, an excess temperature of 1350 °C was used as the highest constant ceiling temperature. This approach yields the minimum design fire related to temperature exposure to the ceiling from a single burning vehicle.

6.4.1 Theoretical Aspects

Following equation was developed for (1) visibility:

$$\dot{Q}_{vis} = Q^*_{vis}\rho_o c_p T_o u W H \tag{6.7}$$

where

$$Q^*_{vis} = \frac{2}{V_{is}\ln 10 D_{mass}}\frac{H_c}{\rho_o c_p T_o}$$

and u is the velocity in m/s, c_p is the specific heat of air at constant pressure (kJ/kg K), T_o is the ambient temperature (K), ρ_o is the ambient density (kg/m^3) and $A = WH$ is the cross-sectional area (m^2) (H is the tunnel height (m) and W is the tunnel width (m)). The visibility V_{is} (m) and mass optical density D_{mass} (m^2/kg) are described in details in Chap. 14.

Following equation was developed for (2) critical velocity:

$$\dot{Q}_{cv} = Q^*_{cv}\rho_o c_p T_o g^{1/2} H^{5/2} \tag{6.8}$$

where $Q^*_{cv} = \dfrac{\dot{Q}}{\rho_o c_p T_o g^{1/2} H^{5/2}}$, $\dot{Q}$ is the total HRR (kW) and g is the gravitational acceleration (m/s^2).

The following equation was developed for (3) maximum excess ceiling gas temperature:

$$\dot{Q}_T = \begin{cases} \left(\dfrac{\Delta T_{\max}}{17.5}\right)^{3/2} H_{ef}^{5/2}, & V' \le 0.19 \\ \Delta T_{\max} u b_{fo} H_{ef}^{5/3}, & V' > 0.19 \end{cases} \tag{6.9}$$

where $V' = u / \left(\frac{g\dot{Q}}{b_{fo}\rho_o c_p T_o} \right)^{1/3}$.

Equation (6.9) relates to the maximum excess temperature $\Delta T_{\max}$ depending on which ventilation region is obtained. The effective tunnel height, H_{ef}, is defined as the height from the bottom of the fuel source to the ceiling, that is $H_{ef} = H - h_{fo}$, where h_{fo} is the height from tunnel floor to bottom of the fuel. For a HGV trailer, h_{fo} can be set to 1.2 m. The effective radius of the fire source, b_{fo} (m), can be obtained by estimating the projected area of the fuel, A_p (m^2), $b_{fo} = \sqrt{A_p / \pi}$. For a HGV trailer this can be the length of the trailer times the width of the trailer.

6.4.2 Calculation

Ingason and Li [34] came up with the following equations depending on the critical conditions for each type of conditions. For (1) visibility, Eq. (6.7) was simplified by using some experimental constant:

$$\dot{Q}_{vis} = 0.15 \cdot \zeta H^{5/2} \tag{6.10}$$

where $\zeta = W/H$ is the aspect ratio, and the critical velocity using Eq. (13.4) was assumed.

For (2) critical velocity, Eq. (6.8) was simplified by using some experimental constants and by using Eq. (13.4):

$$\dot{Q}_{cv} = 0.165 H^{5/2} \tag{6.11}$$

For (3) maximum excess ceiling temperature, Eq. (6.9) was simplified by using some experimental constant and assuming a critical velocity (Eq. (13.4)) in the tunnel:

$$\dot{Q}_T = 11.3 \cdot 10^{-4} \cdot \Delta T_{\max} A_p^{1/6} \sqrt{H} \left(H - h_{fo} \right)^{5/3} \tag{6.12}$$

In Fig. 6.5, Eqs. (6.10)–(6.12) are plotted for a wide range of tunnel heights (H) and widths (W) of tunnels. The input parameters are $A_p = 25$ m^2 (corresponds to 10 m long trailer which is 2.5 m wide), $h_{fo} = 1.2$ m, which is a typical height of the loading area for a HGV trailer and two aspects ratios, $\zeta = 1$–3. The excess ceiling temperature is 1350 °C. The obtained HRRs are the minimum design fire for three different applications and all show a significant influence of the tunnel ceiling height, H. Therefore, this parameter is the single most important parameter for the fire safety design of a tunnel. Other parameters of importance are the tunnel aspect ratio, $\zeta = W/H$ which is important for the visibility but W has no influence on critical velocity and excess ceiling temperature. The geometrical parameters of the fuel, A_p and h_{fo}, were found to be important for the excess ceiling temperature, $\Delta T_{\max}$. In general, the aspect ratio is a parameter that needs to be considered, but its influence varies.

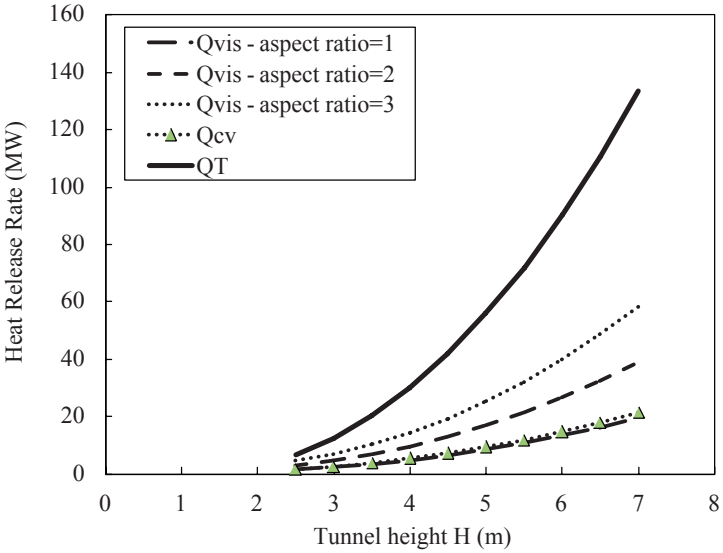

Fig. 6.5 Plot of different design fires for different tunnel heights between 2.5 to 7 m [34]

The lowest HRRs needed to obtain critical conditions in 2.5 m high tunnels is in the range of 2 5 MW. Generally, it was found that the minimum HRRs to obtain critical conditions in 7 m high tunnels varies from 20 to 130 MW. In all cases, the longitudinal velocity in the tunnel corresponds to the critical velocity. This is a very interesting result, as most designers determine their design fires without any type of relation to the geometry of the tunnel or the fuel. The type of vehicle decides the design fire and that can be compared to these results.

Analysis of the equation used in NFPA 502 [2] for critical velocity, Eq. (3.13), where the critical velocity continues to increase as a one third power relation of the HRR, and not becomes constant as with use of Eq. (13.4), indicates that for HRRs above the highest obtained design fire $Q_T = 130$ MW the increase in critical velocity using 130 MW instead of 200 MW for heights varying from 2.5 to 7 m, is in the range of 1–8 %, respectively. If the same comparison is made for an increase from 130 to 300 MW, the change in calculated critical velocity with Eq. (3.13) is 2–13 %. This shows that even for Eq. (3.13) used in the NFPA502 standard, the increase in calculated critical velocity is moderate above the value of 130 MW as a design fire. Consequently, the choice of a design fire higher than 130 MW will not significantly change the results. In the calculations, an aspect ratio $\zeta = 2$ was used.

Of the three different equations derived, Eq. (6.12) yields the highest HRR. This is reasonable and should be considered in the design process for the construction. The equation is also very useful in showing the connection between the HRR and the standardized time–temperatures. To demonstrate this, an example is given in Fig. 6.6 using the standardized time–temperature curves such as ISO, HC and RWS. The corresponding HRR for a tunnel which is 7 m high are calculated. Other parameters used were $h_f = 1.2$ m, $A_p = 25$ m^2 and $T_0 = 20$ °C.

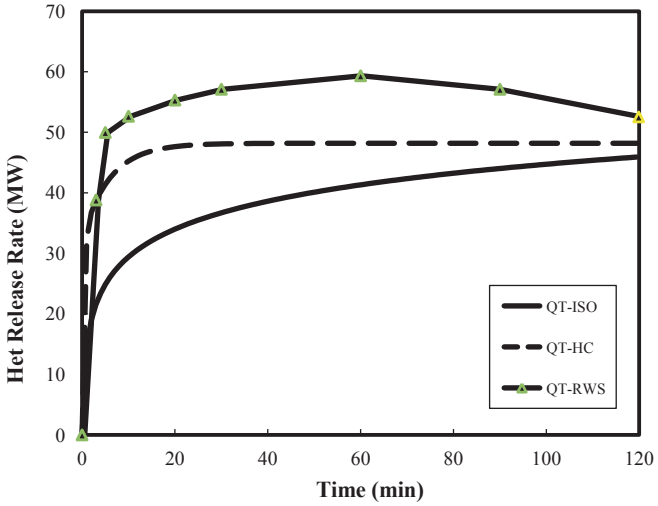

Fig. 6.6 Plot of calculated HRR for some standardized time–temperature *curves* at the critical velocity [34]

The method presented here is very useful tool to estimate the range of minimum design fires for a given tunnel. The values obtained should be put in relation to the actual fire load, that is, the vehicles used in a given tunnel. In other words, an analysis of the potential fire load that will travel through the tunnel should also be carried out. If the tunnel height is relatively low, there is no reason to choose a design fire that is far above the one obtained by the concept given here. On the other hand if the tunnel height is large, there is no reason to choose a design fire that is much lower than the one calculated here, especially if the fire load analysis indicates that the potential for such a fire exists for the tunnel. Altogether, the process has to be put into a context based on the purpose of the design.

6.5 Summary

Design fires are presented for different types of vehicles. Both constant values as well as time dependent values are given. The values correspond well to what is found in the experimental data from different types of tunnels. Mathematical representations of different types of design fire curves are given and discussed. These are linear curves, quadratic curves and exponential curves. The complexity of these expressions varies. Although, the simplest one is the linear representation the equations are discontinuous, and different equations are valid for different periods of the fire development. This representation is most far away from real fire curves obtained from experiments. Improvement is obtained by the quadratic equations, but still it is divided into different equations for different time periods. Although

the exponential curve is the most complicated from the point of view of parameters used, it has the benefit that it can describe the entire fire development. It can also be easily put into a data sheet and used as a summation of numerous objects burning. This makes it easier to reconstruct an entire fire in a vehicle, focusing on each main component that is burning. Examples of such reconstructions are given, with very good results.

Finally, a new concept for design fires is presented which is a very useful tool to estimate the range of design fires for a given tunnel. The minimum values obtained should be put in relation to the actual fire load for a given tunnel. The method shows that the tunnel height is the single most important parameter influencing the choice of a design fire. This is important to consider in the design of tunnel fire protection. Low tunnel heights require lower HRRs to obtain the same conditions as in tunnels with higher tunnel heights. It is possible to use the obtained equations to calculate what HRRs are necessary to obtain a given standardized time–temperature curve for ISO, HC, RWS, RABT or HCM. This provides the key to a clear discussion between designers of ventilation systems and the tunnel construction.

References

1. Fire and Smoke Control in Road Tunnels (1999). PIARC
2. NFPA 502– Standard for Road Tunnels, Bridges, and Other Limited Access Highways (2014). National Fire Protection Association, 2014 Edition
3. Lacroix D Guidelines for Fire Safe Design: Synthesis and Current Harmonisation Processes. In: 1st International Symposium on Safe & Reliable Tunnels, Prague, Czech Republic, 4–6 February 2004. CUR, pp 107–115
4. Richtlinien für Ausstattung und Betrieb von Tunneln (RABT) (1985). Ausgabe 1985 edn. Forschungsgesellschaft für Straßen- und Verkehrswesen
5. Thematic Network on Fires in Tunnels (FIT) – Technical Report Part 1– Design Fire Scenarios (2001–2004). European Commission under the 5th Framework Program
6. Peacock R, Reneke P, Jones W, Bukowski R (1995) Concept for fire protection of passenger rail transportation vehicles:pas, present and future. Fire and Materials 19:71–87
7. Standard for Fixed Guideway Transit and Passenger Rail Systems (2003). 2003 edn. National Fire Protection Association
8. ISO/TS 16733 Fire safety engineering – Selection of design fire scenarios and design fires (2006). International Organisation of Standardization
9. Maevski IY (2011) NCHRP Synthesis 415– Design Fires in Road Tunnels. A Synthesis of Highway Practice. National cooperative highway research program
10. Ingason H Design Fires in Tunnels. In: Conference Proceedings of Asiaflam 95, Hong Kong, 15–16 March 1995. Interscience Communications Ltd., pp 77–86
11. Lacroix D New French Recommendations for Fire Ventilation in Road Tunnels. In: 9th International Conference on Aerodynamics and Ventilation of Vehicle Tunnels, Aosta Valley, Italy, 6–8 October 1997
12. Ingason H (2009) Design fire curves in tunnels. Fire Safety Journal 44 (2):259–265
13. Marlair G, Lemaire T, Öhlin M Fire Scenarios and accidents in the past – Draft final report (1) task 2.1, part 1, UPTUN WP2 Report
14. Opstad K (2005) Fire scenarios to be recommended by UPTUN WP2 Task leader meeting of WP2

15. Ingason H Design fire in tunnels. In: Safe & Reliable Tunnels Innovative European Achievements, Second International Symposium, Lausanne, 2006
16. Fire-resistance tests – Elements of building construction – Part 1: General requirements (1999). First edn. International Organization for Standardization
17. Fire resistance tests – Part 2: Alternative and additional procedures (1999). First edn. European Committee for Standardization
18. Beproeving van het gedrag bij verhitting van twee isolatiematerialen ter bescherming van tunnels bij brand (1979). Instituut TNO voor Bouwmaterialen en Bouwconstructies, Delft, The Netherlands
19. Ingason H Fire Development in Large Tunnel Fires. In: 8th International Symposium on Fire Safety Science, Beijing, China, 18–23 September 2005. International Association for Fire Safety Science (IAFSS), pp 1497–1508
20. Ingason H Modelling of Real World Fire Data. In: 2nd International Symposium on Tunnel Safety & Security (ISTSS), March 15–17, 2006 Madrid, Spain, 2006. pp 7–13
21. Numajiri F, Furukawa K (1998) Short Communication: Mathematical Expression of Heat Release Rate Curve and Proposal of 'Burning Index'. Fire and Materials 22:39–42
22. Hansen R, Ingason H (2012) Heat release rates of multiple objects at varying distances. Fire Safety Journal 52:1–10
23. Hansen R, Ingason H (2011) An Engineering tool to calculate heat release rates of multiple objects in underground structures. Fire Safety Journal 46 (4):194–203. doi:10.1016/j.firesaf.2011.02.001
24. Li YZ, Ingason H A new methodology of design fires for train carriages. In: ISTSS 6th International Symposium on Tunnel Safety and Security, Marseille, 2014.
25. Li YZ, Ingason H, Lönnermark A (2013) Correlations in different scales of metro carriage fire tests. SP Report 2013:13. SP Technical Research Institute of Sweden, Borås, Sweden
26. Li YZ, Ingason H, Lönnermark A Fire development in different scales of a train carriages. In: 11th International Symposium on Fire Safety Science, New Zealand, 2014.
27. Ingason H, Kumm M, Nilsson D, Lönnermark A, Claesson A, Li YZ, Fridolf K, Åkerstedt R, Nyman H, Dittmer T, Forsén R, Janzon B, Meyer G, Bryntse A, Carlberg T, Newlove-Eriksson L, Palm A (2012) The METRO project – Final Report 2010:08. Mälardalen University, Västerås
28. Bowditch P. A., Sargeant A. J., Leonard J. E., Macindoe L. (2006) Window and Glazing Exposure to Laboratory-Simulated Bushfires. CMIT Doc 2006–205. Bushfire CRC, Melbounre, Australia
29. Harada K., Enomoto A., Uede K., T W An experimental study on glass cracking and fallout by radiant heat exposure. In: Fire Safety Science – Proceedings of the 6th International Symposium, London, 3–7 March 2000. IAFSS
30. Mowrer F.W. (1998) Window Breakage Induced by Exterior Fires. National Institute of Standards and Technology, Gaithersburg, MD, USA
31. Strege S. LBY, Beyler C. (2003) Fire Induced Failure of Polycarbonate Windows in Railcars. Fire and Materials
32. Ingason H, Lönnermark A (2005) Heat Release Rates from Heavy Goods Vehicle Trailers in Tunnels. Fire Safety Journal 40:646–668
33. Lönnermark A, Lindström J, Li YZ, Ingason H, Kumm M Large-scale Commuter Train Tests – Results from the METRO Project. In: Proceedings from the Fifth International Symposium on Tunnel Safety and Security (ISTSS 2012), New York, USA, 14–16 March 2012. SP Technical Research Institute of Sweden, pp pp. 447–456
34. Ingason H, Li YZ New concept for design fires in tunnels. In: Proceedings from the Fifth International Symposium on Tunnel Safety and Security (ISTSS 2012), New York, USA, 14–16 March 2012. SP Technical Research Institute of Sweden, pp 603–612
35. Oka Y, Atkinson GT (1995) Control of Smoke Flow in Tunnel Fires. Fire Safety Journal 25:305–322
36. Li YZ, Ingason H (2010) Maximum Temperature beneath Ceiling in a Tunnel Fire. SP Report 2010:51, SP Technical Research Institute of Sweden, Borås, Sweden

Chapter 7
Combustion Products from Fires

Abstract Knowledge of the different species produced during fires is of great importance for estimating the toxicity of the fire gases. In this chapter the main combustion products from different types of fires are presented. This includes carbon monoxide (CO), carbon dioxide (CO_2), hydrogen chloride (HCl), sulphur dioxide (SO_2), volatile organic compounds (VOCs), polycyclic aromatic hydrocarbons (PAHs), polychlorinated dibenzo-p-dioxins and dibenzofurans (PCDDs/PCDFs), total amount of hydrocarbons (THC) and soot/smoke, but yields also for some other species are presented. Results from measurement during fire tests in vehicles and tunnels are summarized and discussed. The importance of the ventilation conditions (equivalence ratio) on the productions of different species is described and relations for different yields and ratios are given and discussed.

Keywords Combustion products · Carbon monoxide · Carbon dioxide · Smoke · Ventilation conditions · Equivalence ratio · Yield · Species

7.1 Introduction

The reason for fatalities in fires is most often due to inhalation of fire gases. In several of the catastrophic fires presented in Chap. 1, people were found dead in their cars. Increased temperature can, however, affect both the physical health and the capacity to escape. Among the fire effluents, carbon monoxide (CO) is seen to be the most important component responsible for causing fatalities, even if the effect of hydrogen cyanide (HCN) has been much discussed during recent years [1–4]. In a comprehensive review, Nelson showed that even if high blood concentrations of HCN were found in fire victims, most fatalities can be explained by the CO concentration [5]. Furthermore, carbon dioxide (CO_2) has an important effect on tenability, not only by being toxic at high levels, but mostly by increasing the uptake of other fire gases, for example, CO, due to increasing the breathing rate.

Even if fire gases do not always lead to fatalities, sublethal effects, for example, incapacitation, reduced egress speed, reduced motor capability, decreased mental acuity, and visual obscuration are also important [6]. Further, many effluents can

H. Ingason et al., *Tunnel Fire Dynamics,* DOI 10.1007/978-1-4939-2199-7_7

cause long-term or chronic effects, which is of particular importance for firefighters and rescue personal.

Another issue becoming increasingly important in the context of fire emissions is the effect on the environment and emissions which may pose potentially long-term hazards to health. Even if they have not typically been considered to be central issues for fires in tunnels, this is an issue related to all fires. More detailed aspects of toxicity and tenability are presented and discussed in Chap. 15.

In the design of tunnel ventilation, even the ventilation of gases in a nonfire situation is an important issue. That is in most cases the main reason why ventilation systems are installed in tunnels in the first place. Traditionally, the concentration of CO exhausted from the vehicles has been used to design the ventilation systems, but because of the development of new vehicles and new fuels, the emissions of CO has decreased significantly [7]. For this reason, concentrations of other species, for examples, NO_x (most often with a guideline concentration for NO_2) have also been included in the design of the ventilation system.

This chapter discusses what species are produced during a fire and how different parameters and conditions, that is, the ventilation conditions and temperature, affect the production. Not only acute toxic species are included in the discussions, but also the production of species interesting for other reasons.

7.2 Combustion and Fire Chemistry

Fire is a field of combustion, often referred to as uncontrolled combustion. Combustion involves a large number of elementary (intermediate) reactions. These different reactions (steps) can be grouped depending on whether or not free radicals are formed or consumed in the reactions. Free radicals are atoms, molecules, or ions that have unpaired valence electrons or an open electron shell and, therefore, in most situations are highly reactive. The following types of reaction can be identified, here exemplified with reactions in the hydrogen–oxygen system [8, 9]:

1. Chain initiating step:

The reaction chain starts with an initiating step where free radicals are formed.

Free radicals (in the reactions marked with a dot) are produced from stable species, for example:

$$H_2 + O_2 = 2\,OH\cdot \tag{7.1}$$

2. Chain propagating (or carrying) steps

A radical reacts with stable species to form a new free radical, for example:

$$OH\cdot + H_2 = H_2O + H\cdot \tag{7.2}$$

3. Chain branching step:

A free radical reacts with a stable species forming two free radicals, that is, the number of free radicals increases, for example:

$$H\cdot + O_2 = OH\cdot + O\cdot \tag{7.3}$$

4. Chain terminating step

Free radicals react to form stable species, that is, free radicals are "consumed", *for example,*

$$2\,H\cdot = H_2 \tag{7.4}$$

Even for relatively simple fuels, there are a large number of elementary reactions, often combined in complex reaction schemes. It is not the aim of this chapter to in detail discuss these elementary reactions. Instead the simplified "global" reaction will be discussed and how this reaction is affected by the fire conditions and how these conditions influences what species are produced during a fire.

If a hydrocarbon fuel, with or without oxygen, is involved in the fire and complete combustion is assumed the following global reaction can be written:

$$C_aH_bO_c + \left(a + \frac{b}{4} - \frac{c}{2}\right)(O_2 + 3.76N_2) \rightarrow aCO_2 + \frac{b}{2}H_2O + \left(a + \frac{b}{4} - \frac{c}{2}\right)3.76N_2 \tag{7.5}$$

In a combustion reaction energy is also released and from the global reaction the heat of combustion can be derived (for example, by assuming all H_2O being released in gas phase). The fuel can also contain other elements (N, S, Cl, Br, etc.). In those cases it must either be known or assumed what species are formed.

In Sect. 7.5, the effect of ventilation conditions on the production of different species is presented. For this often the equivalence ratio, ϕ, is used. To calculate this parameter, the ideal reaction stoichiometric air to fuel ratio for complete combustion, r, can be used. This parameter is defined by:

$$1\,\text{kg fuel} + \text{r kg air} \rightarrow (1 + \text{r})\,\text{kg products} \tag{7.6}$$

For complete combustion it is assumed that there is exactly enough air for the fuel to completely (ideally) react and produce CO_2 and H_2O as described by Eq. (7.5). These conditions are called stoichiometric and the stoichiometric coefficient, r, can be calculated (using the notation in Eq. (7.5)) as[1]:

$$r = \frac{(1+3.76)M_{air}\left[a + (b/4) - (c/2)\right]}{M_C \cdot a + M_H \cdot b + M_O \cdot c} \approx \frac{137.9\left[a + (b/4) - (c/2)\right]}{12 \cdot a + b + 16 \cdot c} \tag{7.7}$$

[1] See also Eq. (2.13).

Table 7.1 Molecular weight of selected species and concentration of main components in air

Species	Molecular weight	Concentration in air (vol-%)	Reference
Carbon dioxide, CO_2	44.010	0.04	[10, 11]
Carbon monoxide, CO	28.010	–	[10]
Carbon, C	12.011	–	[10]
Oxygen, O_2	31.999	20.946	[10, 12]
Nitrogen, N_2	28.013	78.084	[10, 12]
Argon, Ar	39.948	0.934	[12, 13]
Air (dry)[a]	28.967		

[a] Based on the concentrations and molecular weights given in the table

where the molecular weight, M_i, for air and different atoms are given in Table 7.1.

Note that r in some literature is defined as the stoichiometric fuel to air ratio.

The equivalence ratio, ϕ, which is the quotient between the actual fuel/air ratio and the stoichiometric fuel/air ratio, is here defined as[2]:

$$\phi = \frac{\dot{m}_f / \dot{m}_a}{\left(\dot{m}_f / \dot{m}_a\right)_{stoich.}} = \frac{\dot{m}_f \cdot r}{\dot{m}_a} \tag{7.8}$$

where

$\phi = 1$ stoichiometric combustion
$\phi < 1$ well-ventilated combustion
$\phi > 1$ under ventilated combustion

where $\dot{m}_f$ is the mass loss rate of the fuel (kg/s) and $\dot{m}_a$ is the mass flow rate of air (kg/s) and the subscript "stoich" refers to these values under stoichiometric conditions. Note that to calculate ϕ, also the quotient of the actual fuel/oxygen ratio and the stoichiometric fuel/oxygen ratio could be used.

As discussed in Chap. 2, there are different terms used for different ventilation conditions. The situation when more air (oxygen) is available than is needed for stoichiometric combustion, is referred to as overventilated, well-ventilated, fuel lean, or fuel controlled. If insufficient air is available for stoichiometric combustion the situation is termed under ventilated, vitiated, fuel rich, or ventilation controlled. Note that in some publications the words do not mean exactly the same thing. In this chapter, the terms well-ventilated (fuel controlled) and under ventilated (ventilation controlled), respectively, are mainly used and are related to the whole system. Even under well-ventilated conditions, the geometric conditions and flow pattern can be such that fresh air does not reach the combustion zone. Such a situation is here referred to as locally under ventilated. In Sect. 7.5, the effect of the ventilation conditions on the production of different species are further discussed.

[2] see also Eq. (2.14).

To be able to relate the produced amount of a certain species to the consumed mass of fuel, it is of interest to know the net heat of combustion, ΔH_c (kJ/kg), which is defined as the enthalpy change for a complete reaction where 1 kg fuel reacts with O_2 to yield CO_2 and H_2O at a given temperature and pressure (298 K and 1 atm, respectively), that is, the difference between the total enthalpy of formation of the products and the total enthalpy of formation of the reactants. By default, the heat of combustion used here corresponds to product of water in vapour form (often referred to as net heat of combustion). To find ΔH_c the following expression is used:

$$\Delta H_c = \sum_{products} \Delta H_f - \sum_{reactants} \Delta H_f \tag{7.9}$$

where ΔH_c is the enthalpy of formation (kJ/kg).

If energy is released from the reaction, ΔH_c will be negative, but note that in many tables for different fuels, heat of combustion is given as a positive value. If now the heat of combustion is known (or assumed to be an average value) and the heat release is measured, the mass loss of fuel, $\dot{m}_f$, can be calculated as

$$\dot{m}_f = \frac{\dot{Q}}{\chi \cdot \Delta H_c} \tag{7.10}$$

where $\dot{Q}$ is the heat release rate (HRR) (kW) and χ is the combustion efficiency. Through substitution of Eq. (7.10) into Eq. (7.8), one obtains:

$$\phi = \frac{\dot{Q} \cdot r}{\dot{m}_a \cdot \Delta H_c \cdot \chi} \tag{7.11}$$

Hugget showed that $\Delta H_c/r$ is approximately 3000 kJ/kg, consumed air for most carbon-based materials [14]. This leads to the equation[3]

$$\phi = \frac{\dot{Q}}{\dot{m}_a \cdot 3000 \cdot \chi} \tag{7.12}$$

if the HRR is given in kW.

7.3 Yields

To compare the emissions from different materials, yields, Y_i (kg/kg), are introduced and widely used (in most of the tables in this chapter they are given as g/kg). This means the ratio between the mass m_i (kg) of a compound *i* generated by the combustion of a certain mass of material (fuel):

[3] See also Eq. (2.17).

Table 7.2 Yields of CO (g/kg) for different experimental set-up and varied combustion conditions

Material	Large-scale tests[a] [16]	Small-scale method[b] [17]
Wood	58	5[c]
Paper	58	
Textiles	51	
PVC	116	63
PUR	160	20–50[d]
Polystyrene	220	60
Polyethene	60	24

[a] Values taken from a summary of yields during large-scale fire tests. Ventilation conditions might have been different between the different tests performed in large-scale and small-scale
[b] ASTM E2058 fire propagation apparatus
[c] Pine
[d] Rigid PUR

$$Y_i = \frac{\dot{m}_i}{\dot{m}_f} \quad \text{or} \quad Y_i = \frac{m_i}{\Delta m_f} \tag{7.13}$$

where $\dot{m}_i$ is the production rate of compound i (kg/s) and $\dot{m}_f$ is the mass loss rate of fuel (kg/s), Δm_f is the total fuel mass loss (kg) during the studied test period. Equation (7.13) shows that one can use either mass flow rates, $\dot{m}_i$, or total mass, m_i, of the produced species to calculate the yield. However, one must realize that the latter method gives some overall average results and that different materials might be consumed at different times during the fire (or experiment). Therefore, the results obtained might be more useful if these differences could be resolved. In this section, examples of yields of different products from some common materials are presented. Much of the yields below were summarized by Lönnermark et al. [15].

Yields of CO from some common materials used in fire experiments in different scales are presented in Table 7.2. The yields in the table, as well as most of the other tables in this chapter are given with the unit g/kg. Note that the yields in large-scale tests generally are higher than the yields in the small-scale tests. These differences could be due to scaling effects, geometrical differences or differences in ventilation and combustion conditions. It should, however, be noted that the large-scale values in Table 7.2, are based not only on experimental values but also on considerations of chemical composition and experimental conditions.

Hertzberg et al. tested in the cone calorimeter (ISO 5660-1 [18]) a large number of different materials [19]. The yield of particles can be found in Table 7.3.

Butler and Mulholland [20] made a summary of smoke yields (can probably be described as soot yield, but the wording of the authors has been used here) from different plastic materials. A selection of their data is presented in Table 7.4. Yields of

Table 7.3 Yield of particles from materials tested in the cone calorimeter [19]

Material	Particle yield (g/kg)
FR4, brominated laminate	139
Polystyrene (EPS)	126
Teflon-cable	102
Carbon fibre laminate	83
PVC (floor)	57
Polyethene-cable	51
50 % PVC + 50 % Teflon cables	42
PVC-cable	39
Bitumen	38
Polyethene pellets	35
Stone wool	30
Optic cable	29
Glass wool	28
Polyurethane (PUR), rigid	26
Teflon pellets	25
Nitrile rubber	25
Wool (92 % wool, 8 % polyamide)	22
Melamine	18
Particle board	3.9
Wood	2.4

Table 7.4 Yield of smoke from different plastic materials [20]

Material	Fuel surface (m^2)	Smoke yield (g/kg)
PMMA	0.006	15–18
Polystyrene	0.006	41
PVC	0.006	105–185
Rigid PVC	0.006	12
Polypropene	0.006	42
Rigid PUR	0.006	91
Flexible PUR	0.0225	34
HDPE	0.006	18–23

CO, CO_2, total hydrocarbons, and smoke from different plastic materials, based on small-scale experiments, are summarized in Table 7.5.

Tewarson [17] presents yields for CO, total hydrocarbons and smoke for a large number of materials based on small-scale tests. The yields for some liquid fuels are given in Table 7.6.

Table 7.5 Yield of CO, CO_2, total amount of hydrocarbons (THC) and smoke for some common plastic materials (g/kg) [17]

Material	CO	CO_2	THC	Smoke
ABS				105
PMMA	10	2120	1	22
Polyethene	24	2760	7	60
Polypropene	24	2790	6	59
Polystyrene	60	2330	14	164
Nylon	38	2060	16	75
PVC	63	460	23	172
EPS	54	1900		

Table 7.6 Yield of CO, hydrocarbons and smoke from some common liquid fuels (g/kg). The values come from small-scale tests [17]

Material	CO	Hydrocarbons (HC)	Smoke
Methanol	1	–	–
Ethanol	1	1	8
Isopropyl alcohol	3	1	15
Acetone	3	1	14
Heptane	10	4	37
Kerosene	12	4	42
Benzene	67	18	181
Mineral oil	41	12	97

7.4 Emissions from Fires in Vehicles and Tunnels

There are a number of reports and papers on the issue of fires and the environment. Some of them present summaries of emissions from common materials or common types of fires [16, 21, 22], while others focus on emissions from fires in a more general sense or present results from single fires that have had a large impact on the environment [23–25].

The analysis of the smoke gases from an automobile fire (passenger car) shows that emissions with a potentially negative impact on the environment, or humans, are produced in significant concentrations [26]. Three separate, full scale fire tests were performed under SP's large-scale ("industry") calorimeter: a fire ignited and developed in the engine compartment; a fire ignited inside the vehicle that was extinguished in the early stages; and a similar fire ignited inside the vehicle that was allowed to spread until the entire vehicle was involved in the fire. Both fire gases and run-off water were analysed.

The emissions included HCl, SO_2, volatile organic compounds (VOCs; for example, benzene), polycyclic aromatic hydrocarbons (PAHs), and polychlorinated

Table 7.7 Emissions of PCDD/F and PAH from vehicle fires in a tunnel and PCDD/F found in the fire residue [28]. The values are divided by the energy content

Vehicle	Q_{tot}	Fire residue PCDD/F		Tunnel PCDD/F		Tunnel PAH	
	GJ	mg I-TEQ	mg I-TEQ/GJ	mg I-TEQ	mg I-TEQ/GJ	g	g/GJ
Old car	6	0.012	0.002	0.032	0.0053	13	2.2
New car	9	0.008	0.00089	0.044	0.0049	27	3.0
Subway carriage	41	0.54	0.013	2.0	0.049	NA	NA
ICE-wagon	77	1.1	0.014	9.2	0.12	NA	NA

dibenzo-p-dioxins and dibenzofurans (PCDDs/PCDFs). The definition of VOC often depends on the sampling/analysis method, but typically include species with molecular masses between 75 and 200 g/mol. Sources of chlorine in the vehicle for production of HCl and PCDDs/PCDFs included, most probably: upholstering materials, dash board components, and electrical wirings, as indicated from the small-scale experiments conducted on selected materials from an automobile similar to that used for the full scale automobile fire.

Aldehydes and isocyanates were also found in the smoke gases, both compounds with well-documented short-term and long-term effects on humans. Other toxic compounds included: HCN and SO_2. These compounds have a direct effect on people and are of concern for rescue personal and others exposed to smoke from vehicle fires. The health effects, especially time to incapacitating dose for some of the gases, are further discussed in Chap. 15.

The particles emitted from the fire had a particle size distribution with a high number of particles with a diameter below 1 μm. Such small particles can be transported far from the location of the fire and are respirable, implying that the body's defence system against particles (in the nose and throat) cannot provide adequate protection. Analysis of the content of the fire-generated particles revealed that these contained high concentrations of zinc, lead, and chlorine.

Analysis of extinguishing water showed that this was severely contaminated, containing elevated levels of both organic compounds and metals. Comparison with data from other vehicle fires found in the literature showed that contamination of lead, copper, zinc, and antimony appear to be significant in water run-off from these types of fires.

Within the EUREKA EU499 project [27] the release of PCDD/Fs and PAHs were analysed in connection with some of the tests: an old car (1974), a new car (1988), a German subway carriage, and a Deutsche Bahn wagon with a steel body and a modern InterCityExpress (ICE) interior [28], see further Chap. 3, Sect. 3.3.7. The release into the tunnel was estimated by using 1 m^2 passive collectors (cotton and steel, respectively) and active sampling at different positions along the tunnel. In addition, the fire residue was analysed. In Table 7.7 the releases of PCDD/F and PAH into the tunnel from the different vehicle fires are summarized. To better

compare the results with results from other tests, the values have been normalized relative to the energy content of each vehicle. The results show that the PCDD/F from the subway carriage and the ICE-wagon are similar and that these results are approximately one order of magnitude larger than those from the passenger cars. Corresponding values obtained in the passenger car fires described above [26] were 0.023 mg I-TEQ/GJ (0.0868 mg I-TEQ in total) for PCDD/F and 31.3 g/GJ (119 g in total) for PAH, that is, almost an order of magnitude higher than for the cars reported by Wichmann. Apart from actual differences in production between the tests, there are two other possible explanations for the differences. There might be higher collection efficiency in the tests performed beneath the industry calorimeter. There is also a difference in how the total energy was calculated. In the case of the EUREKA 499 tests, the energy content was estimated from the composition of the fuel load, while in the test presented by Lönnermark and Blomqvist [26] the total energy was calculated from the heat release measurements. This latter difference is, however, relatively small. A comparison with the integrated values available for the subway carriage and the ICE-wagon [29], show that the estimated total energy content is approximately 10 % higher than the integrated HRR value for the subway carriage and approximately 30 % higher for the ICE-wagon.

Lönnermark and Blomqvist [26] present yield result from fire tests with a car and materials from a car. The emissions of the main combustion products from selected materials are listed in Table 7.8. The materials were selected to represent the most abundant combustible materials in the car. There was no information available on the amount of respective material in the car. However, in the work done by Persson et al. [22] one assessed that, for example, 9 % of the plastic material of an automobile was PVC and 17 % was PUR.

The test set-up used for the small-scale fire tests was the closed 0.5 m^3 chamber described in ISO 5659. The 75 × 75 mm horizontally mounted sample was exposed to two different levels of external radiation in consecutive tests. A lower radiation level of 25 kW/m^2 was applied to generate pyrolytic conditions, and a higher level of 50 kW/m^2 was applied to give conditions of flaming combustion.

The yields of the inorganic gas components from the full scale tests with a car are presented in Table 7.9.

Much referred to is the work by Lemieux et al. [30–33]. During tests with pieces of car tyres, measurements were made of VOC, semi-VOC, particles, PAH, and some metals. In the tests either “chunk”, (1/4–1/6 tires) or “shred” (5.1 × 5.1 cm) tires were combusted in a “burn pit” [32]. In total 13.6 kg (approximately two tires) were placed on a scale. Between 4.5 and 9.0 kg was combusted. In Table 7.10, selected results from the VOC analyses are presented.

Conesa et al. [34] performed pyrolysis experiments in laboratory scale with pieces of car tyres. The pieces had a diameter of approximately 4 mm. The flow of fuel was 0.5 g/min. By controlling and varying a flow with a mixture of O_2 and N_2, yields under different conditions (pure N_2 or 10 % O_2) could be calculated. Also the temperature was varied: 450, 750, and 1000 °C. The main species found were CO_2, CO, H_2, methane, ethane, propane, propene, isoprene, benzene, and toluene. The results are presented in Table 7.11. There is a clear function of the temperature,

Table 7.8 Yields of compounds generated by the combustion of materials found in cars. Results from small-scale tests [26]

Car component	Test condition	CO_2 (g/kg)	CO (g/kg)	HCN (g/kg)	NO (g/kg)	NH_3 (g/kg)	HCl (g/kg)	SO_2 (g/kg)
Door panel	Pyrolytic	410	43	2.1	–	–	120	–
	Flaming	1500	72	2.9	7.4	-	160	–
Component from ventilation system (polymer)	Pyrolytic	–	360	–	–	–	–	–
	Flaming	2100	27	–	–	–	–	–
Floor material (carpet)	Pyrolytic	–	49	4.9	–	–	–	–
	Flaming	2400	43	0.9	9.5	–	–	–
Dashboard	Pyrolytic	260	25	3.8	–	–	–	–
	Flaming	1800	23	1.2	6.4	–	–	–
Upholster material from driver's seat	Pyrolytic	250	43	1.7	–	–	51	–
	Flaming	1800	78	2.4	5.7	0.4	66	9.9
Upholster material from back seat	Pyrolytic	–	26	3.9	–	–	–	–
	Flaming	1700	88	5.3	7.5	0.35	8.1	10
Lacquered plate from car body	Pyrolytic	–	21	–	–	–	–	–
	Flaming	610	96	2.7	–	–	–	–
Electrical wirings	Pyrolytic	260	32	–	–	–	340	–
	Flaming	1100	86	–	–	–	390	–
Tyre	Pyrolytic	–	81	–	–	–	–	21
	Flaming	1400	30	–	–	2.3	–	11

Table 7.9 Yield for inorganic gas components during full scale tests with a car [26]

Species	Total amount (kg)	Yield (g/kg)
CO_2	265	2400
CO	6.9	63
HCN	0.17	1.6
HCl	1.4	13
SO_2	0.54	5.0

Table 7.10 Yields of selected VOC species from pieces of car tyres during small-scale tests, sampled with two different methods: VOST (Tenax-GC) and XAD-2, respectively [32]

Species	Yield (Chunk) (g/kg)	Yield (Shred) (g/kg)
VOST (Tenax-GC)		
Benzene	2.16	2.20
Phenol	0.0005	0.014
Total	11.2	13.1
XAD-2		
Biphenyl	0.21	0.33
Phenol	0.37	0.70
Total	8.37	16.3

Table 7.11 Yields of selected species in gas phase from pyrolysis tests in laboratory scale with pieces of car tyres (g/kg) [34]. Two different atmospheres were used: 100% N_2 and a mixture of 90% N_2 and 10% O_2. Values are average of two tests if not else stated

Species	450 °C		750 °C		1000 °C	
	0% O_2	10% O_2	0% O_2	10% O_2	0% O_2	10% O_2
CO_2	34	85	41	100	18	45
CO	–	47	12[a]	36	13	89
H_2	0.5	2.9	3.5	4.0	10	13.8
Methane	6.5	11	46	48	79	38
Ethane	2.4	1.3	11	11	1.1	0.4
Ethene	3.9	1.7	24	28	7.1	3.1
Propane	0.9	0.8	1.4	1.4	0.02[a]	–
Propene	2.2	1.0	11	16	0.34	0.06
Isoprene	29	3.6	7.2	3.0	0.15[a]	–
Benzene	–	–	43	45	87	77
Toluene	0.03	15	25	21	–	0.03

[a] Detected only in one test

especially for the last three species. They were, however, analyzed only in the gas phase and the total emissions could have been higher.

Vianello et al. [35] developed a scale-model car (scale 1:30) to perform fire tests in a scale tunnel (total length 5.0 m, radius 0.15 m, height from the floor to the apex 0.21 m, and width 0.30 m). The tunnel was naturally ventilated. The main purpose of the test series was to study the temperature profiles in the tunnel and compare with real scale. During the tests, however, samples for gas analyses were also extracted. Four different types of adsorber/filter were used: Tenax, XAD-2, Silica gel, and PTFE/glass fibre. The results are presented in Table 7.12.

Lemieux et al. [33] presented average values to represent yields from cars, boats, and trains for the following species: CO (62.4 g/kg), particles (50.0 g/kg) and NO (2.0 g/kg).

In the Runehamar tunnel large-scale tests, mixtures of cellulose and plastic materials were used as fuels [36–38]. The test data clearly show that the production rate of CO_2 increases linearly with the HRR (see Fig. 7.1). The relation can be expressed as [36]:

$$\dot{m}_{CO_2} = 0.087\dot{Q} \tag{7.14}$$

where the HRR is given in MW.

Note that different materials were used in the Runehamar tunnel fire tests, including wood pallets, PE materials, PUR mattresses, furniture, and paper cartons with polystyrene cups. It seems that for these types of materials the production rates of CO_2 are independent of the materials and only dependent on the HRR. The

Table 7.12 Results from sampling during fire in a scale-model car in a scale tunnel [35]

Compound	Concentration
Tenax adsorber	[mg/m^3]
Benzene	0.415
Toluene	0.380
Ethyl benzene	0.015
p-zilene	0.056
m-xilene	0.053
o-xilene	0.027
XAD-2 adsorber	[mg/m^3]
Naphtalene	0.607
Acenaphtylene	0.136
Silica gel adsorber	[µg/m^3]
HF	0.087
HCl	0.165
HNO_3	0.707
H_2SO_4	0.790
PTFE filter and glass fibre	[mg/m^3]
Anthracene	0.576
Fenanthrene	0.587
Fluoranthene	0.536
Pyrene	0.437
Benzo[a]anthracene	0.172
Crisene	0.191
Benzo[a]pyrene	0.128
Benzo[b]fluoranthene	0.169
Benzo[k]fluoranthene	0.136
Indeno[1, 2, 3-cd]pyrene	0.114
Benzo[g, h, i]perylene	0.095

reason could probably be that the main fire load consisted of the cellulose materials and that the combustion efficiency was high during large portions of the tests.

However, there was no simple correlation between the production rate of CO and the HRR (see Fig. 7.2). The production rate of CO strongly depends on the type and geometry of the fuels, which influence the access of air and local ventilation and burning conditions. Most of the CO was produced at the beginning of each test in the Runehamar tunnel fire tests when the combustion seems to have been less efficient and in the rest of each test the combustion appears to have been very good, with the possible exception of the test T2, which involved PUR. The short period of less efficient combustion was, however, enough to have significant influence on the CO results.

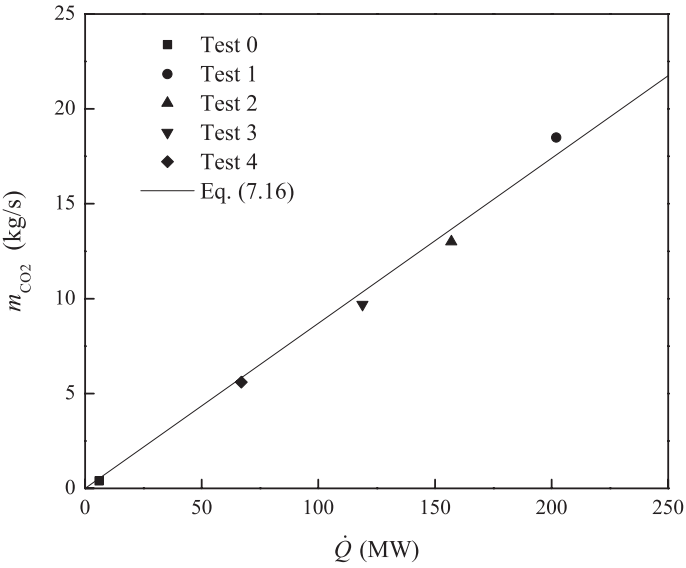

Fig. 7.1 The production rate of CO_2 as a function of the HRR from large-scale tests in the Runehamar tunnel [36]

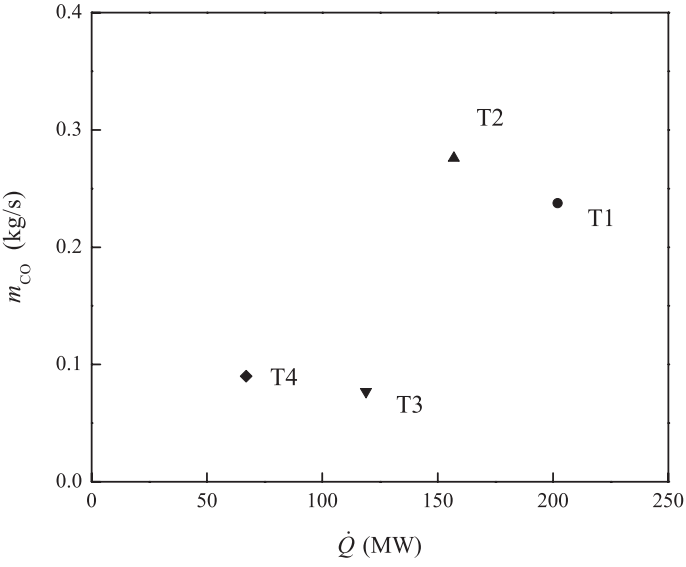

Fig. 7.2 The production rate of CO as a function of the HRR from large-scale tests in the Runehamar tunnel [36]

7.5 Effect of Ventilation Condition

The ventilation conditions are important for the chemical production and the hazards (see Chap. 15). In an under ventilated fire situation the yield of major toxicants (for example, carbon monoxide and hydrogen cyanide) is greater, compared to well-ventilated conditions. Furthermore, the total volume of effluents is greater [39].

The ventilation is an important means to affect, and hopefully improve, the conditions in a tunnel. Longitudinal ventilation can improve the conditions upstream of the fire significantly, making it possible for the rescue service to reach the fire. It is, however, important to remember that the situation downstream of the fire can be exacerbated by the ventilation. In Norway, at least at some places, the ventilation is used as a part of the firefighting tactics where in case of fire the ventilation is used in a predefined direction [40]. Two reasons in particular are given for this methodology: first, the firefighters know in advance the ventilation direction in the tunnel and thereby what portal to attack the fire from, and second, the conditions downstream of the fire are assumed to be of no danger to people being in this part of the tunnel, due to dilution of the fire gases. This strategy is partly based on the results from the experiments with two passenger cars in the Byfjord tunnel in 1998 and the Bømlafjord tunnel in 2000. These results showed that downstream of the car fires, the concentrations of CO and NO_x were not life threatening [41].

In a Swedish study concerning the HRRs from tunnel fires, the ability of the rescue service to rescue people from the tunnel and to attack the fire, and the possibility for people to escape from a tunnel fire showed that the two main effects of longitudinal ventilation on the conditions during a tunnel fire is an increase of the growth rate of the fire and an increased dilution of the gases [42].

The ventilation conditions can be described by the equivalence ratio as defined in Sect. 7.2 and Eq. (7.8). The local ventilation conditions can be very important for the combustion process, but in cases where the spatial variation either can be assumed to be small or when it is difficult to resolve the variations, the overall combustion process is often studied instead. In such cases ϕ can be defined in a more general sense using the equivalence ratio for the total combustion process. This is usually referred to as the global equivalence ratio (GER). Originally, the GER was defined as the ratio of the mass of gas in the upper layer in an enclosure derived from the fuel divided by that introduced from air, normalized by the stoichiometric ratio [43]. Beyler, who was the first to correlate the species concentrations in the upper layer with the equivalence ratio, used a variant called the plume equivalence ratio defined as the ratio of the fuel volatilization rate to the air entrainment rate, normalized by the stoichiometric fuel to air ratio [44–46]. In the work presented by Blomqvist and Lönnermark [47], the definition of the GER is the ratio between the mass loss rate of the fuel and the mass flow of oxygen entering the combustion room normalized by the stoichiometric ratio.

In order to measure the GER in the two different test rooms used by Blomqvist and Lönnermark, a device called “the phi meter” [48, 49], was constructed. The essential parts of the phi meter are the combustor, into which the fire gases and

additional pure oxygen are introduced, and the O_2 analyser. Complete combustion of the fire gases is achieved in the combustor by the high temperature (1000 °C was used in these specific tests) and by using a platinum catalyst and additional oxygen. The readings on the O_2 analyser are compared with background measurements without fire gases through the phi meter. A simple computation gives the equivalence ratio [47].

There are not many cases reported on measured under ventilated conditions in fires in tunnels. Most cases reported can probably be said to be either fuel controlled or ventilation controlled (for example, see [50]). The latter correspond to a case where limited ventilation leads to a decrease (or control) in the fire size, but if the temperature is high, a continuous mass loss can lead to under ventilated combustion. Among the large-scale fire test series, the one in the Ofenegg tunnel is an obvious example of the effect of the ventilation (see Chap. 3), but that case was also rather special due to the blockage at one end of the tunnel.

Ingason [51, 52] performed fire tests in a model tunnel ($1.08 \times 1.2 \times 10.96$ m^3) to study the effect of the ventilation on the fire behaviour. Under ventilated conditions were of special interest and both naturally ventilated and forced ventilated scenarios were studied. In the first series of tests with naturally ventilated scenarios the fire size and the size of the inlet opening were varied, while in the second series of tests with forced ventilated scenarios the fire size and the flow rate of incoming air were varied. The author described the difficulty in achieving under ventilated condition. The transition to such conditions is highly dependent on the temperature and the thermal feedback to the fuel. This was also seen in the test series described by Lönnermark et al. [53], where a case with 0.5 m^2 chlorobenzene (test CB3) gave a very slow developing fire inside a room. The fire reached high temperatures and under ventilated conditions first after approximately 35 min. Increasing the pool size to 0.8 m^2 (test CB4) gave a significantly different fire development with much higher temperatures and under ventilated conditions after approximately 6 min. This illustrates the importance of the fire size. In a tunnel with forced ventilation, the flame tilt also influences the thermal feedback and thereby the fuel mass loss rate.

In the test series presented by Ingason [51, 52] some of the tests, however, became under ventilated. Gas compositions (CO, CO_2, and O_2) were analysed at three different heights (0.15, 0.5, and 0.9 m below the ceiling), 4.5 m downstream of the centre of the fire, which was situated 1.5 m from the tunnel entrance. The results were presented as $\Delta CO/\Delta CO_2$ ratios, which is the ratio between the increase in CO volume concentration and increase in CO_2 volume concentration. Note that in some of the work referred below instead the ratio between the actual CO volume concentration and the actual CO_2 volume concentration (CO/CO_2 ratio) was used. The version used in the original publication has also been used in this chapter.

In most of the tests presented by Ingason, the $\Delta CO/\Delta CO_2$ ratios were rather similar at the different sampling heights. The ratio was, however, often somewhat higher in the highest position (0.15 m below the ceiling) during some period of the tests. In a few cases the $\Delta CO/\Delta CO_2$ ratio was highest in the lowest position (for example, in test 2 and test 8). In Fig. 7.3 the $\Delta CO/\Delta CO_2$ ratios for heptane pool fires are presented as a function of the equivalence ratio. The values were chosen

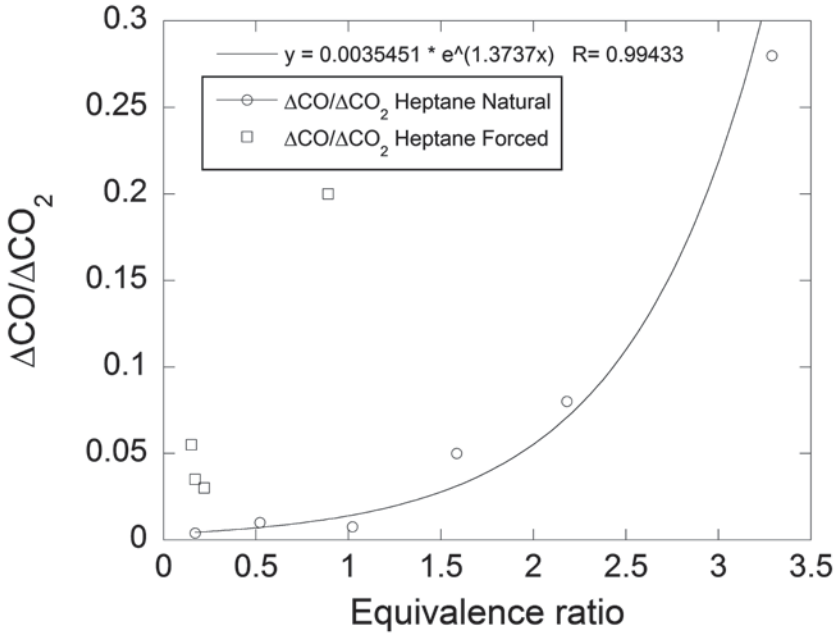

Fig. 7.3 $\Delta CO/\Delta CO_2$ ratio as function of equivalence ratio for heptane pool fires performed by Ingason [51, 52]. The results are given both for natural ventilation and for forced ventilation. Included for illustration is an exponential curve fit of the natural ventilation data [54]. It is, however, based on only six data points

to be representative values for the position with the highest $\Delta CO/\Delta CO_2$ ratio at the selected time. Note that Ingason used an equivalence ratio based on the air to fuel ratio, while throughout this book all equivalence ratios (including those presented in Fig. 7.3) are based on fuel to air ratios. Two different cases are represented in the figure: natural ventilation and forced ventilation. The values of the $\Delta CO/\Delta CO_2$ ratios were determined at the time when the mass loss rate was at its maximum for each test. For the natural ventilation an exponential curve fit is included [54]. It fits the data points very well, but due to the limited number of points it should only be seen as an illustration.

The points for the forced ventilation show a pattern very different from that in the natural ventilation cases. All cases are well-ventilated, but the point at $\phi = 0.89$ shows features of under ventilated fires. This could have two possible explanations. There are studies that indicate that the CO production starts to increase well below $\phi = 1$, at $\phi \approx 0.6$ (see for example, [44, 43]).

Another explanation could be the flow pattern around the fire during forced ventilation. The experimental results, especially the O_2 measurements, show a significant gradient with height, which indicates that even if the tunnel is well-ventilated it could be locally under ventilated in the combustion zone. The three-dimensional flow typically found close to the fire in a tunnel was illustrated by Ingason, showing the main ways for the flows of different density [55].

Table 7.13 $\Delta CO/\Delta CO_2$ ratio as function of equivalence ratio for xylene and methanol pool fires performed by Ingason [51, 52]

Fuel	Ventilation	Fire size [m^2]	Opening [m^2]	ϕ	$\Delta CO/\Delta CO_2$
Xylene	Natural	0.3 × 0.3	0.3 × 0.3	0.37	0.20 (0.38)[a]
Xylene	Natural	0.3 × 0.3	0.15 × 0.15	1.01	0.30 (0.41)[a]
Xylene	Natural	0.3 × 0.3	0.1 × 0.1	1.94	0.36 (0.43)[a]
Xylene	Natural	0.3 × 0.3	0.2 × 0.2	0.70	0.23 (0.31)[a]
Xylene	Forced	0.3 × 0.3	0.2 (ø = 0.5 m)	0.15	0.15 (0.26)[a]
Methanol	Natural	0.4 × 0.4	0.6 × 0.6	0.04	0.003–0.035[b]
Methanol	Forced	0.4 × 0.4	0.2 (ø = 0.5 m)	0.02	−0.01–0.02[b]

[a] The $\Delta CO/\Delta CO_2$ ratio was highest in the beginning of the result period reported and then decreased; the maximum value (within parenthesis) is not used (see discussion of Fig. 7.2) but instead something closer to a steady state value

[b] The $\Delta CO/\Delta CO_2$ ratio is varying significantly; therefore a range is given (including all the three heights)

Results from the experiments with xylene and methanol are summarized in Table 7.13. Compared to the experiments with heptane pool fires presented in Fig. 7.3, xylene results in high values and methanol in low values of $\Delta CO/\Delta CO_2$ ratios. This is in line with the results of Beyler [44] showing that oxygenated hydrocarbons produce small amounts of CO (expressed as yield) at low equivalence ratios. Aromatics (Beyler used toluene) on the other hand, produce a rather constant CO yield independent of the equivalence ratio; only a small increase was reported. This means that aromatics at low equivalence ratios produce relatively high CO yields and at high equivalence ratios produce relatively low CO yields. The variation in $\Delta CO/\Delta CO_2$ ratio with equivalence ratio presented in Table 7.13 might be explained by a decrease in CO_2 production.

Lönnermark et al. [53] performed under ventilated fire experiments in an enclosure (the ISO 5705 room: 2.4×3.6×2.4 m^3), where the size of the opening was varied. Five different fuels were used: Polypropene, Nylon 66, Tetramethylthiuram monosulfide, 3-Chloro-4 nitro-benzoic acid, and Chlorobenzene. In the paper by Blomqvist and Lönnermark [47] results are given for CO and other components in the fire gases, and their dependence on the equivalence ratio. For comparison with the results from model scale tunnel tests presented in Fig. 7.3, CO/CO_2 ratios have been calculated from tests in the enclosure fires [53]. Note that here absolute concentrations have been used, and not changes from background values as in the case presented by Ingason.

In Fig. 7.4, CO/CO_2 ratios for polypropene, Nylon 66, and chlorobenzene pool fires (polypropene and Nylon 66 were solid polymers in form of pellets) are presented as function of the equivalence ratio. For all three materials, results are presented for measurements both in the opening from the enclosure and in the exhaust duct connected to the hood collecting the fire gases. For illustration, an exponential

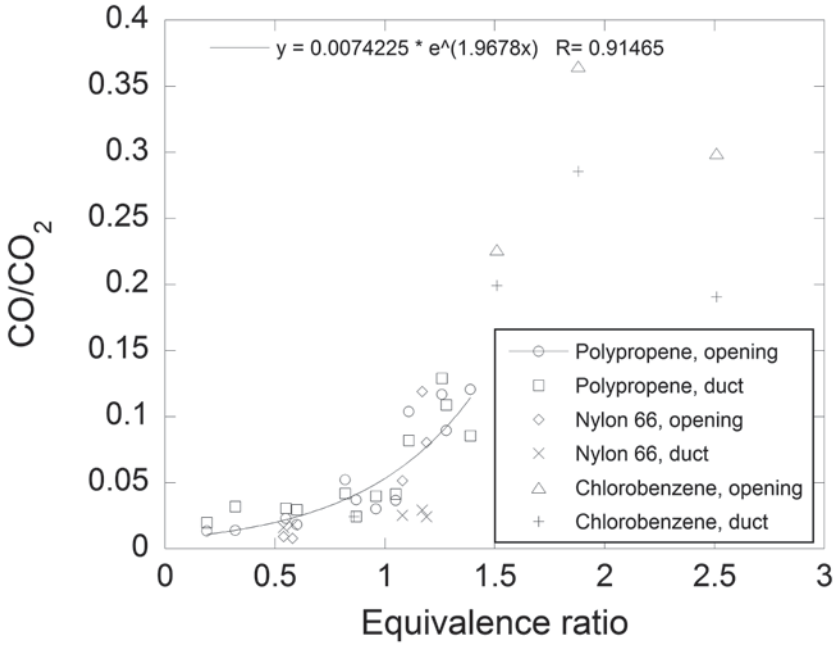

Fig. 7.4 CO/CO_2 ratio as function of equivalence ratio for polypropene, Nylon 66, and chlorobenzene. For all three materials, results are given for measurements in the opening of the enclosure and in the exhaust duct connected to the hood collecting the fire gases. An exponential curve fit is included for polypropene (opening) [54]

curve-fit for the results from the opening for polypropene is included. This fit seems to be qualitatively representative for the other cases also, even if there are differences between the materials.

The effect of combustion outside the opening during under ventilated conditions can be seen for Nylon 66. This effect is also obvious for chlorobenzene. For heptane the CO/CO_2 ratio are rather similar in the opening and the duct for most values of the equivalence ratios reported. From the figure it can be seen that when passing from well-ventilated to under ventilated conditions (passing the point $\phi = 1$), the CO/CO_2 ratios increases above approximately 0.05. This is comparable to the natural ventilated tests with heptane in the model scale tunnel performed by Ingason (see Fig. 7.3). For the cases with forced ventilation the differences are larger. The explanations for this, besides differences between materials, were discussed earlier.

Grant and Drysdale [56] presented analyses of CO and CO_2 for the EUREKA EU499 project. The calculated CO/CO_2 ratios show that high values (maximum 0.2, 30 m downstream of the fire and 0.13, 100 m downstream of the fire) are obtained during the initial phase before the HRR starts to increase rapidly, that is, when the fire spreads to the trailer. During the most intense part of the fire, the CO/CO_2 ratios 100 m downstream stay below 0.02. At 30 m downstream of the fire the CO/CO_2 ratio are also approximately 0.02 or lower, but a clear increase during

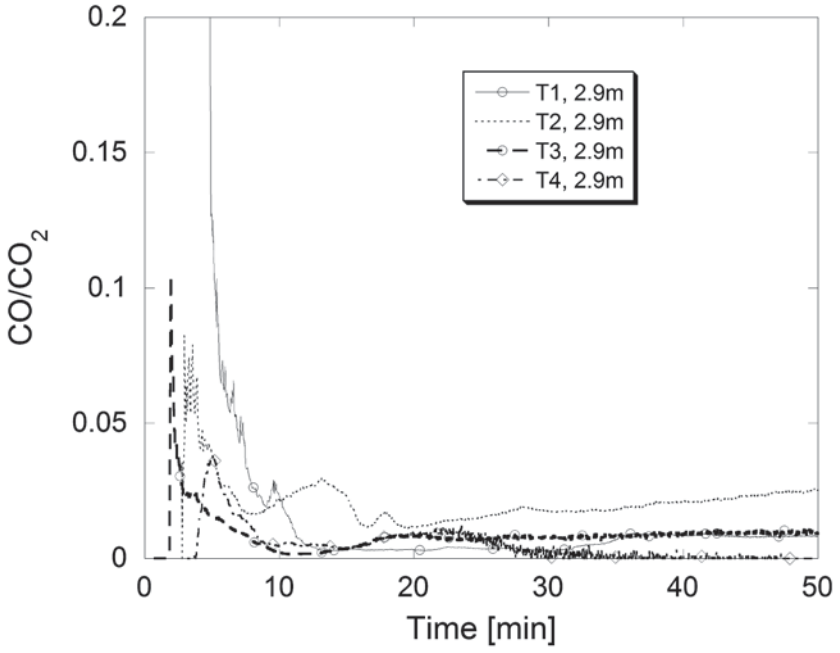

Fig. 7.5 CO/CO_2 ratio as function of time for the Runehamar tests. The gas analyses were performed at 458 m from the centre of the fire, 2.9 m above the road surface [54]

the period when the ventilation was switched off can be seen. The maximum value given is 0.05, but the peak value during this time period could be higher since values are missing for a few minutes. Comparing these results with those presented in Figs. 7.3 and 7.4 indicates under-ventilated combustion during this time period, which is understandable due to low ventilation during a period of high temperatures and probably high mass loss rates.

Similar results were found in the four Runehamar tests, that is, high CO/CO_2 ratios during the initial phase of the fire and low values during the intense fire and the decay period (see Fig. 7.5). The gas analyses (CO and CO_2) were performed at two different heights (2.9 and 5.1 m respectively above the road surface), 458 m from the centre of the fire. Analyses of O_2 were also performed in these positions and at the height 0.7 m (see the work by Ingason et al. [36, 37] for detailed description of the measurement setup and analysers). It can be seen from Fig. 7.5 (in comparison to Fig. 7.4) that all the tests are well-ventilated [54]. The high values at the beginning of the tests can be explained by incomplete combustion. The temperature in the combustion zone may have affected the results. It is known from fire experiments in compartments that both the residence time and the temperature in the upper layer are important factors for the production of CO [57]. Even for well-ventilated conditions, high CO concentrations can be measured if the temperature is below approximately 800 K. The situation looks similar to the one called preflaming combustion

described by Tsuchiya and discussed below [58]. The highest values (not shown in the figure) are also dependent on the absolute relationship between the CO and CO_2 analyses. A small difference in response time or time to reach a concentration above the detection limit, significantly affects the initial values. To be able to compare the CO/CO_2 ratios better with the HRR and the temperature measurements near the fire, the time scales in Fig. 7.5 were corrected for the transport time between the fire and the measurement station. This transport time varies with the HRR and the procedure to calculate this is described by Ingason and Lönnermark [37]. The estimated transport time varies between 1.5 and 2.5 min depending on the HRR.

The results from the Runehamar tests look similar to those reported by Bettis et al. [59] where the tests were well-ventilated, apart from a short period during one of the tests. The CO/CO_2 ratios ranged, in most cases, from 0.005 to 0.025. In a few cases there was a higher value (0.05–>0.1) in the beginning of the test followed by a continuous decrease. A steady state value as high as 0.05–0.06 was reported in only one test (Test 6). The fire was partly sheltered due to the setup and this may have affected the local ventilation conditions.

During ventilated conditions in a tunnel, the situation at the fuel can be ventilation controlled or locally under ventilated if the fuel setup is such that the air flow does not reach the vaporized or pyrolized fuel. This was mentioned in relation to the initial period of fires discussed above.

Tewarson [17] performed an extensive work on collecting data on yield of CO and CO_2, respectively, for different materials, and on how these yields depend on the equivalence ratio. From the result he developed relationships of the ratio of actual yield to well-ventilated yield as function of equivalence ratio. For CO Tewarson suggested the following relation:

$$\frac{Y_{CO,uv}}{Y_{CO,vv}} = 1 + \frac{\alpha}{e^{2.5\phi^{-\xi}}} \tag{7.15}$$

where the values of correlation parameters for some selected fuels are presented in Table 7.14. Combining his results for CO and CO_2 gives the following equation [54]:

$$\frac{X_{CO}}{X_{CO_2}} = \frac{44\left[1 + \dfrac{\beta}{\exp\left(2.5\phi^{-\xi}\right)}\right] Y_{CO,wv}}{28\left[1 - \dfrac{1}{\exp\left(\left(\phi/2.15\right)^{-1.2}\right)}\right] Y_{CO_2,wv}} \tag{7.16}$$

where Y is the yield [kg/kg], β and ξ are correlation coefficients, X is the volume concentration and the index wv corresponds to well-ventilated conditions. The values of the different parameters are given for four selected materials in Table 7.14. The CO/CO_2 ratio as a function of ϕ based on Eq. (7.16) is given for three materials

Table 7.14 Yields of CO and CO_2 during well-ventilated conditions and values of correlation coefficients in Eq. (7.16) given for four materials [17]

Material	$y_{CO,wv}$ [kg/kg]	$y_{CO_2,wv}$ [kg/kg]	α	β	ξ
Polyethene (PE)	0.024	2.76	10	10	2.8
Polypropene (PP)	0.024	2.79	10	10	2.8
Polystyrene (PS)	0.060	2.33	2	2	2.5
Wood	0.005	1.33	44	44	3.5

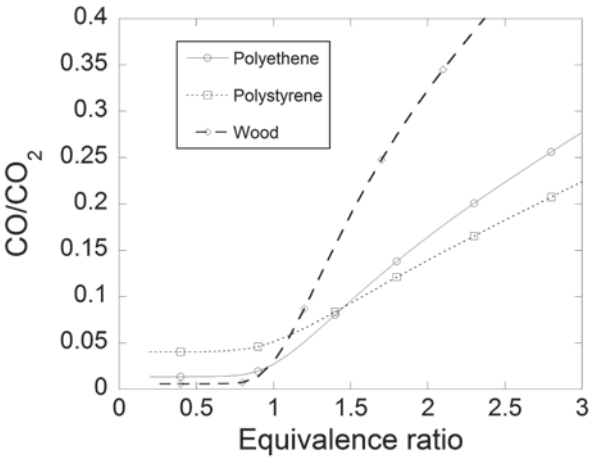

Fig. 7.6 CO/CO_2 ratio for polyethene, polystyrene, and wood as a function of ϕ, based on the work by Tewarson (Eq. (7.16)) [17]

in Fig. 7.6. Polypropene was not included since it is almost identical to polyethene. The curves diverge from each other, but for all three fuels the CO/CO_2 ratio at $\phi = 1$ is between 0.03 and 0.05.

Different fuels utilize available oxygen at high equivalence ratios to very different extents. Beyler [44] reported residual oxygen in exhaust gases from a hood system simulating the upper layer in a two-layer situation at $\phi > 1.2$ for different types of fuels. These results are summarized in Table 7.15. There is a wide range in residual oxygen for the different fuels, from 0.1 % (methanol and ethanol) to 8.0 % (toluene). These values can be compared to the minimum oxygen concentration measured in each test in the Runehamar tunnel: 6.4, 8.6, 11.7, and 15.9 % for T1, T2, T3, and T4, respectively (values corrected for estimated H_2O concentration) [54].

The CO/CO_2 ratio depends on the mode of combustion. For combustion of wood, which is the most common fuel used in large-scale testing in tunnels today, the combustion can be divided into three stages: (1) preflaming pyrolysis, (2) flaming combustion, and (3) char combustion or glowing [58]. Tsuchiya [58] presented mean values of CO/CO_2 ratios for the three phases of combustion for plywood: 0.9

Table 7.15 Residual oxygen for combustion of different fuels at $\phi > 1.2$ [44]

Fuel	Chemical formula	Residual O_2 [%]
Propane	C_3H_8	0.5
Propene	C_3H_6	2.0
Hexanes	C_6H_{14}	3.0
Toluene	C_7H_8	8.0
Methanol	CH_3OH	0.1
Ethanol	C_2H_5OH	0.1
Isopropanol	C_3H_7OH	2.0
Acetone	C_3H_6O	0.7

Table 7.16 CO/CO_2 ratios for selected liquids and noncharforming plastics combusted in normal air in the cone calorimeter [58]

Material	Radiation [kW/m^2]	CO/CO_2
Methanol	5	0.0002
Ethanol	5	0.0004
n-Heptane	5	0.010
Benzene	5	0.065
Xylene	5	0.056
Polypropene	30	0.024
Polypropene	50	0.025
Polystyrene	25	0.046
Polystyrene	40	0.051

(pyrolysis), 0.0035 (flaming combustion), and 0.25 (glowing), respectively. In the discussion above, the mode of combustion has been considered to be flaming in all cases. There is an abrupt transition from preflaming pyrolysis to flaming combustion. Tsuchiya showed that this transition occurred when the O_2 concentration was higher than a certain value that depends on the incident heat flux according to:

$$C_{O_2} = 19.4 - 0.19 \cdot \dot{q}'' \tag{7.17}$$

where C_{O_2} is the concentration of O_2 (in %) and $\dot{q}''$ is the incident heat flux (in kW/m^2).

Modes other than flaming combustion will not be discussed further here. Tsuchiya [58] also presented CO/CO_2 ratios for liquids and noncharring plastics under different levels of incident radiation in the cone calorimeter. Some selected materials of particular interest for the discussion in this section are presented in Table 7.16.

There are large differences between the different types of fuels. When ranking fuels according to their produced CO/CO_2 ratio (from low to high) they can be listed as alcohols and oxygen containing fuels, hydrocarbons, and finally aromatics. This order is valid for well-ventilated conditions. For under ventilated condition the ranking is reversed [60, 44].

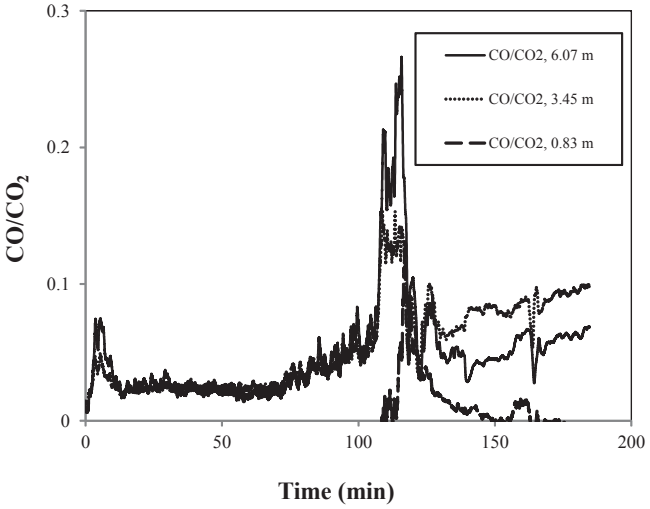

Fig. 7.7 CO/CO_2 ratio at different heights in the tunnel, 100 m downstream of the fire, during test 3 with a commuter train carriage [61]

Lönnermark et al. [61] performed full- scale fire tests with commuter train carriages in a 276 m long tunnel. The concentrations of O_2, CO, and CO_2 were measured at different heights, both in the carriage and in the tunnel. In Fig. 7.7 the CO/CO_2 ratios in the tunnel 100 m downstream of the fire are presented. As can be seen in the figure, the CO/CO_2 ratios clearly exceed the limits discussed above correlating to under ventilated conditions. It was not possible to calculate equivalence ratio in this situation, but this indicates that even if the overall conditions in the tunnel were well-ventilated, the combustion conditions inside the carriage were locally under ventilated. This again illustrates the importance of ventilation conditions on the combustion. The issue of using the CO/CO_2 ratio for determining the ventilation condition is also discussed in Chap. 2.

Example 7.1 A metro carriage is burning in a tunnel. Assume that the fire is locally underventilated with a representative equivalence ratio of $\phi = 1.6$. What would the yields of CO be if the fire could be represented by (1) wood or (2) plastics, for example, polyethene?

Solution:

(1) According to Table 7.14 for wood $y_{CO,\,wv} = 0.005$ *kg/kg,* $\alpha = 44$ *and* $\xi = 3.5$. *Using Eq. (7.15):*

$$y_{CO,wood}(\phi = 1.6) = 0.005 \cdot \left(1 + \frac{44}{e^{2.5 \cdot 1.6^{-3.5}}}\right) = 0.14 \text{ kg/kg}$$

(2) In a similar way for polyethene $y_{CO,\,wv} = 0.024$ kg/kg, $\alpha = 10$ and $\xi = 2.8$ and

$$y_{CO,PE}(\phi = 1.6) = 0.024 \cdot \left(1 + \frac{10}{e^{2.5 \cdot 1.6^{-2.8}}}\right) = 0.38 \text{ kg/kg}$$

To find out the production and concentration of CO both the burning rate (or HRR and combustion efficiency) and air flow in the tunnel need to be known or estimated.

Example 7.2 In a 1.2 km long tunnel, with a width of 9 m and a height of 6 m, an HGV loaded with polypropene is burning in the middle of the tunnel. The fire develops following the "Ultra fast" curve, including a combustion efficiency of 0.9. Estimate the CO/CO_2 ratio after 15 min if the air velocity is 2 m/s and the ambient temperature is 15 °C.

Solution: First the equivalence ratio needs to be calculated. This can be estimated from the HRR according to Eq. (7.12). The fire development can be described as (ultra fast): $\dot{Q} = 0.19 \cdot t^2 = 0.19 \cdot (15 \cdot 60)^2 = 153900$ kW. *The mass flow rate can be calculated from:* $\dot{m}_a = \rho_a \cdot u \cdot A = \frac{353}{288} \cdot 2 \cdot 9 \cdot 6 = 132.4$ kg/s. *Now Eq. (7.12) gives:* $\phi = \frac{\dot{Q}}{\dot{m}_a \cdot 3000 \cdot \chi} = \frac{153900}{132.4 \cdot 3000 \cdot 0.9} = 0.43$. *The fire is well ventilated. Now, studying Fig. 7.4 and7.6, the CO/CO_2 ratio can be estimated to be approximately 0.02. This correlates well also with Table 7.16.*

7.6 Summary

Knowledge of the different species produced during fires is of great importance for estimating the toxicity of the fire smoke. In this chapter the main combustion products from different types of fires are presented. The presentation focuses on CO and the CO/CO_2 ratio, but a large number of species or groups of species are also included, for example, hydrogen chloride (HCl), sulphur dioxide (SO_2), volatile organic compounds (VOCs), polycyclic aromatic hydrocarbons (PAHs), polychlorinated dibenzo-p-dioxins and dibenzofurans (PCDDs/PCDFs), total amount of hydrocarbons (THC) and soot/smoke. The combustion conditions (access of air, temperature, etc.) can vary between different fires in tunnels. Results from measurement during fire tests in vehicles and tunnels are presented in the chapter showing that the ventilation conditions can vary also during the same test leading to very different production rates and yields. The importance of the ventilation conditions on the productions of different species is described and relations for different yields and ratios are given. Especially the relation between the CO/CO_2 ratio and the equivalence ratio is presented and discussed. How to calculate the toxicity when the concentration of a species is known is presented in Chap. 15 on tenability.

References

1. Simonson M, Tuovinen H, Emanuelsson V (2000) Formation of Hydrogen Cyanide in Fires-A Literature and Experimental Investigation. SP Swedish National Testing and Research Institute, Borås, Sweden
2. Purser DA (2000) Toxic product yields and hazard assessment for fully enclosed design fires. Polymer International 49:1232–1255
3. Ferrari LA, Arado MG, Giannuzzi L, Mastrantonio G, Guatelli MA (2001) Hydrogen cyanide and carbon monoxide in blood of convicted dead in a polyurethane combustion: a proposition for the data analysis. Forensic Science International 121:140–143
4. Purser DA (2002) Toxicity Assessment of Combustion Products. In: DiNenno PJ (ed) SFPE Handbook of Fire Protection Engineering. Third Edition edn. National Fire Protection Association, Inc, Quincy, Massachusetts, USA, pp 2–83 -- 82–171
5. Nelson GL (1998) Carbon Monoxide and Fire Toxicity: A Review and Analysis of Recent Work. Fire Technology 34 (1):39–58
6. Gann RG (2004) Sublethal Effects of Fire Smoke. Fire Technology 40:95–99
7. Sader JD, Ou SS (1977) Correlation of the smoke tendency of materials. Fire Research 1 (3)
8. Warnatz J, Maas U, Dibble RW (1996) Combustion-Physical and Chemical Fundamentals, Modeling and Simulation, Experiments, Pollutant Formation. Springer-Verlag, Berlin Heidelberg
9. Glassman I (1996) Combustion. 3rd edn. Academic Press Inc.
10. Atomic Weights of the Elements 1993 (1994). International Union of Pure and Applied Chemistry (IUPAC), Pure & Appl Chem Vol. 66 (No. 12):2423–2444
11. Trends in Atmospheric Carbon Dioxide (2014). Global Greenhouse Gas Reference Network, http://www.esrl.noaa.gov/gmd/ccgg/trends/index.html, Accessed Jan 19. 2014,
12. Weast RC (ed) (1977–78) Handbook of Chemistry and Physics. 58th edn. Chemical Rubber Company
13. Li YZ, Ingason H A new methodology of design fires for train carriages. In: ISTSS 6th International Symposium on Tunnel Safety and Security, Marseille, 2014.
14. Huggett C (1980) Estimation of Rate of Heat Release by Means of Oxygen Consumption Measurements. Fire and Materials 4 (2):61–65
15. Lönnermark A, Stripple H, Blomqvist P (2006) Modellering av emissioner från bränder. SP Sveriges Provnings- och Forskningsinstitut, Borås
16. Persson B, Simonson M, Månsson M (1995) Utsläpp från bränder till atmosfären. SP Sveriges Provnings- och Forskningsinstitut, Borås, Sweden (in Swedish)
17. Tewardson A (2008) Generation of Heat and Gaseous, Liquid, and Solid Products in Fires. In: DiNenno PJ, Drysdale D, Beyler CL et al. (eds) The SFPE Handbook of Fire Protection Engineering. Fourth Edition edn. National Fire Protection Association, Quincy, MA, USA, pp 3–109 -- 103–194
18. ISO (2002) Reaction-to-fire tests-Heat release, smoke production and mass loss rate-Part 1: Heat release rate (cone calorimeter method). 2nd edn. ISO 5660-1
19. Hertzberg T, Blomqvist P, Dalene M, Skarping G (2003) Particles and isocyanates from fires. SP Swedish National Testing and Research Institute, Borås, Sweden
20. Butler K, M., Mulholland GW (2004) Generation and Transport of Smoke Components. Fire Technology 40:149–176
21. Blomqvist P, Persson B, Simonson M (2002) Utsläpp från bränder till miljön-Utsläpp av dioxin, PAH och VOC till luften. Räddningsverket (Swedish Rescue Services Agency), Karlstad, Sweden (in Swedish)
22. Persson B, Simonson M (1998) Fire Emissions into the Atmosphere. Fire Technology 34 (3):266–279
23. Hölemann H Environmental Problems Caused by Fires and Fire-Figthing Agents. In: Fire Safety Science-Proceedings of the Fourth International Symposium, Ottawa, Canada, 13–17 June 1994. International Association for Fire Safety Science (IAFSS), pp 61–77

24. Ahrens M, Rohr KD Fire and the Environment: Issues and Events. In: Proceedings of the Fire Risk and Hazard Assessment Research Application Symposium, Baltimore, Maryland, USA, 9–11 July 2003. The Fire Protection Research Foundation
25. Marlair G, Simonson M, Gann RG Environmental Concerns of Fires: Facts, Figures, Questions and New Challenges for the Future. In: 10th International Fire Science & Engineering Conference (Interflam 2004), Edinburgh, Scotland, 5–7 July 2004. Interscience Communications, pp 325–337
26. Lönnermark A, Blomqvist P (2006) Emissions from an Automobile Fire. Chemosphere 62:1043–1056
27. Fires in Transport Tunnels: Report on Full-Scale Tests (1995). edited by Studiensgesellschaft Stahlanwendung e. V., Düsseldorf, Germany
28. Wichmann H, Lorenz W, Bahadir M (1995) Release of PCDD/F and PAH during Vehicle Fires in Traffic Tunnels. Chemosphere 31 (2):2755–2766
29. Ingason H Heat Release Rate Measurements in Tunnel Fires. In: Ivarson E (ed) International Conference on Fires in Tunnels, Borås, Sweden, October 10–11, 1994 1994. SP Swedish National Testing and Research Institute, pp 86–103
30. Reisman JI (1997) Air Emissions from Scrap Tire Combustion. United States Environmental Protections Agency, EPA-600/R-97-115
31. Lemieux PM, DeMarini D (1992) Mutagenicity of Emissions from the Simulated Open Burning of Scrap Rubber Tires. U.S. Environmental Protection Agency, Control Technology Center, office of Research and Development, EPA-600/R-92-127
32. Lemieux PM, Ryan JV (1993) Characterization of Air Pollutants Emitted from a Simulated Scrap Tire Fire. Journal of the Air & Waste Management Association 43:1106–1115
33. Lemieux PM, Lutes CC, Santoianni DA (2004) Emissions of organic air toxics from open burning: a comprehensive review. Progress in Energy and Combustion Science 30:1–32
34. Conesa JA, Martín-Gullón I, Font R, Jauhiainen J (2004) Complete Study of the Pyrolysis and Gsification of Scrap Tires in a Pilot Plant Reactor. Environmental Science & Technology 38:3189–3194
35. Vianello C, Fabiano B, Palazzi E, Maschio G (2012) Experimental study on thermal and toxic hazards connected to fire scenarios. Journal of Loss Prevention in the Process Industries 25:718–729
36. Ingason H, Lönnermark A, Li YZ (2011) Runehamar Tunnel Fire Tests. SP Technical Research Institute, SP Report 2011:55
37. Ingason H, Lönnermark A (2005) Heat Release Rates from Heavy Goods Vehicle Trailers in Tunnels. Fire Safety Journal 40:646–668
38. Lönnermark A, Ingason H (2005) Gas Temperatures in Heavy Goods Vehicle Fires in Tunnels. Fire Safety Journal 40:506–527
39. Hull TR, Stec AA (2010) Introduction to fire toxicity. In: Stec A, Hull R (eds) Fire Toxicity. CRC
40. Mauring T (2003). Personal communication, Åndalsnes, Norway
41. Nilsen AR, Lindvik PA, Log T Full-scale Fire Testing in Sub Sea Public Road Tunnels. In: Interflam 2001, Edinburgh, Scotland, 17–19 September 2001. Interscience Communications, pp 913–924
42. Ingason H, Bergqvist A, Lönnermark A, Frantzich H, Hasselrot K (2005) Räddningsinsatser i vägtunnlar. Räddningsverket, P21-459/05 (in Swedish)
43. Pitts WM (1994) The Global Equivalence Ratio Concept and the Prediction of Carbon Monoxide Formation in Enclosure Fires. National Institute of Standards and Technology, Gaithersburg, MD, USA
44. Beyler CL (1986) Major Species Production by Diffusion Flames in a Two-layer Compartment Fire Environment. Fire Safety Journal 10:47–56
45. Gottuk DT (1992) Carbon Monoxide Production in Compartment Fires. Journal of Fire Protection Engineering 4 (4):133–150

46. Gottuk DT, Lattimer BY (2002) Effect of Combustion Conditions on Species Production. In: DiNenno PJ (ed) SFPE Handbook of Fire Protection Engineering. Third Edition edn. National Fire Protection Association, Inc, Quincy, Massachusetts, USA, pp 2–54 -- 52–82
47. Blomqvist P, Lönnermark A (2001) Characterization of the Combustion Products in Large-scale Fire Tests: Comparison of Three Experimental Configurations. Fire and Materials 25:71–81
48. Babrauskas V, Parker WJ, Mulholland G, Twilley WH (1994) The phi meter: A simple, fuel-independent instrument for monitoring combustion equivalence ratio. Rev Sci Instrum 65 (7):2367–2375
49. Lönnermark A, Babrauskas V (1997) TOXFIRE-Fire Characteristics and Smoke Gas Analyses in Under-ventilated Large-scale Combustion Experiments: Theoretical Background and Calculations. SP Swedish National Testing and Research Institute, Borås, Sweden
50. Ingason H Fire Development in Catastrophic Tunnel Fires (CTF). In: Ingason H (ed) International Symposium on Catastrophic Tunnel Fires (CTF), Borås, Sweden, 20–21 November 2003. SP Swedish National Testing and Research Institute, pp 31–47
51. Ingason H (1995) Effects of Ventilation on Heat Release Rate of Pool Fires in a Model Tunnel. SP Swedish National Testing and Research Institute, Borås, Sweden
52. Ingason H (1995) Fire Experiments in a Model Tunnel using Pool Fires-Experimental Data. SP Swedish National Testing and Research Institute, Borås, Sweden
53. Lönnermark A, Blomqvist P, Månsson M, Persson H (1997) TOXFIRE-Fire Characteristics and Smoke Gas Analysis in Under-ventilated Large-scale Combustion Experiments: Tests in the ISO 9705 Room. SP Swedish National Testing and Research Institute, Borås, Sweden
54. Lönnermark A (2005) On the Characteristics of Fires in Tunnels. Doctoral Thesis, Doctoral thesis, Department of Fire Safety Engineering, Lund University, Lund, Sweden
55. Ingason H (2005) Fire Dynamics in Tunnels. In: Carvel RO, Beard AN (eds) The Handbook of Tunnel Fire Safety. Thomas Telford Publishing, London, pp 231–266
56. Grant GB, Drysdale D Estimating Heat Release Rates from Large-scale Tunnel Fires. In: Fire Safety Science-Proceedings of the Fifth International Symposium, Melbourne, 1995. pp 1213–1224
57. Gottuk DT, Roby RJ, Beyler CL (1995) The Role of Temperature on Carbon Monoxide Production in Compartment Fires. Fire Safety Journal 24:315–331
58. Tsuchiya Y CO/CO_2 Ratios in Fire. In: Fire Safety Science-Proceedings of the Fourth International Symposium, Ottawa, Canada, 13–17 June 1994. IAFSS, pp 515–526
59. Bettis RJ, Jagger SF, Wu Y (1993) Interim Validation of Tunnel Fire Consequence Models: Summary of Phase 2 Tests. Health and Safety Executive, Buxton, Derbyshire, UK
60. Beyler CL Major Species Production by Solid Fuels in a Two Layer Compartment Fire Environment. In: Fire Safety Science-Proceedings of the First International Symposium, Gaithersburg, USA, 7–11 October 1985. IAFSS, pp 431–440
61. Lönnermark A, Claesson A, Lindström J, Li YZ, Kumm M, Ingason H Gas composition during a fire in a train carriage. In: Proceedings from the Sixth International Symposium on Tunnel Safety and Security (ISTSS 2014), Marseille, France, 12–14 March 2014. SP Technical Research Institute of Sweden

Chapter 8
Gas Temperatures

Abstract Gas temperature is of great importance for assessment of heat exposure to tunnel users and tunnel structures, estimation of fire detection time and possibility of fire spread, and to design ventilation systems. In this chapter, the theory of fire plumes in ventilated flows is presented with a focus on the maximum ceiling gas temperature and its position in tunnel fires. The maximum ceiling excess gas temperature can be classified into two regions, depending on the ventilation velocity. Each can be divided into two subregions. The first subregion exhibits a linear increase which transits into a constant period, depending on the fire size, ventilation, and effective tunnel height. The position of the maximum ceiling gas temperature is directly related to a dimensionless ventilation velocity. A theoretical analysis of the upper smoke layer is presented and correlations for the distribution of ceiling gas temperature along the tunnel are given to support this analysis. Finally, a one-dimensional model of average gas temperatures in tunnel fires with longitudinal ventilation is presented.

Keywords Ventilation flow · Fire plume · Maximum ceiling gas temperature · Position · Flame angle · Temperature distribution · One-dimensional model

8.1 Introduction

The ability to predict gas temperatures in tunnel fires is of great importance. The knowledge can be used to assess heat exposure to humans and tunnel structures, to estimate fire detection time and risk for fire spread, and to design ventilation systems.

In particular, the stability of the tunnel structure is a key design parameter concerning the fire safety in tunnels. For example, a tunnel may be the key transportation line between two countries as in the case of the Mont Blanc or the St. Gotthard tunnels, where several fires have occurred, some with significant consequences [1], see also Chap. 1. A large fire can jeopardize the tunnel construction if the fire becomes too intense over a long period of time. Our knowledge of the impact of thermal exposure from the fire on the tunnel construction and how to calculate the stability of the structure is, therefore, critical. Traditionally, evaluation of heat exposure to a tunnel

H. Ingason et al., *Tunnel Fire Dynamics,* DOI 10.1007/978-1-4939-2199-7_8

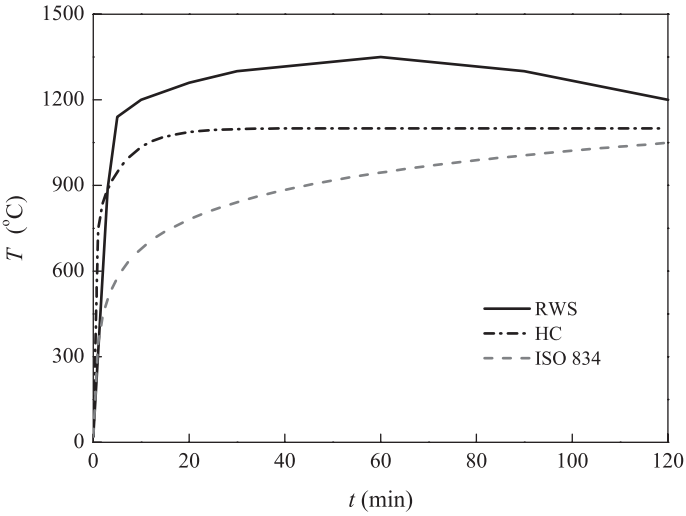

Fig. 8.1 A diagram of the interaction of ventilated flow with fire plume

construction is based on the use of standardized time–temperature curves. Indeed, standard fire temperature curves, such as ISO 834 [2], the hydrocarbon curve (HC) [3], or the RWS curve [4], are widely used to test the fire performance of tunnel linings, see Fig. 8.1.

In the following, a short summary of the mathematical expressions for various standardized time–temperature curves is given. One standard curve used when testing the temperature exposure is the cellulose curve defined in several standards, for example, ISO 834 [2]. This curve applies to materials found in typical buildings and is expressed as:

$$\Delta T(t) = 345\lg(8t+1) \tag{8.1}$$

where t is the time in min.

ISO 834 curve has been used for many years, also for tunnels, but it is clear that this curve does not represent all fire situations including the typical burning performance of important materials, for example petrol, chemicals, etc., and therefore a special curve, the hydrocarbon curve (the HC curve), which was developed in the 1970s for use in the petrochemical and offshore industries, has been applied to tunnels [3]. The main difference between these two curves is that the HC curve exhibits a much faster fire development and is consequently associated with a faster temperature increase than the standard ISO 834 fire curve and has traditionally been seen to be more relevant for a petroleum fire. The HC curve can be expressed as follows [3]:

$$\Delta T(t) = 1080(1 - 0.325\exp^{-0.167t} - 0.675\exp^{-2.5t}) \tag{8.2}$$

where t is the time in min.

Alternative (specific) temperature curves have been developed in some countries to simulate other hydrocarbon fires in tunnels. Examples of such curves are the Rijkswaterstaat Tunnel Curve (RWS curve) [4], the RABT/ZTV Curve [5], and the EBA curve [6]. These temperature curves are discontinuous and cannot be represented with a single mathematical expression as the ISO 834 and the HC curves. All these curves are derived in different ways and usually based on large- or small-scale tests or by consensus of technical committees working nationally or internationally in this field.

When choosing different curves, there is no single guideline document concerning how to choose one curve in relation to the HRRs (HRRs), longitudinal ventilation velocity, or the ceiling heights compared to others. The method is crude and prescriptive and therefore, not applicable to performance based design. Due to this fact, there is a clear need for a reliable engineering tool based on theoretical analysis that can predict the gas temperature as a function of the tunnel geometry, HRR, and ventilation conditions.

8.2 Interaction of Ventilation Flow with Fire Plume

The interaction of the ventilation flow with the fire plume is the most important phenomenon in ventilated tunnel fires. Hoult et al. [7, 8] made a valuable theoretical analysis of the fire plume in a ventilated flow based on the following assumptions:

1. The velocity and temperature defect profiles have the shape of a top hat, and that the cross section of the plume is circular.
2. The plume is slender, that is, the radius is small compared to the centreline radius of curvature.
3. There are basically two entrainment mechanisms: one is due to the difference between the plume velocity, u, and wind velocity component parallel to the plume, $u_o\cos\theta$, and the other to the wind velocity component, $u_o\sin\theta$, normal to the plume. The two mechanisms are additive.
4. The net rate of entrainment is the product of a dimensionless entrainment coefficient times the perimeter of the plume cross section times the corresponding velocity difference.
5. The entrainment coefficients, α and β, are independent of position along the plume.

The fire plume with an initial radius, b_{fo}, rises up and is then deflected by the horizontal ventilated flow, as shown in Fig. 8.2.

For weak plume the governing equations can be described as follows [7, 8, 16]:

Mass:

$$\frac{d}{d\xi}(B^2U) = 2B\left[\alpha\left|U - V'\cos\theta\right| + \beta\left|V'\sin\theta\right|\right] \tag{8.3}$$

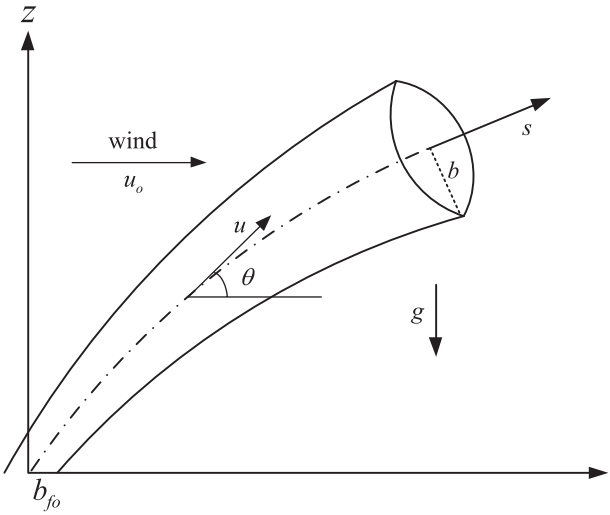

Fig. 8.2 A diagram of the interaction of ventilated flow with fire plume

Momentum:

$$\pi \frac{d}{d\xi}(B^2U^2) = \frac{\sin\theta}{U} + \pi V' \cos\theta \frac{d}{d\xi}(B^2U) \tag{8.4}$$

$$\pi B^2U^2 \frac{d\theta}{d\xi} = \frac{\cos\theta}{U} - \pi V' \sin\theta \frac{d}{d\xi}(B^2U) \tag{8.5}$$

Energy:

$$B^2U\phi = \frac{1}{\pi}\frac{w^{*2}}{b_{fo}g} \tag{8.6}$$

The dimensionless parameters are defined as follows:

The dimensionless plume radius: $B = b / b_{fo}$,
The dimensionless plume velocity: $U = u / w^*$,
The dimensionless plume temperature: $\phi = (T - T_o) / T_o$,
The dimensionless position along the trajectory: $\xi = s / b_{fo}$.
The dimensionless ventilation velocity is defined as:

$$V' = u_o / w^* \tag{8.7}$$

The characteristic plume velocity, w^*, is:

$$w^* = \left(\frac{g\dot{Q}}{b_{fo}\rho_o c_p T_o}\right)^{1/3} \tag{8.8}$$

where b_{fo} is the radius of fire source (m), u is the plume velocity (m/s), u_o is the wind velocity (m/s), s is a trajectory (m), b is the radius of fire plume at a given position (m), g is the acceleration of gravity (m/s^2), $\dot{Q}$ is the HRR (kW), ρ_o is the ambient density (kg/m^3), c_p is the heat capacity (kJ/kgK), T_o is the ambient temperature (K), θ is the angle between plume axis and horizontal axis (°), α is the tangential entrainment coefficient and β is the normal entrainment coefficient.

The above equations show that the dimensionless ventilation velocity is the key parameter in the interaction of ventilated flow with fire plume, with which both ventilation velocity and characteristic plume velocity are correlated.

8.3 Maximum Ceiling Gas Temperature

Extensive research has been conducted on maximum ceiling gas temperatures in tunnel fires. Kurioka et al. [9] proposed an empirical equation to predict the maximum gas temperature rise below the tunnel ceiling and its position relative to the center of the fire. Their equation indicates that the maximum ceiling gas temperature approaches infinite, when the ventilation velocity approaches zero. One consequence of this behavior is that the maximum gas temperature rise below the ceiling cannot be predicted correctly when the ventilation velocity is very low. Moreover, the proposed correlation was originally obtained by empirical correlations rather than theoretical analysis. Li et al. [10–12] conducted a theoretical analysis of the maximum gas temperature rise below the ceiling based on an axisymmetric fire plume theory. The proposed equations for the maximum excess gas temperature beneath the ceiling fits the data from both model- and large-scale tests. The theory of maximum ceiling gas temperature in tunnel fires proposed by Li et al. [10–12] is presented in the following sections.

8.3.1 Fire Plume Mass Flow Rate in a Ventilated Flow

The first approach is to perform a simple theoretical analysis in order to predict the maximum ceiling temperature in a longitudinally ventilated tunnel flow. In order to do that, we assume that we can exclude the virtual source term in the axisymmetric fire plume analysis. The virtual source term is used to compensate for the difference between the actual fire source and the ideal point source [13]. The mass flow rate of an axisymmetric fire plume in the open can then be expressed as [14, 15]:

$$\dot{m}_{p,o}(z) = 0.071\dot{Q}_c^{1/3} z^{5/3} \tag{8.9}$$

where $\dot{Q}_c$ is the convective HRR (kW), z is the height above the fire source (m), and $\dot{m}_{p,o}$ is the mass flow rate of the plume in the open (kg/s).

Normally in a longitudinally ventilated tunnel, the fire plume on the downstream side leans towards the tunnel surface. The air entrainment of the fire plume is stronger than this in the open. Experimental data of air entrainment through ventilated windows from Quintiere et al. [16] supports the trend that the extra air entrainment due to wind increases almost linearly with the air velocity through the ventilated window. The ratio of mass flow rate of the fire plume in a ventilated flow to that in the open can be expressed as [10]:

$$\frac{\dot{m}_p(z)}{\dot{m}_{p,o}(z)} = C_k V' \tag{8.10}$$

where $\dot{m}_p$ is the mass flow rate at a given height in a ventilated flow (kg/s) and C_k is a coefficient. Note that the dimensionless ventilation velocity, V', is defined as the ratio of the ventilation velocity, u_o, to the characteristic plume velocity w^*.

AGA studied the effect of wind on LNG pool fires and proposed a formula to estimate the flame angle due to wind, for methane which can be expressed as [16, 17]:

$$\sin\theta = \begin{cases} 1, & V' \le 0.19 \\ (5.26V')^{-1/2}, & V' > 0.19 \end{cases} \tag{8.11}$$

The flame angle θ in Eq. (8.11) is defined as the angle between the flame axis and a horizontal surface. It is shown that when the ventilation velocity is too small, that is when $V' \le 0.19$, the flame is hardly deflected and the ventilated flow has no effect on the fire plume. Consequently, the plume mass flow rate does not increase. In addition, when the ventilation velocity is greater ($V' > 0.19$), the flame deflects and the ventilated flow induces extra air entrainment into the fire plume in a ventilated flow, so that the plume mass flow rate increases with the ventilation velocity. Consequently, the condition for this transition can be expressed as:

$$V' = 0.19 \tag{8.12}$$

Note that under this condition, the ratio of mass flow rate of the fire plume in a ventilated flow to that in the open, as defined in Eq. (8.10), should be equal to 1, both for the dimensionless ventilation velocity lower than 0.19 ($V' \le 0.19$) and for the dimensionless ventilation velocity greater than 0.19 ($V' > 0.19$). Consequently, the coefficient C_k can be given as:

$$C_k = \begin{cases} 1/V', & V' \le 0.19 \\ 5.26, & V' > 0.19 \end{cases} \tag{8.13}$$

Substituting Eqs. (8.9) and (8.13) into Eq. (8.10) yields:

$$\dot{m}_p(z) = \begin{cases} 0.071\dot{Q}_c^{1/3} z^{5/3}, & V' \le 0.19 \\ 0.3735\dot{Q}_c^{1/3} z^{5/3} V', & V' > 0.19 \end{cases} \tag{8.14}$$

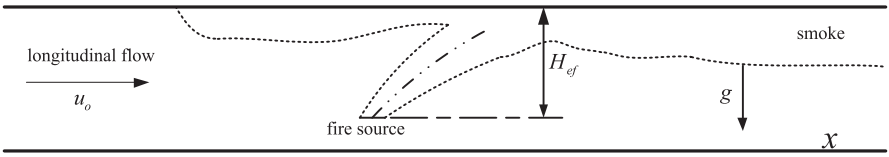

Fig. 8.3 Definition of the effective tunnel ceiling height, H_{ef}

8.3.2 Maximum Ceiling Gas Temperature in a Small Fire

We assume that the velocity and temperature profiles are of similar form, independent of the height. Further, we assume that these profiles are so called top-hat profiles, so that the velocity and temperature are constant over the whole section at a given height. This is a normal assumption for axisymmetric fire plumes in the open.

In addition, the radiative energy is typically in the range of 20–40 % of the total energy released from many common fuel sources. This means that 70 % of the total HRR is a reasonable value to be used as the convective HRR. The average excess temperature of the fire plume above ambient at a given height, $\Delta T(z)$, can therefore be expressed as [10–12]:

$$\Delta T(z) = \frac{\dot{Q}_c}{\dot{m}_p(z)c_p} = \frac{(1-\chi_r)\dot{Q}}{\dot{m}_p(z)c_p} \tag{8.15}$$

where χ_r is the fraction of convective HRR in total HRR.

According to research on plume flow in the open, the weak plume assumptions can be relaxed. In addition, note that the maximum temperature of the fire plume at the tunnel height is the maximum temperature of the buoyancy-driven smoke flow beneath the tunnel ceiling. This means that the effective tunnel height, that is the vertical distance between the bottom of the fire source (flame) and the tunnel ceiling, H_{ef}, is the vertical distance above the fire source bottom, z, under this condition, see Fig. 8.3 for a geometric illustration of these parameters.

The maximum gas excess temperature beneath the ceiling can therefore be expressed as:

$$\Delta T_{\max} = C_T \Delta T(H_{ef}) \tag{8.16}$$

where ΔT_{max} is the maximum ceiling gas excess temperature (K), C_T is a temperature correction factor due to the top hat assumption and H_{ef} is the effective tunnel height.

Substituting Eqs. (8.14) and (8.15) into Eq. (8.16) gives [10–12]:

$$\Delta T_{\max} = \begin{cases} 14.1 C_T (1-\chi_r)^{2/3} \dfrac{\dot{Q}^{2/3}}{H_{ef}^{5/3}}, & V' \le 0.19 \\ \dfrac{2.68 C_T (1-\chi_r)^{2/3} g^{1/3}}{(\rho_o c_p T_o)^{1/3}} \dfrac{\dot{Q}}{u_o b_{fo}^{1/3} H_{ef}^{5/3}}, & V' > 0.19 \end{cases} \tag{8.17}$$

From Eq. (8.17), it is seen that the maximum gas excess temperature beneath the tunnel ceiling can be categorized into two regions. When the dimensionless ventilation velocity, V', is lower than 0.19 (Region I), the plume mass flow rate in a ventilated tunnel can be assumed to be almost equal to that in the open, and so the maximum gas excess temperature is the same, independent of the ventilation velocity. Further, the maximum gas excess temperature varies as two-thirds power of the HRR. This phenomenon occurs at a relatively high HRR or at a very low ventilation velocity. When the dimensionless ventilation velocity, c, is greater than 0.19 (Region II), the mass flow rate of the fire plume in a ventilated tunnel increases linearly with the ventilation velocity and decreases slowly with the HRR. As a consequence, the maximum gas excess temperature is proportional to the HRR, and inversely proportional to the ventilation velocity, as shown in Eq. (8.17). In addition, the maximum excess gas temperature varies as a $-5/3$ power law of the effective tunnel height in both regions.

Equation (8.17) was obtained based on the assumption that the flow profile and the gas temperature profile across the section of the fire plume at any height is a top-hat profile, and that the continuous flame zone is lower than the tunnel height. This implies that the plume gas temperature is assumed to be constant across any section of the plume. In practice, at any given height the center line gas temperature of the fire plume is higher than the average gas temperature. The coefficient, C_T, defined in Eq. (8.16) can be determined from experimental data. The maximum excess gas temperature beneath the tunnel ceiling can be expressed as [10]:

$$\Delta T_{\max} = \begin{cases} 17.5 \dfrac{\dot{Q}^{2/3}}{H_{ef}^{5/3}}, & V' \le 0.19 \\ \dfrac{\dot{Q}}{u_o b_{fo}^{1/3} H_{ef}^{5/3}}, & V' > 0.19 \end{cases} \tag{8.18}$$

Comparing Eqs. (8.17) and (8.18) indicates that the coefficient C_T is equal to 1.57 for Region I and 1.56 for Region II. This means that the condition for this transition that the dimensionless ventilation velocity approaches 0.19, is appropriate to estimate the fire plume properties for fires in longitudinally ventilated tunnels. It is known that this value is around 1.8 for free plumes. The wind could affect the profiles of temperature and velocity at a given cross section and thus the slight difference exists. Further, Lönnermark and Ingason [18] found that the width of the tunnel had no influence on the maximum gas temperature. These finding correlate well with the theoretical model presented here.

8.3.3 Maximum Ceiling Gas Temperature in a Large Fire

The above correlations are not valid when the flames become very large. For a very large fire in the tunnel, the flame impinges on the tunnel ceiling, and the continuous flame volume (combustion zone) extends along the tunnel ceiling, see Fig. 8.4.

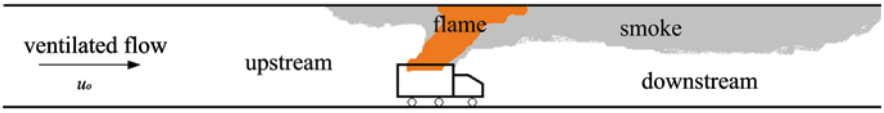

Fig. 8.4 A diagram of turbulent flame impinging on the ceiling in a large tunnel fire

Therefore, the maximum temperature beneath the ceiling should be the flame temperature. In such cases, the mass flow rate of the fire plume is difficult to estimate and Eq. (8.14) collapses. Therefore, prediction of the temperature of a large fire plume in a ventilated flow appears to be impossible to derive theoretically using this methodology.

However, we can assume that Eq. (8.18) should still be fulfilled before the part of the flame volume representing the combustion zone impinges on the tunnel ceiling. After that the maximum temperature beneath the ceiling is assumed to be the flame temperature. This means that in such a case the maximum temperature beneath the ceiling should be a constant, based on a vast majority of research on the flame temperature, such as McCaffrey's fire plume theory [18]. However, gas temperatures over 1000 °C, even up to about 1365–1370 °C, have been measured beneath the tunnel ceiling in full-scale tests such as the Runehamar tests [19] and the Memorial tests [20].

The reason why the maximum temperature beneath the tunnel ceiling is so high is that the scenario is different to that in an open fire or an enclosure fire. In an open fire, the flame and hot gases radiate to the surroundings, approximately without any heat feedback from the surrounding. In an enclosure fire the heat feedback from the surrounding roof and walls is generally limited due to the large space and the possible highest HRR is directly related to opening areas except for a fully developed fire. However, for a large fire in the tunnel, the heat feedback plays an important role in the heat balance of flame and hot gases, and the forced ventilation enhances the combustion. Further, Note that a tunnel fire is normally fuel controlled in a well-ventilated tunnel. As a consequence, the temperature of the flame and hot gases is higher than in an open fire or an enclosure fire.

The maximum temperature beneath the ceiling in a tunnel fire is independent of the ventilation velocity if the ventilation velocity across the fire source is very low compared to the HRR, and the maximum temperature is simply dependent on the HRR; however, it approaches a constant if the part of the flame volume containing the combustion zone is present at the tunnel ceiling. In other words, if $V' \leq 0.19$ (Region I), the maximum excess temperature can be expressed as:

$$\Delta T_{\max} = \begin{cases} \mathrm{DTR\,I}, & \mathrm{DTR\,I} < 1350 \\ 1350, & \mathrm{DTR\,I} \geq 1350 \end{cases} \tag{8.19}$$

where the Delta T in Region I, DTRI, is defined as:

$$\mathrm{DTR\,I} = 17.5\frac{\dot{Q}^{2/3}}{H_{ef}^{5/3}}$$

If the ventilation velocity across the fire source becomes larger, the maximum excess temperature beneath the ceiling depends on both the HRR and the ventilation velocity. However, it also approaches a constant if the continuous combustion zone is present at the tunnel ceiling. In other words, if $V' > 0.19$ (Region II), the maximum excess temperature can be expressed as:

$$\Delta T_{\max} = \begin{cases} \mathrm{DTR\,II}, & \mathrm{DTR\,II} < 1350 \\ 1350, & \mathrm{DTR\,II} \geq 1350 \end{cases} \tag{8.20}$$

where the Delta T in Region II, DTRII, is defined as:

$$\mathrm{DTR\,II} = \frac{\dot{Q}}{u_o b_{fo}^{1/3} H_{ef}^{5/3}}$$

Figure 8.5 and 8.6 show the maximum ceiling excess gas temperatures in tunnel fires in Region I ($V' \leq 0.19$) and Region II ($V' > 0.19$) respectively. Clearly, the tests data are correlated well with Eqs. (8.19) and (8.20).

Although, in theory the maximum excess temperature in the constant regions is also dependent on some other parameters, such as the thermal properties of tunnel wall and vehicles, the figures show that it is close to a constant in the constant regions, and the equations presented above normally produce conservative results suitable for engineering applications.

Note that, there is a parameter called the radius of the fire source b_{fo} used in the above equations. For a circular fire source, the radius of the fire source is easy to determine. For a rectangular fire source, such as a gas fire or pool fire, an equivalent circular radius of the fire source should be used based on equivalent area of fire source, that is $\sqrt{4A/\pi}$ (where A is the area of the fuel source). The same method has been applied to a wood crib fire. In such cases, the projection area (or bottom area) of the fire source can be regarded as an equivalent geometry of the fire source.

It should also be noted that the height used here is not the tunnel height, but the effective tunnel height, H_{ef}, that is the vertical distance between the bottom of the fire source and the tunnel ceiling. This parameter is very important in order to determine the maximum excess temperature beneath the ceiling in a tunnel fire.

The correlations, that is Eqs. (8.19) and (8.20), can be used to calculate the excess gas temperature as a function of the HRR and ventilation velocity at any given tunnel and fire scenario. These equations become the key for converting a standardized time–temperature curve for a given tunnel to the corresponding HRR to obtain this temperature, and vice versa.

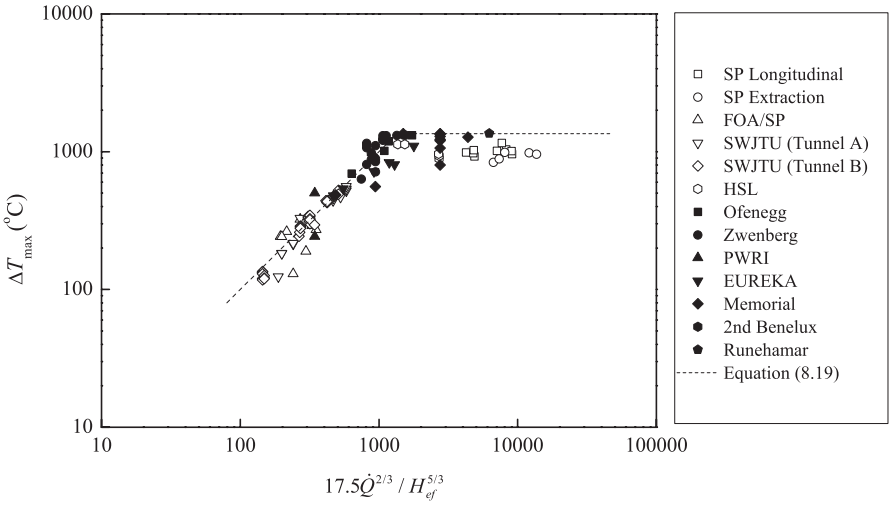

Fig. 8.5 Maximum excess gas temperature beneath the tunnel ceiling (Region I) [11]

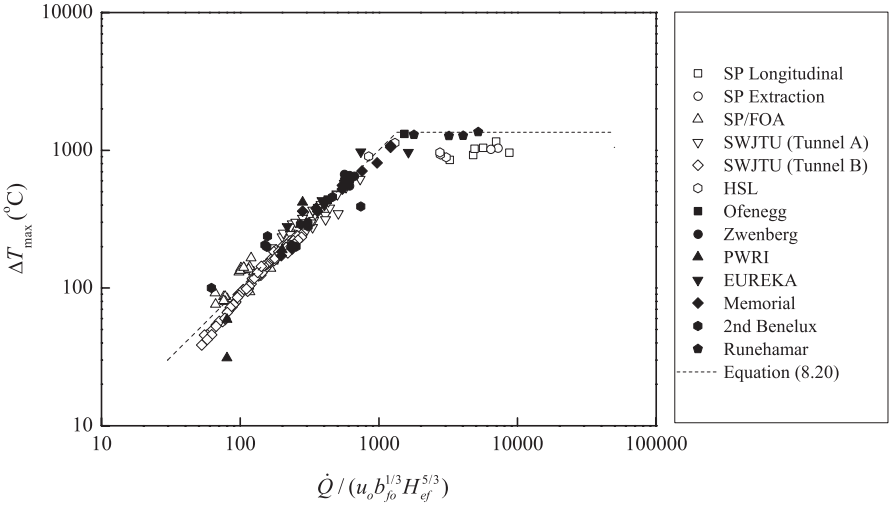

Fig. 8.6 Maximum excess gas temperature beneath the tunnel ceiling (Region II) [11]

Example 8.1 An HGV vehicle (heavy goods vehicle trailer) is assumed to start to burn due to a tyre or engine fire. The tunnel height at its maximum is 6 m and the width is 12 m at its widest part. The height from the bottom of the fire load up to the ceiling is 4.8 m. The radius of the fuel in the vehicle, b_{fo}, is 4 m. The fire is assumed to be fuel controlled (or well-ventilated). The ambient conditions are 10 °C. Calculate the maximum ceiling gas temperature for a 6 m high and 12 m wide tunnel with:

1. Natural ventilation system at a HRR of 10 MW;

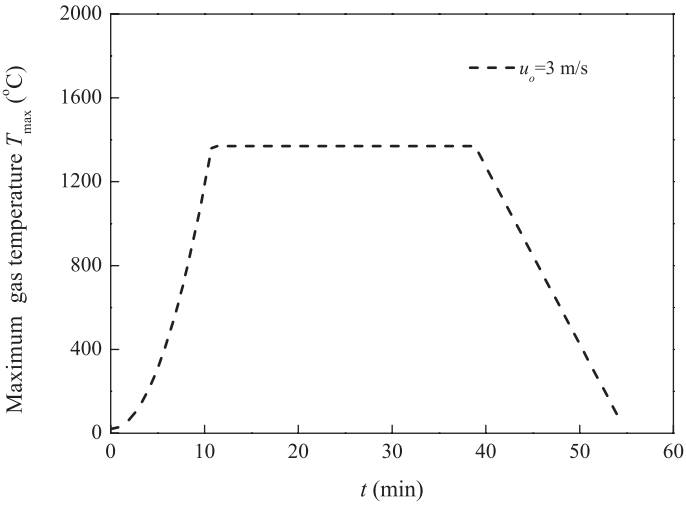

Fig. 8.7 A unique time–temperature curve for Example 8.1

2. Semitransverse ventilation at a longitudinal velocity through the fire of 0.5 m/s and a HRR of 10 MW.
3. Longitudinal ventilation at a longitudinal velocity of 3 m/s. The fire approximately follows the ultra-fast curve to a maximum HRR of 150 MW, and keep for 10 min and then decrease to 0 after further 20 min. Make a time–temperature curve for this tunnel fire. The ultra-fast curve is expressed as $\dot{Q} = 0.19t^2$, where $\dot{Q}$ is HRR in kW, and t is time in seconds.

Solution:

1. *Note that $V' < 0.19$ according to Eqs. (8.7) and (8.8). Therefore, Eq. (8.19) should be used. The estimated maximum ceiling gas temperature is 595 °C.*
2. *For a semitransverse ventilation system, there could still be a longitudinal velocity which is one of the key parameter for us to calculate the maximum ceiling gas temperature. We need to check the value of V', which can be found to be 0.12 using Eqs. (8.7) and (8.8). Therefore, $V' < 0.19$, Eq. (8.19) should be used. The estimated maximum ceiling gas temperature is 922 °C.*
3. *Note that $V' > 0.19$ for the entire time period. By using Eq. (8.20) we can make a unique time–temperature curve, as shown in Fig.* 8.7.

Example 8.2 Assuming that the tunnel in Example 8.1 is designed for the HC curve, estimate the corresponding HRR curve and also if the fire duration is assumed to be 120 min, what is the corresponding fire load in GJ. The longitudinal ventilation is assumed to be 3 m/s. The expression for the Hydrocarbon Curve (HC) can be found in Eq. (8.2).

Solution: First we assume $V' > 0.19$ since $\dot{Q}(t)$ is unknown. This means that Eq. (8.20) is used here. The corresponding HRR can be found in Fig. 8.8. *Then we calculate V' using $\dot{Q}_{max}$, which turns out to be greater than 0.19.This means at any*

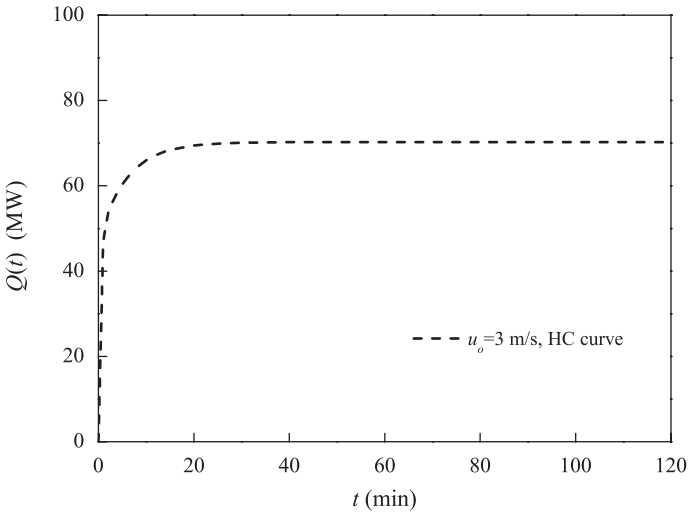

Fig. 8.8 The calculated HRR corresponding to a HC curve in a 6 m high tunnel with ventilation of 3 m/s

time in this scenario, V'>0.19 is fulfilled, which verifies the first assumption. For data with a temperature over 1100 °C*, it is difficult to determine in which region it lies. However, it is clear that the calculated HRR is the minimum value required to obtain such a high temperature.*

If we integrate the curve we find the total energy to be 496 GJ. This would correspond to at least two HGVs. A reasonable conclusion is that this tunnel would be designed to a fire that can resist a collision between two HGVs, and the fire can be very intense for up to 120 min. This shows the practical implication of using Eqs. (8.19) and (8.20). These equations become a key to relate information between the standardized time–temperature curves and the fire load in terms of the HRR and total energy found in the fire load.

8.4 Position of Maximum Ceiling Gas Temperature

A schematic diagram of the position of the maximum ceiling temperature in a tunnel fire is shown in Fig. 8.9. The horizontal distance between the position of the maximum ceiling temperature and the fire source centre is L_{MT}. A flame angle, φ, is defined here as the angle between the horizontal line and the line connecting the fire source centre and the position of the maximum ceiling temperature. Therefore, it should be kept in mind that the flame angle, φ, discussed here is defined based on the position of the maximum ceiling temperature, rather than the real flame angle.

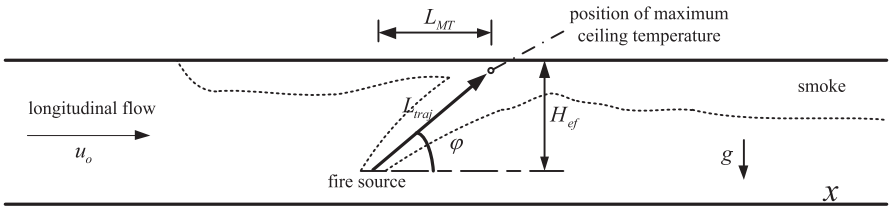

Fig. 8.9 A diagram of flame angle and position of maximum ceiling gas temperature

Experimental data for air entrainment through ventilated windows from Quintiere et al. [16] support the postulate that the mass flow rate of fire plume in a ventilated flow is almost equal to that in the open by use of the inclined flame path as the plume height. In other words, Eqs. (8.14) and (8.9) should be equal to each other when using H_{ef} and L_{traj}, respectively [21]:

$$\dot{m}_p(H_{ef}) = \dot{m}_{po}(L_{traj}) \tag{8.21}$$

where L_{traj} is the length of the trajectory of the plume (m), and H_{ef} is the effective height (m), that is, the vertical distance between the tunnel ceiling and the bottom of the fire source (flame).

Note that when the ventilation velocity is very low, the plume is not inclined by horizontal wind (or at least to a negligible degree), so the flame angle should approach 90°. Under these conditions the continuity of the equations should also be fulfilled.

Therefore, we obtain the following equation [21]:

$$\sin\varphi = \frac{H_{ef}}{L_{traj}} = \begin{cases} 1, & V' \le 0.19 \\ (5.26V')^{-3/5}, & V' > 0.19 \end{cases} \tag{8.22}$$

If the flame angle is known, the horizontal distance between the position of the maximum ceiling temperature and the fire source centre, L_{MT}, can be simply calculated (see Fig. 8.9) [21]:

$$L_{MT} = H_{ef}\cot\varphi \tag{8.23}$$

Based on the above analysis, one can conclude that the position of the maximum ceiling temperature is directly dependent on the dimensionless ventilation velocity in a small tunnel fire. The influence of the tunnel width on the fire plume is supposed to be insignificant and thus ignored since the deflection depends on the interaction of ventilation flow with fire plume, which generally has nothing to do with tunnel width. Instead, the effective tunnel height plays a key role in the position of the maximum ceiling temperature.

When the fire becomes larger, the flame tip reaches the ceiling and extends a certain distance along the tunnel. The influence of the HRR on the position of the maximum ceiling temperature could be different, based on experience from the previous study on smoke control and maximum ceiling temperature [10, 11, 22].

Under low ventilation conditions, the phenomenon of backlayering occurs upstream of the fire. The dimensionless backlayering length, L_b^*, can be expressed as [22]:

$$L_b^* = \frac{L_b}{H} = \begin{cases} 18.5\ln(0.81\mathrm{Ri}^{\prime 1/3}) & Q^* \le 0.15 \\ 18.5\ln(0.43/u^*) & Q^* > 0.15 \end{cases} \tag{8.24}$$

where H is the tunnel height (m). The modified Richardson Number, Ri', dimensionless longitudinal velocity, u^*, and the dimensionless HRR, Q^*, in Eq. (8.24) are respectively defined as [22]:

$$\mathrm{Ri}' = \frac{g\dot{Q}}{\rho_o c_p T_o u_o^3 H}, \quad u^* = \frac{u_o}{\sqrt{gH}}, \quad Q^* = \frac{\dot{Q}}{\rho_o c_p T_o g^{1/2} H^{5/2}} \tag{8.25}$$

It should be kept in mind that these equations do not take the geometry of the fire source into account. However, Eq. (8.24) implies that for a large fire in a tunnel, that is when $Q^*>0.15$, the backlayering length is independent of HRR and only related to the ventilation velocity.

Note that, the modified Richardson Number in Eq. (8.25) can be related to the dimensionless ventilation velocity [21]:

$$\mathrm{Ri}' = \frac{b_{fo}}{H} V'^{-3} \tag{8.26}$$

where b_{fo} is the radius of fire source (m).

For a small fire in a tunnel, it can be seen that both the flame angle and the backlayering length are directly related to the modified Richardson Number. It can therefore be speculated that for a large fire in a tunnel, the flame angle is also independent of the HRR, drawing an analogy to the backlayering length. Due to the continuity of the equations at the transition point, the full expression of the flame angle can be expressed as [21]:

$$\sin\varphi = \frac{H_{ef}}{L_{traj}} = \begin{cases} 1, & V' \le 0.19 \\ (5.26V')^{-3/5}, & V' > 0.19 \,\&\, Q^* \le 0.15 \\ 0.25(b_{fo}u^{*3}/H)^{-1/5} & V' > 0.19 \,\&\, Q^* > 0.15 \end{cases} \tag{8.27}$$

According to Eq. (8.27), it can be seen that the flame angle can be categorized into three zones. The flame angle is 90° if the dimensionless ventilation velocity is lower than 0.19. If V' increases, the flame angle varies as −3/5 power law of V' when $Q^* \le 0.15$, and is independent of HRR when $Q^*>0.15$.

Figure 8.10 shows a plot of tests data related to the position of maximum ceiling gas temperature [21]. The data correlate well with the proposed equations.

Example 8.3 Estimate the positions of the maximum ceiling gas temperatures in a 6 m high and 10 m wide tunnel at HRRs of 10 MW and 50 MW respectively. The

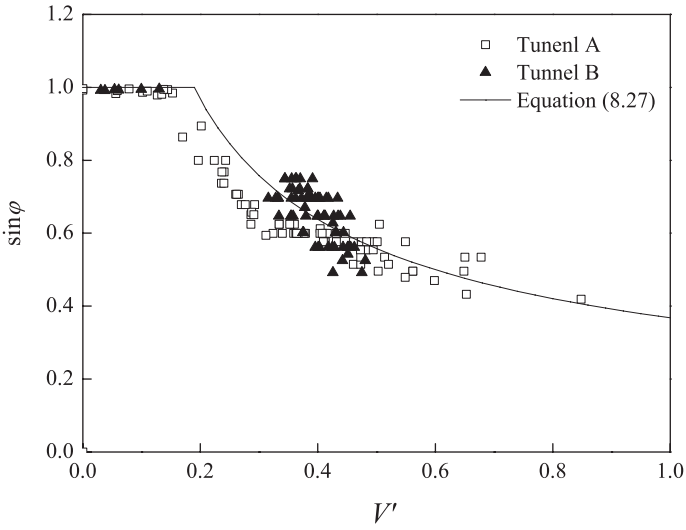

Fig. 8.10 Flame angle and dimensionless ventilation velocity [21]. Tunnel A and Tunnel B are two model tunnels with different cross section

longitudinal ventilation velocity is 3 m/s. The fire source has an equivalent radius of 2 m and its bottom is 1 m above the floor.

Solution:

1. *For the 10 MW fire, V' can be estimated to be 0.58 using Eq. (8.7), lower than 0.19, and the dimensionless HRR Q^* is 0.10 using Eq. (8.25), lower than 0.15. This means that the second conditions in Eq. (8.27) are valid for this case. The estimated horizontal distance between the position of the maximum ceiling gas temperature and the fire source center using Eq. (8.27) is therefore 8.4 m.*
2. *For the 10 MW fire, V' can be estimated to be 0.34, greater than 0.19, and the dimensionless HRR Q^* is 0.51, greater than 0.15. This means that the third conditions fulfill the requirement in Eq. (8.27) and should therefore be used. The estimated horizontal distance between the position of the maximum ceiling gas temperature and the fire source center using Eq. (8.27) is 7.6 m, slightly shorter than that in the first example due to that the larger fire in this example creates larger buoyancy force.*

8.5 Ceiling Gas Temperature Distribution

First, let us carry out a theoretical analysis of the stratified smoke flows in the upper layer at a quasi-steady state. Similar to the vertical plume entrainment, it can be assumed that the entrainment velocity is proportional to the relative velocity of the

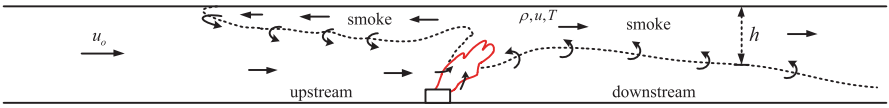

Fig. 8.11 A schematic diagram of smoke spread upstream and downstream of the fire

smoke flow, see more in Chap. 12. A schematic view of smoke spread upstream and downstream of the fire is shown in Fig. 8.11.

Downstream of the fire, the smoke flow at the upper layer entrains the air from the lower layer. Assuming that no heat source is introduced into the ceiling smoke flow (no combustion in the ceiling flow), the mass and energy equations can be expressed as:

$$\frac{\mathrm{d}}{\mathrm{d}x}(\rho uA) = \rho_o W v_e \tag{8.28}$$

$$\frac{\mathrm{d}}{\mathrm{d}x}(\rho Auc_p T) = \rho_o W v_e c_p T_o - h_t w_p (T - T_o) \tag{8.29}$$

The entrainment velocity, v_e (m/s), for downstream smoke flow could be expressed as (see details in Chap. 12):

$$v_e = \beta(u - u_o) \tag{8.30}$$

In the above equations, u is the smoke velocity (m/s), u_o is the air velocity (m/s), A is the cross-sectional area of the smoke flow (m^2), W is the tunnel width at the bottom of the smoke layer (m), h_t is the total net heat transfer coefficient on tunnel walls (kW/m^{2}K), w_p is the wet perimeter of the smoke flow (M), β is the entrainment coefficient, ρ and T are the average density (kg/m^3) and temperature of the smoke flow (K).

It is known that the dominating term in the differential energy equation, that is, Eq. (8.29), is the heat loss to the tunnel structure. Therefore, the effect of entrainment on the energy equation is ignored while solving the differential equations. To obtain an analytical solution, it is also assumed that the net heat transfer coefficient, h_t, and wet perimeter, w_p, (or the term $h_t w_p$) are constant. Therefore, we have:

$$\frac{\Delta T(x)}{\Delta T_{\max}} = \exp\left(-\frac{h_t w_p + \rho_o v_e W c_p}{\rho u A c_p} x\right) \tag{8.31}$$

where h is the smoke layer height (m). The above equation can be approximately expressed as:

$$\frac{\Delta T}{\Delta T_{\max}} \approx \exp\left(-a\frac{x}{h}\right) \tag{8.32}$$

For rectangular cross-sections ($A = hW$), the dimensionless parameter a in the above equation can be expressed as:

$$a = \frac{h_t(1+2h/W)+\rho_o v_e c_p}{\rho u c_p} \propto \frac{h_t}{\rho u c_p} \tag{8.33}$$

where x is the distance from the fire source (m). Note that, the smoke layer height is generally much smaller than the width and also the ratio h/W varies in a narrow range.

This suggests that the ceiling gas temperature varies as an exponential equation of the dimensionless distance from the fire if the parameter a is constant.

Upstream of the fire, the behavior of smoke flow is slightly different from that downstream of the fire. The fresh air flow at a high velocity could be considered to entrain the smoke from the upper layer and blow it away from the fire. In the case that the fresh air flow has a great enough velocity, it could arrest the smoke front and prevent any further spread, see Fig. 8.11. Close to this point, the mass flow rate of the smoke flow decreases to 0. Assuming that no heat source is introduced into the horizontal smoke flow, the mass and energy equation can be expressed as:

$$\frac{\mathrm{d}}{\mathrm{d}x}(\rho u A) = -\rho W v_e \tag{8.34}$$

$$\frac{\mathrm{d}}{\mathrm{d}x}(\rho A u c_p T) = -\rho W v_e c_p T - h_t w_p (T - T_w) \tag{8.35}$$

The entrainment velocity for the upstream smoke flow could be expressed as:

$$v_e = \beta(u + u_o) \tag{8.36}$$

Similar to the treatment to the downstream smoke flow, the analytical solution can be expressed as follows:

$$\frac{\Delta T}{\Delta T_{\max}} = \exp\left(-\frac{h_t w_p}{\rho A u c_p} x\right) \tag{8.37}$$

The above equation can then be simplified into:

$$\frac{\Delta T}{\Delta T_{\max}} = \exp\left(-b\frac{x}{h}\right) \tag{8.38}$$

where, for rectangular cross sections, the dimensionless parameter, b, is defined as:

$$b = \frac{h_t(1+2h/W)}{\rho u c_p} \propto \frac{h_t}{\rho u c_p} \tag{8.39}$$

From the above analysis, it is expected that for smoke flows both downstream and upstream of the fire, the temperature distribution can be approximated using an exponential function.

Note that the Stanton number *St* is correlated with the skin friction coefficient, which can expressed approximately as follows:

$$\mathrm{St} = \frac{h_c}{\rho u c_p} = \frac{1}{2} C_f \tag{8.40}$$

where h_c is the convective heat transfer coefficient (kW/m^{2}K), C_f is the friction coefficient. This suggests that for small fires where the convective heat transfer dominates, the decrease of the ceiling gas temperature follows an exponential equation.

However, the heat transfer coefficient in Eqs. (8.31) and (8.37) is the total heat transfer coefficient on a tunnel wall, h_t, rather than the convective heat transfer coefficient, h_c. For most tunnel fires that are relevant, the radiative heat transfer dominates heat transfer to the tunnel walls in the near field of the fire source. In such cases, the term in the numerator of *a* and *b* should be 2+2 instead of 1+2 *h*/*W*. In reality, the conductive heat transfer plays an important role in the total heat transfer from hot gases to the tunnel wall, and its importance increases with time. In other words, at the early stages of a fire, the conduction has an insignificant influence on the heat transfer but the importance of the heat conduction increases with time, see Chap. 10.

Therefore, the total heat transfer coefficient is not constant along the tunnel. Instead, it should be greater close to the fire but less far away from the fire. Similarly, it should be greater at the early stage of the fire and less as time goes on. If the tunnel walls are exposed to hot gases for a long time, heat conduction will dominate the heat transfer, and then the coefficient approaches a constant along the tunnel. Despite this, based on the test data, it has been found that the ceiling temperature distribution along the tunnel can be well represented by the sum of two exponential equations, and the tunnel height could be used to represent the smoke layer height, *h*. This is in good correlation to the theory, that is, Eqs. (8.32) and (8.38).

The dimensionless excess gas temperature beneath the tunnel ceiling downstream of the fire can be plotted as a function of a dimensionless distance from the fire, as shown in Fig. 8.12. Data from model-scale tunnel fire tests conducted at SP and full-scale tunnel fire tests including the Runehamar tunnel tests and the Memorial tunnel tests have been used. Note that, data for both high and low ventilations are plotted in Fig. 8.12. It is shown that all the experimental data correlates well with the sum of two exponential equations, which can be expressed as:

$$\frac{\Delta T(x)}{\Delta T_{\max}} = 0.55 \exp(-0.143 \frac{x - x_v}{H}) + 0.45 \exp(-0.024 \frac{x - x_v}{H}) \tag{8.41}$$

where x_v is the distance between the virtual origin and the fire source (m).

Cleary, Fig. 8.12 shows that the ceiling gas temperature decreases more rapidly with distance in the vicinity of the fire than further away from the fire. This has

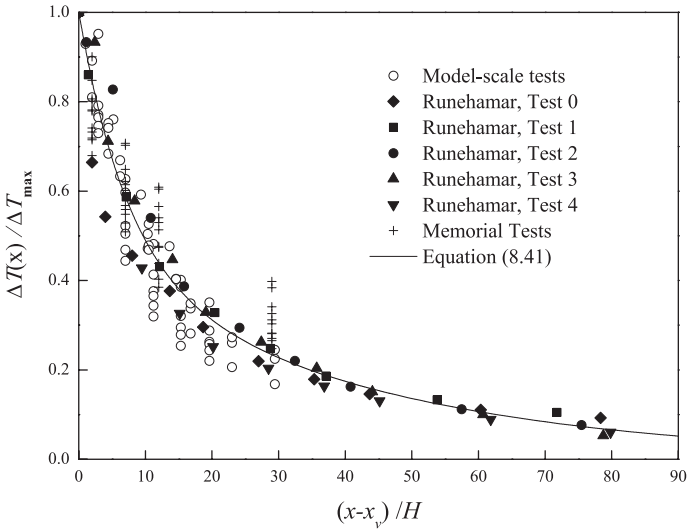

Fig. 8.12 Distribution of dimensionless ceiling excess gas temperature along the tunnel

been explained as being due to the fact that the total heat transfer coefficient in the vicinity of the fire is much greater than further downstream.

It should be kept in mind that in the above analysis, it has been assumed that no heat is introduced to the ceiling smoke flow. In large fires, the ceiling flame exists and continuously releases heat along the tunnel. This indicates that in the vicinity of the fire the gas temperatures could decrease much more slowly. This phenomena has been observed by Ingason and Li [23]. In the analysis of test data from model- and full-scale tunnel fire tests conducted by SP, they found [23] that there is a virtual origin for large fires, that is, the gas temperatures between the fire source center and the virtual origin decrease very slowly. They postulated that this is due to the fact that the continuous flame continually introduces a large amount of heat into the smoke flow although the smoke flow releases heat along the tunnel. Given that a gas temperature of 600 °C could represent a ceiling flame tip, the distance between a ceiling gas temperature of 1200 and 600 °C is approximately ten times the tunnel height, according to Eq. (8.41). The distance between the fire source center and the virtual origin, x_v, can therefore be estimated using:

$$x_v = \begin{cases} L_f - 10H, & L_f > 10H \\ 0, & L_f \le 10H \end{cases} \tag{8.42}$$

where L_f (m) is the flame length that can be estimated using equation proposed in Chap. 9 on flame length. The above equation indicates that the virtual origin needs to be accounted for only when the fire is very large and the flame length is over ten times the tunnel height. Otherwise, the virtual origin does not exist and can be considered zero in Eq. (8.41).

Note that ceiling gas temperatures in a range of 600–1200 °C could correspond to the intermittent flame region, that is, a less intense combustion region compared to the continuous flame region. On one hand, heat is continuously introduced to the smoke flow along the ceiling, which lessens the decrease in the ceiling gas temperature. On the other hand, this region corresponds to a higher heat transfer coefficient and more heat is lost in this region compared to the nonflaming region, which could aggravate the temperature decrease. However, these two opposite effects seem to cancel out to a certain degree. The overall effect can be neglected, although a slightly more rapidly increase in the vicinity of the fire which could suggest that the radiation loss effect still dominates.

Equation (8.41) together with Eq. (8.42) could be used to estimate the temperature attenuation along the tunnel with both high and low ventilations.

Example 8.4 Calculate the ceiling gas temperature at 100, 200, and 300 m downstream of a bus fire with a constant HRR of 30 MW in a 6 m high and 10 m wide tunnel at 30 min. The bus is 3 m wide and 10 m long. The ventilation velocity is 3 m/s and ambient temperature is 10 °C. The fire source can be assumed to be 0.5 m above the tunnel floor (bus floor).

Solution: At 30 min, the properties within 300 m can be considered as quasi-steady stage. Firstly, the maximum ceiling gas temperature needs to be calculated.The equivalent diameter of the bus fire is 6.18 m. Then calculate $V' = 0.46 > 0.19$. *Therefore, Eq. (8.17) should be used. The estimated maximum ceiling excess gas temperature is 405 °C. Estimate the flame length* $L_f = 6.4\ m < 10H$, *therefore* $x_v = 0$. *Calculate the ceiling gas temperature at 100 m using Eq. (8.39):* $T(100m) = 10 + 405 \times [0.55 \times \exp(-0.143 \times 100/6) + 0.45 \times \exp(-0.024 \times 100/6)] = 153°C$. *The ceiling gas temperature at 200 and 300 m are 94 and 65 °C respectively.*

8.6 One-Dimensional Simple Model

In tunnel fires with longitudinal ventilation, that is, when the longitudinal air velocity is over a certain value (such as 1 m/s), the smoke flows inside the tunnel downstream of the fire can be considered as one-dimensional flow. Using this simplification, simple equations can be obtained which are very convenient and useful in evaluation of the gas temperature, buoyancy force, etc.

The mass flow rate, $\dot{m}$ (kg/s), can be simply calculated by:

$$\dot{m} = \dot{m}_o = \rho_o u_o A_T \tag{8.43}$$

The energy equation can be expressed as follows:

$$\dot{m} c_p \frac{\mathrm{d}T_{avg}}{\mathrm{d}x} = -h_t w_p (T_{avg} - T_o) \tag{8.44}$$

where A_T is the tunnel cross-sectional area (m^2), w_p is the perimeter of the whole tunnel cross-section (m), T_{avg} is the average temperature of the whole cross-section (K), h_t is the total heat transfer coefficient (kW/m^{2}K).

Noting that the mass flow rate is constant, the average gas temperature at x m downstream of the fire source at time t can be estimated using:

$$\Delta T_{avg}(x,t) = \Delta T_{avg}(0,\tau) e^{-\frac{h_t w_p}{\dot{m}_o c_p} x} \tag{8.45}$$

where t is the time (s), and τ is the actual time corresponding to the fire source(s).

Assuming that 2/3 of the total HRR is convective HRR, the maximum average temperature, that is, the average temperature at the fire source, can be estimated using the following equation:

$$\Delta T_{avg}(0,\tau) = \frac{2\dot{Q}(\tau)}{3\dot{m}_o c_p} \tag{8.46}$$

Note that in the above calculation, the transportation time has been taken into account. The actual time, τ, at location x can be approximated with aid of the following equation [12]:

$$\tau = t - \int_0^L \frac{dx}{u_{avg}(x)} \tag{8.47}$$

where L is the distance between fire and measurement location, u_{avg} is the average velocity of the whole cross-section.

The variation of the velocity along the tunnel can be approximated using the mass balance equation and the ideal gas law, assuming constant cross-sectional area and neglecting the fuel mass flow compared to the airflow in the tunnel:

$$u_{avg}(x) = \frac{u_o}{T_o} T_{avg}(x) \tag{8.48}$$

Given that, the average temperature of the smoke flow at a given distance, x, downstream of the fire can be estimated using Eqs. (8.45) and (8.46), the actual time can, therefore, be expressed as [12]:

$$\tau = t - \frac{L}{u_o}\left[\frac{1}{\xi}\ln\left(\frac{\psi + e^{\xi}}{\psi + 1}\right)\right] \tag{8.49}$$

where the two variables are defined as:

$$\xi = \frac{h w_p L}{\dot{m}_o c_p}, \quad \psi = \frac{2}{3}\frac{\dot{Q}}{\dot{m}_o c_p T_o}$$

Another simple method to correct the time is to directly estimate the time consumed when travelling between the fire source and the measurement station at the longitudinal ventilation velocity. This simple method is accurate enough when the distance is short.

In summary, the average gas temperature downstream of the fire can be reasonably well described using the one-dimensional method. However, it should be kept in mind that if the ventilation velocity is too low, the one-dimensional model is not applicable. Instead, Eq. (8.41) can still be used to the maximum ceiling gas temperature at a given position.

Example 8.5 Calculate the average gas temperature and average gas velocity at 100 m downstream of a bus fire with a HRR of 50 MW following the fast curve in a 6 m high and 12 m wide tunnel at 10 min. The ventilation velocity is 2 m/s and ambient temperature $T_o = 20\,°C$.

Solution: First we simply calculate the actual time $\tau = t\text{-}x/u_o = 600–100/2 = 550$ *s and the mass flow rate* $\dot{m}_o = 1.2 \times 2 \times 6 \times 12 = 173$ *kg/s. Thus, the average temperature at* $x = 0$ *becomes* $T_{avg}(0) = 20 + 2/3 \times 50000/(173 \times 1) = 213\,°C$. *The average temperature 100 m from the fire at time* $t = 10$ *min can be calculated using Eq. (8.45).* $T_{avg}(100) = 20 + (213–20) \times \exp[-0.025 \times 32 \times 100/(144 \times 1)] = 115\,°C$, *where* $h_t = 0.025$ *kW/m*^{2}*K,* $w_p = 36$ *m and* $x = 100$ *m. Therefore, the average temperature 100 m from the fire is* $u_{avg}(100) = 2 \times (273 + 115)/(273 + 20) = 2.65$ *m/s.*

8.7 Summary

Gas temperature is of great importance for assessment of heat exposure of humans and tunnel structures, estimation of fire detection time, and possibility of fire spread.

A theory of maximum ceiling gas temperature in tunnel fires and useful correlations have been presented. The main influencing parameters were found to include the HRR, ventilation velocity, effective tunnel height, and geometry of the fire source. The maximum gas excess temperature beneath the tunnel ceiling varies as the two-thirds power of the HRR, independent of the longitudinal ventilation velocity, and with high ventilation, for a small fire in a tunnel with low ventilation, and it increases linearly with the HRR and is inversely proportional to the longitudinal ventilation velocity for a small fire in a tunnel with high ventilation. In both cases, the maximum gas excess temperature varies as a $-5/3$ power law of the effective tunnel height. For a large fire in a tunnel, that is, when the flame impinges on the ceiling and extends along the tunnel ceiling, it was found that the maximum excess gas temperature beneath the ceiling approaches a constant value, regardless of the ventilation velocity.

The position of the maximum ceiling gas temperature was found to be directly related to the dimensionless ventilation velocity. Moreover, it becomes insensitive to the HRR for a large tunnel fire, similar to the backlayering length. The reason is that these two terms are both directly related to the dimensionless ventilation

velocity. A flame angle has been defined here based on the position of the maximum ceiling temperature in a tunnel fire. For a given tunnel and fire source, the flame angle under critical conditions is almost of the same value, independent of the HRR, and the maximum ceiling temperature under critical condition (critical velocity) always corresponds to the same position. Generally, the horizontal distance between the position of the maximum ceiling temperature and the fire source center is about 1.5 times the effective tunnel height.

A theoretical analysis of hot smoke flow results in a simple equation for gas temperature attenuation along the tunnel. In a large fire, the ceiling flame exists and continuously releases heat along the tunnel which results in a much slower decrease of the gas temperature along the ceiling in the vicinity of the fire. When the fire is very large and the flame length is over ten times tunnel height, a virtual origin needs to be accounted for. Note that, the proposed equations can be used for both high and low ventilations.

In tunnel fires with longitudinal ventilation, the smoke flows inside the tunnel could be considered as one-dimensional flow since the smoke layer generally descends to the floor level at a certain distance downstream of the fire under high ventilation. Simple equations are presented for evaluation of average gas temperature, buoyancy force, and et cetera. Note that, the one-dimensional simple model cannot be used if the ventilation velocity is too low, for example, lower than a certain value such as 1 m/s.

References

1. Carvel RO, Marlair G (2005) A history of fire incidents in tunnels. In: Beard AN, Carvel RO (eds) The Handbook of Tunnel Fire Safety. Thomas Telford Publishing, London, UK, pp 3–41
2. Fire-resistance tests—Elements of building construction—Part 1: General requirements (1999). First edn. International Organization for Standardization
3. Fire resistance tests—Part 2: Alternative and additional procedures (1999). First edn. European Committee for Standardization, EN 1363-2
4. Beproeving van het gedrag bij verhitting van twee isolatiematerialen ter bescherming van tunnels bij brand (1979). Instituut TNO voor Bouwmaterialen en Bouwconstructies, Delft, The Netherlands
5. Richtlinien für Ausstattung und Betrieb von Tunneln (RABT) (1985). Ausgabe 1985 edn. Forschungsgesellschaft für Straßen- und Verkehrswesen
6. Abschlussbericht zum BMVBS/ BASt Forschungsvorhaben 15.0391/2003/ERB: Brandschutzverhalten von selbstverdich-tendem Beton (SVB) im Straßentunnelbau (2005). MFPA Leipzig, März
7. Hoult DP, Fay JA, Forney LJ (1969) A Theory of Plume Rise Compared with Field Observations. Journal of the Air Pollution Control Association 19:585–590
8. Hoult DP, C. WJ (1972) Turbulent plume in a laminar cross flow. Atmospheric Environment 6 (8):513–530
9. Kurioka H, Oka Y, Satoh H, Sugawa O (2003) Fire properties in near field of square fire source with longitudinal ventilation in tunnels. Fire Safety Journal 38:319–340
10. Li YZ, Lei B, Ingason H (2011) The maximum temperature of buoyancy-driven smoke flow beneath the ceiling in tunnel fires. Fire Safety Journal 46 (4):204–210

11. Li YZ, Ingason H (2012) The maximum ceiling gas temperature in a large tunnel fire. Fire Safety Journal 48:38–48
12. Li YZ, Ingason H (2010) Maximum Temperature beneath Ceiling in a Tunnel Fire. SP Report 2010:51, SP Technical Research Institute of Sweden, Borås, Sweden
13. Karlsson B, Quintier JG (2000) Enclosure Fire Dynamics. CRC Press, New York
14. Heskestad G (2008) Fire Plumes, Flame Height, and Air Entrainment. In: DiNenno PJ, Drysdale D, Beyler CL et al. (eds) The SFPE Handbook of Fire Protection Engineering. Fourth Edition edn. National Fire Protection Association, Quincy, MA, USA, pp 2–1–2–20
15. Zukoski EE Smoke movement and mixing in two-layer fire models. In: The 8th UJNR Joint Panel Meeting on Fire Research and Safety, Tsukuba, 13–17 June 1985.
16. Quintiere JG, J. RW, W JW (1981) The effect of room openings on fire plume entrainment. Combustion Science and Technology 26:193–201
17. Raj P. P. K., Moussa A. N., K A (1981) Experiments involving pool and vapor fires from spills of liquidified natural gas on water. Prepared for U.S. Dept. of Transportation, U.S. Coast Guard, Rept. No. CG-D-55–79.
18. McCaffrey BJ (1979) Purely Buoyant Diffusion Flames: Some Experimental Results. NBSIR 79-1910. National Bureau of Standards, Washington, D.C., USA
19. Ingason H, Lönnermark A, Li YZ (2011) Runehamar Tunnel Fire Tests. SP Technicial Research Institute, SP Report 2011:55 Borås, Sweden
20. Memorial Tunnel Fire Ventilation Test Program—Test Report (1995). Massachusetts Highway Department and Federal Highway Administration, Massachusetts
21. Li YZ, Ingason H (2014) Position of Maximum Ceiling Temperature in a Tunnel Fire. Fire Technology 50:889–905
22. Li YZ, Lei B, Ingason H (2010) Study of critical velocity and backlayering length in longitudinally ventilated tunnel fires. Fire Safety Journal 45:361–370
23. Ingason H, Li YZ (2010) Model scale tunnel fire tests with longitudinal ventilation. Fire Safety Journal 45:371–384

Chapter 9
Flame Length

Abstract In a large tunnel fire, the flame impinges on the ceiling and then extends along the tunnel ceiling. When the longitudinal ventilation rate is high, flames only exist on the downstream side of the fire source, while under low ventilation rate, flames exist both upstream and downstream of the fire source. In a large tunnel fire the horizontal distance between the fire source and the flame tip is defined as a flame length. A theoretical model of flame length in a large tunnel fire is proposed in this chapter. A large amount of data relevant to the flame length from model- and large-scale tunnel fire tests are used to verify the model. The results show that the downstream flame length increases approximately linearly with the heat release rate (HRR) but is insensitive to the longitudinal ventilation velocity. The flame length under high ventilation rate approximately equals the downstream flame length under low ventilation rate. As the longitudinal ventilation velocity decreases, the upstream flame length increases and so does the total flame length. Dimensionless equations that correlate well with test data are proposed.

Keywords Flame length · Large fire · Downstream flame length · Upstream flame length · Heat release rate (HRR) · Longitudinal ventilation velocity

9.1 Introduction

Relatively large fires are needed in order for flames to extend along a tunnel ceiling. This corresponds to HRRs that are usually over 20 MWs for most tunnels. Due to the confined tunnel space, the ceiling flame length is normally longer than that in an open fire or a room fire. This horizontal extension results in higher risk for fire spread to the neighbouring vehicles. As the risk of fire spread increases with flame length, it is identified as a key parameter that needs to be thoroughly investigated.

The visible flame is a product of combustion which emits visible radiation. The flames indicate regions with high gas temperatures. Note that, the room or enclosure fires are always related to vertical buoyancy driven turbulent diffusion flames. In some special scenarios the fires could be related to turbulent jet flames, for example, a liquefied gas tank ejects burning gases from small orifices to several hundred times the orifice diameter. Therefore, the focus will be on turbulent diffusion flames

H. Ingason et al., *Tunnel Fire Dynamics,* DOI 10.1007/978-1-4939-2199-7_9

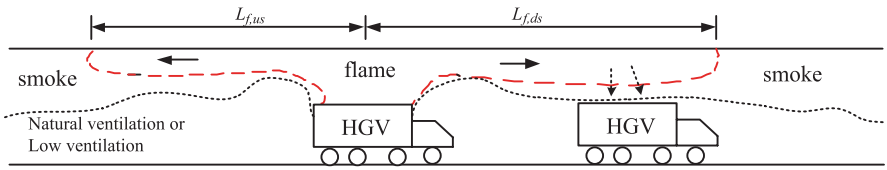

Fig. 9.1 Flame length in a large tunnel fire under low ventilation rate or natural ventilation

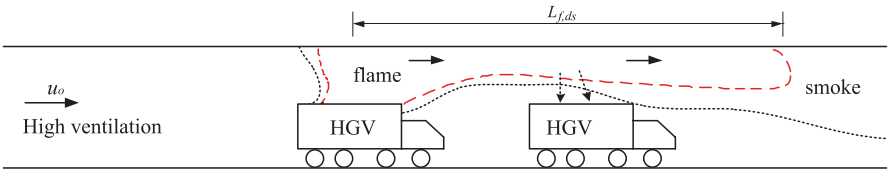

Fig. 9.2 Flame length in a large tunnel fire under high ventilation rate

as they are more likely in large tunnel fires. The existence of the turbulent diffusion flame along the tunnel ceiling is mainly due to insufficient air entrainment.

The combustion of the fuels can be categorized into two parts. In the vertical flame zone, part of the combustible gas burns and flows upward until it impinges on the tunnel ceiling. In the horizontal flame zone, another part of combustible gas burns along the ceiling to a certain distance downstream of the fire source. The flame length, L_f, discussed in this chapter is defined as the horizontal distance from the impingement point of the fire source center to the flame tip.

In a tunnel fire with natural ventilation or a low ventilation rate, the horizontal flame could exist both upstream and downstream of the fire source, as shown in Fig. 9.1. Note that generally, the flames on the two sides are not symmetrically distributed since, even under natural ventilation there is a dominating wind direction. Here, the downstream side refers to the region with a slightly longer flame length.

In a tunnel fire with a high ventilation rate, the ceiling flame only exists downstream of the fire source, see Fig. 9.2. Compared to the fire under a low ventilation rate, more heat is blown to the downstream side and the smoke layer height is lower. The distinction condition between the low ventilation rate and high ventilation rate will be discussed later.

9.2 Overview of Flame Length in Open and Enclosure Fires

For buoyancy driven turbulent diffusion flames in a quiescent environment (no wind), the flame length or flame height has been found to be well correlated with the Froude number defined using the parameters of the fuel gas and the flame length, L_f, can be estimated using [1]:

$$L_f = 0.235\dot{Q}^{2/5} - 1.02D_f \tag{9.1}$$

where $\dot{Q}$ is the HRR (kW), D_f is the equivalent diameter of the fire source (m). Note that, this equation is only suitable for turbulent diffusion flames. It is widely used in fire safety engineering.

The work on flame lengths under unconfined ceilings gives us some valuable information about the flame length in a large tunnel fire. When the flame impinges on an unconfined ceiling, the unburnt gases spread radialy and a circular disc flame can be observed under the ceiling. You and Faeth [2] carried out small-scale experiments and the results show that the ceiling flame length is about half the difference between the free flame height in an open fire and the ceiling height. However, this estimation is very rough since the tested HRRs were very small. Heskestad and Hamada [3] carried out fire tests using larger HRRs ranging from 93 to 760 kW and the tests results show that the flame length below the ceiling is about the same as the difference between the free flame height and the ceiling height. In other words, the total flame length, that is, sum of the ceiling height and the ceiling flame length in an enclosure fire equals the free flame height in an open fire.

The flame length in a corridor fire is more similar to a large tunnel fire. Hinkley [4] carried out an experimental investigation of flames spreading under an incombustible ceiling in a corridor with one closed end. The fire source was a town gas burner placed at one end of the simulated corridor and covered the whole corridor width. Hinkley [4] considered the flame length in a corridor as the distance between the flame tip and a virtual origin. The horizontal distance between the virtual origin of the horizontal flames and the fire source appeared to be twice the ceiling height above the fire source, however, more test data are required to support this. Based on a dimensional analysis and investigation of the test results, Hinkley [4] presented a correlation for the flame length in a corridor with one closed end and an open bottom (no floor). For a dimensionless parameter $m^* < 0.024$ with either no front end screen or a 150 mm deep screen fitted to the end of a 7.3 m long corridor, and for $m^* < 0.018$ with a 230 mm deep front end screen, the flame length in a corridor with one closed end can be expressed as:

$$\frac{L_f'}{H} = 220m^{*2/3} \tag{9.2}$$

where the dimensionless parameter, m^*, is defined as:

$$m^* = \frac{m'}{\rho_o g^{1/2} H^{3/2}}$$

In the above equation, m' is the fuel flow rate per cm corridor width (kgcm^{-1} s^{-1}), H is the ceiling height above the fire source (m), L_f', is the horizontal flame length from the virtual origin estimated based on an empirical equation to account for the vertical flame part (m). The results showed that when $m^* > 0.024$ the flame lengths

were underestimated. Note that according to the above equation, the horizontal flame length is actually independent of the smoke thickness or corridor height. The flame length in the above equation was estimated based on a virtual origin which was not well defined. Further, the fire source was attached to the closed end of the corridor and covered the whole corridor width, and the corridor had an open bottom (no floor). Moreover, the tests were carried out under no ventilation. Therefore, the scenario is different to a fire in a tunnel.

Based on Alpert's work [5] on infinite line plume impinging on a ceiling and flowing equally in both directions of a corridor, Babrauskas [6] presented a method to estimate the horizontal flame length, assuming that the total entrained mass flow rate required for ceiling combustion is the same as that required for vertical combustion flames in the open. Results from Hinkley et al.'s [4] and Atallah's tests [7] were used in the analysis. However, this assumption of entrainment cannot be reasonable for the tunnel/corridor case since the air flow that can be entrained is much smaller in a tunnel fire compared to in an open fire.

9.3 Overview of Flame Length in Tunnel Fires

Limited research has been carried out on the flame length in tunnel fires. The focus has been on flame lengths on the downstream side. Rew and Deaves [8] presented an equation for flame length in tunnels, which included HRR and longitudinal velocity but not the tunnel width or height. Much of their work was based on the investigation of the Channel Tunnel Fire in 1996 and test data from the HGV-EUREKA 499 fire test [9] and the Memorial Tests [10]. They defined the horizontal flame length, L_f, as the distance of the 600 °C contour from the center of the HGV or the pool, or from the rear of the HGV. The flame length from the rear of the HGV was represented by the following equation:

$$L_f = 0.02\left(\frac{\dot{Q}}{120}\right)\left(\frac{u_o}{10}\right)^{-0.4} \tag{9.3}$$

where u_o is the longitudinal air velocity (m/s). Note that in the above equation, the HRR $\dot{Q}$ is expressed in MW. This equation is a conservative fit to a limited data obtained from the HGV-EUREKA 499 test. The weakness of Eq. (9.3) is that no geometrical parameter has been taken into account, which makes it impossible to predict the flame length for other tunnels due to different geometries of tunnel and fire source.

Lönnermark and Ingason [11] investigated the flame lengths of the Runehamar tests. Alpert's equation for ceiling jet temperatures [12] were used to estimate the form of the equation for the flame length, and the uncertain coefficients were determined by regression analysis which gave a best fit for an exponent of 0.8 for the

HRR. Data from the Runehamar tests and some data from the Memorial tests were used in the analysis. The proposed equation was expressed as follows:

$$L_f = \frac{1370\dot{Q}^{0.8}u_o^{-0.4}}{(T_f - T_o)^{3/2}H^{3/2}} \tag{9.4}$$

where $\dot{Q}$ is the HRR (kW), L_f is the horizontal flame length (m), T_f is the flame tip temperature (K) and H is the tunnel height (m). Given, that the ceiling jet equation used in the analysis is only suitable for ceiling jets under unconfined ceilings, the generic use of the equation is limited.

Both equations above imply that the effect of longitudinal ventilation velocity on flame length is not as important as the HRR. This phenomenon was observed by Ingason and Li [13] in their model-scale tests that flame length is insensitive to the longitudinal ventilation velocity.

9.4 Flame Lengths in Tunnel Fires

9.4.1 Transition Between Low and High Ventilation Rate

If the longitudinal ventilation velocity is much lower than the critical velocity, there exist two parts of horizontal flame regions, that is, upstream region ($L_{f,\,ds}$) and downstream region ($L_{f,\,us}$). For high ventilation velocities, the flames only exist downstream of the fire. The transition point is therefore, defined as the longitudinal velocity under which no ceiling flame exists upstream of the fire source. Accordingly, the "high ventilation" for the flame length is defined as the case with the ventilation velocity larger than the transition point, and the "low ventilation" corresponds to the ventilation velocity less than the transition point.

Based on Li et al.'s study [14], the ratio of back-layering length to the tunnel height is related to the ratio of the ventilation velocity to the critical velocity at a given HRR. For high HRRs, the back-layering length is only dependent on the ventilation velocity, regardless of the HRR. Note that the upstream flame length is part of the back-layering length, and the fires with ceiling flames only correspond to high HRRs. Therefore, similar to the critical velocity, a dimensionless ventilation velocity at the transition point is defined:

$$u_{tp}^* = \frac{u_{o,tp}}{\sqrt{gH}} \tag{9.5}$$

A dimensionless HRR was defined according to the following equation:

$$Q^* = \frac{\dot{Q}}{\rho_o c_p T_o g^{1/2} H^{5/2}} \tag{9.6}$$

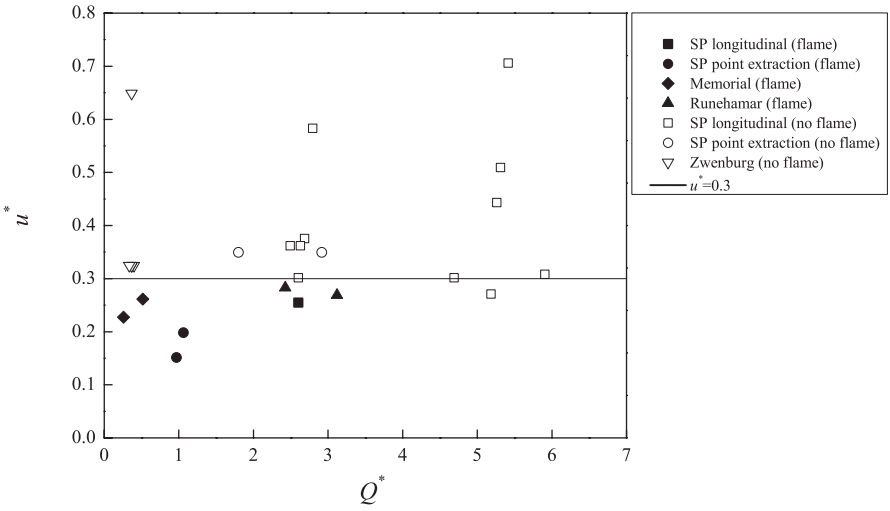

Fig. 9.3 Transition line between low ventilation rate and high ventilation rate

where u_o is the longitudinal velocity (m/s), g is the gravitational acceleration (m/s^2), H is the tunnel height (m), $\dot{Q}$ is the HRR (kW), ρ_o is an ambient air density (kg/m^3), c_p is the heat of capacity (kJ/kg K), T_o is an ambient air temperature (K). Subscript *tp* indicates transition point.

Figure 9.3 shows a plot of data with and without upstream flames. Data from longitudinal tunnel fire tests conducted at SP [13], point extraction tests also conducted at SP [15], the Memorial tunnel tests [10] and the Runehamar tests [16] are used in the analysis. For further information about large- and model-scale tests see Chap. 3. The solid data points represent a situation when the flames existed on the upstream side in the tests, and the hollow data points indicate when no flames were obtained on the upstream side for different longitudinal velocities. The data show that there is a clear transition line that exists between the solid and hollow data points. This line can be expressed as:

$$u_{tp}^{*} = 0.3 \tag{9.7}$$

Given that the dimensionless critical velocity approaches 0.43 for large fires [14], the results shown in Fig. 9.3 indicate that the transition point corresponds to a longitudinal velocity of approximately 70 % of the critical velocity.

Example 9.1 Estimate the location of the ceiling flames for a 150 MW fire in a tunnel with dimensions of 6 m high and 6 m wide at a longitudinal velocity of 1 and 3 m/s, respectively. What are the scenarios if the tunnel instead is 6 m high and 12 m wide.

Solution: Calculate the dimensionless longitudinal velocity using Eq. (9.5), $u^* = 0.13 < 0.3$ for the velocity of 1 m/s and $u^* = 0.39 > 0.3$ for the velocity of 3 m/s.

Therefore, we know that both upstream and downstream flames exist for 1 m/s and only downstream flame exists for 3 m/s. If the tunnel width is 12 m instead, it means that the scenarios are the same as the tunnel width does not influence the results.

9.4.2 Model of Flame Length in Tunnel Fires

Under low ventilation rate conditions, two parts of the flame exist: upstream and downstream of the fire, respectively.

In the ceiling flame zone, relatively good stratification probably exists, that is, there appears to be a clear layer interface between the fire and the fresh air. The total mass flow rate at the flame tip in the horizontal combustion region can be estimated as follows:

$$\dot{m}_{hr} = \int_0^{L_f} \rho_o v W dx \tag{9.8}$$

where $\dot{m}_{hr}$ is the mass flow rate of the entrained air from the lower layer by the horizontal flame (kg/s), ρ_o is the density of the entrained air (kg/m^3), v is the entrainment velocity (m/s), W is the tunnel width (m), x is the distance from the fire, and L_f is the horizontal flame length (m).

The combustion in the horizontal flame is mainly dependent on the entrainment of the air flow and the mixing at the interface. The entrainment velocity for the mixing layer is given in the same form as that for the vertical plume. More information can be found in Chap. 12. The upstream and downstream entrainment velocities, can be expressed as:

$$v_{t,us} = \beta \left| u_{us} + u_o \right|, \quad v_{t,ds} = \beta \left| u_{ds} - u_o \right| \tag{9.9}$$

where subscripts *us* and *ds* represent upstream and downstream, respectively, "+" indicates opposite directions between longitudinal flow and smoke, and vice versa.

Note that, the entrainment coefficient in a vertical plume is assumed to be a constant. For simplicity, we also assume the average entrainment coefficient along the flame β is a constant.

Thus, the mass flow rate of total entrained air downstream, $\dot{m}_{ds}$ (kg/s), and upstream of the fire, $\dot{m}_{us}$ (kg/s), can be respectively expressed as:

$$\dot{m}_{ds} = \rho_o v_{ds} W L_{f,ds}, \quad \dot{m}_{us} = \rho_o v_{us} W L_{f,us} \tag{9.10}$$

We also know from the research on open fires that there is a relationship between the HRR and the entrained air, that is, the HRR should be intimately related to the mass of entrained air flows. Here, we assume that the ratio of air flows involved in reaction and total entrained air flows is k. Therefore, the energy equation can be expressed as:

$$\dot{Q} = \dot{Q}_{vt} + (\xi_{ds} \dot{m}_{ds} Y_{O_2,ds} + \xi_{us} \dot{m}_{us} Y_{O_2,us}) \Delta H_{O_2} \tag{9.11}$$

where $\dot{Q}_{vt}$ is the heat released in the vertical flame region (kW), ξ is the ratio of the oxygen involved in the combustion to the oxygen entrained (or the ratio of air flow involved in the combustion to the total entrained air flow), ΔH_{O2} is the heat released while consuming 1 kg of oxygen (kJ/kg), Y_{O2} is the mass concentration of oxygen in the air flow at the lower layer. The second term on the right-hand side means the heat released in the horizontal flame regions.

Inserting Eq. (9.10) into Eq. (9.11) gives:

$$\dot{Q} = \dot{Q}_{vt} + (\xi_{ds}\rho_o W L_{ds}\beta Y_{O_2,ds}\left|u_{ds} - u_o\right| + \xi_{us}\rho_o W L_{us}\beta Y_{O_2,us}\left|u_{us} + u_o\right|)\Delta H_{O_2} \quad (9.12)$$

For upstream and downstream ceiling flames, the ratio *k* should be approximately the same, that is $\xi_{ds} = \xi_{us} = \xi$. Therefore, we have

$$L_{f,ds}Y_{O_2,ds}(u_{ds} - u_o) + L_{f,us}Y_{O_2,us}(u_{us} + u_o) = \frac{\dot{Q} - \dot{Q}_{vt}}{\xi\rho_o\beta W\Delta H_{O_2}} \quad (9.13)$$

The mass flow rate in the vertical flame region under different ventilation conditions has not yet been explored thoroughly. Li et al. [17, 18] carried out a theoretical analysis of the maximum gas temperature beneath a tunnel ceiling and the mass flow rate of the fire plume in a ventilated flow based on a plume theory. The HRR, longitudinal ventilation velocity and tunnel geometry were taken into account. Test data were also used to verify the theoretical model and good agreement was obtained between the theory and test data. However, the entrainment of the flame zone is very different compared to the plume zone. Due to lack of information, we may assume that the entrainment inside the flame region in tunnel flows is similar to that in open fires. Delichatois [19] proposed simple correlations for the mass flow rate inside the flame:

$$\dot{m}(z) \propto D_F^2 z^{1/2} \quad \text{for } z / D_F < 1 \quad (9.14)$$

where *z* is the height above the fire source (m), $\dot{m}(z)$ is the mass flow rate inside the flame at height *z* (kg/s), and D_F is the diameter of the fire source (m). Note that, the equation for the mass flow at height *z* can also be expressed as:

$$\dot{m}(z) \propto \rho u D(z)^2 \quad (9.15)$$

where *u* is the vertical gas velocity (m/s) and *D(z)* is the diameter of the plume at height *z* (m). It can be expected that the fire plume diameter is proportional to the diameter of the fire source, that is, $D(z) \propto D_F$, and the temperature inside the continuous flame zone can be reasonably considered as constant. Combining the above two equations suggests that the maximum vertical gas velocity, $u_{\max,v}$, can be expressed as:

$$u_{\max,v} \propto H_{ef}^{1/2} \quad (9.16)$$

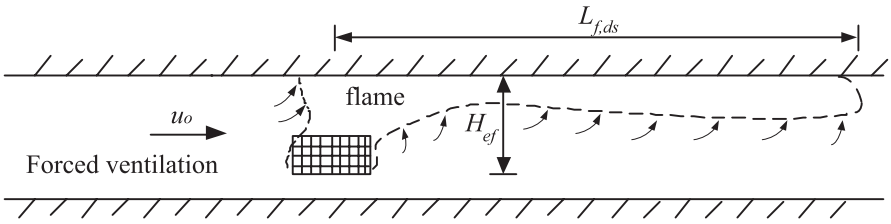

Fig. 9.4 A schematic diagram of entrainment under high ventilation

where $u_{max,v}$, is the maximum velocity of the vertical flame (m/s), H_{ef} is the effective tunnel height (m), that is, the tunnel height above the fire source. For vehicle fires or solid fuel fires, the effective tunnel height is the vertical distance between the bottom of the fire source and the tunnel ceiling. The above relationship correlates well with Thomas' equation for gas velocities in the flame zone [20].

The velocity of the fire plume after impingement on the ceiling slightly decreases, however, it can be assumed to be proportional to the maximum velocity in the vertical plume, as proved in the research on ceiling jets [12]. This indicates the maximum horizontal gas velocity, $u_{max,h}$, could also be expressed as:

$$u_{\max,h} \propto H_{ef}^{1/2} \tag{9.17}$$

where $u_{max,h}$, is the maximum velocity of the horizontal flame (m/s). The horizontal maximum gas velocity could be considered as a characteristic velocity for the ceiling flames.

9.4.3 Flame Length with High Ventilation Rate

According to the previous definition, the high ventilation here corresponds to the ventilation velocity under which no ceiling flame exists upstream of the fire source, that is, a dimensionless ventilation velocity greater than $0.3u^*$. In such cases, the ceiling flames only exist downstream of the fire, see Fig. 9.4.

Note that, generally the longitudinal ventilation velocity is around 3 m/s for a tunnel with longitudinal ventilation during a fire and even less for transverse and semi-transverse ventilation. For a large tunnel fire with a relatively long ceiling flame length, the smoke velocity right above the fire could range from 6 to 12 m/s or even higher. Apparently, this velocity is relatively low compared to the gas velocity in the ceiling flame region. Therefore, we may use the gas velocity under natural ventilation to approximately express the velocity difference between the ceiling flame layer and lower layer, that is

$$u_{ds} - u_o \propto H_{ef}^{1/2} \tag{9.18}$$

For a HGV fire, the horizontal flame could be very long, that is several times or even over ten times the tunnel height. The combustion in the vertical flame region could be limited due to the confinement of the tunnel configuration. Moreover, the flame was deflected and thus, the vertical flame region also contributes to the flame length. Therefore, as a first attempt, the combustion in the vertical flame region is ignored. Given that the air entrained from the lower layer is generally not highly vitiated, the oxygen concentration for the entrained air is considered to be constant, that is close to ambient. Thus from Eq. (9.13) one gets:

$$L_{f,ds} = \frac{\dot{Q}}{\xi \rho_o \beta \Delta H_{O_2} Y_{O_2} W H_{ef}^{1/2}} \propto \frac{\dot{Q}}{W H_{ef}^{1/2}} \tag{9.19}$$

For a rectangular tunnel, $A = WH$. For other shapes, the tunnel width could vary with the flame layer height above the floor. For simplicity, let us estimate the tunnel width using $W = A/H$. The above equation can therefore, be written as:

$$L_{f,ds} \propto \frac{\dot{Q}H}{AH_{ef}^{1/2}} \tag{9.20}$$

To normalize the results, two dimensionless parameters are defined here. The dimensionless flame length is defined as:

$$L_f^* = \frac{L_f}{H} \tag{9.21}$$

The dimensionless heat release rate is defined as:

$$Q_f^* = \frac{\dot{Q}}{\rho_o c_p T_o g^{1/2} A H_{ef}^{1/2}} \tag{9.22}$$

Therefore, we expect that the dimensionless flame length is proportional to the dimensionless HRR:

$$L_{f,ds}^* = C_f Q_f^* \tag{9.23}$$

where C_f is a coefficient which will be determined by experimental data. It can be seen that the flame length is independent of the ventilation velocity, under the above assumptions. This conclusion is in accordance with the previous findings presented in Sect. 9.3. Figure 9.5 shows the dimensionless flame lengths under high ventilation as a function of the dimensionless HRR. Test data from longitudinal tunnel fire tests conducted at SP [13], point extraction tests also conducted at SP [15], EUREKA 499 programme [9], Memorial tunnel tests [10], and Runehamar tests [16] were plotted. Clearly, the proposed equation correlates well with the test data. The correlation can be expressed as:

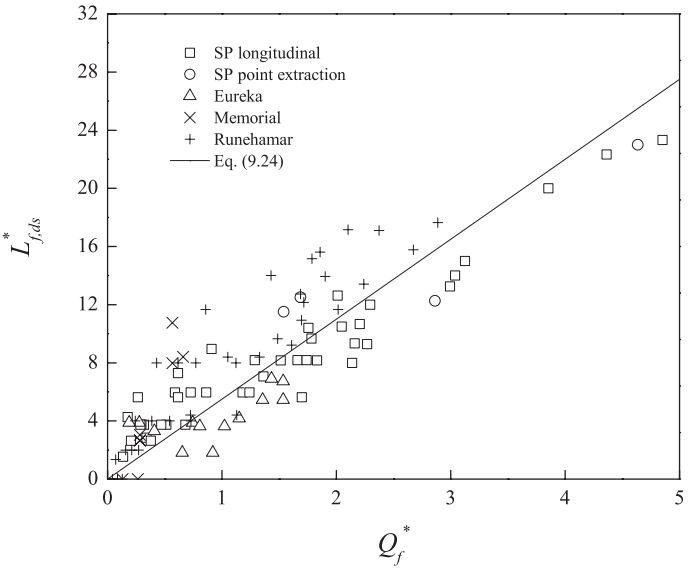

Fig. 9.5 Flame lengths under high ventilation rate

$$L^*_{f,ds} = 5.5Q^*_f \tag{9.24}$$

It can be concluded that under high ventilation, the flame length in a tunnel fire is mainly dependent on the HRR, tunnel width and the effective tunnel height, and insensitive to the ventilation velocity.

Example 9.2 Calculate the flame length for a 150 MW fire in a tunnel with dimensions of 6 m high and 6 m wide ($H \times W$) at a longitudinal velocity of 3 m/s, respectively. The bottom of the fire sources is 1 m (H_{ef}=5 m) above the tunnel floor. What is the flame length ($L_{f,ds}$) if the tunnel instead is 6 m high and 12 m wide?

Solution: From Example 9.1, we know that for the tunnel with a width of either 6 or 12 m, only downstream flame exists at a longitudinal velocity of 3 m/s. The dimensionless HRR can be estimated using Eq. (9.22): $Q^*_f = (150 \times 1000)/(1.2 \times 1 \times 293 \times 9.8^{0.5} \times 6 \times 6 \times 5^{0.5}) = 1.69$. *For 3 m/s, the downstream flame length can be calculated using Eq. (9.21) and Eq. (9.24), that is,* $L_{f,ds} = 5.5 \times 1.69 \times 6 = 56$ *m. If the tunnel width is 12 m instead, the flame lengths calculated will reduce by 50%, since the width is in the denominator in Eq. (9.22), that is,* $L_{f,ds} = 28$ *m.*

9.4.4 Flame Length Under Low Ventilation Rate

Under low ventilation rate conditions, two parts of horizontal flame regions exist, that is the upstream and downstream regions. The relative velocity can be estimated using:

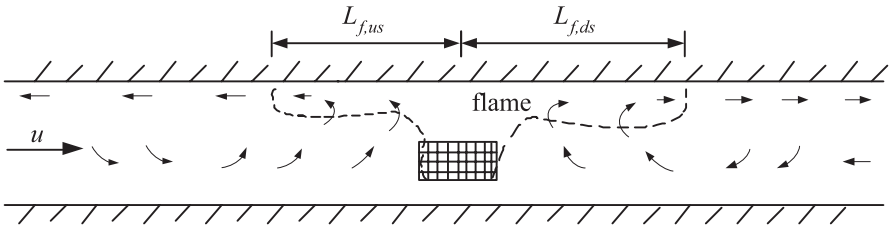

Fig. 9.6 A schematic diagram of the vitiated gas entrained into the ceiling flame region under natural ventilation or low ventilation

$$\left|u_{ds}-u_o\right| \propto H_{ef}^{1/2}, \quad \left|u_{us}+u_o\right| \propto H_{ef}^{1/2} \tag{9.25}$$

The combustion in the vertical flame region is also considered as being limited and thus, ignored as a first approximation.

For a slightly higher ventilation velocity, for example, 1.5 m/s, the length of the upstream flame and the back-layering is short, and therefore, the entrained air in the upstream flame region will only be slightly vitiated (inerted). However, the air could be highly vitiated in the downstream flame region. If no dominating ventilation direction exists, the fresh air will be entrained from both sides of the tunnel by thermal pressure created by the hot smoke. The air entrained into the flame region on both upstream and downstream sides could be highly vitiated, see Fig. 9.6. This phenomenon has not been clearly understood and needs to be further investigated. As a first approximation, the oxygen concentration will be implicitly accounted for in the following analysis. Therefore, we have:

$$L_{f,tot} = L_{f,ds} + L_{f,us} = \frac{\dot{Q}-\dot{Q}_v}{\xi\beta\rho_o W\bar{Y}_{O_2}\Delta H_{O2}H_{ef}^{1/2}} \tag{9.26}$$

where $\bar{Y}_{O_2}$ is the average oxygen concentration of the entrained air, $L_{f,tot}$ is the total flame length (m).

Therefore, the dimensionless total flame length could be expressed as:

$$L_{f,tot}^{*} = C_f' Q_f^{*} \tag{9.27}$$

where C_f' is a coefficient which will be determined by experimental data.

Figure 9.7 shows the dimensionless total flame lengths under low ventilation conditions as a function of the dimensionless HRR. Test data from EUREKA 499 programme [9], Memorial tunnel tests [10], and Hinkley's tests [4] were used. Note that in Hinkley's tests [4] the fire sources were attached to one closed end, and thus the scenario could be considered as being symmetrical, that is both the flame lengths and HRRs are doubled while plotting in the figure. It is clearly shown that the proposed equation correlate very well with the test data. The correlation can be expressed as:

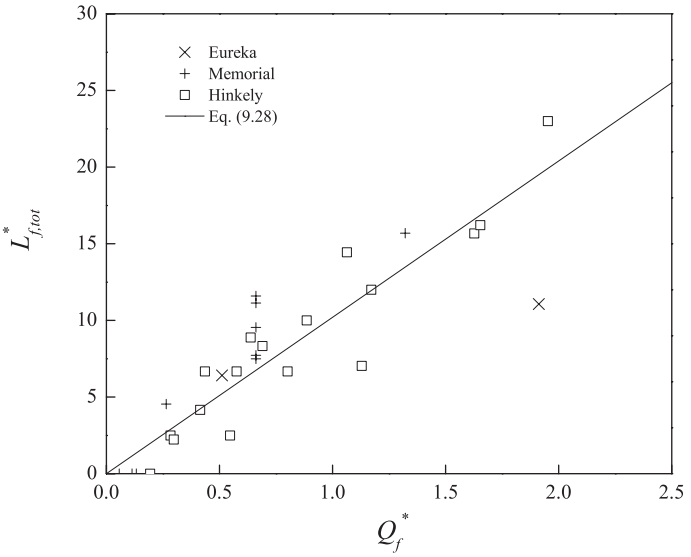

Fig. 9.7 Total flame length under low ventilation rate

$$L^*_{f,tot} = 10.2Q^*_f \tag{9.28}$$

We may also want to know how the downstream flame length varies with the longitudinal ventilation velocity. Figure 9.8 shows the dimensionless downstream flame lengths under high ventilation as a function of the dimensionless HRR.

Test data from EUREKA 499 programme [9], Memorial tunnel tests [10], and Hinkley's tests [4] were used, see Chap. 3. For test data from Hinkley's tests [4], the HRRs are doubled in the figure. Under natural ventilation or very low ventilation, the air entrained into the ceiling flame region is vitiated, as shown in Fig. 9.6. Especially in the vicinity of the fire the air quality gets worse. This suggests that more gas needs to be entrained into the flame region for combustion, that is, the flame length could be longer than with high ventilation, which will be discussed later.

The downstream flame length under low ventilation rate can be expressed as:

$$L^*_{f,ds} = 5.2Q^*_f \tag{9.29}$$

Comparing the above equation to the equation for flame length under high ventilation shows a very small difference. This suggests that the downstream flame length is insensitive to the ventilation velocity. In other words, the flame length under high ventilation is approximately equal to the downstream flame length under low ventilation. For simplicity, the downstream flame length can be estimated using Eq. (9.24), regardless of the ventilation conditions.

Thus, as the ventilation velocity decreases, the total flame length increases, although, the downstream flame length is approximately invariant. In other words,

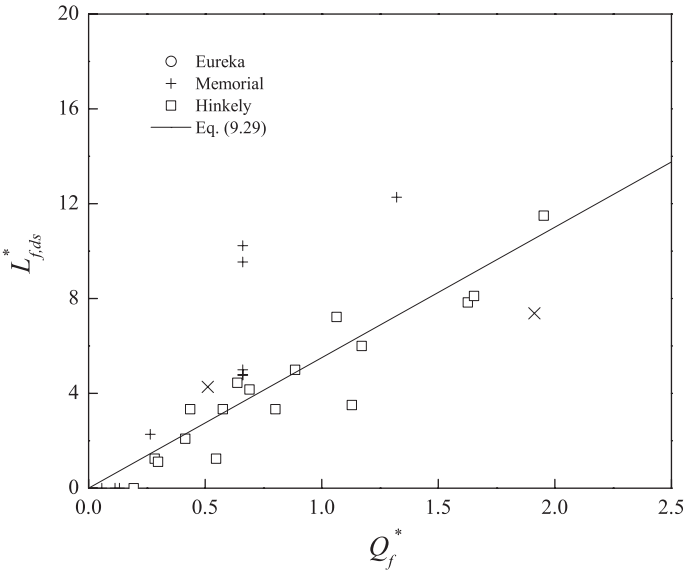

Fig. 9.8 Downstream flame length under low ventilation

the increase of total flame length due to a lower ventilation velocity is due to the existence of the upstream flame.

Example 9.3 Calculate the flame length in the same scenarios as described in Example 9.2 but at a longitudinal velocity of 1 m/s.

Solution: *From Example 9.1, we know that both upstream and downstream flames exist for the velocity of 1 m/s. The dimensionless heat release rate is* $Q_f^* = (150 \times 1000)/(1.2 \times 1 \times 293 \times 9.8^{0.5} \times 6 \times 6 \times 5^{0.5}) = 1.69$. *For 1 m/s, the maximum total flame length can be calculated using Eq. (9.28), that is* $L_{f,tot} = 10.2 \times 1.69 \times 6 = 103$ *m, and the downstream flame length can be calculated using Eq. (9.21) and Eq. (9.24) although the results could tend to be conservative, that is,* $L_{f,ds} = 5.2 \times 1.69 \times 6 = 53$ *m. The upstream flame length can be estimated as:* $L_{f,us} = 103 - 53 = 50$ *m. In reality, the upstream flame length could be slightly shorter than this value for a velocity of 1 m/s. If the tunnel width is 12 m instead, the flame lengths calculated will reduce by 50% since the width is in the denominator in Eq. (9.22).*

9.5 Summary

In a large tunnel fire, the flame impinges on the ceiling and then extends along the tunnel ceiling for a certain distance. Under high ventilation rate conditions only downstream flame exists, and under low ventilation rate conditions, both upstream

and downstream flames exist. The horizontal distance between the fire source and the flame tip is called the flame length in a tunnel fire. A simple theoretical model for the flame length in a large tunnel fire was proposed. A large amount of experimental data relevant to the flame length was used to verify the model.

The downstream flame length was found to be directly related to the HRR, tunnel width and effective tunnel height, and insensitive to the ventilation velocity. The downstream flame length can be estimated using Eq. (9.24), regardless of the ventilation conditions.

Under low ventilation, that is, $u^* < 0.3$, the total flame length increases with the decreasing ventilation velocity, despite that the downstream flame length is approximately invariant. This indicates that increase in the total flame length due to a lower ventilation velocity is only due to the existence of the upstream flame. The maximum total flame length is obtained when there is no ventilation in the tunnel, and it is approximately twice the downstream flame length in tunnel fires under high ventilation. The maximum total flame length under low ventilation can be estimated using Eq. (9.28).

References

1. Heskestad G (2008) Fire Plumes, Flame Height, and Air Entrainment. In: DiNenno PJ, Drysdale D, Beyler CL et al. (eds) The SFPE Handbook of Fire Protection Engineering. Fourth Edition edn. National Fire Protection Association, Quincy, MA, USA, pp 2–1–2–20
2. You HZ, Faeth GM (1981) An Investigation of Fire Impingement on a Horizontal Ceiling. NBS-GCR-81-304. National Bureau of Standards, Washington, D.C., USA
3. Heskestad G, Hamada T (1993) Ceiling Jets of Strong Fire Plumes. Fire Safety Journal 21:69–82
4. Hinkley PL, Wraight HGH, Theobald CR (1984) The Contribution of Flames under Ceiling to Fire Spread in Compartments. Fire Safety Journal 7:227–242
5. Alpert L (1971) Fire induced turbulent ceiling-jet. Report 19722–2. Factory Mutual Research Corporation, Norwood, Massachusetts, USA
6. Babrauskas V (1980) Flame Lengths under Ceiling. Fire and Materials 4 (3):119–126
7. Atallah S (1966) Fires in a model corridor with a simulated combustible ceiling, Part I-Radiation, temperature and emissivity measurements. Fire Research Note No 628. Fire Research Station
8. Rew C, Deaves D Fire spread and flame length in ventilated tunnels—a model used in Channel tunnel assessments. In: Proceedings of the International Conference on Tunnel Fires and Escape from Tunnels, Lyon, France, 5–7 May 1999. Independent Technical Conferences Ltd, pp 397–406
9. Fires in Transport Tunnels: Report on Full-Scale Tests (1995). edited by Studiensgesellschaft Stahlanwendung e. V., Düsseldorf, Germany
10. Memorial Tunnel Fire Ventilation Test Program—Test Report (1995). Massachusetts Highway Department and Federal Highway Administration, Massachusetts
11. Lönnermark A, Ingason H (2006) Fire Spread and Flame Length in Large-Scale Tunnel Fires. Fire Technology 42 (4):283–302
12. Alpert RL (2002) Ceiling Jet Flows. In: DiNenno PJ (ed) SFPE Handbook of Fire Protection Engineering. National Fire Protection Association, Quincy, MA, USA, pp 2–18–12–31
13. Ingason H, Li YZ (2010) Model scale tunnel fire tests with longitudinal ventilation. Fire Safety Journal 45:371–384

14. Li YZ, Lei B, Ingason H (2010) Study of critical velocity and back-layering length in longitudinally ventilated tunnel fires. Fire Safety Journal 45:361–370
15. Ingason H, Li YZ (2011) Model scale tunnel fire tests with point extraction ventilation. Journal of Fire Protection Engineering 21 (1):5–36
16. Ingason H, Lönnermark A, Li YZ (2011) Runehamar Tunnel Fire Tests. SP Technicial Research Institute, SP Report 2011:55, Borås, Sweden
17. Li YZ, Lei B, Ingason H (2011) The maximum temperature of buoyancy-driven smoke flow beneath the ceiling in tunnel fires. Fire Safety Journal 46 (4):204–210
18. Li YZ, Ingason H (2012) The maximum ceiling gas temperature in a large tunnel fire. Fire Safety Journal 48:38–48
19. Delichatsios MA (1987) Air Entrainment into Buoyant Jet Flames and Pool Fires. Combustion and Flame 70:33–46
20. Thomas PH The Size of Flames from Natural Fires. In: 9th Int. Combustion Symposium, Pittsburg, PA, 1963. Comb. Inst., pp 844–859

Chapter 10
Heat Flux and Thermal Resistance

Abstract Heat flux is a major issue that must be considered for evacuation, fire spread, and structure protection in tunnel fires. The three heat transfer mechanisms: convective, radiative, and conductive heat transfer are described with a focus on correlations related to tunnel fires. The Reynolds–Colburn analogy is introduced as a basis for calculation of convective heat transfer. Characteristics of the absorbing, emitting, and scattering gases are summarized, together with radiation between multiple surfaces. Analytical solutions for heat conduction into tunnel walls are summarized for different types of simplified boundary conditions. The overall heat transfer from flames and gases to the tunnel structure involves all three heat transfer mechanisms; their correlations are illustrated using an electrical circuit analog. Simple models for calculating heat flux in small and large tunnel fires are presented with a focus on radiation. Correlations for incident heat flux are proposed and verified for small and large fires in tunnels, taking radiation from both flames and smoke into account.

Keywords Heat transfer · Convection · Radiation · Conduction · Heat flux · Boundary condition · Flame radiation · Tunnel fire

10.1 Introduction

There are three basic modes of heat transfer: convective heat transfer, radiation heat transfer, and heat conduction. The internal driving force of all the heat transfer modes is the temperature gradient among substances or mediums. Convective heat transfer is attributed to the temperature difference between gas flow and a solid or liquid surface. Radiative heat transfer is driven by temperature differences among substances or mediums that have a clear line of sight between them. Heat conduction is triggered by the temperature difference in solid substances. A large amount of literature on heat transfer is available, see for example textbook references [1–5].

Other fire safety phenomena, such as evaporation of liquid fuels or water droplets, sublimation of solid fuels, and gas phase chemical reactions are also effected by heat transfer.

H. Ingason et al., *Tunnel Fire Dynamics,* DOI 10.1007/978-1-4939-2199-7_10

In the fire research community many useful heat flux equations have been proposed for simple estimation of the heat flux from fires and hot gases to walls and ceilings [6]. However, most of these equations are empirical and only suitable for specific scenarios and not necessarily tunnel fires. This chapter focuses on the three basic modes of heat transfer and applies the basic theory to solve problems in tunnel fire safety.

10.2 Convective Heat Transfer

Convective heat transfer is the heat exchange in the boundary layer between a fluid and a solid or liquid surface. The heat loss, to or from the surface follows Fourier's law on both sides of the surface. By introducing a convective heat transfer coefficient, h_c, the convective heat flux at the boundary can be expressed as:

$$\dot{q}''_{w,c} = -k\frac{\partial T}{\partial z}\Big|_{z=0} = h_c(T_w - T_\infty) \tag{10.1}$$

In the above equation, $\dot{q}''_{w,c}$ is the convective heat flux (kW/m^2), k is the conductivity (kW/(mK)), h_c is the convective heat transfer coefficient (kW/(m^{2}K), T is the temperature (K) and z is the distance normal to the surface (m). Subscript w specifies the wall surface and ∞ the surrounding fluid. Note that the fluid temperature T_∞ in the above equation is the ambient fluid temperature outside the boundary layer.

After introducing a characteristic length l (m) and normalizing the above equation, the convective heat transfer coefficient can be correlated with the Nusselt number, Nu:

$$\frac{\partial(T_w - T)/(T_w - T_\infty)}{\partial(z/l)}\Big|_{z/l=0} = \frac{h_c l}{k} = \mathrm{Nu} \tag{10.2}$$

The above equation indicates that in reality the Nusselt number, Nu, is correlated with a characteristic temperature layer thickness, δ'_t (m), by the following equation:

$$\mathrm{Nu} = \frac{l}{\delta'_t} \tag{10.3}$$

In other words, the Nusselt number is inversely proportional to the temperature thickness. The boundary layers for laminar flow and turbulent flow will be discussed in the following section.

For engineering applications, the convective heat transfer coefficient is a single key parameter to be determined, which can be estimated based on the Nusselt number:

$$h_c = \frac{k}{l}\mathrm{Nu} \tag{10.4}$$

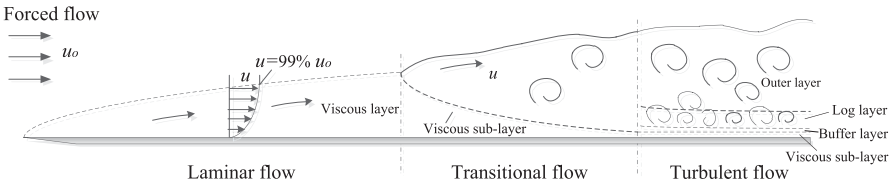

Fig. 10.1 Boundary layers on a flat plate with sharp edge

Therefore, the Nusselt number must be known for estimation of convective heat transfer. Further, it should be noted that the characteristic length differs from one application to another, and that the characteristic length in the above equation and in the correlation for the Nusselt number should be the same. Comparing Eq. (10.3) with Eq. (10.4) gives the expression for the thermal thickness: $\delta'_t = k/h_c$.

10.2.1 Boundary Layer

Convective heat transfer occurs in the boundary layer. Therefore, the thickness of the boundary layer and the flow modes within it are very important in determining the convective heat flux. For a simple geometry, an analytical solution can be obtained by analysis of the controlling equations, based on some simplifications. A good example is the flow over a flat plate with a sharp leading edge, see Fig. 10.1. Near the leading edge the flow is purely laminar with small thickness; then the flow enters a transitional phase, and finally becomes fully turbulent as the distance away from the leading edge increases.

For laminar flows, the boundary layer is viscous and therefore the viscous force controls the velocity distribution normal to the surface. In other words, there is only one layer for laminar flows, see Fig. 10.1. However, for turbulent flows, the boundary layer mainly consists of four sub-layers, that is, the viscous sub-layer, the buffer layer, the log layer, and the outer layer, see Fig. 10.1. In the viscous sub-layer, eddy diffusivity is small compared to viscous diffusivity and thus can be ignored. The buffer layer is a transitional layer between the viscous sub-layer and the log layer. In the log layer turbulent eddy diffusivity becomes dominant. In the outer layer, inertial forces dominate the flow and thus the layer is only weakly influenced by the wall. Despite this, the main thermal resistance of the boundary layer results from the viscous sub-layer for turbulent flows. For rough walls the viscous sub-layer can be easily disrupted, therefore the thermal resistance decreases significantly and the heat transfer increases accordingly.

The thickness of the flow boundary, δ (m), for laminar flows on a flat plate [2] can be estimated using:

$$\delta = 4.92 x \, \mathrm{Re}_x^{-1/2} \tag{10.5}$$

For turbulent flows on a flat plate it becomes [2]:

$$\delta = 0.16x\,\mathrm{Re}_x^{-1/7} \tag{10.6}$$

where the Reynolds number, Re, is defined as:

$$\mathrm{Re}_x = \frac{ux}{v} \tag{10.7}$$

In the above equations, x is the distance from the upstream edge of the plate (m), u is the fluid velocity (m/s), v is the kinematic viscosity (m^2/s), δ is the flow boundary layer thickness (m), and Re_x is the Reynolds number at location x.

The Reynolds number characterizes the influence of inertial force and viscous force in a flow. It can be used to determine whether the flow is laminar flow, transitional flow, or turbulent flow.

The characteristic length in the equations for the thickness is the distance away from the entrance. However, the turbulent length in a tunnel is restricted by the tunnel diameter. Note that these results are obtained based on smooth surfaces. The thickness of the turbulent flows in reality corresponds to the log layer since the viscous sub-layer is very thin at a high Reynolds number.

10.2.2 Reynolds–Colburn Analogy

The momentum equation for the flow boundary layer and the energy equation for the temperature boundary layer have the same form with similar boundary conditions, except for a difference in the diffusivity coefficients. The kinematic viscosity v is used for the flow boundary and the thermal diffusivity a is used for the temperature boundary in *laminar flows*, while the eddy diffusivity ε_m is used for the flow boundary, and the eddy diffusivity of heat ε_T is used for the temperature boundary in *turbulent flows*. The high similarity between momentum and convective heat transfer provides an easy way of estimating the convective heat transfer based on knowledge of the flow boundary.

The Reynolds–Colburn analogy for laminar flows, transitional flows, and turbulent flows not too far above the transition can be approximated as follows [1]:

$$\mathrm{St} = \frac{1}{2} C_f\,\mathrm{Pr}^{-2/3} \tag{10.8}$$

where the Stanton number, St, is defined as

$$\mathrm{St} = \frac{h_c}{\rho c_p u} = \frac{\mathrm{Nu}}{\mathrm{Re}\,\mathrm{Pr}} \tag{10.9}$$

and the skin friction coefficient:

$$C_f = \frac{\tau_w}{\rho u^2 / 2} \tag{10.10}$$

The Reynolds number, Re, is defined as:

$$\mathrm{Re} = \frac{\rho u l}{\mu} \tag{10.11}$$

The Prandtl number, Pr, is defined as:

$$\mathrm{Pr} = \frac{v}{a} \tag{10.12}$$

In the above equations, C_f is the skin friction coefficient, ρ is the gas density (kg/m^3), c_p is the heat capacity (kJ/(kgK)), u is the gas velocity (m/s), τ_w is the wall shear stress (N/m^2), l is the characteristic length (m), μ is the dynamic viscosity (kg/ms) and a is the thermal diffusivity (m^2/s).

Note that the Stanton number represents the ratio of the convective heat flux to the total heat flux capacity of the flow. The Prandtl number characterizes the influence of viscous diffusivity and thermal diffusivity in a flow.

The Nusselt number can be expressed as:

$$\mathrm{Nu} = \mathrm{St} \cdot \mathrm{Re} \cdot \mathrm{Pr} \tag{10.13}$$

or

$$\mathrm{Nu} = \frac{1}{2} C_f \, \mathrm{RePr}^{1/3} \tag{10.14}$$

However, it should be kept in mind that the equation is based on complete similarity between the temperature boundary layer and flow boundary layer, that is, it is assumed that Pr is equivalent to 1, or the flow boundary layer and temperature boundary layer have the same thickness. In reality, Pr is lower than 1 for air, which results in a thicker temperature boundary layer. The ratio of the thickness of the temperature boundary layer and the flow boundary layer for laminar flows can be approximated by:

$$\frac{\delta_t}{\delta} = \mathrm{Pr}^{-1/3} \tag{10.15}$$

where δ_t and δ are the thickness of the thermal boundary layer (m) and the thickness of the flow boundary layer (m) respectively.

The boundary layers in laminar flow, transitional flow, and turbulent flow are different. Thus, the expression of the Nusselt number could be very complicated in order to cover the different flow modes.

The Reynolds analogy for turbulent flows can be expressed as follows [7]:

$$\mathrm{St} = \frac{C_f / 2}{1.07 + 12.7(\mathrm{Pr}^{2/3} - 1)\sqrt{C_f / 2}} \tag{10.16}$$

The difference between this equation for turbulent flows and Eq. (10.8) for laminar flows is apparent. Note that these equations are for smooth surfaces. If the wall is rough, the second term in the denominator must be revised to account for the roughness.

10.2.3 Forced Convection

In tunnel fires, longitudinal flows moving into and out of the tunnel usually exist in one way or another due to either mechanical ventilation, natural ventilation, or buoyancy force resulting from the fire itself. Therefore, in tunnel fires convective heat transfer is always related to forced convection and turbulent flows of, for example, the hot gases flowing along the tunnel ceiling or the cold air flowing along the heated tunnel floor.

The Nusselt number for forced convection generally has a form of [1]:

$$\mathrm{Nu} = C\,\mathrm{Re}^{m}\,\mathrm{Pr}^{n} \tag{10.17}$$

where m, n, and C are coefficients depending on the scenarios.

For a flat plate in forced convection, for example, the tunnel floor, the equation for the Nusselt number can be expressed as [2]:

$$\mathrm{Nu}_{l} = 0.037\,\mathrm{Re}_{l}^{4/5}\,\mathrm{Pr}^{0.43} \tag{10.18}$$

In Eq. (10.18), the characteristic length l is the distance from the edge of the solid surface. However, the turbulent length in a tunnel is restricted by tunnel geometry, and generally the hydraulic diameter of the tunnel can be used as a characteristic length. Therefore, although Eq. (10.18) was not proposed for tunnel flows, it can be used to roughly estimate the convective heat transfer in a tunnel.

Note that the above equations are all for smooth surfaces, which indicates that the roughness is considered as 0 or at least so small that its influence on the heat transfer is negligible. For a wall having a rough surface, the viscous sub-layer is disrupted and the thermal resistance of the sub-layer decreases significantly. The convective heat transfer coefficient on a wall with a rough surface can be twice that of a smooth wall for the same flow situation.

In the analysis of heat flux problems in tunnel fires, the convective heat transfer equations for tube flows are recommended to be used. For tubes with rough surfaces, the friction is generally expressed in terms of the Darcy–Weisbach friction factor, f, which is defined as:

$$f = \frac{\Delta p}{\frac{1}{2}\frac{L}{D}\rho u^{2}} = \frac{1}{4}C_{f} \tag{10.19}$$

where Δp is the pressure loss (Pa), L is the length (m), and D is the diameter (m).

The Nusselt number for a wall with a rough surface is well correlated by the following relationship [8]:

$$\mathrm{Nu}_D = \frac{(f/8)\,\mathrm{Re}_D\,\mathrm{Pr}}{1+(4.5\,\mathrm{Re}_\varepsilon^{0.2}\,\mathrm{Pr}^{0.5}-8.48)\sqrt{f/8}} \tag{10.20}$$

The relationship applies for the following ranges of Re and the relative roughness of the surface ε/D:

$$Re_D > 10^4 \; and \; 0.002 \le \varepsilon / D \le 0.05.$$

The Reynolds number depends on the relative roughness of the surface and is defined as:

$$\mathrm{Re}_\varepsilon = \mathrm{Re}_D \frac{\varepsilon}{D}\sqrt{\frac{f}{8}} \tag{10.21}$$

The Darcy–Weisbach friction factor is correlated with the roughness and the Reynolds number by [9]:

$$f = \frac{1}{\left\{1.81\lg\left[\frac{6.9}{\mathrm{Re}_D}+\left(\frac{\varepsilon}{3.7D}\right)^{1.11}\right]\right\}^2} \tag{10.22}$$

In the above equations, ε is the root mean square roughness of the surface (m), and ε/D is the relative roughness of the surface. Note that for fully developed turbulent flows, the Darcy–Weisbach friction factor is not sensitive to the Reynolds number.

In the above equations, all properties are estimated at the flow temperature. This makes the above equations easy to use.

Generally, the tunnel diameter can be used as the characteristic length in the heat transfer analysis of the whole system. Also the hydraulic diameter can be used in the analysis of heat loss to walls surrounding the hot gases where clear stratification exists. The hydraulic diameter can be calculated by:

$$D = \frac{4A}{P} \tag{10.23}$$

where A is the flow area (m^2), and P is the wet perimeter of the flow (m).

Note that the convective heat transfer is not very sensitive to the characteristic length scale in a tunnel. Therefore, the error introduced by slight differences in choosing the characteristic length scale should be quite limited in most cases.

10.2.4 Natural Convection

Natural convection suggests that the flow movement is induced internally or inherently. Although the natural convection mode is not so important in tunnel fires, it is shortly described here for completeness.

The Nusselt number for natural convection generally has a form of:

$$\mathrm{Nu}_l = C\,\mathrm{Ra}_l^m \tag{10.24}$$

where the Rayleigh number, Ra_l, is defined as:

$$\mathrm{Ra}_l = \mathrm{Gr}_l\,\mathrm{Pr} \tag{10.25}$$

and the Grashof number, Gr_l, is defined as:

$$\mathrm{Gr}_l = \frac{g\beta\Delta T l^3}{\nu^2} \tag{10.26}$$

where g is the gravitational acceleration, ΔT is the difference between gas temperature and wall surface temperature, β is the thermal expansion coefficient (1/K), and superscript m is a coefficient.

For a vertical plate heated by radiation from flames and hot gases under natural convection, the Nusselt number can be expressed as [2]:

$$\mathrm{Nu}_l = 0.678\,\mathrm{Ra}_l^{1/4}\left(\frac{\mathrm{Pr}}{\mathrm{Pr}+0.952}\right) \approx 0.55 Ra_l^{1/4} \tag{10.27}$$

All the properties in Eq. (10.27) should be evaluated at $T=(T_w+T_\infty)/2$, with the exception of the expansion coefficient which should be evaluated at T_∞ (temperature of the main flow stream).

10.2.5 Gas Properties

Generally atmospheric air properties can be used as properties for smoke flows, due to the inertia dominance of nitrogen gas in the smoke flow. The gas properties, for example, conductivity, thermal, and kinematic viscosity vary significantly with temperature. They can be obtained from tables or estimated using some simplified expressions which are proposed in the following equations.

Based on the data from reference [10], approximate expressions for air temperature in a range of 0–2000 °C at standard atmospheric pressure are given here for convenience. The conductivity, k (W/(m K)), could be expressed as:

$$k = 1.16\times10^{-11}T^3 - 4.1\times10^{-8}T^2 + 10^{-4}T \tag{10.28}$$

and the thermal diffusivity, a (m^2/s),:

$$a = 2.3 \times 10^{-9} T^{1.62} \tag{10.29}$$

and the kinematic viscosity, v (m^2/s),:

$$v = 1.43 \times 10^{-9} T^{1.64} \tag{10.30}$$

where T is the gas temperature in Kelvin (K).

According to the definition of thermal diffusivity, the heat capacity, c_p (J/(kg·K)), could be simply estimated by:

$$c_p = \frac{k}{\rho a} \tag{10.31}$$

Note that, the Prandtl number is insensitive to temperature and can be approximated as:

$$\mathrm{Pr} = \frac{v}{a} = 0.7 \tag{10.32}$$

These expressions can be conveniently used to estimate the gas properties.

Example 10.1 A 6 m high and 10 m wide rock tunnel is full of 1000 °C sooty gases. The rock tunnel has an average roughness of 10 cm. The smoke flow velocity is assumed to be 7 m/s. Estimate the convective heat transfer coefficient.

Solution: Eq. (10.4) can be used to estimate the convective heat transfer. First, calculate the gas properties using Eqs. (10.28)–(10.31): $k = 0.095$ W/(m·K), $a = 0.00033$ m^2/s, $v = 0.00024$ m^2/s, and $c_p = 1250$ J/(kg·K). The hydraulic diameter of the tunnel D is 7.5 m (Eq. (10.23)). Given that this rock tunnel is very rough, Eq. (10.20) can be used to estimate the Nusselt number. We first calculate the relative roughness $\varepsilon/D = 0.013$, then $Re_D = 218750$ with the aid of Eq. (10.11), $f = 0.042$ with the aid of Eq. (10.22) and finally $Re_\varepsilon = 212$ with the aid of Eq. (10.21). Now we can estimate the Nusselt number using Eq. (10.20) that is $Nu_D = 683$. The convective heat transfer coefficient is finally estimated to be $h_c = k \cdot Nu_D/D = 8.65$ W/(m^2K) (Eq. (10.4)).

10.3 Radiative Heat Transfer

All bodies emit energy by electromagnetic radiation. The intensity mainly depends on the temperature and properties of the emitting surface. Further, smoke emits, absorbs, and even scatters radiation from flames and hot surfaces.

10.3.1 Simplification in Engineering Application

Generally, all surfaces can be simplified into diffuse surfaces in which all energy is reflected or radiated equally in every solid angle. Although, radiation is strongly dependent on the wavelength of the emitted energy, this influence is eliminated by introducing simple assumptions in engineering applications which are discussed in the following text.

A black body is an idealized surface which absorbs all incident radiation. The total emissive power from a blackbody per unit area, e_b (kW/m^2), can be calculated by:

$$e_b = \sigma T^4 \tag{10.33}$$

where the Stefan–Boltzmann constant, σ, is 5.67×10^{-11} kW/(m$^2 \cdot$ K^4), and T is the temperature in Kelvin (K).

Realistic surfaces are not blackbodies and cannot absorb all incident radiation. Instead, part of the incident radiation is reflected.

For simplicity, the gray body approximation is introduced here. This means that all properties of the surface are independent of the wavelength. The emissive power from a gray body per unit area, e, can be calculated by introducing the emissivity, ε:

$$e = \varepsilon e_b \tag{10.34}$$

Note that incident radiation can be absorbed, reflected, or passed through the surface, thus the following equation is obtained:

$$\alpha + \tau + \gamma = 1 \tag{10.35}$$

The emissivity is ε, absorptance is α, transmittance is τ, and reflectance is γ.

For most solid surfaces, the radiation cannot penetrate the solid surface. Therefore, following equation is obtained:

$$\alpha + \gamma = 1 \tag{10.36}$$

According to the Kirchhoff's law, the emissivity of all diffusive gray bodies is equal to the absorption, or

$$\varepsilon = \alpha \tag{10.37}$$

The above equation works for most practical surfaces in engineering applications.

10.3.2 View Factor

The radiation from blackbody i to another blackbody j can be expressed as:

$$\dot{Q}_{i-j} = A_i F_{i-j} \sigma (T_i^4 - T_j^4) \tag{10.38}$$

where the view factor is defined as:

$$F_{i-j} = \frac{1}{A_i}\int_{Ai}\int_{Aj}\frac{\cos\beta_i \cos\beta_j}{\pi s^2} dA_j dA_i \tag{10.39}$$

where A is the surface area (m^2), F is the view factor, $\dot{Q}$ is the radiative heat (kW), β is the angle between the light of sight and the surface normal, and s is the distance (m) between dA_i and dA_j. Subscripts i and j indicate ith and jth surface. The physical meaning of the view factor F_{i-j} is the fraction of radiation emitted by ith surface that is received by jth surface.

The following two equations are always fulfilled:

$$A_i F_{i-j} = A_j F_{j-i} \tag{10.40}$$

and

$$\sum_j A_i F_{i-j} = 1 \tag{10.41}$$

The view factor represents the percentage of radiation from one object to another. The analytical solution, even for a simple case, is difficult to obtain although the definition is very clear.

10.3.3 Radiation Among Multiple Surfaces

Radiation among multiple surfaces can be very complicated. To express it clearly, the electrical circuit analog is introduced. Figure 10.2 shows a diagram of the surface radiation balance. The irradiance (incident heat flux), $\dot{q}''_{inc}$ (kW/m^2), and the radiosity, J (kW/m^2), can be expressed as:

$$J = \gamma \dot{q}''_{inc} + \varepsilon e_b \tag{10.42}$$

The net radiation at the surface, $\dot{Q}_{net}$ (kW), is:

$$\dot{Q}_{net} = \dot{q}''_{net} A = (J - \dot{q}''_{inc})A = \frac{e_b - J}{(1-\varepsilon)/(\varepsilon A)} \tag{10.43}$$

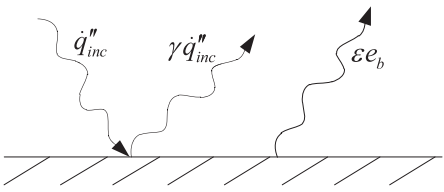

Fig. 10.2 A diagram of surface radiation balance

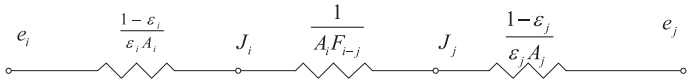

Fig. 10.3 An electrical circuit analog of radiation between any two surfaces

We can consider that the radiation J is emitted from an equivalent blackbody beside the realistic surface with the same view factor from ith surface to jth surface. Thus, the radiation between J_i and J_j can be expressed simply by:

$$\dot{Q}_{net,i-j} = (J_i - J_j) A_i F_{i-j} = \frac{J_i - J_j}{A_i F_{i-j}} \tag{10.44}$$

The form of the above two equations suggests an electrical circuit with potentials e or J, current $\dot{Q}$, and resistors. For example, the radiation between two parallel infinite plates can be shown in Fig. 10.3. This method of expressing the heat transfer process is called the electrical circuit analog.

The net heat flux between surface i and surface j can be simply calculated as:

$$\dot{Q}_{net,i-j} = \frac{e_i - e_j}{(1-\varepsilon_i)/(\varepsilon_i A_i) + 1/A_i F_{i-j} + (1-\varepsilon_j)/(\varepsilon_j A_j)} \tag{10.45}$$

For a more complicated case when multiple surfaces are involved, the net heat flux $\dot{Q}_{net}$ at the surface can be obtained by solving the following equation:

$$\sum_{j=1}^{n} \left(\frac{\delta_{ij}}{\varepsilon_i} - \frac{1-\varepsilon_j}{\varepsilon_j A_j} A_i F_{i-j}\right) \dot{Q}_{net,j} = \sum_{j=1}^{n} A_i F_{i-j} (\sigma T_i^4 - \sigma T_j^4) \tag{10.46}$$

where the Kronecker delta, δ_{ij}, is defined as:

$$\delta_{ij} = \begin{cases} 1 & for\ i = j \\ 0 & for\ i \neq j \end{cases} \tag{10.47}$$

For n surfaces involved in the radiation, N equation can be solved for the n unknown values of $\dot{Q}_{net,j}$.

10.3.4 Absorbing, Emitting and Scattering Gas

Smoke absorbs, emits and even scatters the radiation from flames and hot surfaces. In a fire producing very sooty smoke, radiation from the walls could be mostly absorbed and the smoke layer itself acts similar to a gray body or a "gray gas". In these scenarios, the properties of the smoke must be considered. The gray gas approximation works in many engineering applications. All properties of the gases, including emissivity and absorptance are assumed to be independent of the wavelength.

Generally, the smoke can be considered as a nonscattering gas. Thus we obtain the following equation:

$$\alpha_g + \tau_g = 1 \tag{10.48}$$

where the subscript g indicates gas (including both gas molecules and smoke particles).

Ignoring the scattering effect, the radiation transport equation (RTE) along path s, can be simply expressed as:

$$\frac{dI}{ds} = \kappa(I_b - I) \tag{10.49}$$

where I is the radiation intensity (kW/m^2·steradian), κ is the absorption coefficient (1/m) and s is the path length (m). The radiation intensity from a blackbody is:

$$I_b = \frac{\sigma T^4}{\pi} \tag{10.50}$$

Equation (10.49) suggests that along a path s, the radiation intensity is absorbed by the gas, however, the gas volume also emits the radiation. If the scattering effect is taken into account, the absorption coefficient in the second term on the right-hand side must be replaced by the sum of the absorption coefficient α and a scattering coefficient.

Assuming that one gas volume is homogeneous, the RTE equation, that is Eq. (10.49), can be integrated and the following equation is obtained:

$$\frac{I(s) - I_b}{I(0) - I_b} = e^{-\kappa s} \tag{10.51}$$

Equation (10.49) can be transformed into:

$$I(s) = I(0)e^{-\kappa s} + I_b(1 - e^{-\kappa s}) \tag{10.52}$$

Note that the terms on the right-hand side of the above equation corresponds to heat transmitted through and heat emitted from a gas volume. Note that *I(0)* and I_b appear to be independent and thus it is simple to obtain the definitions of transmittance, τ, and emissivity, ε, for the gas volume:

$$\tau_g = e^{-\kappa s},\ \varepsilon_g = 1 - e^{-\kappa s} \tag{10.53}$$

Note that the Kirchoff's law also works for gas, which suggests that the emissivity of the medium equals its absorptance. This can be easily checked from Eqs. (10.48) and (10.53).

In engineering applications, to estimate the overall emissivity of a large gas volume, the path length, s, is normally replaced by a mean beam length, L_m (m), which is defined as:

$$L_m = 3.6\frac{V_m}{A_m} \tag{10.54}$$

where the volume containing the hot gases is V_m (m^3) and the bounding area A_m (m^2). This simple method significantly simplifies the calculation of heat radiation and has been widely used in different fields of fire safety science.

In a fire, the radiation absorbed by the hot gases is mainly attributed to the soot. Other combustion products, for example, CO_2 and H_2O, play a much less important role. The total emissivity of the medium can be estimated using [11]:

$$\varepsilon_t = \varepsilon_s + \varepsilon_g - \varepsilon_s \varepsilon_g \tag{10.55}$$

where

$$\varepsilon_g = \varepsilon_{CO_2} + \varepsilon_{H_2O} - \varepsilon_{CO_2}\varepsilon_{H_2O} \approx \varepsilon_{H_2O} + \frac{1}{2}\varepsilon_{CO_2} \tag{10.56}$$

In the above equation, subscript t indicates total, s is soot, g is gas, CO_2 is carbon dioxide, and H_2O is water vapor. The absorption coefficient for soot, κ_s, is proportional to the volume fraction of the absorbing medium, which can be expressed as [5]:

$$\kappa_s = 3.72 \frac{C_o}{C_2} X_s T \tag{10.57}$$

where X_s is the soot volume fraction, T is the smoke temperature (K), C_o is a constant varying between 2 and 6, depending on the refractive index, C_2 is the Planck's second constant, 1.4388×10^{-2} m K. Equation (10.57) applies only to small particles, that is, the complex refractive index of the particles is assumed to be independent of wavelength. The absorption coefficient of the particles can increase for aggregates if the primary particle sizes are over the Rayleigh scattering limits. Generally the soot produced by fires is small enough for the Rayleigh scattering limits.

The absorption coefficients of CO_2 and H_2O can be obtained directly from charts in the literature, for example reference [5] and [11], given that the partial pressure, temperature of the species, and the mean beam length are known.

In a complicated scenario, a three-dimensional radiation model must be employed, taking solid angles and wavelength bands into account. Further, the local absorption coefficients and path length should be used rather than the global absorption coefficient and mean beam length.

Example 10.2 Estimate the radiation between two infinite plates parallel to each other. One plate has a temperature of 1000 °C and an emissivity of 0.92. The corresponding parameters are 300 °C and 0.8 for the other plate.

Solution: First estimate the emissive powers using Eq. (10.33): $e_{b,1} = 5.67 \times 10^{-11} \times (273 + 1000)^4 = 148.9$ kW/m^2 and $e_{b,2} = 5.67 \times 10^{-11} \times (273 + 300)^4 = 6.1$ kW/m^2. The view factor between the two infinite plates is one because two face-to-face surfaces can only see each other. The net heat flux between the plates can be estimated using Eq. (10.45):

$$\dot{q}_{net,i-j} = \frac{\dot{Q}_{net,i-j}}{A} = \frac{148.9 - 6.1}{(1-0.92)/0.92 + 1/1 + (1-0.8)/0.8} = 106.8 \text{ kW/m}^2.$$

Example 10.3 A 30 MW fire occurs in a 6 m high and 10 m wide tunnel having a longitudinal ventilation velocity of 3 m/s. The downstream is full of smoke. The fire source mainly consists of polyethylene with an effective heat of combustion of 40 MW/kg. The average soot yield is 0.06, that is, 1 kg fuel produces 0.06 kg soot. The density of the pure particles (pure soot without gas) is 1000 kg/m^3. Assuming that CO_2 and H_2O have no effect, estimate the emissivity of the smoke volume for a gas temperature of 300 °C. The incoming air flow is 20 °C under a normal pressure of 1 atm.

Solution: First estimate the mass flow rate: $\dot{m} = \rho_o u_o A = 1.2 \times 3 \times 6 \times 10 = kg/s$. *Then calculate the total fuel mass loss rate:* $\dot{m}_f = 30/40 = 0.75 kg/s$. *The mass flow rate of the soot is:* $0.75 \times 0.06 = 0.045$ *kg/s. The mass fraction of the soot in the flow on the downstream side is:* $Y_s = 0.045/216 = 0.00208$ *kg/kg. The density of the gas is:* $1.2 \times 293/(273 + 300) = 0.614$ *kg/m*^{3}. *The volume fraction of the soot can therefore be estimated by:* $X_s = 0.00208 \times 0.614/1000 = 1.28 \times 10^{-6}$ *m*^{3}*/m*^{3}. *The absorption coefficient can be calculated using Eq. (10.57):* $\kappa_s = 3.72 \times (4/1.4388 \times 10^{-2}) \times 1.28 \times 10^{-6} \times (273 + 20) = 0.39$. *The length of the bounded volume can be assumed to be 1 m (This value has no influence on the results. It can also be 2 or 3 m). Therefore, the mean beam length is:* $L_m = 3.6 \times 6 \times 10/(6 \times 2 + 10 \times 2) = 6.75$ *m. The emissivity can then be estimated:* $\varepsilon_g = 1 - e^{(-0.39*6.75)} = 0.93$. *The value is close to 1 which indicates that the gas volume is similar to a black body and the radiation transfer between the ceiling and wall is very limited.*

10.4 Heat Conduction

In tunnel fire safety, the heat losses to the tunnel walls and the temperature inside the tunnel walls are the key issues in the design of both active and passive fire safety systems. Generally it can be assumed that the substance is isotropic, that is, the thermal properties of the substance are independent of the direction.

The controlling equation for one-dimensional heat conduction can be expressed as:

$$\frac{\partial T_s}{\partial t} = a_s \frac{\partial^2 T_s}{\partial z^2} \tag{10.58}$$

where the thermal diffusivity of the solid, a (m^2/s), is defined as:

$$a_s = \frac{k_s}{\rho_s c_s}$$

where t is the time (s) and z is the depth below surface (m). Subscript s indicates solid.

Boundary conditions on one side or both sides must be given to get a solution of the temperatures inside the substance or on the surface.

There are four typical wall boundary conditions:

- First boundary condition—Fixed surface temperature: T_w = Constant.
- Second boundary condition—Constant net heat flux on the wall:

$$-k\frac{\partial T_s}{\partial z}|_{z=0} = \dot{q}''_{net} \tag{10.59}$$

- Third boundary condition—Constant heat transfer coefficient:

$$-k_s\frac{\partial T_s}{\partial z}|_{z=0} = h(T_g - T_w) \tag{10.60}$$

- Fourth boundary condition—Constant heat flux and constant convective heat transfer coefficient:

$$\dot{q}''_w = -k\frac{dT}{dz}|_{z=0} = \dot{q}''_{net} + h_c(T_g - T_w) \tag{10.61}$$

According to Fourier's law, the solution for a steady-state one-dimensional heat conduction problem can be obtained by:

$$\dot{q}''_k = \frac{k_s}{\delta_s}(T_w - T_{bw}) \tag{10.62}$$

where δ_s is the thickness of the solid (m). Subscript *w* means exposed wall surface and *bw* means backside wall surface.

For a complicated geometry or a complicated boundary condition an analytical solution is not possible to obtain. However, in many cases, the boundary conditions can be simplified to heat conduction in an infinite plate with one of the four basic boundaries. Analytical solutions can be obtained for these cases which are discussed in the following sections.

10.4.1 Thermally Thin Materials

For thermally thin materials such as a thin steel plate, the heat conduction is fast compared to the heat transfer to the surface. Therefore, it is normally assumed that the material always has the same temperature throughout (no temperature gradient inside the material). Note that the first boundary (that is the boundary condition with fixed surface temperature) has no meaning for thermally thin materials.

For thermally thin materials with the second boundary condition (fixed heat flux at the surface), the temperature can be estimated using:

$$\Delta T_s = T_s - T_i = \frac{\dot{q}''_w t}{\rho_s \delta_s c_s} \tag{10.63}$$

Therefore, the ignition time for thermally thin fuel, t_{ig} (s), can be estimated using:

$$t_{ig} = \frac{\rho_s \delta_s c_s \Delta T_s}{\dot{q}''_w} \tag{10.64}$$

For thermally thin materials with the third boundary condition (constant heat transfer coefficient), the temperature can be estimated using:

$$T_\infty - T_s = (T_\infty - T_o)\exp(-\frac{ht}{\rho_s \delta_s c_s}) \tag{10.65}$$

For thermally thin materials with the fourth boundary condition (a constant heat flux and constant convective heat transfer coefficient), the temperature can be estimated using:

$$T_\infty - T_s = (T_\infty + \frac{\dot{q}''}{h_c} - T_o)\exp(-\frac{h_c t}{\rho_s \delta_s c_s}) \tag{10.66}$$

In the above equations, t is time (s), T_s is the temperature of the thermally thin material (K), T_i is the initial temperature (K), T_∞ is the gas temperature (K), $\dot{q}''_w$ is the net heat flux absorbed by surface (kW/m^2), h is the heat transfer coefficient (kW/(m^{2}K)), δ is the thickness of the thermally thin material (m), c_s is the heat capacity of the material (kJ/(kgK)). Subscripts s indicates solid, c convective heat transfer and ig ignition.

10.4.2 Thermally Thick Materials

Thermally thick materials indicate, that there always exists a temperature gradient normal to the surface of the material. In a heat conduction process, the heat travels into the material through the surface continuously, eventually reaching the back side of the plate. This is defined as thermal penetration for a given thickness. To determine whether a material has been penetrated by heat, the thermal penetration depth, δ_s, can be estimated using:

$$\delta_s = C_k \sqrt{a_s t} \tag{10.67}$$

where C_k is a coefficient. For estimation of whether the material is thermally thick or not, the value of 3.6 corresponding to a relative temperature rise of 1% is recommended for use. While, determining whether the material has been fully penetrated, the value of 2 corresponding to a relative temperature rise of 16% is recommended for use. After the full thermal penetration (C_k=2), the temperature gradient inside the material is constant, and the heat flux can be calculated using

Eq. (10.63). The corresponding conductive heat transfer coefficient, h_k, can be directly expressed as:

$$h_k = k_s / \delta_s \tag{10.68}$$

Before thermal penetration, the material could be considered as an infinite plate. This is generally a good assumption in tunnel fires as the walls are often very thick and may have concrete linings or they could be infinite in depth as in rock tunnels.

For heat conduction inside thermally thick materials, two key dimensionless parameters are defined first:

$$\zeta = \frac{z}{2\sqrt{a_s t}} \tag{10.69}$$

and

$$\beta = \frac{h\sqrt{a_s t}}{k_s} = h\sqrt{\frac{t}{k_s \rho_s c_s}} \tag{10.70}$$

For the four typical boundary conditions for heat conduction mentioned previously, analytical solutions can be obtained and are presented in the following sections.

10.4.2.1 First Boundary Condition

Recall the first boundary condition is constant surface temperature. This boundary condition is not realistic, but could be reasonable if an object is exposed to gas with a rapidly increasing temperature that becomes constant in a short time, or if an object is suddenly exposed to a constant temperature.

Assume that the gas temperature, T_g, is equivalent to the wall surface temperature, the temperature inside the wall material can be estimated by:

$$\frac{T_s(z,t) - T_o}{T_g - T_o} = 1 - \text{erf}(\zeta) = \text{erfc}(\zeta) \tag{10.71}$$

where z is the depth below the surface (m), t is the time (s), erf is Gauss error function, and erfc its complimentary function.

The heat flux at the surface can be estimated as:

$$\dot{q}''_w = \sqrt{\frac{k_s \rho_s c_s}{\pi t}}(T_g - T_o) \tag{10.72}$$

If the plate or wall is not infinite and the heat has penetrated to the backside of the plate, then the heat flux can be simplified to:

$$\dot{q}''_w = \frac{k_s}{\delta_s}(T_g - T_{bw}) \tag{10.73}$$

where T_{bw} is the backside wall temperature.

10.4.2.2 Second Boundary Condition

Recall that the second boundary condition is a constant net heat flux to the wall. The internal temperature can be calculated by [1]:

$$T_s(z,t) - T_i = \frac{2\dot{q}''_{net}}{k_s}\sqrt{\frac{a_s t}{\pi}}\exp(-\zeta^2) - \frac{z}{2}\operatorname{erfc}(\zeta) \tag{10.74}$$

The surface temperature can be calculated by:

$$T_w - T_o = \frac{2\dot{q}''_{net}}{k_s}\sqrt{\frac{a_s t}{\pi}} = 2\dot{q}''_{net}\sqrt{\frac{t}{\pi k_s \rho_s c_s}} \tag{10.75}$$

The above equation has been widely used in the fire safety research to estimate the ignition time, t_{ig} (s), by modifying it into the following form:

$$t_{ig} = \frac{\pi}{4} k_s \rho_s c_s \frac{(T_{ig} - T_o)^2}{\dot{q}''^2_{net}} \tag{10.76}$$

Despite its wide use, the net heat flux at a surface is in fact not constant and thus a numerical solution is usually required to solve the problem.

10.4.2.3 Third Boundary Condition

The third boundary condition is a surface exposed to convective heat transfer with a constant heat transfer coefficient, which can be expressed as:

The internal temperature can be calculated by [1]:

$$\frac{T(z,t) - T_o}{T_g - T_o} = erfc(\zeta) - \exp(2\zeta\beta + \beta^2)\operatorname{erfc}(\zeta + \beta) \tag{10.77}$$

The surface temperature, T_w or $T(0,t)$, can therefore be calculated by:

$$\frac{T_w - T_o}{T_g - T_o} = 1 - \exp(\beta^2)\operatorname{erfc}(\beta) \tag{10.78}$$

Consequently the heat flux at the surface can be obtained by the following equation:

$$\dot{q}''_w = h(T_g - T_w) = h(T_g - T_o)\exp(\beta^2)\operatorname{erfc}(\beta) \tag{10.79}$$

10.4.2.4 Fourth Boundary Condition

The fourth boundary condition is a surface which absorbs heat by radiation at a constant radiative heat flux and by convection with a constant convective heat transfer coefficient. This boundary condition is not commonly used.

Note that, the fourth boundary condition is very similar to the third boundary and thus the solution can be easily obtained.

The temperature inside the solid can be expressed as:

$$\frac{T(z,t)-T_o}{T_g+\dot{q}''_{net}/h_c-T_o}=erfc(\zeta)-\exp(2\zeta\beta+\beta^2)\,\mathrm{erfc}(\zeta+\beta) \tag{10.80}$$

where the surface temperature is:

$$\frac{T_w-T_o}{T_g+\dot{q}''_{net}/h_c-T_o}=1-\exp(\beta^2)\,\mathrm{erfc}(\beta) \tag{10.81}$$

10.4.2.5 Complicated Boundary

The four boundary conditions described above are highly simplified, although they can be applied to some specific cases. In reality, boundary conditions are always very complicated and deviate from the four boundary conditions discussed above, for example, a transient boundary. In these cases, the Duhamel integral method or numerical simulation must be applied to give a solution. Such numerical methods for fluid flow and heat flux transfer will be discussed further in Chap. 17.

Example 10.4 Calculate the maximum concrete temperature at 5 cm below the ceiling surface, which is exposed to a 100 MW HGV fire for 10 min in a 6 m high and 20 m wide tunnel with a ventilation velocity of 2 m/s. The pool fire was set at 0.5 m above the tunnel floor. The HGV is 3 m wide and 10 m long. The ambient temperature is 10 °C. (Concrete lining: density ρ = 2100 kg/m^3, c_p = 880 J/(kg·K), k = 1.37 W/(m·K))

Solution: The maximum temperature exists at the ceiling above the fire. Calculate the maximum gas temperature near the ceiling surface using Eqs. (8.19) and (8.20): $T_{max}=T_o+\Delta T_{max}=10+1350\,°C$. *We could use two methods to estimate the temperature at 5 cm below tunnel ceiling, that is, the first boundary condition or the third boundary condition. Calculate* $\zeta=1.185$ *by Eq. (10.69). For the first boundary condition, calculate T(z = 0.05 m, t = 600 s) = 136 °C by Eq. (10.71), and* $\dot{q}''=49kW/m^2$ *by Eq. (10.72). For the third boundary condition, estimate the lumped heat transfer coefficient by* $h_t=h_c+\sigma(T_g^2+T_w^2)\times(T_g+T_w)=998\,W/(m^2K)$ *and* $\beta=15.4$, *then calculate T(z = 0.05m, t = 600s) = 136 °C by Eq. (10.77).*

Note that, the same results are obtained from both boundary conditions. This is because the heat conduction inside the concrete lining dominates the heat transfer. The boundary cannot be simplified to the second boundary since the net heat flux into the surface decreases significantly with time due to the increase in surface temperature. Further, caution should be taken when using the equations that include error functions, which can be numerically unstable and result in large errors. Therefore, is recommended to check whether the values obtained are realistic and possible.

10.5 Thermal Resistance

In this section, the thermal resistance of the heat transfer process from hot gases to the tunnel walls is discussed. A tunnel wall can be considered as an infinite plate even including concrete linings, given that the heat penetration to the backside of the lining generally takes a long time.

The convective heat flux can be expressed as:

$$\dot{q}_c'' = \frac{T_g - T_w}{1/h_c} \tag{10.82}$$

The conductive heat flux on the surface of a thermally thick material can be expressed as:

$$\dot{q}_k'' = \frac{(T_w - T_o)}{1/h_k} \tag{10.83}$$

where the heat transfer coefficient for thermally thick materials before the thermal penetration occurs is:

$$h_k = \sqrt{\frac{k_s \rho_s c_s}{\pi t}} \tag{10.84}$$

and the heat transfer coefficient after thermal penetration becomes:

$$h_k = \delta_s / k_s \tag{10.85}$$

The radiative heat flux on the wall surface may be expressed as:

$$\dot{q}_r'' = \frac{T_g - T_w}{1/h_r} \tag{10.86}$$

with

$$h_r = \varepsilon\sigma(T_g^2 + T_w^2)(T_g + T_w) \tag{10.87}$$

where the subscripts c, k, and r indicate convective, conductive, and radiative heat transfer respectively. Note that the conductive heat transfer coefficient, h_k, increases very rapidly with time. Further, the radiative heat transfer coefficient, h_r, may vary significantly with time.

The net heat flux through the surface, consisting of both radiative and convective net heat flux, should be equivalent to the net heat flux into the wall surface by heat conduction, which can be expressed as

$$\dot{q}_w'' = \dot{q}_r'' + \dot{q}_c'' = \dot{q}_k'' \tag{10.88}$$

The electrical circuit analog of the overall heat transfer from the gas to the wall surface is shown in Fig. 10.4. Note that the thermal resistances are the reciprocals

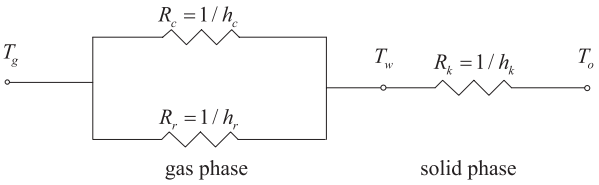

Fig. 10.4 The electrical circuit analog of global heat transfer from gas to the wall

of the heat transfer coefficients. Therefore, the overall heat flux through the surface can be expressed as:

$$\dot{q}'' = \frac{T_g - T_o}{1/h_k + 1/(h_c + h_r)} \tag{10.89}$$

The electrical circuit analog shown above is very simplified. The objective is only to clearly show the relationship among these three heat transfer mechanisms in the heat transfer from gas to wall and improve the understanding.

Example 10.5 A 6 m high and 10 m wide rock tunnel is full of 1000 °C sooty gases. The rock tunnel has an average roughness of 10 cm. The emissivity of the hot gases can be estimated to be 1. The smoke flow velocity is assumed to be 7 m/s. Calculate the thermal resistance of convective heat transfer, radiative heat transfer, and heat conduction at the time of 600 s and 3600s. (Rock properties: density $\rho = 2500$ kg/m^3, $c_p = 900$ J/kg K, $k = 1.3$ W/m·K)

Solution: Note that the scenario is the same as that in Example 10.1, we obtain the convective heat transfer coefficient $h_c = k \cdot Nu_D/D = 8.65$ *W/(m²K). At 600 and 3600 s, the wall surface temperature should approach the gas temperature. Therefore the radiative heat transfer coefficient can also be estimated by* $h_r \approx \varepsilon\sigma(T_g^2 + T_g^2)(T_g + T_g) = 4\varepsilon\sigma T_g^3 = 801 W/(m^2K)$. *Calculate the conductive heat transfer coefficient* $h_k = 36.6$ *W/(m²K) at 600 s and* $h_k = 15.0$ *W/(m²K) at 3600 s by using Eq. (10.84). Now we can estimate the thermal resistance* $R_c = 1/h_c = 0.116$, $R_r = 1/h_r = 0.0012$. *The lumped thermal resistance of convective and radiative heat transfer is* $\overline{R} = 1/(1/h_c + 1/h_r) = 0.0012$. *This suggests that radiation dominates the heat transfer from gas to wall surfaces. Then calculate the conduction resistance* $R_k = 0.027$ *for 600 s and* $R_k = 0.067$ *for 3600s. Therefore, the total thermal resistance is* $R_t = 0.0012 + 0.027 = 0.028$ *at 600 s, and* $R_t = 0.0012 + 0.067 = 0.068$. *Note that the total thermal resistance increases with time, and it is dominated by conductive heat transfer in this case.*

10.6 Heat Flux Measurement

Heat flux meters (HFMs) are used routinely in fire tests to measure the heat flux. The most popular types are the Gardon gauge (GG) and Schmidt–Boelter (SB) meters. Recently the use of plate thermometers (PT) for heat flux measurement has been developed and widely spread due to its simplicity and robustness.

Both GG and SB measure the total heat flux to a water cooled surface by measuring the temperature difference. The relationship between the measured heat flux and the incident radiation can be approximated as:

$$\dot{q}''_m = \varepsilon_m(\dot{q}''_{inc} - \sigma T_w^4) \tag{10.90}$$

where the subscript *m* indicates the value is measured by a HFM and w is the cooling water temperature. The emissivity is mostly dependent on the paint on the sensing surface of the HFM, but is generally in the range of 0.9–0.95. HFMs can be very sensitive to local convection since the surface temperature is reduced by the cooling water. Therefore the placement of these types of HFMs in hot gases could induce large errors, which must be corrected after the measurement.

The PT was initially developed by Wickström in the 1980s for controlling fire resistance furnaces to harmonize the test results. The PT has since been specified in the relevant international (ISO 834) and European (EN 1363-1) standards. At that time, the PT was not thought to be a HFM but to measure an effective temperature, assuring the same heat transfer to specimens in various types of fire resistance furnaces. Later, Ingason and Wickström [12] developed the methodology to use the PT for heat flux measurement. Wickström et al. [13] carried out further work to refine the model. Based on the equation for energy conservation, Ingason and Wickström proposed the following equation for calculating the incident heat flux [12]:

$$\dot{q}''_{inc} = \frac{\varepsilon_{PT}\sigma T_{PT}^4 + (h_{c,PT} + K_{cond})(T_{PT} - T_\infty) + (\rho c\delta)_{PT}\dfrac{\Delta T_{PT}}{\Delta t}}{\varepsilon_{PT}} \tag{10.91}$$

where the conduction correction factor $K_{\text{cond}} = 8.43\ \text{W/m}^2 \cdot \text{K}$, the surface emissivity of PT $\varepsilon_{PT} = 0.8$, and the lumped heat capacity coefficient $(\rho c\delta)_{PT} = 4202\text{J/m}^2 \cdot \text{K}$ [13]. The subscript ∞ indicates the surrounding gas. The terms in the numerator on the right-hand side are emissive radiation, convective heat loss, conductive heat loss, and accumulative heat gain, respectively. Note that the PTs do not need water to cool the surface, which make it very suitable for use in large-scale fire testing, for example, full scale tunnel fire tests.

10.7 Calculation of Heat Fluxes in Tunnel Fires

The total net heat flux on a surface is the sum of convective heat flux and radiative heat flux, which can simply be expressed as:

$$\dot{q}''_{net} = \dot{q}''_{net,c} + \dot{q}''_{net,r} \tag{10.92}$$

In large tunnel fires, generally the radiative heat flux is much higher than the convective heat flux. Also, note that the convective heat flux can be easily calculated using the equations proposed in the previous section. Therefore the calculation of the radiative heat flux is the focus of the following sections.

10.7.1 Exposed Tunnel Ceiling and Walls at Upper Layer

The surfaces at the upper layer are surrounded by smoky gases or flames in a large fire. The emissivity of the walls is assumed to be close to 1. Further, the view factor between the smoke and ceiling or walls can also be assumed to be 1. This is suitable for large fires but for small fires these assumptions can result in a conservative estimation. The net radiative heat flux can then be estimated using:

$$\dot{q}''_{net,w} = \frac{\dot{Q}_{g-w}}{A_w} = \frac{(e_{b,g} - e_{b,w})/A_w}{(1-\varepsilon_g)/(\varepsilon_g A_g) + 1/A_w F_{w-g} + (1-\varepsilon_w)/(\varepsilon_w A_w)} \tag{10.93}$$

where the subscript w indicates wall and g indicates hot gases.

Note that for $A_w = A_g$ and $F_{o-g} = 1$, we have:

$$\dot{q}''_{net,w} = \frac{e_{b,g} - e_{b,w}}{1/\varepsilon_g + (1-\varepsilon_w)/\varepsilon_w} \tag{10.94}$$

The incident heat flux received at the ceiling or wall surfaces can be estimated by:

$$\dot{q}''_{inc,w} = \frac{\dot{q}''_{net,w}}{\varepsilon_w} + e_{b,w} = \frac{\sigma(T_g^4 - T_w^4)}{\varepsilon_w/\varepsilon_g + 1 - \varepsilon_w} + \sigma T_w^4 \tag{10.95}$$

Given that the emissivity of the wall and the objects normally ranges from 0.85 to 0.95, an emissivity of 1 for the ceiling and upper walls can be assumed. Therefore, the incident heat flux at the upper layer can be simply written in the following form:

$$\dot{q}''_{inc,w} \approx \varepsilon_g \sigma T_g^4 \tag{10.96}$$

For large tunnel fires, the gas emissivity, ε_g, approaches 1. A comparison of the estimated and measured incident heat fluxes in the Runehamar tunnel fire tests carried out in 2003 [14] is presented in Fig. 10.5. All data lie close to the equality line which suggests a very good match.

Example 10.6 Estimate the incident heat fluxes at the ceiling in a 6 m high and 12 m wide tunnel with a heat release rate (HRR) of 30 and 100 MW respectively. The longitudinal flow velocity is 3 m/s and the ambient temperature is 20 °C. The bottom of the fire source is assumed to be 1 m above tunnel floor. The equivalent radius of the fuel is assumed to be 3 m. The emissivity can be assumed to be 1 for these two large fires.

Solution: First the maximum ceiling gas temperatures can be estimated using Eq. (8.17) in Chap. 8 on gas temperature, given that V′ > 0.19. The maximum excess gas temperature can be calculated to be 474 °C for 30 MW and 1350 °C for 100 MW. Therefore the corresponding maximum gas temperatures are 494 and 1370 °C respectively. The incident heat fluxes can then be estimated using Eq. (10.96) with an emissivity of 1. The calculated values are 19.6 kW/m² for 30 MW and 413 kW/m² for 100 MW.

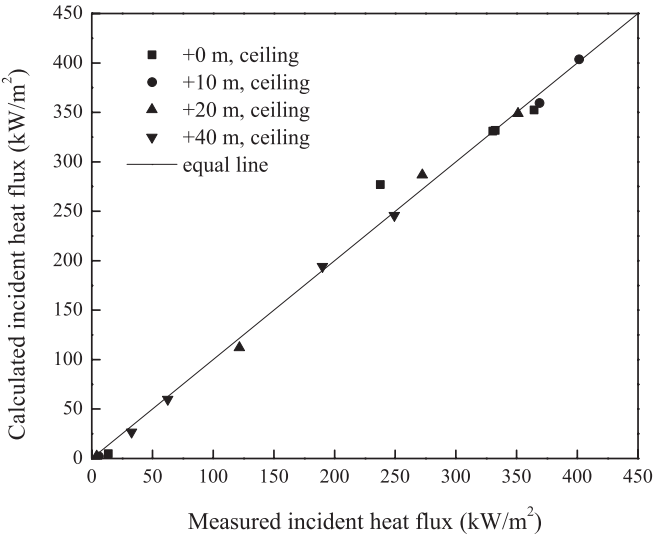

Fig. 10.5 Comparison of calculated and measured incident heat fluxes in Runehamar tests

10.7.2 Heat Flux in Lower Layer

10.7.2.1 Horizontal and Vertical Object Surfaces

The smoke flow in a tunnel fire is sometimes divided into two layers, that is, a relatively hot upper layer and a relatively cool lower layer. There is always temperature stratification, even in well mixed conditions at a position far away from the fire. The heat flux to an object in the lower layer is mainly attributed to the radiation from upper layer hot gases. Note that the gas temperature does not vary significantly along the length of a tunnel section of two or three times the tunnel height. Therefore, a three-dimensional radiation problem can be simplified into a two-dimensional problem. The radiation surfaces can be divided into three types, that is, hot gas surface in the upper layer (g), object in the tunnel (o), and cold walls and floors in the lower layer (w). A diagram of surface radiation to an object in the lower layer is shown in Fig. 10.6. Note that the hot gases surrounded by the upper tunnel walls as a whole are considered as one surface in Fig. 10.6.

Note that, the radiation between the object and the lower wall is limited compared to the radiation emitted from the hot gases. We may assume $e_{b,w} \approx e_{b,o}$. The radiation to an object in the lower layer can be represented by an electrical circuit analog as shown in Fig. 10.7.

The view factor from the gas to the wall F_{g-w} is much larger than the view factor from the gas to the object F_{g-o}, therefore the most of the heat goes to the wall. Thus the heat flux to object can be expressed as:

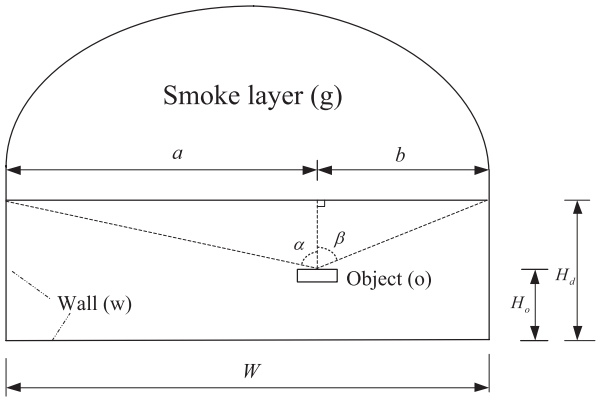

Fig. 10.6 A diagram of radiation to an object at the lower layer

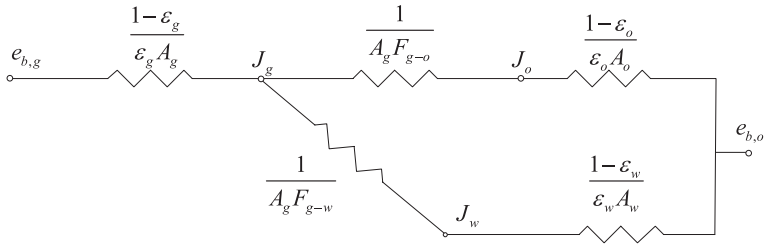

Fig. 10.7 Electrical circuit analog of radiation to an object in the lower layer

$$\dot{Q}_{net,g-o} = \frac{\dfrac{1}{F_{g-w}A_g} + \dfrac{1-\varepsilon_w}{\varepsilon_w A_w}}{\dfrac{1}{F_{g-o}A_g} + \dfrac{1-\varepsilon_o}{\varepsilon_o A_o}} \frac{e_{b,g} - e_{b,o}}{\dfrac{1-\varepsilon_g}{\varepsilon_g A_g} + \dfrac{1}{F_{g-w}A_g} + \dfrac{1-\varepsilon_w}{\varepsilon_w A_w}} \tag{10.97}$$

Note that $F_{g-w} = 1$ but $F_{w-g} \neq 1$, and $F_{g-o}A_g = F_{o-g}A_o$. The radiation heat flux from the smoke layer to the object can be expressed as:

$$\dot{q}''_{net,g-o} = \frac{\dot{Q}_{net,g-o}}{A_o} = \left(\frac{\dfrac{1}{A_g} + \dfrac{1-\varepsilon_w}{\varepsilon_w A_w}}{\dfrac{1}{\varepsilon_g}\dfrac{1}{A_g} + \dfrac{1-\varepsilon_w}{\varepsilon_w A_w}}\right) \frac{e_{b,g} - e_{b,o}}{\dfrac{1}{F_{o-g}} + \dfrac{1}{\varepsilon_o} - 1} \tag{10.98}$$

Recall most of the radiation to the object comes from the smoke layer beside the object within a tunnel length of two or three tunnel heights, and the gas temperature within this range does not vary significantly. Therefore the characteristic radiation temperature can be considered constant. By considering a longitudinal length of dx (m), we know the exposed area for the smoke layer, A_g (m^2), and the lower layer, A_w (m^2):

$$A_g = W dx \tag{10.99}$$

$$A_w = (W + 2H_d)dx = P_w dx \tag{10.100}$$

Therefore, the equation for net heat flux from the smoke layer to the object surface can be simplified to:

$$\dot{q}''_{net,g-o} = C_{r1}C_{r2}\sigma(T_g^4 - T_o^4) \tag{10.101}$$

where coefficients C_{r1} and C_{r2} are defined as:

$$C_{r1} = \left(\frac{\frac{1}{W} + \frac{1-\varepsilon_w}{\varepsilon_w P_w}}{\frac{1}{\varepsilon_g W} + \frac{1-\varepsilon_w}{\varepsilon_w P_w}}\right) \approx \varepsilon_g, \quad C_{r2} = \frac{\varepsilon_o F_{o-g}}{\varepsilon_o + (1-\varepsilon_o)F_{o-g}}$$

The incident heat flux can be estimated using:

$$\dot{q}''_{inc,o} = \frac{\dot{q}''_{net,g-o} + \dot{q}''_{net,w-o}}{\varepsilon_o} + e_{b,o} \tag{10.102}$$

The radiation between the object and the walls is limited, that is, the net heat flux between the walls and object is much smaller than the heat flux between the gas and object. Therefore Eq. (10.102) can be written as:

$$\dot{q}''_{inc,o} = C_{r1}C_{r2}\sigma(T_g^4 - T_o^4) / \varepsilon_o + \sigma T_o^4 \tag{10.103}$$

The above equations can further be simplified, given that the emissivity of the wall and the object normally ranges from 0.85 to 0.95, with an average value of 0.9. In such cases, C_{r1} is nearly the same as ε_g and C_{r2} is approximately the same as $0.9F_{o-g}$. Using these assumptions, the net heat flux on the target surface can now be expressed in the following equation:

$$\dot{q}''_{net,o} = \dot{q}''_{net,g-o} \approx 0.9\varepsilon_g F_{o-g}\sigma(T_g^4 - T_o^4) \tag{10.104}$$

Given that the temperature of the object surface is generally much lower than the smoke layer temperature, the incident heat flux received on the object surface can be simplified to:

$$\dot{q}''_{inc,o} \approx \varepsilon_g F_{o-g}\sigma T_g^4 \tag{10.105}$$

When the object is immersed in the smoke layer, the view factor equals 1 and the above equation becomes the same equation as that for exposed tunnel ceiling and walls at upper layer. As a rough estimation, the height of a characteristic smoke layer can be set at 50 % of the tunnel height (H_d in Fig. 10.7), unless information indicating a better estimation is available. This assumption could work well if the ceiling gas temperature is used as the characteristic temperature of the smoke layer.

The emissivity depends on local soot concentrations which is dependent on the soot production of the fire. Usually this term is difficult to determine. The smoke layer can be considered as optically thick in most tunnel fires, indicating that the emissivity approaches 1. In large tunnel fires, it is certain that the emissivity can be considered as 1. In a small fire or at the early stage of a large fire, the emissivity is much lower. However, over time the upper wall surface temperature approaches the gas temperature even for a small fire, for example, a 5 MW fire with relatively low ceiling height, or for a tunnel with fire protection linings. The emissivity in the above equations in reality is a property of the whole upper smoke layer including the tunnel ceiling and walls surrounded by the smoke. In thermally thin cases, most of the radiation from the upper ceiling and walls will be emitted to the lower layer as the radiation absorbed by smoke could be limited. Therefore, the emissivity of the whole upper layer is slightly higher, than what would be expected. In summary, the total emissivity of the upper layer can also be assumed to be 1 in such cases, although it could result in a slightly conservative estimation.

Therefore, the main parameter that must be determined is the view factor from the object to the smoke layer, which will be discussed in the following text for different placements of the object.

View Factors in Tunnels For an object on the tunnel floor or a certain height above the floor with its surface facing upward, the view factor can be calculated using:

$$F_{o-g} = \frac{1}{2}(\sin\alpha + \sin\beta) \tag{10.106}$$

where α and β are the angles plotted in Fig. 10.6.

The object could also be placed on the wall with its surface facing the opposite wall, for example, placed on the right wall in Fig. 10.6, in which case the view factor can be calculated using:

$$F_{o-g} = \frac{1}{2}(1 - \cos\alpha) \tag{10.107}$$

If the object is placed on the left wall in Fig. 10.6, the angle in the above equation should be β instead of α.

If the object surface is facing one side of the tunnel, the view factor can be estimated by:

$$F_{o-g} = \frac{1}{2\pi}(\alpha + \beta) = \frac{1}{2\pi}\left[\tan^{-1}\left(\frac{a}{H_d - H_o}\right) + \tan^{-1}\left(\frac{b}{H_d - H_o}\right)\right] \tag{10.108}$$

where $H_d - H_o$ is the distance between the hot layer and the object surface center, a and b are the horizontal distances between the target center and the side walls, see Fig. 10.6. When the object is surrounded by hot gas having a characteristic gas temperature, the view factor is close to 1, especially if the object's surface is facing upward. Recall the smoke layer height, can be estimated as 50% of tunnel height. One reason for this assumption is that ceiling gas temperature is used as the

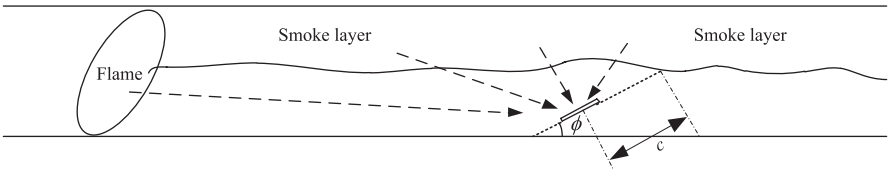

Fig. 10.8 A diagram of radiation from flame and smoke layer to the object

characteristic gas temperature in the calculation of the heat flux. In reality, there always exists a temperature difference between upper gas layer and lower floor layer even when the so-called smoke destratification has occurred. Therefore, the decrease of view factor somewhat compensates for the probable overestimation of the characteristic gas temperature.

The key parameters in the heat flux Eq. (10.103), for example, C_{r1} and C_{r2}, are dimensionless and not sensitive to tunnel geometry. This insensitivity indicates that the model is mainly related to the shape of the lower floor layer and the position of the object. Therefore, it is suitable for tunnels with different geometries.

Equation (10.103) can be used to estimate heat fluxes received by evacuees, firefighters, or neighboring vehicles in case of a tunnel fire. Further, it can be used to estimate the possibility of fire spread to neighboring vehicles or other objects.

10.7.2.2 Inclined Target Surfaces

In some cases, the surface is neither horizontal nor vertical, as shown in Fig. 10.8. There can be an inclination angle between the object surface and smoke layer surface. If such an inclined surface is in the vicinity of the fire source, the flames can also contribute to the heat radiation to the surface. Therefore, the total heat flux received on the surface should consist of both the smoke layer and the fire source. In this section we only discuss the heat flux from smoke layer; the flame radiation will be described in Sect. 10.7.3.

In calculation of heat fluxes received by inclined surfaces, the effect of inclination must be accounted for. The model for estimation of view factor from rectangular radiators to differential areas at various plane angles can be used here, see Fig. 10.9. The object lies on a plane normal to the line of intersection between the planes with its origin at one corner of the rectangle.

The radiation from the rectangular radiator to the object can be expressed using the view factor, $F_{o-radiator}$ or F_{o-g}, which is given in the following equation [15, 16]:

$$F_{o-radiator} = \frac{1}{2\pi}\left\{\tan^{-1}\left(\frac{1}{L}\right) + V(N\cos\phi - L)\tan^{-1}(V) + \frac{\cos\phi}{W}\left[\tan^{-1}\left(\frac{N - L\cos\phi}{W}\right) + \tan^{-1}\left(\frac{L\cos\phi}{W}\right)\right]\right\} \tag{10.109}$$

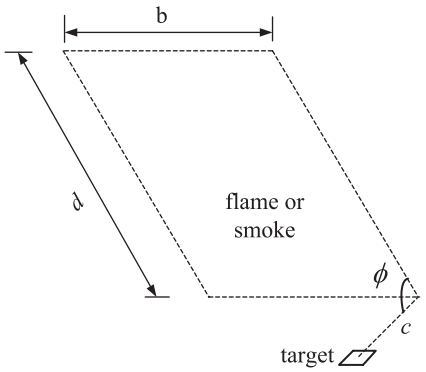

Fig. 10.9 A diagram of radiation from flame and smoke layer to the object

where

$$V = \frac{1}{\sqrt{N^2 + L^2 - 2NL\cos\phi}}$$

$$W = \sqrt{1 + L^2 \sin^2 \phi}$$

$$N = \frac{d}{b}$$

$$L = \frac{c}{b}$$

In the above equation, b and d are side lengths of the radiator (m), c is the distance from the object to the intersection line of the two planes (m), and ϕ is the angle between the two planes (°).

The angle can vary between 0 and 180°. Note that when the angle approaches 0 or 180°, numerical instabilities could result in unreasonable value for the view factor. Therefore it should be kept in mind that the overall view factor obtained from a calculation should never be less than 0 or greater than 1.

Equation (10.109) can be used to estimate the heat fluxes from both the vertical flame and the smoke layer to an inclined surface.

For radiation from the smoke layer which can be considered as an infinitely long plate above the object, Eq. (10.109) can be simplified into:

$$F_{o-radiator} = \frac{1}{2\pi}\left\{\tan^{-1}\left(\frac{1}{L}\right) + \frac{\cos\phi}{W}\left[\frac{\pi}{2} + \tan^{-1}\left(\frac{L\cos\phi}{W}\right)\right]\right\} \tag{10.110}$$

In the above equation, the parameter d, has been eliminated. Therefore the view factor is only a function of b, c, and angle ϕ. For an object placed at the centerline of the tunnel, radiation from two radiation planes to the object must be summed, that is:

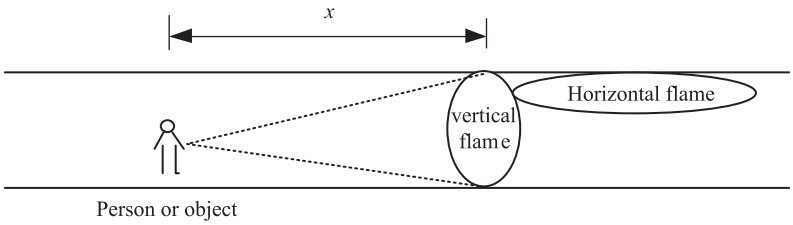

Fig. 10.10 A diagram of flame radiation to an object in a large tunnel fire

$$F_{o-g} = F_{o-g,1} + F_{o-g,2} \tag{10.111}$$

For each radiation plane, the equation for an infinitely long plate is used. The only difference in calculation of the two view factors is the parameter b. The sum of this parameter, b, for these two view factors should be equal to the tunnel width.

10.7.2.3 Radiation from Vertical Flames in Large Tunnel Fires

For a large tunnel fire, people (such as firefighters) located upstream of the fire can see the flame occupying the whole tunnel cross-section at the fire site, see Fig. 10.10. Here the radiation from the vertical part of the flames is discussed.

The incident radiative heat flux received by the person at L meters away from the fire can be estimated using the following equation:

$$\dot{q}''_{inc,F-o} \approx \varepsilon_F \sigma T_F^4 F_{o-F} \tag{10.112}$$

In most cases, especially for a large fire, the emissivity of the flame is approximately 1, that is, $\varepsilon_F = 1$. The average flame temperature can be assumed to be between 1000 and 1100 °C.

The flame can be considered as a radiating plane by a person some distance away from the fire. This plane can be divided into four parts, as shown in Fig. 10.11.

The four areas plotted in the figure, correspond to the part of flame which is visible to the object located either upstream or downstream. The areas correspond to the whole tunnel cross-sectional area only if there is no smoke along the path, for example, the back-layering has been prevented by forced flows.

Note that the total view factor is the sum of the four parts, that is

$$F_{o-F} = \sum_{i=1}^{4} F_{o-F,i} = F_{o-F,1} + F_{o-F,2} + F_{o-F,3} + F_{o-F,4} \tag{10.113}$$

where the view factor, F_{o-F}, for flame part 1 is:

$$F_{o-F,1} = \frac{1}{2\pi}\left[\frac{a}{\sqrt{a^2+x^2}}\tan^{-1}\left(\frac{b}{\sqrt{a^2+x^2}}\right) + \frac{b}{\sqrt{b^2+x^2}}\tan^{-1}\left(\frac{a}{\sqrt{b^2+x^2}}\right)\right]$$

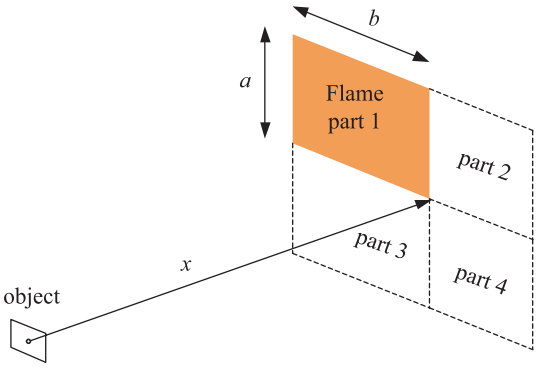

Fig. 10.11 A diagram of view factor between the object and the flame plane

where a and b are dimensions (m) of part 1 of the flame (see Fig. 10.11.), and x is the distance between object and the flame (m). The arctan function is represented by $\tan^{-1}$.

For a smaller fire, the area, A_T, can be replaced by the estimated flame area having a line of sight to the object. However, the point source method is recommended for estimation of radiation from a small tunnel fire, see Sect. 10.7.3.

Equation (10.113) suggests that for a very large tunnel fire, that is, a significant horizontal flame exists, the heat flux received at a certain distance, increases with the tunnel cross-sectional area. In comparison, the heat radiation in a small fire can be assumed to be independent of the tunnel width.

For an inclined surface, for example, Fig. 10.8, the actual heat flux from the flame to the object surface is reduced as follows:

$$\dot{q}''_{inc,F} = \dot{q}''_{inc,F,vertical} \cos\beta \tag{10.114}$$

where $\dot{q}''_{inc,F,vertical}$ is the incident heat flux received at a vertical surface facing the flame (kW/m^2), and β is the angle between the radiation and the normal line of the object surface (°).

Example 10.7 Estimate the heat fluxes received by a horizontal object surface located at a height of 1.5 m and at 20 m downstream of a 30 and 100 MW fire in a 6 m high and 12 m wide tunnel. The longitudinal flow velocity is 3 m/s and the ambient temperature is 20 °C. The bottom of the fire source is assumed to be 1 m above tunnel floor and the equivalent radius of the fuel is assumed to be 3 m. The object is located at the center line of the tunnel. At 20 m it is reasonably assumed that the smoke layer height is 50 % of the tunnel height. Also estimate the maximum heat fluxes that are received by an object located at 20 m downstream.

Solution: From Example 10.6, we already know that the maximum ceiling excess gas temperature is 474 °C for 30 MW and 1350 °C for 100 MW, so the ceiling gas temperature at 20 m downstream of the fires can be estimated using Eq. (8.39) and Eq. (8.40). First the flame lengths are estimated to be 5.6 m for 30 MW and 42 m for 100 MW using Eq. (9.26). Note that, the flame lengths are all less than 10 times tunnel height, the virtual origin $x_v = 0$ according to

Eq. (8.40). Using Eq. (8.39) the ceiling gas temperature at 20 m can be calculated to be 380 °C for the 30 MW fire and 1046 °C for the 100 MW fire. The view factor can be estimated using Eq. (10.106), that is, $F_{o-g} = 0.97$. *The radiation from the upper smoke layer for the 30 MW fire can be estimated using Eq. (10.105), that is,* $\dot{q}''_{inc,o,1} = 1 \times 0.97 \times 5.67 \times 10^{-11} \times (273+380)^4 = 10.0\, kW/m^2$ *The flame radiation can be estimated using Eqs. (10.112) and (10.113). The view factor is the sum of four parts:* $F_{o-F} = F_{o-F,1} + F_{o-F,2} + F_{o-F,3} + F_{o-F,4} =$ *0.053. The radiation from the vertical flame can be estimated using:* $\dot{q}''_{inc,o,2} = 0.053 \times 5.67 \times 10^{-11} \times (273+1000)^4 \times \cos\left\{\tan^{-1}\left[20/(3-1.5)\right]\right\} = 0.6 kW/m^2$. *Therefore the total incident heat flux received by the horizontal object surface for the 30 MW fire is: 10.0 + 0.6 = 10.6 kW/m². Similarly, for the 100 MW fire the total incident heat flux is: 166.5 + 0.6 = 167.1 kW/m². The contribution of the vertical flame to the radiation on the horizontal object surface is quite limited due to the large angle β.*

To calculate the maximum heat flux, the influence of the inclination angle φ must be estimated. The radiation from the upper smoke layer to an inclined surface can be estimated using Eqs. (10.110) and (10.111). For the 30 MW fire, the total incident heat flux on the inclined object surface increases with the inclination angle until around 70°, where a maximum heat flux of 21.2 kW/m² is achieved. For the 100 MW fire, the total incident heat flux on the inclined object surface stays at the same level until about 10°, after which the total incident heat flux decreases rapidly. The maximum value for the 100 MW fire is approximately 168 kW/m². Comparing this result to the 167.1 kW/m² heat flux for the horizontal surface shows nearly no difference.

By comparing the maximum contribution from the vertical flame part (force $\cos\beta = 1$) and the smoke layer (horizontal surface), the influence of the inclination angle can be estimated. In the above example, the maximum possible incident radiation from the vertical flame part is 1.6 times (160 %) that from the smoke layer for the 30 MW fire, but only 9.5 % for the 100 MW fire. Therefore, the vertical flame part plays a key role for the 30 MW fire but is negligible for the 100 MW fire in the above calculations.

In practice, the maximum heat flux received by a target can be approximately estimated using the following equation:

$$\dot{q}''_{inc,\max} = \sqrt{\dot{q}''^2_{inc,o,horizontal} + \dot{q}''^2_{inc,O,vertical}} \tag{10.115}$$

Note that a person in the vicinity of the fire absorbs radiative heat from all directions. Therefore the maximum incident heat flux should be used for estimation of tenability at evacuation or for firefighting operations.

10.7.2.4 Verification of the Heat Flux Models in the Lower Layer

In the following section, the heat flux equations for objects in the lower layer proposed in the previous analyses is verified using data from both full scale and model scale tests.

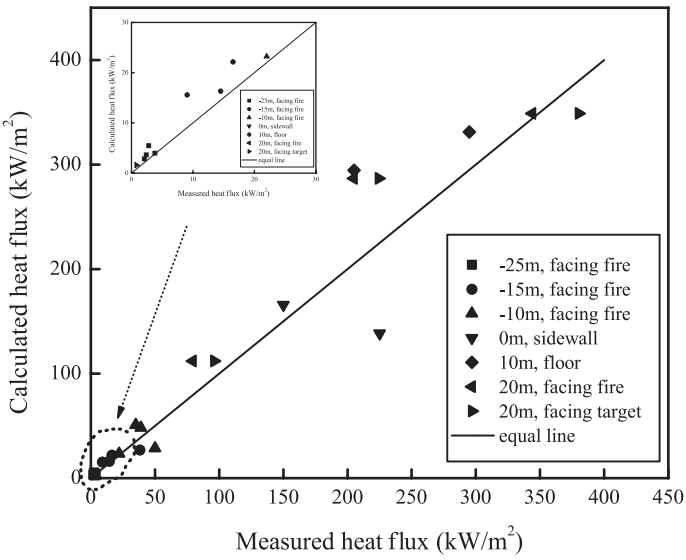

Fig. 10.12 Comparison of calculated and measured heat fluxes in Runehamar tunnel tests

Figure 10.12 shows a comparison of calculated and measured heat fluxes in the Runehamar tunnel fire tests [14]. Data measured by seven HFMs are plotted in the figure. There were two HFMs placed 20 m from the fire beside a pallet pile (the object), with one HFM facing the fire and another flush with the wall facing the object. All HFMs were placed 1.6 m above the tunnel floor with the exception of the one at 10 m which was placed on the floor. Only the HFM placed at 20 m facing the fire was a PT measuring incident heat flux. The others were SB gauges measuring net heat fluxes using water cooling of the surface of the probe. An emissivity of 0.9 for the SB gauges was assumed. For the HFM at 0 m it can be assumed that this HFM was surrounded by the flames and thus a view factor of 1 was used in the calculations. Further, the view factor for the two HFMs at 20 m can also be expected to be 1 since the large object also placed at 20 m was burning during the tests. The heat fluxes measured at 20 m increased significantly when the object started to burn. For all the other positions, it was assumed that the characteristic upper smoke layer was at 50 % of the tunnel height. The flames were very sooty and the emissivity was assumed to be 1 for all the tests. Note that, this assumption works in most engineering applications while estimating the heat fluxes although it could result in slightly conservative values for small fires. For HFMs facing fire, heat flux from the upper smoke layer and from the vertical flame section were superposed as the total heat flux. For the HFM at the floor, the vertical flame radiation was ignored.

It is shown in Fig. 10.12 that most of data points fall in the vicinity of the equality line, which suggests that the measured and calculated heat fluxes correlate reasonably well.

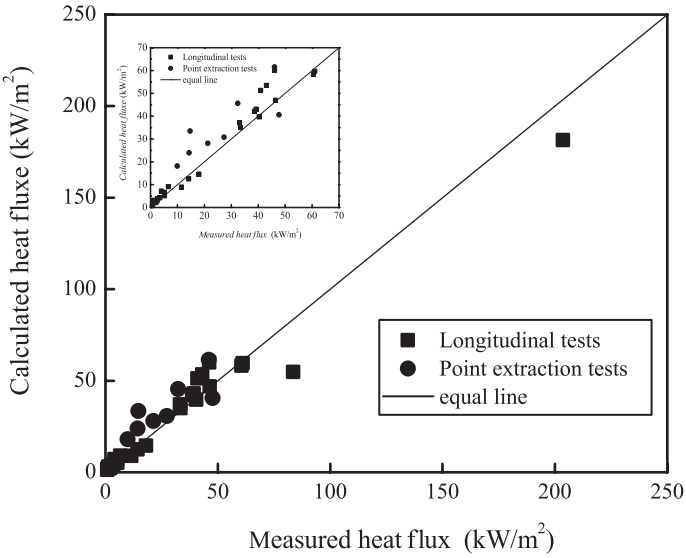

Fig. 10.13 Comparison of measured and calculated heat fluxes in model scale fire tests

Figure 10.13 shows the comparison of calculated and measured heat fluxes in model scale tests with longitudinal [17] and point extraction ventilation [18]. The heat fluxes were measured by SB gauges placed on the tunnel floor. The aspect ratio, that is, ratio of width to height, of the tunnel tested was 1.5 and 2.0. In these tests, the flames were very sooty, so the emissivity is assumed to be 1 for all the tests. The characteristic upper smoke layer was assumed to be at 50% of tunnel height. Figure 10.13 shows that the calculated heat fluxes correlate very well with the measured values.

10.7.3 Flame Radiation in Small Tunnel Fires

When the fire size is very small, the point source method is recommended to be used in estimation of the heat flux received from flames. A small fire is defined as a fire having flames that don't reach the ceiling. A schematic drawing of the radiation from flames to an object in a tunnel fire is shown in Fig. 10.14.

Radiation is the main mechanism of heat transfer for an object placed near the fire, that is, convective heat transfer can usually be ignored when considering the heat flux received at an object surface near the fire. The radiation received by an object's surface in such a scenario mainly consists of radiation from flames, and the radiation from other objects or the environment is comparatively insignificant.

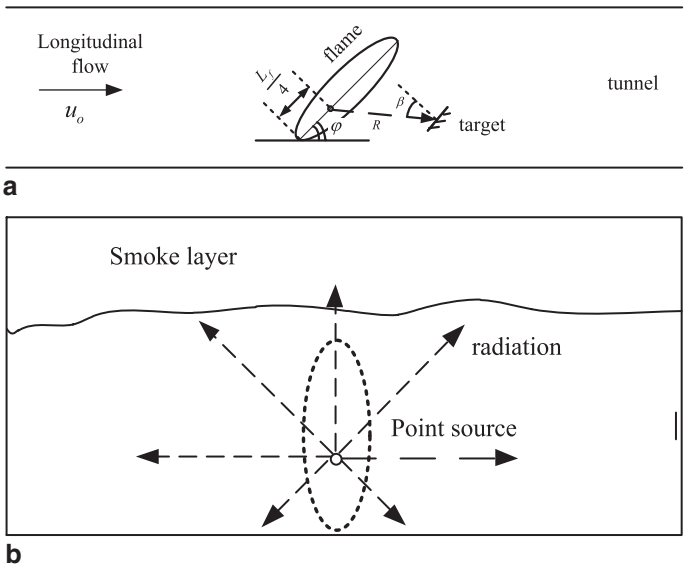

Figure . 10.14 A sketch of radiation from the flame to an object

The flame length equation for open fires can still be used but in a tunnel the whole flame is tilted in the downstream direction. Therefore, the fire source centre lies at a position downstream of the fire. The flame length can be calculated using [19]:

$$L_f = 0.235\dot{Q}^{2/5} - 1.02C \tag{10.116}$$

where L_f is flame length (m), $\dot{Q}$ is HRR (kW) and D is diameter (m).

The vertical height and horizontal length of the tilted flame for small tunnel fires can be approximated using the following equation:

$$H_{Flame} = L_f \sin\varphi, \quad L_{Flame} = L_f \cos\varphi \tag{10.117}$$

where φ is the flame angle, see Fig. 10.14. Subscripts v and h indicate vertical and horizontal flame components, respectively. The flame angle, φ, can be estimated using Eq. (8.27). The flame can be simplified to a point source at 1/4 of the flame length and 35% of the total HRR can be considered as the radiation source, that is, X_r=0.35. Therefore, the incident heat flux at an object on the tunnel wall can be calculated using the following equation:

$$\dot{q}'' = \frac{\chi_r \dot{Q}}{4\pi R^2} \tag{10.118}$$

where χ_r is the fraction of the total HRR that is lost by flame radiation, and R is the distance between the flame centre and the object (m).

This equation is only valid when the vertical flame height, $L_{f,v}$, is less than the tunnel height (for small fires), otherwise the flame radiation should be estimated using the method proposed in Sect. 10.7.2.3. Further, note that Eq. (10.118) can only be used to roughly estimate the flame radiation. It is not valid when the object is too close to the fire, for example, when the target is surrounded by flames. More specifically, the validity can be checked after the calculation, considering that the heat flux from a tunnel fire is generally not greater than 400 kW/m^2, which corresponds to a gas temperature of about 1360 °C.

Note that the heat flux received by a surface is related to the surface orientation. The incident heat flux received by the surface must be multiplied by a factor of cosβ (the angle between the incident radiation and the object surface), that is, Eq. (10.118) must be corrected by:

$$\dot{q}'' = \frac{\chi_r \dot{Q}}{4\pi R^2} \cos\beta \tag{10.119}$$

where β (°) is the angle between the incident radiation and a line normal to the object surface, see Fig. 10.14. Note that when the object surface can see part of the flame, the angle will be close to 0.

In the following text, data from two series of tests performed by SP Fire Research are used for validation of the proposed equations. These include one lab test without wind and eight tests in a road tunnel under different ventilation conditions.

In the lab test a gas burner, consisting of two octagon rings with each having an equivalent diameter of 1 m, was used as the fire source. The fuel outlet surface was 0.95 m above the floor. The fire size was designed to follow the fast curve (Q(kW)=0.047t^2, t in seconds) until it reached approximately 5 MW. The lab test set ups are presented in Fig. 10.15. A large plate thermometer was located 2 m from the fire center and 0.3 m above the floor to measure the heat fluxes at different locations and orientations. At 7 m above the floor, one normal PT (PT1) was placed facing the fire, and one shielded thermocouple and one unshielded thermocouple were placed beside it. PT2 and PT3 were placed 5 m and 7 m from the fire center respectively, and 1.75 m above the floor. PT4 was placed beside the large PT with the same height as TC4. PT5 was placed 3 m from the fire center and 1.65 m above the floor.

In the road tunnel fire tests, the fire source was the same as that used in the lab tests, with the fire size also following the fast curve until the fire reached 6 MW. A total of 8 fire tests, including 4 tests with a water spray system, were carried out in a 7 m high tunnel with a longitudinal velocity of 3–5.5 m/s, see Fig. 10.16. The tunnel width varied from 11 to 14 m in different sections. The large PT was placed at different locations, that is, in a range of 2 and 3.8 m downstream of the fire source. One normal PT was placed beside TC3 and another was placed on the side wall (5.5 m from the fire center in one section of the test tunnel and 7 m in another section of the tunnel).

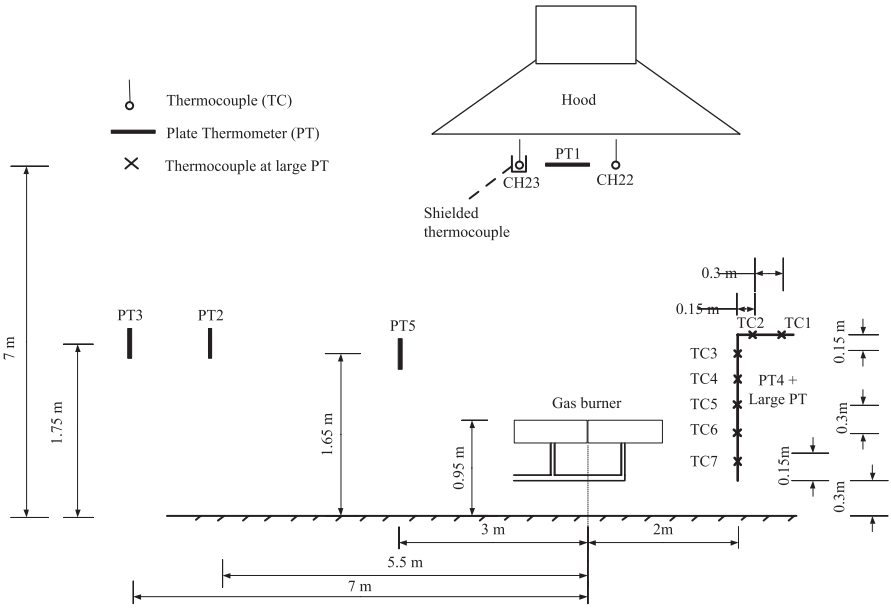

Fig. 10.15 A sketch of the SP Fire Research lab test

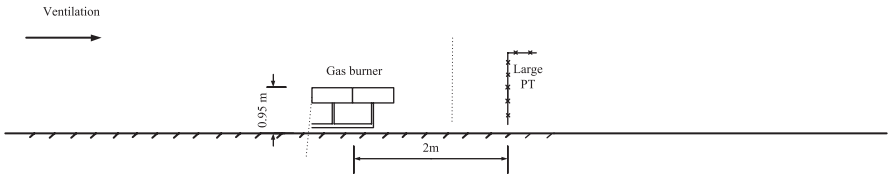

Fig. 10.16 A sketch of the road tunnel fire test

Figure 10.17 shows a comparison of measured incident heat fluxes in the lab test, with the calculated values using the point source method. Clearly, it shows that there is a very good agreement between calculated and measured values.

Figure 10.18 shows a comparison of measured incident heat fluxes in the road tunnel fire tests, with the calculated values using the point source method. Only data from the nonsprinkler tests are used here. Good agreement can be found although the data scatters slightly.

It can be concluded that the point source method can be used to estimate heat flux in both open fires and tunnel fires with or without ventilation. The flame could be simplified to a point source at 1/4 of the flame height (no wind) or flame length (wind).

Example 10.8 Estimate the maximum heat fluxes received by a firefighter located at 5 m upstream of a 6 MW fire in a 6 m high and 12 m wide tunnel. The longitu-

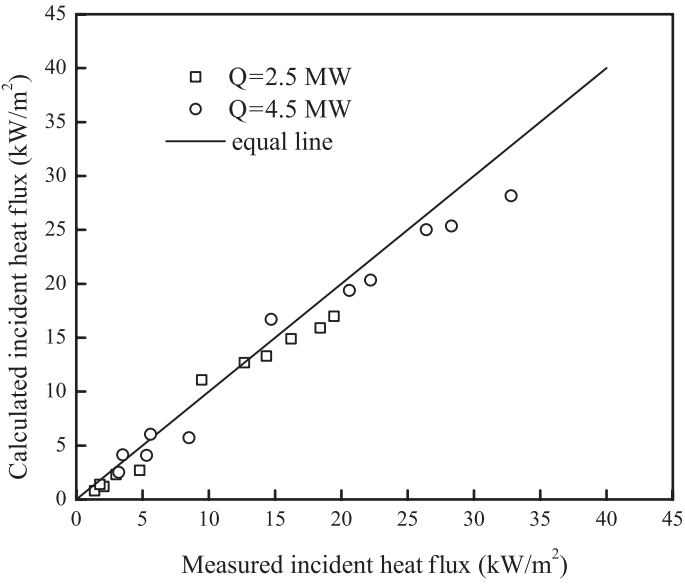

Fig. 10.17 Comparison of measured heat flux with calculated values in lab test

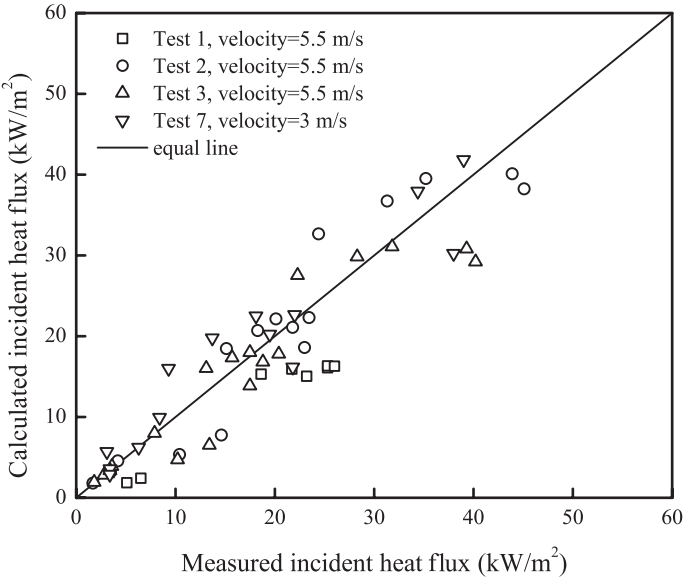

Fig. 10.18 Comparison of measured incident heat fluxes to calculated values in tunnel tests

dinal flow velocity is 3 m/s and the ambient temperature is 20 °C. The firefighter were located at the center line of the tunnel. The fuel is 0.5 m above floor with a radius of 1 m.

Solution: Firstly we know there is no back-layering after estimating the critical velocity $u_c = 2.45$ m/s by Eq. (13.4). The flame length can be estimated using Eq. (10.116), that is, $L_f = 0.235 \times 6000^{0.4} - 1.02 \times 1 \times 2 = 5.9$ m. It is clear that the radiation received by a fire fighting 5 m upstream is mainly the flame radiation in this case. The flame angle can be calculated using Eq. (8.27), that is, $\sin\varphi = 0.53$ and $\cos\varphi = 0.85$. The horizontal flame length, $L_{f,h}$, and vertical flame length, $L_{f,v}$, can be estimated to be 3.5 and 5.6 m. By setting the fuel surface center at coordinates of (0, 0.5), the location of the flame center can be determined, that is, at (1.4, 1.6). Given that the vertical axis is probably less than the height of the firefighter, the maximum heat flux is achieved when $\cos\beta = 1$. The maximum heat flux can then be estimated using Eq. (10.119), that is, $\dot{q}''_{inc} = 0.35 \times 6000 / 3.14 \times (5 + 1.4)^2 \times 1 = 4.1 kW/m^2$, less than the tenable limit of 5 kW/m^2 for protective clothing. Therefore, the firefighter is able to stay at a distance of 5 m upstream of a 6 MW fire in the tunnel with a longitudinal flow velocity of 3 m/s.

For a person or target located downstream of the fire, or for a fire with back-layering, the radiation from upper smoke layer must be accounted for. The same method used in the above example can be used here, with the only exception being that the vertical flame radiation is estimated based on the point source method for small fires rather than the vertical plane radiation method. The reason for this is that when the vertical flame height is greater than the tunnel height, the ceiling flame exists but it contributes to the total radiation to a target in a different way.

10.8 Summary

Basic knowledge about the three modes of heat transfer, that is, convective, radiative, and conductive heat transfer, are presented in detail.

Convective heat transfer occurs in the boundary layer where heat and momentum transfer coexist. The correlation between the heat and momentum transfer on the boundary is well expressed by the Reynolds–Colburn analogy which significantly facilitates the calculation of convective heat transfer. For different scenarios, for example, forced ventilation and natural ventilation, the Nusselt number is calculated and then used to estimate the convective heat transfer coefficient.

Radiation is a heat transfer mechanism between surfaces and/or mediums. For engineering applications, the gray body approximation is widely used in which all properties related to radiation are independent of the wavelength. For radiation among multiple surfaces the view factors can be estimated and the radiative heat transfer can be solved. However, the radiation from flames and hot smoke involves absorbing, emitting, and scattering gas which makes the estimation much more complicated.

In fire safety engineering, heat conduction is generally considered as one dimensional heat transfer in isotropic mediums. Analytical solutions for heat conduction into tunnel walls are summarized for different types of simplified boundary conditions, which can be used to estimate the heat response of the ceiling

and tunnel walls or estimate the possibility of fire spread, combined with the estimated heat fluxes.

The theories are applied to solve thermal issues in tunnel fire safety. Simple models of heat fluxes in small and large tunnel fires are presented and verified using test data.

The tunnel surfaces in the upper smoke layer are surrounded by smoky gases and/or flames in a large fire. The incident heat flux in the upper smoke layer can be simply correlated with the smoke temperature and the emissivity of the smoke volume. For large fires, the emissivity can be assumed to be 1. To calculate the incident heat flux in the lower layer, the view factor must be accounted for, together with the upper layer smoke temperature and the emissivity of the smoke volume. The incident heat flux is highly dependent on the orientation of the target surface.

In the vicinity of the fire source, radiation from the vertical flame can also play an important role in the incident heat flux. For an object close to a small fire, the flame radiation could be the main mechanism of heat transfer. In these cases, the point source method is recommended. The flame can be simplified to a point source at 1/4 of the flame length, and 35 % of the total HRR can be considered as the radiation source. In the case of a large fire when the vertical flame height is greater than the tunnel height, the point source method is not valid due to the existence of the ceiling flame. Instead, the vertical part of the flame can be assumed to be a vertical flame plane and the view factor method can be directly used to estimate the heat flux from the flame.

References

1. Holman JP (1992) Heat Transfer. 7th edn. McGraw-Hill, Singapore
2. Lienhard IV JH, Lienhard V, John H. (2012) A heat transfer textbook, Phlogiston Press, Cambridge, Massachusetts
3. Siegel R, Howell JR (1992) Thermal Radiation Heat Transfer. Third edn. Hemisphere Publishing Corporation,
4. Wickström U (2004) Heat transfer by radiation and convection in fire testing. Fire and Materials 28, 411–415
5. Tien CL, Lee KY, Stretton AJ (2002) Radiation heat transfer. In: DiNenno PJ (ed) SFPE Handbook of Fire Protection Engineering. National Fire Protection Association, Quincy, MA, USA, pp 1-73 -- 71–89
6. Lattimer BY (2002) Heat fluxes from fires to surfaces. In: DiNenno PJ (ed) SFPE Handbook of Fire Protection Engineering. National Fire Protection Association, Quincy, MA, USA, pp 2-269 -- 2–296
7. Petukhov BS (1970) Heat Transfer and Friction in Turbulent Pipe Flow with Variable Physical Properties. Advances in Heat Transfer 6:504–565
8. Bhatti MS, Shah RK (eds) (1987) Turbulent and transition convective heat transfer in ducts. Handbook of Single-phase Convective Heat Transfer. John Wiley, New York
9. Haaland SE (1983) Simple and explicit formulas for the friction factor in turbulent pipe flow. Journal of Fluids Engineering-transactions of The ASME 105:89–90
10. DiNenno PJ (2002) SFPE Handbook of Fire Protection Engineering. National Fire Protection Association, Quincy, MA, USA
11. Karlsson B, Quintier JG (2000) Enclosure Fire Dynamics. CRC Press, New York

12. Ingason H, Wickström U (2007) Measuring incident radiant heat flux using the plate thermometer Fire Safety Journal Vol. 42 (2):161–166
13. Andreas H, Johan S, Wickström U (2013) Using plate thermometer measurements to calculate incident heat radiation. Journal of Fire Sciences 31 (2):166–177
14. Ingason H, Lönnermark A, Li YZ (2011) Runehamar Tunnel Fire Tests. SP Technicial Research Institute, SP Report 2011:55, Borås, Sweden
15. Hamilton DC, and Morgan WR (1952) Radiant-interchange configuration factors. NASA,
16. Chung BTF, Kermani MM (1989) Radiation view factors from a finite rectangular plate. Journal of Heat Transfer 111 (4):1115–1117
17. Ingason H, Li YZ (2010) Model scale tunnel fire tests with longitudinal ventilation. Fire Safety Journal 45:371–384
18. Ingason H, Li YZ (2011) Model scale tunnel fire tests with point extraction ventilation. Journal of Fire Protection Engineering 21 (1):5–36
19. Heskestad G (1983) Virtual Origins of Fire Plumes. Fire Safety Journal 5:109–114

Chapter 11
Fire Spread

Abstract Fire spread is a very important issue during fires in tunnels. The elongated geometry of a tunnel with a relatively low ceiling height makes the flames and hot gases follow the ceiling over long distances, increasing the risk for fire spread. The use of ventilation in the tunnel as well as different types of vehicles, commodities, and materials influences the fire spread. This chapter contains both a summary of traditional ignition and fire spread theory and experiences especially related to situations in tunnels with risk for fire spread. Different aspects of spread and burning of liquids are presented and discussed.

Keywords Fire spread · Ignition · Radiation · Ignition temperature · Spill fire

11.1 Introduction

Fire spread is one of the most important processes during fires in tunnels. In many cases it determines the duration of a fire, the hazards for the evacuees and the possibilities for the fire and rescue services to fight the fire. As soon as the fire has spread to more than one vehicle, the situation becomes more severe. This is especially true when heavy goods vehicles (HGVs) are involved.

Rew and Deaves identified five different types of mechanisms for fire spread between wagons in a rail tunnel [1]:

1. Flame impingement
2. Flame spread (that is, flame spread across a surface)
3. Remote ignition/"flashover." Here they discussed spread from one wagon to another due to flashover. In many cases this means ignition by radiation. It also includes convective heating leading to auto ignition despite the fact that this may be combined with heating by radiation from flames, hot gases, or hot surfaces.
4. Fuel transfer. This includes both spread by burning liquid and by burning debris ("fire brands") transported downstream of the fire.
5. Explosion, which can spread fuel and fire.

Flame impingement relates to what is termed piloted ignition. There are two types of piloted ignition: (1) a pilot flame impinging directly on the surface, which is

H. Ingason et al., *Tunnel Fire Dynamics,* DOI 10.1007/978-1-4939-2199-7_11

heated by convection and/or radiation and (2) a pilot flame (or spark) in the gases near the surface, but without heating the object. For fire spread between vehicles in a tunnel, the first type of piloted ignition is the dominating process, while the second type can be involved in the first ignition process.

An extended flame along the ceiling in a tunnel is an important factor to consider when studying fire spread in a tunnel. It will influence both mechanisms 1 and 3. It can also increase the flame spread along a surface (mechanism 2). Therefore, it is important to be able to estimate the flame length in different fire situations in tunnels. This subject is extensively discussed in Chap. 9.

11.2 Introduction to the Theory of Ignition

11.2.1 Solids

Fire spread can be seen as a sequence of ignition processes and, therefore, an introduction to the theory of ignition is given here. For solids there are a number of different types of ignition [2]:

1. Ignition of fuel vapors from the material.
2. Smoldering ignition. An example of this is self heating of a porous material.
3. Direct ignition of the surface of a solid material. An example of this is ignition of some metals.
4. Ignition by a chemical reaction taking place directly in the solid phase. An example of this is explosives and pyrotechnics

Ignition type 1 is the most common type for solids and for fire spread in tunnels. The process of producing fuel vapors is often called pyrolysis, that is, the breakage of large molecules to smaller molecule fragments that can be released as gases. Some materials vaporize without pyrolizing. For ignition to take place, the material needs to be heated enough to produce gases in concentrations suitable for ignition. The fuel vapors then need to mix with air (or other oxidizer) to form a flammable mixture. This means that ignition can take place first after the production of fuel vapors is such that the concentration of the mixture reaches above the lower flammability limit (LFL). A schematic drawing of heat and mass transfer in solid materials is presented in Fig. 11.1.

For ignition to occur, the temperature of the fuel/air mixture needs to be increased to obtain an auto-ignition. Alternatively, an external heat/energy source can be applied to the mixture, for example, a spark or a flame. This is called piloted or forced ignition. If a material is affected by external heating, the ignition in most cases (for most solids) takes place in the gas phase. The heat drives off volatiles, which then burns outside the material.

One parameter often used to define or characterize the ignition properties of a material is the ignition temperature. The ignition temperature is, however, defined

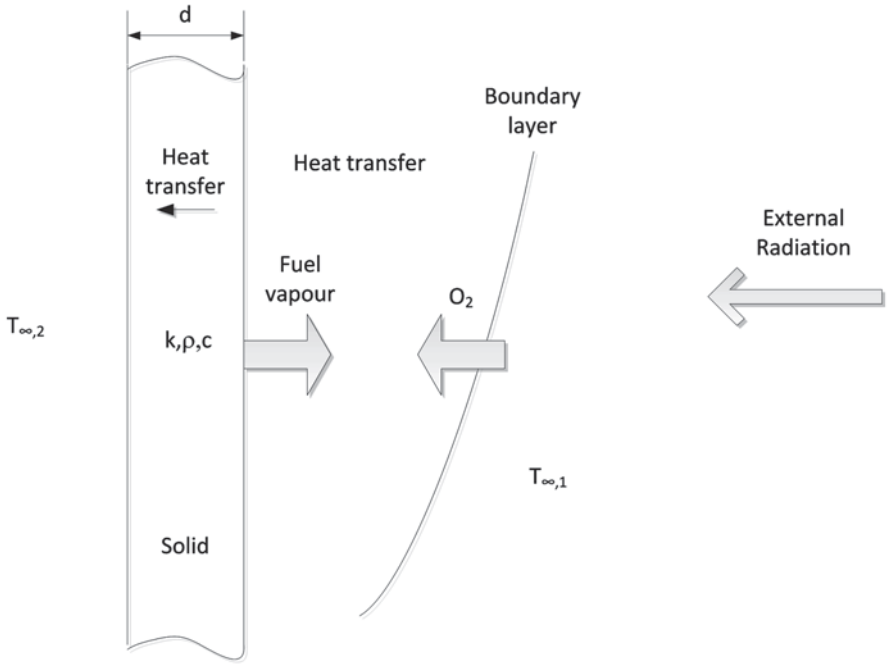

Fig. 11.1 Simplified schematics of the processes involved in ignition of a solid

mainly in two different ways depending on the situation. First, in fire testing situations the furnace temperature is often used, for example, the gas temperature near the object needed for the specimen to ignite. Second, in many studies the surface temperature of the specimen at the time for ignition is used. The problem with the latter definition is that the surface temperature is often very difficult to measure.

The first definition is convenient to use for studies of the ignition temperature using furnaces with homogenous gas temperature. It is, however, important to note that when tested in a furnace, the surface temperatures of the object and the gas temperature in the furnace are not necessarily the same. There are, however, measurements of the temperatures at the surface and in the gas phase right before ignition and in these cases these temperature were essentially the same [2]. Another important issue is that in a real case the conditions may be such that the fuel is heated by radiation but cooled by convection, that is, there is no homogenous high-temperature media surrounding the fuel. Irrespective of whether small thermocouples or optical methods are used to measure the surface temperature there are risks for significant errors, for example, that the thermocouple is not measuring exactly at the surface and the surface temperature of the material or that the optical properties (emissivity) of the material are not known all through the process of heating the surface. The surface temperature at ignition also depends on whether the material is thermally thin or thick.

Thermally thin means that the material is physically thin or has high thermal conductivity (k) so that it can be assumed that the temperature is the same throughout the material. The basic theory can be found in Chap. 10 on heat fluxes and thermal resistance. To distinguish the thermally thin materials from thermally thick materials, one can introduce the Biot number, which is defined as:

$$Bi = \frac{hd}{k} \tag{11.1}$$

where h is the heat transfer coefficient (kW/(m^2 K)), d is the thickness (m) of the material (see Fig. 11.1) and k is the thermal conductivity (kW/(m K)). For Bi smaller than 0.1, the material is considered thermally thin. This means that the conduction of heat inside the object is much faster than the convective heat transfer at its surface. This means that a uniform body temperature can be assumed and this is often referred to as the *lumped heat capacity* model.

Fire scenarios, for example, with significant radiation and high levels of irradiance, often involve only short time scales of the heat transfer mechanisms which are relevant for the important processes. This means that only the surface can be assumed to be important for the ignition process. In these situations the materials are said to be thermally thick and can approximately be treated as a semi-infinite plate. This means that when the front side of a material is heated, for the time of consideration a significant temperature rise has not occurred at the back side. The parameters important for determining whether a material is to be considered thermally thick are the thermal properties of the material (k, ρ, c), the thickness of the material and the time of interest, where ρ is the density (kg/m^3) and c is the heat capacity (kJ/(kg K)). One way of expressing this is by calculating the thermal penetration depth, δ_p (m). This is used to calculate how far the heat wave has reached into the material and is expressed as distance reached where a certain fraction of the temperature rise is reached in relation to the surface temperature rise. Wickström [3] gave two such penetration depths relating to a relative temperature rise of 5 and 1 %, respectively:

$$\delta_{p,0.05} = 2.8\sqrt{\alpha t} \tag{11.2}$$

and

$$\delta_{p,0.01} = 3.6\sqrt{\alpha t} \tag{11.3}$$

where α is the thermal diffusivity ($\alpha = k/(\rho c)$; m^2/s) and t is the time (s).

This means, of course, that the penetration depth depends on how it is defined and what relative temperature rise is used.

Irrespective of which one is selected, one should remember that they are developed for a situation with single-sided heating and that the penetration depth for a case with heating from both sides needs to be less than half of the corresponding value calculated from the single-side equation.

Whether a composite material with a thin outer layer should be considered thermally thin or thick depends on the density of the substrate or material behind the

outer layer. With a much lower density of the material behind, the ignition behavior is determined by the outer layer alone, while a substrate with high density can make the composite thermally thick even if the substrate is incombustible.

Note that most fuels present in vehicles are thermally thin. Babrauskas [2] gives a rule of thumb that products with thickness ≤ 1 mm will be thermally thin while products with a thickness ≥ 20 mm will be thermally thick (foam materials are excluded from this generalization).

The behavior of a material also depends on the heat flux. For a very high irradiance it can behave thermally thick, while for low irradiance it can behave thermally thin.

To complicate things, the ignition is not only controlled by the surrounding temperature and the ignition temperature but also the geometry and thermal inertia of the fuel, that is , how the heat is transferred into the object. This also depends on the properties of the heating source, for example, the level of radiation. It is important to note that in many cases the time to ignition is what is of specific interest. In these cases, the thermal inertia may play a more significant role than the ignition temperature. The time to ignition for thick homogenous objects is proportional to the thermal inertia. The thermal inertia is dependent on the heat conductivity (k), density (ρ), and specific heat capacity (c). In the literature, one can find two different definitions:

$$I_1 = k\rho c \tag{11.4}$$

$$I_2 = \sqrt{k\rho c} \tag{11.5}$$

In this chapter the first definition ($kJ^2/(s\ m^4\ K^2)$) has been used when presenting data in different tables. Values of heat conductivity, density, specific heat capacity, and thermal inertia for some selected materials are presented in Table 11.1.

The exact ignition temperature varies depending on apparatus used for the measurement. However, the temperature for piloted ignition is lower than the corresponding auto-ignition temperature. Examples for this are presented by Babrauskas for thermoplastics with ignition temperature of 369 °C (+/− 73 °C) for piloted ignition and 457 °C (+/− 63 °C) for auto-ignition. The corresponding average ignition temperatures for thermosetting plastics are given as 441 °C (+/− 100 °C) and 514 °C (+/− 92 °C) [2]. There are also examples where the measured ignition temperature (for wood) was higher than the measured furnace temperature which means that self heating occurred.

It has been observed that the surface temperature for wood at ignition depends on the situation [5, 6]. This is summarized in Table 11.2.

To exemplify the influence of the thermal inertia on the ignition of a solid, some material and ignition properties of expanded polystyrene (EPS) will be discussed. In Table 11.3 results from cone calorimetry tests with different types of EPS are presented [2, 7, 8] and are also compared with some other selected materials.

Table 11.1 Material properties of some selected solid materials [3, 4]

Material	Heat conductivity, k (kW/(m K))	Density, ρ (kg/m^3)	Specific heat capacity, c (kJ/(kg K))	Thermal inertia, $k\rho c$ (kJ^{2}m^{-4}s^{-1}K^{-2})
Polyurethane foam	0.0003	20	1.400	0.000840
Fiber insulating board	0.00004	100	2.000	0.007920
Wood, pine	0.00014	500	2.800	0.196000
Wood, oak	0.00017	700	2.800	0.333000
Gypsum plaster	0.0005	1400	0.840	0.588000
Concrete	0.0017	2300	0.900	3.53
Steel (mild)	0.046	7850	0.460	166
Aluminum	0.20	2700	0.900	486
Copper	0.39	8930	0.390	1360

Table 11.2 Surface temperature for wood at ignition [5, 6]

Mode of heat transfer	T_s, spontaneous ignition (°C)	T_s, pilot ignition (°C)
Radiation	600	300–410
Convection	490	450

The time to ignition for a material exposed to radiation depends on the level of radiation, that is, with increasing radiation the ignition time decreases. At the other end of the scale, the ignition time increases so that below a certain radiation level ignition does not occur, at least not within a specific and long time period of exposure. This minimum heat flux, $\dot{q}''_{\min}$ (kW/m^2), is defined as the minimum heat flux needed for the surface temperature to reach the ignition temperature, T_{ig} [2], which can be determined experimentally for different materials. Cleary and Quintiere [8] performed tests in a cone calorimeter and found that $\dot{q}''_{\min}$ was 15 kW/m^2, for polystyrene foam, both expanded and extruded, fire retarded and nonfire retarded. In another study, also with the cone calorimeter, Dillon [7] analyzed two different fire retarded polystyrene foams, for example, EPS and reached $\dot{q}''_{\min}$ of 8 and 23 kW/m^2, respectively. At a first glance at the values in Table 11.3 it appears to be that 15 kW/m^2 could be used as a representative value of $\dot{q}''_{\min}$ irrespective of type of EPS. However, in the two test series the thermal properties of the materials differed, that is, the thermal inertia ($k\rho c$) was different. This could explain why the fire-retarded and the nonfire retarded materials showed the same $\dot{q}''_{\min}$ in the work by Cleary and Quintiere. As can be seen in Fig. 11.2, there is a large difference in the correlation whether the nonfire retarded value is included or not. If the nonfire retarded value is left out, the following expression can be used:

$$\dot{q}''_{\min} = 27.2 \cdot \left(k\rho c\right)^{-0.5} - 13.4 \tag{11.6}$$

Table 11.3 Results for cone calorimetry tests with expanded polystyrene (EPS). Some other materials are included for comparison [2, 7, 8]

Material	Thickness, mm	ρ, kg/m^3	$k\rho c$, kJ^{2}m^{-4}s^{-1}K^{-2}	T_{ig}, meas, °C	T_{ig}, comp[a], °C	$\dot{q}''_{min}$, kW/m^2	References
Polystyrene foam, EPS	50	32	0.58		376	15	[8]
Polystyrene foam, FR EPS	50	16	0.96		376	15	[8]
Polystyrene foam, FR EPS	50	32	0.91		376	15	[8]
Polystyrene foam, FR EPS	40	30	1.594		295	8	[7]
Polystyrene foam, FR EPS	80	30	0.557		490	23	[7]
Polystyrene foam, FR XPS	50	32	0.91		376	15	[8]
Polyethene			1.834	315–330	300		[9]
PVC, FR	3	1505	1.306		415	16	[7]
Wood, beech	15	749	0.504		358		[10]
Wood, beech 9% MC			0.463	380			[11]
Wood, Douglas fir 0% MC	16.8	465	0.159	350			[12]
Wood, mahogany			0.512		407	18	[2, 13]
Wood, Monterey pine 0% MC	17.5	460	0.156	349			[12]
Wood, Monterey pine 11% MC			0.593	340			[11]
Wood, oak			0.447		301		[2, 14]
Wood, spruce	15	468	0.208		375		[10]
Wood, spruce			0.214		358		[15]
Wood, spruce			0.181		352		[2, 14]

[a] Computed ignition temperature

Since the ignition temperature can be difficult both to define and measure, other means for comparing ignition conditions for different materials have been studied. One such parameter is the mass loss rate at ignition. However, it can also be difficult to measure this accurately at ignition and the values can be apparatus dependent

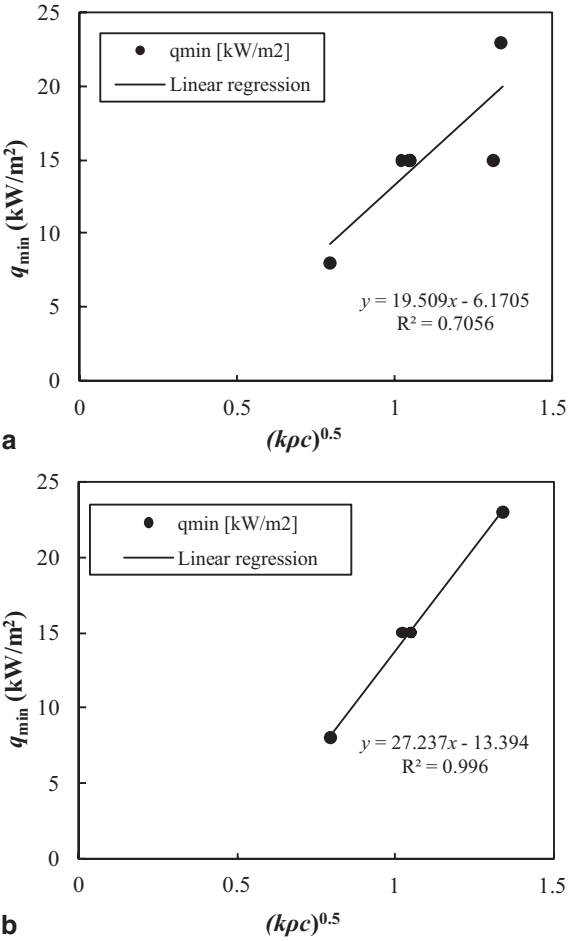

Fig. 11.2 Minimum heat flux for ignition of EPS as function of thermal inertia. In the *upper* Figure (**a**) there is an outlier corresponding to a non-fire retarded case. If this outlier is removed the correlation is much better as can be seen in the *lower* Figure (**b**)

[2]. Another parameter that could be useful is the heat release rate (HRR), where a span between 25 and 50 kW/m^2 are given for some common materials at piloted ignition [2].

The geometry of the object and the position of the heat source (flame) are important since it is easier to ignite a corner than an edge or a flat surface. The reason for this is that in the case with a corner the surface temperature is raised more quickly since the heat can flow into the body along three directions [2]. A vertical surface will in most cases ignite at the top. There are two reasons for that: First, a convective flow will be formed along the surface. At ambient temperature, this flow will cool the surface. The boundary layer will be thicker at the top, reducing the cooling. For fires in tunnels in most cases the heating will also come from the hot gases and flames along the ceiling, heating the surfaces from above. Second, for a very high radiation, the effect of convection on ignition will be negligible. If a large surface is exposed to radiation, the time to ignition will be shorter than the time to ignition for a small surface for a given irradiance.

Another phenomenon that can influence the ignition is charring. This process can both increase ignition time and increase the critical heat flux below which ignition will not take place.

A third mechanism for ignition, in addition to radiative and convective heating, is direct contact with a hot body. It has been shown, however, that this requires significantly higher ignition temperatures (around 600 °C for several materials) than both piloted and auto-ignition.

Effect of Velocity Air flow can affect ignition and fire spread in several different ways. If a material is heated by radiation, a flow of air at relatively low temperature cools the object and the gases near the material by convection. It also dilutes the fuel/air mixture. An air flow leads in these cases to a higher ignition temperature needed for ignition compared to a case with lower velocity or without forced airflow. This effect is highest at the lowest irradiances leading to ignition.

If the air flow has a temperature leading to convective heating, there is an optimum velocity leading to the shortest ignition time. For low velocities, an increased velocity leads to faster pyrolysis and better mixing and in turn faster ignition, while at higher velocities an increased velocity decreases the residence time and thereby the time for chemical reaction. As for cold flows, it also dilutes the fuel vapors. There is a limit for the velocity above which ignition will not occur. This limit depends on the temperature and oxygen concentration.

If the geometry is three dimensional and complex or if the material is ignited in the glowing mode, the addition of air via an increased air flow will affect the ignition, increase the reaction rate, and increase the rate of flame spread. The reason for this is that it can be difficult for the air (oxygen) to reach the pyrolysates and the combustion zone. This can be the case in a tunnel fire when an increased air flow can make it easier for the air to reach the combustion zone in for example an HGV cargo.

In a tunnel, an airflow can also tilt the flames in such a way that they are either closer to a combustible surface or forced into a three-dimensional fuel. In both these cases it will increase the flame and fire spread. There are also other situations where an increased velocity will decrease the size of a fire. The effect of the ventilation on the fire size is discussed in more detail in Chap. 4.

11.2.2 Liquids

Combustible liquids are in tunnels available in different form, both as fuels for the individual vehicles and as goods transported in large bulk volumes. Therefore, it is important to understand also the ignition of liquids. In most cases the materials do not ignite in the form of liquid, but instead in the form of vapors mixing with the air, forming a combustible mixture. Liquids are also classified according to their flash point, that is, the lowest temperature at which a liquid can produce enough vapors to form a flammable vapor/air mixture. It should be noted that there are different test methods for determining the flash point, for example, closed cup or open cup flash point, and that these do not give the same values. Flash points for some selected

Table 11.4 Flash point and fire point temperatures for liquid fuels [2, 5]

Material	Closed cup flash point (°C)	Open cup flash point (°C)	Fire point (°C)
Gasoline (100 Octane)	−38[a]		
n-Hexane	−22[a, b]	−26[b]	
Cyclohexane	−20[a]		
n-heptane	−4[b]	−1[b]	2[b]
n-octane	12[b], 13[a]		
Iso-octane	−12[a]		
n-nonane	31[b]	37[b]	42[b]
n-decane	46[a], 44[b]	52[a, b]	61.5[a, b], 66[b]
n-dodecane	74[a, b]		103[a, b]
m-xylene	25[b]		44[b]
o-xylene	32[b]	36[b]	42[b]
p-xylene	27[a], 25[b]	31[a, b]	44[a, b]
Methanol	11[a], 12[b]	1[a] (13.5)[a, c]	1[a] (13.5)[a, c]
Ethanol	13[a, b]	6[a], (18)[a, c], 22[b]	6[a] (18)[a, c], 22[b]
Propanol	26[a], 29	16.5[a] (26)[a, c]	16.5[a] (26)[a, c]
n-butanol	35[a]	36[a, b] (40)[a, c]	36[a] (40)[a, c], 36–50[b]
Sec-butanol	24[b]		29[b]
i-pentanol	41[a]		57[a]
Glycerol	160[b]		207[b]
JP6		38[b]	43[b]
Fuel oil, No. 2	124[b]		129[b]
Fuel oil, No. 6	146[b]		177[b]
Motor oil	216[b]		224[b]

[a] Drysdale [5]. Closed-cup flash points comes from work by NFPA [16], while the open-cup flash point and fire points come from work by Glassman and Dryer [17]
[b] Babrauskas [2]
[c] Values in parentheses refer to ignition by a spark and not pilot flame

liquid fuels are presented in Table 11.4. Since the processes are different, there is no relation between the flash point and the auto ignition temperature. The fire point, which is also included in Table 11.4, is the lowest temperature for which ignition leads to sustained burning.

A burning liquid fuel can constitute a hazard in itself, but also be an important source for fire spread to other vehicles. An important parameter is also the thickness of the fuel; either it is burning on the road surface or in a bulk transport. The effects of the boundaries underneath the fuel bed are important but are seldom considered as a parameter that can influence the burning conditions.

11.2.2.1 Release of Liquids

Liquid fuels can be released in tunnels in different ways: small leakages from fuel tanks or fuel hoses, ruptured tanks, leakage from a tanker carrying a flammable liquid, etc.

To estimate the extent of an unconfined spread of a liquid fuel, one needs to know the resulting thickness of the spill. Gottuk and White [18] summarize the results from several tests in the following relationships:

$$\begin{cases} A/V_s = 1.4 \text{ m}^2/\text{L Spill} < 95 \text{ L} \\ A/V_s = 0.36 \text{ m}^2/\text{L Spill} \geq 95 \text{ L} \end{cases} \tag{11.7}$$

where A is the area (m^2) and V_s is the volume in liters (L) of the spill

As conservative minimum depths δ (mm), the following values were given:

$$\begin{cases} \delta = 0.7 \text{ mm} \quad \text{Spill} < 95 \text{ L} \\ \delta = 2.8 \text{ mm} \quad \text{Spill} \geq 95 \text{ L} \end{cases} \tag{11.8}$$

When the area of unconfined spill is calculated it is important to note that the area increases after being ignited. That means if cold spill area is denoted A_s, the fire area, A_f, can be calculated as [18]:

$$A_f = 1.55 A_s \tag{11.9}$$

The discussion above, regards a momentary release of a certain volume of fuel. If there is continuously flowing spill, the situation will be different. After ignition a balance will be reached between the volumetric burning and flow rates of the liquid release, $\dot{V}_L$ (m^3/s). From this balance a steady state diameter, D_{ss} (m) can be derived [18]:

$$D_{ss} = \left(\frac{4\dot{V}_L \rho}{\pi \dot{m}''} \right)^{1/2} \tag{11.10}$$

Based on empirical data, Gottuk and White recommend that for high fuel release rates (>10 L/min), confined pool burning rates are used, while for lower rates spill burning rates are used, that is, one fifth of the pool burning rates. Burning rates in kg/(m^2 s) for pool fires are discussed in more details in Chaps. 3 and 4.

Ingason [19] performed spillage tests on roadway asphalt and painted particle board with different slopes, leakage hole diameter, and volume flow rates.

The volume flow rate, $\dot{V}$ (m^3/s), of a leakage from a circular hole in a vehicle trailer tank can be calculated from:

$$\dot{V} = 2A_T K(\sqrt{h_1} - Kt) \tag{11.11}$$

where

$$K = \frac{C_v \pi D^2 \sqrt{2g}}{8A_T} \tag{11.12}$$

and A_T is the horizontal surface area of the leaking compartment (m^2), D is the hole diameter of the leakage (m), h_1 is the initial height (m) of the fuel (gasoline) at $t=0$ s, C_v is the flow contraction coefficient (=0.7), g is gravitational acceleration (m/s^2) and t is the time (s).

Ingason found that the area of the spill can be estimated by

$$A = BL \tag{11.13}$$

where B (m) is an average width between the impingement point of the leakage and the side where the drainage system is and L is the center line distance from the impingement point to the drainage system (m). The test results showed that for a spill onto asphalt B can be estimated by the following empirical correlation:

$$B = 48\dot{V}^{0.46} \tag{11.14}$$

The length L depends on the slope but Ingason gave an expression for the maximum spillage area [19]:

$$A_{\max} = \frac{\dot{V}\rho_f}{\dot{m}''} \tag{11.15}$$

where ρ_f is the density of the fuel (kg/m^3) and $\dot{m}''$ the burning rate of the spillage ($kg/s/m^2$). For a circular pool spillage with a diameter D_{ss}, Eq. (11.15) gives the same results as Eq. (11.10). The actual spillage area depends on the design of and distance to the drainage system.

Example 11.1 A tanker carrying 20,000 m^3 of gasoline starts to leak through a pipe connected to one of the five tanker compartments. The surface area A_T of each compartment is 3 m^2. The diameter of the leaking opening is 0.05 m and the distance to the drainage system is 6 m. What is the potential fire size, or HRR (in MW) on the road surface if the fire starts after 30 s?

Solution: As there are five compartments, each carries 4 m^3 of gasoline. The initial height h_1 is therefore $4m^3/3m^2 = 1.33$ m. Using Eq. (11.12) *and $C_v = 0.7$ we obtain $K = 0.001$ and with aid of* Eq. (11.11)*, we obtain the volume flow after 30 s, $\dot{V} = 0.0067$ m^3/s (6.7 l/s or 405 l/min). The width B of the spillage at this time is obtained by using* Eq. (11.14)*, or 4.8 m. The total area A is obtained by* Eq. (11.13)*, or 28.8 m^2. The maximum spillage area A_{max} that can exist is obtained with* Eq. (11.15)*. From* Table 11.4 *we obtain for gasoline $\rho_f = 740$ kg/m^3, $\dot{m}'' = 0.055$ $kg/(m^2\,s)$ and $\Delta H_{c,eff} = 43.7$ MJ/kg (assuming $\chi = 1$). The maximum area that can burn is $0.0067 \times 740/0.055 = 90$ m^2 which is larger than 28.8 m^2. Thus, the HRR will be $28.8 \times 0.055 \times 43.7 = 69$ MW. Here we have not considered the effects of pan size or the depth of the fuel.*

11.2.2.2 Flame Spread over a Liquid Surface

It has been shown that both the flame spread rate and the fire intensity decreases significantly when the fuel depth decreases below a couple of centimeters [18, 20].

In tests on JP-5 fuel, the HRR for a thin fuel layer was 20–25 % of the HRR for the thick-layer case [20]. There are also studies indicating that the flames do not spread from the source of ignition when the fuel layer thickness is below 1.5 mm [20].

The spreading rate of a fire over a liquid fuel surface depends on the temperature of the fuel. Above a certain initial surface temperature the flame spread is controlled by the gas phase and flame propagation velocities in the order of 1 m/s can be observed [18]. Below that temperature, different regions were observed. The different temperature intervals and the observed velocities might vary between fuels and setup, but the effect of the fuel temperature is clear from the reported experiment. It is also important to remember that the flame spread rate decreases with the pan width [20].

White et al. [20] studied the effect of the temperature on the flame spread rate, but for isopentanol. They also observed a significant increase in the flame spread when the liquid temperature increases. As the temperature increased, three different regions were identified: the liquid-controlled, the gas phase-controlled, and the asymptotic gas phase-controlled regions. In the first region (I), where the flame is spread with surface tension-induced flow, there is a slow increase in flame spread rate with temperature. In the second region (II) there is a steep increase in flame spread rate with temperature while in the third region (III) the flame spread rate is approximately constant with increased temperature (see Fig. 11.3). The transitions between the different regions occur at the temperatures T_{go} and T_{gm}, respectively. The regions are defined in Fig. 11.3.

The experimental results indicate that the parameters most important for the flame spread are the initial fuel temperature (before ignition), T_l, the flash point of the fuel, T_{fl}. and the difference between them. For JP-8, for example, the transition between region I and region II occurred when $T_l - T_{fl} = T_{go} - T_{fl} \approx 18\,°C$. The results for different fuels are summarized in Table 11.5. Flash points for other fuels are given in Table 11.4.

For hydrocarbons tested, the maximum flame-spread rate in region I was 0.1 m/s and in region III between 1.20 and 2 m/s. This was the case also for alcohols, but there the span limits in region III were 1.5 and 2 m/s. When the flame spread rate is known, the fire area can be described:

$$\begin{cases} A_f = \pi v^2 t^2 \text{ (circular flame spread)} \\ A_f = wvt \text{ (rectangular flame spread)} \end{cases} \tag{11.16}$$

where v is the flame spread velocity (m/s) and w is the width (m) of the confinement of the fuel, for example, walls.

The burning rate of a spill fire is lower than the corresponding confined pool fire with a significantly larger fuel depth (centimeters rather than millimeters). For diameters larger than 1 m, the burning rate of a spill fire is approximately one fifth of the burning rate of the corresponding confined pool fire [18].

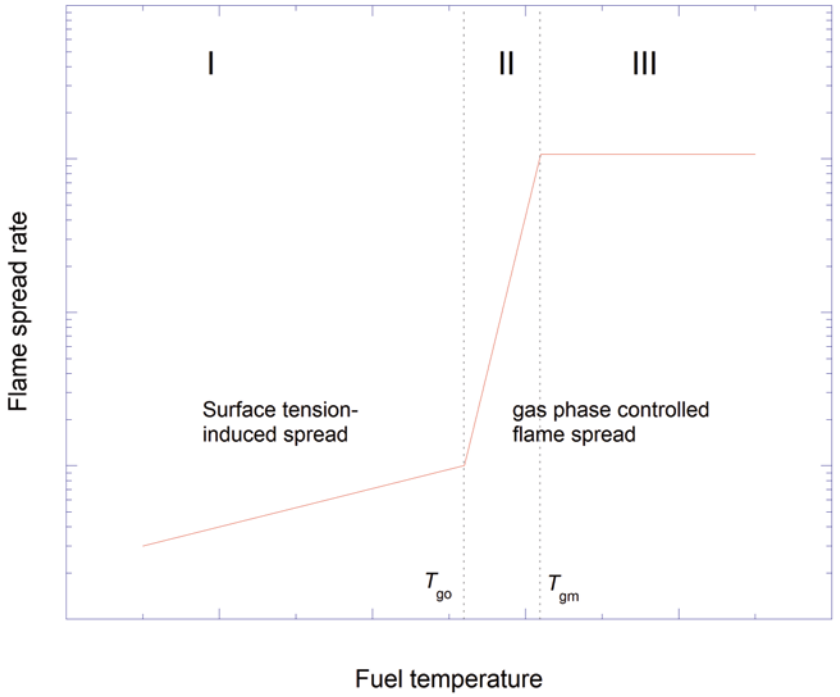

Fig. 11.3 Presentation of the regions of flame spread as function of fuel temperature and definition of T_{go} and T_{gm}. (After Gottuk and White [18])

Table 11.5 Summary of transition temperature between different regions for some selected fuels [18]

Fuel	T_{fl} (°C)	T_{go} (°C)	$(T_{go}-T_{fl})$	T_{gm} (°C)	$(T_{gm}-T_{go})$	$(T_{gm}-T_{fl})$
JP-8	39	57	18	62	5	23
25/75 JP-8/5	42	60	18	66	6	24
50/50 JP-8/5	48	65	17	72	7	24
75/25 JP-8/5	54	68	14	74	6	20
JP-5	63	76	13	79	3	16
Decane	44	56	12	62	6	18
Average of 1–6 above			15		6	21
1-Pentanol	48	52	4	62	10	14

11.2.2.3 The Effect of Macadam

The burning rate of a liquid fire depends on the depth of the fuel layer. The effects of different thicknesses on the HRR have been discussed in detail in Chap. 4. The burning rate is also dependent on the surface type, that is, if a fuel spillage is released onto a hard asphalt surface or onto a surface with a layer of macadam as is often used in rail tunnels.

Lönnermark et al. [21] performed a test series to study the effect of the relation between the fuel height and macadam on the burning rate. The test series, performed with different depth of liquid fuel (heptane and diesel) in a pool with macadam, showed that the macadam had a significant influence on the burning rate of the fuel.

The fire tests were performed using a pool with an area of 3.1 m^2 (2 m diameter). The pool was placed beneath an industry calorimeter to measure the HRR. Macadam was included in the pool up to a height of 0.15 m. Railway macadam of Class I (washed; 32–64 mm) was used. The bulk volume of the macadam was approximately half the free volume of the pool with the same height, that is, half the amount of liquid could be used to reach the same height in the pool compared to the case without macadam in the pool.

Heptane was used as the main fuel. During the test series the volume and depth of fuel were varied. The main parameter varied was the depth of fuel in relation to the depth of macadam, that is, the level of the upper surface of the fuel in relation to the upper layer of the macadam. To limit the time for each test, a water layer was added beneath the fuel in the pool. Two tests were also performed with diesel oil as fuel to study the influence of the fuel characteristics on the results. For each fuel a free-burning test without macadam was performed.

From the analyses it can be seen that the HRR for all cases with macadam are affected relative to the free-burning cases. When the upper fuel level is a distance below the upper macadam level there is a significant effect. This effect increases with the distance between the fuel surface and the upper level of macadam. This is shown graphically in Fig. 11.4. The influence of macadam can be used in rail tunnels or in other situation with macadam where the effect of a fuel release should be assessed.

11.3 Fire Spread in Tunnels

The different ways of fire spread in a tunnel were presented in Sect. 11.1:

1. Flame impingement
2. Flame spread
3. Remote ignition
4. Fuel transfer
5. Explosion.

Some of these points have been briefly discussed as separate issues in the sections above. In this section, the specific situation with a fire in a tunnel and ways and

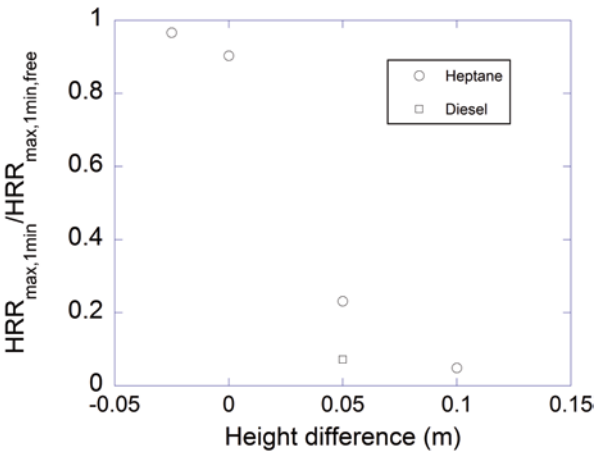

Fig. 11.4 The ratio between the peak 1 min average of the HRR for tests with macadam and a free-burning test without macadam, presented as function of the height difference between the level of macadam and the level of the *upper* surface of the liquid fuel. A positive height difference indicates the liquid surface is *below* the level of macadam

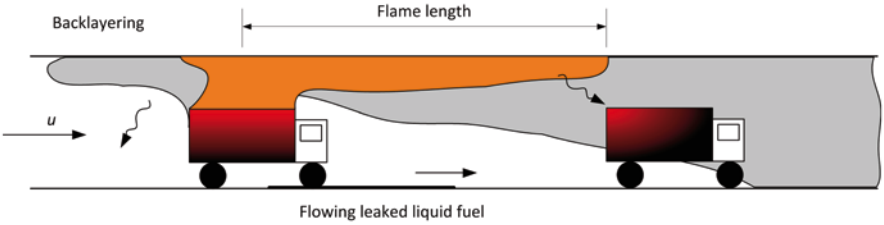

Fig. 11.5 Examples of different processes in fire spread in a tunnel

consequences of fire spread are discussed. In Fig. 11.5 some of the ways of fire spread given in the list above are exemplified.

The specific geometry of a tunnel with its *semi-confined* space with walls and often very limited ceiling height makes the fire spread situation very much different from fires freely burning above ground. Initially, the fire starts to spread inside the vehicle and the flames and hot gases extend to the ceiling. With limited ventilation the flames and hot gases are then guided in two directions along the tunnel tube. If a significant ventilation flow is present, the flames and fire gases are directed in mainly one direction. The extent of the flow of hot gases depends on the type of ventilation system and where the extraction points are positioned (see Chap. 13).

In road tunnels the main reasons for large fires are collisions between vehicles or with the tunnel wall. In the latter case, the vehicle can catch fire directly or due to subsequent collision with other vehicles. Some other causes are overheating (engine, brakes), faults in the engine or gear box, leakage of flammable liquids, etc.

A stop in a tunnel, due to a single-vehicle stop or collision, often results in a long queue of vehicle or even a multivehicle pileup, which could lead to further fire spread. This is also the situation if there is a queue downstream of the fire as well. This could be the case in a city tunnel during rush hours or because of a stop in the traffic due to another accident.

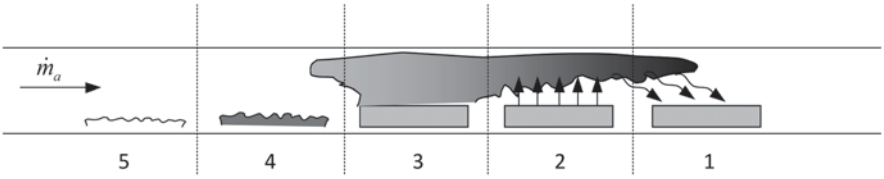

Fig. 11.6 Schematic description of the fire spread and burning process in a ventilation controlled fire in a tunnel. (After Ingason [22])

The main reasons for fires in rail tunnel are not as obvious as those in road tunnels. There are, however, fires due to collisions also in rail tunnels. Furthermore, derailment is the cause of several fires. In some cases the event has started with an explosion. Some have electrical causes, not only underneath the train (for example, due to short circuit) but also inside the train, for example, in a cabinet. Some causes are not fully described while several were due to arson. Examples of key fire incidents in rail tunnels are given in Chap. 1.

In many cases, fires in tunnels are not ventilation controlled, but if there are several vehicles involved in the fire a ventilation-controlled situation can occur. The fire spread and burning process in such a situation is schematically presented in Fig. 11.6. The process can be divided into five different steps as shown in the figure:

1. Preheating of unburnt fuel downstream of the fire
2. Pyrolysis leading to a region with excess fuel
3. Combustion (fully-developed fire)
4. Glowing ember
5. Burnt out/cooling

If there are more vehicles positioned further downstream in the tunnel the described process will continue and move in the downstream direction in the tunnel, starting from point 1 again.

If the fire is assumed to radiate as a point source, the radiation from the fire can be estimated by

$$\dot{q}'' = \frac{\chi_r \dot{Q}}{4\pi r^2} = K_r \frac{\dot{Q}}{r^2} \tag{11.17}$$

where χ_r is the fraction of the total HRR, $\dot{Q}$ (kW), that is emitted as radiation and K_r is a constant based on χ_r. In Table 11.6 χ_r and K_r are given for some selected materials. For the gases and several of the liquids the average of χ_r is approximately 0.3, which is a value commonly used. However, as seen in the table, the values vary from 0.14 for methane upto 0.64 for one of the rigid PU foams. Also some of the liquids have high values. Therefore, it is important not to use 0.3 in all situations, but try to relate the value to what is actually burning. The average for all the values of χ_r in the table is 0.40 (53 different materials), but this value of course depends on what materials are included. One should, however, note that the data were obtained from small-scale tests which differ from large-scale fires. Full-scale test data are recommended for use if they are available. For many of the common hydrocarbon

Table 11.6 Radiation fraction from different burning materials, calculated based on data from Tewarson [24]

Material	χ_r	K_r
Methane	0.14	0.011
Ethane	0.25	0.020
Propane	0.29	0.023
Butane	0.31	0.024
Ethylene	0.34	0.027
Propylene	0.37	0.029
Average common gases	0.28	0.022
Methyl alcohol	0.16	0.012
Ethyl alcohol	0.25	0.020
Isopropyl alcohol	0.29	0.023
Acetone	0.27	0.022
Heptane	0.33	0.026
Octane	0.33	0.027
Kerosene	0.35	0.028
Benzene	0.60	0.048
Toluene	0.60	0.047
Styrene	0.53	0.042
Average common liquids	0.37	0.030
Tissue paper	0.41	0.033
Wood (red oak)	0.37	0.030
Wood (Douglas fir)	0.38	0.030
Wood (pine)	0.30	0.024
Average cellulosic materials	0.36	0.029
POM	0.22	0.018
PMMA	0.31	0.025
PE	0.43	0.034
PP	0.41	0.033
PS	0.59	0.047
Silicone	0.31	0.025
Polyester-1	0.48	0.038
Nylon	0.40	0.032
Average synthetic solids	0.40	0.031
PU (flexible) foam GM21	0.52	0.041
PU (flexible) foam GM23	0.46	0.036
PU (flexible) foam GM25	0.58	0.046
PU (flexible) foam GM27	0.54	0.043
Average flexible PU foams	0.52	0.042
PUR (rigid) foam GM29	0.59	0.047

Table 11.6 (continued)

Material	χ_r	K_r
PU (rigid) foam GM31	0.55	0.044
PU (rigid) foam GM35	0.56	0.044
PU (rigid) foam GM37	0.51	0.041
PU (rigid) foam GM41	0.64	0.051
PU (rigid) foam GM43	0.57	0.045
Average rigid PU foams	0.57	0.045
PS foam GM47	0.56	0.045
PS foam GM49	0.61	0.049
PS foam GM51	0.58	0.046
PS foam GM53	0.57	0.045
Average PS foams	0.58	0.046
Corrugated paper boxes, empty	0.25	0.020
Corrugated paper boxes w. PVC (62 %-thick)	0.11	0.009
Corrugated paper boxes w. PC (59 %-thick)	0.27	0.021
Corrugated paper boxes w. PS (58 %-thick)	0.23	0.018
Corrugated paper boxes w. PS (60 %-thin)	0.48	0.038
Corrugated paper boxes w. PS (40 %-thin)	0.36	0.029
Corrugated paper boxes w. ABS (59 %-thick)	0.21	0.017
Corrugated paper boxes w. PET (41 %-thin)	0.41	0.032
Corrugated paper boxes w. PU (40 %-foam)	0.40	0.032
Average corrugated paper boxes w/wo polymers	0.30	0.024

fuels the radiative fraction decreases with increasing pool diameter. Koseki [23] reports that when the fire diameter is smaller than about 2 m, the radiative fraction for these fuels is 0.3–0.5, while when increasing the diameter to 10 m the radiative fraction decreases to 0.07–0.2. Further, note that the assumption that a fire is a radiation point source is a simplification that can be useful in some situations to estimate the risk for fire spread. However, in other situations a more detailed analysis is needed, for example, when there are long flames radiating toward an object. For information on more general methods for calculating radiation, see Chap. 10.

Large-scale tests simulating HGV fires were performed in the Runehamar tunnel, 2003 [25]. The radiation given by Eq. (11.17) was calculated for the maximum HRR during the mentioned Runehamar tests. The values were measured on the upstream side of the fire. In Fig. 11.7 these calculated values were compared to measured values [26]. In these calculations, a value of 0.3 was used for χ_r. A relatively good correlation can be seen.

In the tests in the Runehamar tunnel, fire spread was studied using targets downstream of a mock-up simulating an HGV fire [27]. Different types of targets were used: large targets with the same type of commodity as used in each of the full-scale tests and smaller wooden and plastic targets placed on the ground at different dis-

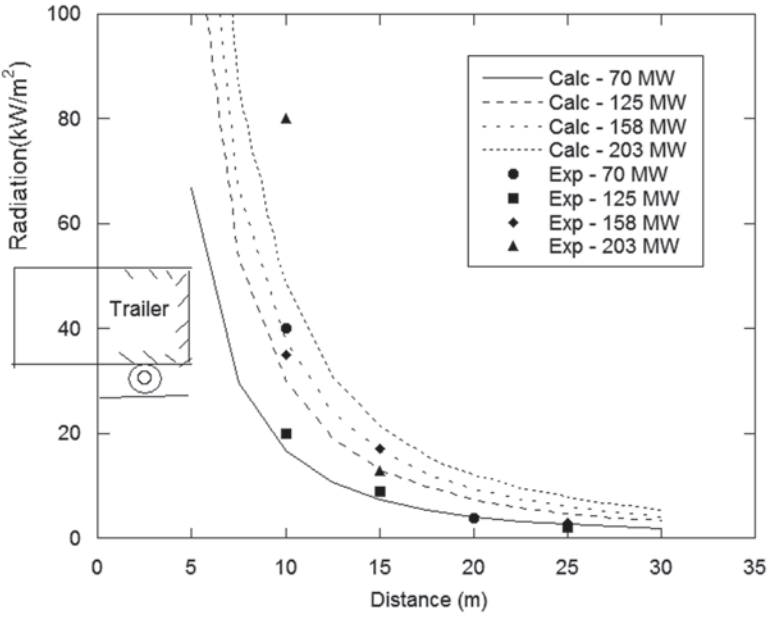

Fig. 11.7 Calculated (*Calc*) and experimental (*Exp*) radiation levels upstream of experimental setup in the Runehamar tests. The calculated values are based on the maximum HRR and the distance from the center of the fire (trailer mock-up) [26]

tances from the seat of the fire. The plastic targets were affected approximately up to the flame length while the fire spread to the pieces of wood occurred up to a distance of about (or somewhat more than) 70 % of the flame length. For the 202 MW fire in test T1 this corresponds to fire spread distances of 95 m for plastic targets and 70 m for wooden targets. This corresponds to spontaneous ignition due to radiation dominated fire spread from the upper layer to the road surface. With a higher target, for example, a vehicle with a cargo, the fire might spread even further distances between the initial fire and the target since convective heating and high temperature in the upper layer influence the target to a larger extent. Also direct impingement of flames onto the target can occur. The radiation will, however, still be an important factor for the fire spread. When the fire spreads to the large target (20–22 m downstream of the center of the fire), the HRR was in the range of 20–40 MW. This was obtained in a longitudinal flow of about 2–3 m/s.

The fire spread results from the Runehamar tests can be compared to the observations from the fire in the Fréjus tunnel in June 2005. The fire started in the engine of an HGV loaded with tyres [28]. The fire then spreads to an HGV loaded with cheese 60 m away. An HGV with scrap metal another 60 m away was also ignited. A fourth HGV, 350 m from the initial fire was ignited, but this was extinguished before the tank containing toxic glue was ruptured [29]. This HGV was extinguished approximately 6 h after the driver of the first HGV pressed the SOS button [28]. These observations correlate well with the results from the Runehamar tests. It

shows the long distances this type of fire can spread and, once again emphasizes the importance of HGVs on the outcome of tunnel fires.

A number of road tunnels fires have occurred throughout Europe with catastrophic results. These are described in Chap. 1, Tables 1.1 and 1.2. In all these fires, the cargo in HGV trailers played a major role in the outcome. The main reason being that the trailers contain a very high-fire load and the fire could easily spread within the cargo and further to adjacent vehicles due to the tunnel ventilation and the long flames created. Fire spread between vehicles is, therefore, of great concern inside a tunnel. An interesting thing to note is that, typically, fires involving only one HGV lead to no fatalities. There are many such examples, for example, Fréjus 1983, St. Gotthard 1984, Fréjus 1993, St. Gotthard 1994, and St. Gotthard 1997. On the other hand as soon as two or more HGVs are involved, the severity of the situation increases leading to fatalities, for example, in Velsen 1978, Nihonzaka 1979, Gumefens 1987, Serra a Ripoli 1993, St. Gotthard 2001, and Fréjus 2005. One important exception is the fire in the Channel tunnel in 1996, which involved in total ten HGVs, but did not lead to any fatalities. However, there are some important features of this fire that make it different. The HGVs were transported on a train and all the drivers and other people travelling on the train were sitting in a special passenger coach in the front of the train. With a supplementary ventilation system, the operator managed to reverse the air flow making the fire spread in the opposite direction. This made it possible for the people to escape with only minor effects of the smoke.

It can be worth noting that both in the St. Gotthard tunnel, where one of the catastrophic fires occurred, and in the Fréjus tunnel with fatalities during a fire in 2005, there have previously been fires not leading to fatalities and the main difference between these cases seems to be the number of HGVs. In the St. Gotthard tunnel HGVs/lorries were involved in fires on 14 separate occasions between 1992 and 1998 [30].

The analysis of the fires in tunnels presented in Tables 1.1 and 1.2 showed the importance of the number of vehicles involved in a fire, and even when the number of HGVs involved in a fire in a tunnel increased from one to two, the risk for a catastrophic outcome seems to increase significantly. This underlines the importance of fire spread for the severity of a fire in a tunnel. In the Mont Blanc tunnel fire in 1999, a total of 15 HGVs entering from the French side were burnt over a distance of 500 m (another 8 HGVs entering from the Italian side were also involved in the fire) [31, 32]. The distance between the HGVs varied between 3 and 45 m. In the fire in the St. Gotthard tunnel 2001, 13 HGVs and 10 cars over a distance of 550 m were involved in the fire.

There are several reasons why the fire spread and involvement of more than one vehicle are important for the outcome of the fire. One reason is that as soon as two or more vehicles are involved it can be very difficult for the rescue services to reach the site of the fire, both due to the increased radiation and to the fact that the rescue services would need to be able to come between the burning vehicles to be able to fight the fire. The ventilation can have a crucial impact on this situation since ventilation can make the conditions upstream of the first vehicle endurable for the rescue

services approaching the fire, while the conditions downstream of the first vehicle can become more severe and the fire can spread more easily.

One conclusion from fires in tunnels presented and discussed above is that goods that are considered to be nonhazardous transported on an HGV must be considered to be hazardous when involved in a fire in a tunnel. As soon as more than one HGV is involved in a fire in a tunnel, the situation becomes severe and often leads to fatalities. Both real fires in tunnels and fire experiments have shown that there are risks of fire spread over long distances when HGVs are involved in the fire.

Example 11.2 A HGV trailer carrying tissue paper is burning. The peak HRR is estimated to be 75 MW. How close to the fire can the fire fighters reach if their protecting clothes can withstand 5 kW/m^2 during their operation?

Solution: We rearrange Eq. (11.17) *to obtain the distance r. This means that* $r = \sqrt{K_r \frac{\dot{Q}}{\dot{q}''}}$ *. We obtain* K_r *from* Table 11.6 *for tissue paper,* $K_r = 0.033$*. Thus, the critical distance for the fire fighters is* $\sqrt{0.033 \frac{75000}{5}} = 22$ *m.*

11.4 Modeling of Fire Spread

Much of the modeling performed for tunnels include CFD modeling to calculate the temperature distribution and flow of hot gases and smoke (see Chap. 17). It is possible to use results from such models or from hand calculations to estimate the risk for fire spread, for example, by estimating the radiation (see for example, Sect. 11.3).

Ignition of a solid, however, involves many different processes and it can be difficult to model in detail. It is, therefore, common to make a number of assumptions and simplifications to be able to derive an equation that is possible to solve. In addition, many of those expressions are related to a specific test method with controlled conditions. The most common representations and assumptions for piloted ignition of solids are presented and discussed by Torero [33] and Babrauskas [2].

The main assumptions are:

- The solid remains inert until ignition, that is, the time delay before ignition is mainly related to heating the solid. This means that ignition will occur at the onset of pyrolysis. The ignition process can be represented by an ignition temperature T_{ig} (surface temperature at ignition) and an ignition delay time, t_{ig} (s), which is the time delay from start of exposure to ignition.
- Constant thermal material properties, both in space and time, that is, for k (kW/(m K)), ρ (kg/m^3), and c (kJ/(kg K)).
- Most of the incident heat flux, $\dot{q}_e''$ (kW/m^2), is absorbed by the solid at the surface, that is, absorptance $\alpha_r \approx 1$.
- Linearizing of the surface radiation and lumping the reradiation term together with the convective term using a total or effective heat transfer coefficient, h_{eff} (kW/(m^2 K)).

- Assumptions regarding the backside losses, for example semi-infinite (thermally-thick body)

Note that Torero uses the name minimum heat flux for ignition while Babrauskas denotes it as critical heat flux, $\dot{q}''_{cr}$ (kW/m^2). Babrauskas describes that there actually is a minimum heat flux $\dot{q}''_{\min}$ (higher than $\dot{q}''_{cr}$) at the time of ignition below which ignition does not occur. This means that there is a finite maximum t_{ig} for ignition to occur. Still, if it is assumed that $t_{ig} \to \infty$ (under the critical condition), the following equation can be derived:

$$T_{ig} = T_0 + \frac{\dot{q}''_{cr}}{h_{eff}} \tag{11.18}$$

Assuming a constant external heat flux, the following equation for the case with high-incident heat flux can be derived [33] (see also Chap. 10):

$$\frac{1}{\sqrt{t_{ig}}} = \frac{2}{\sqrt{\pi}\sqrt{k\rho c}} \frac{\dot{q}''_e}{\left(T_{ig} - T_0\right)} \tag{11.19}$$

This case is valid for $t_{ig} << t_c$, where

$$t_c = \frac{k\rho c}{h_{eff}^2} \tag{11.20}$$

The corresponding equation for a case with low incident heat flux ($t_{ig} \geq t_c$) [33]:

$$\frac{1}{\sqrt{t_{ig}}} = \frac{\sqrt{\pi}\sqrt{k\rho c}}{h_{eff}} \left[1 - \frac{h_{eff}\left(T_{ig} - T_0\right)}{\dot{q}''_e}\right] \tag{11.21}$$

To correlate the derived equation with experimental results different procedures and relations have been suggested. Janssens derived the following equation [2]:

$$\dot{q}''_e = \dot{q}''_{cr} \left[1 + 0.73 \left(\frac{k\rho c}{h_{eff}^2 t_{ig}}\right)^{0.55}\right] \tag{11.22}$$

Note the different exponent of the thermal inertia and t_{ig}.

The ignition time delay can from Eq. (11.22) be written as:

$$t_{ig} = \frac{0.56 \cdot k\rho c}{h_{eff}^2 \left[\frac{\dot{q}''_e}{\dot{q}''_{cr}} - 1\right]^{1.82}} \tag{11.23}$$

For thermally thin solids Babrauskas presents three different cases where the front face in all cases is exposed to radiant heat flux and there is re-radiation and convective cooling:

1. The back face is perfectly insulated.
2. The back face undergoes reradiation and convective cooling.
3. The back face is exposed to identical heat flux as the front face and undergoes reradiation and convective cooling

Note that for the discussions above, piloted ignition has been assumed. For cases without pilot, the air velocity and temperature strongly affect the time to ignition. This is extensively discussed by Babrauskas [2].

For tunnels the situations in many cases are extreme and significantly different from the conditions in the different test methods used when determining values for, for example, $\dot{q}''_{cr}$. The high air flow around the object for the fire to spread to may cool and disperse the mixture of pyrolysis gases at the surface and thereby delay the ignition process. Therefore, much care must be taken when taking these values into a real tunnel fire situation. However, the table values presented in this chapter together with the presented equation can give information on important influencing factors and relative differences between various materials.

One of the few models specifically developed for fire spread in tunnels is the one developed by Beard [34–38]. The model (FIRE-SPRINT) was created to model the fire spread from a burning HGV to a second HGV. There has been a continuous development of the model through different versions as summarized below (if nothing is mentioned the next version of the model has the same assumptions as the one before):

FIRE-SPRINT A1 [34]: It was assumed that the fire does not extend over or around the target vehicle, but is retained near the region of the initially burning vehicle (no flames extend downstream of the initial fire). A flow of air of ambient temperature exists in the tunnel due to forced ventilation. No smoke is assumed to move upstream. No radiative heat transfer occurs from the fire to the gases, but radiative feedback exists on the fire from the gases.

FIRE-SPRINT A2 [35]: A flame is assumed to extend to the upper part of the tunnel, also above the target, but there is a region above the target with no flame (between the target and the flame). It is assumed that no direct radiative heat transfer occurs between the downstream flame and the target.

FIRE-SPRINT A3 [36]: As in FIRE-SPRINT A2, but with a thicker flame in the region between the fire and the target. Thermal radiation is assumed to exist between the downstream flame section and the top of the target object.

FIRE-SPRINT B1 [37]: Flame impingement onto the target is assumed to exist (a persistent flame impingement is assumed).

The models have been used to estimate the fire spread by calculating the limits of stability of the system (correlated with a jump in the temperature) by means of nonlinear dynamics, and investigating how these limits depend on the HRR, the air flow velocity and the distance between the fire and the target. In each of the above mentioned cases, the limit for HRR to reach an unstable condition (fire spread) has decreased, which is in line with what can be expected. For a case with 6.45 m distance between the fire and the target and an air velocity of 2 m/s, the critical value of the HRR was calculated to be 55.2, 45.3, 38.6, and 14 MW, respectively, for the four different model versions.

The differences in results obtained with the different versions show both the impact different processes can have on the results, and the importance of large-scale fire tests to validate both models used and assumptions made. There are also cases when flame impingement onto the target (for example, another vehicle) does not exist, which means that knowledge about the actual situation is needed to make the correct assumptions (that is, to choose the correct version of the fire spread model).

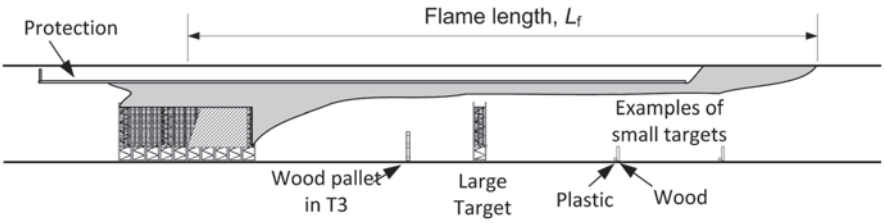

Fig. 11.8 A diagram of the fire load and the targets placed downstream of the fire. (From Lönnermark and Ingason [6])

To shed some light on the issue regarding whether flame impingement is probable during a certain fire situation or not, Carvel et al. [39] collected experimental information from the literature and used Bayes' Theorem to calculate the probability of impingement.

The authors scale the experimental results and draw the conclusion that the flames from a majority ("a large portion") of HGV fires will impinge on another HGV up to 20 m downstream of the fire. For a car fire (assumed to have a HRR less than 8 MW) it is unlikely that the flame will impinge on another vehicle more than 5 m downstream. In both cases the results are assumed to be valid for air velocities between 1 and 4 m/s.

Hansen and Ingason [40, 41] studied the fire risks in mines and developed a methodology to calculate fire spread among multiple objects to calculate HRR development in vehicles in underground structures. The modeling uses summation of individual HRR curves for different burning objects. The method, which was suggested by Ingason [42], is based on work by Numajiri and Furukawa [43]. It assumes a fire with a negligible constant period of maximum HRR and is useful only for fuel controlled fires. The model includes different parameters: maximum HRR, a retard index, an amplitude coefficient, and a time width coefficient. Several of these parameters can be related to the maximum HRR or the total energy content, but the retard index is determined by curve fitting. See Chap. 6 for further detailed information on fire curves.

To model fire spread it is also necessary to decide when a second object is ignited due to the flames from the first object. Three different methods to determine or model the ignition of a second object were evaluated as ignition criteria: one method with critical external heat flux and two methods using a surface ignition temperature. The first method was shown to be best for short distances between objects while the ignition temperature methods worked better for longer distances between the objects. Another issue is to find relevant values for critical heat flux and ignition temperatures as discussed earlier in the chapter. However, with suitable values good correlation can be found between the model and the experimental results for the selected scenarios.

Lönnermark and Ingason [27] investigated the fire spread in the Runehamar tests [25]. Several targets were placed at different locations downstream of the fire, see location of small targets of Plastic and Wood pieces at floor level in Fig. 11.8. Models of the average temperature for the cross-section were used to study the

connection of this parameter to fire spread. For the region of fire spread, a large temperature difference between the temperature in the upper layer and the calculated average temperature of the cross-section exists. This temperature difference has an important effect on the incident radiation, which in most cases is the cause of fire spread. The use of an average temperature in fire spread calculations might, therefore, be misleading.

In the vicinity of a fire, the radiation dominates the heat transfer. The incident heat flux represents the intensity of incident radiation from surroundings. The incident heat flux received on the target surface can be approximately estimated using the following equation (see Chap. 10 on heat flux):

$$\dot{q}''_{inc} = \varepsilon_g F_{o-g} \sigma T_g^4 \tag{11.24}$$

where ε_g is the gas emissivity, T_g is the gas temperature (K), $F_{o\text{-}g}$ is the view factor from the target to smoke layer. Note that T_g must be expressed in degrees Kelvin for this equation to be valid and ε_g in most cases can be considered as 1 for estimation of fire spread due to the sooty smoke layer. The view factor is equal to one if the target is immersed in the layer or else it is lower than 1, for example, a surface at the floor level. How to calculate this view factor can be found in Chap. 10 on heat flux.

The critical condition for ignition is difficult to identify. The critical ignition criterion varies significantly, including ignition temperature, critical heat flux, critical fuel mass flow rate, etc. In spite of the significant difference in determination of the critical ignition condition, it can be expected that there is a strong correlation between the ignition and the ceiling gas temperature in a ventilated tunnel fire. Ingason et al. [25] analyzed the ignition condition using the critical ceiling gas temperature, that is, the minimum ceiling gas temperature required to ignite the target material of plastic and wood material. At the ignition state, the controlling equation for the energy in the surface layer of the sample can be expressed as:

$$\dot{q}''_{ig} = \varepsilon_s (\dot{q}''_{inc,cr} - \sigma T_{ig}^4) + h_c (T_\infty - T_{ig}) \tag{11.25}$$

where $\dot{q}''_{ig}$ is the critical net heat flux at ignition (kW/m^2), $\dot{q}''_{inc,cr}$ is the critical incident heat flux at ignition (kW/m^2) from Eq. (11.24), ε_s is the surface emissivity of the sample and T_{ig} is the ignition temperature (K). Since the emissivities of the common materials, such as wood and PE plastic, are generally in a range of 0.8–0.95, the surface emissivity of the sample is not supposed to have a strong influence on the total heat flux absorbed by the sample, except for some special materials. The above equation in fact indicates that there exists a critical incident heat flux corresponding to the ignition state in a given condition.

Ingason et al. [25] found that the location of wood crib surface relative to the smoke layer height plays an important role in the fire spread. It can be argued that the fire spread to the second vehicle is unlikely to occur if a tunnel height is very high, say up to twice the vehicle height. They found that for wood the ceiling gas temperature at the edge of fire spread, that is, the critical ceiling gas temperature, is in a range of 709–955 °C in the Runehamar test T2, 674–740 °C in T3 and 674–740 °C in T4. This means that a ceiling gas temperature of about 700 °C is required to ignite the wood crib placed on the floor level. The mechanism of ignition should

be the spontaneous ignition by thermal radiation. According to Li et al. [44], a surface temperature of 600 °C should be obtained for wood before its spontaneous ignition. Given the differences between experimental conditions in the tunnel and those in the reference, these temperatures correlate well with each other. In a study of the fire spread using model scale tests [45], the critical ceiling gas temperature for fire spread to the second wood cribs is about 600 °C for fire spread to the wood with *surface close to the ceiling* in a tunnel fire. It is therefore concluded that the critical ceiling gas temperature is about 700 °C for fire spread to a wood *at floor level* and about 600 °C for fire spread to the wood with *surface closer to the ceiling (mid tunnel height)* in a tunnel fire.

For plastic material the critical ceiling gas temperature, is below 1001 °C in the Runehamar tunnel fire test T1, below 710 °C in T2, below 672 °C in T3 and in a range of 466–514 °C in T4. Compared to the wood, the plastic material in these tests was much easier to ignite. It was concluded that the critical ceiling gas temperature for fire spread to the plastic materials placed at the floor level can be considered to be 490 °C, that is, an average value of 466–514 °C in T4.

11.5 Summary

In the chapter different parameters affecting the ignition and fire spread are presented and discussed. For tunnels the situations in many cases are extreme and significantly different from the conditions in the test methods used when determining values, for example, $\dot{q}''_{cr}$. Therefore, much care must be taken when applying these values to a real tunnel fire situation. However, the table values presented in this chapter together with the presented equations can give information on important influencing factors and relative differences between various materials. A few fire spread models specifically developed for tunnels or vehicles are also presented.

It is also shown that ordinary cargo can be hazardous in tunnels, both due to fast developing and high HRR fire and due to the high risk for fire spread. The involvement of more than one HGV in a fire significantly increases the risk for severe outcomes, for example, fatalities. This emphasizes the importance of fire spread in tunnels and the effect on the fire development, possibilities for the fire and rescue services to fight the fire and on the final outcome of the fire.

References

1. Rew C, Deaves D Fire spread and flame length in ventilated tunnels—a model used in Channel tunnel assessments. In: Proceedings of the International Conference on Tunnel Fires and Escape from Tunnels, Lyon, France, 5–7 May 1999. Independent Technical Conferences Ltd, pp 397–406
2. Babrauskas V (2003) Ignition Handbook. Fire Science Publishers, Issaquah, WA, USA
3. Wickström U (To be published) Heat Transfer in Fire Technology. Draft 26 March 2013 edn.

4. Quintiere JG (1998) Principals of Fire Behavior. Delmar Publishers
5. Drysdale D (1994) An Introduction to Fire Dynamics. John Wiley & Sons
6. Kanury AM (1972) Ignition of cellulosic materials: a review. Fire Research Abstracts and Reviews 14:24–52
7. Dillon SE (1998) Analysis of the ISO9705 Rom/Corner Test: Simulations, Correlations and Heat Flux Measurements M.S. Thesis, Department of Fire Protection Engineering, University of Maryland
8. Cleary TG, Quintiere JG (1991) Flammability Characterization of Foam Plastics. NIST
9. Hopkins Dj, Quintiere JG (1996) Material Fire Properties and Predictions for Thermoplastics. Fire Safety Journal 26:241–268
10. Grexa O, Janssens M, White R, Dietenberger M Fundamental Thermophysical Prperties of Materials Derived from Cone Calorimeter Measurements. In: Wood & Fire Safety: 3rd International Scientific Conference, 1998. The High Tatras, Slovak Republic, pp 139–147
11. Henderson A (1998) Predicting Ignition Time under Transient Heat Flux Using Results from Constant Heat Flux Experiments. School of Engineering, Univ. Canterbury, Christchurch, New Zealand
12. Janssens ML (1991) Fundamental Thermophysical Characteristics of Wood and Their Role in Enclosure Fire Growth. Ph.D dissertation, University of Gent, Belgium
13. Harkleroad M. Unpublished NIST data
14. Grexa O, Horváthová E, Osvald A Cone Calorimeter Studies of Wood Species. In: International Symposium on Fire Science and Technology, Seoul, 1997. Korean Institute of Fire Science & Enginering, pp 77–84
15. Dietenberger M, Grexa O Analytical Model of Flame Spread in Full-scale Room/Corner Tests (ISO 9705). In: Fire & Materials ’99, 6th International Conference, 1999. Interscience Communications Ltd, pp 211–222
16. NFPA (1981) NFPA Handbook. National Fire Protection Association
17. Glassman I, Dryer F (1980/81) Flame spreading across liquid fuels. Fire Safety Journal 3:123–138
18. Gottuk DT, White DA (2008) Liquid Fuel Fires. In: DiNenno P (ed) The SFPE Handbook of Fire Protection Engineering. Quincy: National Fire Protection Association, pp 2–337 – 332–357
19. Ingason H Small Scale Test of a Road Tanker Fire. In: Ivarson E (ed) International Conference on Fires in Tunnels, Borås, Sweden, October 10–11 1994. SP Swedish National Testing and Research Institute, pp pp. 238–248
20. White D, et al. (1997) Flame Spread on Aviation Fuels Fire Safety Journal Volume 28:pp. 1–31
21. Lönnermark A, Kristensson P, Helltegen M, Bobert M Fire suppression and structure protection for cargo train tunnels: Macadam and HotFoam. In: Lönnermark A, Ingason H (eds) 3rd International Symposium on Safety and Security in Tunnels (ISTSS 2008), Stockholm, Sweden, 12–14 March 2008. SP Technical Research Institute of Sweden, pp 217–228
22. Ingason H (2012) Fire Dynamics in Tunnels. In: Beard AN, Carvel RO (eds) In The Handbook of Tunnel Fire Safety, 2nd Edition ICE Publishing, London, pp 273–304
23. Koseki H (1989) Combustion Properties of Large Liquid Pool Fires. Fire Technology 25 (August):241–255
24. Tewardson A (2008) Generation of Heat and Gaseous, Liquid, and Solid Products in Fires. In: DiNenno PJ, Drysdale D, Beyler CL et al. (eds) The SFPE Handbook of Fire Protection Engineering. Fourth Edition edn. National Fire Protection Association, Quincy, MA, USA, pp 3–109–103–194
25. Ingason H, Lönnermark A, Li YZ (2011) Runehamar Tunnel Fire Tests. SP Technicial Research Institute, SP Report 2011:55
26. Ingason H, Bergqvist A, Lönnermark A, Frantzich H, Hasselrot K (2005) Räddningsinsatser i vägtunnlar. Räddningsverket, P21-459/05 (in Swedish)
27. Lönnermark A, Ingason H (2006) Fire Spread and Flame Length in Large-Scale Tunnel Fires. Fire Technology 42 (4):283–302

28. BEA-TT (2006) Rapport provisoire d'enquête technique sur l'incendie de poids lours survenu dans le tunnel du Fréjus le 4 juin 2005. Bureau d'Enquêtes sur les Accidents de Transport Terrestre, France
29. Brinson A (2005) Fire in French Tunnel Kills Two. Eurosprinkler
30. Bettelini M, Neuenschwander H, Henke A, Gagliardi M, Steiner W The Fire in the St Gotthard Tunnel of October 24, 2001. In: Ingason H (ed) International Symposium on Catastrophic Tunnel Fires (CTF), Borås, Sweden, 20–21 November 2003. SP Swedish National Testing and Research Institute, pp 49–68
31. Ingason H Fire Development in Catastrophic Tunnel Fires (CTF). In: Ingason H (ed) International Symposium on Catastrophic Tunnel Fires (CTF), Borås, Sweden, 20–21 November 2003. SP Swedish National Testing and Research Institute, pp 31–47
32. Duffé P, Marec M (1999) Report on the Technical Enquiry into the Fire on 24 March 1999 in the Mont Blanc Tunnel. Ministry of the Interior, Ministry for Equipment, Transport and Accommodation, France
33. Torero JL (2008) Flaming Ignition of Solid Fuels. In: DiNenno P (ed) The SFPE Handbook of Fire Protection Engineering. Quincy: National Fire Protection Association, pp 2–260 – 262–277
34. Beard AN, Drysdale DD, Bishop SR (1995) A Non-linear Model of Major Fire Spread in a Tunnel. Fire Safety Journal 24:333–357
35. Beard AN (1997) A Model for Predicting Fire Spread in Tunnels. Journal of Fire Sciences 15 (July/August):277–307
36. Beard AN Major Fire Spread in a Tunnel: A Non-linear Model. In: Vardy AE (ed) Fourth International Conference on Safety in Road and Rail Tunnels, Madrid, Spain, 2–6 April 2001. University of Dundee and Independent Technical Conferences Ltd., pp 467–476
37. Beard AN Major Fire Spread in a Tunnel: A Non-linear Model with Flame Impingement. In: Proceedings of the 5th International Conference on Safety in Road and Rail Tunnels, Marseille, France, 6–10 October 2003. University of Dundee and Independent Technical Conferences Ltd., pp 511–521
38. Beard AN Major Fire Spread in a Tunnel, Assuming Flame Impingement: Effect of Separation and Ventilation Velocity. In: Fifth International Conference on Tunnel Fires, London, UK, 25–27 October 2004. Tunnel Management International, pp 317–326
39. Carvel RO, Beard AN, Jowitt PW The Influence of Longitudinal Ventilation on Fire Spread between HGV Fires in Tunnels. In: Fifth International Conference on Tunnel Fires, London, UK, 25–27 October 2004. Tunnel Management International, pp 307–316
40. Hansen R, Ingason H (2011) An Engineering tool to calculate heat release rates of multiple objects in underground structures. Fire Safety Journal 46 (4):194–203. doi:10.1016/j.firesaf.2011.02.001
41. Hansen R, Ingason H (2012) Heat release rates of multiple objects at varying distances. Fire Safety Journal 52:1–10
42. Ingason H (2009) Design fire curves in tunnels. Fire Safety Journal 44 (2):259–265. doi:10.1016/j.firesaf.2008.06.009
43. Numajiri F, Furukawa K (1998) Short Communication: Mathematical Expression of Heat Release Rate Curve and Proposal of 'Burning Index'. Fire and Materials 22:39–42
44. Li YZ, Lei B, Ingason H (2011) The maximum temperature of buoyancy-driven smoke flow beneath the ceiling in tunnel fires. Fire Safety Journal 46 (4):204–210
45. Ingason H, Li YZ (2011) Model scale tunnel fire tests with point extraction ventilation. Journal of Fire Protection Engineering 21 (1):5–36

Chapter 12
Smoke Stratification

Abstract The phenomena and formation mechanisms of smoke stratification and engineering solutions to estimate smoke stratification in tunnel fires are described. Smoke stratification is an important issue for evacuation and fire fighting in tunnel fires. Smoke released from a fire contains some hazardous combustion products. If the smoke stratification in a tunnel section dissolves, tunnel users in this region could be in great danger. In no ventilation or very low ventilation conditions, smoke exists on both sides of the fire, and good stratification could exist at the early stages but generally not after the fire becomes larger. For a ventilation velocity slightly lower than the critical velocity, smoke backlayering and good stratification exist upstream of the fire, however, the smoke stratification downstream becomes worse. Under high ventilation rates, all the smoke flows towards the downstream side and stratification is difficult to maintain even at a short distance downstream. The theory of the smoke movement along the tunnel is introduced. An empirical model of smoke stratification in tunnels with longitudinal ventilation is also presented.

Keywords Stratification · Ventilation velocity · Entrainment · Smoke layer height · Smoke backlayering · Simple model · Froude number

12.1 Introduction

Smoke stratification is dependent on the longitudinal ventilation velocity and the buoyancy forces created by the fire. Due to the buoyancy forces, the hot smoke flows upward and occupies the upper region of a tunnel cross section. Therefore, a clear stratification may exist in some cases.

Smoke released from a fire is a combination of combustion products and air. The four factors affecting tenable conditions are asphyxiant fire gases, irritant fire gases, heat, and visual obscuration. More detailed information on these parameters is given in Chaps. 14 and 15. All of these factors are intimately related to smoke, with the exception of flame radiation in the vicinity of a fire source. In the early stages of a fire the heat could be a minor problem, but high concentrations of some combustion products such as carbon monoxide and other toxic gases could easily cause deaths. In any case, after the smoke descends to the head height of the tunnel

H. Ingason et al., *Tunnel Fire Dynamics,* DOI 10.1007/978-1-4939-2199-7_12

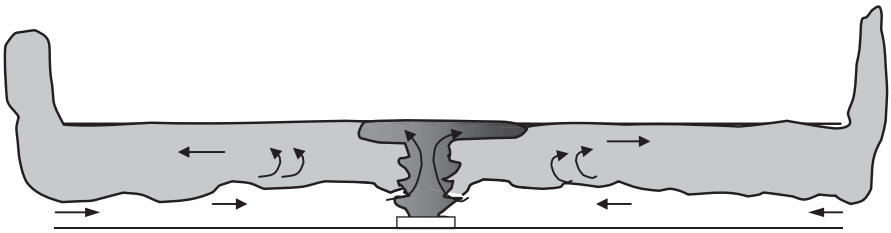

Fig. 12.1 A sketch showing the smoke stratification in a tunnel with a very low air velocity, typically 0–0.5 m/s for group 1

users, people inside the region will be in great danger. In engineering applications in building fires, maintaining the smoke layer height above head height is a key task. In tunnel fires, this issue is even more important due to the limited possibilities for evacuation and often unfamiliar surroundings for the users.

The phenomena and formation mechanisms of smoke stratification are described, and engineering solutions to estimate the smoke stratification in tunnel fires are presented in the following sections.

12.2 Phenomenon of Smoke Stratification

In tunnel fires, the characteristics of the smoke spread are highly dependent on the air velocity inside the tunnel, especially in the vicinity of the fire site. In order to illustrate this, we can identify three typical air velocity ranges (groups):

- low or no forced air velocity (0–1 m/s),
- moderate forced air velocity (1–3 m/s), and
- high forced air velocity (> 3 m/s).

Note that the values of 1 and 3 m/s inside the parentheses are only approximate values. Specifically, 3 m/s is an estimate of the critical velocity under which no backlayering exists. The critical velocity in tunnel fires is defined as the minimum longitudinal ventilation velocity required to prevent any backlayering of smoke. The concept of critical velocity is discussed thoroughly in Chap. 13. The critical velocity in a tunnel fire could in reality be greater than 3 m/s for a large fire or less than this value for a small fire.

In the *first group* (low air velocity) the stratification of the smoke is usually high in the vicinity of the fire source. Tunnels with natural ventilation normally fall into this group. The backlayering length of the smoke is relatively long and in some cases the smoke travels nearly uniformly in both directions, see Fig. 12.1. When the velocity increases and is close to about 1 m/s the smoke upstream of the fire is inhibited by the ventilation and prevented from further spreading, and the length of this backlayering smoke layer from the fire site could be of the order of 25 times the tunnel height, see Fig. 12.2. The estimation of the backlayering length can be found in Chap. 13 on tunnel fire ventilation, and is therefore not discussed further here.

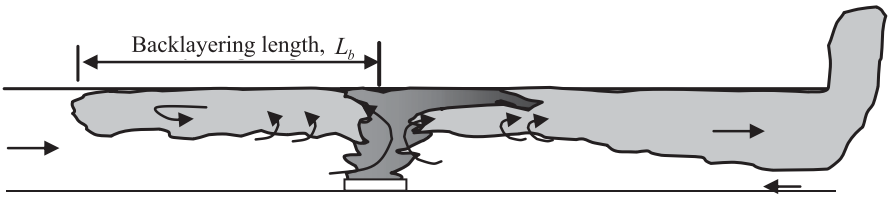

Fig. 12.2 A sketch showing the smoke stratification with a flow velocity of 1 m/s

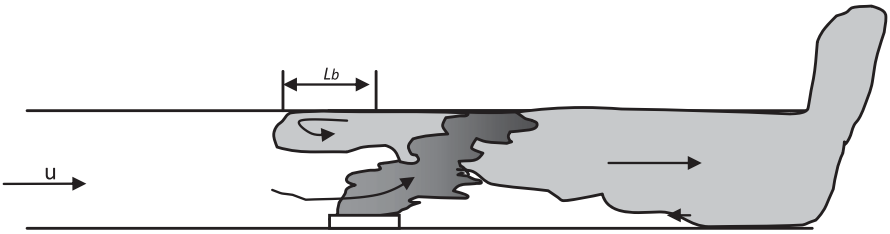

Fig. 12.3 A sketch showing a typical smoke stratification for group 2

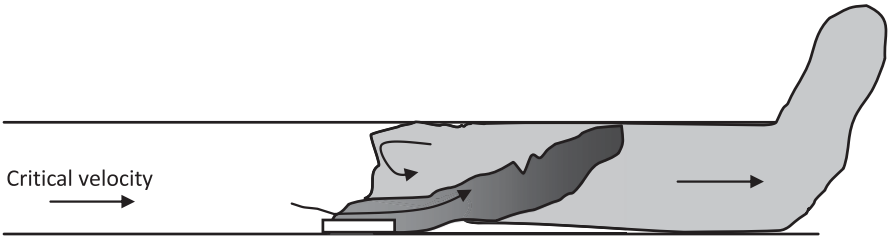

Fig. 12.4 A sketch showing a typical smoke stratification for group 3, i.e. a flow velocity larger than the critical flow velocity, u_c

In the *second group* (moderate flow) the stratification in the vicinity of the fire is strongly affected by the air velocity, especially at the higher velocities. Tunnels with natural ventilation or forced ventilation can reside in this group. The backlayering length could vary from 0 up to around 25 times the tunnel height, see Fig. 12.3.

In the *third group* (high flow velocity) the stratification of the smoke downstream usually disappears and no backlayering exists upstream of the fire, see Fig. 12.4. This group generally corresponds to tunnels with forced ventilation [13].

The stratification downstream from the fire is a result of the mixing process between the cold air stream and the hot plume created by the fire. The phenomenon is three-dimensional in the region close to the fire plume. The principal pathways of the two flows are indicated in Fig. 12.5. The gravitational forces tend to suppress turbulent mixing between the two flows having different densities.

This explains why it is possible for cold unreacted air to bypass the fire plume without mixing, even though the flow is turbulent. The longitudinal dimension of

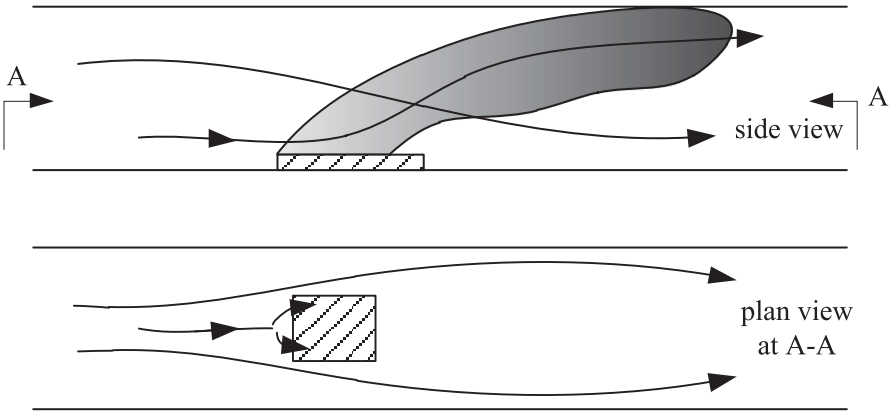

Fig. 12.5 The principal flow pathways in the vicinity of a fire plume [13]

the fuel involved in the fire may therefore, play an important role for the mixing process between the longitudinal flow and the fuel vapours generated by the fire.

12.3 Mechanism of Smoke Stratification

Stratification is a common phenomenon, for example, floating oil on water. Hot smoke flows have lower density which produces a pressure difference between the hot gas and ambient air, that is, thermal pressure. Due to the thermal pressure or buoyancy force, the hot smoke flows upward, impinges on the tunnel ceiling, and then flows along the tunnel ceiling longitudinally. As the smoke travels along the ceiling, the smoke temperature decreases rapidly with distance mainly due to heat loss to the tunnel structure. This indicates that the thermal pressure also decreases with distance. Therefore, smoke stratification becomes more and more difficult to maintain as the distance from the fire increases.

Inertia forces also play a role in formation of stratification. Consider a cold air jet beneath the tunnel ceiling at ambient temperature. There will be no heat transfer between the air jet and the homogenous environment. However, as the distance from the injection outlet increases, the air jet continually entrains air from the layer beneath and the thickness of the layer increases gradually. This suggests that the inertia forces tend to destroy the stratification of the layer.

This means that the thermal pressure tends to maintain the smoke stratification but the inertia force tends to destroy the smoke stratification. A nondimensional parameter to describe the balance between these two forces is the global Richardson number, Ri, defined as:

$$\mathrm{R\,i} = \frac{\Delta\rho g h}{\rho \Delta u^2} \tag{12.1}$$

where ρ is the hot gas density (kg/m^3), $\Delta\rho$ is the density difference (kg/m^3), g is the gravitational acceleration (m/s^2), h is the layer thickness (m), and Δu is the gas velocity difference between the layers (m/s). The characteristic depth, h, in fact should be the depth of the mixing layer, however, for smoke flow beneath the ceiling it is reasonable to use the layer thickness instead. It can be expected that as the Richardson number increases, the smoke stratification becomes more stable.

12.3.1 Entrainment

An important phenomenon observed in density stratified flows is the entrainment between the layers. For upperlayer smoke flows in tunnel fires, it can be expected that the entrainment of air flows into the upper smoke layer is mainly due to turbulent mixing between the two layers, that is, the entrained air is mainly carried by the large vortices produced by turbulence.

The entrainment coefficient based on the mixing theory is introduced in the following set of equations. By applying mixing length turbulent theory [1] to the mixing layer between the hot smoke layer and the lower layer, it is known that the turbulent mixing velocity, u_t (m/s), can be expressed as:

$$u_t = Cl_m \frac{\partial u}{\partial z} \tag{12.2}$$

where C is a proportionality constant, l_m is the mixing length (m) and z is the vertical distance (m). The entrainment velocity, v_e, can be expected to approximate the turbulent mixing velocity. Further, given that the mixing length is proportional to the thickness of mixing layer, that is, $l_m = 0.07\,\delta$ [1], the entrainment velocity, u_e (m/s), can be expressed as follows:

$$u_e = 0.07C\delta\frac{\Delta u}{\delta} = 0.07C\Delta u \tag{12.3}$$

The entrainment coefficient, β, can therefore be expressed as:

$$\beta = \frac{u_e}{\Delta u} = 0.07C \tag{12.4}$$

The entrainment coefficient has been extensively investigated in different scenarios in the last several decades. The entrainment coefficient for isothermal jet flows is close to constant, however, for density stratified flows, buoyancy affects the entrainment. The entrainment coefficient for the stratified layer has been found to be a function of the Richardson number, Ri.

There is a large amount of research on the entrainment of stratified layers in the field of fluid dynamics.

Ellison and Turner [2] carried out a classic study on mixing between a turbulent fluid and a stationary fluid and correlated the entrainment coefficient β with the Richardson number in the following relationship:

$$\beta = \alpha_1 \exp(-\alpha_2 \,\mathrm{Ri}) \tag{12.5}$$

where α_1 could be considered as the entrainment coefficient for vertical fire plumes and α_2 is a correction coefficient. Alpert [3] found that the above equation with $\alpha_2 = 3.9$ is a good fit to Ellison and Turner's [2] data, that is, the expression can be [4, 5]:

$$\beta = 0.12 \exp(-3.9\,\mathrm{Ri}) \tag{12.6}$$

Based on a numerical study and a comparison with test data, Alpert [3] proposed alternative equations for the entrainment coefficient:

$$\beta = 0.075 \exp(-5\,\mathrm{Ri}) \tag{12.7}$$

and in the form of distance:

$$\beta = 0.12[1 - \exp(-0.6H/x) \tag{12.8}$$

You and Faeth [4] carried out a numerical study of ceiling fire plumes and compared numerical results to their test data. The equation for entrainment has the same form as Ellison and Turner's [2] but with different coefficients. They found that the following equation best test results best for weak plume [4]:

$$\beta = 0.14 \exp(-1.5\,\mathrm{Ri}) \tag{12.9}$$

Ding and Quintiere [6] pointed out that the density ratio also needed to be accounted for and corrected Alpert's equation [3] to:

$$\beta = 0.075\rho/\rho_o \exp(-5\,\mathrm{Ri}) \tag{12.10}$$

where ρ_o is the density of the gas in the lower layer and ρ is the smoke density.

The equations presented above are basically of the same form as proposed by Ellison and Turner [2]. However, the expression proposed by Ellison and Turner [2] is only valid for $\mathrm{Ri} < 0.8$ [7]. Further, nearly all the equations presented above date back to Ellison and Turner's [2] liquid experiments. For entrainment into hot smoke flows, especially into flame flows, the validity of these equations must be confirmed. According to Fernando [7], for intermediate Richardson numbers ranging from 0.1 to 10, the entrainment law was proposed to be $\beta \sim \mathrm{Ri}^{-1}$ and within this range the Kelvin–Helmholtz instabilities are active.

Wilkinson and Wood [2] investigated the possible density jump in density stratified flows and related it to a critical Froude number below which entrainment will not occur, based on which Delichatsios [8] analyzed smoke flow under a beamed ceiling. However, according to Kunsch's study on smoke movement in tunnel fires [9], no density jump occurred in the tunnel fire cases that were studied, although further study was recommended. Fernando [7] conducted a systematic review of turbulent mixing in stratified flows. The analysis showed that for a Richardson number ranging from 0 to 100, the entrainment coefficient ranged from 10^{-1} to 10^{-5} This appears to be contrary to the definition of density jump. It could be interpreted that, as the Richardson number increases to a certain number the entrainment will decrease to a very low level which could be ignored.

For smoke flows in tunnel fires, the smoke flow could be very different from the ceiling flow in the open or in a short corridor due to the confinement of the tunnel geometry and ventilation. The entrainment in these scenarios needs to be further investigated.

12.3.2 Smoke Layer Height

Although this chapter discusses smoke stratification in tunnel fires, the variance of smoke layer height along the tunnel is more meaningful. In tunnel fires, the smoke released from a fire impinges on the ceiling and then flows along the ceiling, and the depth of smoke flow generally increases with distance from the fire. In reality, the descent of the smoke layer is the outcome of a combination of mass entrainment, momentum loss, and heat transfer.

The profile of gas velocity and density for smoke flows is complicated and could differ from one location to another. For simplicity, top hat profiles are assumed for these parameters. For smoke flow in a tunnel with natural ventilation, the time-resolved differential controlling equations for mass, momentum, and energy can approximately be expressed as:

Mass:

$$\frac{\partial}{\partial t}(\rho A)+\frac{\partial}{\partial x}(\rho u A)=\rho_o u_e W \tag{12.11}$$

Momentum:

$$\frac{\partial}{\partial t}(\rho u A)+\frac{\partial}{\partial x}(\rho u^2 A)+\frac{\partial}{\partial x}\left(\frac{1}{2}\Delta\rho g h A\right)=-\frac{1}{2}C_f \rho u^2 w_p \tag{12.12}$$

Energy:

$$\frac{\partial}{\partial t}(\rho A c_p T)+\frac{\partial}{\partial x}(\rho u A c_p T)=\rho_o u_e W c_p T_o - h_t w_p (T-T_w) \tag{12.13}$$

where A is the cross sectional area of smoke flow (m^2), t is the time (s), x is a distance along the tunnel length axis (m), h is the smoke layer depth (m), h_t is the total heat transfer coefficient (kW/(m^2 K)), w_p is the wet perimeter of the smoke layer (m), C_f is the skin friction coefficient, T_w is the wall temperature (K).

It is evident from the momentum equation that the definition of the Richardson number in fact is the ratio of buoyancy to momentum in a steady state. The controlling equations imply that besides the initial conditions, the three factors that affect the smoke layer height are heat transfer, wall friction, and entrainment. Note that the influence of heat transfer and momentum on stratification has been discussed previously and integrated into a global Richardson number.

For a steady smoke flow, the mass flow rate along the tunnel, $\dot{m}$ (kg/s), can be approximated using:

$$\dot{m}(x)=\dot{m}_o+\beta W\int|u-u_o|dx \tag{12.14}$$

where u_o is the air velocity at lower layer (m/s) and β is the entrainment coefficient between the layers.

As a rough approximation, the entrainment coefficient could be assumed to be around 0.01 based on the equations presented previously and the resulting mass flow should be conservative.

The tunnel length is an influencing factor, especially after the smoke front reaches the exit.

The smoke layer depth at a position x m from the fire before the smoke descends to the floor level can be estimated using:

$$h(x) = \frac{\dot{m}(x)(T_o + \Delta T(x))}{\rho_o T_o u(x) W} \tag{12.15}$$

where ΔT is smoke excess gas temperature (K).

The smoke layer height can be expressed as:

$$H_{smoke}(x) = H - h(x) \tag{12.16}$$

Note that the tunnel height is the upper limit for the smoke layer depth.

The initial conditions of the ceiling jets must be known, however, there is a lack of this knowledge for tunnel fires, especially for large fires in longitudinal ventilated tunnels. Further, in a tunnel fire with longitudinal ventilation, the controlling equations become more complicated. Moreover, as mentioned in the previous section, the validity of the entrainment equations needs to be confirmed in such an environment before any practical use.

Therefore, the purpose of this section is mainly to improve understanding of the mechanisms of smoke stratification and smoke layer height. Further research on this topic is needed.

12.4 Simple Model of Smoke Stratification in Tunnels

Although the theoretical model and the related key parameters have been discussed in the previous section, the solution is complex and some of the key parameters required for the solution cannot be accurately estimated.

As an alternative, a simple model is presented in this section for estimation of smoke stratification in tunnels according to Newman [10] and Nyman and Ingason's work [11].

Newman [10] has shown, for duct fires, that there is a correlation between the local temperature stratification and the local mass concentration of chemical compounds. Further, Ingason and Persson [12] have shown that there is a correlation between local smoke optical density (or visibility) and the local density (or temperature) and the oxygen concentration in tunnels. Therefore, it is reasonable to assume that there is a correlation between the local temperature stratification as given by Newman and the gaseous composition (CO, CO_2, O_2 etc) and smoke stratification in tunnels. The temperature stratification is not only related to the air velocity but also to the heat release rate (HRR) and the tunnel height. These parameters can be related through the local Froude number (*Fr*) or Richardson number (Ri).

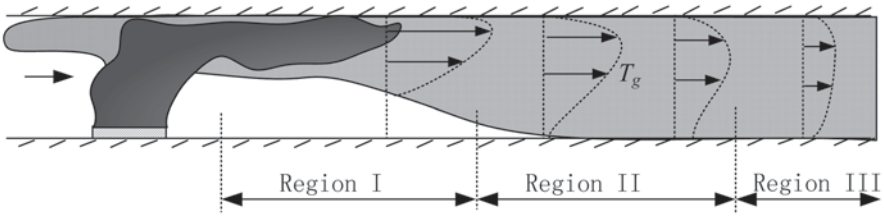

Fig. 12.6 A sketch of three stratification regions after Ingason [13]

Newman [10] presented a very simple method to identify three distinct regions of smoke stratification in terms of a specific Froude number, Fr, which is defined as follows:

$$\mathrm{Fr} = \frac{u_{avg}^2}{\sqrt{gH\Delta T_{cf} / T_{avg}}} \tag{12.17}$$

where H is the tunnel height (m), T_{avg}, the average gas temperature over the entire cross-section at a given position (K), $\Delta T_{cf} = T_c - T_f$, gas temperature difference between ceiling and floor (K) and $u_{avg} = uT_{avg}/T_a$ (m/s). The average temperature at a specific location can be estimated using the one dimensional equations proposed in Chap. 8, Sect. 8.6, on gas temperatures. The definition of the Froude number has a similar physical meaning to the Richardson number defined previously: both of them correlate buoyancy force with inertia force somehow, but in an inverse way to each other.

A sketch of the temperature stratification regions is shown in Fig. 12.6. The vertical temperature profile varies significantly from Region I to Region III. Newman's classification for smoke stratification [10] is described in the following. In the first region (Region I), when $Fr \leq 0.9$, there is severe stratification in which hot combustion products travel along the ceiling. For Region I, the gas temperature near the floor is essentially ambient. This region consists of buoyancy dominated temperature stratification. The second region (Region II) $0.9 \leq Fr \leq 10$ is dominated by strong interaction between imposed horizontal flow and buoyancy forces. Although not severely stratified or layered, it has vertical temperature gradients and is mixing controlled. In other words, there is significant interaction between the ventilation velocity and the fire-induced buoyancy. The third region (Region III), $Fr > 10$, has insignificant vertical temperature gradients and consequently insignificant stratification.

Newman [10] also established correlations for the excess temperatures near the ceiling at $0.88 \times \mathrm{H}$ (ceiling) and temperatures near the floor at $0.12 \times \mathrm{H}$ (floor) for the different regions of stratification, which are based on a weighted average of the gas temperature (T_{avg}) and the gas velocity (u_{avg}) over the entire cross section. He postulated that these correlations could be used for various applications, such as in assessing flame spread and detector response. These correlations have not been tested for tunnel fires and are therefore not presented here. The majority of the tests used to identify these stratification regions were performed in a large scale (rectan-

gular) duct measuring 2.4 m wide (B), 2.4 m high (H), and 47.6 m long (L) with $D_h/L = 19.8$ m, where D_h is the hydraulic diameter. The hydraulic diameter is defined as $\sqrt{4A/P}$ where A is the cross sectional area (m^2) and P is the perimeter (m).

To estimate the smoke stratification according to the Froude number defined above, the temperature difference between the ceiling and floor must be known. Nyman and Ingason [11] investigated Newman's temperature correlations based on a large amount of data from small- and large-scale tunnel fire tests. It was concluded that Newman's equation for ceiling temperatures did not fit the large-scale data, and a new equation in Region II was proposed for estimation of the temperature difference between the ceiling and floor, ΔT_{cf} (K), which can be expressed as:

$$\Delta T_{cf} = 0.225 \frac{gH\Delta T_{avg}^2}{T_{avg} u_{avg}^2} \tag{12.18}$$

The average temperature and average gags velocity in the above equation can be estimated using Eqs. (8.45) and (8.48). Afterward, the temperature difference between the ceiling and floor can be estimated using Eq. (12.18). The calculated values can thereafter be used to calculate the Froude number by Eq. (12.17) and then the smoke stratification can be estimated for any specific location downstream of a fire.

It should be kept in mind that there is no clear distinction between Region II and Region III. A Froude number of 10 and ratio of $\Delta T_{cf}/\Delta T_{avg}$ of 0.1 is used by Newman [10] as an approximation. However, if the work done by Nyman and Ingason [11] is applied here and the same criteria of $\Delta T_{cf}/\Delta T_{avg} = 0.1$ is used, the value of the Froude number at the Region II–III interface can then be determined as 3.2, compared to a value of 10 proposed by Newman. In general, the Froude number of 3.2 should be a more reasonable value for the interface between Region II and Region III in tunnel applications.

Therefore, the first region (Region I) corresponds to $Fr \leq 0.9$, results in severe stratification. Region II corresponds to $0.9 \leq Fr \leq 3.2$ where strong interaction between imposed horizontal flow and buoyancy forces exists. Region III corresponds to $Fr > 3.2$ where smoke stratification is insignificant. For practical use, the calculated Froude number should be less than 0.9 to ensure severe stratification, that is,

$$Fr \leq 0.9 \tag{12.19}$$

Further, it should be kept in mind that the gas temperature equations proposed in this section are purely empirical without any physical meaning, which, therefore, cannot be used in estimation of ceiling gas temperatures and instead should be used only for estimation of the Froude number.

Example 12.1

What is the stratification region after 10 min (600 s) at $x = 150$ m from the fire location? The longitudinal ventilation is 2 m/s, ambient temperature $T_o = 20$ °C, the tunnel geometry is $H = 6$ m and $W = 9$ and the fire grows linearly and reaches a peak HRR of 120 MW after 10 min.

Solution: First the simple method proposed in Sect. 8.6 to correct the time is applied here, that is, $\tau = t - x/u_o = 600 - 150/2 = 525$ s, which means $\dot{Q}(\tau) = 105$ MW. Thus,

By using Eq. (8.46), the average temperature at $x=0$ becomes: $T_{avg}(x=0,\tau)=560\,°C$ where $\dot{m}_a = 1.2\times 2\times 6\times 9=130$ kg/s. The reader must note that the corresponding ceiling temperature may be much higher than 560 °C (~ 1000 °C), but since this is an average bulk temperature used as input for determine the Fr number it is acceptable. The average temperature 150 m from the fire at time $t=600$ s can be calculated using Eq. (8.45): T_{avg} ($x=150$, $t=600$ s) = 247 °C where $h=0.025$ kW/(m^2 K), $P=30$ m, $x=150$ m, $\dot{m}_a = 130$ kg/s, $T_o=20\,°C$ and $c_p=1$ kJ/(kg K). The temperature difference is $\Delta T_{cf}=123\,°C$ by Eq. (12.18). Thus, the Froude number can be determined using Eq. (12.17), that is, $Fr=3.4>3.2$. This corresponds to Region III, that is, smoke stratification is insignificant. It could be expected that at this moment the whole tunnel is full of smoke and evacuation here is very difficult.

12.5 Summary

Smoke stratification is an important phenomenon for evacuation and fire fighting in tunnel fires. Smoke released from a fire contains some deadly combustion products. If smoke stratification disappears, people in the region could be in great danger.

The phenomenon of smoke stratification in a tunnel fire is illustrated. Under no ventilation or very low ventilation, smoke exists on both sides of the fire, and good stratification could exist at the early stages but generally not after the fire becomes larger. For a ventilation velocity slightly lower than the critical velocity, smoke backlayering and good stratification exist upstream of the fire. However, the smoke stratification downstream becomes worse. Under high ventilation, all smoke flows toward downstream and stratification is difficult to maintain even at a short distance downstream of the fire.

The mechanism of the smoke stratification is closely related to the global Richardson number, which indicates the stability of the smoke layer. Entrainment is a key mechanism that causes the descent of the smoke layer. The entrainment velocity is proportional to the velocity difference between layers.

The time-resolved controlling equation for smoke movement is proposed. From the controlling equations, it is known that besides the initial conditions, the three factors that affect the smoke layer height are heat transfer, wall friction, and entrainment. At present, there is a lack of knowledge on initial conditions for ceiling jets and the applicability of the entrainment equations, especially for large fires in longitudinal ventilated tunnels. Further, in a tunnel fire with longitudinal ventilation, the controlling equations become more complicated. Moreover, as mentioned in the previous section, the validity of the entrainment equations must be confirmed in such an environment before practical use.

A simple model of smoke stratification in tunnels is described in Sect. 12.4 which could be used for estimation of smoke stratification in tunnels with longitudinal ventilation.

References

1. Versteeg HK, Malalasekera W (1995) An Introduction to Computational Fluid Dynamics. Longman, England
2. Wilkinson DL, Wood IR (1971) A rapidly varied flow phenomenon in a two-layer flow. Journal of Fluid Mechanics 47:241–256
3. Alpert RL (1971) Fire induced turbulent ceiling-jet. Report no. 19722-2. Factory Mutual Research Corp., Norwood
4. You HZ, Faeth GM (1985) An investigation of fire plume impingement on a horizontal ceiling 2– Impingement and ceiling-jet regions. Fire and Materials 9 (1):46–56
5. Babrauskas V (1980) Flame Lengths under Ceiling. Fire and Materials 4 (3):119–126
6. Ding H, Quintiere JG (2012) An integral model for turbulent flame radial lengths under a ceiling. Fire Safety Journal 52:25–33
7. Fernando HJS (1991) Turbulent mixing in stratified fluids. Annual Review of Fluid Mechanics 23:455–493
8. Delichatsios MA (1981) The Flow of Fire Gases under a Beamed Ceiling. Combustion and Flame 43:1–10
9. Kunsch JP (1999) Critical velocity and range of a fire-gas plume in a ventilated tunnel. Atmospheric Environment 33:13–24
10. Newman JS (1984) Experimental Evaluation of Fire-Induced Stratification. Combustion and Flame 57:33–39
11. Nyman H, Ingason H (2012) Temperature stratification in tunnels. Fire Safety Journal 48:30–37
12. Ingason H, Persson B (1999) Prediction of Optical Density using CFD. In: Curtat M (ed) Fire Safety Science—Proceedings of the 6th International Symposium, Poitiers. pp 817–828
13. Ingason H (2005) Fire Dynamics in Tunnels. In: Carvel RO, Beard AN (eds) The Handbook of Tunnel Fire Safety. Thomas Telford Publishing, London, pp 231–266

Chapter 13
Tunnel Fire Ventilation

Abstract Ventilation is the most common measure to mitigate the effect of fire and smoke in a tunnel. Various normal ventilation systems for removal of heat and contaminants from the tunnels are introduced at first. In case of a tunnel fire, fire ventilation systems are required to control smoke flows and create paths for evacuation and firefighting. The fire ventilation systems used in tunnels mainly include longitudinal ventilation systems and smoke extraction ventilation systems, which are discussed in great detail in this chapter. Two key parameters for tunnels with longitudinal ventilation, that is, critical velocity and back-layering length are investigated in full details. For smoke extraction systems, sufficient fresh air flows are required to be supplied from both sides to prevent further smoke spread. Further, fire ventilation systems in tunnel cross-passages and rescue stations are discussed. A simple model of longitudinal flows is introduced for calculation of longitudinal ventilation velocity in a tunnel fire.

Keywords Normal ventilation · Fire ventilation · Longitudinal ventilation · Smoke extraction · Critical velocity · Back-layering length · Cross-passage · Rescue station · Ventilation flows

13.1 Introduction

Ventilation in tunnels has a history as long as one hundred years with different ventilation systems being developed during different periods.

The original aim of mechanical tunnel ventilation was to cope with the contaminant produced by vehicles, such as diesel locomotives and the full transverse ventilation systems were therefore developed. Later, to reduce the cost, semi transverse ventilation systems were developed. In the 1980s, the longitudinal ventilation systems were developed and started to be widely used all over the world due to their relatively simple mechanism and low cost.

Fire safety in tunnels was not in focus, however, in the past few decades many catastrophic tunnel fire accidents have occurred and attracted much attention from the public, and accordingly many regulations have been built to cope with fire safety issues in tunnels. Different fire ventilation systems have been developed and used

H. Ingason et al., *Tunnel Fire Dynamics,* DOI 10.1007/978-1-4939-2199-7_13

as one of the major measures to mitigate the effect of fire and smoke in tunnels. This will be discussed in detail after the introduction of "normal" ventilation systems.

13.2 Normal Ventilation

Under normal conditions, the vehicles passing through the tunnels introduce a large amount of contaminants, dust and heat, which are harmful to tunnel users, tunnel equipments, and vehicle devices themselves. Therefore, normal ventilation systems are designed to reduce the concentration of contaminants and dust, and/or remove heat from the tunnels under normal operation. In road tunnels and in rail tunnels with diesel locomotives running inside, the main concern of normal ventilation is the contaminants and dust caused by the vehicles. However, in modern railway or metro tunnels with high speed electric locomotives running inside, the key objective of the ventilation design has shifted to taking away the heat produced by the locomotives.

The normal ventilation systems can be divided into two types: natural ventilation and mechanical ventilation systems.

For road tunnels with high traffic flows or for railway tunnels with high speed trains, the piston effect could produce a high enough air flow to remove the heat and reduce the concentration of contaminants and dust and therefore, mechanical ventilation systems could not be necessary under normal ventilation. Further, for very short tunnels or tunnels with many large shafts, the mechanical ventilation systems may not be required under normal ventilation. These types of ventilation systems without mechanical fans are called natural ventilation systems.

However, mechanical ventilation systems generally need to be installed in long tunnels to take away contaminants and heat from vehicles or other equipments. Clearly, mechanical ventilation systems are robust, and are not as dependent on the environments as natural ventilation systems do. Therefore, they are much more widely used as tunnel ventilation systems. Typical mechanical ventilation systems include longitudinal ventilation systems, transverse ventilation systems, semi-transverse systems and combined ventilation systems, which will be discussed in detail below.

13.2.1 Longitudinal Ventilation

In a longitudinal ventilation system, the jet fans and/or normal fans are used to create a longitudinal flow to remove the contaminants, dust and heat.

Jet fans are widely used in tunnels with longitudinal ventilation due to the relatively low cost and simple installation, especially in very long tunnels where construction of shafts or other ventilation tubes is difficult and not cost-effective. Figure 13.1 shows a schematic drawing of a longitudinal ventilation system solely consisting of jet fans. The jet fans are mainly located at the portals of a tunnel, below the ceiling or attached to the side walls. Generally two or three jet fans form

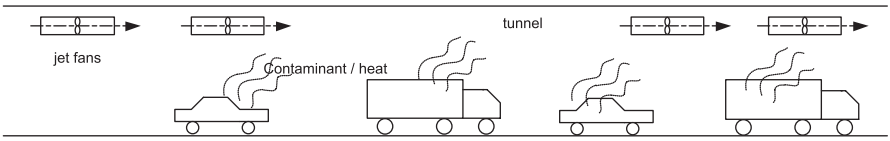

Fig. 13.1 A schematic diagram of longitudinal ventilation solely with jet fans

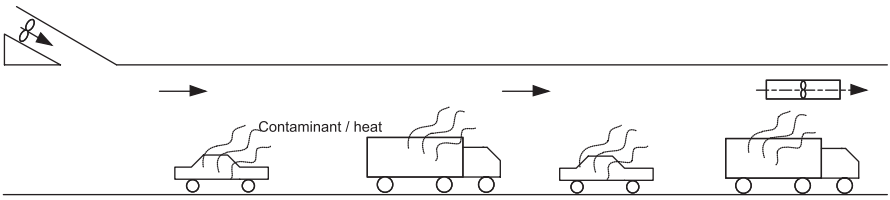

Fig. 13.2 A schematic diagram of longitudinal ventilation with Saccardo nozzle and jet fans

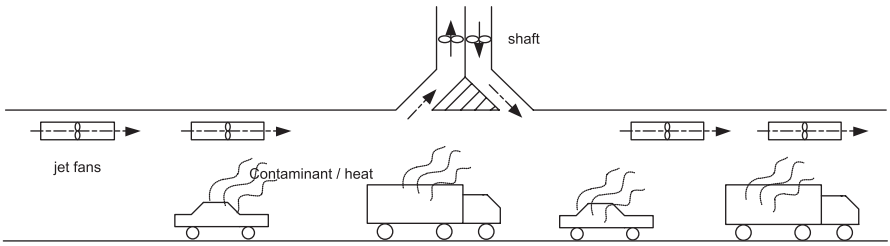

Fig. 13.3 A schematic diagram of longitudinal ventilation with shaft and jet fans

a group. The spacing between two groups is approximately 100 m, depending on the characteristics of the jet fans and the tunnel geometry.

Saccardo nozzles at the entry portals could also be used to produce longitudinal flows, see Fig. 13.2. Large fans are installed in the nozzle to introduce fresh air flows to the tunnel through the nozzle. However, a Saccardo nozzle only produces a limited pressure rise and therefore, this method is only suitable for short tunnels unless it is installed together with other ventilation equipments, such as jet fans (see Fig. 13.2).

In a tunnel with longitudinal ventilation, the contaminants released from vehicles or other equipment are not eliminated but only transported by the longitudinal flow. Therefore, the contaminant concentrations increase with the distance from the entry portal and generally the heat also follows this trend. This suggests a practical limit for the length of a tunnel equipped with a longitudinal ventilation system. In other words, long tunnels may not be able to use a purely longitudinal ventilation system. Instead, one shaft or more may need to be constructed to exhaust the contaminant and heat and to supply fresh air (see Fig. 13.3).

In some cases when the dust concentration is the key determining parameter in the environmental limits, an electrostatic precipitator could be used to eliminate dust particles in the air. This can be used to extend the limit for the length of a tunnel

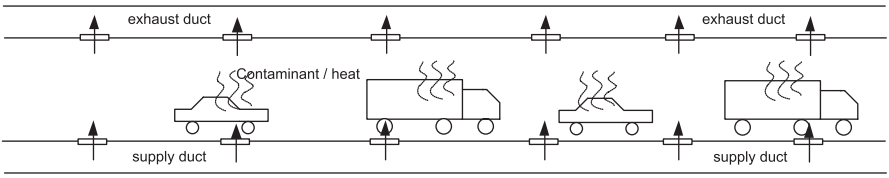

Fig. 13.4 A schematic diagram of transverse ventilation (Longitudinal)

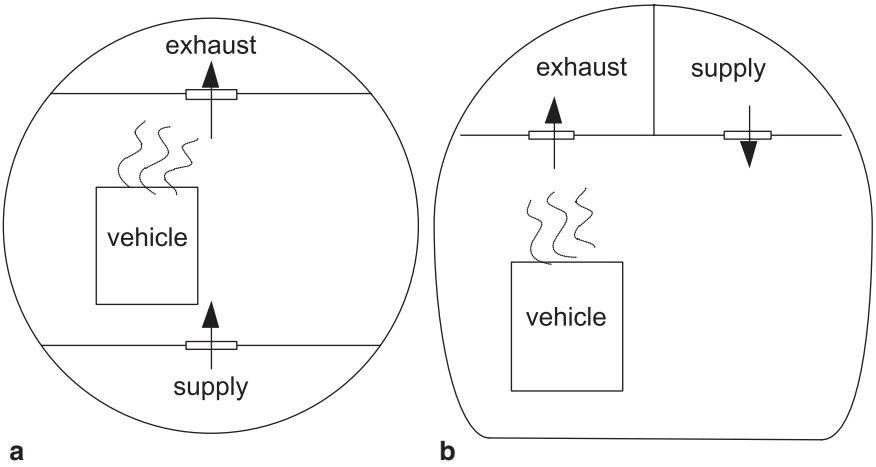

Fig. 13.5 A schematic diagram of transverse ventilation (Cross section)

equipped with a longitudinal ventilation system or reduce the cost of the ventilation system. However, it does not work if a gaseous contaminant concentration or heat is the key issue.

13.2.2 Transverse Ventilation

A transverse ventilation system suggests that the air flows are transversely transferred from supply vents into exhaust vents. Such a system consists of many vents positioned along the tunnel for supplying fresh air into the tunnel and exhausting the contaminants as shown in Figs. 13.4 and 13.5. The exhaust vents are generally placed at the ceiling but the supply vents could be placed either at the floor (see Fig. 13.5a) or at the ceiling level (see Fig. 13.5b). The ducts can be either connected to a shaft located between the tunnel portals or a fan room nearby a tunnel portal. The exhaust vents are generally placed at upper part of the tunnel cross section while the supply vents could be placed either in the upper or lower part, depending on the location of the supply duct.

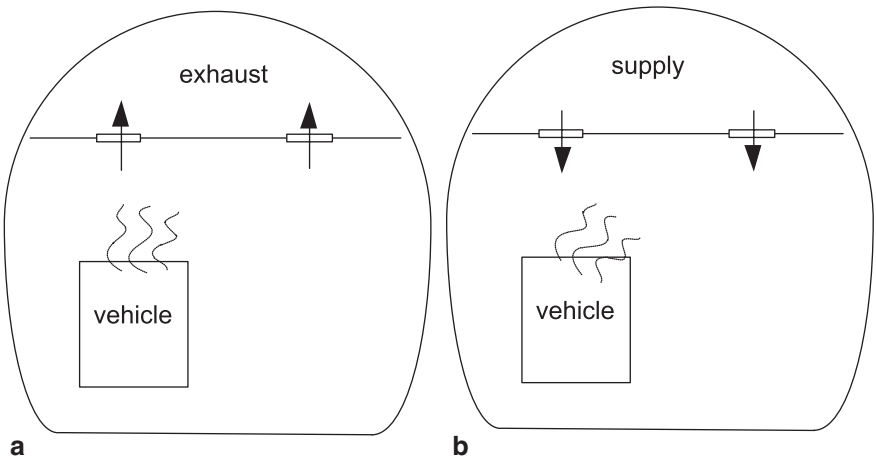

Fig. 13.6 A schematic diagram of semi-transverse ventilation (Cross section view)

13.2.3 Semi-transverse Ventilation

A semi-transverse ventilation system is very similar to a transverse ventilation system. The only difference is that for a semi-transverse system, only supply vents or only exhaust vents are in operation. In other words, only fresh air is supplied into the tunnel (see Fig. 13.6a) or only contaminant air is extracted into the extraction duct (see Fig. 13.6b).

13.3 Longitudinal Fire Ventilation

In the following sections the ventilation systems are discussed in relation to a fire situation.

The normal ventilation system generally needs to be modified to the fire ventilation mode. The objective of a fire ventilation system is to control smoke flow and mitigate the effect of fire and smoke, to aid evacuation, emergency response, and firefighting operations. To reduce the cost and simplify the construction of a tunnel structure, the fire ventilation system should, if at all possible, always be combined with the normal ventilation system.

The fire ventilation modes can be categorized into longitudinal ventilation, smoke extraction ventilation, and combined fire ventilation. Further, special constructions and ventilation strategies are designed to mitigate the effect of fire and smoke flows, such as cross-passages and rescue stations inside the tunnels. The longitudinal fire ventilation system is illustrated in this section and other emergency systems will be presented in the following sections.

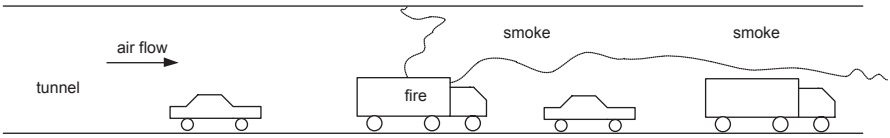

Fig. 13.7 Fire ventilation in a tunnel with longitudinal ventilation

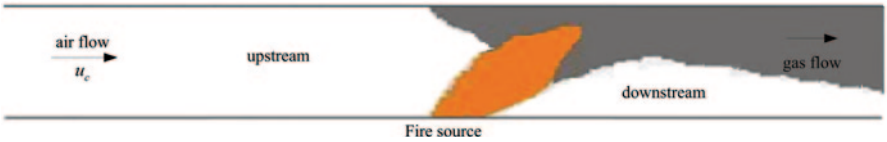

Fig. 13.8 A diagram of critical velocity in a tunnel fire

In case of a fire, a longitudinal ventilation system is designed to produce a longitudinal flow to create a smoke-free path upstream of the fire. Therefore, at least upstream of the fire, the tunnel users can escape. However, the tunnel users located downstream of the fire are exposed to heat and smoke flow. For road tunnels, it is assumed that they are able to escape out of the tunnel by driving their vehicles. However, the scenarios could be completely different if they get trapped in a queue and cannot escape by use of the vehicles. Further, in railway tunnels, the tunnel users downstream of the fire could either pass the fire and escape to the upstream side or keep running downstream to a cross-passage or to the tunnel portal. In such cases, the longitudinal ventilation can potentially severely worsen the situation for tunnel users located downstream of the fire.

However, as a longitudinal ventilation system needs no extra space for ducts, it provides a very cheap solution for tunnel ventilation and is, therefore, attractive despite its limitations as a tunnel fire ventilation system. This is the main reason why the longitudinal ventilation is becoming more and more widespread nowadays. Note that in some tunnels with large slopes, natural ventilation could even produce air flows with air velocity greater than the critical velocity in case of a fire, and therefore, no mechanical fans would be required (Fig. 13.7).

The two most important parameters for a tunnel with longitudinal ventilation are the critical velocity and the back-layering length, which are discussed in detail in the following sections.

13.3.1 Critical Velocity

The critical velocity is defined as the minimum longitudinal ventilation velocity to prevent reverse flow of smoke from a fire in the tunnel (see Fig. 13.8). The problems of critical velocity and back-layering are important design parameters that have been investigated by many researchers [1–7].

There are mainly two types of models to estimate the critical velocity, that is, the critical Froude model and the nondimensional model, which will be discussed in the following in sequence.

13.3.1.1 Critical Froude Model

Thomas [1, 2] proposed that the velocity head of fresh air flow should be comparable or greater than the buoyancy head of smoke flow in order to prevent backlayering, and defined a critical Froude number, Fr_c, which could be expressed as follows:

$$\mathrm{Fr}_c = \frac{\Delta\rho g H}{\rho_o u_c^{\ 2}} \tag{13.1}$$

where $\Delta\rho$ is the density difference (kg/m^3), g is the gravitational acceleration (m/s^2), H is the tunnel height (m), ρ_o is the ambient density (kg/m^3), u_c is the critical velocity (m/s). Thomas [1, 2] suggested that the smoke backflow disappears as the critical Froude Number approaches 1. The proposed equation to predict the critical velocity was expressed as follows:

$$u_c = \left(\frac{g\dot{Q}H}{\rho_o c_p T_f A}\right)^{1/3} \tag{13.2}$$

where $\dot{Q}$ is the total heat release rate (HRR) (kW), c_p is the heat of capacity (kJ/(kg K)), T_f is the average downstream temperature (K), and A is the tunnel cross-sectional area (m^2).

Danziger and Kennedy [3, 4] argued that based on Lee et al.'s experiments [8], the critical Froude Number varied over a range of 4.5–6.7 and thus a critical Froude Number of 4.5 was recommended. Further, the convective HRR should be used in the equation rather than the total HRR. The equation including the critical Froude number can be expressed as:

$$u_c = \left(\frac{g\dot{Q}_c H}{\rho_o c_p T_f A \mathrm{Fr}_c}\right)^{1/3} \tag{13.3}$$

where the average downstream temperature is expressed as:

$$T_f = \frac{Q_c}{\rho_o c_p A u_c} + T_o$$

In the above equation, $\dot{Q}_c$ is the convective HRR (around 60–80 % of total HRR) and T_o is the ambient temperature (fresh air temperature).

However, note that Eq. (13.3) is the same as Thomas' equation with the exception that the critical Froude number is explicitly embedded and the convective HRR

is used. Further, only several data points from Lee et al.'s experiments with long ceiling flame lengths [8] were used in determining the critical Froude number.

According to Li et al.'s work [7], the critical Froude number is approximately a constant of 1.15 for small fires but varies significantly with the HRR for larger fires, with a value of around 4.5 for a very large tunnel fire.

Note that in Lee et al.'s experiments [8], only very large fires with long ceiling flame lengths were tested, and the Froude number of 4.5 also corresponds to a very large fire, with a dimensionless HRR of around 1.0. Using the data from Lee et al.'s tests we can obtain a dimensionless critical velocity of 0.43, which correlates very well with Li et al.'s work [7]. In other words, the critical value of 4.5 concluded by Kennedy [4] is not suitable for the entire range of fires, but only an approximation for some large tunnel fires.

In summary, a constant critical Froude number does not exist, and thus the critical Froude number is not a reasonable way to estimate the critical velocity for smoke control in longitudinally ventilated tunnel fires although it has been widely used historically.

Example 13.1 Calculate the critical velocity using Danziger and Kennedy's equation, that is Eq. (13.3), for a 5 MW car fire and a 30 MW bus fire, respectively, in a 6 m high and 10 m wide tunnel. The ambient temperature is 20 °C. Assume that the fraction of convective part in the HRR is 70 % and the ambient temperature is 20 °C.

Solution: In each case, an iteration procedure is generally required to obtain an exact solution of the critical velocity using Eq. (13.3).

1. *Firstly we assume that the critical velocity is 1.5 m/s and then the average gas temperature can be calculated:* $T_f = 0.7 \times 5000/(1.2 \times 1 \times 6 \times 10 \times 2.5) + 273 + 20 = 325$ *K. The critical velocity is estimated using Eq. (13.3), that is,* $u_c = [9.8 \times 0.7 \times 5000 \times 6/(1.2 \times 1 \times 410 \times 6 \times 9 \times 4.5)]^{1/3} = 1.25$ *m/s. This indicates the guessed value of 1.5 m/s is too high, and thus we should reduce it and recalculate the critical velocity. Repeat the process until the difference between guessed and calculated values are closely the same. The solution in this case is approximately 1.24 m/s.*
2. *Firstly we assume the critical velocity as 2.5 m/s and then the average gas temperature can be calculated:* $T_f = 0.7 \times 30000/(1.2 \times 1 \times 6 \times 10 \times 2.5) + 273 + 20 = 410$ *K. The critical velocity is estimated using Eq. (13.3), that is,* $u_c = [9.8 \times 0.7 \times 30000 \times 6/(1.2 \times 1 \times 410 \times 6 \times 9 \times 4.5]^{1/3} = 2.1$ *m/s. It can be concluded that the guessed value of 2.5 m/s is too high. Reduce it and repeat the process. The solution in this case is approximately 2.06 m/s.*

In reality, Danziger and Kennedy's equation is not recommended for use in estimation of the critical velocity. The reason why this example is given here is to make a comparison with other equations which will be further discussed in Example 13.2.

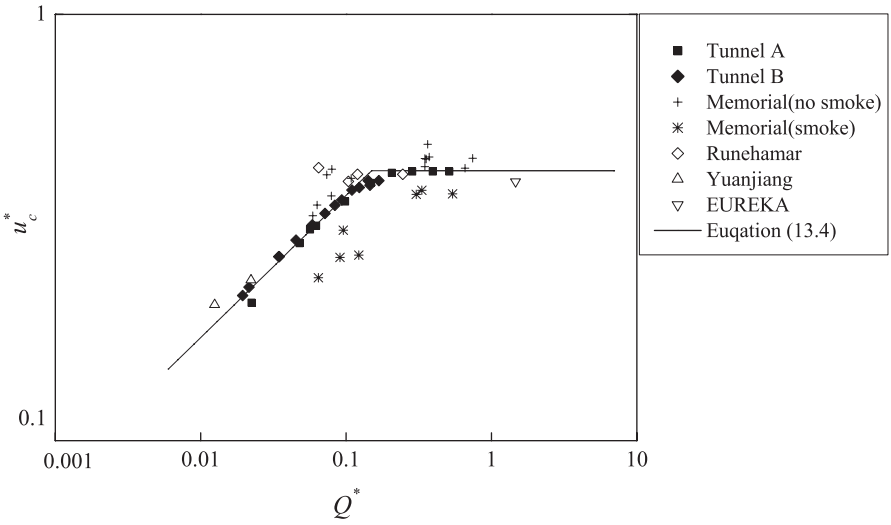

Fig. 13.9 Dimensionless critical velocity vs. dimensionless HRR

13.3.1.2 Non-dimensional Model

Oka and Atkinson [5] carried out a series of model-scale experiments to examine the relationship between the critical velocity and the HRR, taking different geometries and placements of the fire source into account. A dimensionless HRR and a dimensionless critical velocity were defined and a piecewise function was used to correlate their data. They found that the critical velocity becomes independent of the HRR in large fires. Wu and Bakar [6] carried out a series of model-scale experiments to investigate the critical velocity, accounting for varying tunnel cross sections, and correlated their results using hydraulic diameter instead of tunnel height. However, their test data for tunnel aspect ratio over one do not really support the use of the hydraulic diameter. The effect of tunnel width on critical velocity will be discussed later. Note that, in the above two series of experiments carried out by Oka and Atkinson [5] and Wu and Bakar [6], water spray devices were placed above the fire source to cool down the tunnel walls. This strategy is questionable due to the fact that the water spray significantly increases heat losses to the surroundings.

Li et al. [7] carried out experiments and theoretical analyses to investigate the critical velocity together with the back-layering length in tunnel fires. Two series of model-scale tests were carried out. Full-scale tunnel fire test data were also used for comparison. The results were correlated using the dimensionless HRR and the dimensionless critical velocity, as shown in Fig. 13.9. It can be seen that all the test data correlates reasonably well with the proposed equation. The critical velocity increases continuously, but more slowly, as the dimensionless HRR approaches 0.15, and then remains almost constant, independent of the HRR. A piecewise function was proposed to correlate the experimental data of these two tunnels, which can be expressed as [7]:

$$u_c^* = \begin{cases} 0.81Q^{*1/3}, & Q^* \le 0.15 \\ 0.43, & Q^* > 0.15 \end{cases} \tag{13.4}$$

where the dimensionless HRR, Q^*, and the dimensionless critical velocity, $u_c{}^*$, are defined as:

$$Q^* = \frac{\dot{Q}}{\rho_o c_p T_o g^{1/2} H^{5/2}}, \quad u_c^* = \frac{u_c}{\sqrt{gH}}$$

Example 13.2 Calculate the critical velocity using Li et al.'s equation, that is, Eq. (13.4), for a 5 MW car fire and a 30 MW bus fire, respectively, in a 6 m high and 10 m wide tunnel. The ambient temperature is 20 °C.

Solution:

1. *At first calculate* $Q^* = 5000/(1.2\times1\times293\times9.8^{1/2}\times6^{5/2}) = 0.051 < 0.15$, *then use Eq. (13.4):* $u_c^* = 0.81\times0.031^{1/3} = 0.30$. *For a 5 MW car fire, the critical velocity can be estimated:* $u_c = 0.25\times\sqrt{9.8\times6} = 2.3$ m/s.
2. *At first calculate* $Q^* = 30000/(1.2\times1\times293\times9.8^{1/2}\times6^{5/2}) = 0.31 > 0.15$. *According to Eq. (13.4):* $u_c^* = 0.43$. *For a 30 MW bus fire, the critical velocity can be estimated:* $u_c = 0.43\times\sqrt{9.8\times6} = 3.30$ m/s.

Comparing the values obtained using Li et al.'s equation (Example 13.2) to those obtained using Danziger and Kennedy's equation (Example 13.1) clearly shows that Danziger and Kennedy's equation gives very low critical velocities for both a 5 MW car fire and a 30 MW bus fire. Even for the 30 MW fire in the 6 m high tunnel, the critical velocity calculated using Danziger and Kennedy's equation is only 2.06 m/s. The selection of $Fr_c = 4.5$ for all fires may explain this difference. If the value of $Fr_c = 1.15$ for small fires [7] is used, the corresponding velocities would have been 1.95 m/s for the 5 MW and 3.25 m/s for the 30 MW, which is much closer to the values presented in Example 13.2.

The values obtained by Eq. (13.3) are apparently too low according to full-scale test data for small fires. For example, in the Runehamar tunnel fire test T0, the fire was a 6 MW pool fire at longitudinal velocity of 2.5 m/s, however, even under these conditions a small range of back-layering existed [9].

13.3.1.3 Influence of Vehicle Obstruction

Li et al. [7] systematically investigated the effect of vehicle obstruction on the critical velocity. They defined a reduction ratio for the critical velocity due to vehicle obstruction, ε to analyze their test data, which can be expressed as [7]:

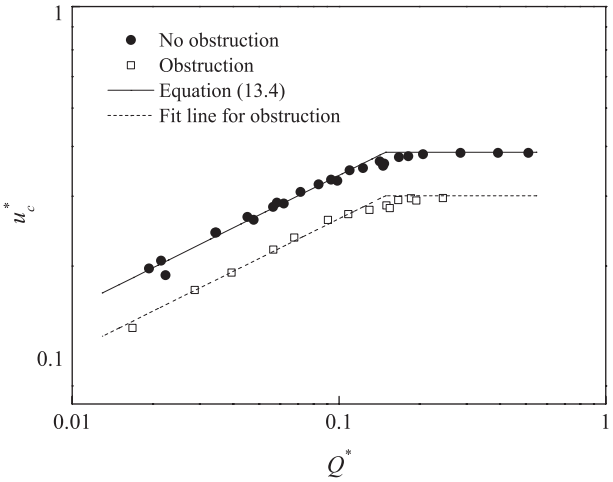

Fig. 13.10 Effect of vehicle obstruction on critical velocity [7]

$$\varepsilon = \frac{u_c - u_{c,ob}}{u_c} = \frac{u_c^* - u_{c,ob}^*}{u_c^*} \tag{13.5}$$

where the subscript *ob* indicates vehicle obstruction. The reduction ratio indicates how much the critical velocity is reduced due to the vehicle obstruction.

A comparison of the critical velocity in a tunnel with vehicle obstruction at the fire location and without vehicle obstruction is shown in Fig. 13.10. The ratio between the critical velocity in a tunnel with and without vehicle obstruction, is around 0.23, which means that the reduction ratio of the critical velocity due to the obstruction is 23%. In these tests, the blockage ratio, that is, the dimension ratio of model vehicle to model tunnel, is approximately 0.2, or 20% for both model tunnels. Consequently, the reduction ratio of critical velocity due to obstruction approximately equals the blockage ratio. In other words, the local critical velocity is almost the same, regardless of the vehicle obstruction. Oka and Atkinson's test data [5] show a similar trend. They found that the reduction ratio of critical velocity is 15% when a vehicle occupies around 12% of the tunnel cross section, and 40–45% when a vehicle occupies around 32% of the tunnel cross section. However, note that in their tests with a vehicle occupation of 32% of tunnel cross section, the fire source was significantly raised above the floor, and the effect could be equivalent to lower the tunnel height, which also reduces the critical velocity. Li et al. [7] concluded that as a conservative rule of thumb, the blockage ratio could be regarded as the reduction ratio of the critical velocity due to obstruction near the fire site, ε, from which the critical velocity for smoke control in an obstructed tunnel can be extrapolated.

The work by Li et al. [7] has further been verified by Lee and Tsai [10]. The obstructions were placed immediately upstream of the fire source, which also significantly increases the local velocity across the fire source and similar results were obtained.

In summary, the reduction ratio of the critical velocity due to vehicle obstruction near the fire site, ε, is approximately the same as the blockage ratio, that is, the dimension ratio of obstruction to tunnel.

13.3.1.4 Influence of Heat Release Rate in Large Fires

According to the above analysis, it is known that the critical velocity tends to be independent of the HRR for large fires. There have been many different explanations for this phenomenon. The phenomenon has been verified by large-scale tunnel fire tests, such as the Runehamar tunnel fire tests [9] and the Memorial tunnel fire tests [11].

Oka and Atkinson [5] argued that for large fires, the gas temperature is constant and as is the buoyancy force. However, according to the work by Li and Ingason [12, 13], the maximum ceiling gas temperatures under the critical conditions are much lower than the temperatures within the continuous flame zone, which indicates that the critical HRRs estimated using the constant flame temperature are much higher than the value obtained from the tests. Therefore, the explanation of constant gas temperatures is not plausible.

Wu and Bakar [6] attributed this to the appearance of an intermittent region where the gas velocity is constant. However, it should be kept in mind that the total pressure, that is, the sum of static pressure and dynamic pressure, controls the movement of smoke flows, rather than the gas velocity. Note that the dynamic pressure is not only a function of the gas velocity, but also related to the gas density.

Kunsch [14] carried out a theoretical analysis of smoke movement in a tunnel under no ventilation based on Alpert's work on ceiling jets under unconfined ceilings [15], and obtained a simple equation for estimation of the critical velocity. However, the equation predicts a very low critical HRR where the critical velocity starts to become independent of HRR. Further, to propose the explicit solution, the energy equation for weak plumes was used, which is not appropriate for large tunnel fires. Despite the theoretical weaknesses, the proposed equation is interesting in that it shows how the critical velocity varies with HRR and tunnel geometry.

It is known that the movement of smoke flows is controlled by the total pressure, that is, the sum of static pressure and dynamic pressure. Therefore, the critical velocity should be directly related to the total pressure. It can be speculated that the total pressure of smoke flows close to the impingement point should be almost constant for large fires. At the impingement point, part of dynamic pressure transforms to static pressure, and a large amount of energy is lost due to the impingement, especially for the part of smoke flowing to the upstream side. At present, a detailed understanding of ceiling smoke flow characteristics in tunnel fires is not available, and thus a complete theory of critical velocity cannot yet be fully developed.

13.3.1.5 Influence of Tunnel Width

As mentioned earlier the movement of smoke is controlled by the total pressure. Further, both the static pressure and dynamic pressure are intimately related to the fire properties such as gas temperature and flow. One of the key parameter for the fire plume in a tunnel fire is the maximum ceiling gas temperature. According to Chap. 8 on gas temperature, the maximum ceiling gas temperature in a tunnel fire is mainly related to the effective tunnel height, HRR and ventilation velocity, and almost independent of the tunnel width. This could also suggest that at the impingement position, the other fire properties are also independent of tunnel width, including the total pressure. Therefore, it can be speculated that the critical velocity to prevent the smoke back-layering, should also be approximately independent of the tunnel width.

There has been some experimental work on the influence of tunnel width on the critical velocity. Wu and Bakar [6] carried out a series of tests in model tunnels with aspect ratios (width/height) from 0.5 to 4.0. They correlated their results using the hydraulic diameter instead of the tunnel height. However, note that in most tunnels, the tunnel aspect ratio is in a range of 1–3. By analyzing their data in this range, it can be found that the average difference in the critical velocity is 1.0% between the tunnel aspect ratio of 1 and 2 and 7.0% between aspect ratio of 1 and 4. One may expect that the average difference is much lower than 7% between the aspect ratio of 1 and 3, and could be around 4%. Based on the above analysis of the test data, the influence of tunnel width can be ignored for most of tunnels.

Vauquelin and Wu [16] further investigated the influence of tunnel width on the critical velocity. The results of cold gas tests using a mixture of helium and air to simulate the hot gases and results from Wu and Bakar's tests [6] were analyzed. It was found that in both series of tests, for aspect ratios greater than unity, it is noticed that the critical velocity decreases when the width increases. They also found that for the aspect ratio lower than one and for high enough HRRs, the critical velocity significantly increases with tunnel width. By analyzing their data, it can also be found that the difference in the critical velocity for a tunnel aspect ratio in a range of 1–3 is also very small.

It should be kept in mind that in Wu and Bakar's [6] tests, the use of water sprays in the vicinity of the fire source could result in large error, especially when the tunnel is very wide, and in Vauquelin's tests [16] the cold gas was used which could differ significantly from a realistic fire.

Despite this, the test data show that the critical velocities in tunnels with aspect ratios of 1 to 3 are almost the same, and the effect of tunnel width on the critical velocity can be ignored. Only when the tunnel aspect ratio is significantly lower than 1 or greater than 3, should the effect of tunnel width be considered. According to the previous theoretical analysis, the critical velocity should be approximately independent of tunnel width, which correlates reasonably well with the test data.

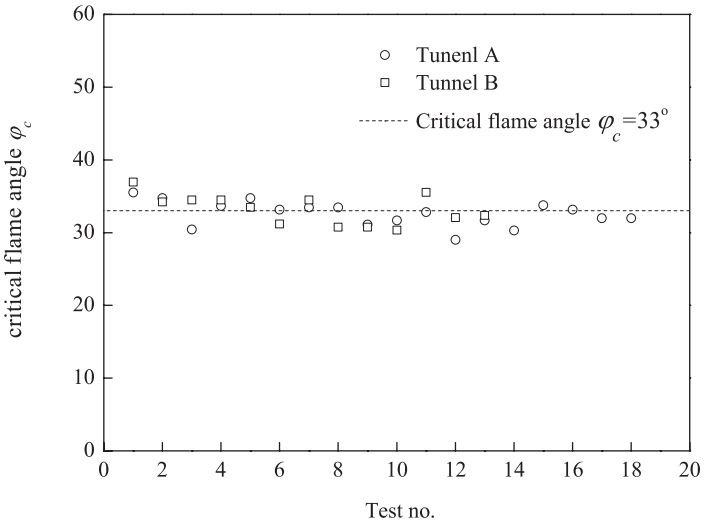

Fig. 13.11 The critical flame angle in a ventilated tunnel fire [17]

13.3.1.6 Critical Flame Angle

Li et al. [17] carried out a theoretical and experimental study of flame angles and found that there exists a critical flame angle corresponding to the critical velocity when the back-layering just disappears, and this critical flame angle is independent of the HRR. The critical flame angle can be simply expressed as [17]:

$$\sin \varphi_c = k_c \left(\frac{b_{f0}}{H} \right)^{-1/5} \tag{13.6}$$

where k_c is a coefficient, 0.42, b_{fo} is the radius of fire source (m) and H is the tunnel height (m). This means that for a given tunnel and fire source, the flame angle is always of the same value in a tunnel fire, independent of the HRR. Consequently, the position of the maximum temperature beneath the tunnel ceiling remains the same. Figure 13.11 plots two series of test data [17] which clearly shows that the critical angle approaches a constant.

The critical flame angle is a very interesting phenomenon. It could correspond to a state of balance between momentums of a plume and a ventilation flow. This should also relate to the momentum change before and after impingement of the fire plume, and distribution of the flows upstream and downstream after impingement.

13.3.1.7 Short Summary

The critical velocity in a tunnel fire can be estimated using Eq. (13.4). If the tunnel blockage ratio due to a burning vehicle or a vehicle right upstream of the fire is of

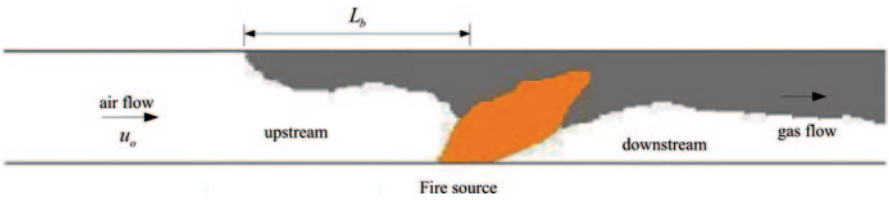

Fig. 13.12 A schematic diagram of back-layering in a tunnel fire

a significantly great value, the critical velocity could be multiplied by a correction factor, $(1-\varepsilon)$.

13.3.2 Back-Layering Length

The back-layering length, L_b (m), is defined as the length of the smoke back-layering upstream of the fire when the ventilation velocity is lower than the critical velocity (see Fig. 13.12).

In a longitudinally ventilated tunnel, a fresh air flow with a velocity not lower than the critical velocity at the designed HRR is created to prevent smoke back-layering, which means that the tunnel is free of smoke upstream of the fire site. However, smoke stratification downstream of the fire may not persist as the ventilation velocity is too high. For this reason, a new term, "confinement velocity", has been introduced. This is the velocity needed to prevent back-layering at a certain position, that is, to prevent further spreading upstream. Vauquelin and Telle [18] defined the "confinement velocity" as the longitudinal velocity, as induced by the extraction ventilation system, which is necessary to prevent smoke layer development after the last exhaust vent has been activated. The reason for using such a velocity is the attempt to control back-layering and, at the same time, to preserve certain stratification. Limited research has been performed on the confinement velocity and the back-layering length.

Thomas [1] gave a simple one dimensional theoretical analysis of the back-layering length in case of a fire in a longitudinally ventilated tunnel. He correlated the back-layering length with the Froude Number. Based on data of the back-layering length from small-scale experiments and one large-scale experiment, a correlation for the dimensionless back-layering length, L_b^*, that is, the ratio of back-layering length (L_b) to tunnel height (H), was proposed as follows:

$$L_b^* = \frac{L_b}{H} = 0.6\left(\frac{2gH\dot{Q}}{\rho_o T_o c_p u_o^3 A} - 5\right) \tag{13.7}$$

Vantelon et al. [19] carried out small-scale experiments in a 1.5 m long semicircular pipe with 0.15 m radius, and found that the ratio of back-layering length to tunnel height tended to vary as 0.3 power of a modified Richardson Number, which is defined as:

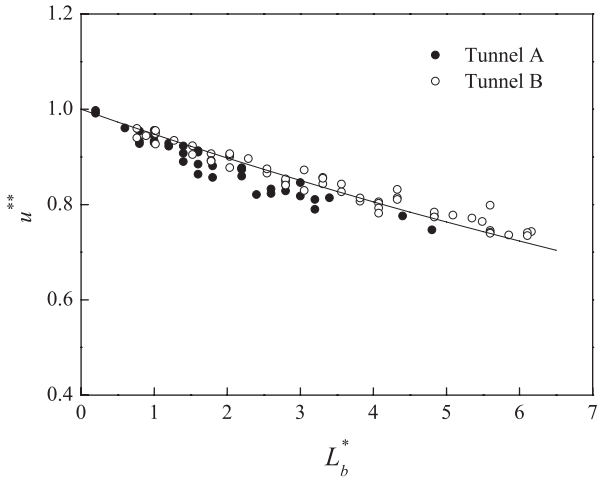

Fig. 13.13 Dimensionless confinement velocity vs. dimensionless back-layering length [7]

$$\mathrm{Ri}' = \frac{g\dot{Q}}{\rho_o T_o c_p u_o^3 H} \tag{13.8}$$

However, in Vantelon's tests, the HRRs were very small. Further, no equation was proposed to correlate all the test data.

Deberteix et al. [20] made detailed measurements of the back-layering length as well as the critical velocity in a model of the Paris metro with 0.163 m height, and related the back-layering length with a Richardson Number. However, according to their equation, the back-layering length is a negative value for a HRR of zero, which is not consistent with any physical laws.

Li et al. [7] carried out two series of tests in model-scale tunnels based on a dimensional analysis, and found that the back-layering length increases with the HRR for low HRRs and is nearly independent of HRR and dependent only on the ventilation velocity at higher HRRs. According to a dimensional analysis, the dimensionless back-layering length, L_b^*, was correlated with the ratio of longitudinal ventilation velocity to critical velocity, u^{**}, [7]:

$$L_b^* = \frac{L_b}{H} \propto f(u^{**}) = f(u^*/u_c^*) \tag{13.9}$$

The plot of dimensionless back-layering length against dimensionless confinement velocity u^{**} for two series of model-scale tests [7] is shown in Fig. 13.13. Clearly, it shows that the experimental data of back-layering length can be correlated into a universal form, which can be expressed as [7]:

$$u^{**} = \exp(-0.054 L_b^*) \tag{13.10}$$

It is shown that the relationship between the ratio of longitudinal ventilation velocity to critical velocity and the dimensionless back-layering length approximately follows an exponential relation. When the dimensionless HRR is less than 0.15, the back-layering length varies as one-third power of the modified Richardson number and is almost independent of the dimensionless HRR, that is, it depends only on the ventilation velocity at higher HRRs.

The dimensionless back-layering length in a tunnel fire can, therefore, be expressed as [7]:

$$L_b^* = \begin{cases} 18.5\ln(0.81Q^{*1/3}/u^*), & Q^* \le 0.15 \\ 18.5\ln(0.43/u^*), & Q^* > 0.15 \end{cases} \tag{13.11}$$

Note that the term $Q^{*1/3}/u^*$ equals the one-third power of the modified Richardson Number, and Eq. (13.10) could be transformed into [7]:

$$L_b^* = \begin{cases} 18.5\ln(0.81\mathrm{Ri}^{-1/3}) & Q^* \le 0.15 \\ 18.5\ln(0.43/u^*) & Q^* > 0.15 \end{cases} \tag{13.12}$$

This suggests that when the dimensionless HRR is lower than 0.15 the dimensionless back-layering length is indeed related to the modified Richardson number, however, at higher HRRs depends only on the ventilation velocity.

Li et al. [7] also investigated the effect of vehicle obstruction on the back-layering length. A very long vehicle was placed continuously along the tunnel. The results show that the back-layering length was reduced when the vehicle was placed inside the tunnel for a certain dimensionless confinement velocity. In other words, a small change in velocity will result in a greater change in back-layering length. The main reason is the enhanced heat transfer to the vehicle body which results in sharp decreases of gas temperature and buoyancy force, and thus the smoke front is arrested more easily. In reality, the blockage ratio is normally a small value and the vehicles upstream are generally located separately. Under these conditions, the effect of blockage on the back-layering length can be neglected.

Example 13.3 Calculate the back-layering length for a 30 MW bus fire in a 6 m high and 10 m wide tunnel at a longitudinal velocity of 2 m/s. The ambient temperature is 20 °c.

Solution: At first calculate $Q^* = 30000/(1.2 \times 1 \times 293 \times 9.8^{1/2} \times 6^{5/2}) = 0.31 > 0.15$, *then use Eq. (13.11):* $L_b^* = 18.5 \times \ln[0.43/(2/\sqrt{9.8 \times 6})] = 9.3$. *The back-layering length can therefore be estimated:* $L_b = L_b^* H = 9.3 \times 6 = 55.8$ m.

13.4 Smoke Extraction

Smoke extraction suggests that smoke flows (plume flow) arising from a fire are directly exhausted using extraction vents in the vicinity of the fire, see Fig. 13.14 where only three vents nearby the fire are activated to extract smoke flows.

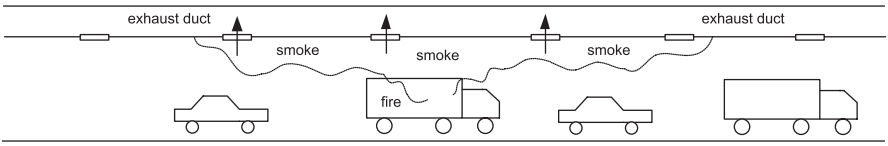

Fig. 13.14 Fire ventilation in a tunnel with point extraction ventilation

When designing an extraction system in a tunnel, the traditional method is to estimate a "smoke release rate" corresponding to the maximum design fire size, and then use this value to determine the capacity of the extraction system. However, in the fire community the smoke release rate generally refers to the production rate of smoke particles. This production rate is related to the mass flow rate of the fuel in kg/s and multiplied by the yield of smoke; see Eq. (7.13) and Table 7.4. The extraction systems should be designed to extract all the smoke flows. However, the smoke flow rate is not only dependent on the HRR, but also strongly depends on the ventilation and geometry of the tunnel. In other words, the smoke flow rate is not constant. Further, the traditional method always tries to avoid plugholing, that is, the smoke flows is extracted slowly in order to improve the efficiency, rather than efficiently to control the smoke flows. Ingason and Li [21] have shown that in order to efficiently control the smoke flow, that is, confine the smoke between the vents and the fire source, an extraction ventilation system must be powerful enough to create longitudinal flows from both sides. Otherwise the smoke flow will continually travel along the ceiling until finally the smoke front is trapped by the incoming flows, which could results in high risk of fire spread in a large tunnel fire.

The smoke extraction systems can be categorized into single point extraction system, two point extraction system, three points extraction system, etc., by the number of opened extraction vents during a fire. The configurations of these systems are different. However, the concept is essentially the same that incoming air flows with sufficiently large ventilation velocity should be supplied from both sides of these systems to successfully prevent smoke from spreading further [21]. Unfortunately in most practical applications, the main objective is only to partly remove the smoke flow. Therefore, the extraction capacity and the cost are significantly reduced. As the smoke flow cannot be completely controlled within a small region between vents and the fire source, it spreads to a much larger region. In the following, we focus on a discussion of how to completely control the smoke flow within a small region between vents and the fire source.

In a tunnel with a semi-transverse ventilation system or a transverse ventilation system as normal ventilation systems, the normal ventilation systems could be easily changed to smoke extraction systems, although the exhaust capacity generally needs to be raised. For a tunnel with a transverse ventilation system under normal ventilation, both vents can be designed to extract the smoke flow if possible, that is, by keeping the exhaust fans running and reversing the supply fans. However, in case that the supply vents are placed at floor level, these supply vents should not be used to extract the smoke flows or else the smoke layer will be destroyed

immediately, instead they should be closed to avoid the supply of too much oxygen to the fire site and to increase the efficiency of the smoke extraction system. For a tunnel with a semi-transverse ventilation system, if the vents are placed at the upper level of a tunnel cross-section, the vents nearby the fire site can be used to extract smoke flows.

A smoke extraction system needs to be operated with the assistance of a manual or an automatic fire detection system. In case of a fire, the location of the fire is determined by the fire detection system and then the extraction vent or vents nearby the fire site can be opened to extract smoke flows. The number of open vents will then depend on the fire size and the designed volume flow rate for each vent. Meanwhile, the other vents should remain closed, see Fig. 13.14.

In operation, other ventilation equipments, such as jet fans installed beneath the ceiling, may need to be operated together with the point extraction systems to produce the longitudinal flows from both sides to suppress smoke from spreading further.

Given that the fire and smoke flow will spread further, if more extraction vents with the same interval between two extraction vents are used at a given total exhaust flow rate, the smoke zone of a multipoint extraction system will inherently be wider than that with a single-point extraction system. Further, from the practical point of view, it is much easier to control an extraction system with smaller number of activated extraction vents, or densely distributed vents. In the following, a single point extraction system and two point extraction system are discussed. The general requirements for these two systems can be applied to extraction systems with more point vents.

13.4.1 Single Point Extraction Volume

In a single point extraction system, as shown in Fig. 13.15, the exhaust volume flow rate through the extraction vent is one key parameter. However, the exhaust volumetric flow rate varies significantly with the gas temperature of the smoke flow. This implies that different exhaust volume flow rates (m^3/s) will be present at different locations of the duct relative to the extraction vent, especially for a large fire which produces smoke flows with a very high gas temperature. Therefore, it is more reasonable to use the exhaust mass flow rate (kg/s) as a characteristic parameter of the extraction vent, rather than the exhaust volume flow rate.

An effective extraction system has been shown to be established when sufficient fresh air flows are supplied from both sides, to confine the fire and smoke to the zone between the fire source and the extraction vent for a single point extraction ventilation system. The fire and smoke flow cannot be confined if only the flow rate in the extraction vents are controlled, regardless of the ventilation velocities on both sides.

If the ventilation velocity is smaller than the critical velocity, the phenomenon of back-layering occurs. The distance between the smoke front on the left-hand side

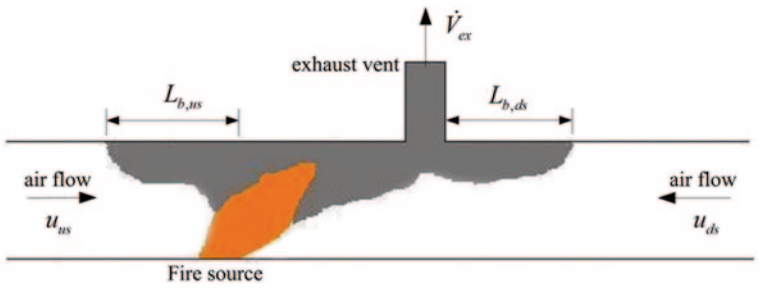

Fig. 13.15 Schematic diagram of single point extraction system

(in Fig. 13.15) and the fire source is defined as the back-layering length upstream of the fire source, $L_{b,\,us}$, and the distance between the extraction vent and the smoke front on the right-hand side is defined as the back-layering length downstream of the extraction vent, $L_{b,\,ds}$, as shown in Fig. 13.15.

It has been found from model-scale tests that in a single extraction system, fire and smoke flows upstream and downstream of the fire source can be fully controlled, if the ventilation velocity upstream of the fire source is at least 2.9 m/s in real-scale (0.6 m/s in model-scale), and the ventilation downstream of the extraction vent is above about 3.8 m/s (0.8 m/s), for a HGV fire or even several HGVs with HRR up to about 500 MW. Note that the critical velocity for smoke control in this tunnel with longitudinal ventilation is around 2.9 m/s in large-scale (0.6 m/s) according to the test data. This suggests the critical velocities for both sides are closely the same as the critical velocity for smoke control in a longitudinal ventilated tunnel fire. According to the law of mass conservation, the critical extraction mass flow rate of the extraction vent required for confining the smoke into a small region between the fire and the extraction vent, $\dot{m}_{ex}$, could approximately be estimated using:

$$\dot{m}_{ex} = 2\rho_o u_c A \tag{13.13}$$

where ρ_o is the fresh air density (kg/m^3), u_c is the critical velocity (m/s) and A is the tunnel cross-sectional area (m^2).

13.4.2 Two Point Extraction

In a two point extraction system, the system is designed such that fire and smoke is to be confined to the zone between the two extraction vents. Figure 13.16 gives a schematic diagram of a two point extraction system. The ventilation velocity across the fire source is dependent on the ventilation system of the specific tunnel. In most cases the systems is not symmetrical, and there is always a longitudinal flow across the fire source. In that case the fire source leans toward one side, as shown in Fig. 13.16. If the ventilation velocity across the fire source is very small, the smoke

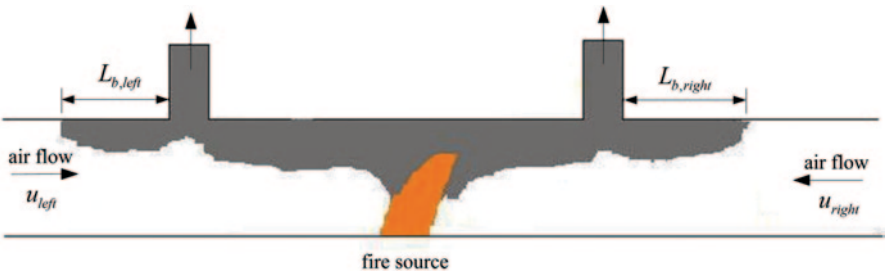

Fig. 13.16 Schematic diagram of a two point extraction system

stratification could be preserved relatively well in the zone between the two extraction vents at least at the early stage. Of course, the gas temperature in this zone is very high. However, the dangerous region can be confined by reducing the distance between two extraction vents, as the environment in the vicinity of the fire is not the focal point, but rather the environment outside this region.

In a two point extraction system, as shown in Fig. 13.16, the back-layering length on the left-hand side is defined as the distance between the smoke front and the left extraction vent. In a similar way the definition of the back-layering length on the right-hand side can be made.

In a two point extraction system, sufficient fresh air flows need to be supplied from both sides, to confine the fire and smoke to the zone between two extraction vents. The longitudinal ventilation velocities on both sides should be greater than about 2.9 m/s in large-scale (0.6 m/s in the model-scale), in HGV fires up to about 500 MW. In other words, the critical velocities for both sides are closely the same as the critical velocity for smoke control in a longitudinal ventilated tunnel fire. Therefore, Eq. (13.13) can also be used here to estimate the total extraction mass flow rate required for smoke control for a two point extraction system, and for each vent the extraction mass flow rate is approximately 50 % of the total value estimated.

13.4.3 Short Summary

In both single point and two point extraction systems, an effective smoke extraction system has been shown to be established when sufficient fresh air flows are supplied from both sides, to confine the fire and smoke to either the zone between the fire source and the extraction vent in a single point extraction ventilation system, or between two extraction vents in a two point extraction ventilation system. The ventilation velocities of fresh air flows from both sides required for smoke control in point extraction systems are approximately the same as the critical velocity for smoke control in a longitudinally ventilated tunnel fire. This general requirement could also be applied to extraction systems with more extraction vents. Further, it can be expected that the equations for back-layering length could also be applied to these types of systems.

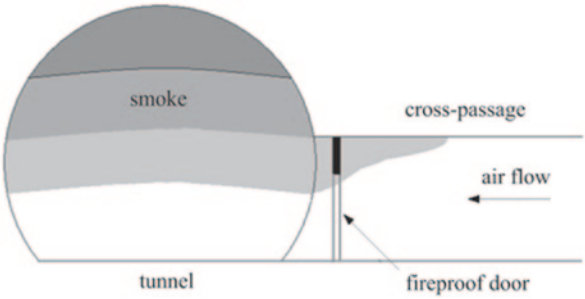

Fig. 13.17 The schematic diagram of smoke ingress into the cross-passage

Moreover, an efficient smoke extraction system significantly reduces the risk of the fire spreading outside the fire and smoke zone, as a result of efficiently removing the flame and heat produced by the fire from the tunnel.

Example 13.4 A 5 m high and 6 m wide submersed tunnel is designed with a single point extraction ventilation system for smoke control. Estimate the critical extraction mass flow rate required for confining the smoke into a small region between the fire and the extraction vent. The design fire is a HGV fire with a maximum heat releaser ate of 100 MW. The ambient temperature is 20 °c.

Solution: At first calculate $Q^* = 100000/(1.2\times1\times293\times9.8^{1/2}\times5^{5/2}) = 1.62 > 0.15$. *According to Eq. (13.4):* $u_c^* = 0.43$. *The critical velocity can be estimated:* $u_c = 0.43\times\sqrt{9.8\times5} = 3.0$ m/s . *The critical extraction mass flow rate can be estimated by:* $\dot{m}_g = 2\times1.2\times3.0\times5\times6 = 216$ kg/s *which corresponds to 177* m^3/s *under normal conditions.*

13.5 Cross-Passages

A tunnel cross-passage connects the main tunnel to a safe place, and provides a safe route for evacuation and rescue operations in a tunnel fire. The interval between two cross-passages ranges from 100 to 500 m. This distance could be determined based on analysis of smoke movement and evacuation in a given scenario.

In the event of a fire, enough fresh air should be supplied to keep the cross-passages free of smoke as shown in Fig. 13.17. The minimum ventilation velocity through an opened fireproof door that can prevent smoke from spreading into a cross-passage is defined as the critical velocity for smoke control in a cross-passage.

There has been some research on the critical velocity in a cross-passage, defined as the minimum ventilation velocity through the fireproof door that can prevent smoke ingress. Tarada [22] proposed a performance-based method to calculate a specific critical velocity for a cross passage located downstream of the fire, and simply regarded the critical Froude number as 4.5 which was found by Danziger

and Kennedy [3, 4] for use in smoke control in tunnels with longitudinal ventilation. In reality, according to the analysis in Sect. 13.3.1.1 we know that this value was wrongly determined by Danziger and Kennedy from Lee et al.'s small-scale experiments [8]. Despite this, based on the critical Froude number, Li et al. [23] proposed the following equation for the critical velocity in a tunnel cross-passage, u_{cc}, as:

$$u_{cc} = \frac{gH_d\dot{Q}_c}{\rho_o c_p A_d T_f Fr_{cc} V_{cc}^{\ 2}} - \frac{A_t}{A_d}u_t \tag{13.14}$$

where

$$T_f = \frac{\dot{Q}_c}{\rho_o c_p (u_t A_t + u_{cc} A_d)} + T_o, \qquad Fr_{cc} = \frac{gH_d(\rho_o - \rho_f)}{\rho_o u_{cc}^{\ 2}}$$

In the above equation, H_d is the height of the fireproof door (m), A_d is the cross-sectional area of the fireproof door (m^2), A_t is the tunnel cross-sectional area (m^2), u_t is the longitudinal velocity in the tunnel (m/s), T_f and ρ_f are the average gas temperature (K) and average gas density (kg/m^3) respectively.

Li et al. [23] carried out a series of model-scale tests, and the results showed that the critical Froude number varied significantly in a range of 4–17, and also decreased with the door height. Therefore, it was concluded that the critical Froude number method is not suitable for estimation of the critical velocity in a tunnel cross-passage. Note that if the critical Froude number is constant, the critical velocity in a cross-passage approximately varies as square root of the door height.

Based on a large amount of test data obtained, Li et al. [23] conducted a parametric study of critical velocity in a tunnel cross-passage, taking the fireproof door geometry, HRR, longitudinal ventilation velocity and fire source location all into account. It was found that the critical velocity in a tunnel cross-passage varies approximately as 3/2 power of the fireproof door height, as 1/3 power of the HRR and as exponential law of the ventilation velocity, and is almost independent of the fireproof door width. Based on the parametric study of the influencing factors on the critical velocity and a dimensional analysis, Li et al. [23] proposed a robust nondimensional equation to predict the critical velocity for smoke control in a cross-passage:

$$u_{cc}^* = 1.65H_d^* Q_t^{*1/3} \exp(-u_t^*) \tag{13.15}$$

where

$$u_{cc}^* = \frac{u_{cc}}{\sqrt{gH_d}}, \; H_d^* = \frac{H_d}{H_t}, \; Q_t^* = \frac{\dot{Q}}{\rho_o c_p T_o g^{1/2} H_t^{5/2}}, \; u_t^* = \frac{u_t}{\sqrt{gH_t}}$$

In the above equation, u_{cc}^* is the dimensionless critical velocity in the cross-passage, H_d^* is the dimensionless door height, Q_t^* is the dimensionless HRR in the tunnel, u_t^* dimensionless velocity in the tunnel.

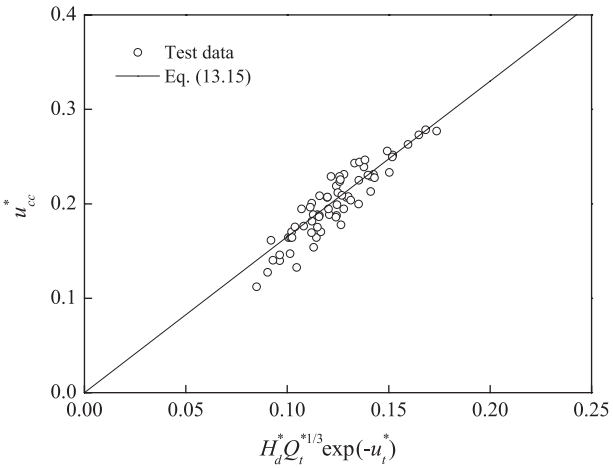

Fig. 13.18 Critical velocity for smoke control in cross-passages [23]

The results of critical velocity in the cross-passages with various geometries of fireproof doors (eight doors) [23] are shown in Fig. 13.18. It can be seen that all the experimental data correlates well with Eq. (13.15).

According to Li et al.'s [23] findings, the critical velocity in a tunnel cross-passage varies approximately as 3/2 power of the fireproof door height, and is independent of the fireproof door width. However, assuming that the critical Froude number is constant, the critical velocity in a cross-passage approximately will vary as square root of door height, which is contrary to the finding. This also proves that in reality the critical Froude number does not exist for smoke control in a tunnel cross-passage.

For very large fires, the equation proposed has not been verified, partly due to the fact that from the point of view of safety design, in such a large fire, the door in the cross-passage nearby the fire source will not be opened. Referring to the effect of HRR on critical velocity for smoke control in longitudinally ventilated tunnels, it could be expected that the critical velocity in a tunnel cross-passage estimated using Eq. (13.15) could be slightly conservative for very large fires.

Example 13.5 Two unidirectional tunnels are connected by cross-passages with an interval of 250 m. Longitudinal ventilation systems are used both under normal and emergency conditions. In case of a fire, a longitudinal flow with a velocity of around 3 m/s is created in the fire tunnel, and the other tunnel will be pressurized by the operation of jet fans installed at the exits and/or shaft fans. Estimate the critical ventilation velocity through the 2.2 m high fireproof door in the cross-passages, for a bus fire with a maximum heat releaser rate of 30 MW, and for a 5 MW car fire and a 100 MW HGV fire. The tunnels are both 6 m high and 10 m wide and the ambient temperature is 20 °c.

Solution: At first we calculate $Q^* = 30000/(1.2\times1\times293\times9.8^{1/2}\times6^{5/2}) = 0.31$, $H_d^* = 2.2/6 = 0.367$ *and* $u_t^* = 3/\sqrt{9.8\times6} = 0.39$, *then use Eq. (13.15), that is,* $u_{cc}^* = 1.65\times0.367\times0.31^{1/3}\exp(-0.39) = 0.276$. *The critical velocity in the tunnel cross-passage is:* $u_{cc} = 0.39\times\sqrt{9.8\times6} = 1.25$ m/s. *The fire ventilation system can be designed based on this value. Accordingly, the critical velocity in the tunnel cross-passage is 0.71 m/s for a HRR of 5 MW and 1.9 m/s for 100 MW.*

13.6 Rescue Station

The safety level in a very long tunnel can be significantly improved by use of a rescue station since the passengers can evacuate efficiently through the numerous cross-passages with a short spacing that would be expected in such a rescue station. Geber [24] studied the risk of the case that the incident train cannot arrive at any of emergency exits, that is, tunnel exits or emergency rescue stations, during an accident, assuming that the train can still travel over 20 km after an accident. The results show that the risk is around 30 % if the interval between the emergency exits is 30 km, and about 0.01 % if the interval is 20 km.

Nowadays, rescue stations are mainly specified in long railway tunnels. The main reason is the difficulty in evacuation of large amounts of passengers on a train during a short period. In case of a fire, a rescue station provides routes for evacuees at the evacuation stage and also provides the fire brigade a shortcut to attack the fire during the firefighting stage. In a rescue station in a long tunnel, emergency communication, emergency lights, fire hoses and other safety facilities are also provided. It can also be used as a construction site during the construction stage and as a maintenance station under normal condition. In a summary, a rescue station can be used for emergency evacuation, firefighting, maintenance, and construction.

Although rescue stations are not that common, they are of great interest from the point of view of smoke control, and therefore, we have added as special section for these types of systems.

13.6.1 Configuration and Function of Rescue Station

Table 13.1 gives a summary of the rescue stations constructed or under construction worldwide. All these tunnels are very long with a length from 16.2 to 53.9 km. It is shown clearly in Table 13.1 that most of these tunnels are twinbore single-track tunnels, except the Seikan tunnel. The length of the rescue stations ranges from 400 to 540 m. At least 6 cross-passages are available or planned in each rescue station in these very long tunnels.

Figure 13.19 shows an example of ventilation system in one rescue station of a long railway tunnel. One inclined shaft and one vertical shaft were built for emergency ventilation. In case of a fire in one tunnel, the inclined shaft supplies air flow

Table 13.1 The rescue stations constructed or under construction [25]

Tunnels	Year	Tunnel length	Tunnel type[a]	Rescue stations					
		(km)		Number	Type[b]	Length (m)	Interval (m)	Number of cross-passages	Ventilation
Seikan [26]	1988	53.9	Single	2	External + Service	480	40	13	Service supply
Gotthard Base [27]	2012/2013	57	Twin	2	External + Service	440/450	90	6	Shafts supply/exhaust
Lötschberg [27]	2007	34	Twin	1	Internal	450	90	6	Shafts supply/exhaust
Young Dong [28]	2000	16.2	Single	1	Internal	–	–	8	Shafts supply/exhaust
Koralm [29]	2016	32.8	Twin	1	Internal	400	50	8	Shafts supply
Guadarrama [30]	2007	28.4	Twin	1	Internal + Service	500	50	11	Service supply
Taihangshan [25]	2007	39.4[c]	Twin	2	Internal	540	60	9	Shafts supply/exhaust

[a] "Single" corresponds to a single-bore double-track tunnel, and "twin" correspond to twinbore single-track line tunnel

[b] "External" and "internal" correspond to external rescue station and internal rescue station respectively, and "service" means there is at least one additional service tunnel besides the main tunnels

[c] One 27.8 km long tunnel and one 11.6 km long tunnel are connected through a viaduct thus these two tunnels are considered together as one tunnel from the safety point of view

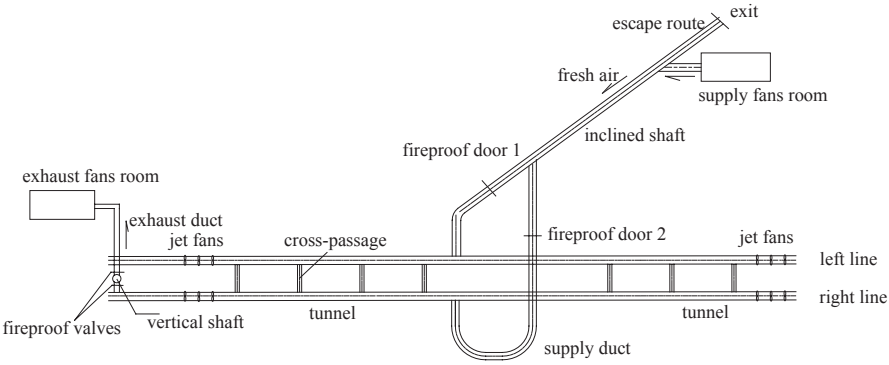

Fig. 13.19 A schematic view of the ventilation in rescue station of a tunnel

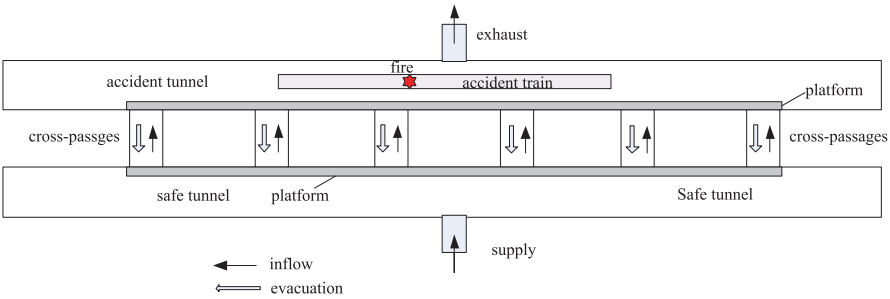

Fig. 13.20 The internal rescue station in a long tunnel

to the safe tunnel (nonincident tunnel) together with the jet fans, and the fresh air flows are forced to flow into the fire tunnel (incident tunnel). Part of the smoke flows are exhausted by the vertical shaft and the others are exhausted by the tunnel flows.

According to the placement of platforms and safe regions, the rescue stations in the long tunnels in Table 13.1 can be categorized into two types: internal rescue station and external rescue station, as shown in Fig. 13.20 and 13.21. Note that only six cross-passages are plotted here, in practice there could be more. In an internal rescue station, the two neighboring tunnels are connected together by cross-passages, and the neighboring tunnel is regarded as a safe region. In an external rescue station, the two running tunnels are independent and extra regions connected to the incident tunnel are regarded as safe regions. The extra regions could be a service tunnel or a pilot tunnel or a large space specifically built for the rescue station.

Note that for both types of rescue stations, the safe region is pressurized to push fresh air flow into the incident tunnel to prevent the smoke spread from the incident tunnel to the escape path or the safe region. Meanwhile, the smoke in the incident tunnel could be exhausted by the exhaust shaft available in the incident tunnel, or be blown away along a preferred direction by the forced longitudinal flow in the

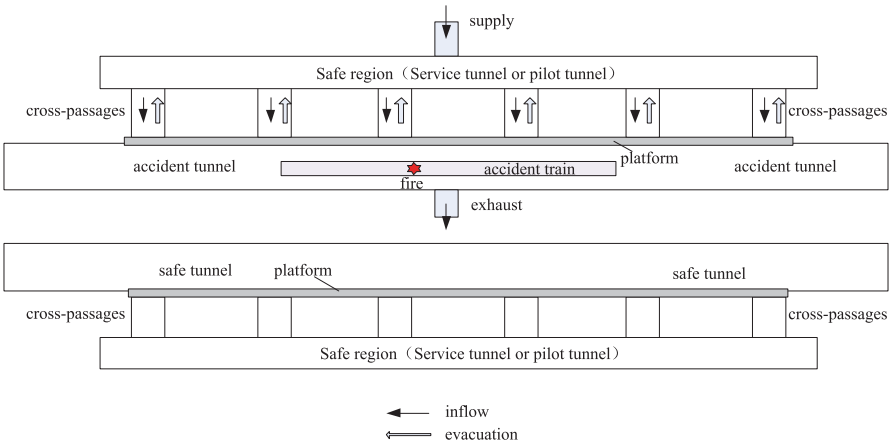

Fig. 13.21 The external rescue station in a long tunnel

fire tunnel. This is the basic pattern of smoke control in a rescue station in a very long tunnel.

13.6.2 Smoke Control

The main method of smoke control in a rescue station fire is to supply fresh air toward the incident tunnel to keep the cross-passages free of smoke. The smoke flow in the fire tunnel could also be exhausted through vertical shafts or blown out by the longitudinal flows.

Note that the main method of smoke control in a rescue station is similar to that in normal tunnel cross-passages nearby a fire. Therefore, the same model can be used for estimation of the critical velocities for smoke control in a rescue station.

Li et al. [25] carried out 54 model-scale rescue station fire tests to investigate the smoke control issues in the rescue station fires. The effects of HRR, train obstruction, fire source location, and ventilation condition on smoke control of the cross-passages in a rescue station were tested and analyzed. Their results show that the critical velocity in the cross-passage beside the fire source is the highest, and the critical velocity in cross-passages decreases with the distance away from the fire source. The critical velocities in the two neighboring cross-passages are about 80 to 90% of the maximum critical velocity. The critical velocities in the cross-passages approximately vary as 1/3 power law of the HRR and decreases due to the obstruction of the train. The average reduction ratio of critical velocity due to vehicle obstruction is about 14% on average, that is, slightly lower than the blockage ratio of the vehicle which was 20% in the tests [25]. The results of the critical velocity for smoke control in the rescue station correlate well with that in the normal cross-passages [23], despite the fact that the values obtained from the rescue station fire tests are slightly higher due to that the method of testing tended to conservative [25].

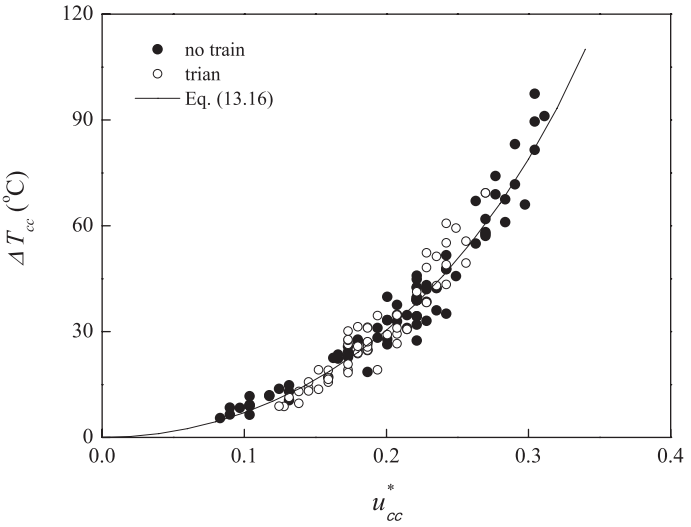

Fig. 13.22 Critical smoke temperatures vs. critical velocities in the cross-passages [25]

13.6.3 Gas Temperature Beside the Door

Smoke temperature and smoke layer height beside a door are key parameters to determine whether evacuees can evacuate through the door. Li et al. [25] conducted both theoretical and experimental analyses of the critical gas temperature beside the door of a cross-passage, which is defined as the smoke layer temperature beside the fireproof door under the critical condition. The critical gas temperature can be correlated well with the critical velocities in the cross-passages. A simple equation, which correlates very well with the experimental data (see Fig. 13.22) was obtained to estimate the critical gas temperature, ΔT_{cc}, which is expressed as [25]:

$$\Delta T_{cc} = \frac{T_o u_{cc}^{*2}}{0.42 - u_{cc}^{*2}} \tag{13.16}$$

The smoke layer height beside the door under the critical condition was also investigated and it has been shown that the smoke layer height beside the door is directly related to the critical gas temperature. Li et al. [25] also found that the gas temperature beside the door is insensitive to the flow velocity through the door and the critical gas temperature can be regarded as a characteristic gas temperature beside the door in a cross-passage. Therefore, based on the calculation of critical velocity in a cross-passage, the characteristic gas temperature beside the door can be estimated using the above equation.

13.6.4 Fireproof Door Height

Li et al. [25] also investigated the smoke layer height beside the door under critical conditions. It has been shown that the smoke layer height beside the door is directly related to the critical gas temperature. The fireproof door height should not be lower than 2.2 m to ensure a smoke layer height above approx. 1.74 m [25]. From this view point, the fireproof door height should be as high as possible. However, in order to reduce the critical velocity for smoke control in the cross-passages, the fireproof door height should be as low as possible. As a consequence, a fireproof door height of 2.2 m is proposed as a reasonable tradeoff value [25].

Example 13.6 Estimate the critical ventilation velocity through the 2.2 m high fireproof doors in the cross-passages of a rescue station in a railway tunnel and estimate the gas temperature right beside the door, assuming that the design fire is 30 MW. Extraction vents placed along the tunnel ceiling with an interval of 50 m are opened to extract the smoke flows, and the longitudinal velocity across the fire is around 0.5 m/s. The cross sections on each side of the rescue station are 8 m high and 8 m wide and the ambient temperature is 20 °C.

Solution: The equation for normal tunnel cross-passage, Eq. (13.15), can be used for estimation of critical velocity for smoke control in the cross-passages in a rescue station. At first calculate $Q^* = 30000/(1.2 \times 1 \times 293 \times 9.8^{1/2} \times 8^{5/2}) = 0.15$, $H_d^* = 2.2/8 = 0.275$ *and* $u_t^* = 0.5/\sqrt{9.8 \times 6} = 0.056$, *then use Eq. (13.15), that is,* $u_{cc}^* = 1.65 \times 0.275 \times 0.15^{1/3} \exp(-0.056) = 0.23$. *The maximum critical velocity in the cross-passage downstream is:* $u_{cc} = 0.23 \times \sqrt{9.8 \times 6} = 1.07$ m/s. *The critical velocity for smoke control is slightly lower than this value in the other cross-passages, however, this value should be used for design of the fire ventilation system in a rescue station since, the location of a fire is arbitrarily distributed along the rescue station.*

The excess gas temperature beside the door can be estimated using Eq. (13.16), that is, $\Delta T_{cc} = (273 + 20) \times 0.23^2/(0.42 - 0.23^2) = 42\,°c$, *and the gas temperature beside the door is:* $T_{cc} = 20 + 42 = 62\,°c$. *This temperature is not so high due to that the tunnel is very high compared to the height of the fireproof door. This also indicates that the thermal environment for evacuation through cross-passages is much better in a railway tunnel than a metro tunnel for a given HRR.*

13.7 A Simple Model of Longitudinal Flows

A simple theoretical model of ventilation flows in tunnel fires has been proposed by Ingason et al. [31] to calculate the ventilation velocity in a tunnel under natural ventilation or longitudinal ventilation. This model is based on the general flow theories for one-dimensional turbulent duct flow (Bernoulli's law). The pressure

equilibrium in the tunnel during a fire under external wind toward the portals can be expressed as follows:

$$\Delta p_{fan} \pm \Delta p_w \pm \Delta p_T = \Delta p_{in} + \Delta p_e + \Delta p_{fr} + \Delta p_{HGV} + \Delta p_{ob} \tag{13.17}$$

where Δp_{fan} is the pressure change created by the fan (Pa), Δp_w, is the wind pressure difference between the portals (Pa) where the $\pm$ sign determines by the direction of the main flow within the tunnel, Δp_T is the pressure difference due to density variation created by the fire (Pa) where the ± sign determines if the thermal pressure force is enhancing or oppose the main flow within the tunnel, Δp_{in} and Δp_e are the pressure loss (Pa) at the inlet and the exit of the tunnel, respectively, Δp_{fr} is the pressure loss due to wall friction (Pa), Δp_{HGV}, is the pressure loss due to the presence of the HGV mock-up (Pa), and Δp_{ob} is the total pressure loss due to other flow obstruction inside the tunnel (Pa). In the following each term in the equation will be discussed in more details.

The pressure change created by the mobile fan, $\Delta p_{fan,\,i}$, can be expressed as:

$$\Delta p_{fan} = \eta \frac{I_{fan}}{A_t} \tag{13.18}$$

where the momentum flux, that is, impulse force of the fan, $I_{fan} = \dot{m}_{fan} u_{fan}$ (N), and η is the efficiency of the impulse force of the fan to create the longitudinal flow in the tunnel, $\dot{m}$ is the mass flow rate of the fan (kg/s), A_t is the tunnel cross-sectional area (m^2). For jet fans placed separately in the tunnel, the efficiency is normally around 0.9.

The pressure difference due to buoyancy created by the fire, Δp_T, can be expressed as:

$$\Delta p_T = \left(1 - \frac{T_e}{T_m}\right) \rho_e g \Delta h \tag{13.19}$$

The stack height difference, Δh (m), can be calculated as $\Delta h = \theta \times L_{ds}/100$ where θ is the slope in percent and L_{ds} is the tunnel length downstream of the fire (m). For simplicity we use a mean temperature, T_m (K), as a representative temperature of the region between the fire source and downstream exit which will be discussed later.

The static pressure loss due to the inflow at the entrance of the tunnel, Δp_{in}, can be obtained by the following equation:

$$\Delta p_{in} = \xi_{in} \frac{1}{2} \rho_o u_o^2 \tag{13.20}$$

and the static pressure loss due to the outflow of the tunnel, Δp_e, is:

$$\Delta p_e = \xi_e \frac{T_e}{T_o} \frac{1}{2} \rho_o u_o^2 \tag{13.21}$$

where u_o is the average longitudinal fresh air velocity over the cross section (m/s) and T_e is the hot gas temperature in Kelvin (K) at the outlet of the tunnel. The pressure loss coefficient at the inlet is $\xi_{in}=0.5$ and at the exit $\xi_e=1$ [32].

The pressure loss due to friction can be obtained from the following equation:

$$\Delta p_{fr} = \frac{f}{D}\left[L + L_{ds}\left(\frac{T_m}{T_0}-1\right)\right]\frac{1}{2}\rho_0 u_0^2 \tag{13.22}$$

where L is the tunnel length (m), L_{ds} is the downstream tunnel length (m), f is the Darcy–Weisbach friction factor.

The wind pressure difference between the portals, Δp_w, can be expressed as:

$$\Delta p_w = \left(\zeta_{in} + \zeta_e + f\frac{L}{D}\right)\frac{1}{2}\rho_o u_i^2 \tag{13.23}$$

where the initial wind velocity inside the tunnel before the fire occurs is u_i. This velocity has to be measured or known. The friction coefficient, f, can be found from the Moody chart [32] or using other equations for flow resistance (see Chap. 10 on heat flux), based on the relative roughness of the tunnel surfaces and the Reynold number in a specific case. The total local friction coefficient ζ in a tunnel mainly consists of the pressure losses at the inlet and exit.

The burning vehicles induce a certain hydraulic resistance to the airflow. There could be some obstructions located inside the tunnel such as vehicles trapped in a tunnel fire or measuring cabins in a test. The pressure loss due to vehicles and obstructions can be approximated by the following equation:

$$\Delta p_{ob} = \xi_{ob}\frac{T_g}{T_o}\frac{1}{2}\rho_o u_o^2 \tag{13.24}$$

where T_g is the average gas temperature in Kelvin close to the vehicle or obstruction, and the pressure loss coefficient for a flow passing an obstruction in a tube can be calculated according to the following equation [32]:

$$\xi_{ob} = 1.15 c_x \frac{A_{ob}/A_p}{(1-\gamma A_{ob}/A_p)^3}\left(1-\frac{2y}{D}\right)^{1/3} \tag{13.25}$$

where the drag coefficient, c_x, is determined from tables given by Fried and Idelchick [32], y is the distance between the centre of the body and the wall (m), D is the height or diameter of the cross section (m) and γ is the correction factor for the effect of the body shape and contraction of the transverse cross section of the tube. For simplicity, generally it could be assumed that the object is a cube which means that c_x is 1.05 and γ is 1.5.

Combing all the equations in this section, we have a solution for the average longitudinal velocity under ambient conditions:

$$u_0 = \sqrt{\frac{2}{\rho_0}} \sqrt{\frac{\eta \frac{I_{fan}}{A_t} \pm \rho_o g \Delta h \left(1 - \frac{T_o}{T_m}\right) \pm \Delta p_w}{\xi_{in} + \xi_e \frac{T_e}{T_o} + \frac{f}{D}\left[L + L_{ds}\left(\frac{T_m}{T_o} - 1\right)\right] + \xi_{HGV} \frac{T_f}{T_o} + \xi_{ob} \frac{T_g}{T_o}}} \tag{13.26}$$

This suggests that the mass flow rate of the ventilation flow in the tunnel, $\dot{m}$ (kg/s), can be estimated using:

$$\dot{m} = \rho_o u_o A_t \tag{13.27}$$

The gas temperatures in the above equations need explicit expression in order to calculate the average longitudinal velocity. Assuming that the radiative energy occupies 1/3 of the total HRR, the average gas temperature at the fire site, T_f (K), can be calculated according to the following equation [31]:

$$T_f = T_o + \frac{2}{3} \frac{\dot{Q}}{\dot{m} c_p} \tag{13.28}$$

The mean temperature, existing in the expressions of the friction pressure loss and the thermal pressure difference, plays a key role in the calculation of longitudinal velocity inside the tunnel. The mean temperature is a representative temperature of the region between the fire source and downstream exit. Ingason et al. [31] proposed two possibly feasible methods to calculate the mean temperature. The first method is to use the average temperature at the middle point between the fire source and the downstream exit by the following equation [33]:

$$\Delta T_m = \Delta T_f \exp\left(-\frac{h w_p}{\dot{m} c_p} x\right) \tag{13.29}$$

where h is the total heat transfer coefficient (kW/(m^2 K)) and w_p is the wet perimeter of the tunnel (m).

The second method is to use an average temperature based on the energy equilibrium of the downstream region. Considering the region between the fire source and downstream exit as a control volume, the conservation of energy can be expressed as follows [31]:

$$\Delta T_m = \frac{2}{3} \frac{\dot{Q}}{\dot{m} c_p + h w_p L_{ds}} \tag{13.30}$$

Ingason et al. [31] compared these two methods and found that the first method gave a best fit to the data from Runehamar tunnel fire tests, while the second method overestimated the mean temperature despite its clearer physical meaning. How-

ever, it could be expected that if the mean temperature based on the first method is close to ambient, a larger error could be induced and the second method could produce better results.

Ingason and Lönnermark [33] validated this equation and the results from Runehamar tunnel fire tests show that a total heat transfer coefficient of 0.025 kW/m^2 gives the best fit to the test data.

The above equations have been validated by Ingason et al. [31] using data from the Runehamar tunnel fire tests, and can be used to simply estimate the ventilation flows in a tunnel fire.

Note that under natural ventilation, the proposed equations could still be valid. The only difference is the absence of the fans.

However, it should always be kept in mind that the one-dimensional theoretical model presented here is not valid if the longitudinal velocity is very low, for example, lower than 1 m/s.

Example 13.7 What is the average longitudinal ventilation velocity at the ambient condition in a submersed tunnel with a 50 MW fire at 500 m from the right tunnel portal? The tunnel has a 3 % downward slope to the middle of the tunnel and then a 3 % upward slope to the exit. The tunnel geometry is $L = 2$ km, $H = 6$ m, $W = 9$ m. The ambient temperature is 20 °C. The sprayed tube walls have a roughness of around 5 cm on average and the friction coefficient is around 0.018 for turbulent flows.

Solution: Note that in a sloping tunnel, the buoyancy force is only attributed to the section between the fire source and the exit of smoke flow. Therefore, the stack height difference: $\Delta h = 3 \times 500/100 = 15$ *m.*

Since the mean temperature *needs to be estimated based on the mass flow rate, we firstly assume* $u_o = 2.5$ *m/s. Then estimate the mass flow rate using Eq. (13.27):* $\dot{m} = 1.2 \times 2.5 \times 6 \times 9 = 162$ *kg/s, and the maximum temperature using Eq. (13.28):* $\Delta T_f = (2/3) \times 50000/(162 \times 1) = 206$ *K.*

Assuming $h = 0.025$ *kW/(m*^{2} *K), the mean temperature can be estimated using the first method, that is, Eq. (13.29):* $\Delta T_m = 206 \times \exp(-0.025 \times 30 \times (500/2)/(162 \times 1) = 65$ *K.*

In a similar way, the exit temperature can be estimated to be 313 K. The equivalent diameter of the tunnel is 7.2 m. Therefore, according to Eq. (13.26), the longitudinal velocity can be calculated:

$$u_0 = \sqrt{\frac{2}{1.2}} \sqrt{\frac{1.2 \times 9.8 \times 15 \times \left(1 - \dfrac{293}{293+25}\right)}{0.5 + 1 \times \dfrac{313}{293} + \dfrac{0.018}{7.2}\left[1500 + 500\left(\dfrac{293+65}{293} - 1\right)\right]}} = 2.79 \text{ m/s}$$

Note that the obtained value of 2.79 m/s is greater than the assumed value of 2.5 m/s, therefore, we need to assume a lower value for the longitudinal velocity. Second cal-

culation using a value of 2.79 m/s gives a value of 2.80 m/s, which correlate well with each other. The exact solution is 2.80 m/s.

We may check the second method for the mean temperature. The calculated longitudinal velocity is 2.69 m/s. Clearly, the value is lower than that obtained using the first method, as observed by Ingason et al. [31].

If there are jet fans or exhaust fans existing in the tunnel or shaft, we may simply estimate the pressure rise using Eq. (13.18).

13.8 Summary

Ventilation is one of the major measures at tunnel designers disposal to mitigate the effect of fire and smoke, to aid evacuation, rescue services, and firefighting in a tunnel fire. In this Chapter, various normal ventilation systems are briefly described before the introduction of fire ventilation systems. Further, fire ventilation systems, including longitudinal ventilation and point extraction ventilation systems, are discussed in great detail.

For longitudinal ventilation, critical velocity and back-layering length are the two key issues for smoke control. It is shown that a constant critical Froude number does not exist, and thus the critical Froude number is not a reasonable estimate of the critical velocity. Instead, a nondimensional model, that is, Eq. (13.4), gives better prediction of the critical velocity. The effect of vehicle obstruction and tunnel width, influence of HRR on critical velocity are also investigated, and the critical flame angles are shortly discussed. The back-layering length is correlated well with the critical velocity using Eq. (13.10) which can be used to estimate the back-layering length in a tunnel fire.

Further, fire ventilation in tunnel cross-passages is discussed. The critical velocity for smoke control in a tunnel cross-passage varies approximately as 3/2 power of the fireproof door height, as one-third power of the HRR and as exponential law of the ventilation velocity, almost independent of the fireproof door width. A useful equation, Eq. (13.14), is proposed to estimate the critical velocity in a tunnel cross-passage.

Smoke control in rescue stations is also investigated. There are two types of rescue stations, that is, internal rescue station and external rescue station. For both types of rescue stations, the safe tunnel is pressurized to push fresh air flow into the fire tunnel to prevent smoke spread into the safe region. Meanwhile, the smoke in the incident tunnel could be exhausted by the exhaust shaft or be blown away by the forced longitudinal flows. Note that the main method of smoke control in a rescue station is similar to that in the normal cross-passages nearby a fire. Therefore, the same model can be used for estimation of the critical velocities for smoke control in a rescue station. Based on the calculation of critical velocity, the gas temperature beside the door can also be estimated using Eq. (13.15).

A simple one-dimensional model of longitudinal flows is introduced for calculation of longitudinal ventilation velocity in a tunnel fire with natural ventilation or mechanical ventilation. However, it should always be born in mind that the one-

dimensional theoretical model presented here is not valid if the longitudinal velocity is very low.

References

1. Thomas P (1958) The movement of buoyant fluid against a stream and the venting of underground fires. Fire Research Note No. 351. Fire Research Station, Boreham Wood
2. Thomas PH (1968) The Movement of Smoke in Horizontal Passages Against an Air Flow. Fire Research Note No. 723. Fire Research Station, Boreham Wood
3. Danziger NH, Kennedy WD Longitudinal Ventilation Analysis for the Glenwood Canyon Tunnels. In: Fourth International Symposium on the Aerodynamics & Ventilation of Vehicle Tunnels, York, UK, 23–25 March 1982. BHRA Fluid Engineering, pp 169–186
4. Kennedy W. D. Critical velocity: Past, Present and Future. In: Seminar of Smoke and Critical Velocity in Tunnels, London: JFL Lowndes, 1996, pp. 305–322, 9–11 March 1996. JFL Lowndes, pp 305–322
5. Oka Y, Atkinson GT (1995) Control of Smoke Flow in Tunnel Fires. Fire Safety Journal 25:305–322
6. Wu Y, Bakar MZA (2000) Control of smoke flow in tunnel fires using longitudinal ventilation systems—a study of the critical velocity. Fire Safety Journal 35:363–390
7. Li YZ, Lei B, Ingason H (2010) Study of critical velocity and backlayering length in longitudinally ventilated tunnel fires. Fire Safety Journal 45:361–370
8. Lee CK, Chaiken RF, Singer JM (1979) Interaction between duct fires and ventilation flow: an experimental study. Combustion Science and Technology 20:59–72.
9. Ingason H, Lönnermark A, Li YZ (2011) Runehamar Tunnel Fire Tests. SP Technicial Research Institute, SP Report 2011:55
10. Lee Y-P, Tsai K-C (2012) Effect of vehicular blockage on critical ventilation velocity and tunnel fire behavior in longitudinally ventilated tunnels. Fire Safety Journal 53:35–42
11. Memorial Tunnel Fire Ventilation Test Program—Test Report (1995). Massachusetts Highway Department and Federal Highway Administration, Massachusetts
12. Li YZ, Ingason H (2012) The maximum ceiling gas temperature in a large tunnel fire. Fire Safety Journal 48:38–48
13. Ingason H, Li YZ New concept for design fires in tunnels. In: Proceedings from the Fifth International Symposium on Tunnel Safety and Security (ISTSS 2012), New York, USA, 14–16 March 2012. SP Technical Research Institute of Sweden, pp 603–612
14. Kunsch JP (2002) Simple Model for Control of Fire Gases in a Ventilated Tunnel. Fire Safety Journal 37:67–81
15. Alpert RL (1975) Turbulent ceiling-jet induced by large-scale fires. Fire Technology 11:197–213
16. Vauquelin O, Wu Y (2006) Influence of tunnel width on longitudinal smoke control. Fire Safety Journal 41:420–426
17. Li YZ, Ingason H (2014) Position of Maximum Ceiling Temperature in a Tunnel Fire. Fire Technology 50:889–905
18. Vauquelin O, Telle D (2005) Definition and experimental evaluation of the smoke "confinement velocity" in tunnel fires. Fire Safety Journal 40:320–330
19. Vantelon JP, Guelzim A, Quach D, Son D, K., Gabay D, Dallest D Investigation of Fire-Induced Smoke Movement in Tunnels and Stations: An Application to the Paris Metro. In: IAFSS Fire Safety Science-Proceedings of the third international symposium, Edinburg, 1991. pp. 907–918

20. Deberteix P., Gabay D., Blay D. Experimental study of fire-induced smoke propagation in a tunnel in the presence of longitudinal ventilation. In: Proceedings of the International Conference on Tunnel Fires and Escape from Tunnels, Washington, 2001. pp 257–265
21. Ingason H, Li YZ (2011) Model scale tunnel fire tests with point extraction ventilation. Journal of Fire Protection Engineering 21 (1):5–36
22. Tarada F. Critical Velocities for Smoke Control in Tunnel Cross-passages. In: 1st International Conference on Major Tunnel and Infrastructure Projects, Taiwan, 2000.
23. Li YZ, Lei B, Ingason H (2013) Theoretical and experimental study of critical velocity for smoke control in a tunnel cross-passage. Fire Technology 49:435–449
24. Gerber P. Quantitative risk assessment and risk-based design of the Gotthard Base Tunnel. In: Proceedings of the 4th International Conference Safety in Road and Rail Tunnels, Madrid, Spain, 2006. pp 395–404
25. Li YZ, Lei B, Ingason H (2012) Scale modeling and numerical simulation of smoke control for rescue stations in long railway tunnels. Journal of Fire Protection Engineering 22 (2):101–131
26. Ozawa S. Ventilation and Fire Countermeasure in Seikan Tunnel. In: 6th Int. Symp. on Aerodynamics and Ventilation of Vehicle Tunnels, England, 1988. pp 481–493
27. Rudin C. Fires in long railway tunnels—the ventilation concepts adopted in the AlpTransit projects. In: 10th Int. Symp. on Aerodynamics and Ventilation of Vehicle Tunnels, Boston, 2000. pp 481–493
28. Tarada F., Bopp R., Nyfeler S. Ventilation and risk control of the Young Dong Rail Tunnel in Korea. In: 1st International Conference on Major Tunnel and Infrastructure Projects, Taiwan, 2000.
29. Bassler A., Bopp R., Scherer O., et al. Ventilation of emergency station in the Koralm tunnel. In: 12th International Symposium on Aerodynamics and Ventilation of Vehicle Tunnels, Portoroz, Slovenia, 2006.
30. Hilar M., Srb M. Long railway tunnels—comparison of major projects. In: WTC 2009, Budapest, Hungary, 2009.
31. Ingason H, Lönnermark A, Li YZ (2012) Model of ventilation flows during large tunnel fires. Tunneling and Underground Space Technology 30:64–73
32. Fried E., Idelchick I.E. (1989) Flow Resistance: A Design Guide for Engineers. Hemisphere Publishing Corporation, New York
33. Ingason H, Lönnermark A (2005) Heat Release Rates from Heavy Goods Vehicle Trailers in Tunnels. Fire Safety Journal 40:646–668

Chapter 14
Visibility

Abstract Visibility is very important for evacuation during a fire and, therefore, a very important parameter for fire safety in a tunnel. There are different methods for estimating the visibility in smoke-filled spaces, using mass-specific extinction coefficient or the mass optical density. For both methodologies there are experimental values available for some materials of interest. First, the mass extinction coefficient methodology is presented and at the end compared and correlated to the mass optical density methodology. Values of these parameters for selected materials are presented and conversion of values for one of the parameters into the other is discussed. Finally, the effect on the walking speed during egress is discussed.

Keywords Visibility · Extinction coefficient · Optical density · Egress

14.1 Introduction

Fire safety in tunnels relies to a large extent on the principle of self-evacuation. Visibility is one of the most important parameter affecting the possibilities for safe egress. Although reduced visibility in itself does not lead to incapacitation, visibility is an important parameter in tenability analysis. With the most common criteria used for visibility, the "tenability limits" for visibility are in most cases reached before similar limits are reached for other parameters of interest (gas concentrations, temperature, and radiation) as shown in Chap. 15. Therefore, good knowledge of visibility phenomena and the processes affecting it are very important for the safety of escaping people.

As with other parameters relating to perception, it is not easy to find a single mathematical equation describing the relation between visibility and smoke density. The situation is complicated by the fact that the typical size and shape of the particles in smoke from fires varies and depends on the burnt material and combustion conditions [1, 2]. This has led to different suggestions about how to calculate visibility, that is, how to relate a measurable (or estimated) physical parameter to visibility. In the next section different approaches are presented, compared, and discussed.

H. Ingason et al., *Tunnel Fire Dynamics,* DOI 10.1007/978-1-4939-2199-7_14

14.2 Different Methods of Predicting Visibility

One common way to express the smoke density is by the extinction coefficient, C_s (1/m):

$$C_s = \frac{1}{L}\ln\left(\frac{I_0}{I}\right) \tag{14.1}$$

where I_0 is the intensity of the incident light, I is the intensity of the light through smoke, and L is the path length of the light (m).

The relationship between the transmitted and incident intensities is a function of the mass-specific extinction coefficient of smoke σ (m^2/kg), the mass concentration of smoke, ρ_{sm} (kg/m^3), and L (m) as expressed by Bouguer's law [3]:

$$\frac{I}{I_0} = \exp(-\sigma\rho_{sm}L) \tag{14.2}$$

Jin [4, 5] developed several relationships between the visibility (V_s) and the extinction coefficient. For a *light-emitting sign* the relationship is given as:

$$V_s \approx \frac{1}{C_s}\ln\left(\frac{B_{EO}}{\delta_c k\Pi}\right) \tag{14.3}$$

where,

B_{EO}	brightness of the sign (cd/m^2)
δ_c	contrast threshold of signs in smoke at the obscuration level (-)
$k = \sigma_s/C_s$	
$C_s = \sigma_s + \sigma_{ab}$	extinction coefficient (1/m)
σ_s	scattering coefficient (1/m)
σ_{ab}	absorption coefficient (1/m)
Π	$1/\pi$ of mean illuminance of light radiating from all directions in smoke (m/m^2)

The contrast threshold (δ_c) is in the range 0.01–0.05, and a value of 0.02 is often used (For example, ISO 13571). For *reflecting signs* the corresponding equation can be written as [4, 5]:

$$V_s \approx \frac{1}{C_s}\ln\left(\frac{\alpha}{\delta_c k}\right) \tag{14.4}$$

where α is the reflectance of the sign.

Jin also showed that, at the obscuration threshold (for visibilities between 5 and 15 m) the visibility can be expressed as [5]:

$$V_s = \frac{K}{C_s} \tag{14.5}$$

where K is a constant which is 5–10 for a light-emitting sign and 2–4 for a reflecting sign.

If the smoke is an irritant, the visibility is reduced and both the smoke density and the irritation affect the walking speed. There is a linear decrease in visibility as the extinction coefficient increases, in the same way as for nonirritant smoke for $0.1 \leq C_s \leq 0.25$. For $C_s \geq 0.25$ the visibility in irritant smoke can be written as [4, 5]:

$$V_s = (K / C_s)(0.133 - 1.47 \lg C_s) \tag{14.6}$$

The experiments for which the correlation above was developed, showed that a value of $K = 6$ gave best agreement [5]. Note that those tests were performed with a lighted FIRE EXIT sign.

Since

$$C_s = \sigma \cdot \rho_{sm} \tag{14.7}$$

one can write

$$V_s = \frac{K}{\sigma \rho_{sm}} \tag{14.8}$$

where

$$\rho_{sm} = Y_s \frac{\Delta m_f}{V} \text{ or} \tag{14.9}$$

$$\rho_{sm} = Y_s \frac{\dot{m}_f}{\dot{V}} \tag{14.10}$$

depending on whether the object of interest is defined by a volume, V (m^3; for example, a train without openings) or an air flow rate, $\dot{V}$ (m^3/s; for example, a tunnel). Y_s is the soot yield (kg/kg) for the burning material under prevailing conditions. The change in mass of fuel can be given as a mass difference, Δm_f (kg) as in Eq. (14.9) or as a mass flow, $\dot{m}_f$ (kg/s) as in Eq. (14.10). In Table 14.3 the soot yield Y_s is given for some selected materials in kg/kg. In Chap. 7 the soot yield and the effect of the equivalence ratio are discussed further.

The extinction coefficient, C_s, can be obtained either from measurements using Eq. (14.1) or from values of σ and ρ_{sm} using Eq. (14.7).

If one-dimensional smoke flow in a tunnel is assumed, the visibility can be calculated from

$$V_s = \frac{KuA_t}{\sigma Y_s \dot{m}_f} \tag{14.11}$$

where u is the velocity of air in the tunnel (m/s) and A_t is the cross section area of the tunnel (m^2). The heat release rate, $\dot{Q}$ (kW), from a fire can be described as

$$\dot{Q} = \chi \Delta H_c \dot{m}_f \tag{14.12}$$

where χ is the combustion efficiency and ΔH_c is the heat of combustion (kJ/kg). This means that

$$V_s = \frac{KuA_t \chi \Delta H_c}{\sigma Y_s \dot{Q}} \tag{14.13}$$

Note the difference between the optical density (OD), and the extinction coefficient (C_s), where

$$OD = \lg \frac{I_0}{I} = \frac{C_s \cdot L}{\ln 10} \approx \frac{C_s \cdot L}{2.303} \tag{14.14}$$

This is discussed in more detail below, when relating the specific extinction coefficient to the mass optical density, D_{mass} (m^2/kg).

Both the mass-specific extinction coefficient and the soot yield depend on the type of fuel and therefore it is important to have data for different types of fuels. Note that there are different definitions and different ways of presenting this type of data.

Mulholland et al. [6, 7] have studied the specific extinction coefficient and presented an average value of 8700 m^2/kg (wavelength = 632.8 nm) for postflame smoke production from well-ventilated fires. Table 14.1 and 14.2 summarize the mass-specific extinction coefficients for gases/liquids and solids, respectively, with values from different studies. The value 8700 m^2/kg (with an expanded uncertainty of 1100 m^2/kg and 95 % confidence interval) mentioned above is an average of all the included studies. One can note that for some fuels, for example, heptane there is some spread in the specific extinction coefficient between the different studies. This could be an effect of the experimental setup or the scale. However, for some fuels, for example, PS, PVC, and rubber, there are relatively good agreement between the different setups.

Note that the standard SS-ISO 13571:2007 suggests an average value of 10,000 m^2/kg [8].

Tewarson [9] presented data for many different types of fuels. There the information is given as

$$D_{mass} = \frac{OD \cdot Y_s}{L \cdot \rho_s} \tag{14.15}$$

Using Eqs. (14.7), (14.14) and (14.15), a relationship between the specific extinction coefficient and D_{mass} can be found:

$$\sigma = \frac{\ln 10 \cdot D_{mass}}{Y_s} \tag{14.16}$$

In Table 14.3 and 14.4 Y_s and D_{mass} for a number of fuels and building materials are listed. Equation (14.16) is then used to calculate the mass-specific extinction coefficient. In the table, there are two columns with soot yield. The reason for this is that, the more recent version of the SFPE handbook has somewhat different values

Table 14.1 Examples of mass-specific extinction coefficients (at 632.8 nm) for burning gases and liquids [6]

Fuel	σ [m^2/g]	Description
Gases		
Propane	8000	170–350 kW
Ethene	7800	Turbulent diffusion burner, 5–10 kW
Ethene	8800	5 cm diameter burner, 2.0 kW
Propene	7000	Turbulent diffusion burner, 5–10 kW
Butadiene	7500	Turbulent diffusion burner, 5–10 kW
Acetylene	5300	Turbulent diffusion burner, 5–10 kW
Acetylene	7800	Premixed burner at equivalence ratio of 2.5
Acetylene	7800	5 cm diameter burner, 2.6 kW
Liquids		
Heptane	10,300	Small-scale to large-scale
Heptane	7800	30 cm (60 kW) and 50 cm (250 kW) pools
Heptane	6400	Turbulent diffusion burner, 5–10 kW
Benzene	7800	Turbulent diffusion burner, 5–10 kW
Styrene	9700	2 cm diameter pool
Cyclohexane	7500	Turbulent diffusion burner, 5–10 kW
Toluene	7000	Turbulent diffusion burner, 5–10 kW
Kerosene	10,100	Small-scale to large-scale
Kerosene	9200	Small-scale, 1–5 kW
Petrol	11,200	5 mL of fuel
Diesel	10,300	5 mL of fuel
Fuel oil	11,600	5 mL of fuel
Fuel oil	7200	Small-scale, 1–5 kW
Fuel oil	9400	Small-scale, 1–5 kW
Paraffin oil	9100	5 mL of fuel
Butane	9900	5 mL of fuel
Crude oil	8800	40 cm (60 kW) and 60 cm (180 kW) pools

compared to the 1st edition. The 1st edition version is included since those values correspond to the reported values of D_{mass}.

For some materials there is a large variation in the values of the specific extinction coefficient calculated from D_{mass} in Table 14.3 and 14.4 compared to the measured values listed in Table 14.1 and 14.2. The specific extinction coefficient depends on the experimental setup and the size of the fire as shown by the values in Table 14.1 and 14.2. In some cases there is a good correlation between the values in Table 14.1 and 14.2 and Table 14.3 and 14.4.

Table 14.5 shows the difference in soot yield for some fuels at different fire sizes. It can be seen that the mass-specific extinction coefficient depends on the fuel type, but does not seem to depend on the flame conditions (laminar or turbulent) [3].

Table 14.2 Examples of mass-specific extinction coefficients (at 632.8 nm) for burning solids [6]

Fuel	σ [m²/g]	Description
Solids		
Douglas fir	10,300	Small-scale to large-scale
Oak	7600	Small-scale, 1–5 kW
Wood crib	8500	1 crib (50 kW), 3 cribs (250 kW)
HDPE	8800	Small-scale, 1–5 kW
PP	7400	Small-scale, 1–5 kW
PMMA	10,500	Small-scale to large-scale
PMMA	7900	Small-scale, 1–5 kW
Polycarbonate	10,200	Small-scale to large-scale
Polycarbonate	7600	Small-scale, 1–5 kW
PVC	9900	Small-scale to large-scale
PVC	9000	Small-scale, 1–5 kW
PS	10,000	Small-scale to large-scale
PS	9600	Small-scale, 1–5 kW
Styrene-butadiene rubber	10,400	Small-scale to large-scale
Rubber	10,100	Small-scale, 1–5 kW
Polyurethane crib	8100	1 crib (100 kW), 3 cribs (300 kW)

PE polyethene, *PP* polypropene, *PS* polystyrene, *PUR* polyurethane

Using Eqs. (14.13) and (14.16) one can derive an equation for visibility based on D_{mass}:

$$V_s = \frac{K \cdot \chi}{\ln 10} \frac{uA\Delta H_c}{D_{mass}\dot{Q}} \tag{14.17}$$

If a combustion efficiency of unity is assumed, Eq. (14.17) reduces to:

$$V_s = \frac{K}{2.3} \frac{uA\Delta H_c}{D_{mass}\dot{Q}} \tag{14.18}$$

and if a value of $K=2$ is assumed, one obtains the following expression:

$$V_s = 0.87 \frac{uA\Delta H_c}{D_{mass}\dot{Q}} \tag{14.19}$$

which is the same equation presented by Ingason [11]. Ingason also summarized mass optical densities for different vehicles. These are given in Table 14.6.

In a test series in the Runehamar tunnel in Norway, Ingason et al. [13] performed tests simulating fires in heavy goods vehicle (HGV) cargos. Except for a pool fire test using diesel, different mixtures of cellulosic materials and plastics (18–19% plastics in each test) were used as fuel to simulate the cargo. During these tests the extinction coefficient was measured. The mass optical density estimated from the

Table 14.3 Soot yield, D_{mass} and specific extinction coefficient for selected materials

Material	Y_s (kg/kg)	Y_s (kg/kg)	D_{mass} (m^2/kg)	σ (m^2/kg)
Reference	[9]	[10]	[9]	Calculated, Eq. (14.16)
Ethane	0.008	0.013	24	6900
Propane	0.025	0.024	81	7500
Butane	0.026	0.029	155	13,700
Ethene	0.045	0.043	201	10,300
Propene	0.103	0.095	229	5100
1,3-Butadiene	0.134	0.125	319	5500
Acetylene	0.129	0.096	315	5600
Heptane	0.037	0.037	190	11,800
Octane	0.039	0.038	196	11,600
Benzene	0.175	0.181	361	4700
Styrene	0.184	0.177	351	4400
Kerosene	NA	0.042	NA	NA
Isopropylalcohol	0.014	0.015	NA	NA
Wood (red oak)	0.015	0.015	37	5700
Wood (hemlock)	NA	0.015	NA	NA
Toluene	NA	0.178	NA	NA
ABS	NA	0.105	NA	NA
PE	0.060	0.06	230	8800
PP	0.059	0.059	240	9400
PS	0.164	0.164	335	4700
Nylon	0.075	0.075	230	7100

NA not available

measurements for different types of materials (cargo) is presented in Table 14.7. The values correlate well with the values given for "truck" in Table 14.6. The values for diesel are similar to those given for benzene and styrene in Table 14.3.

For the estimation of the visibility in a tunnel either Eq. (14.13) or Eq. (14.17) can be used depending on which information is available on the involved parameters. If the visibility is to be determined for a line of sight having a distance x m downstream of a fire with a nonconstant HRR, it is important to take the transport time into account and relate the transient visibility to the relevant HRR. This was discussed also in Chap. 8 on gas temperatures, where a relation for the actual time and its dependency on a nonconstant velocity was presented. If for simplicity, a constant velocity, u, is assumed, the actual time τ (s) for the fire development at the distance x from the fire can be calculated as

$$\tau = t - \frac{x}{u} \tag{14.20}$$

where t (s) is the measured time from the ignition of the fire.

Table 14.4 Soot yield, D_{mass} and specific extinction coefficient for selected building materials

Material	Y_s (kg/kg)	Y_s (kg/kg)	D_{mass} (m²/kg)	σ (m²/kg)
Reference	[9]	[10]	[9]	Calculated, Eq. (14.16)
PUR foam, flexible, GM21	0.131	0.131	NA	NA
PUR foam, flexible, GM23	0.227	0.227	326	3300
PUR foam, flexible, GM25	0.194	0.194	286	3400
PUR foam, flexible, GM27	0.198	0.198	346	4000
PUR foam, rigid, GM29	0.130	0.13	304	5400
PUR foam, rigid, GM31	0.125	0.125	278	5100
PUR foam, rigid, GM35	0.104	0.104	260	5800
PUR foam, rigid, GM37	0.113	0.113	290	5900
Polystyrene foam, GM47	0.180	0.18	342	4400
Polystyrene foam, GM49	0.210	0.21	372	4100
Polystyrene foam, GM51	0.185	0.185	340	4200
Polystyrene foam, GM53	0.200	0.2	360	4100
PVC-1 (LOI = 0.50)	NA	0.098	NA	NA
PVC-2 (LOI = 0.50)	NA	0.076	NA	NA
PVC (LOI = 0.35)	NA	0.088	NA	NA
PVC (LOI = 0.30)	NA	0.098	NA	NA
PVC (LOI = 0.25)	NA	0.078	NA	NA
Cable, PE/PVC 1	0.076	0.076	242	7300
Cable, PE/PVC 2	0.115	0.115	NA	NA
Cable, PE/PVC 5	0.136	0.136	NA	NA

NA not available

For estimation of the soot yield, the $\dot{Q}(\tau)$ is used in Eq. (14.13) or Eq. (14.17), that is, the transportation time should be accounted for in this case.

Example 14.1 An HGV loaded with polypropene ($\Delta H_c = 38.6$ MJ/kg) is burning in a tunnel with the cross section $W = 9$ m and $H = 6$ m. The air velocity in the tunnel is 2 m/s. The HRR of the fire increases linearly at 210 kW/s for 12 min. What is the visibility after 6 min at a distance of 500 m downstream of the fire? Assume nonirritant smoke.

Solution: Start with calculating the actual time using (14.20): $\tau = 360 - 500/2 = 110$ s. This gives $\dot{Q}(\tau) = 210 \times 110 = 23100$ kW. From Table 14.3 the $D_{mass} = 240$ m²/kg for polypropene can be found. Using Eq. (14.18) and assuming $K = 2$ gives

$$V_s = \frac{2}{2.303} \frac{2 \cdot 9 \cdot 6 \cdot 38600}{240 \cdot 23100} = 0.65 \text{ m}.$$

In this solution we used $K = 2$ (lower end of the interval for reflecting signs), which often is used, but note that in many cases other values are used, for example, $K = 3$, that is, the centre of the interval for reflecting signs.

Table 14.5 Yield of soot for different fuels and different HRR [7]

Material	Y_s (kg/kg)
Propane, 50 kW	0.0106
Propane, 200 kW	0.0063
Propane, 450 kW	0.0052
Heptane, 300 kW	0.0129
Toluene, 250 kW	0.100
Heptane/Toluene, 320 kW	0.082

Table 14.6 Mass optical densities (D_{mass}) for different types of vehicles [11, 12]

Type of vehicle	D_{mass} (m²/kg)
Road	
Car (steel)	381
Car (plastic)	330
Bus	203
Truck	76–102
Rail	
Subway (speed)	407
Subway (aluminium)	331
IC type (steel)	153
ICE type (steel)	127–229
Two joined half-vehicles (steel)	127–178

Table 14.7 Mass optical densities (D_{mass}) for different types of HGV cargo materials [13]

Type of cargo/material	D_{mass} (m²/kg)
Diesel	360–450
Wood/PE	13–82
Wood/PUR	47–138
Furniture/rubber	10–87
Cartons/PS cups	30–120

14.3 The Influence of Visibility on Egress

One of the most well-known and used relationships between visibility (extinction coefficient) and walking speed is presented by Jin [4]. The values are presented in Fig. 14.1 and also included in Fig. 14.2. These tests were performed with a limited number of participants.

Frantzich and Nilsson [14] performed tests in a tunnel with these dimensions: 36.75 m long, 5.0 m wide and 2.55–2.70 m high. In total 46 persons participated in the study, with an average age of approximately 22 years. The extinction coefficient was measured using a 5 mW diode laser with a wavelength of 670 nm. The measurements were performed at a height of 2 m in the tunnel with a sight distance of 1 m.

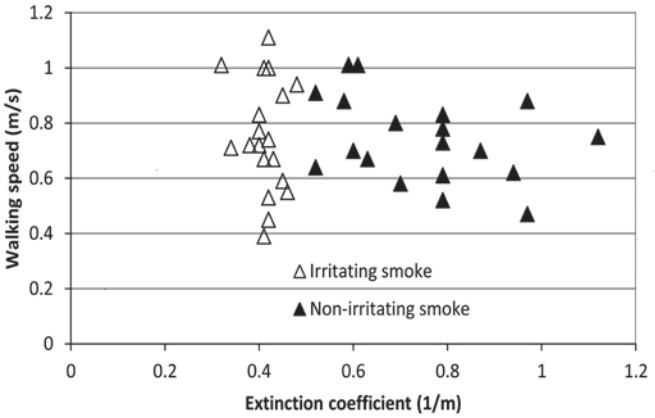

Fig. 14.1 Relationship between the walking speed and the extinction coefficient for irritant and nonirritant smoke after Jin [4]

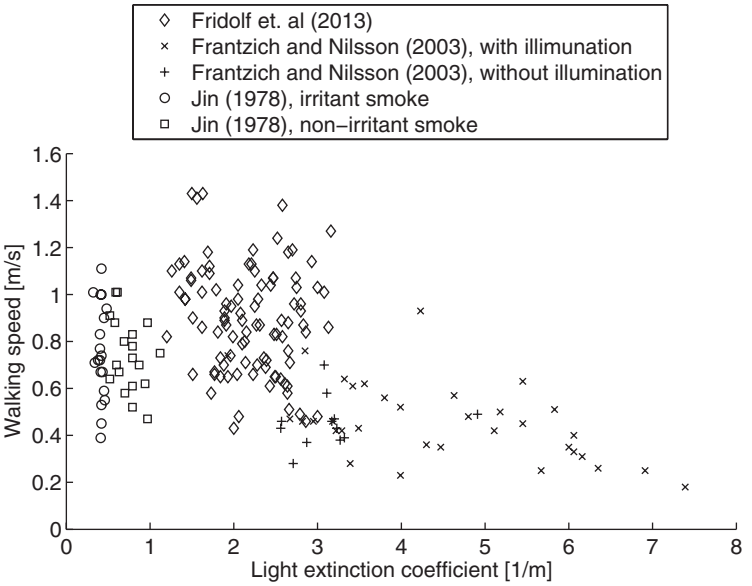

Fig. 14.2 Relationship between the walking speed and the extinction coefficient for irritant and nonirritant smoke [15]. The graph is based on several different sources [16, 14, 17]

In their tests, Frantzich and Nilsson used the value $K=2$ in Eq. (14.5) for calculating the visibility, that is, at the lower end of the interval reported to be valid for reflecting signs. One aim of the study was to verify the results by Jin. However, the extinction coefficient in the tests by Frantzich and Nilsson was found to be between 2 m^{-1} and 8 m^{-1}, while in the tests by Jin it was below 1.2 m^{-1}. Another difference between the tests was that Jin used black fire smoke while Frantzich and Nilsson

used white artificial smoke with addition of acetic acid. It is difficult to say what these differences mean for the results. Frantzich and Nilsson have, however, shown that the equation for visibility is valid both for black fire smoke and for white artificial smoke [14]. The results from the walking speed tests are included in Fig. 14.2.

Based on the tests, Frantzich and Nilsson found the following relation [14]:

$$u_w = -0.057 \cdot C_s + 0.706 \tag{14.21}$$

when the general lighting (normal lighting inside the tunnel) was used, where u_w is the walking speed. When the general lighting was not used, there was no statistically significant influence of the extinction coefficient on the walking speed. Furthermore, Frantzich and Nilsson showed that there was an influence on the walking speed of the choice of walking along a wall or not [14].

The walking speeds registered by Frantzich and Nilsson were lower (varied between 0.2 and 0.8 m/s) than those measured by Jin. This is expected since the visibility was higher in Jin's test series. Frantzich and Nilsson also argued that the measured walking speed should be multiplied by a factor lower than 1 to get an effective walking speed, taking into account both stops on the way and the fact that the persons did not take the closest way to the escape route. There was a large variation in this factor between the people participating in the tests with an average value of approximately 0.9. Also, the dependency of the extinction coefficient has a high uncertainty. Furthermore, it was concluded that the walking speed was in general higher for those walking along the tunnel wall for at least two thirds of the walking distance studied in the tests. The dependency on the extinction coefficient was also more evident in the cases where the test participants walked along the wall. The choice of route, therefore, seems important for determining the effective walking speed and there might also be other properties or conditions affecting the walking speed such as a person's height and gender.

To increase the number of data points, Fridolf et al. performed tests similar to Frantzich and Nilsson with a span in extinction coefficients between 1.2 m^{-1} and 7.5 m^{-1}. The results are included in Fig. 14.2. They then combined their results with those of Frantzich and Nilsson and derived a new relationship for walking speed:

$$u_w = -0.1423 \cdot C_s + 1.177 \tag{14.22}$$

or if visibility is used as the independent parameter:

$$u_w = 0.5678 \cdot V_s + 0.3033 \tag{14.23}$$

where $K = 2$ was used when calculating the visibility. The correlation with the extinction coefficient is statistically somewhat better ($R^2 = 0.4132$) than the correlation with the visibility ($R^2 = 0.3612$). Using the extinction coefficient directly also avoids the use of the constant K. In Fig. 14.3 the walking speed is shown as a function of visibility for the test series mentioned above [15]. Note that $K = 3$ was used when producing Fig. 14.3.

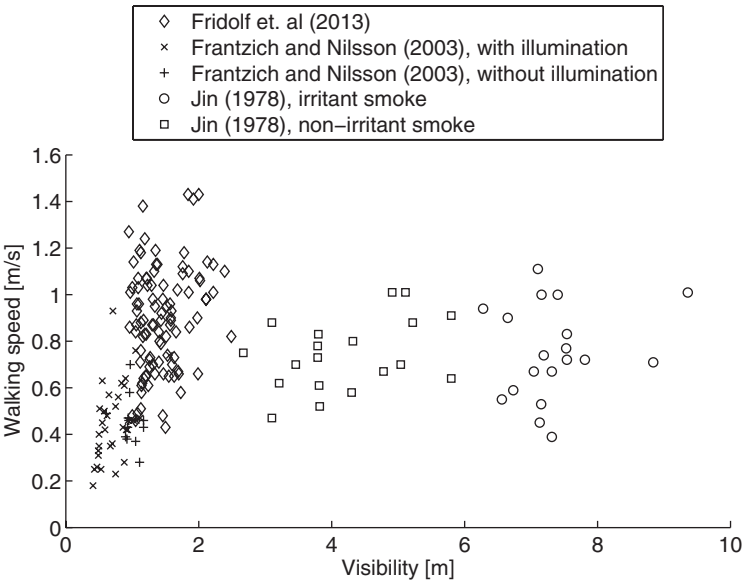

Fig. 14.3 Walking speed as function of visibility [15]. The graph is based on several different sources [16, 14, 17]. Note that a value $K=3$ was used to produce these results

In the guidelines to the Swedish building code there are suggestions for walking speeds to be used in performance based design of means for evacuation [18]. Note that these guidelines are for buildings rather than tunnels. However, the basic unhindered walking speed is set to 1.5 m/s. Note also that the influence of visibility is not discussed in these guidelines, probably since high visibility (10 m for areas >100 m^2) is one of the design criteria. For children or people with disabilities (in mobility or orientation) the walking speed is set to 0.7 m/s. There is also a decrease in walking speed in stairways (0.6 m/s up and 0.75 m/s down) in relation to the basic unhindered walking speed.

Frantzich [19] has also shown an effect of people getting used to the surface and the conditions. In tests with evacuation of metro trains the walking speed near the train was 1.0–1.4 m/s while further away (130 m from the train) it was 1.0–1.8 m/s. The tests were run without smoke and with emergency lighting, but Frantzich argues that this adaption effect should exist also during evacuation in fire smoke or darkness. When the tests were performed in darkness (without smoke) the walking speed varied between 0.5 and 1.0 m/s.

Example 14.2 What is the walking speed in Example 14.1?

Solution: Using the equation proposed by Fridolf et al., Eq. (14.23) gives $u_w = 0.568 \cdot V_s + 0.3 = 0.568 \cdot 0.65 + 0.3 = 0.47$ m/s. *One should here again note that this is based on* $K=2$ *and that a value* $K=3$ *is used to derive the graph in Fig.* 14.3. *One can still see that the visibility in this case is in the lower end of the graph and that the resulting walking speed is not very much higher than the constant value given by Eq. (14.23).*

Example 14.3 At what time has the fire in Example 14.1 reached a point where the walking speed is 0.9 m/s at a position 150 m downstream of the fire?

Solution: The heat release rate $\dot{Q}(\tau) = 210 \cdot \tau$ *and* $\tau = t - 150/2$. *Using this together with Eq. (14.18) give after some algebraic steps:*

$$t = \frac{1}{210} \cdot \frac{K}{2.3} \frac{uA\Delta H_c}{D_{mass} V_s} + \frac{150}{2} = \frac{1}{210} \cdot \frac{2}{2.303} \frac{2 \cdot 9 \cdot 6 \cdot 38600}{240 \cdot 0.9} + \frac{150}{2} = 155 \text{ s}$$

14.4 Summary

Visibility is very important for evacuation during a fire and, therefore, a very important parameter for fire safety in a tunnel. In this chapter different methods to define and describe visibility have been presented and discussed. The main methods for estimating the visibility in smoke-filled spaces are to use either the mass-specific extinction coefficient or the mass optical density. For both methodologies there are experimental values available for some materials of interest. The focus has been on the mass extinction coefficient methodology, but at the end this method was compared and correlated to the mass optical density methodology. Values of these parameters for selected materials were presented and conversion of values for one of the parameters into the other was discussed. Finally, the effect on walking speed during egress was discussed and some methods for estimating walking speed were presented.

References

1. Mulholland GW, Liggett W, Koseki H (1997) The Effect of Pool Fire Diameter on the Property of Smoke Produced by Crude Oil Fires. Fire Science and Technology 17 (1):64–69
2. Widmann JF, Yang JC, Smith TJ, Manzello SL, Mulholland GW (2003) Measurement of the optical extinction coefficients of post-flame soot in the infrared. Combustion and Flame 134:119–129
3. Mulholland GW, Choi MY Measurement of the Mass Specific Extinction Coefficient for Acetylene and Ethene Smoke Using the Large Agglomerate Optics Facility. In: Twenty-Seventh Symposium (International) on Combustion, 1998. The Combustion Institute, pp 1515–1522
4. Jin T, Yamada T (1985) Irritating Effects of Fire Smoke on Visibility. Fire Science and Technology 5 (1):79–89
5. Jin T (2008) Visibility and Human Behavior in Fire Smoke. In: The SFPE Handbook of Fire Protection Engineering. National Fire Protection Engineering, pp 2–54 -- 52–66
6. Mulholland G, Croarkin C (2000) Specific Extinction Coefficient of Flame Generated Smoke. Fire and Materials 24:227–230
7. Mulholland GW, Johnsson EL, Fernandez MG, Shear DA (2000) Design and Testing of a New Smoke Concentration Meter. Fire and Materials 24:231–243
8. ISO (2007) Life-threatening components of fire—Guidelines for estimation of time available for escape using fire data. ISO 13571:2007
9. Tewarson A (1988) Generation of Heat and Chemical Compounds in Fires. In: DiNenno PJ, Beyler CL, Custer RLP, Walton WD, Watts JM (eds) SFPE Handbook of Fire Protection Engineering. First Edition edn. NFPA, pp 1–179 -- 171–199

10. Tewardson A (2008) Generation of Heat and Gaseous, Liquid, and Solid Products in Fires. In: SFPE Handbook of Fire Protection Engineering. NFPA, pp 2–109 – 103–194
11. Ingason H (2012) Fire Dynamics in Tunnels. In: Beard AN, Carvel RO (eds) In The Handbook of Tunnel Fire Safety, 2nd Edtion ICE Publishing, London, pp 273–304
12. Steinert C Smoke and Heat Production in Tunnel Fires. In: The International Conference on Fires in Tunnels, Borås, Sweden, 10–11 October 1994. SP Swedish National Testing and Research Institute, pp 123–137
13. Ingason H, Lönnermark A, Li YZ (2011) Runehamar Tunnel Fire Tests. SP Report 2011:55. SP Technicial Research Institute of Sweden, Borås, Sweden
14. Frantzich H, Nilsson D (2003) Utrymning genom tät rök: beteende och förflyttning. Avd. för brandteknik, Lunds tekniska högskola, Lund
15. Fridolf K (2014) Walking speed as function of extinction coefficient. Personal communication, Jan. 10
16. Jin T (1978) Visibility through smoke. Journal of Fire & Flamability 9:135–157
17. Fridolf K, Andrée K, Nilsson D, Frantzich H (2013) The impact of smoke on walking speed. Fire and Materials
18. BFS (2011) Boverkets allmänna råd om analytisk dimensionering av byggnaders brandskydd. Boverkets Författningsamling, BFS 2011:27 BBRAD (in Swedish)
19. Frantzich H (2000) Utrymning av tunnelbanaetåg—Experiemntell utvärdering av möjligheten att utrymma i spårtunnel. Räddningsverket, Karlstad

Chapter 15
Tenability

Abstract One of the most important issues during a fire in a tunnel is the possibility for a safe escape. During an evacuation, tunnel users may be exposed to toxic gases, radiation, high temperatures and dense smoke. In this chapter the most important consequences of exposure to gas components, radiation and convective heat are presented. Examples of asphyxiant and irritant gases and the effect on evacuating people are presented. Different models for estimating time to incapacitation and other endpoints due to exposure are discussed.

Keywords Tenability · Toxicity · Gas concentration · Carbon monoxide · Carbon dioxide · Oxygen · Hydrogen cyanide · Radiation · Convective heat

15.1 Introduction

During a fire, occupants in a building or a tunnel, or passengers in a train can be exposed to heat (high gas temperature or radiation), smoke, or toxic gases (toxicants). This can inhibit evacuation, but also lead to incapacitation and finally death.

The levels of the production of smoke and different species are dependent on mainly three different parameters: the burning material, temperature and the ventilation conditions (oxygen concentration). The latter parameter is not only dependent on the overall availability of oxygen, but also on the spatial/geometrical arrangement of the burning material and the possibility for the oxygen to reach the combustion zone and mix with the pyrolysis gases. This is discussed in more detail in Chap. 7. Further, the effect of smoke on visibility, the escape and walking speed is presented in Chap. 14.

UK statistics show that "smoke" and "burns/smoke" (where the cause of death was ambiguous) cause a significant proportion of the UK fire deaths [1]. There was a peak in fire deaths in the UK in 1979, and since 1985 there has been an almost constant decrease. Some suggested explanations for this reduction are the increased use of fire retarded furniture and the increased availability of low-cost smoke alarms. Also for nonfatal fire injuries the portion of hospital admissions caused by toxic gas inhalation is significant. Although these statistics are not specifically for tunnel

H. Ingason et al., *Tunnel Fire Dynamics,* DOI 10.1007/978-1-4939-2199-7_15

fires, the effect of smoke is very important for conditions during a tunnel fire and as mentioned above the fire smoke affects the possibilities for a safe escape, both due to reduced visibility and increased risk for incapacitation.

For a long time, carbon monoxide has been seen as the only important toxicant. The reason for this is that it was easily quantified in the blood and was routinely analysed for in forensic investigations. However, it has been shown that also other toxicants are important, for example, hydrogen cyanide and this chapter summarizes the most common fire smoke toxicants, their effects and how to calculate the fraction of an incapacitation dose.

15.2 Combustion Products Related to Toxicity

The different parameters affecting the production of different toxic species are discussed in Chap. 7. In that chapter, it is concluded that the ventilation conditions are important for the chemical production and the hazards. In an under-ventilated fire situation the yield of major toxicants is higher. Furthermore, the total volume of effluents is greater [1]. The fire smoke toxicants can be divided into two groups: asphyxiant (or narcotic) gases and irritant gases. Particulates are also important.

Asphyxiant gases are the gases that prevent the uptake of oxygen or decrease the amount of oxygen delivered to the body tissue (For example, the brain tissue) and thereby cause hypoxia [1, 2]. This can lead to loss of consciousness and death. One can divide this group into two subgroups: simple and chemical asphyxiants, respectively [2]. The first group simply displaces oxygen, leading to a lower oxygen concentration. Examples are nitrogen (N_2) and carbon dioxide (CO_2). Note, however, that CO_2 in a fire situation can have other effects such as increasing the breathing rate leading to a faster inhalation of other more toxic gases. The CO_2 can also have toxic effects at higher concentrations. At concentrations above 7 % there is risk for unconsciousness within a few minutes [3]. Chemical asphyxiants, on the other hand, affects a step in the electron transport chain system of the mitochondria, resulting in tissue hypoxia [2]. Examples of chemical asphyxiants are carbon monoxide (CO) and hydrogen cyanide (HCN). In a fire situation also the consumption of oxygen can lead to a low O_2 situation resulting in asphyxiant effects. In most fire situations toxic gases, for example CO, are present in lethal concentration before the oxygen concentration decreases to levels preventing survival. However, there are additive effects and the effects of low O_2 concentrations should be included in calculations of incapacitations.

Irritant gases can affect the eyes and the upper respiratory tract, leading to immediate incapacitation [1], but could also give long-term effects. Examples of irritants are given in Table 15.1.

The smoke also contains particles which are hazardous to health. Particulates in the smoke can prevent escape due to visual obscuration. The decreased visibility due to smoke slows down the walking speed of the people trying to escape from a fire. Furthermore, small particulates can also be inhaled and pose hazards to the

Table 15.1 Examples of asphyxiant and irritant gases

Asphyxiants		Irritants
Simple	Chemical	
Nitrogen (N_2)	Carbon monoxide (CO)	Hydrogen fluoride (HF)
Carbon dioxide (CO_2)	Hydrogen cyanide (HCN)	Hydrogen chloride (HCl)
		Hydrogen bromide (HBr)
		Nitrogen dioxide (NO_2)
		Sulphur dioxide (SO_2)
		Acrolein (C_3H_4O)
		Formaldehyde (CH_2O)

respiratory system. Depending on the size of the particulates, they can enter and affect different parts of the respiratory system. Examples of effects are fluid release and inflammation. Particulates smaller than 0.5 μm can cause interstitial and luminal oedema or enter the blood where they can trigger hazardous immune responses [1]. Particulates can also carry other hazardous species deep into the respiratory system. The particles are not discussed further here, while the visibility and the walking speed are discussed in Chap. 14.

In this introduction, as well as in the rest of this chapter, the main components of fire gases and those with known effects are presented and discussed. There might be other gases that are not often analysed for or with unknown effects that could be important for the overall toxicity in some situations.

15.3 Toxicity

15.3.1 Asphyxiants

Carbon monoxide is an asphyxiant gas and an important gas in connection with a fire. The toxic effect of CO is due to its combination with haemoglobin in the blood to form carboxyhaemoglobin (COHb). In Table 15.2, health effects at different COHb concentrations in the blood are summarized.

The toxicity of CO and its relationship to COHb and effects on the oxygen-carrying blood capacity is well-known, but CO can have other adverse effects, for example interruption of energy production of cells, interference of oxygen delivery and other cellular activities [4]. These latter effects are not as well understood or widely discussed as the binding of CO producing COHb, resulting both in the haemoglobin not being able to transport as much oxygen and the oxygen being more tightly bonded to the haemoglobin. The values in Table 15.2 should be seen as examples and not as exact limits. A concentration of 50 % COHb is often taken as a threshold for lethality [3]. Nelson, however, reports that a larger variety can be expected and that the actual limit depends on the situation [4]. A lower level and

Table 15.2 Summary of health effects at different COHb levels [5]

COHb level [%]	Effect
10	Asymptomatic or headache
20	Dizziness, nausea and dyspnea
30	Visual disturbance
40	Confusion and syncope
50	Seizures and coma
≥60	Cardiopulmonary dysfunction and death

longer exposure can result in effects on the cellular processes and this can lead to fatalities at lower levels of COHb than if a person is subjected to shorter and higher exposures.

While CO decreases the possibilities for the blood to take up, carry and deliver oxygen to the tissues, HCN decreases the ability to use the oxygen delivered to the tissues [3]. By the formation of cyanide ions in the blood, hydrogen cyanide is approximately 25 times more toxic than CO [1]. The dynamics of HCN in the human body are, however, poorly understood and blood cyanide is not analysed as routinely as COHb. This is partly due to difficulties associated with the measurement of HCN in the blood of a fire victim and the decay of HCN levels in the blood after mortality.

Low oxygen concentrations can cause hypoxia effects similar to those caused by CO and HCN. In most cases, heat exposure or toxic cases have reached lethal limits before oxygen concentration has decreased below tenable levels (approximately 6 %) [1]. CO_2 affects the time to incapacitation in two ways. At low concentrations, CO_2 stimulates breathing, that is, increases the breathing rate (RMV = Respiratory minute volume rate). This increases the uptake of other toxic gases. At high concentrations (above approximately 5 %) CO_2 becomes an asphyxiant, although not additive to the effects of CO and HCN.

15.3.2 Irritants

Irritant gases are important when determining the possibility for people to escape from a fire. These gases can be both inorganic (For example, hydrogen chloride (HCl)) and organic (For example, acrolein).

The inorganic irritants halides HCl and HBr dissociate totally in water and are strong acids. Hydrogen fluoride (HF), another halide, is a very irritating gas. Furthermore, nitrogen dioxide (NO_2) can form nitric and nitrous acid when dissolved. These acids can at high concentrations cause pulmonary oedema and death [1]. The effects of different concentrations of HCl and HF are given in Tables 15.3 and 15.4, respectively.

The main effect is irritation of mucous membranes, for example, in the eyes, upper respiratory tract, and to some extent the lungs. The effects include tears and

Table 15.3 Effects of different concentrations of HCl

HCl concentration [ppm]	Effect	References
10	Tolerable exposure	[1]
10–50	Perceived as irritant, but work is possible	[3]
50–100	Tolerable for one hour	[1]
100	Severe irritant effects	[1]
200	Predicted to impair escape in half the human population	[3]
309	Mouse RD_{50}	[3]
900	Incapacitation in half the human population	[3]
1000–2000	Thought to be dangerous for humans for short exposures	[1, 3]
2600	Lethal concentration for mice after 30 min exposure	[1]
3800	Lethal concentration for rats after 30 min exposure	[3]
4700	Lethal concentration for rats after 30 min exposure	[1]
15000	5-min lethal exposure limit concentration in rats and baboons	[3]

Table 15.4 Effects of different concentrations of HF

HF concentration [ppm]	Effect	References
62	30 min AEGL-3	[6, 7]
170	10 min AEGL-3	[6, 7]
200	Predicted to impair escape in half the human population	[3]
500	Incapacitation	[8]
900	Incapacitation in half the population	[3]
2900	30-minute exposure LC_{50} concentration	[3]

reflex blinking, pain in the nose, throat and chest, breath-holding and laryngeal spasm. Another effect is that the gases can cause oedema and inflammation in the lungs, leading to death 6 to 24 h after exposure [3]. In Table 15.5, limiting values are summarized for irritant organic gases as presented by different references.

15.4 Fractional Effective Dose, FED

The general method when estimating the toxicity of a smoke composition is to assume that the effects of the individual toxicants are additive, and in this sum for each toxicant express the concentration as its fraction of the lethal concentration (LC_{50} value), the latter estimated to be lethal for 50 % of the population for a 30 min exposure. To calculate this, one uses the fractional effective dose (FED) which according to ISO 13344 is defined as “ratio of the exposure dose for an asphyxiant toxicant to that exposure dose of the asphyxiant expected to produce a specified

Table 15.5 Limiting values (irritant and lethal concentrations) for irritant organic gases

Substance	IDLH (ppm)	OEL, 15 min (ppm)	RD_{50} Mouse[c] (ppm)	Severe sensory irritancy in humans (ppm)	30-min LC_{50} Mammal (ppm)
Reference	[9]	[10]	[3]	[3]	[3]
Acetaldehyde	2000	50[a]	4946	>1500	20000–128000
Acrolein	2	0.3[a]	1.7	1-5.5	140–170
Acrylonitrile	6	85	10–100	>20	4000–4600
Benzene	500	3[a]	–	–	–
Crotonaldehyde	50	–	10–100	4–45	200–1500
Formaldehyde	20	0.6[b]	3.1	5–10	700–800
Phenol	250	2[a]	10–100	>50	400–700
Styrene	700	20[a]	980	>700	10000–80000
Toluene	500	100[a]	–	–	–
Toluene 2,4-diisocyanate	2.5	0.005[b]	0.20	1.0	100

[a] Short-term value
[b] Ceiling limit value
[c] Where spans are given, ranked according to their reported irritancy in humans [3]

effect on an exposed subject of average susceptibility", that is in this case 50% lethality. This can be described mathematically as

$$FED = \sum_{i=1}^{n} \int_0^t \frac{C_i}{(C \cdot t)_i} dt \tag{15.1}$$

where C_i is the concentration of the toxic component i. One model often used is the N-gas model presented in ISO 13344 [11]:

$$FED = \frac{m \cdot [CO]}{[CO_2] - b} + \frac{21 - [O_2]}{21\text{-}LC_{50,O_2}} + \frac{[HCN]}{LC_{50,HCN}} + \frac{[HCl]}{LC_{50,HCl}} + \frac{[HBr]}{LC_{50,HBr}} \tag{15.2}$$

where m is the slope of the CO-vs-CO_2 curve and b is the intercept of the CO-vs-CO_2 curve, which depicts the increasing toxicity of CO as the CO_2 concentration increases. [CO], [CO_2] and [O_2] are concentrations expressed in percent by volume, while [HCN], [HCl] and [HBr] are concentrations expressed in ppm by volume. The values of the gas concentrations are the integrated product values $(C \cdot t)$ over a 30-min test period divided by 30 min. FED in Eq. (15.2) describes the fractional effective dose based on lethality.

The values of the parameters m and b in Eq. (15.2) depend on the concentration of CO_2. If [CO_2] $\leq 5\%$, $m = -18$ and $b = 122000$. If [CO_2] $> 5\%$, $m = 23$ and

Table 15.6 LC_{50} concentrations (30 min) for selected gases common during fires

Compound	Rats (Levin) [12]	Rats (ISO 13344) [3, 11]	Rats [1]	Mice [1]	Primates [1]
CO (ppm)		5700	5300–6600	3500	2500–4000
low O_2 (%)	5.4		7.5	6.7	6–7
HCN (ppm)	150	165	110–200	165	170–230
HCl (ppm)	3700	3800	3800	2600	5000
HBr (ppm)	3000	3800			
HF (ppm)		2900			
SO_2 (ppm)		1400			
NO_2 (ppm)		170			
Acrolein (ppm)		150			
Formaldehyde (ppm)		750			

$b = -38600$. Note that in ISO 13344, the values used as LC_{50}-values in Eq. (15.2) are those presented for rats by Levin (see Table 15.6, where LC_{50} values from other sources are also given). According to ISO 13344, 5700 ppm leads to death (rats) for a 30 min exposure [11].

As can be seen in Eq. (15.2), the effect of the increased respiration rate due to high concentration of CO_2 was only assigned to alter the effect of CO. Purser developed a model where the effect of hyperventilation influences the effect of all the toxic species. Furthermore, carbon dioxide can be toxic by itself and this effect is included as an acidosis factor Z_A.

$$FED = \left(\frac{[\mathrm{CO}]}{\mathrm{LC}_{50,\mathrm{CO}}} + \frac{[\mathrm{CN}]}{\mathrm{LC}_{50,\mathrm{HCN}}} + \frac{[X]}{\mathrm{LC}_{50,X}} + \frac{[Y]}{\mathrm{LC}_{50,Y}} \right) \times V_{\mathrm{CO}_2} + Z_{\mathrm{A}} + \frac{21 - [\mathrm{O}_2]}{21\text{-}5.4} \tag{15.3}$$

where [CN] is the HCN concentration, expressed in ppm, corrected for the presence of other nitriles and the protective effect of NO_2, and is given by Eq. (15.4).

$$[\mathrm{CN}] = [\mathrm{HCN}] + [\text{total organic nitriles}] - [\mathrm{NO}_2] \tag{15.4}$$

[*X*] is the concentration (ppm) of each acid gas irritant and [*Y*] is the concentration (ppm) of each organic irritant. The multiplication factor for CO_2-driven hyperventilation is expressed as

$$V_{\mathrm{CO}_2} = 1 + \frac{\exp\left(0.14[\mathrm{CO}_2]\right) - 1}{2} \tag{15.5}$$

Z_A is an acidosis factor equal to $[CO_2] \times 0.05$.

Table 15.7 Activity dependant variation in parameters for the fractional effective dose for incapacitation by carbon monoxide [13]

Activity	RMV (L/min)	I (%COHb)
Resting or sleeping	8.5	40
Light work—walking to escape	25	30
Heavy work—slow running, walking up stairs	50	20

15.5 Fractional Effective Dose for Incapacitation

In Sect. 15.4, the lethal exposures are discussed. In this section, the focus is the time to incapacitation (or partial incapacitation), that is, the conditions that will lead to incapacitation (and not immediate death), which will prevent evacuation and in turn significantly increase the risk for lethality in the end. For this a fractional effective dose (FED) for incapacitation (or fraction of an incapacitating dose) is calculated. The fraction of an incapacitating dose for all asphyxiant gases (excluding effects of irritants), F_{IN}, can then be written (for a certain time step):

$$F_{IN,n} = \left(F_{I_{CO},n} + F_{I_{CN},n}\right) \cdot V_{CO_2,n} + F_{I_{O_2},n} \tag{15.6}$$

where the total fraction of an incapacitation dose is calculated from the contributions from CO, HCN and low concentration of O_2. In addition, CO_2 affects the breathing rate increasing the effect of CO and HCN. The different contributions are described and explained below.

The calculations are based on the expressions given by Purser [3]:

$$F_{I_{CO},n} = \frac{3.317 \cdot 10^{-5} \cdot [\mathrm{CO}]^{1.036} \cdot RMV \cdot \left(t_n - t_{n-1}\right)}{I} \tag{15.7}$$

where F_I is the fraction of an incapacitating dose, [CO] is the concentration of CO (in ppm) during the time step, RMV is the breathing rate (25 L/min for light activity), $t_n - t_{n-1}$ is the length of the time step (min), and I is the COHb (carboxyhaemoglobin) concentration at incapacitation (30 % for light activity). Using values for light work, Eq. (15.7) can be simplified to:

$$F_{I_{CO},n} = 2.7642 \cdot 10^{-5} \cdot [\mathrm{CO}]^{1.036} \cdot \left(t_n - t_{n-1}\right) \tag{15.8}$$

Values to be used in Eq. (15.7) for other levels of activity can be found in Table 15.7. Death is likely to occur for COHb above 50 %. Note, however, that the RMV decreases (to approximately 6 L/min) after incapacitation.

For the effect of HCN on the fractional effective dose of incapacitation the following equation has been derived [3]:

$$F_{I_{CN},n} = \frac{t_n - t_{n-1}}{\exp\left(5.396 - 0.023\left[\mathrm{HCN}\right]_n\right)} \tag{15.9}$$

where $[HCN]_n$ is the concentration of HCN (in ppm) during the time step.

Simplified expressions for $F_{I_{CN},n}$ have been developed and Purser suggests the following expression [14]:

$$F_{I_{CN},n} = \frac{\left(t_n - t_{n-1}\right)}{1.2 \cdot 10^6 \cdot \left[\mathrm{HCN}\right]^{-2.36}} \tag{15.10}$$

which is also described in ISO 13571 [8].

A correction similar to the one expressed in Eq. (15.4) could be done, that is, considering additional effects of other nitriles and some protective effects of the presence of NO_2. However, their effects are small in comparison to the effect by HCN and Purser suggests that one could ignore the effects of other nitriles and NO_2 and only take the concentration of HCN into account, as described in Eq. (15.10) [14].

To calculate the effect of decreased concentration of oxygen, the following equation can be used [3]:

$$F_{I_{O_2},n} = \frac{t_n - t_{n-1}}{\exp\left(8.13 - 0.54\left(20.9 - \left[\mathrm{O_2}\right]\right)\right)} \tag{15.11}$$

where $[O_2]$ is the concentration of O_2 (in vol-%) during the time step.

The fraction of an incapacitating dose for all asphyxiant gases (excluding effects of irritants), F_{IN}, can then be calculated using Eq. (15.6) for each time step with

$$V_{CO_2,n} = \frac{\exp\left(0.1903\left[\mathrm{CO_2}\right] + 2.0004\right)}{RMV_r} \tag{15.12}$$

as the multiplying factor for the enhanced uptake of asphyxiant gases (other than CO_2) due to induced hyperventilation where $[CO_2]$ is the concentration of CO_2 (in vol-%) during the time step, and RMV_r is the resting RMV (7.1 L/min is used).

A simplified equation has been suggested [3]:

$$V_{CO_2,n} = \exp\left(\frac{C_{CO_2,n}}{5}\right) \tag{15.13}$$

The total fraction of an incapacitating dose is calculated as the sum of many time steps:

Table 15.8 Summary of tenability limits for incapacitation or death for some in fire gases common asphyxiants [3]

Species	Five minute exposure		Thirty minute exposure	
	Incapacitation	Death	Incapacitation	Death
CO (ppm)	6000–8000	12000–16000	1400–1700	2500–4000
HCN (ppm)	150–200	250–400	90–120	170–230
Low O_2 (%)	10–13	<5	<12	6–7
CO_2 (%)	1–8	>10	6–7	>9

$$FI\left(t = t_N\right) = \sum_{n=2}^{N} F_{IN,n} \tag{15.14}$$

Since the asphyxiant effect of CO_2 is not additive to the effects of the other gases it is not included in Eq. (15.6). However, the fraction of an incapacitating dose of CO_2 can be calculated separately as

$$F_{I_{CO_2},n} = \frac{t_n - t_{n-1}}{\exp\left(6.1623 - 0.5189\left[CO_2\right]\right)} \tag{15.15}$$

Purser [3] summarized tenability limits for incapacitation or death when exposed to some common asphyxiants in fire gases. These are presented in Table 15.8.

If a situation with constant gas concentrations is assumed the time to incapacitation can be calculated as:

$$t_{IN} = \frac{1}{\left(\frac{3.317 \cdot 10^{-5} \cdot \left[CO\right]^{1.036} \cdot RMV}{I} + \frac{\left[HCN\right]^{2.36}}{1.2 \cdot 10^{6} \cdot}\right) V_{CO_2} + \frac{1}{\exp\left(8.13 - 0.54\left(20.9 - \left[O_2\right]\right)\right)}} \tag{15.16}$$

Example 15.1 An escaping person is during 5 min exposed to an environment containing 1000 ppm CO, 0.5% CO_2, and 20.2% O_2 followed by a period with the composition 5000 ppm CO, 3% CO_2 and 16.5% O_2 during an additional 2.5 min. of exposure Calculate the total fraction of an incapacitating dose for the escaping person.

Solution: Since the asphyxiant effect of CO_2 is not additative to the effects of the other gases and becomes an asphyxiant above approximately 5%, we do not include CO_2 in the calculations more than for the multiplying factor according to Eq. (15.13). This gives together with Eqs. (15.7), (15.10) and (15.11):

$$\begin{aligned} FI &= F_{I,0-5\,\mathrm{min}} + F_{I,5-7.5\,\mathrm{min}} = F_{I_{CO},0-5\,\mathrm{min}} \cdot V_{CO_2,0-5\,\mathrm{min}} + F_{I_{O_2},0-5\,\mathrm{min}} \\ &\quad + F_{I_{CO},5-7.5\,\mathrm{min}} \cdot V_{CO_2,5-7.5\,\mathrm{min}} + F_{I_{O_2},5-7.5\,\mathrm{min}} = \\ &= 0.177 \cdot 1.105 + 0.002 + 0.470 \cdot 1.822 + 0.008 = 1.06 \end{aligned}$$

Table 15.9 Required radiant exposure dose for different exposure dose endpoints [3]

r [(kW/m^2)$^{4/3}$]	Exposure dose endpoints
1.33	Tolerance limit, pain, first-degree burns
10	Severe incapacitation and second-degree burns
16.7	Fatal exposure and third-degree burns

This (FI > 1) means that it is probable that the escaping person will be incapacitated before reaching a safe haven.

The discussion above focused on the gas composition. However, the temperature (heat exposure) also affects an escaping occupant. There are mainly three different ways heat exposure can be a threat: body surface burns, hyperthermia and respiratory tract burns. The heat exposure can cause both incapacitation and death due to hyperthermia.

In dry air, respiratory tract burns do not appear without skin burns, that is, the tenability limits for skin burns are in most cases lower than corresponding limits for respiratory tract burns. However, in cases with air saturated with water vapour, respiratory tract burns can occur when inhaling air with a temperature higher than 60 °C [1]. A convective heat flow with a temperature above 120 °C could be very painful and give skin burns within minutes. The tenability limit for radiant heat flux on skin is, according to Purser, approximately 2.5 kW/m^2 [3]. The same level is used in the Swedish building regulations [15]. It has been noted that below this limit, the heat flux can be tolerated for at least several minutes and does not affect the possibilities for evacuation. However, at this level (2.5 kW/m^2) the radiation can be tolerable for approximately 30 s and for a radiation of 10 kW/m^2 the time limit is 4 s [3].

Above the level 2.5 kW/m^2 the time to different effects due to the exposure can be calculated by

$$t_{Irad} = \frac{r}{\dot{q}''^{4/3}} \tag{15.17}$$

where r is the radiant heat exposure dose [(kW/m^2)$^{4/3}$] required to reach a certain endpoint. In Table 15.9, values of r for some endpoints are given [3].

For convective heat, Purser presents a relationship that is the same as the one for a unclothed or lightly clothed person according to SS-ISO 13571:2012 [8]

$$t_{I_{conv\_L},n} = 5 \cdot 10^7 T^{-3.4} \tag{15.18}$$

where T is the gas temperature (°C). In the ISO standard, there is also an expression for exposure of convective heat for a fully clothed person:

$$t_{I_{conv\_F},n} = 4.1 \cdot 10^8 T^{-3.61} \tag{15.19}$$

The convective effect depends on the humidity and Eq. (15.18) tends to follow the 100 % humidity line (worst case). Purser also presented another equation for time tolerance under mid-humidity conditions [3]:

$$t_{tol} = 2 \cdot 10^{31} \cdot T^{-16.963} + 4 \cdot 10^{8} \cdot T^{-3.7561} \tag{15.20}$$

which also fits better to empirical data.

The selected equation for the effect of the convective heat exposure can be used together with Eq. (15.17) to calculate the fractional effective dose of heat:

$$\mathrm{FED} = \int_{t_1}^{t_2} \left(\frac{1}{t_{Irad}} + \frac{1}{t_{Iconv}} \right) \Delta t \tag{15.21}$$

15.6 Large-Scale Example of Fraction of an Incapacitation Dose

In 2003, tests were performed in the Runehamar tunnel [16–18] with a set-up simulating a heavy goods vehicle (HGV) with cargo. The tunnel is a 1600 m long abandoned road tunnel. During the four tests performed, different mixtures of cellulosic material and plastics were used as fuel. Gas was sampled at different heights at a measurements station, 458 m from the centre of the fire. Since some of the measurements are only available at the height 2.9 m above the road, all gas concentrations has been evaluated as this height. This is higher than the height representative for a person in the tunnel, but this choice was made to be able to compare the different contributions to the fraction of an incapacitating dose.

The HCN analyses are described by Brandt [19]. The HCN concentrations are affected with some uncertainties. The HCN concentration is, for example, below zero during different time periods in the tests T1, T3 and T4 (only positive values were used in the calculations). Therefore, the total fraction of an incapacitating dose is given both with and without the effect of HCN. For the calculation, Eqs. (15.6), (15.8) and (15.10) were used. In Fig. 15.1, the individual contributions of O_2 and CO, respectively, are presented separately for test T2 (mainly wood pallets and PUR mattresses). In Fig. 15.1, also the fraction of an incapacitating dose due to the asphyxiant effect of CO_2 (Eq. (15.15)) is included. This effect is not additive to the effect of the other gases and is not included in the total fraction of an incapacitating dose.

The HCN concentration significantly affects the time to incapacitation ($F_I = 1$). In these tests, incapacitation is quickly reached (within a few minutes from the start of the increase). In all four tests, significant amounts of HCN were produced. HCN is formed in a fire during combustion of nitrogen-containing materials. In the Runehamar test series, the polyurethane mattresses in test T2 are the most obvious nitrogen source (analyses show 4.6 % (by weight) is nitrogen). Further, the fuel was placed on particle boards in all the tests. The nitrogen content of these boards were

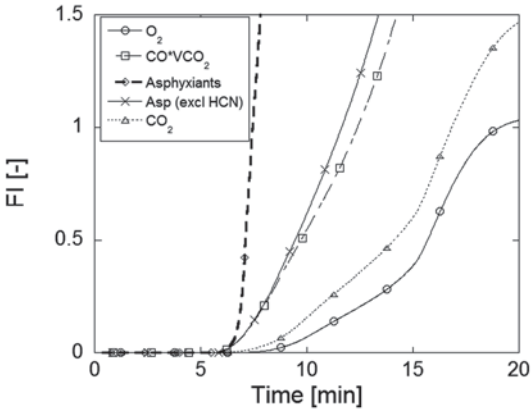

Fig. 15.1 Fraction of an incapacitating dose for asphyxiant gases analysed during test T2 in the Runehamar tunnel 2003 [18]

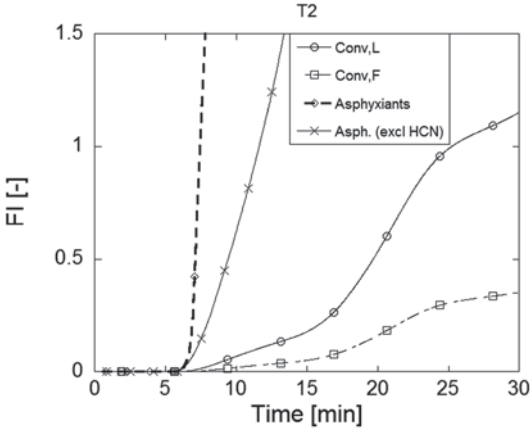

Fig. 15.2 Fraction of an incapacitating dose for convective heat exposure compared with asphyxiant gases for test T2 in the Runehamar tunnel test series from 2003 [18]

not analysed, but a nitrogen content of the order of a few percent has been reported in other cases [20, 21]. Wood also contains nitrogen, but to a lower extent, 0.1 to 0.2 % (by weight) [22, 20, 23]. The formation of HCN is affected by the combustion conditions. High temperatures and under-ventilated or vitiated condition favour the formation of HCN [24–26].

Even without HCN included, incapacitating dose is reached fairly quickly, approximately 5 min after the start of the increase. It should be noted that the transport time is not subtracted, that is, the time in the graphs is the time at the measurement station after ignition.

The fraction of an incapacitating dose (FI) for heat exposure based on the Runehamar test T2 is compared with the results for asphyxiant gases in Fig. 15.2. Incapacitating dose for a lightly clothed person (Conv, L) is reached after 25 min, that is, in T2 the convection curve is far behind the one for asphyxiant gases. In the case with a fully clothed person (Conv, F), the level of incapacitating dose is not reached. It should be remembered that the calculations presented here are based

on measurements performed 458 m from the seat of the fire. The effect of the heat exposure will increase closer to the fire. In the work presented by Ingason et al. [27] it was shown that in most cases (scenarios), the temperature and radiation quickly increases above critical values for the occupants in the tunnel. Another conclusion from the same work was that the calculations showed a critical value of 75 MW above which it can be difficult for the occupants in the tunnel to reach the escape routes and survive the fire. If no evacuation is started, only the smallest fire (8 MW) can be survived. During a bus fire (25 MW), critical levels can be reached after long exposure times and for larger fires, the critical values are relatively rapidly reached. The occupants in the cases of no evacuation were assumed to be either 70 or 150 m from the fire.

The results given in this section should be seen as an example of the influence of gas composition and heat on the fraction of an incapacitating dose. The conditions in a specific situation during a fire in a tunnel are very complex and several parameters, for example, the degree of activity of the occupants, affect the results. It should also be noted that age and different kinds of impairment (For example, disease and physical conditions) significantly affects the critical COHb level (COHb levels found in victims) [4]. The results do confirm, however, the importance of the first minutes during a tunnel fire for the ability of the occupants in the tunnel to escape the incident. Note that, the criteria FI = 1 relates to a limit at which 50 % of the population would be expected to experience tenable conditions, while 50 % would be expected to experience compromised tenability [8]. Therefore, it is important to use more conservative numbers for a designer, authority or fire safety engineer. On the other hand, the fast increase (t^2) of many fires means that uncertainties due to variations in the individual susceptibility have a relatively small effect on the predicted times to incapacitation [3].

15.7 Irritant Gas Model

For evaluating the effect of irritant gases, often the concept of fractional effective concentration (FEC) is used. This means that the FEC is determined for each time step for each irritant and the time when the sum of the FEC for each irritant exceeds a certain threshold represents the time when a specific tenability limit is exceeded. This can be expressed as [8]

$$\mathrm{FEC} = \frac{\mathrm{HCl}}{\mathrm{IC}_{\mathrm{HCl}}} + \frac{\mathrm{HBr}}{\mathrm{IC}_{\mathrm{HBr}}} + \frac{\mathrm{HF}}{\mathrm{IC}_{\mathrm{HF}}} + \frac{\mathrm{SO_2}}{\mathrm{IC}_{\mathrm{SO_2}}} + \frac{\mathrm{NO_2}}{\mathrm{IC}_{\mathrm{NO_2}}} + \\ + \frac{\mathrm{acrolein}}{\mathrm{IC}_{\mathrm{acrolein}}} + \frac{\mathrm{formaldehyde}}{\mathrm{IC}_{\mathrm{formaldehyde}}} + \sum \frac{\mathrm{irritant}}{\mathrm{IC}_{\mathrm{irritant}}} \tag{15.22}$$

Table 15.10 IC values for some irritants [8]

Irritant	IC (ppm)
HCl	1000
HBr	1000
HF	500
SO_2	150
NO_2	250
Acrolein	30
Formaldehyde	250

Table 15.11 Yields of some irritant gases from a car fire [28]

Irritant	Yield (g/kg)
HCl	2400
SO_2	5.0
Acrolein	<0.3
Formaldehyde	1.1

where the values of IC (incapacitating concentration) for each irritant represent a concentration (ppm) when the tenability is seriously compromised. In Table 15.10, values are presented for IC for the irritants in Eq. (15.22).

Except for HCl, many of the gases in Eq. (15.22) and Table 15.10 are not analysed for or not detected in most fire tests. Lönnermark and Blomqvist, however, reported yields for some of the species in connection with a car fire test [28]. These yields are presented in Table 15.11.

15.8 Acceptance Criteria

In Sect. 15.5, different aspects of tenability were presented. The fraction of an incapacitation dose can be used when modelling an evacuation situation in performance-based design using advanced computer models or one dimensional dynamic fire development and change in the tunnel environment at different positions. In addition to this, there are several sources of acceptance criteria or acceptable exposure. The main issue is to ensure safe egress. There are several different factors affecting escape from a tunnel. The parameters that will be included here are visibility, gas temperature, radiation and toxic gases. Visibility was also discussed in detail in Chap. 14.

Different acceptance criteria have been suggested for these parameters. In the EU project UPTUN an analysis of different aspects were performed and the values given in Table 15.12 were suggested [29].

Within a Swedish project aiming at developing a proposal for a Swedish performance-based design guide for fire safety in road tunnels different acceptance criteria were also discussed [30]. These are also included in Table 15.12. The Swedish

Table 15.12 Examples of acceptance criteria for different types of exposure

Parameter	UPTUN [29]	FKR-BV12 [30]	TRVR [31]	BBRAD1 [15]
Visibility	≥10 m		10 m in unknown env. 5 m in known env. Height below smoke layer > 1.6 m + H × 0.1 m	10 m in spaces > 100 m^2 5 m in spaces ≤100 m^2 Height below smoke layer > 1.6 m + H_{room} × 0.1 m
Gas temperature	≤60 °C	<80 °C	<80 °C	≤80 °C
Radiation (kW/m^2)	≤2 kW/m^2	<2.5 kW/m^2	<2.5 kW/m^2 or short duration of <10 kW/m^2	≤2.5 kW/m^2
Toxic gases	FI_{tot} < 1[a]	$[CO_2]$ 5 % [CO] > 2000 ppm $[O_2]$ > 15 % during max 1 min or FI_{tot} 0.3 (including at least CO, CO_2, O_2 and HCN)		$[CO_2]$ > 5 % [CO] > 2000 ppm $[O_2]$ > 15 %
Heat			≤60 kJ/m^2 + the energy from a radiation of 1 kW/m^2	≤60 kJ/m^2 + the energy from a radiation of 1 kW/m^2

[a] In a similar way as described by Eq. (15.6)

Transport Administration (Trafikverket) has published advice related to technical requirements for road and rail tunnels in Sweden [31]. These are presented under TRVR in Table 15.12. For comparison also values to be used for performance-based (analytical) design of buildings in Sweden (BBRAD 1) [15] are included in Table 15.12.

In the UPTUN report, specific acceptance criteria were also given for the fire and rescue services [29]:

- Gas temperature ≤ 100 °C
- Radiation ≤ 5 KW/m^2
- Toxic gases: no limitation due to breathing apparatus (BA)
- Visibility: No limitation due to infra-red cameras

15.9 Summary

Occupants in a tunnel can during escape be exposed to different types of hazards. In this chapter, the most important consequences of exposure to main gas components, radiation and heat are presented. The effects of the most common asphyxiant (CO and HCN) and irritant gases are given. Since one of the most important issues during a fire in a tunnel is the possibility for a safe escape, different exposures affecting the escape are discussed. The effects often depend on both the concentration and the time of exposure. Different models for estimating time to incapacitation and other endpoints due to exposure are discussed. These models are useful when estimating the possibilities for escape from a fire situation. This is exemplified by using data from full-scale fire tests. In some guidelines, there are absolute levels given for exposure and in this chapter some such examples are given and discussed.

References

1. Hull TR, Stec AA (2010) Introduction to fire toxicity. In: Stec A, Hull R (eds) Fire Toxicity. CRC
2. Tan K-H, Wang T-L (2005) Asphyxiants: Simple and Chemical. Annals of Disaster Medicine 4 (1):S35-S40
3. Purser DA (2008) Assessment of Hazards to Occupants from Smoke, Toxic Gases, and Heat. The SFPE Handbook of Fire Protection Engineering, 4th ed. edn. Quincy: National Fire Protection Association., 2–96 -- 2–193
4. Nelson GL (1998) Carbon Monoxide and Fire Toxicity: A Review and Analysis of Recent Work. Fire Technology 34 (1):39–58
5. Varon J, Marik PE, Fromm RE, Gueler A (1999) Carbon Monoxide Poisoning: A Review for Clinicians. The Journal of Emergency Medicine 17 (1):87–93
6. EPA (2012) Acute Exposure Guideline Levels (AEGLs): Hydrogen fluoride Results. United States Environmental Protection Agency, http://www.epa.gov/oppt/aegl/pubs/results53.htm, Updated Jan. 11 2012, Accessed Jan. 14 2014
7. Acute Exposure Guideline Levels for Selected Airborne Chemicals, Volume 4 (2004).
8. ISO (2012) Life-threatening components of fire – Guidelines for the estimation of time to compromised tenability in fires. International Organization for Standardization, SS-ISO 13571:2012
9. IDLH (1994) Documentation for Immediately Dangerous To Life or Health Concentrations (IDLHs) – Chemical Listing and Documentation of Revised IDLH Values (as of 3/1/95). NIOSH
10. AFS (2011) Occupational Exposure Limit Values. The Swedish Work Environment Authority, AFS 2011:18
11. ISO (2004) Estimation of the lethal toxic potency of fire effluents. International Organization for Standardization, ISO 13344, Second edition
12. Levin BC, Paabo M, Gurman JL, Clark HM, Yoklavich MF Further Studies of the Toxicological Effects of different Time Exposures to the Individual and Combined Fire Gases: Carbon Monoxide, Hydrogen Cyanide and Reduced Oxygen. In: Polyurethane ’88, Proceedings of the 31st Society of Plastics Meeting, Lancaster, PA, 1988. Technomic Publishing Co., pp 249–252

13. Purser DA (2010) Toxic hazard calculation models for use with fire effluents data. In: Stec A, Hull R (eds) Fire toxicity. CRC
14. Purser D (2014) Models for toxicity and tenability limits. Personal communication, Jan. 5,
15. BFS (2011) Boverkets allmänna råd om analytisk dimensionering av byggnaders brandskydd. Boverkets Författningsamling, BFS 2011:27 BBRAD 1 (in Swedish)
16. Ingason H, Lönnermark A, Li YZ (2011) Runehamar Tunnel Fire Tests. SP Technicial Research Institute, SP Report 2011:55
17. Ingason H, Lönnermark A (2005) Heat Release Rates from Heavy Goods Vehicle Trailers in Tunnels. Fire Safety Journal 40:646–668
18. Lönnermark A (2005) On the Characteristics of Fires in Tunnels. Doctoral Thesis, Doctoral thesis, Department of Fire Safety Engineering, Lund University, Lund, Sweden
19. Brandt AB Presentation of test result from large scale fire tests at the Runehamar tunnel. In: Ingason H (ed) International Symposium on Catastrophic Tunnel Fires (CTF), SP Report 2004:05, Borås, Sweden, 20–21 November 2003. SP Swedish National Testing and Research Institute, pp 117–120
20. Lighty JS, Pershing DW (1993) Control of Pollutant Emissions from Waste Burning. University of Utah, Project number AQ93-4
21. Risholm-Sundman M, Vestin E (2005) Emissions during combustion of particleboard and glued veneer. Holz als Roh- und Werkstoff 63:179–185
22. Grønli M (1996) A Theoretical and Experimental Study of the Thermal Degradation of Biomass. Doctoral Thesis, The Norwegian University of Science and Technology, Trondheim, Norway
23. Zevenhoven R, Axelsen EP, Kilpinen P, Hupa M Nitrogen oxides from nitrogen-containing waste fuels at FBC conditions – Part 1. In: The 39th IEA FBC meeting, Madrid, Spain, 22–24 November 1999.
24. Simonson M, Tuovinen H, Emanuelsson V (2000) Formation of Hydrogen Cyanide in Fires – A Literature and Experimental Investigation. SP Swedish National Testing and Research Institute, Borås, Sweden
25. Tuovinen H, Blomqvist P (2003) Modelling of Hydrogen Cyanide Formation in Room Fires. SP Swedish National Testing and Research Institute, Borås, Sweden
26. Hansson K-M, Samuelsson J, Tullin C, Åmand L-E (2004) Formation of HNCO, HCN, and NH3 from the pyrolysis of bark and nitrogen-containing model compounds. Combustion and Flame 137:265–277
27. Ingason H, Bergqvist A, Lönnermark A, Frantzich H, Hasselrot K (2005) Räddningsinsatser i vägtunnlar. Räddningsverket,
28. Lönnermark A, Blomqvist P (2006) Emissions from an Automobile Fire. Chemosphere 62:1043–1056
29. Ingason H (ed) (2005) TG2.2– Target criteria. UPTUN Report WP2– task Group 2,
30. Gehandler J, Ingason H, Lönnermark A, Frantzich H, Strömgren M (2013) Performance-based requirements and recommendations for fire safety in road tunnels (FKR-BV12). SP Technical Research Institute of Sweden
31. TRV (2011) TRVR Tunnel 11: Trafikverkets tekniska råd Tunnel. Trafikverket, TRV publ nr 2011:088 (in Swedish)

Chapter 16
Fire Suppression and Detection in Tunnels

Abstract The basic concepts of fire suppression systems are depicted. There are mainly two water-based fire suppression systems used in tunnels, that is, water spray systems and water mist systems. The main differences are the water density, pressure, and droplet size. The extinguishment mechanisms are explored and the critical conditions at extinction are discussed. Further, suppression of realistic fires is discussed considering both the water flow rate and the total water flow rate used for fire suppression. A summary of fire suppression tests carried out in tunnels is presented followed by a short discussion of tunnel fire detection.

Keywords Fire suppression · Deluge · Water spray · Water mist · Surface cooling · Gas cooling · Extinction · Critical water flow rate · Fire detection · Fire tests

16.1 Introduction

Sprinkler systems in buildings and warehouses have now been used for over 100 years. The definition of a sprinkler system for buildings is found in NFPA13 [1]. The use of sprinklers in tunnels began in Japan in 1963 [2], however, there is still confusion about how to design sprinkler systems in tunnels. The most common system to date used in tunnels is the Fixed Fire Fighting Systems (FFFS), which includes all types of fixed *water-based systems* and *foam-based systems*. This classification depends on what the main extinguishing medium is. If the system uses a foam agent as the main extinguishing medium (light water foam, compressed air foam) it is referred to as a 'foam system'. On the other hand, if the system uses water as the main extinguishing medium (even with a small amount of foam additives), it is referred here to as a "water-based system".

The nomenclature used also depends on how the systems are constructed, activated, and operated. The most common systems applied in tunnels nowadays operate in zones (*deluge systems*), however, a few systems are activated by individual bulbs (*automatic systems*) which are the same as those used in buildings.

H. Ingason et al., *Tunnel Fire Dynamics,* DOI 10.1007/978-1-4939-2199-7_16

For clarification, when discussing “FFFS” or “sprinklers” in this chapter it means all types of water-based FFFS by default.

Water-based systems can be divided into *water spray systems* and *water mist systems*, depending on the operating pressure and the water droplet size. If the system operates under low pressure (generally several atmospheric pressure), it is usually called a ‘water spray system’, whereas if it operates under high pressure (generally over 10 atm) with very small droplets it is referred to as a ‘water mist system’. Water mist systems can be subdivided into low pressure water mist systems (around 10 atm) and high pressure water mist systems (For example, 80 atm). Water spray systems and water mist systems (that is, water-based systems) are usually operated in zones that are remotely controlled by valves. More details on different types of systems are given in Sect. 16.2.

Depending on the performance in relation to a given fire, FFFS can be classified in different ways, however, there are no standard design fires against which the performance of the FFFS in tunnels can be tested or classified. Usually, one discusses the performance of water based FFFS in tunnels in terms of

- suppression of the fire,
- control of the fire, or
- thermal management of the fire.

The word ‘fighting’ from the acronym FFFS can be misleading in terms of performance of the system. The first priority is activation of the system (if necessary), then to protect the tunnel structure, reduce and prevent further development of the fire, and to mitigate the hazardous situation for tunnel users. It also should be a complement to firefighting operations.

Fire suppression, according to NFPA13 [1], is defined as “sharply reducing the heat release rate (HRR) of a fire and preventing its regrowth by means of direct and sufficient application of water through the fire plume to the burning fuel surface”. In the road tunnel standard NFPA 502, Standard for Road Tunnels, Bridges, and Other Limited Access Highways [3], suppression is explained in the informative part of the standard as “Fire suppression systems are designed to arrest the rate of fire growth and significantly reduce the energy output of the fire shortly after operation”. This text is more general than that written in NFPA13 [1].

Fire control is defined in NFPA 13 as “Limiting the size of the fire by distribution of water so as to decrease the HRR and pre-wet adjacent combustibles, while controlling ceiling gas temperatures to avoid structural damage”. NFPA502 [3] reads “Fire control systems are designed to significantly reduce or stop the rate of fire growth, but not necessarily to reduce the energy output of an established fire”. Here again, the text in NFPA13 is more detailed and specific.

The term *thermal management* could be related to the term “volume cooling systems” described in the Annex of NFPA502: “Volume cooling systems are designed to reduce the temperature of heated products of combustion, and of systems and tunnel structures, but may not have any direct effect on fire size or fire growth rate.”

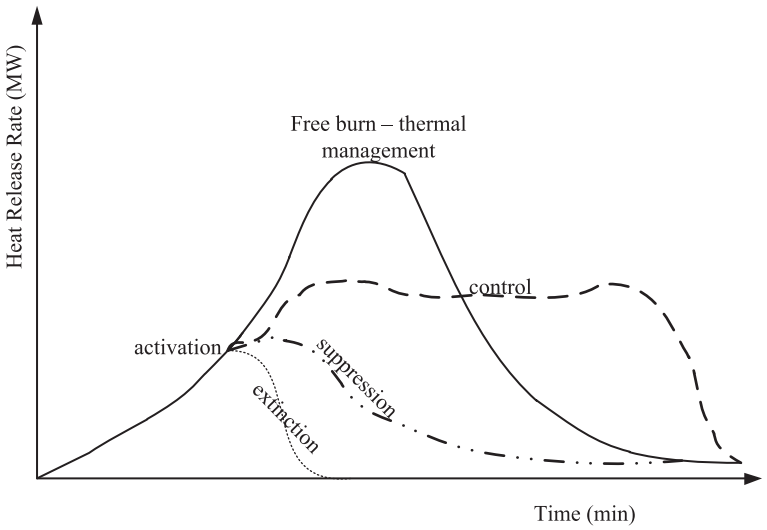

Fig. 16.1 A schematic of the performance objectives of water-based FFFS

There is one more performance possibly achieved by sprinkler systems, namely *extinguishment* or *extinction*. This means, a complete elimination of the fire HRR and protection of all the surfaces shortly after the system is activated. However, in tunnels extinguishment is mostly not the FFFS design objective. Further, most systems work in deluge mode, that is, operate in zones with a given water density. In contrast, in buildings extinguishment is much more easily obtained because most sprinkler heads operate automatically. This means that at the early stages of a fire the sprinklers right above the fire can operate with a very high water density. In Fig. 16.1, a sketch explaining each of the terms is given.

The terminology of "suppression" commonly used in tunnel fire safety may be slightly misleading as it is generally not meant to extinguish the fire or suppress it completely or efficiently. The idea is to arrest the flame volume so that the heat feedback is reduced immediately. At the same time, there is a need for delivery of water to cool the fuel surface to such a degree that the pyrolysis process is reduced significantly, although not completely. Usually, fires in solids are deep-seated and in order to extinguish the fire additional water density is required. The main difference between suppression and extinction is therefore the amount of water that reaches the fuel surfaces per unit area. When automatic sprinkler heads activate at an early fire stage in buildings they usually have an overcapacity in relation to their design criteria whereas deluge systems in tunnels do not. They simply deliver the designed amount of suppression media in each zone. On the other hand, they can cover larger areas and the risk that the fire will escape is significantly reduced. The idea of controlling fires instead of suppressing them comes from the awareness that a sprinkler system is designed to cover a certain area when all the nozzles have activated. In

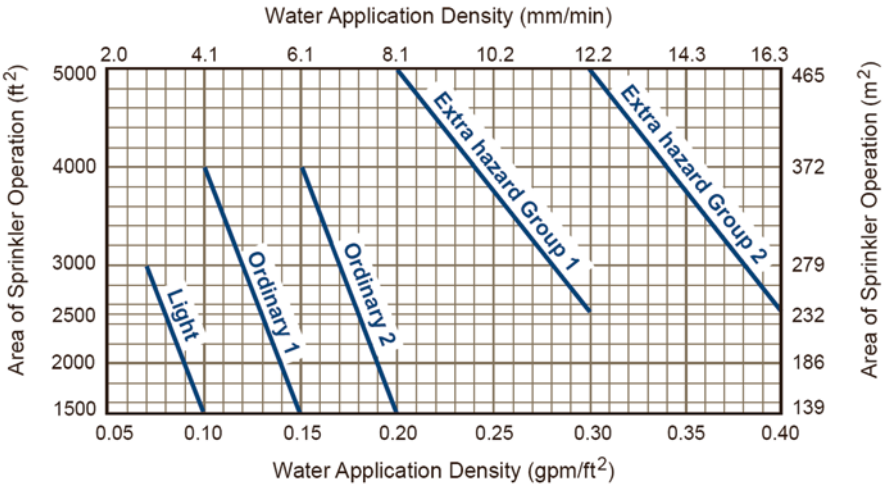

Fig. 16.2 A graph of necessary water density for sprinkler systems given in NFPA13

any case, the applied water density should be enough to control the fire, that is, control the rate of burning, and protect the structure.

The terminology of water density is related to the fuel that should be protected, however, it has been adapted to tunnels without any clear correspondence to the type of fuel. Numerous experiments were conducted in 1960–1990 with pool fires (sometimes referred to as Class B fires), and cars, small trucks and buses [2] (sometimes referred to as solid material or Class A fires). These results provided a basis for designing tunnels with 6 mm/min (6 l/(min m^2)) water density, which implies that a water density of 6 mm/min for a deluge system should be enough to control and prevent fire spread. In Australia, the water density in deluge systems is in the range of 7.5–10 mm/min, although tests using deluge systems with that density were not carried out in tunnels when adopting it. Large-scale tests using 8 and 12 mm/min have been conducted by the Land Transport Authority (LTA) in Singapore with good results [4, 5]. In the Benelux tests [6], water density of 12 mm/min were used. Most water mist systems use much lower water density, on the order of 1–4 mm/min.

It is interesting to compare these water densities with the NFPA13 standard for buildings. Figure 16.2 shows the water design area of the sprinkler system as a function of the water density. As the design area increases the water density requirement decreases, although the total applied water flow rate increases. The choice of a design line is based on the classification of the expected fuel load and activity in the building. The hazard groups are divided into different categories, see Fig. 16.2. Examples are given of different occupancy groups (three examples for each group are given here, for others see NFPA13):

- light hazard occupancies
  - churches
  - hospitals
  - restaurant areas
- Ordinary hazard occupancies (group 1)
  - Automobile parking
  - Electronic plants
  - Laundries
- Ordinary hazard occupancies (group 2)
  - Chemical plants
  - Machine shops
  - Paper process plants
- Extra hazard occupancies (group 1)
  - Plywood and particle board manufacturing
  - Saw mills
  - Upholstering with plastic foam
- Extra hazard occupancies (group 2)
  - Flammable liquid spraying
  - Plastic processing
  - Solvent cleaning

It is clear from this classification that there is a correlation to tunnel occupancy in the form of vehicles and other types of fuel load, for example in the cargo of a heavy goods vehicle (HGV). The sprinkler systems are designed to control the fire within a given design area (area of operating sprinklers). According to NFPA13, this area varies from 140 to 465 m^2, as shown in Fig. 16.2. If we assume that we have a tunnel that is 10 m wide, this would correspond to a zone length of about 15–50 m, which is within the size of zone lengths designed for tunnels today. In Sect. 16.2, these zone lengths will be discussed in more detail. In tunnels, the average fuel density over the protected zone is usually much lower than in buildings, although the local fuel density in tunnels could be higher. Further, the ventilation conditions are very much different in tunnels and can play an important role. It is, however, clear that the water density design for tunnels has a reasonable correspondence with building water density.

16.2 Basic Concepts of Fire Suppression Systems

In the following text, a detailed description of different types of FFFS is given. As mentioned earlier, the fire suppression systems in tunnels can be categorized into water-based FFFS and foam systems. Water-based FFFS can be subdivided into deluge water spray systems and water mist systems, both with and without the use of foam additives. All of these systems have been applied to tunnels, although deluge systems without additives represent the vast majority of the installed systems.

16.2.1 Deluge Water Spray System

16.2.1.1 General Description

Deluge water spray systems consist of open sprinklers[1] or water spray nozzles[2] attached to pipework at the tunnel ceiling. The pipework consists of mains pipes, manifold pipes, feed mains, and branch pipes. The sprinklers or nozzles are attached to the branch pipes, which are typically arranged in a uniform pattern at the ceiling to distribute spray to all sections of the roadway. The branch pipes are connected to a feed main which is connected to a deluge valve. The deluge valve is mounted on a manifold attached to a mains pipe that is supplied by one or more water reservoirs or fire pump stations. Mains pipes are normally water-filled up to the point of connection to the deluge valve. Therefore, the mains pipe and the deluge valves must be protected against freezing. The deluge valve separates the water-filled mains pipe from the empty (dry) feed main and branch pipes supplying the sprinklers or spray nozzles. When the deluge valve is opened, water flows into the feed main and branch pipes and discharges from the open sprinklers.

The branch piping is divided into deluge zones, typically 25–50 m in length, each served by its own deluge valve. An independent fire detection system that is capable of locating a fire accurately is required, so that the deluge valve serving the zone where the fire is located can be released. The deluge valve can be opened either automatically by the detection system, or manually by a signal from the tunnel operator. If an incident occurs on the boundary between two deluge zones, both zones may need to be activated. When the deluge valve opens, water flows into the feed main and branch piping and discharges from all sprinklers or nozzles in that deluge zone. As the water spray nozzle (or sprinkler head) orifices are open, the branch piping is at atmospheric pressure until water is introduced. A water spray system has a time delay between detection of a fire and the discharge of water from the sprinklers or nozzles due to the time required to operate the valve (which depends on whether activation is automatic or manual) and to fill the branch piping network with water and reach the desired operating pressure.

According to recommendations provided in NFPA 502 [3], standard water spray nozzles should be spaced such that the coverage of the water spray extends to the roadway shoulders and, if applicable, maintenance and patrol walkways. The system should be designed with sufficient water capacity to allow simultaneous operation of at least two consecutive deluge zones, but depending on the precision provided by the detection system, it may be necessary to design for three operating zones, one in the incident area, and the adjacent upstream and downstream zones.

[1] An open sprinkler is a sprinkler that does not have actuators or heat-responsive elements.

[2] An open spray nozzle is an open water discharge device that will distribute the water in a specific, directional pattern. Spray nozzles are typically used in applications requiring special water discharge patterns, directional spray, or other discharge characteristics.

The length of the deluge zones should be coordinated with the pumping capability as well as the fire detection and ventilation zones. Piping should be designed to allow drainage of water from all piping between the deluge valve and the sprinklers or nozzles after the flow is stopped.

16.2.1.2 Specific Technical Information

The length of deluge zones typically varies from 25 to 50 m. Standard water spray nozzles, which typically require a minimum operating pressure of 1.5–5 bar are used and they discharge a uniform pattern of water droplets over the protected area with droplet sizes less than 2 mm in diameter. The water discharge density over the length of the deluge zone or predefined area commonly in tunnel fires is in the range of 6–12 mm/min (l/(min m^2)). The K-factor of the nozzles is typically 80 L/(min $bar^{1/2}$). Tests with fires having potential free burning HRRs in the order of 25–140 MW have been conducted with deluge water spray systems.

The most suitable length of the deluge zones must be based on the width of the tunnel and the capacity of the water supply. Large zones will reduce the number of control valves but require a higher total water demand [7]. The typical application rates and zone sizes can result in flow demands in the range of 7500–15,000 L/min, which can have a significant impact on supply and drainage system requirements [8]. This value is very much dependent on the tunnel width. For example in a 15 m wide tunnel, a density of 10 mm/min, and a two operating deluge zones each having a length of 50 m would require 15,000 L/min. If the tunnel width is 10 m instead, the corresponding flow would be 10,000 L/min, which is significantly lower.

The type of fire detection device is selected, mainly, based on the hazard (For example, smoke detectors, heat detectors, CCTV, or optical flame detectors). The initiation device signals the fire alarm panel, which in turn signals the deluge valve to open. Activation can also be manual, depending on the fire protection objectives of the system. Manual activation is usually done via an electric or pneumatic fire alarm pull station, which signals the fire alarm panel, which in turn signals the deluge valve to open. According to the SOLIT guidelines [9], water spray systems may be activated and operated manually or automatically depending on the availability of trained personnel, the risks expected, the type of water spray system, the control systems used, and applicable legislation. NFPA 502 [3] recommends that the time delay should not exceed 3 min in order to prevent the development of a major fire. NFPA 502 also say that automatic fire detection system should be able to detect a tunnel fire incident of 5 MW or less within 90 s or better in testing environment of 3 m/s. More information on fire detection in tunnels is presented in Sect. 16.5.

The UPTUN [10, 11], and SOLIT [9] guidelines recommend that the installation of pumps shall comply with the manufacturer's documented requirements. Pumps shall be installed in a dedicated pump room or other designated area. Adequate ventilation and drainage shall be provided. The pump room shall be lockable to prevent access of unauthorized personnel. Deluge water spray systems shall be designed to

provide at least 110% of the nominal flow rate required for the most demanding protection area in the tunnel. This flow rate shall be calculated at the minimum nozzle pressure as tested in large-scale fire tests and shall be provided by one or more pumps.

According to the SOLIT guidelines [9], the duration time shall be determined in a specific risk analysis for every individual tunnel. The system shall be capable of a minimum activation time of 30 min, although longer activation times are normally required. A minimum of 60 min shall be used for tunnels longer than 500 m, however, in practice 90–120 min are probably necessary to account for the response capabilities of the fire department.

Deluge water spray systems are mostly installed in Australia and Japan.

Australian Deluge Systems Australia has installed FFFS systems into its road tunnels since the Sydney Harbour Tunnel was opened in 1992. Currently, there are 19 tunnels with water spray systems in operation. A deluge valve station is generally located every 120 m along the tunnel length. This location coincides with the location of cross passages or egress passages and therefore the valves are located inside a fire rated space. The deluge valves are designed and timed to open and close automatically as the valves are at a considerable distance from the tunnel operations control room. This means that the operator can open and close deluge valves as required during a fire scenario, especially if the fire moves or spreads.

The deluge zone length can vary but has generally been designed around a deluge zone area of 300 m^2 which covers the full width of the roadway. Consequently, the length of the deluge zone can vary according to tunnel width. The system is designed for simultaneous activation of, however, many zones are required to provide complete coverage of the maximum length vehicle that uses the tunnel plus allowance to cover the possibility that the vehicle may be at the boundary of two zones. Currently, common practice is to provide a water discharge density of between 7.5–10 mm/min in road tunnels. Australia also has some tunnels which are only used by buses. The water discharge density for these tunnels is generally 6 mm/min. In a fire scenario, the system flow rate is designed to operate for 60 min at full flow while a number of hydrants operate simultaneously. Pumps and tanks (if required) are duplicated so that no single failure can affect the water spray system performance.

Activation of the water spray system is usually by manual operation from a remote Control Room. The operator receives an alarm from one or a number of detection systems such as a Video Automatic Incident Detection (VAID) system, linear heat detection system, other Closed Circuit TV (CCTV) cameras and/or manual alarm calls. On receipt of the alarm, the operator confirms that there is a fire event and activates the water spray system. Most systems are configured so that on alarm, unless the operator intervenes, the water spray system activates. However, the operator can initiate the system prior to automatic operation. The operational intent is to activate the FFFS as soon as possible while the fire is still small, that is, less than 10–20 MW [12].

Japanese Deluge Systems Japan introduced deluge systems into its high risk urban tunnels 40 years ago, and currently there are over 120 systems in operation. Different technical solutions are applied, depending on the owner of the tunnel. The Japanese deluge water spray systems are designed for 6 mm/min. The pressure at the nozzle location is between 3 and 3.5 bars. There are either 50 m spray zones or 100 m spray zones. Depending on the owner there are different distances between nozzles in each zone. Water reservoir capacity should be designed as 40 min for the operation time for two deluge zones (50 or 100 m) [14]. System design and operation is as follows [13]:

1. Flame detectors are located on tunnel side walls at 1.1–1.3 m height with 10–13 m spacing within the whole section for initial detection of the fire
2. The fire location is confirmed in the Control Room by CCTV, at which time the deluge system is manually activated for a 50 m zone around the seat of the fire until the fire brigade arrives to the fire site
3. To minimize the risk of fire spread, one additional deluge zone will be activated.

Technically, the Japanese water and foam sprinkler systems are automatic in design in combination with fire detector and automatic valve control. However, as automatic operation of sprinklers could cause a traffic accident, the tunnel operator must recognize the fire and confirm its existence by CCTV, before starting the sprinkler system. Once the fire has been visually confirmed, the sprinkler system is started manually as quickly as possible [13].

Swedish Simplified Deluge Water Spray System In 2012, the Swedish Traffic Administration started to install a simplified deluge water spray system in the tunnel of the Northern Link. An improved version of the concept is also planned to be used in the Stockholm Bypass when it will open in 2020. In total, the system will be installed in 50 km of tunnels.

The design considerations were: simplicity, robustness, investment cost, and maintenance issues. To meet these design requirements the system consists of:

- A single pipe in the centre line of the tunnel ceiling, fitted with two extended coverage nozzles (large K-factor nozzles) directed horizontally toward each of the tunnel walls. The entire cross section of the 14 m wide tunnel is covered with only one pipe. The nozzles used for the Northern Link have a K-factor of 240 (L/(min·bar$^{1/2}$)) and the nozzles for the Stockholm Bypass have a K-factor of 360 (L/(min·bar$^{1/2}$)).
- Long sections of 50–75 m are used and they are designed to deliver 5–10 mm/min without the use of any water additives. A lower water density is acceptable if two sections are activated due to a fire between them,
- The deluge water spray system is combined with the fire hydrant system, reducing the need of water mains in the tunnel to only one,

- The water supply is obtained by connection to the public water supply, and no additional pumps are required. This means that the duration time of the water supply is virtually unlimited.
- Thermoplastic-coated steel pipes and clamp couplings instead of welded stainless steel pipes have been used.

The main purpose of the system is to limit the fire size and prevent fire spread during the evacuation period in congested traffic situations. When the traffic is flowing freely the need for the system is regarded as minor. The system can be manually operated from the Traffic Control Centre based on detection by CCTV, or from the tunnel escape routes where the deluge valves are located. The system also starts automatically if a heat sensing cable detects high temperatures from a fire. The sprinkler pipes are self-draining due to the risk of freezing. In winter, the temperature in the traffic space is expected to drop below −20 °C.

16.2.2 Water Mist Systems

Water mist systems are fundamentally similar to deluge water spray systems, that is, the pipework consists of a water-filled mains pipe, manifold, deluge valves, dry feed main, and branch pipes to which the nozzles are attached. The mains pipe is connected to a water supply and the pressure is generated by pumps. Water mist deluge systems may vary with respect to their working pressures, that is, low and high pressure mist systems. The piping or tubing utilized in the system must be designed for the corresponding operating pressure. To protect against plugging of small orifice nozzles, water mist systems utilize corrosion resistant materials such as stainless steel pipe or tubing. The primary difference between the systems are the percentage of smaller droplet sizes (as a rough estimation the droplet size is inversely proportional to the pressure applied), and the momentum of the spray ejected from the nozzles (for a given water flow rate the spray from a high pressure nozzle has a higher momentum than that from a low pressure nozzle).

According to the definition given in UPTUN guidelines [10] the general principle of the low pressure water mist system is to produce a fog (or mist) of small water droplets at a nozzle pressure of 3–10 bar. The high pressure water mist system produces a fog (or mist) with a mix of different sizes of water droplets at a nozzle pressure of 60–120 bar.

According to the Annex table in the UPTUN document [11], the total water flow rate per 25 m zone for low pressure systems (without additives) is in the range of 221–683 L/min, and for high pressure systems, 140–550 L/min. Note, however, that the total water flow rate depends on the tunnel width, zone length and the number of zones operating. One zone of 25 m in a 10 m wide tunnel, at 2.3 mm/min, would require 575 L/min. Designing for two zones would require a pumping capacity of 1150 L/min (+10 % of the nominal flow required), and for three 25 m zones, 1725 L/min (+10 %). If the tunnel is more than 10 m wide and the zones longer than 25 m, the hydraulic demand and pump capacity is much higher. The discharge rate

for low pressure systems is in the range of 1.1–3.3 mm/min and for high pressure systems 0.5–2.3 mm/min. Note that the design application densities are based on a density per unit area of coverage (l/(min m^2) or mm/min). They are sometimes converted to another measure often used when discussing water mist systems, namely a volumetric density expressed as a flow rate per volume (L/(min m^3)) by dividing mm/min by the ceiling height of the tunnel in meters. This means that for two tunnels with the same width but different tunnel heights, the water spray densities are identical when expressed in terms of tunnel area, but very different when expressed in terms of volume. The K-factor for a high pressure system can vary between 4.0–5.5 L/(min $bar^{1/2}$). The length of each zone can vary from 20 to 25 m and up to three zones can be used at once.

The water mist systems use significantly less water than deluge water spray systems. On the other hand, they require significantly higher pressure, especially the high pressure system. As a result, pipes, tanks, and pump capacities can be smaller, and the water demand be lowered. Likewise, drainage volumes can potentially be lowered [12].

According to the SOLIT guidelines [9], a high pressure water mist system applies nozzle pressures above 35 bars. Low pressure water mist systems apply nozzle pressure of less than 12 bars. The medium pressure water mist systems apply nozzle pressure between 12–35 bar. Water mist systems apply small water droplets as the firefighting agent. The diameter of drops contained in a volume of spray from a water mist nozzle, that is, the "Dv0.90" value (meaning that 90 % of the volume of the spray is contained in drop sizes of less than 1 mm) is measured in a plane 1 m from the nozzle at its minimum operating pressure [9]. NFPA 750 uses a "Dv099" value instead of a "Dv0.90" value to define a "water mist". The NFPA 750 definition ensures that almost no drops are larger than 1 mm in diameter.

Centrifugal pumps are typically used for low pressure and medium pressure systems, whereas positive displacement (PD) pumps (or assemblies of PD pumps) are typically used for medium and high pressure systems. For the pump capacity, the same rule should be applied as for water spray systems. The minimum output capacity for positive displacement pumps, or assemblies of PD pumps, shall be 90 L/min. The minimum capacity for centrifugal pumps shall be 750 L/min. The water tank shall be suitable for providing water for all simultaneously activated sections (typically two or three) with the required flow rate based on the defined minimum period of operation [9].

16.2.3 Foam Systems

There are mainly three types of foam systems. A foam water spray system with injected foam concentrates into the water supply, a high expansion foam system (Hi-Ex), and compressed air foam (CAF).

A foam water spray system is a specific application system, discharging low expansion foam, resulting in a foam spray from the sprinkler. Foam water spray

systems are effective in controlling fires involving flammable liquid spills in tunnels, but they are also effective against conventional lorry fuel load fires [15]. Systems using injected foam concentrates can be both deluge water spray systems and water mist systems, as described in Sect. 16.1.

The discharge density needed in order to extinguish or control flammable liquid fires using water with a film forming additive is reasonably well established. Information is given in NFPA 16, which recommends an average discharge density of 6.5 mm/min. Large-scale fire suppression tests in tunnels show good performance for foam-water sprinkler systems. In tests conducted by Arvidson in 2010 [16] water and foam additives (3% AFFF) were pumped from a container to the deluge zone with nozzles. The tests showed that the effectiveness of the deluge foam-water spray system was not negatively affected by a longitudinal ventilation velocity of 4.2 m/s. The test fires were extinguished in less than 30 s.

Technology involving CAF [17] or Hi-Ex [18] has been tested against both solid and liquid fuel fires. These foam system tests demonstrated a good degree of fire control. As pointed out by Mawhinney [15] neither the CAF nor Hi-Ex systems have been widely accepted for use in tunnels. One reason is uncertainty about the potential loss of visibility for firefighting and rescue operations, particularly with Hi-Ex foam.

16.2.4 Mode of Operation

There are different types of operation modes presented by different manufacturers. The most common is the deluge mode. Mawhinney and Telles [19] presented three modes of operation: the deluge mode, the sprinkler mode, and the hybrid mode. The major difference between the modes is the amount of water discharged outside the immediate fire region. This forms the basis for the attempt to reduce costs without weakening firefighting performance.

In the deluge mode, all nozzles are open. Opening the zone valve leads to water discharge from all the nozzles in the zone as soon as the piping is filled and pressurized. This mode applies the highest total amount of water compared to the other two modes.

In the sprinkler mode, automatic nozzles are used, meaning each nozzle is individually activated by heat from the fire. Water flow into the branch pipes serving the automatic nozzles is controlled by a zone control valve. Under normal conditions, the nozzles are covered with protective caps that protect the heat sensitive glass bulbs from dirt and mechanical impact and, in case of fire, prevent bulbs from breaking by heat in inactive zones further away from the fire. The branch piping does not contain water unless the zone control valve is opened, either manually or automatically by an independent fire detection system. At activation, the branch piping in the zone is filled with water, and the protective caps within the pressurized zone are hydraulically released. Nozzles will begin to activate in areas with sufficient heat. Even if heat spreads beyond the fire zone, water will only be released

from nozzles where the zone control valve has been opened. The sprinkler mode applies the lowest total amount of water of the three concepts.

The hybrid mode is a combination of deluge and sprinkler modes, with half of the nozzles being automatic nozzles and the other half open nozzles. Open nozzles and automatic nozzles are spaced sequentially along each branch pipe. Opening the zone valve leads to immediate discharge of water from the open nozzles as well as removal of the protective caps from the automatic nozzles. This approach ensures that only the automatic nozzles closest to the seat of the fire discharge water, such that the maximum water discharge density is focused on the actual fire region while additional cooling is obtained remotely from the fire region within the activated zones. The hybrid mode of operation could use significantly less water than a deluge system.

There are water-based FFFS available which are designed to share the pipe and pump units with a hydrant system.

The operation of foam systems is similar but not discussed further here.

16.3 Tunnel Fire Suppression Tests

There have been many FFFS tests conducted in full-scale or large-scale tunnels. Several tests were carried out in Japan, for example, Futatsugoya tunnel fire tests in 1969 [14], Kakeitou Tunnel fire tests in 1980 [20], and New Tomei Expressway tests in 2001 [14]. However, these tests were not well documented and technical information was very limited. After 2000, several series of large-scale fire suppression tests have been conducted in tunnels, most of which were performed in Europe. These reasonably well documented tests are summarized in Table 16.1, and the results are briefly discussed below. There are also some model-scales tests that have been conducted, for example [21, 22], but not included here.

16.3.1 Second Benelux 2000–2001

During 2000 and 2001, 14 large-scale fire tests were conducted in the Second Benelux Tunnel near Rotterdam in the Netherlands [6].

The test tunnel had a rectangular cross section with the width 9.8 m, the height 5.1 m, and a length of 980 m. The intended traffic direction was unidirectional. The slope of the tunnel was maximum 4.4% and its lowest point was in the middle of the tunnel. The tube had two traffic lanes. Six fans were installed in the upstream tunnel opening to create longitudinal ventilation air flows up to 6 m/s. The test area was located 265 m from the downstream portal. Measurements were taken in an area ranging from 50 m upstream to 200 m downstream of the fire.

Table 16.1 A summary of tunnel fire tests with water-based fire suppression systems

Test	Year	Number of suppression tests	Fire suppression	Tunnel length (m)	Tunnel width (m)	Tunnel height (m)	System configuration	Water flow rate (mm/min)	Activation time or type	V (m/s)	Fire source	HRR Free-burn (MW)
2nd Benelux, Netherland	2000–2001	4	Water spray	980	9.8	5.1	17.5 m+ 20 m	12.5	4–21 min	0–6	Simulated truck load	5–30
IF tunnel, Norway, UPTUN	2002–2004	19 low, 56 high[a]	Low pressure mist High pressure	100	8	6	24 m 36 m	1.1–3.3	Mostly 2 or 3 min	3	Pool, pallets, vehicle	2–25
IF tunnel, Norway, Marioff	2004	24	High pressure	100	8	6	24 m (1 zone)	1.4–3.7	2 or 3 min	3	Pool, pallets	5–25
VSH Hagerbach, Marioff	2005	10	HI-FOG	200	9.3	2.55	NA	NA	10 min	3	Automobile car	5–30
San Pedro de Annes, Spain, Marioff	2006	40	HI-FOG	600	9.5	5.2	72 m (3 Zones)	3.7–4.3	Hybrid Most 5–7 min	3.5	Pallets	75/90
Runehamar, SINTEF and Effectis	2007	5		1600	9	6	75 m (3 Zones)	NA	1.5–7	3–4	Pallets, pool	200

Table 16.1 (continued)

Test	Year	Number of suppression tests	Fire suppression	Tunnel length (m)	Tunnel width (m)	Tunnel height (m)	System configuration	Water flow rate (mm/min)	Activation time or type	V (m/s)	Fire source	HRR Free-burn (MW)
San Pedro de Annes, Spain, SOLIT	2008	50	Water mist	600	9.5	5.2	NA	NA	NA	NA	Pallets, pool	200
San Pedro de Annes, Spain, SOLIT2	2011–2012	30	Water mist	600	7.5	5.2	60 m	NA	3 min	2–3	Pallets, pool	5–160
Singapore tests	2011–2012	7	Water spray	600	7.2–9.5	5.2	50 m	8–12	4 min[b]	3	Pallets	150
Runehamar, SP	2013	6	Water spray	1600	9	6	30 m	10	2–12 min[b]	3	Pallets	100

NA Not Available

[a] 19 Low pressure mist tests and 56 high pressure mist tests with 8 free-burn reference tests

[b] delay time after "fire detection"

The performance of open deluge water spray systems was tested in four fire tests with simulated truck loads, tests 11–14. Test 11 consisted of one van loaded with 18 wood pallets having a total weight of 400 kg (18) pallets, with three tyres placed on top. Tests 12 and 13 had an aluminum covered truck load and test 14 had an open truck load. The open truck load consisted of 72 wood pallets and six tires having a total weight of 1600 kg. The aluminum covered truck loads consisted of 36 wood pallets with four tires on top and had a total weight of 800 kg stacked under an aluminum cover with the rear side open.

The open deluge system was designed with a water discharge density of 12 mm/min and consisted of two sections. Section 1 was directly above the fire and contained two parallel rows of sprinklers along the tunnel. Each row had a length of 17.5 m. Section 2 contained two rows of sprinklers, each with a length of 20 m, and was placed downstream of the fire next to Section 1.

In tests 11, 12, and 13, both sections were activated after 14, 4, and 10 min, respectively. In test 14, Section 1 was activated after 21 min and Section 2 was delayed by 10 min, that is, it was activated after 31 min. The chosen activation time was determined based on the objective of the test. The purpose of test 11 was to examine steam production by heating the van as much as possible before activation of sprinklers. The purpose of tests 12 and 13 was to determine the visibility reduction due to water droplets, steam, and smoke. The systems were activated as soon as possible after detection or after the time required to stop the traffic and evacuate the tunnel. In test 14, the effects of heating a tanker or truck near the fire and then cooling it with sprinklers were investigated. For all the tests, the systems were activated manually.

In test 11, the fire reached approximately 7.2 MW at 14 min when the two sections of spray systems were activated. After activation, the HRR decreased to 5 MW at around at 20 min and to 1.6 MW at 25 min. In test 12, the fire reached 6.3 MW at around 4 min and the two sections of water sprays were activated. After activation, the HRR was not measured. In test 13, the HRR reached around 13.5 MW at 10 min and then the two sections of water sprays were activated. After activation, the data were again not available. However, it can be seen from the temperature measurements that all the thermocouples measured ambient temperatures. Therefore, the fire should have been effectively suppressed, that is, extinguishment was achieved. In test 14, the fire reached its peak value of 26 MW at 11.5 min and started to decrease from 18 min. Section 1 was activated when the HRR decreased to 14 MW and the HRR continued to decrease. The fire was 1 or 2 MW at 30 min when Sect. 2 was activated. Note that based on the fuel types and configurations, one may estimate the peak HRRs for tests 11 to 13 to be 7.2, 14, 14 MW. Therefore, in all the tests except test 12, the water sprays systems were activated after the fires had approximately reached their peak HRRs.

Further, the water spray systems reduced gas temperatures significantly and the risk of fire spread was also reduced. The temperature downstream did not attain lethal tenability and steam production was insignificant. However, the visibilities in these tests were reduced so that escape routes were difficult to detect.

16.3.2 IF Tunnel, UPTUN 2002–2004

In the framework of the UPTUN project [23], two series of fire suppression tests were carried out in the IF tunnel, primarily a training tunnel, located the south of Oslo in Norway, including 19 low pressure water mist tests and 56 high pressure water mist tests. In each series of tests, eight free-burn tunnel fire tests were conducted for reference.

The fire sources were mainly diesel pool fires in pans. This creates a relatively thick fuel bed and the mass burning rate per square meter fuel will be much higher compared to thin fuel layers that float on a road surface. Further, the water sprayed into the fire source is contained in the pan along with the fuel, rather than washing the flammable liquids away as in a realistic leakage fire. Therefore, these types of liquid pools cannot simulate realistic fire sources in tunnels. Besides the pool fires, in each series of tests, two tests were carried out using 80 wood pallets as the fire sources and one test using small vehicles.

The low pressure water mist system had one row of nozzles below the ceiling with a length of 20 m, and two rows placed in the corner between the floor and the tunnel wall, with a length of 16 m. The high pressure mist systems had three rows of nozzles at the ceiling level.

The low pressure water mist systems had an operating pressure ranging from 5 to 9 bar, and the high pressure systems had an operating pressure ranging from 60 to 120 bar. It was reported that the water droplets produced by the nozzles used in both systems were much smaller than 1000 μm (1 mm). The applied water flow rates were in a range of 1.1–3.3 mm/min for low pressure water mist systems, and in a range of 0.5–2.3 mm/min for high pressure water mist systems. In most of the tests, the fires were only controlled but not extinguished.

16.3.3 IF Tunnel, Marioff, 2004

In 2004, Marioff [24] conducted 24 fire suppression tests in the IF tunnel in Norway. The tunnel cross-section has a shape of a horse shoe. Three rows of sprinklers were installed consisting of one at the center line of the tunnel and right below the ceiling, and the others placed on sides of the wall. The spacing between the nozzles, that is, spray heads, was 3 m in most of the tests and 4 m for the last five tests.

Trays of diesel and/or different numbers of wood pallets were used as the fire sources. Each tray had a dimension of 1.4, 1.6, and 0.4 m. There was always a 1.1 m high wall vertically placed in the front of the first two pools to simulate a blocking effect. Further, in some tests, a steel plate was placed at a short distance above the pool fires and covered 75% of the pool area. The HRRs ranged from 5 to 25 MW. The water flow rate can be estimated to be in a range of 1.4–3.7 mm/min.

In most of the tests, the fires were controlled but not extinguished. However, gas temperatures were reduced significantly.

16.3.4 VSH Hagerbach, Marioff, 2005

Mawhinney [25] and Tuomissaari [24] described a series of tests involving passenger automobiles in a tunnel with a low ceiling height, carried out in 2005 at the Versuchstollen Hagerbach (Hagerbach) tunnel research facility in Sargans, Switzerland. The test tunnel was representative of the "A86" passenger vehicle tunnel on a highway encircling Paris, France. The A86 passenger vehicle tunnel was approximately 9 m wide and 2.5 m high. The tunnel sloped upward in the direction of travel at approximately 2% slope, with a transverse gradient from left to right. Fuel from ruptured fuel tanks drained downhill and across the tunnel floor. The tests simulated the fire scenario in the tunnel involving a collision of two or more passenger cars.

Instrumentation was installed near the tunnel discharge to measure oxygen depletion in order to estimate the HRR. These tests showed that fires in passenger automobiles in a tunnel (before activation of the water mist system) typically exceeded the peak HRR from NFPA 502 of 5 MW per automobile. With tunnel ventilation at approximately 3 m/s, a group of three passenger cars created fires with peak HRR between 25 and 35 MW. The HRR for three vehicles would have been approximately 15 MW. With a peak HRR two times larger than the design fire, the additional heat and buoyancy may overwhelm the ventilation system and the time available for egress and rescue decreases. The risk of fire propagation to additional vehicles in the tunnel increases.

The fire scenarios consisted of a three-automobile fire in a two-lane and three-lane configuration. The primary differences included the number of vehicles surrounding the group involved in the fire and the relationship of the vehicles to the overhead lines of nozzles. In the "two lane" scenario, there were no vehicles to the right of the fire group.

The water mist system consisted of two zones of 33 m length with three lines of nozzles attached to the ceiling. The water mist system was activated manually based on a visual assessment of the size of the fire. All nozzles were 90° spray cone nozzles operating at approximately 80 bar pressure. The distance between the lines of nozzles was 2.8 m. The system operated as a deluge system with all nozzles flowing.

In the tests, the longitudinal velocity was initially 6 m/s, and then reduced to 3 m/s over a 4 min period after ignition. The tests results show that the fire spread to adjacent vehicles was prevented after activation of the fire suppressions system.

16.3.5 San Pedro de Anes tests, Marioff, 2006

Marioff Corporation conducted a series of full-scale fire tests in the San Pedro de Anes Test Tunnel facility in Asturias, in northern Spain, between February 2 and 27, 2006 [24, 25]. The objective of the tests was to evaluate the performance of a HI-FOG water mist system against very large fires in fuel packages similar to HGV trailer loads. Eleven tests were conducted—most using standard European wood

pallets placed on a platform to simulate the elevated load of a HGV trailer. These were referred to as "standard severity" fire packages. Two of the fire tests were conducted using wood pallets interspersed with high density polyethylene pallets (16 % by weight); these are referred to as "high severity" fire packages.

The fuel packages with wood-pallets only could potentially reach 75 MW under unsuppressed conditions. Similarly, the high severity-fire fuel packages with polyethylene pallets were estimated to have a potential peak HRR of 95 MW under unsuppressed conditions. In addition to the type of fuel package, the wind conditions in the tunnel, the location of the fuel load relative to the lines of nozzles, and water pressure were varied. The longitudinal wind-speed varied from less than 2–3.5 m/s; the fuel load was placed under the middle line or between two lines; and the water mist system was operated at nominally 100 bar or 80 bar end nozzle pressure. In addition, the fuel load was tested with and without a wind-break panel on the rear face of the fuel package—intended to simulate the effect of the solid rear doors and solid forward cab that are typically found on HGV trailers.

The water system consisted of three consecutive sections of 24 m each. Each section was equipped with three lines of sprinklers with a horizontal spacing of 4 m and longitudinal spacing of 3 m. Three modes of activation were tested, that is, the deluge mode, sprinkler mode, and the hybrid mode. The sprinkler mode used a dedicated protective cap for each section. After a section valve was opened all the protective caps in that section were released and the sprinklers were exposed to the hot gases. The hybrid mode was a mixture of deluge and sprinkler systems. Every other sprinkler was a closed sprinkler nozzle. The nominal volumetric flux density in all cases was nearly constant, ranging between 3.7 and 4.3 mm/min.

In every test, the fires were prevented from achieving their full potential by the water mist system. The water mist system reduced the HRR of the "standard severity" fires to between 20 and 37 % of their peak potential HRR of 75 MW. For the two high severity tests, the water mist system reduced the fires to 68 and 29 % of the peak potential HRR of 95 MW.

The thermal management of the water mist system was evaluated based on the ceiling temperatures at the end of the water mist zone, and in the 15 m section directly over the fuel package. The temperatures at the ceiling at the end of the water mist zone were typically as low as 80 °C, although in one test the temperature was as high as 213 °C. At an elevation of 1.5 m above the roadway and from 8 to 15 m downstream from the end of the mist zone, the average temperatures were below 65 °C.

In five out of 11 tests, between 28 and 60 % of the available fuel remained unburned after the test. In the remaining 6 tests, all available fuels on the platform burned. The high severity fuel packages were entirely consumed in both tests.

The water mist system prevented the ignition of target arrays in all but one fire. In that fire (T14, between two lines), the top three pallets on the target located 4 m away ignited. No ignition occurred in any targets located more than 4 m away from the end of the fuel package [24, 25].

16.3.6 SINTEF Runehamar Tunnel 2007

SINTEF, together with Efectis Nederland BV [26], conducted several fire suppression tests during December 2007 and January 2008 in the Runehamar tunnel in Norway. The fire scenarios were pool fires and solid fuel fires, each with a nominal HRR of up to 200 MW. The prime objective of these tests was to determine the suppression and extinguishing effect of a water mist system on fully developed fires. These tests were carried out by SINTEF NBL and Aquasys upon request of Rijkswaterstaat, the department within the Ministry of Public Works of The Netherlands that is also responsible for tunnel safety. These tests were designed to serve as a unique opportunity to obtain experimental data on the risk of a BLEVE (Boiling Liquid Expanding Vapor Explosion) in the area immediately downwind of the fire, and also to perform measurements on the tenability conditions along the first few 100 m downstream of the fire.

The largest solid fire load consisted of 720 pallets, configured to represent a loaded HGV. The fire pool consisted of diesel fuel and had a surface area of 100 m^2. The BLEVE-risk and the tenability conditions were investigated. However, no data about the HRR in the fire suppression tests are available.

16.3.7 SOLIT 2008 and SOLIT2 2012

In the SOLIT project [27], more than 50 fire tests were carried out in the San Pedro de Anes test tunnel with water mist systems. The tests included 25 truck fires with a potential HRR of almost 200 MW and pool fires with surfaces partly covered creating a HRR of up to 35 MW. The HRRs of two tests were presented. The water mist systems in both tests were activated 4 min after ignition, when the HRR was less than 10 MW. After activation, the covered fire increased slowly to around 50 MW and was extinguished manually, and the uncovered fire increased to 30 MW at 11 min and then decreased gradually. The data have shown that the fires in these two tests had been effectively controlled, however, the technical information is not available.

In the SOLIT2 project [9], more than 30 tests were conducted in the San Pedro de Anes test tunnel with water mist systems. In the vicinity of the fire, additional walls were installed resulting in a tunnel width of 7.5 m. Wood pallets and diesel pools were used as fire sources. The peak HRRs for the wood pallet fires was estimated to be 150 MW. The nominal HRRs for the pool fires were 5, 60, and 100 MW. The water mist system was installed over a length of 60 m. Two rows of nozzles were installed along the tunnel. Both longitudinal ventilation and semi-transverse ventilation systems were tested. The semi-transverse ventilation is designed to deal with free-burn fires of approximately 30 MW. Data of five tests were presented in the report. Under longitudinal ventilation, the fire size was restricted to 30 MW for a wood pallet fire with a PVC tarpaulin cover and 15 MW for a wood pallet fire without cover. The activation time was around 7 and 3 min in the tests and the corresponding activation HRRs were around 8 and 5 MW, respectively. For the pool fires

with longitudinal ventilation, the activation time was also 3 min, and the corresponding activation HRR was approximately 25 MW. The peak HRR was approximately 70 MW. Note that in this test the nominal HRR was 60 MW. Therefore, the fire was not controlled except that the gas temperature was lowered due to gas cooling.

In the two pool fire tests with semi-transverse ventilation and flow rates of 120 and 80 m^3/s, the activation time was approximately 4 and 3 min, and the corresponding HRRs were approximately 15 and 35 MW, respectively. The peak HRRs in these two tests were approximately 65 and 70 MW, respectively. The nominal HRRs in these two tests are unknown. However, from the HRR curves it can be expected that the nominal HRRs were also 60 MW in these two tests. In summary, the water mist system effectively controlled or suppressed the wood pallet fires but had limited influence on the fire development of pool fires. It should be kept in mind that the water flow rates used in these tests are unknown.

16.3.8 Singapore tests 2011–2012

In 2011, Land Transport Authority (LTA) Singapore commissioned Efectis to conduct a fire test programme [4, 5] to investigate the effect of fire suppression on the HRR and tunnel ventilation, to reduce the risk of vehicular fire spread, and to acquire information on the appropriate design parameters to adopt. A total of seven large-scale fire tests were conducted in the San Pedro de Anes test tunnel with water spray systems.

The fire sources consisted of 228 wooden (80 %) and plastic (20 %) pallets. The HGV mock up was 2 m wide, 3 m high, and 7.5 m long covered by a tarpaulin. The tunnel had a ventilation velocity of around 3 m/s. Two piles of pallets were placed 5 m behind the edge of the HGV mock-up to investigate the possibility of fire spread to adjacent targets.

The water spray systems consisted of three rows of nozzles were used in these tests. The nozzles had a K-factor of 80 and an operating pressure of 1–2 bar. The water flow rate was 8–12 mm/min. The system was activated 4 min after the "fire detection", corresponding to 60 °C gas temperature measured below the ceiling.

The test data showed that the peak HRRs were below 40 MW if the deluge system was activated 4 min after detection. Note that the HRR in the free-burn test stayed near 115 MW for about 5 min period and had a peak HRR of 150 MW during a short period (1–2 min). The reason for the peak has not been given, but one can speculate that it has to with a sudden collapse of parts of the fuel stack. This will increase the exposed fuel surface directly, and consequently the HRR may rise. The reduction of the HRR from 115/150 to less than 40 MW shows that the system controlled the fire effectively. However, the duration time was prolonged and most of the fuels were consumed in the tests. If the deluge system was activated 8 min after detection, the HRR was as high as 100 MW and the curve was similar to the free-burn test. The ceiling gas temperature in test 1 was reduced to 300 °C, compared to 1200 °C in the free-burn test, and the heat flux can also be expected to be reduced significantly although the measurement could fail while being exposed to the water sprays.

16.3.9 SP Runehamar Tunnel Fire Suppression Tests 2013

In 2013, SP Sweden [28] carried out a series of fire suppression tests in the Runehamar tunnel in Norway to investigate the performance of the Swedish simplified deluge water spray system before its application in the Stockholm Bypass. A total of six tests were carried out. Wood pallets were used as fuel with an estimated peak HRR of 100 MW. A total length of 30 m was covered by the fire suppression system equipped with TN (Tunnel Nozzle)-25 manufactured by TYCO (Prior to the notation it was called T-Rex). A 1.1 bar water pressure at the nozzles with K-360 ($L/(min\ bar^{1/2})$) yielded a water flow rate of 375 L/min. The coverage area was 37.5 m^2, which corresponds to a water density of 10 mm/min. The criterion for the "fire detection" was a ceiling gas temperature of 141 °C. The activation of the fire suppression system was delayed by 2–12 min after the "fire detection".

The results showed that the HRR upon activation ranged from approximately 10–30 MW. The HRR was controlled after activation for a period of 10–20 min. After that the fire was suppressed over a period of 10–30 min, which means that the system prevented further fire spread inside the fuel. The FFFS resulted in peak HRRs lower than 50 MW in all five cases, which was one of the original questions postulated by the LTA. The maximum temperatures at the ceiling were never higher than 400–800 °C after activation. In all experiments, the fire was controlled in the first period after activation and then suppressed with a considerable amount of fuel still remaining. A target consisting of a pile of pallets stood 5 m from one end of the fire. It was used to assess the risk of fire spread to adjacent vehicles. In all cases with the FFFS operating, the target was unaffected by the main fire.

The experiments also showed the importance of early activation of the FFFS. Despite this, it was clear from the experiments that the system has a sufficient safety margin to allow delayed response while retaining the ability to fight the more severe fires produced by such a delay. The system was able to prevent the spread of the fire beyond the main fire load, and was clearly able to lower the gas temperatures in the tunnel. This has important implications for the design and safety of the evacuation. The tests show that the design fire of 100 MW as originally planned can be reduced to lower than 50 MW by the presence of a FFFS, which translates into significant savings in investment costs for the ventilation system. The experiments show that if the system activates late, an increase of toxic substances and smoke is produced, but the impact of this effect can be mitigated by activating the system early.

16.3.10 A Short Discussion

Water spray systems normally use a water flow rate of 10–12.5 mm/min. Water mist systems normally use a water flow rate of 1–4 mm/min. The ratio of the water flow rates used in these two systems is in a range of 3–4. However, these values of water flow rate are mainly applied from fire suppression in residence and industrial buildings. The main mechanisms of fire suppression using these two types of systems

are different. A deluge water spray system suppresses a fire mainly by fuel surface cooling; a water mist system suppresses a fire mainly by dilution and gas cooling.

Compared to normal building fires, the fuel load density for a HGV tunnel fire is much higher. Further, ventilation reduces the dilution effect significantly. Therefore, in suppression of fires in tunnels with longitudinal ventilation, the systems with low water flow rates and small droplets, which extinguish fire mainly by dilution, cannot perform as well as in building fires in a quiescent environment.

In most of the tests discussed here, the fires were neither extinguished nor suppressed, and instead were only controlled, especially for the water mist systems tested. There have been some popular arguments that fire suppression systems cannot suppress tunnel fires, but only mitigate the fire effect. However, we can only conclude that most of the systems tested cannot successfully suppress or extinguish the tunnel fires. The main problem is that the design of fire suppression systems used in buildings has been applied to tunnel fires, which corresponds to low water flow rate, especially for the water mist systems. In other words, in order to successfully suppress tunnel fires, the performance of fire suppression systems needs to be improved.

There are also arguments that the performance of a water mist system is better than a water spray system. However, under the tested water flow rates, the performance of the water sprays systems was much better than the water mist systems. Further, it should always be kept in mind that the water spray systems and water mist systems discussed here use significantly different water flow rates. Therefore, it is apparently not fair to make the comparison so simply.

The use of fire suppression systems in a tunnel is always a cost-effectiveness issue. The capability of fire suppression systems needs to be improved to effectively suppress the fires, rather than only control the fires. However, the cost will definitely increase. Research on the minimum capacity to suppress the fire is of special interest from an economic point of view.

16.4 Theory of Fire Suppression

16.4.1 Extinguishment Mechanism

The mechanism of extinguishment of fires using water-based fire suppression systems can be classified into two types: condensed phase suppression and gas phase suppression. In the condensed phase, surface cooling is the main mechanism. In the gas phase, the extinguishment mechanisms can be categorized into gas cooling, heat capacity and dilution effects, and kinetic effects.

16.4.1.1 Surface Cooling

The water droplets arriving at the fuel surfaces evaporate and take the heat away, which results in lower burning rates or extinction of the fire. This process is called surface cooling. Note that 1 kg of water can take away around 2.6 MJ heat by

evaporation to water vapor at a temperature of 100 °C. For water-based fire suppression systems in tunnel fires, fuel surface cooling can be regarded as the primary mechanism of suppression of solid fuel fires.

For surface cooling to be effective the water droplets must be able to penetrate the fire plumes. During this process, both the momentum and the evaporation of the water droplets dominate. Further, the flow rate of the water droplets surviving in this process and arriving at the fuel surfaces must be great enough to suppress the fire. For exposed solid fuels, traditional water spray systems could have better performance due to the large water flow rate and large water droplets. The amount of water required for fire suppression only needs to approximately equal the heat absorbed by the fuel surface, rather than the total HRR.

In a tunnel fire, surface cooling delays the fire growth rate by pre-wetting the nearby un-burnt fuels. Further, the nozzles away from the fire source discharge water to the surface of the nearby vehicles, inhibiting vehicular fire spread. Surface cooling can easily delay or prevent ignition. Many tests have shown that even a small amount of water is capable of preventing fire spread to neighboring targets.

Water sprays discharged to the tunnel walls also provide protection for the tunnel structure. As a consequence, the requirement for passive protection could be lowered.

16.4.1.2 Gas-Phase Cooling

The water discharged from the nozzle is atomized into a large number of water droplets, and the total droplet surface areas are very large. Droplet evaporation results in efficient cooling of the flame and hot gases. The cooling of the flame raises the lower flammability limit of the oxygen and reduces combustion intensity. Further, heat feedback to the fire source is reduced. In a tunnel fire, the cooling of hot gases could increase the tenability conditions for evacuations, although the vapor introduced slightly lowers down the tenability limit for the respiratory gas temperatures. For large tunnels fires the HRR is very high so extinction purely by gas phase cooling would require a very large amount of water, which is almost impossible. Therefore, this is not the main mechanism of fire suppression in tunnel fires.

The nozzles upstream of the fire source also contribute to fire suppression by cooling the gases flowing to the fire source if back-layering exists, and a small amount of the injected water droplets could also be blown to the nearby fire source.

16.4.1.3 Dilution Effects and Heat Capacity

Dilution effects in water-based fire suppression systems are created by the evaporation of water drops. Note that due to the evaporation, the volume of water droplets expands by a factor of around 2700 at a temperature of 300 °C, which dilutes the concentration of both fuel and oxygen in the vicinity of the fuel surfaces and in the flame. At the same time, the higher heat capacity of water vapor compared to air reduces the gas temperatures.

Dilution effects could be the key mechanism of suppression of gas and liquid fires, especially for water mist systems. However, in tunnel fires with forced ventilation, the water vapour could be blown away and the dilution effect could be significantly reduced.

16.4.1.4 Radiation Attenuation

Similar to soot, water sprays and water vapors also absorb radiation. The radiation attenuation due to the water sprays depends on the water flow rate and the droplet sizes. For a continuous water curtain, the radiation attenuation could be very effective due to the high absorptance of the water. It is known that water vapor has a low absorptance, however, it could still play a key role due to the large volume.

Radiation attenuation reduces heat feedback to the fuel surface and lowers the HRR. It can also delay the fire growth rate and prevent fire spread to nearby vehicles in a tunnel fire.

On the other hand, water vapors produced by evaporation perform as a radiation medium, which absorbs heat from flames and hot gases, and also re-radiates the heat at a lower radiation intensity.

16.4.1.5 Kinetic and Other Factors

Kinetic effects include the impingement of water droplets on the fuel surface, turbulence induced by the water sprays, the interaction between the nozzles, and the effect of droplets on the flame temperature limit.

Other factors could include the effect of tunnel ventilation on the movement of water droplets and water vapors and the effect of tunnel walls.

These are only secondary effects and are not expected to significantly affect the performance of water spray fire suppression systems in tunnels, and therefore are not discussed further.

16.4.2 Critical Conditions for Extinction

16.4.2.1 Condensed Phase Extinction

The fire point equation is widely used in fire suppression theories, which in reality is the energy equation applied to the fuel surface and can be expressed as:

$$\dot{q}''_{net} - \dot{m}''_f L_g - \dot{m}''_w L_{v,w} = 0 \tag{16.1}$$

where $\dot{q}''_{net}$ is the net heat flux absorbed by the fuel surface (kW/m^2), L_g is the heat of gasification of the fuel (sum of heat of vaporization and increase of heat enthalpy,

kJ/kg), $\dot{m}_f''$ is the fuel mass burning rate (kg/(m^{2}s)), $\dot{m}_w''$ is the water flow rate per unit fuel surface area (kg/(m^{2}s)), and $L_{v,w}$ is the heat of vaporization of the water (kJ/kg).

The terms on the left hand side are the net heat flux absorbed by the fuel surface, heat absorbed for gasification, and the heat absorbed for evaporation of water droplets, respectively.

The heat flux absorbed by the fuel surface can be divided into two parts, that is, the heat flux from the self-sustained flame itself (no external flux) and the heat flux from other flames (at other locations) or heat sources. The heat flux from the self-sustained flame could be expressed in the form of the local HRR by multiplying a kinetic parameter, φ. Therefore, the above equation can also be expressed as:

$$\dot{m}_f''(\varphi \Delta H_{c,eff} - L_g) + \dot{q}_e'' - \dot{q}_l'' - \dot{m}_w'' L_{v,w} = 0 \tag{16.2}$$

where $\dot{q}_e''$ is the radiation from external sources or other flames (kW/m^2) and $\dot{q}_l''$ is the radiation loss (kW/m^2). The kinetic parameter, φ, in the above equation is defined as the ratio of heat absorbed by the fuel surface to the HRR [29]:

$$\varphi = \frac{\Delta H_g}{\Delta H_{c,eff}} \tag{16.3}$$

where ΔH_g is the heat of the self-sustained flame transferred to the fuel surface per unit mass of fuel gasified (kJ/kg), and $\Delta H_{c,eff}$ is the effective heat of combustion (kJ/kg). It should be noted that the kinetic parameter, φ, is not constant. However, the equation expressed in such a form is useful when analyzing the critical fire point equation.

In the following text, we discuss the critical conditions for extinction, that is, the critical fuel mass burning rate and the critical water flow rate that are required for fire extinction.

Note that for a self-sustained flame at extinction, we may assume that no radiation loss exists and the fuel surface obtains heat for gasification only by convective heat transfer from the small burning flame. Therefore, the critical fire point equation is expressed as:

$$\dot{m}_{cr}''(\varphi \Delta H_{c,eff} - L_g) = 0 \tag{16.4}$$

where $\dot{m}_{cr}''$ is the critical fuel mass burning rate for a self-sustained burning material (kg/(m^{2}s)).

The critical mass burning rate at extinction for a self-sustained flame is determined by convective heat feedback. According to Spalding's B number theory, it is given by [30]:

$$\dot{m}_{cr}'' = \frac{h_c}{c_p} \ln(1 + B_{cr}) \tag{16.5}$$

The critical B number at extinction, B_{cr}, is defined as [30]:

$$B_{cr} = \frac{Y_{O2,\infty}\Delta H_{O2}}{\varphi \Delta H_{c,eff}} \tag{16.6}$$

In the above equations, h_c is the convective heat transfer coefficient (kW/(m^{2}K)), c_p is the heat capacity of the air, $Y_{O2,\infty}$ is the surrounding oxygen mass concentration, ΔH_{O2} is the heat released by consuming 1 kg oxygen (kJ/kg).

Note that the Spalding's B number theory is only an approximate theory. The physical meaning of the above equation is that burning is sustained only by the convective heat transfer, that is, heat conduction to the fuel surface. Here it is assumed that all the oxygen is consumed near the fuel surface, and also assumed that the heat gain from the flame at extinction equals the heat required for obtaining the critical mass burning rate, that is

$$L_g = \varphi \Delta H_{c,eff} \tag{16.7}$$

The critical mass burning rate per unit area for normal plastics at extinction is in a range of 2.5–4.4 g/(m^{2}s) under forced convection and 1.9–3.9 g/(m^{2}s) under natural convection [31]. Tewarson and Pion [32] defined a term called ideal mass burning rate assuming that no heat is lost from the surface or the heat loss has been compensated by the external heat flux. Ingason and Li [33] compared these values to the data obtained from their tests and found they correlate well with each other. The corresponding ideal mass burning rate per unit area for these normal plastics is in a range of 14–35 g/(m^{2}s). The ratio between the critical and ideal mass burning rate per unit area ranges from 10 to 18%. However, according to the model described above, the critical mass burning rate is a variable and sometimes a very high mass burning rate could be obtained, although it may not be realistic. As a first estimation, considering it as a fixed value or a variable is acceptable.

An expression for the critical water flow rate required for fire suppression can be obtained from Eq. (16.2):

$$\dot{m}''_{w,cr} = \frac{\dot{m}''_{cr}(\varphi \Delta H_{c,eff} - L_g) + \dot{q}''_e - \dot{q}''_l}{L_{v,w}} \tag{16.8}$$

The model presented above is only an approximate solution and the uncertainty is high. However, the model correlates many parameters and is very useful for understanding the mechanism of the fire suppression.

16.4.2.2 Gas Phase Extinction

Beyler [30] assumed that the analogy of flammability limit for premixed and diffusion flames works, and proposed an equation to estimate the fraction of enthalpy

of reaction that can be lost before extinction occurs at the stoichiometric limit, φ_{SL}, which can be expressed as:

$$\varphi_{SL} = 1 - \frac{c_p(T_{AFT} - T_o)(1 + 1/r)}{Y_{O2,\infty}\Delta H_{O2}} \tag{16.9}$$

where T_{AFT} is the adiabatic flame temperature for diffusion flames (K), and r is the mass-based stoichiometric air to fuel ratio which can be ignored in most cases.

Beyler [30] proposed the following equation to account for the effect of dilution and heat capacity on fire suppression:

$$\varphi = k\varphi_{SL} = k1 - \frac{c_p(T_{AFT} - T_o) + Y_{ext}\Delta c_p(T_{AFT} - T_o)}{Y_{O2,\infty}\Delta H_{O2}(1 - Y_{ext})/(1 + 1/r)} \tag{16.10}$$

where k is the correction ration between the actual and stoichiometric limit (closely 1), Y_{ext} is the mass fraction of the extinguishing agent, Δc_p is the difference in heat capacity between the diluents and ambient gas (kJ/(kgK)). Note that the stoichiometric parameter term in the above equation has been corrected based on the original equation [30].

Although Beyler [30] referred to the parameter T_{AFT} as the adiabatic flame temperature at the stoichiometric limit, the temperature of 1700 K was used, that is, the adiabatic flame temperature at the flammability limit. The physical meaning of the parameter also suggests that the latter temperature should be used.

Note that the fraction must be positive to sustain a flame. This in reality suggests the controlling equation for flammability limit for diffusion flames. Both the ambient oxygen mass concentration and the ambient temperature are key parameters.

Note that the introduction of diluents, that is, water vapor or other extinguishing agents, results in a decrease of the oxygen concentration, which is accounted for by the term $(1-Y_{ext})$ in the denominator. The effect of heat capacity is represented by the additional term in the numerator, and the difference in the heat capacity between the diluents and the ambient gas is Δc_p.

The expression of the fraction of enthalpy of reaction that can be lost before extinction could be questionable. Further, the assumptions made in Eq. (16.9) may not work in case of fire suppression.

For water-based fire suppression systems, the inerting gas is water vapor. Given that the fuel mass is normally negligible compared to the total mass in a flame volume, the parameter r can be ignored in Eq. (16.10). Assuming that the concentration of water vapor is Y_w and $k=1$, the fraction of enthalpy of reaction can be expressed as:

$$\phi = 1 - \frac{c_p(T_{AFT} - T_o) + Y_w\Delta c_p(T_{AFT} - T_o)}{Y_{O2,\infty}\Delta H_{O2}(1 - Y_w)} \tag{16.11}$$

The gas phase extinction can be linked to the condensed phase extinction by applying the above equation in combination with Eqs. (16.8), (16.5) and (16.6).

Based on the above equation, the extinction criterion for flames with fire suppression can be obtained, which is expressed as:

$$Y_{O2,\infty}\Delta H_{O2}(1-Y_w) < c_p(T_{AFT}-T_o)+Y_w\Delta c_p(T_{AFT}-T_o) \tag{16.12}$$

The above criterion indicates the oxygen level needs to be higher for possible ignition in case of fire suppression. This criterion is very valuable in determining the combustion conditions for under-ventilated fires and suppressed fires.

Example 16.1 Estimate the critical mass burning rate for a small wood sample under normal conditions. Assume that the heat of combustion is 15 MJ/kg, and heat of vaporization is 2.5 MJ/kg, and the convective heat transfer coefficient is 10 W/(m^{2}K).

Solution: First calculate the critical B number using Eq. (16.6)*, that is,* $B_{cr} = 0.023 \times 13.1/2.5 = 0.12$*. Then calculate the critical mass burning rate using* Eq. (16.5)*, that is,* $\dot{m}''_{cr} = 10/1 \times \ln(1+0.12) = 0.00114$ *kg/(m*^{2}*s) or 1.14 g/(m*^{2}*s).*

16.4.3 Fire Suppression

Note that the critical mass burning rate and critical water flow rate correspond to the critical state of fire suppression when the fire is almost extinguished, and the corresponding extinguishment time could be infinite. To effectively suppress a well developed fire the water flow rate needs to be greater to assure either that enough the water droplets are able to penetrate the fire plume and reach the fuel surfaces before evaporation, or that enough water vapor is produced to cool the flame and dilute the combustible mixture.

16.4.3.1 Suppression of Gas and Pool Fires

Rasbash et al. [34, 35] carried out a series of tests on extinction of liquid pool fires. Two groups of extinction processes with water sprays were identified, that is, cooling the burning fuel surface to the fire point and action of spray on the flames causing rapid disappearance of the flames. It was concluded that except for alcohol fires, which were extinguished by surface dilution, the liquid fires were extinguished by fuel surface cooling. The extinction time was reported to decrease with increasing water flow rate and increased with water droplet size. The critical water flow rates associated with fuel surface cooling increased linearly with droplet size.

Kung [36] reported on suppression of hexane pool fires by cooling the flames in a ventilated room where the pool was placed in the corner and the water nozzle was placed at the centre of the room. Extinction occurred when the mole fraction of steam

generated immediately after discharge of the water spray was greater than a value that was between 0.3 and 0.39. The water evaporation rate was proportional to the HRR and the water flow rate, and it varied by the −0.73 power of the mean droplet size.

Heskestad [37] conducted a series of water spray tests using liquid pool fires, accounting for the nozzles that are not geometrically scaled. He proposed an equation for gas and pool fires to predict the critical water flow rate, which is exponentially proportional to an effective nozzle diameter, nozzle height, and free-burn HRR. The equation for the critical water density can be expressed as:

$$\dot{q}_w = 0.312 D_{ne}^{1.08} H^{0.4} \dot{Q}^{0.41} \tag{16.13}$$

where $\dot{q}_w$ is the volumetric water flow rate (L/min), H is the clearance height between the nozzle and the pool surface (m), $\dot{Q}$ is the HRR (kW), and D_{ne} is the outlet diameter of the nozzle (mm). For comparison of nozzles with different geometries, an effective nozzle diameter should be used instead of the outlet diameter. Based on the conservation of mass and momentum equations, the effective nozzle diameter, D_{ne} (mm), is defined as:

$$D_{ne} = \left[4\dot{m}_w^2 / (\pi M \rho_w) \right]^{1/2} \tag{16.14}$$

where M is the momentum (N) and ρ_w is the density of water (kg/m^3). Heskestad [37] argued that spray-induced dilution of the flammable gas is a major factor in extinguishing gas fires, and that a liquid pool fire needs higher water rates to be extinguished compared to a gas fire.

It should be kept in mind that Heskestad's equations presented above are only suitable for extinguishment of pool fires using a water spay nozzle directly above the pool.

Example 16.2 Estimate the water density required for one nozzle to extinguish a 5 MW pool fire in a 5.5 m high tunnel. The nozzle has an outlet diameter of 7 mm is placed 5 m above the pool and is designed to cover 25 m^2 of tunnel area.

Solution: The required water flow rate can be estimated using Eq. (16.13)*, that is,* $\dot{V}_w = 0.312 \times 7^{1.08} \times 5^{0.4} \times 5000^{0.41} = 160$ *L/min. The water density can then be calculated:* $q''_w = 160/25 = 6.4$ *l/(m^2 min) or 6.4 mm/min.*

In case of a water mist nozzle with several small outlets, Eq. (16.14) could be used to roughly estimate the effective nozzle diameter, although such a use has not been validated.

16.4.3.2 Suppression of Solid Fuel Fires

The suppression of solid fires normally takes a longer time due to the three-dimensional characteristics of the solid fire source. The time that is required for extinction of a fire is correlated to the water flow rate. A higher water flow rate can reduce the extinguishment time and less fuel will be consumed.

Kung and Hill [38] investigated the extinction of wood crib and pallet fires and obtained some useful empirical equations. They conducted a series of experiments on extinguishment of wood crib fires by water applied directly on the top of the cribs and wood pallets. The water was applied on the top by means of a rake consisting of perforated stainless steel tubes. They presented interesting nondimensional variables which basically account for variations in the preburn percentage and crib height, showing nondimensional fuel consumption and total water evaporated as functions of non-dimensional water flow rate. More specifically, it was shown that a single empirical correlation, for three types of cribs with the same stick size, but different crib height can be established between the ratio of crib mass consumed during the extinction period and combustible material remaining at the beginning of the water application, R, and the ratio of true water application rate and the fuel burning rate at the activation of water application, which is expressed as:

$$R = \frac{\Delta m_{f,ex}}{m_{f,a}} = \xi \left[\frac{\dot{m}_w (1-c)}{\dot{m}_{f,a}} \right]^{-1.55} \tag{16.15}$$

where $\Delta m_{f,\,ex}$ is the mass consumed during the extinction period (kg), $m_{f,\,a}$ is the combustible fuel mass at the activation (kg), $\dot{m}_w$ is the applied water flow rate (kg/s), c is the fraction of water applied that fell directly through the shafts of the crib, $\dot{m}_{f,a}$ is the fuel burning rate at activation (kg/s), ξ is a correlation coefficient. Note that the factor c is introduced into the equation by Ingason [22].

In Kung and Hill's work [38], the correlation coefficient ξ is a variable, which is 0.312 for the center-shaft ignited wood crib fires, 0.26 for the full-bottom ignited wood crib fires, and 0.15 for the wood pallet fires if the factor c is set to 0. Kung and Hill [38] also presented a single linear relationship between the ratio of total water evaporated and the total mass consumed during extinguishment and the ratio of the "true" water application rate versus the maximum free burning rate of the wood crib based on wood crib tests:

$$\frac{\Delta m_{w,ev}}{\Delta m_{ex}} = \psi \frac{\dot{m}_w (1-c)}{\dot{m}_{f,\max}} \tag{16.16}$$

where $\Delta m_{w,\,ev}$ is the total water evaporated (kg), $\dot{m}_{f,\max}$ is the maximum burning rate in a free-burn test (kg/s) and Ψ is a correlation coefficient which is determined by Kung and Hill [38] to be 2.5.

Ingason [22] carried out a series of model-scale tunnel fire tests with a deluge system and a water curtain system using hollow cone nozzles, in order to improve the basic understanding of water spray systems in a longitudinal tunnel flow. The water spray system used consisted of commercially available axial-flow hollow

cone nozzles. Based on Kung and Hill's work [38], Ingason [22] proposed the following equation to correlate the energy content with the HRR:

$$\frac{\Delta E_w}{\Delta E_{ex}} = \psi \frac{\dot{Q}_w(1-c)}{\dot{Q}_{f,\max}} \tag{16.17}$$

where ΔE_w is the total energy taken by water evaporation (kJ), ΔE_{ex} is the total energy content at the activation (kJ), $\dot{Q}_w$ is the heat flux taken by the water (kW) and $\dot{Q}_{f,\max}$ is the peak HRR in a free-burn test (kW). Ingason [22] correlated the non-dimensional ratio of HRR, excess gas temperature, fuel consumption, oxygen depletion and heat flux downstream of the fire to the non-dimensional water flow variable (the term on the right-hand side in the above equation), and good agreement was found. In Ingason's work [22], a value of 0.89 for the factor c provided a good fit to Kung and Hill's equation [38]. This value is reasonable because in Ingason's work [22] the wood cribs were loosely packed.

Tamanini [39] also investigated the application of water sprays to the extinguishment of wood crib fires. A corrected water flow rate was used to correlate the results. It was also found that the mass consumed during extinguishment varied with a power law of the water flow rate, where the power of −1.55 was used by Kung and Hill and was in the range of −1.86 to −2.18 according to Tamanini [39]. The time to extinction was also correlated with the corrected water flow rate and the activation parameters which suggests that the time to extinction prolongs significantly as the water flow rate decreases.

Yu et al. [9] made a theoretical analysis of extinguishment of rack-storage fires by cooling of the fuel surface. A thin layer of fuel undergoing pyrolysis was treated as a plate where the temperature was evenly distributed, that is, similar to a steel plate. It is also assumed that the energy absorbed by the surface of this "plate" resulted in an increase of the burning area. Despite the simplicity, these assumptions seemed to work well. A fire suppression parameter, k, was identified to correlate the fire suppression results obtained from large-scale tests conducted using two different commodities arranged in steel racks of different height. The estimated critical water flow rate is about 6 g/(m^{2}s) for Class II commodities and 17–20 g/(m^{2}s) for plastic commodities. Note that these values were estimated based on the fuel surface area rather than the injection area at the top of the fuels. The HRR at a certain time after activation can be estimated using:

$$\frac{\dot{Q}(t)}{\dot{Q}_a} = \exp\left[-k(t-t_a)\right] \tag{16.18}$$

where the fire suppression parameter, k, is defined as:

$$k = \frac{C_o(\dot{m}''_w L_{v,w} - \varphi \dot{m}''_f \Delta H_c + \dot{m}''_f L_p)}{\rho_f c_p (T_p - T_o)}$$

where C_o is a coefficient related to the effective pyrolysis thickness, L_p is the heat of pyrolysis (kJ/kg), T_p is the temperature of pyrolysis (K), t is the time (s) and t_a is the activation time (s), $\dot{Q}_a$ is the HRR at activation (kW).

Xin and Tamanini [11] also conducted a series of fire suppression tests using representative fuels to assess the classification of commodities for sprinkler protection. They defined a critical sprinkler discharge flux as the minimum water flux delivered to the top of the fuel array capable of suppressing/preventing further fire development, and obtained it by linear interpolation of the tests data. An empirical correlation was proposed for a ceiling clearance of 3.05 m to estimate the actual water flux discharged to the fuel surfaces, which was correlated with the sprinkler discharge flux and the convective HRR. A similar equation to Eq. (16.14) was proposed to correlate the energy consumed during extinguishment with the water flow rate. The estimated critical sprinkler discharge flux was 6.9 mm/min for Class II commodities, 19.9 mm/min for Class 3 and Class 4 commodities, 25.6 mm/min for plastic commodities, and 26.9 mm/min for the cartoned meat trays. Note that these values correspond to the injection area at the top of the rack storages. It is concluded that classifications based on sprinkler discharge flux represents the fire hazard levels of the commodities of interest.

We can also get some indication from the equation for the critical water flow rate, Eq. (16.8). Note that at activation the local fuels could probably have been fully involved in burning, and the radiation heat flux should be much higher than the convective heat flux. Further, for a three-dimensional fire source, the radiation loss could be very limited for the fuels, most of which are located inside the flame. Therefore, Eq. (16.8) can be simplified into:

$$\dot{m}''_{w,cr} = \frac{\dot{q}''_{net,r}}{L_{v,w}} \tag{16.19}$$

This suggests that the critical water flow rate is proportional to the net heat flux, which mainly consists of radiation heat flux. Further, in order to extinguish such a fire within a short time, the applied water flow rate must be much higher than the critical water flow rate discussed earlier.

In summary, the HRR and the energy consumed during extinguishment have been correlated with either the discharge water flow rate or the actual water flow rate. Some useful equations have been obtained, however, most of these equations are empirical and they must be used with caution.

Example 16.4 Roughly estimate the water flow rate required to effectively suppress a wood pallet fire in a 9 m wide tunnel. The potential fire size is 100 MW but is 20 MW at the activation of the water spray system. Here we define the effective suppression as only 20% of the fuel mass at activation consumed during the extinction period. The wood pallet piles are 3 m wide and 8 m long, and its heat of combustion is approximately 15 MJ/kg.

Solution: The water flow rate applied on the wood pallets can be estimated using Eq. (16.16). *First we need to estimate the fraction of water applied that not fall onto*

the fuel surfaces c. Given that the wood pallets are densely packed, it is reasonable to assume that all water droplets falling on the wood pallets do not penetrate the fuel and reach the tunnel floor. The parameter c therefore can be estimated as: c = (9 − 3)/9 = 2/3. This indicates 2/3 water applied does not have direct effect on the burning of the fuels. Note that the correlation coefficient ξ is 0.15 for wood pallets and the parameter R = 0.2 according to this assumption. Now use Eq. (16.16) *to estimate the water flow rate, that is,* $\dot{m}_w = \dot{m}_{f,a}(R/\xi)^{-0.645}/(1-c)$ *= (20/15) × (0.2/0.15)*$^{-0.645}$*/ (1 − 2/3) = 3.32 kg/s or 199 L/min. The tunnel section length with fuels burning can roughly be estimated as: 20/100 × 9 × 8 = 14.4 m*^{2}*. Therefore the water density can be estimated: 199/14.4 = 13.8 mm/min or L/(min m*^{2}*).*

16.4.4 A Short Discussion

In an open fire and a compartment fire, vaporized water vapor can surround the fire and flame, and the dilution effect could be significant enough to behave as the main mechanism of fire extinction. However, in a ventilated tunnel fire, water vapor will be blown away from the fuel surfaces, and thus the dilution effect is reduced significantly. Small droplets can also be blown away. In any case, the models and equations developed for suppression of open fires and enclosure fires must be verified in tunnel fires. Further, research on the mechanisms of fire suppression in tunnels is highly recommended.

16.5 Tunnel Fire Detection

All the fire suppression systems used in tunnels need fire detection systems for activation. The only exception is a system solely consisting of automatic sprinklers in which thermal heads are embedded.

In the following sections, different types of fire detection systems used in tunnels are shortly summarized, and then a summary of tunnel fire detection tests is presented.

16.5.1 Types of Fire Detection

The fire detection systems used in tunnels include line type heat detection, smoke detection, flame detection, visual image fire detection, CCTV system, spot heat detection, and/or CO2/CO sensing fire detection.

Line type heat detection (LTHD) have been used in road tunnels for fire detection for approximately 40 years. Line type heat detection detect fires by absolute temperature value or temperature changes. There are four types of line type heat detection systems used in tunnels, that is, electrical cable, optical fiber, thermocouple,

and pneumatic heat detection systems. The electrical cable heat detectors are subdivided into four types, that is, thermistor type, analog integrating circuit, digital circuit, and semiconductor circuit. Optical fiber cable detects cable deformation due to exposure to heat through a change in light transmission or a change in back scattering. Line type thermocouple detection has the measuring junction unfixed and when it is subjected to an increase in temperature it becomes concentrated at the hottest point anywhere along the sensor's entire length. Pneumatic heat detection systems detect the pressure rise due to gas expansion after the tube is exposed to flames or hot smoke flows. Among these systems, the fiber optic heat detection is the most widely used LTHD system in tunnels. These systems respond differently but this topic has not been systematically studied except for the spot heat detector which will be discussed in the following text.

Smoke detectors detect smoke particles either by light extinction sensors, light scattering sensors, or by ionization attenuation sensors. A light extinction smoke detector detects smoke by measuring extinction of the light due to absorption of the smoke particles, while a light scattering smoke detects smoke by measuring light signals caused by scattering due to the smoke particles. An ionization smoke detector uses a radioisotope to produce ionization and the difference over a certain level caused by smoke can be detected, however, it has been found that it is not sensitive to smouldering fires. Similar to heat detectors, the response of the smoke detectors has a delay, which can be estimated using some validated models, for example, the model proposed by Cleary et al. [40]. In practice, the dust sensors for air quality control can be used as complementary smoke detectors in case of a fire.

Flame detectors sense electromagnetic radiation and are designed to discriminate flame radiation from the other sources. The radiation wavelengths can be in the ultraviolet, visible, or infrared portions of the spectrum. Protection against false alarms due to sunlight, the lighting system in the tunnel, and the light from the vehicles is necessary.

Visual Image flame and/or smoke detectors digitize the video images from cameras and use computer software to identify flames or smoke. The algorithms used can become very complicated in order to distinguish the flame and/or smoke from the other items such as light and dust.

CCTV monitors have been used in many tunnels mainly for traffic control but can also be used for monitoring fire accidents and for triggering an alarm manually.

Spot heat detection measures the heat inside the tunnel at a certain interval, for example, placement of thermocouples every 30 m. The response of spot heat detectors has been systematically investigated. Heskestad [41] proposed the use of the Response Time Index (RTI) to rank different types of automatic sprinklers and detectors.

The CO_2 and CO sensors have been used in many tunnels for controlling air quality inside the tunnel under normal ventilation. Although they are not designed for fire detection, they can be used as a complementary system for fire detection in tunnels.

Besides these detection systems, the fire could also be detected immediately by a driver or passenger, who could sound the alarm afterward by either pushing the fire alarm button inside the tunnel or communicating with tunnel managers or fire

brigade in other ways. More information on fire detection can be found in the literature, for example, Schifiliti et al. [42], Maciocia and Rogner, and Zalosh and Chantranuwat [43].

In summary, different detection systems are used in tunnels, mainly depending on the designed safety level for the specific tunnel. For a detection system in combination with a fire suppression system, it must be able to exactly determine the location of fire site. From this view point, LTHD is required. Further, the use of dust detectors and CO/CO_2 measurement equipment designed for normal ventilation as complement to fire detectors is a good combination, but the distance between installations should be shortened for better performance.

16.5.2 Summary of Fire Detection Tests in Tunnels

A summary of fire detection tests in tunnels is presented in Table 16.2. Most of the tests were carried out in Europe focusing on LTHD systems. Quite limited information is available in the literature.

Only the three well documented test series, that is, the 2nd Benelux tunnel fire detection tests in 2000/2001, the Runehamar tunnel fire detection tests in 2007 and the Viger tunnel fire detection tests in 2007 are discussed in detail in the following.

16.5.2.1 Second Benelux tunnel fire detection tests—2000/2001

During 2000–2001, 13 fire detection tests were carried out in the 2nd Benelux tunnel [45] consisting of eight small fires and five larger fires (three pool fires, one van fire, and one simulated truck load fire. Three different LTHD systems were placed both close to the wall and around 3.5 m from one wall (based on estimation). One detection system consisted of a glass fiber detector cable and the other two were electronic sensors on regular distances of several meters. Three different fire source locations were tested. The ventilation velocity varied from 0–5 m/s. The sizes of the pools used in the tests varied from 0.5 to around 2 m^2.

The maximum temperature measured by the systems for each test were in the range of 20–30 °C, however, the detection location differed more than 20 m in some tests with high velocities. The difference between the detection location and the fire location is mainly due to the effect of ventilation, and partly due to the placement between the fire location and the detectors and the measurement error of the LTHDs.

16.5.2.2 Runehamar Tunnel Fire Detection Tests—2007

A total of eight tests were carried out to investigate the performance of different LTHD and smoke detection in the Runehamar tunnel in 2007 [46]. In seven of the tests, the fire sources were a square heptane pool with a side length of 0.4–1 m and

Table 16.2 Summary of fire detection tests in tunnels [43–47]

Year	Tunnel	Country	Type of detection	Fire source	HRR (MW)	Ventilation velocity, u_o (m/s)
1992	Mositunnel	Switzerland	Line type heat detector, spot heat detector, and smoke detectors	Pool fire 0.5–4 m^2		Mostly 1
1999	Schonberg and Gubrist tunnel	Switzerland	Line type heat detector (fiber optic)	Gasoline		
1999	Colli Berici unused tunnel	Italy	Line type heat detector			
1999	CSIRO	Australia	Line type heat detector	Hot smoke	1.36	
2000	Hagerbach model tunnel	Switzerland		Gasoline 0.25–0.75 m^2	0.42–1	0.75–2.8
2000	Felbertauern Tunnel	Switzerland		Diesel 2 m^2, 3 m^2 and ethano l m^2		3.5–11.0
2000	Boemlafjord Tunnel	Finland				3
2001	Shimizu Tunnel	Japan		Gasoline, car, 1–9 m^2		2–3
2001	Second Benelux Tunnel	Netherlands	Line type heat detector	Gasonline, van, simulated truck	1–25	0–5
2007	Runehamar Tunnel	Norway	Line type heat, smoke detector	Heptance, car	0.2–3	1.1–1.8
2007	Viger tunnel	Canada	Line type heat, flame detector and Visual image fire detection	Gasoline pool, 0.09–0.36 m^2	0.125–0.65	0–2.5

in one test the fire source was a real car. For the LTHD, a fixed alarm limit was set to 3 °C in 4 min, while for smoke detectors, the soot or dust density was generally greater than 3000 μg/m^3. The smoke detectors were placed 62.5 and 125 m downstream of the fire source. The results showed that for heptane pool fires the heat detection worked very well but not for the car fire test, and the smoke and dust detectors worked well in the car fire test but not as good as the heat detection for pool fires. It was concluded that the airflow increases the time to detect for heat detection

systems and decreases the detection time for smoke detection. However, this conclusion could be questionable. Note that the pool fires resulted in a rapid increase in temperature at the early stage, and thus could not be representative of typical vehicle fires. In such cases, using the temperature increase rate as the criteria for fire detection is not comparable to smoke detection. Further, the better performance of smoke detection in case of a car fire is mostly attributed to the slowly growing fire which cannot trigger the heat detectors. The smoke detectors tested were more sensitive compared to the heat detectors, however, the disadvantages of smoke detectors are the long delay of measurement due to smoke transportation, tube suction and measurement in the collector, and the disability in determining the exact fire location for the fire suppression system or evacuation or fire fighting. In case of a fast growing fire, heat detection can be expected to perform better.

16.5.2.3 Viger Tunnel Fire Detection Tests—2007

In 2007, nine tests were carried out in Tube A of Carré-Viger Tunnel located in downtown Montreal, Canada [47]. The section of the tunnel used in the tests was 400 m long, 5 m high, and 16.8 m wide (four traffic lanes). Six fire detection systems were evaluated in the test series, including two linear heat detection systems, one optical flame detector, and three video image detection (VID) systems. Two LTHDs were installed on the ceiling of the tunnel.

Gasoline was used as fuel in all the tests. The fire scenarios used in the tests included a small gasoline pool fire (0.09 m^2), a gasoline pool fire (0.36 m^2) located underneath a simulated vehicle, and a gasoline pool fire (0.36 m^2) located behind a large simulated vehicle. The HRRs varied from 125–650 kW as measured using a calorimeter. Four tests were conducted with a small gasoline pool fire (0.09 m^2) at different locations in the tunnel. The peak HRR produced by the fire was approximately 125 kW. The tests were designed to study the effect of changing fire location on the response of the detection systems to a small open pool fire. There was minimal airflow in the tunnel during these tests. In this scenario, the fire developed very quickly and substantial smoke was produced. Three tests were conducted with a pool fire located underneath a simulated vehicle. The tests were used to study the impact of airflow on the response of detection systems to a small fire (0.6 m × 0.6 fuel pan) located underneath a vehicle. The average airflow velocities varied from 0–2.5 m/s.

16.5.3 A Short Discussion

A detection system used in combination with a fire suppression system needs to be able to exactly determine the location of fire site. From this viewpoint, LTHD is required. Further, smoke detectors could be good supplementary detectors in tunnels, and use of normal dust detectors as smoke detectors in case of a fire could be a good option. Further, CCTV used for traffic control can also be used to confirm

the exact location of the fire accident. Other detection technology can be used as aids. In short, a combination of different detection systems which include at least LTHD, smoke/dust detectors and/or CCTV monitoring forms a reliable fire detection system.

16.6 Summary

The basic concepts of fire suppressions systems are described. There are mainly two water-based fire suppression systems used in tunnels, that is, water spray systems and water mist systems. The main difference is the pressure and water droplet size.

The mechanisms of extinguishment of fires using water-based fire suppression systems are introduced, which can be classified into two types: condensed phase suppression and gas phase suppression. In the condensed phase, surface cooling is the main mechanism. In the gas phase, it can be categorized into gas cooling, heat capacity and dilution effects, and kinetic effects. In a ventilated tunnel fire, the vaporized water vapor will be blown away from the fuel surfaces, and thus the dilution effect is reduced significantly. Small droplets could also be blown away. The main extinguishment mechanism is fuel surface cooling in tunnel fires. This suggests that the water spray systems with larger water flow rates will have better performance in suppression of tunnel fires with longitudinal ventilation.

The critical conditions at extinction are discussed. Further, suppression of realistic fires are discussed where both the water flow rate and the total water flow used for fire suppression are discussed.

A summary of fire suppression tests carried out in tunnels, and their main findings, is presented. The use of fire suppression systems in a tunnel is always a cost-effectiveness issue. The capability of fire suppression systems must be improved to effectively suppress fires rather than merely control them.

References

1. NFPA 13—Standard for the Installation of Sprinkler Systems (2013). National Fire Protection Association
2. Carvel RO, Marlair G (2005) A history of experimental tunnel fires. In: Beard AN, Carvel RO (eds) The handbook of tunnel fire safety. Thomas Telford Publishing, London, pp 201–230
3. NFPA 502—Standard for Road Tunnels, Bridges, and Other Limited Access Highways (2011 Edition). National Fire Protection Association
4. Cheong MK, Cheong WO, Leong KW, Lemaire AD, Noordijk LM (2014) Heat Release Rates of Heavy Goods Vehicle Fire in Tunnels with Fire Suppression System. Fire Technology 50:249–266
5. Cheong MK, Cheong WO, Leong KW, Lemaire AD, Noordijk LM, Tarada F Heat release rates of heavy goods vehicle fires in tunnels. In: 15th International Symposium on Aerodynamics, Ventilation & Fire in Tunnels, Barcelona, Spain, 2013. BHR Group, pp 779–788

6. Lemaire T, Kenyon Y (2006) Large Scale Fire Tests in the Second Benelux Tunnel. Fire Technology 42:329–350
7. Arvidson M Fixed Fire suppression System Concepts for Highway Tunnels. In: International Conference on Tunnel Fires and Escape from Tunnels, Lyon, France, 5–7 May 1999. Independent Technical Conferences Ltd., pp 129–136
8. Harris KJ Water Application Rates for Fixed Fire Fighting Systems in Road Tunnels. In: Fourth International Symposium on Tunnel Safety and Security, Frankfurt am Main, Germany, 2010.
9. SOLIT (2012) Engineering Guidance for a Comprehensive Evaluation of Tunnels with Fixed Fire Fighting Systems Scientific report of the SOLIT² research project, prepared by the SOLIT² consor-tium. Annex 3—Engineering Guidance for Fixed Fire Fighting Systems in Tunnels.
10. UPTUN (2008) Workpackage 2 Fire development and mitigation measures—D251. Engineering Guidance for Water Based Fire Fighting Systems for the Protection of Tunnels and Sub Surface Facilities.
11. UPTUN (2008) Workpackage 2 Fire development and mitigation measures—D253. Summary of Water Based FireSafety Systems in Road Tunnelsand Sub Surface Facilities.
12. Jönsson J, Johnson P Suppression System—Trade-offs & Benifits. In: Fourth International Symposium on Tunnel Safety and Security, Frankfurt am Main, 2010. pp 271–282
13. OTA O (December 2002) Automatic fire extinction (sprinkler) system. OTA Engineering, Tokyo, Japan
14. Stroeks R (2001) Sprinklers in Japanese Road Tunnels. Bouwdienst Rijkswaterstaat, Directoraat-Generaal Rijkswaterstaat, Ministry of Transport, The Netherlands
15. Mawhinney J (2013) Fixed Fire Protection Systems in Tunnels: Issues and Directions. Fire Technology 49:477–508
16. Arvidson M Large-Scale Water Spray and Water Mist Fire Suppression System Tests. In: Fourth International Symposium on Tunnel Safety and Security, Frankfurt am Main, 2010. pp 283–296
17. Brandt A, Wighus R (2006) Real-scale tests of compressed air foam system in Runehamar test tunnel 2005. Sintef NBL
18. Lönnermark A, Kristensson P, Helltegen M, Bobert M Fire suppression and structure protection for cargo train tunnels: Macadam and HotFoam. In: Lönnermark A, Ingason H (eds) 3rd International Symposium on Safety and Security in Tunnels (ISTSS 2008), Stockholm, Sweden, 12–14 March 2008. SP Technical Research Institute of Sweden, pp 217–228
19. Mawhinney JR, Trelles J (2007) Computational fluid dynamics modelling of water mist systems on large HGV fires in tunnels. Paper presented at the Journée d'Etude Technique: Brouillard d'Eau—Quoi de Neuf?, at Pôle Européen de Sécurité CNPP -. Vernon, France, 22 Nov
20. State of the Road Tunnel Equipment in Japan—Ventilation, Lighting, Safety Equipment (1993). Public Works Research Institute, Japan
21. Li YZ, Ingason H (2013) Model scale tunnel fire tests with automatic sprinkler. Fire Safety Journal 61:298–313
22. Ingason H (2008) Model scale tunnel tests with water spray. Fire Safety Journal 43 (7):pp 512–528
23. Development of new innovative technologies (2006). UPTUN Work Package 2
24. Tuomisaari M Full Scale fire testing for raod tunnel applications—evaluation of acceptable fire protection performance. In: Lönnermark A, Ingason H (eds) Third International Symposium on Tunnel Safety and Security, Stockholm, 2008. pp 181–193
25. Mawhinney JR Evaluating the performance of water mist systems in road tunnels. In: IV Congreso Bienal Apci Ingenieria de Pci Madrid, 21–23rd of February 2007.
26. Lemaire AD, Meeussen VJA (2008) Effects of water mist on real large tunnel fires: Experimental determination of BLEVE-risk and tenability during growth and suppression. Efectis Nederland BV,

27. Kratzmeir S, Lakkonen M Road Tunnel Protection by water mist systems—Implementation of full scale fire test results into a real project. In: Third International Symposium on Tunnel Safety and Security, Stockholm, 2008. SP pp 195–203
28. Ingason H, Appel G, Li YZ, Lundström U, Becker C Large scale fire tests with a Fixed Fire Fighting System (FFFS). In: ISTSS 6th International Symposium on Tunnel Safety and Security, Marseille, 2014.
29. Rasbash DJ The Extinction of Fire with Plane Water: A Review. In: Fire Safety Science—Proceedings of the First International Symposium, 1985. pp 1145–1163
30. Beyler C (1992) A unified model of fire suppresssion. Journal of Fire Protection Engineering 4 (1):5–16
31. Tewarson A (2002) Generation of Heat and Chemical Compounds in Fires. In: DiNenno PJ, Drysdale D, Beyler CL et al. (eds) The SFPE Handbook of Fire Protection Engineering. Third edition edn. National Fire Protection Association, Quincy, MA, USA, pp 3–82 – 3–161
32. Tewarson A, Pion RF (1976) Flammability of plastics. I. Burning intensity. Combustion and Flame 26:85–103
33. Ingason H, Li YZ (2010) Model scale tunnel fire tests with longitudinal ventilation. Fire Safety Journal 45:371–384
34. Rasbash DJ, Rogowski ZW, Stark GWV (1960) Mechanisms of Extinction of Liquid Fires and Water Sprays. Combustion and Flame 4:223–234
35. Rasbash DJ (1962) The extinction of fires by water sprays. Fire Research Abstracts and Reviews 4:17–23
36. Kung H-C (August 1977) Cooling of Room Fires by Sprinkler Spray. Jounal of Heat Transfer 99 (No. 3):353–359
37. Heskestad G (2003) Extinction of gas and liquid pool fires with water spray. Fire Safety Journal 38:301–317
38. Kung H-C, Hill JP (1975) Extinction of Wood Crib and Pallet Fires. Combustion and Flame 24:305–317
39. Tamanini F (1976) The Application of Water Sprays to the Extinguishemnt of Crib Fires. Combustion Science and Technology 14:p. 17
40. Cleary T, Chernovsky A, Grosshandler W, Anderson M Particulate Entry Lag in Spot-Type Smoke Detectors. In: Fire Safety Science—Proceedings of the Sixth International Symposium, Poitiers, France, 5–9 July 1999. IAFSS, pp 779–790
41. Heskestad G (1988) Quantification of thermal responsiveness of automatic sprinklers including conduction effects. Fire Safety Journal 14:113–125
42. Schifiliti RP, Meacham BJ, Custer RLP (2002) Design of Detection Systems. In: DiNenno PJ (ed) The SFPE Handbook of Fire Protection Engineering (2nd ed). National Fire Protection Association, Quincy, MA, pp 4–1–4–43
43. Zalosh R., Chantranuwat P. (2003) International road tunnel fire detection research project—Phase I, Review of prior test programs and tunnel fires. The Fire Protection Research Foundation, Massachusetts, USA
44. Ingason H (2006) Fire Testing in Road and Railway Tunnels. In: Apted V (ed) Flammability testing of materials used in construction, transport and mining. Woodhead Publishing, pp 231–274
45. Huijben Ir. J.W. (2002) Tests on Fire Detection and Sprinkler. Paper presented at the ITC Conference, Basel, 2–4 December
46. Aralt T.T., Nilsen A.R. (2009) Automatic fire detection in road traffic tunnels. Tunnelling and Underground Space Technology 24:75–83
47. Liu Z.G., Crampton G.P., Kashef A., Lougheed G., Muradori S. (2008) International road tunnel fire detection research project—Phase II, Task 4: Field Fire Tests on Performance of Fire Detection Systems in an Operating Road Tunnel in Montreal. The Fire Protection Research Foundation, Massachusetts, USA

Chapter 17
CFD Modeling of Tunnel Fires

Abstract Computational fluid dynamics (CFD) modeling has been widely used for performance-based tunnel fire safety design in engineering applications. A CFD tool divides a computation domain into a large number of small cells, and solves a set of differential equations with sub-models using different solution algorithms. The CFD users need to not only efficiently use CFD tools, but also to understand the embedded mechanisms. The basics of CFD modeling are introduced including controlling equations, different turbulence models, and numerical methods. Sub-models important for tunnel fires are then described, that is gas phase combustion models, condensed phase pyrolysis models, fire suppression models, wall functions, and heat transfer models. Despite the rapid development and completeness of these models related to fire phenomena, many limitations exist which should be always kept in mind by the users. Recommendations for CFD modeling of tunnel fires are presented.

Keywords CFD · Turbulence · Discretization · Combustion · Pyrolysis · Fire suppression · Wall function · Heat transfer · Limitation · Suggestion

17.1 Introduction

In the past several decades, CFD modeling has been rapidly developed together with significantly increased capacities of the computers.

There have been some commercial CFD tools widely used in a variety of application fields, for example, ANSYS Fluent, ANSYS CFX, PHOENICS, STAR-CCM+. Although, these general CFD tools embed many models and have strong capability of modeling different phenomena, they are generally not well tailored for fire modeling.

There have also been some specific CFD tools developed for use in fire modeling, such as JASMINE, SMARTFIRE, SOFIE, Fire Dynamics Simulator (FDS) [1], and FireFoam [2]. Among these, FDS developed by NIST [1] has become the standard in the fire community.

To date, CFD modeling has been widely used in performance-based fire safety design. Many research and application papers on CFD modeling of tunnel fires can

H. Ingason et al., *Tunnel Fire Dynamics,* DOI 10.1007/978-1-4939-2199-7_17

be found in the literature. For example, Cheong et al. [3] simulated the burning of wood pallets, and Li et al. [4] simulated smoke characteristics of the large fires in the Runehamar tunnel fire tests carried out by Ingason et al. [5, 6].

CFD modeling simulates complex phenomena by use of numerous models. The CFD users are required to not only efficiently use the tool, but also to understand the embedded mechanisms. In this chapter, the basics of CFD modeling and the models related to fire dynamics are introduced, and limitations and recommendations are presented.

17.2 CFD Basics

The fundamental idea of CFD modeling is to divide a computation domain into a large number of small cells, and to solve a set of differential equations with sub-models using different solution algorithm. Within each cell, the properties are assumed to be uniform. The phenomena at a scale larger than the cell size are directly solved using the controlling equations but those at a smaller scale are simulated using sub-models.

17.2.1 Controlling Equations

The controlling equations describing the conservation of mass, momentum, and energy can be written as follows:

Mass:

$$\frac{\partial \rho}{\partial t}+\frac{\partial(\rho u)}{\partial x}+\frac{\partial(\rho v)}{\partial y}+\frac{\partial(\rho w)}{\partial z}=S_m \tag{17.1}$$

or in terms of individuals species (mass fraction Y):

$$\begin{aligned}&\frac{\partial \rho Y_i}{\partial t}+\frac{\partial(\rho u Y_i)}{\partial x}+\frac{\partial(\rho v Y_i)}{\partial y}+\frac{\partial(\rho w Y_i)}{\partial z}\\&=\frac{\partial}{\partial x}(\rho D_i \frac{\partial Y_i}{\partial x})+\frac{\partial}{\partial y}(\rho D_i \frac{\partial Y_i}{\partial y})+\frac{\partial}{\partial z}(\rho D_i \frac{\partial Y_i}{\partial z})+S_{m,i}\end{aligned} \tag{17.2}$$

Momentum:

$$\begin{aligned}&\frac{\partial(\rho u)}{\partial t}+\frac{\partial(\rho u u)}{\partial x}+\frac{\partial(\rho u v)}{\partial y}+\frac{\partial(\rho u w)}{\partial z}\\&=\frac{\partial}{\partial x}(\mu \frac{\partial u}{\partial x})+\frac{\partial}{\partial y}(\mu \frac{\partial u}{\partial y})+\frac{\partial}{\partial z}(\mu \frac{\partial u}{\partial z})-\frac{\partial p}{\partial x}+S_{M,x}\end{aligned} \tag{17.3}$$

$$\frac{\partial(\rho v)}{\partial t}+\frac{\partial(\rho uv)}{\partial x}+\frac{\partial(\rho vv)}{\partial y}+\frac{\partial(\rho vw)}{\partial z}$$
$$=\frac{\partial}{\partial x}(\mu\frac{\partial v}{\partial x})+\frac{\partial}{\partial y}(\mu\frac{\partial v}{\partial y})+\frac{\partial}{\partial z}(\mu\frac{\partial v}{\partial z})-\frac{\partial p}{\partial y}+S_{M,y} \tag{17.4}$$

$$\frac{\partial(\rho w)}{\partial t}+\frac{\partial(\rho uw)}{\partial x}+\frac{\partial(\rho vw)}{\partial y}+\frac{\partial(\rho ww)}{\partial z}$$
$$=\frac{\partial}{\partial x}(\mu\frac{\partial w}{\partial x})+\frac{\partial}{\partial y}(\mu\frac{\partial w}{\partial y})+\frac{\partial}{\partial z}(\mu\frac{\partial w}{\partial z})-\frac{\partial p}{\partial z}+S_{M,z} \tag{17.5}$$

Energy:

$$\frac{\partial(\rho h)}{\partial t}+\frac{\partial(\rho uh)}{\partial x}+\frac{\partial(\rho vh)}{\partial y}+\frac{\partial(\rho wh)}{\partial z}=\frac{\partial}{\partial x}(k\frac{\partial T}{\partial x})+\frac{\partial}{\partial y}(k\frac{\partial T}{\partial y})+\frac{\partial}{\partial z}(k\frac{\partial T}{\partial z})+S_h \tag{17.6}$$

where

$$S_m=\dot{m}'''_{net},\ S_{m,i}=\dot{m}'''_{net,i}$$

$$S_{M,x}=\frac{\partial}{\partial x}(\mu\frac{\partial u}{\partial x})+\frac{\partial}{\partial y}(\mu\frac{\partial u}{\partial y})+\frac{\partial}{\partial z}(\mu\frac{\partial u}{\partial z})-\frac{2}{3}\frac{\partial}{\partial x}\left[\mu(\frac{\partial u}{\partial x}+\frac{\partial v}{\partial y}+\frac{\partial w}{\partial z})\right]+\rho g_x+\sum F_x$$

$$S_{M,y}=\frac{\partial}{\partial x}(\mu\frac{\partial v}{\partial x})+\frac{\partial}{\partial y}(\mu\frac{\partial v}{\partial y})+\frac{\partial}{\partial z}(\mu\frac{\partial v}{\partial z})-\frac{2}{3}\frac{\partial}{\partial y}\left[\mu(\frac{\partial u}{\partial x}+\frac{\partial v}{\partial y}+\frac{\partial w}{\partial z})\right]+\rho g_y+\sum F_y$$

$$S_{M,z}=\frac{\partial}{\partial x}(\mu\frac{\partial w}{\partial x})+\frac{\partial}{\partial y}(\mu\frac{\partial w}{\partial y})+\frac{\partial}{\partial z}(\mu\frac{\partial w}{\partial z})-\frac{2}{3}\frac{\partial}{\partial z}\left[\mu(\frac{\partial u}{\partial x}+\frac{\partial v}{\partial y}+\frac{\partial w}{\partial z})\right]+\rho g_z+\sum F_z$$

$$S_h=\dot{Q}'''_{net}+\Phi+\frac{\partial p}{\partial t}+u\frac{\partial p}{\partial x}+v\frac{\partial p}{\partial y}+w\frac{\partial p}{\partial z}$$

$$\Phi=\mu\left\{2[(\frac{\partial u}{\partial x})^2+(\frac{\partial v}{\partial y})^2+(\frac{\partial w}{\partial z})^2]+(\frac{\partial u}{\partial y}+\frac{\partial v}{\partial x})^2+(\frac{\partial u}{\partial z}+\frac{\partial w}{\partial x})^2+(\frac{\partial v}{\partial z}+\frac{\partial w}{\partial y})^2\right\}$$
$$-\frac{2}{3}\mu(\frac{\partial u}{\partial x}+\frac{\partial v}{\partial y}+\frac{\partial w}{\partial z})^2$$

In the above equations, ρ is the density (kg/m^3), t is the time (s), x, y, z are the cartesian axis (m) and u, v, w are the velocity in the x, y, and z direction respectively (m/s). D is the mass diffusivity (m^2/s), μ is the viscosity (kg/(m s)), k is the heat conductivity (kW/(m K)), p is the pressure (Pa), g is the gravitational acceleration(m^2/s), h is the specific enthalpy (kJ/kg), S is the source term, F is the force term (N/m^3), Y is the species mass fraction and Φ is the dissipation function. Subscripts m is the mass, M is the momentum, h is the enthalpy, F is the external force such as drag exerted by water droplets, and i is the ith species. Superscript (·) indicates per unit time and ("') per unit volume.

Note that the kinetic energy has been replaced by tensors and force terms, and g is the gravity vector. The stress sensors are solved by the deformation rate of the fluid volume.

17.2.2 Equation of state

Thermodynamic equilibrium can be assumed for an ideal gas. The state equation for pressure can be expressed as:

$$p = \frac{\overline{R}}{M}\rho T \tag{17.7}$$

with ambient pressure distribution:

$$\frac{dp_o}{dz} = -\rho_o g \tag{17.8}$$

The state equation for internal energy, e, and enthalpy, h, can be written as:

$$e = c_v T \text{ and } h = c_p T \tag{17.9}$$

For gases consisting of N species, the pressure can be summed as:

$$p = \sum_{i=1}^{N} p_i = \sum_{i=1}^{N} \left(\frac{\overline{R}\rho_i T_i}{M_i}\right) \tag{17.10}$$

and the total enthalpy can be estimated by:

$$h = \sum_{i=1}^{N} \int_{T_o}^{T} c_{p,i} dT \tag{17.11}$$

In the above equations, $\overline{R}$ is the universal gas constant (8.314 kJ/(kmol K)), M is the molecular weight (kg/kmol), T is the gas temperature in Kelvin (K), e is the specific internal energy (kJ/kg), h is the enthalpy (kJ/kg), c_p is the specific heat at

constant pressure (kJ/(kg K)), c_v is the specific heat at constant volume(kJ/(kg K)), p_o is the ambient pressure (Pa) and z is the altitude height (m). Subscript i represent the ith species.

17.2.3 Turbulence

All flows are stable below a certain Reynolds number ($\mathrm{Re}=\rho ul/\mu$, l is length scale), referred to as laminar flow. However, above a certain Reynolds number, the flows become unstable and turbulent, referred to as turbulent flow. Between these regimes, the flows are called transitional flows.

There are different models that can be used in CFD simulations to simulate the turbulence. They can be primarily classified into three types, Navier–Stokes models, large eddy simulation (LES) and direct numerical simulation (DNS).

In turbulent flows, the fluctuations results in additional stresses on the fluid, called Reynold stresses. The mechanism for diffusion of momentum and energy is different between laminar and turbulent flows.

17.2.3.1 Averaged Navier–Stokes models

Averaged Navier–Stokes models solve the averaged controlling equations, and introduce sub-models to solve the terms related to fluctuating components in momentum and energy equations. The flow variables, that is, velocity and pressure, are decomposed into two components: a mean component and a fluctuating component, for example, $\varphi = \overline{\varphi} + \varphi'$. There are two averaging methods that could be used: the Reynolds averaged Navier–Stokes (RANS) model or Favre averaged Navier–Stokes (FANS) model. The Reynolds averaged method solves the time averaged controlling equations while the Favre averaged method solves the weighted averaged equations based on Reynolds averaged controlling equations. If the density fluctuations are small in some specific cases, we can obtain the same equations using both methods. Compared to RANS, FANS is much better in handling compressible flows. Here, the Favre averaged Navier–Stokes model is presented. The Favre averaging is a weighting averaging method, which is given by

$$\tilde{\varphi}(x,t) = \frac{\overline{\rho\varphi}}{\overline{\rho}} \tag{17.12}$$

where φ is a variable property. Superscript "-" indicates average value over a small time increment and "~" indicates favre averaged value.

The controlling equations in Cartesian coordinates can, therefore, be expressed as:

Mass:

$$\frac{\partial \overline{\rho}}{\partial t} + \frac{\partial(\overline{\rho}\tilde{u})}{\partial x} + \frac{\partial(\overline{\rho}\tilde{v})}{\partial y} + \frac{\partial(\overline{\rho}\tilde{w})}{\partial z} = S_m \tag{17.13}$$

or in terms of individuals species:

$$\frac{\partial(\overline{\rho}\tilde{Y})}{\partial t}+\frac{\partial(\overline{\rho}\tilde{u}\tilde{Y})}{\partial x}+\frac{\partial(\overline{\rho}\tilde{v}\tilde{Y})}{\partial y}+\frac{\partial(\overline{\rho}\tilde{w}\tilde{Y})}{\partial z}=\frac{\partial}{\partial x}(\overline{\rho}D\frac{\partial\tilde{Y}}{\partial x})+\frac{\partial}{\partial y}(\overline{\rho}D\frac{\partial\tilde{Y}}{\partial y})$$
$$+\frac{\partial}{\partial z}(\overline{\rho}D\frac{\partial\tilde{Y}}{\partial z})-\left[\frac{\partial(\widetilde{\overline{\rho}u''Y''})}{\partial x}+\frac{\partial(\widetilde{\overline{\rho}v''Y''})}{\partial y}+\frac{\partial(\widetilde{\overline{\rho}w''Y''})}{\partial z}\right]+\tilde{S}_{m,Y} \tag{17.14}$$

Momentum:

X axis:

$$\frac{\partial(\overline{\rho}\tilde{u})}{\partial t}+\frac{\partial(\overline{\rho}\tilde{u}\tilde{u})}{\partial x}+\frac{\partial(\overline{\rho}\tilde{u}\tilde{v})}{\partial y}+\frac{\partial(\overline{\rho}\tilde{u}\tilde{w})}{\partial z}=\frac{\partial}{\partial x}(\mu\frac{\partial\tilde{u}}{\partial x})+\frac{\partial}{\partial y}(\mu\frac{\partial\tilde{u}}{\partial y})+\frac{\partial}{\partial z}(\mu\frac{\partial\tilde{u}}{\partial z})$$
$$-\frac{\partial\tilde{p}}{\partial x}-\left[\frac{\partial(\widetilde{\overline{\rho}u''^2})}{\partial x}+\frac{\partial(\widetilde{\overline{\rho}u''v''})}{\partial y}+\frac{\partial(\widetilde{\overline{\rho}u''w''})}{\partial z}\right]+\tilde{S}_{M,x} \tag{17.15}$$

Y axis:

$$\frac{\partial(\overline{\rho}\tilde{v})}{\partial t}+\frac{\partial(\overline{\rho}\tilde{u}\tilde{v})}{\partial x}+\frac{\partial(\overline{\rho}\tilde{v}\tilde{v})}{\partial y}+\frac{\partial(\overline{\rho}\tilde{v}\tilde{w})}{\partial z}=\frac{\partial}{\partial x}(\mu\frac{\partial\tilde{v}}{\partial x})+\frac{\partial}{\partial y}(\mu\frac{\partial\tilde{v}}{\partial y})+\frac{\partial}{\partial z}(\mu\frac{\partial\tilde{v}}{\partial z})$$
$$-\frac{\partial\tilde{p}}{\partial y}-\left[\frac{\partial(\widetilde{\overline{\rho}u''v''})}{\partial x}+\frac{\partial(\widetilde{\overline{\rho}v''^2})}{\partial y}+\frac{\partial(\widetilde{\overline{\rho}v''w''})}{\partial z}\right]+\tilde{S}_{M,y} \tag{17.16}$$

Z axis:

$$\frac{\partial(\overline{\rho}\tilde{w})}{\partial t}+\frac{\partial(\overline{\rho}\tilde{u}\tilde{w})}{\partial x}+\frac{\partial(\overline{\rho}\tilde{v}\tilde{w})}{\partial y}+\frac{\partial(\overline{\rho}\tilde{w}\tilde{w})}{\partial z}=\frac{\partial}{\partial x}(\mu\frac{\partial\tilde{w}}{\partial x})+\frac{\partial}{\partial y}(\mu\frac{\partial\tilde{w}}{\partial y})+\frac{\partial}{\partial z}(\mu\frac{\partial\tilde{w}}{\partial z})$$
$$-\frac{\partial\tilde{p}}{\partial z}-\left[\frac{\partial(\widetilde{\overline{\rho}u''w''})}{\partial x}+\frac{\partial(\widetilde{\overline{\rho}v''w''})}{\partial y}+\frac{\partial(\widetilde{\overline{\rho}w''^2})}{\partial z}\right]+\tilde{S}_{M,z} \tag{17.17}$$

Energy:

$$\frac{\partial(\overline{\rho}\tilde{h})}{\partial t}+\frac{\partial(\overline{\rho}\tilde{u}\tilde{h})}{\partial x}+\frac{\partial(\overline{\rho}\tilde{v}\tilde{h})}{\partial y}+\frac{\partial(\overline{\rho}\tilde{w}\tilde{h})}{\partial z}=\frac{\partial}{\partial x}(k\frac{\partial\tilde{T}}{\partial x})+\frac{\partial}{\partial y}(k\frac{\partial\tilde{T}}{\partial y})+\frac{\partial}{\partial z}(k\frac{\partial\tilde{T}}{\partial z})$$
$$-\left[\frac{\partial(\widetilde{\overline{\rho}u''h''})}{\partial x}+\frac{\partial(\widetilde{\overline{\rho}v''h''})}{\partial y}+\frac{\partial(\widetilde{\overline{\rho}w''h''})}{\partial z}\right]+\tilde{S}_{h} \tag{17.18}$$

Note that the main difference between the above equations for turbulent flows and for laminar flows is the presence of additional terms on the right-hand sides of the momentum equations Eqs. (17.15–17.17), the species transport equation Eq. (17.14) and the energy equation Eq. (17.18). These terms indicate the additional diffusion of momentum and mass, and extra dissipation of energy. The terms in the momentum equation are called the Reynolds stress and therefore, the momentum equations are called the Reynolds equations. The Navier–Stokes turbulence models are proposed to correlate these turbulent terms with the mean values of the flows. The source terms can be easily obtained by averaging the original terms.

The averaged Navier–Stokes turbulence models mainly include: the zero equation model (mixing length model), two equation k-ε model, Reynolds stress equation model, and algebraic stress model. The most widely used and validated standard *k-ε* model is briefly depicted here.

The turbulent kinetic energy, K (m^2/s^2), and viscous dissipation rate, ε (m^2/s^3), respectively are defined as:

$$K = \frac{1}{2}\widetilde{u_i' u_i'} = \frac{1}{2}(\widetilde{u'^2} + \widetilde{v'^2} + \widetilde{w'^2}),\ \varepsilon = \frac{\mu_t}{\bar{\rho}}\widetilde{\frac{\partial u_i'}{\partial x_j}\cdot\frac{\partial u_i'}{\partial x_j}},\ i,\ j = 1,\ 2,\ 3 \tag{17.19}$$

where μ_t is the turbulent viscosity (kg/(m s)), which is assumed to be isotropic in the *k-ε* model. u', v', and w' are the fluctuating component of velocity u, v, and w respectively (m/s). Subscripts i and j indicate x (1), y (2), or z (3) axis.

The Reynolds stress in the momentum equation, τ_{ij} (kg/(m s^2)), is linked to the mean rates of deformation by:

$$\tau_{ij} = -\bar{\rho}\widetilde{u_i' u_j'} = \mu_t\left(\frac{\partial \tilde{u}_i}{\partial x_j} + \frac{\partial \tilde{u}_j}{\partial x_i}\right) - \frac{2}{3}\left(\mu_t \frac{\partial \tilde{u}_i}{\partial x_j} + \bar{\rho}K\right)\delta_{ij} \tag{17.20}$$

where the Kronecker delta, $\delta_{i,j}$, is defined as:

$$\delta_{ij} = \begin{cases} 1 & i = j \\ 0 & i \neq j \end{cases} \quad i,\ j = 1,\ 2,\ 3 \tag{17.21}$$

Note that the turbulent terms in the momentum equation have been correlated with the mean terms. The main task left is to estimate the turbulent viscosity, μ_t. In the standard *k-ε* model, it is assumed that the turbulent eddy viscosity is proportional to the turbulent velocity scale and length scale which can be replaced by the turbulent kinetic energy and viscous dissipation rate. This assumption leads to:

$$\mu_t = \rho C_\mu \frac{k^2}{\varepsilon} \tag{17.22}$$

The k equation can be expressed as:

$$\frac{\partial(\bar{\rho}K)}{\partial t}+\frac{\partial(\bar{\rho}\tilde{u}_j K)}{\partial x_j}=\frac{\partial}{\partial x_j}(\frac{\mu_t}{\sigma_k}\frac{\partial K}{\partial x_j})+\mu_t\frac{\partial\tilde{u}_i}{\partial x_j}(\frac{\partial\tilde{u}_i}{\partial x_j}+\frac{\partial\tilde{u}_j}{\partial x_i})-\frac{2}{3}\frac{\partial\tilde{u}_i}{\partial x_j}(\mu_t\frac{\partial\tilde{u}_i}{\partial x_j}+\bar{\rho}K)\delta_{ij}-\bar{\rho}\varepsilon \tag{17.23}$$

And the ε equation can be expressed as:

$$\begin{aligned}&\frac{\partial(\bar{\rho}\varepsilon)}{\partial t}+\frac{\partial(\bar{\rho}\tilde{u}_j\varepsilon)}{\partial x_j}=\frac{\partial}{\partial x_j}(\frac{\mu_t}{\sigma_\varepsilon}\frac{\partial\varepsilon}{\partial x_j})\\&+C_{\varepsilon 1}\frac{\varepsilon}{K}\left[\mu_t\frac{\partial\tilde{u}_i}{\partial x_j}(\frac{\partial\tilde{u}_i}{\partial x_j}+\frac{\partial\tilde{u}_j}{\partial x_i})-\frac{2}{3}\frac{\partial\tilde{u}_i}{\partial x_j}(\mu_t\frac{\partial\tilde{u}_i}{\partial x_j}+\bar{\rho}K)\delta_{ij}\right]-C_{\varepsilon 2}\bar{\rho}\frac{\varepsilon^2}{K}\end{aligned} \tag{17.24}$$

where

$$C_\mu=0.09,\ C_{\varepsilon 1}=1.44,\ C_{\varepsilon 2}=1.92,\ \sigma_{\mathrm{k}}=1.0,\ \sigma_\varepsilon=1.30$$

The turbulent terms in other equations are directly correlated with the turbulent viscosity by analogy. The turbulent terms in energy equation can be expressed as:

$$-\bar{\rho}\widetilde{u_i'h}=k_t\frac{\partial\tilde{h}}{\partial x_i} \tag{17.25}$$

The turbulent terms in species scalar equation is expressed as:

$$-\bar{\rho}\widetilde{u_i'Y}=(\rho D)_t\frac{\partial\tilde{Y}}{\partial x_i} \tag{17.26}$$

The corresponding turbulent conductivity, k_t, can be estimated by:

$$k_t=\frac{\mu_t}{\mathrm{Pr}_t} \tag{17.27}$$

And the turbulent mass diffusivity, $(\rho D)_t$, is:

$$(\rho D)_t=\frac{\mu_t}{\mathrm{Sc}_t} \tag{17.28}$$

where Pr_t is turbulent Prandtl number and Sc_t is turbulent Schdmit number. It should be kept in mind that the standard k-ε model is only suitable for flows with high Reynolds numbers, that is turbulent flows. There are also k-ε equations for low Reynold numbers where the viscous diffusivity term needs to be accounted for.

17.2.3.2 Large Eddy Simulation (LES)

As described in the last section, RANS introduces extra equations to model the turbulence, and both large and small eddies are modeled using turbulence sub-models. In contrast, LES directly simulates the mean flow and the largest eddies and only simulate the small eddies using sub-grid scale models. LES models can use explicit filter functions to filter the small eddies. The spatial filtering operation could be expressed as follows:

$$\hat{\varphi}(x,t) = \int_{\Delta} \varphi(r,t) G(|x-r|) dr \tag{17.29}$$

where G is the filter function and Δ is the filter width which is generally equal to the cell size. The most common filter functions include: the Top hat filter function, the Gaussian filter function, and the Fourier Cut-Off filter function [7].

Similar to the Navier–Stokes turbulent models, the Favre averaging is used here, which is given by

$$\tilde{\varphi}(x,t) = \frac{\widehat{\rho\varphi}}{\hat{\rho}} \tag{17.30}$$

The controlling equations for large eddy simulation are similar to those for the FANS model except the turbulent stress terms:

Mass:

$$\frac{\partial \hat{\rho}}{\partial t} + \frac{\partial(\hat{\rho}\tilde{u}_j)}{\partial x_j} = S_m \tag{17.31}$$

or in terms of individuals species:

$$\frac{\partial(\hat{\rho}\tilde{Y})}{\partial t} + \frac{\partial(\hat{\rho}\tilde{u}_j\tilde{Y})}{\partial x_j} = \frac{\partial}{\partial x_j}(\hat{\rho}D\frac{\partial \tilde{Y}_j}{\partial x_j}) - \frac{\partial}{\partial x}(\widehat{\rho u_j Y} - \hat{\rho}\tilde{u}_j\tilde{Y}) + \tilde{S}_{m,Y} \tag{17.32}$$

Momentum:

$$\frac{\partial(\hat{\rho}\tilde{u})}{\partial t} + \frac{\partial(\hat{\rho}\tilde{u}_i\tilde{u}_j)}{\partial x_j} = -\frac{\partial}{\partial x}\left[\tilde{p}\delta_{ij} - \mu_t\frac{\partial \tilde{u}_i}{\partial x_j}(\frac{\partial \tilde{u}_i}{\partial x_j} + \frac{\partial \tilde{u}_j}{\partial x_i}) + \frac{2}{3}(\mu_t\frac{\partial \tilde{u}_i}{\partial x_j})\delta_{ij}\right] - \frac{\partial(\widehat{\rho u_i u_j} - \hat{\rho}\tilde{u}_i\tilde{u}_j)}{\partial x_j} + S_{M,i} \tag{17.33}$$

Energy:

$$\frac{\partial(\hat{\rho}\tilde{h})}{\partial t} + \frac{\partial(\hat{\rho}\tilde{u}_j\tilde{h})}{\partial x_j} = \frac{\partial}{\partial x_j}(\frac{k}{c_p}\frac{\partial \tilde{h}}{\partial x_j}) - \frac{\partial}{\partial x}(\widehat{\rho u_j h} - \hat{\rho}\tilde{u}_j\tilde{h}) + \tilde{S}_h \tag{17.34}$$

It should be kept in mind that all the variables are filtered values. Also, note that the turbulent stress terms in the controlling equations for LES are different with the Reynolds stress terms for FANS owing to the different definitions. Despite the difference, the turbulent stresses also need to be solved using sub grid scale (SGS) models. The commonly used SGS models mainly include the Smagorinsky model, structure function model, mixed scale model, dynamic SGS models, and one-equation SGS models [7]. Here, the basic Smagorinsky model which is used in FDS [1] is depicted briefly.

In the Smagorinsky model, the turbulent eddies are assumed to be isotropic. The subgrid turbulent stresses are modeled as:

$$\tau_{ij} = \widehat{\rho u_i u_j} - \hat{\rho}\tilde{u}_i\tilde{u}_j = -2\mu_{SGS}\tilde{S}_{ij} \tag{17.35}$$

where the rate-of-strain tensor, $\tilde{S}_{ij}$, is defined as:

$$\tilde{S}_{ij} = \frac{1}{2}\left(\frac{\partial\tilde{u}_i}{\partial x_j} + \frac{\partial\tilde{u}_j}{\partial x_i}\right) - \frac{1}{3}\frac{\partial\tilde{u}_n}{\partial x_n}\delta_{ij}, \quad n = 1,\ 2,\ 3 \tag{17.36}$$

It is assumed that the turbulent viscosity can be described in terms of a length scale and the average strain rate of the flow, which suggests:

$$\mu_{SGS} = \rho(C_s\Delta)^2\left[2\tilde{S}_{ij}\cdot\tilde{S}_{ij} - \frac{2}{3}\left(\frac{\partial\tilde{u}_n}{\partial x_n}\right)^2\right]^{\frac{1}{2}} \tag{17.37}$$

where C_s is a coefficient ranging between 0.065 and 0.3. This value is set to 0.2 in FDS [1].

Similar to the Favre averaged Navier–Stokes models, the turbulent terms in other equations are also correlated with the turbulent viscosity by analogy. The turbulent terms in energy equation can be expressed as:

$$\widehat{\rho u_i h} - \hat{\rho}\tilde{u}_i\tilde{h} = -k_{SGS}\frac{\partial\tilde{T}}{\partial x_j} \tag{17.38}$$

The turbulent terms in scalar equation is expressed as:

$$\widehat{\rho u_i Y} - \hat{\rho}\tilde{u}_i\tilde{Y} = -(\rho D)_{SGS}\frac{\partial\hat{Y}}{\partial x_j} \tag{17.39}$$

The corresponding turbulent conductivity and mass diffusivity can be simply estimated by:

$$k_{SGS} = \frac{\mu_{SGS}c_p}{\mathrm{Pr}_{SGS}} \tag{17.40}$$

and

$$(\rho D)_{SGS} = \frac{\mu_{SGS}}{\mathrm{Sc}_{SGS}} \tag{17.41}$$

In FDS, both the turbulent Prandtl number and the Schmidt number are set to be 0.5.

17.2.3.3 Direct Numerical Simulation

Direct numerical simulation (DNS) directly solves the controlling equations and directly simulates both the largest and smallest eddies. Note that the controlling equations for DNS are the same as the equations for laminar flows. Therefore, the mesh size should be smaller than the smallest eddy in the flow, where the Reynolds number is equivalent to unity. The grid number in three-dimensional simulations scales as 9/4 power of the Reynold number. As the Reynolds number increases, the difference between the smallest and largest eddies also increases, and the required grid numbers increases rapidly. Although, some investigations suggest that a reduction by a factor of 100 in the number of the cells is possible without significant loss of accuracy, it is apparent that a DNS calculation is very costly.

Note that use of DNS only suggests the possibility of modeling the flow perfectly, rather than modeling the fire-induced flows perfectly since, the later depends not only the flow models but the other sub-models which will be discussed later.

17.2.4 Discretization Methods

The controlling equations need to be discretized and solved over the cells. Three discretization methods are widely used, that is: the finite volume method (FVM), finite element method (FEM) and finite difference method (FDM). Additionally, the boundary element method, spectral element method, and other high-resolution discretization schemes could be used. Here, we focus on the finite volume method which is widely used in computational fluid dynamics owing to its clear physical meaning and completeness. First we discretize a computation domain into a large amount of small control volumes.

Note that the controlling equations for mass, momentum, and energy can be written in a simple form:

$$\frac{\partial(\rho\varphi)}{\partial t} + div(\rho\varphi\mathbf{u}) = div(\Gamma grad(\varphi)) + S \tag{17.42}$$

where φ is a variable property (1 for mass, u for momentum and h for energy), u is the velocity vector and S is a source term. The symbol *div* is the divergence and *grad* is the gradient.

Integrating the above equation from time t to $t+\Delta t$ for the control volume (CV) suggests:

$$\int_{CV}\int_{t}^{t+\Delta t}\frac{\partial(\rho\varphi)}{\partial t}dtdV+\int_{CV}\int_{t}^{t+\Delta t}div(\rho\varphi\mathbf{u})dtdV$$
$$=\int_{CV}\int_{t}^{t+\Delta t}div(\Gamma grad(\varphi))dtdV+\int_{CV}\int_{t}^{t+\Delta t}SdtdV \tag{17.43}$$

17.2.4.1 Temporal Discretization

The integration of the terms in the above equation, except the first term on the left-hand side signifying the rate of change, from time to t+ Δt can be expressed in such a way:

$$\int_{t}^{t+\Delta t}\varphi dt=\Delta t\left[\xi\varphi(t+\Delta t)+(1-\xi)\varphi(t)\right] \tag{17.44}$$

where Δt is time step (s) and ξ is a coefficient for the discretization.

If $\xi=0$, the term φ at time $t+\Delta t$ is estimated fully based on the values at time t, and the resulting scheme is called fully explicit or Euler explicit scheme. If $\xi=1$, the term φ at time t+Δt is estimated fully based on the values at time $t+\Delta t$, and the resulting scheme is called fully implicit or Euler implicit scheme. If $\xi=1/2$, the scheme is called the Crank–Nicolson scheme. However, note that the first term in Eq. (17.43) signifying the rate of change includes the derivative of time and the time increment can be depleted, and thus it always has the same form, regardless of the schemes.

For fully explicit scheme, stability conditions, that is, Courant–Friedrichs–Lewy (CFL) condition and Von Neumann criterion, need to be fulfilled to avoid instability.

For structured grids, the CFL condition can be simply expressed as:

$$\Delta t\max(\frac{|u|}{\Delta x},\frac{|v|}{\Delta y},\frac{|w|}{\Delta z})<1 \tag{17.45}$$

and the Von Neumann criterion is:

$$\Delta t\max(D,v,a)(\frac{1}{\Delta x^2}+\frac{1}{\Delta y^2}+\frac{1}{\Delta z^2})<\frac{1}{2} \tag{17.46}$$

where Δx, Δy, Δz are the size of the grid cell in the x, y, and z direction respectively, D is the mass diffusivity (m^2/s), v is the kinematic viscosity (m^2/s) and a is the thermal diffusivity (m^2/s).

These limitations are used to stabilize the solution by forcing the coefficients in the numerical equations above zero. The physical meaning is to avoid the flow of mass, momentum, and energy transferring too fast.

A fully implicit scheme indicates that the obtained results are always stable in theory. However, small time steps are required to reduce computation errors since the accuracy of the fully implicit scheme is generally first order or second order in time. For example, the fully implicit Euler scheme is only first order. Further, small time steps could also be required in case of a transient flow involving time dependent boundaries or very complicated phenomena.

17.2.4.2 Spatial Discretization

For the convection term and the diffusion terms, we need to discretize the term as a derivative of the volume size. Let us consider, a control volume enclosed by two neighboring volume west (W) and east (E) and the two corresponding boundaries are called *w* and *e* (*x* axis from w to e).

$$\int_{CV} \frac{\partial \varphi}{\partial x} dV = (\Delta y \Delta z)(\varphi_e - \varphi_w) \tag{17.47}$$

The values at the boundaries need to be replaced using the values of the cells beside the control volume. There are many schemes for discretization of the boundary terms, including: the central differencing scheme, upwind differencing scheme, hybrid differencing scheme, power-law scheme, QUICK scheme, and other high order schemes, for example the Superbee scheme for convection [8].

The central differencing scheme for this volume can be expressed as:

$$\varphi_w = \frac{\varphi_W + \varphi_{CV}}{2} \text{ and } \varphi_e = \frac{\varphi_{CV} + \varphi_E}{2} \tag{17.48}$$

For a convection and diffusion problem, the central differencing scheme may result in instability unless it fulfills the condition for the Peclet number:

$$Pe = \frac{\rho u}{\Gamma \Delta x} < 2 \tag{17.49}$$

The physical meaning is that the directionality of influencing is not expressed well using the central differencing scheme in a flow.

The upwind scheme suggests that the value of the upwind mesh is used as the boundary value, for example, if the wind is from west to east, we have

$$\varphi_w = \varphi_W \text{ and } \varphi_e = \varphi_{CV} \tag{17.50}$$

Although the upwind scheme is so simple and its accuracy is only first order, it is useful for convection problems. To increase accuracy at a high *Pe* number, the hybrid differencing scheme of Spalding can be used. The hybrid differencing scheme is a combination of the upwind scheme and central differencing scheme, and is valid for the whole range of the Peclet number.

The accuracy of hybrid and upwind schemes is only first order. Higher order differencing schemes could be used to speed up the computation. The quadratic upwind differencing scheme (QUICK) [9] is a good example:

$$\varphi_w = \frac{6}{8}\varphi_P + \frac{3}{8}\varphi_W - \frac{1}{8}\varphi_E \text{ and } \varphi_e = \frac{6}{8}\varphi_E + \frac{3}{8}\varphi_P - \frac{1}{8}\varphi_{EE} \tag{17.51}$$

where *EE* is the further east mesh.

17.2.5 Solution Algorithms

After the discretization of the equations we can obtain several discretized equations for each mesh. To solve these large numbers of algebraic equations, special algorithms need to be applied. The core of the solution is to solve the momentum equation.

Solution algorithms include the full coupling method and the pressure–velocity linkage method. The full coupling method solves the system of all the algebraic equations. The problem is that the system is highly nonlinear. Therefore, the full coupling method is much less efficient compared to the pressure–velocity coupling method. Most commercial CFD software only adopts the pressure–velocity linkage method.

The pressure–velocity linkage method could be divided into two sets, the pressure-based methods and the density-based methods. The pressure-based methods are more often used in incompressible flows while the density-based methods in compressible flows. The pressure-based methods can be classified into: the SIMPLE-based algorithms and the Poisson algorithms. The SIMPLE-based algorithms include SIMPLE, SIMPLER, SIMPLEC, and PISO. They calculate the pressure on the staggered grid arrangement following a guess-and-correct procedure. The SIMPLER algorithm is more efficient at correcting the pressure than the SIMPLE algorithm and thus regarded as the standard algorithm in many CFD codes. The Poisson algorithms consist of, for example,the Marker-And-Cell (MAC) method [10], the simplified MAC method SMAC [11], and ALE [12]. These direct-solve the Poisson equation for the pressure and show high efficiency. However, the SIMPLE-based methods are more widely used in the general CFD codes.

17.3 Sub-Models Related to Tunnel Fires

17.3.1 Gas Phase Combustion

The gas-phase combustion theoretically, always takes a discrete amount of time. However, compared to the flow time the reaction time can generally be ignored. The Damköhler number is used to characterize these two times [13, 14]:

$$D_a = \frac{t_{turbulent}}{t_{combustion}} \tag{17.52}$$

We may classify the gas phase combustion models in two ways, that is: the *generalized finite rate combustion* and *infinite rate conserved scalar combustion*.

The generalized finite rate combustion model requires accurate modeling of the diffusion of fuel and oxygen, which accordingly requires very fine meshes and small time steps. The generalized finite rate combustion model includes the laminar finite rate chemistry model, the eddy breakup and dissipation model, etc. [7, 15]. The finite rate chemistry model uses the Arrhenius kinetic expression for the reaction rate. The eddy breakup and dissipation models assume that the local strain rate of turbulence dominates the reaction rate in turbulent flames. The eddy breakup reaction rate is taken to be simply based on the species concentration fluctuations and the rate of eddy breakup.

The conserved scalar combustion models have no chemical source terms in the scalar equations due to the introduction of a mixture fraction. Such models includes: the infinite rate mixture fraction model, the laminar flamelet model, the probability density function model, etc. The infinite rate mixture fraction model assumes that the reaction of fuel and oxygen completes immediately after mixing. The laminar flamelet model considers a flame as an ensemble of laminar flamelets. The probability density function model applies the probability function to account for the interaction between the turbulence and the combustion.

For CFD modeling of a tunnel fire, the computation domain is very large compared to the dimensions of the fire source. A finite rate combustion model requires very fine grid sizes and small time steps for modeling of the fire domain, which suggests that modeling of a flame using the finite rate method and modeling of smoke movement in a tunnel are at different scales and the finite rate combustion models are not particularly suitable for use in engineering applications at present. Instead, the infinite rate mixture fraction model is more practical and has already been widely used in modeling of tunnel fires. The mixture fraction model used in FDS [1] is briefly described below.

The chemistry equation is assumed to be:

$$v_F \text{ Fuel} + vo\,\text{O}_2 \rightarrow \sum_i v_{P,i} \text{ Products} \tag{17.53}$$

Thus

$$\frac{\dot{m}_F'''}{v_F M_F} = \frac{\dot{m}_O'''}{v_O M_O} \tag{17.54}$$

The mixture fraction, Z, is defined as:

$$Z = \frac{sY_F - (Y_O - Y_O^\infty)}{sY_F^I + Y_O^\infty} \tag{17.55}$$

where

$$s = \frac{v_O M_O}{v_F M_F}$$

Mass conservation:

$$\rho \frac{DZ}{Dt} = \nabla \cdot \rho D \nabla Z \tag{17.56}$$

Define the flame surface as:

$$Z(x,t) = Z_f = \frac{Y_O^\infty}{sY_F^I + Y_O^\infty} \tag{17.57}$$

The conditions for the flame surface:

$$Y_O(Z) = \begin{cases} Y_O^\infty (1 - Z / Z_f) & Z < Z_f \\ 0 & Z > Z_f \end{cases} \tag{17.58}$$

In the above equations, v_F, v_O, and v_p are the stoichiometric coefficient for the fuel, oxygen, and combustion products, $\dot{m}'''$ is a mass source term (kg/(m^3 s)), M is the molecular weight (kg/kmol), Y is the fuel mass fraction in the volume, Z is the mixture fraction. Subscript F is the fuel, f is the flame, O is the oxygen, and P is the combustion product. Superscript ∞ indicates ambient condition and I indicates inlet.

The mixture fraction model has proven to be simple and robust, and coarse meshes are allowed, however, the flammability conditions are difficult to determine in the coarse meshes.

17.3.2 Condensed Phase Pyrolysis

In most engineering applications, we simply simulate a tunnel fire using a gas burner producing a fixed heat release rate (HRR) or a HRR curve. Therefore, only gas combustion is simulated.

In some cases, modeling of a pool fire or a solid fire may also be of some interest. For example, to investigate the performance of a fire suppression system using CFD, a pool fire or a more realistic solid fire generally needs to be modeled. Unfortunately, the present capability of CFD tools seldom succeeds in these tasks due to lack of understanding of mechanisms of these condensed phase pyrolysis. Here, only a short description of the pyrolysis models is presented for information only.

17.3.2.1 Solid Phase

The pyrolysis rate of a solid fuel is mainly related to the fuel temperature and mass concentration and could be correlated with the Arrhenius expression [16, 17] for a small volume inside the fuel:

$$\frac{dY_f}{dt} = -A_{pef} Y_f \exp(-\frac{E_A}{RT_f}) \tag{17.59}$$

where Y_f is the fuel mass fraction, T_f is the fuel temperature (K), A_{pef} is the preexponential factor (pef), and E_A is the activation energy (kJ/kmol). Both the activation energy and the preexponential factor are generally considered as constant for a specific fuel, and could be obtained from small-scale tests.

Heat conduction inside the fuel needs to be appropriately modeled. The heat is absorbed by the fuel surfaces and conducted into the fuel to support the pyrolysis. The fuel vapor evaporates, penetrates to the surface, mixes with oxygen and burns in the air. Note that for thermoplastic materials the mechanism of heat transfer into the fuels is slightly different.

17.3.2.2 Liquid Phase

The volume fraction of the vapor right above the surface of a liquid pool or a liquid droplet can be estimated according to the Clausius–Clapeyron relation as follows [18]:

$$X_f = \exp\left[-\frac{L_v M_f}{R}(\frac{1}{T_s} - \frac{1}{T_b})\right] \tag{17.60}$$

where T_s is the liquid surface temperature (K), T_b is the boiling temperature (K), L_v is the heat of vaporization (kJ/kg) and X_f is the volume fraction of fuel vapour. The produced fuel vapour leaves the fuel surface, mixes with air and burns. By comparing the difference between the estimated fuel vapour concentration, according to the Clausius–Clapeyron relation and the actual volume fraction of fuel vapor above the fuel surface the mass burning rate could be estimated. It can be expected from the above equation that the fuel evaporation rate is very sensitive to the surface temperature. The movement of liquid fuels is at a much smaller scale and difficult to model.

17.3.3 Fire Suppression

Recently, the interest in using water-based fire suppression systems in tunnels has increased significantly. For modeling of fire suppression in tunnels, generally a solid fire is required to be modeled. However, as discussed previously, the current CFD

technique cannot model the condensed phase pyrolysis well. Similarly, fire suppression in tunnels cannot be modeled well. Nonetheless, the basic theory related to water-based fire suppression is illustrated here and can be useful on occasion.

The water droplets are discharged into the tunnel, exchanges momentum and heat with the hot gases in the air, and on the fuel surfaces. All these processes need to be modeled. At a very short distance after the water is discharged from a nozzle, it is transformed into a large number of small droplets with different sizes. The cumulative volume distribution of the water droplets can be expressed as: [28]

$$F_v(d) = \begin{cases} \dfrac{1}{\sqrt{2\pi}} \displaystyle\int_0^D \frac{1}{\sigma d'} \exp\left(-\frac{[\ln(d'/d_m)]^2}{2\sigma^2}\right) dd', & d \le d_m \\ 1 - \exp[-0.693(\dfrac{d}{d_m})^{\gamma}], & d > d_m \end{cases} \tag{17.61}$$

where d is the water droplet diameter (m), d_m is the median volumetric droplet diameter corresponding to half the mass (m), γ and σ are the empirical constants equal to approximately 2.4 and 0.6, respectively. The median water droplet diameter depends on the characteristics of the nozzle, see Sect. 18.6.4.

Note that a water spray consists of millions of droplets with different sizes. In CFD modeling, only a limited number of water droplets with different sizes can be modeled to represent the characteristics of all the water droplets discharged from one nozzle. This simplification can cause some errors especially when only a very small amount of droplets are modeled. The water droplets discharged into the tunnel exchange mass, momentum, and energy with the hot gases. The controlling equations for the water droplets are described in Sect. 18.6.1.

For fire suppression modeling, the extinction criteria adopted play the key role. The theory of fire suppression has been described in detail in Chap. 16. There are two extinction mechanisms: gas phase extinction and condensed phase extinction. For gas phase extinction, Eq. (16.12) can be applied. In FDS, the same model is used but the effect of water is neglected. Another choice is to use the model proposed by Willians [13] although its use relies on accurate modeling of the finite rate gas phase combustion. The interaction between the water droplets and fuel surfaces is the key mechanism of fire suppression in tunnels. However, the models available for the condensed phase extinction are too empirical. For example, FDS adopts the simple model for fire suppression proposed by Yu et al. [19]. The local HRR per unit area, $\dot{q}''(t)$, is expressed in the form [1]:

$$\dot{q}''(t) = \dot{q}_0''(t)\, \mathrm{e}^{-\int k(t)dt} \tag{17.62}$$

where the coefficient *k(t)* is expressed as:

$$k(t) = a\dot{m}_w''(t)$$

In the above equation, $\dot{q}_0''(t)$ is the HRR per unit area when no water is applied (kW/m^2), $\dot{m}_w''$ is the water density (mm/min), and a is an empirical coefficient that is dependent on the material properties of the solid fuel and its geometrical configuration.

17.3.4 Wall Function

The tunnel wall results in the main pressure loss in normal ventilation, which is also the key source for the pressure loss in fire ventilation. It is also a key boundary for the tunnel flows, which makes the tunnel fires differ from the other enclosure fires. Note that the shear stress and heat transfer at the boundary layer could be solved reasonably well only using very fine grids. In most cases, sub-models are used for modeling of the near-wall region.

A dimensionless wall-normal distance, y^+, is defined first:

$$y^+ = \frac{\rho u^* y}{\mu} \tag{17.63}$$

where $u^* = \sqrt{\tau_w / \rho}$ (m/s) is the friction velocity, y is the wall-normal distance (m) and τ_w is wall stress (N/m^2). As discussed in Chap. 10, the boundary layer consists of three sublayers, that is, the viscous sublayer, the buffer layer and the log layer. The buffer layer lies between the viscous layer and log layer, however, it is generally incorporated into the other two layers in the wall function. At the viscous sublayer, that is, $y^+ < 11.63$, the viscous force dominates and the velocity can be obtained [20]:

$$\frac{u}{u^*} = y^+ \tag{17.64}$$

At the log layer, that is, $11.63 < y^+ < 500$, the velocity can be expressed as:

$$\frac{u}{u^*} = 2.4 \ln(9.8 y^+) \tag{17.65}$$

The shearing stress at the wall can be obtained from estimation of the parameter, u/u^*. For rough tunnel walls, the roughness can easily disrupt the viscous sublayer, and thus its effect needs to be accounted for. In such cases, the coefficient of 9.8 is usually reduced and an appropriate value needs to be set for it. More information can be found in the references [21, 22].

17.3.5 Heat Transfer

17.3.5.1 Convective Heat Transfer

According to the Reynolds' analogy, similar treatment can be made for the heat transfer to the wall. Launder and Spalding [23] found that the convective heat flux at the wall exposed to air flow at high Reynolds number, $\dot{q}_c''$ (kW/m^2), can be correlated with the local parameters as follows:

$$\frac{(T_p - T_w)\rho c_p \sqrt{\tau_w / \rho}}{\dot{q}_c''} = \mathrm{Pr}_t \left[\frac{u}{u^*} + P\left(\frac{\mathrm{Pr}}{\mathrm{Pr}_t}\right) \right] \tag{17.66}$$

where T_p is the temperature at near wall point p (K), T_w is the wall temperature (K), Pr is the Prandtl number and Pr_t is the turbulent Prandtl number (0.85 for most non-metallic fluids [24]). The function P is called "pee-function", a correction function dependent on the ratio of the two Prandtl numbers. In reality, the above equation is another form of the Reynold analogy. Similar models can be found in the literature, for example, reference [25].

Another method could be to use the convective heat transfer coefficient equations directly, regardless of near-wall parameters, for example, the model used in FDS [1]. This simplified method could result in large error in modeling of a large tunnel fire, as pointed out by Li et al. [4].

17.3.5.2 Radiation Heat Transfer

The radiation transport equation (RTE) could be written in the following form:

$$\begin{aligned} \mathbf{s} \cdot \nabla I_\lambda(\mathbf{r}, \mathbf{s}) = & -\left[\kappa(\mathbf{r}, \lambda) + \sigma_s(\mathrm{r}, \lambda)\right] I_\lambda(\mathbf{r}, \mathbf{s}) + \kappa(\mathbf{r}, \lambda) I_b(\mathbf{r}, \lambda) \\ & + \frac{\sigma_s(\mathbf{r}, \lambda)}{4\pi} \int_{4\pi} \psi(\mathbf{s}, \mathbf{s}') I_\lambda(\mathbf{r}, \mathbf{s}') d\Omega \end{aligned} \tag{17.67}$$

where I is the radiation intensity radiation intensity (kW/(m^2·steradian)), $\mathbf{r}$ is a positionvector (m), $\mathbf{s}$ is a direction vector (m), s' is the scattering direction vector (m), κ is an absorption coefficient (1/m), σ_s is the scattering coefficient (1/m), Ψ is the probability that incident radiation in the direction s will be scattered into the increment of solid angle $d\Omega$ Subscript λ indicates wavelength, b indicates blackbody.

Generally we may ignore the scattering effect and assume the smoke is gray gas. The absorption coefficient of the gas needs to be estimated based on the local mass fraction of the smoke and combustion products, see Chap. 10. Note that a tunnel fire generally produces a large amount of smoke particles which dominates the total absorption coefficient rather than CO_2 and H_2O. Further, note that the soot absorbs

heat continuously, independent of the wavelengths. Therefore, generally it could be quite reasonable to simplify the description to one band model and the assumption of gray gas is quite reasonable in most cases.

At the wall surface, the incident heat flux can be expressed as:

$$\dot{q}''_{w,in}(x) = \int_{2\pi} I(x,s)ds = \int_{\phi=0}^{2\pi}\int_{\theta=0}^{\pi/2} I_{w,in}(\theta,\phi)\cos\theta\sin\theta d\theta d\phi \tag{17.68}$$

and the total outgoing heat flux can be expressed as:

$$\dot{q}''_{w,out}(x) = \varepsilon_w \sigma T_w^4 + (1-\varepsilon_w)\dot{q}''_{w,in}(x) \tag{17.69}$$

where θ is the angle between the incident radiation and the normal line of the wall (radian), φ is the angle between the projection incident radiation line on the surface and a reference line (radian), and ε_w is the wall emissivity.

Different radiation models may be used, primarily including: the P-1 radiation model, the Discrete Ordinates Model, the Finite Volume Method model, the Discrete Transfer Radiative Model, and the Monte Carlo model with the computation cost increasing gradually.

The P-1 radiation model uses the first-order spherical harmonic approximation. It is accurate for optically thick or dense cases, however, not accurate for optically thin cases where the high order differential approximation is required to improve the accuracy.

The discrete ordinates model discretizes the entire solid angle using a finite number of ordinate directions with weight factors. The discretized equation can be obtained by integrating over a control volume, and the edge fluxes of the control volume can be correlated with the fluxes at the volume center by the spatially weighted approximation.

The finite volume method model is quite similar to the discrete ordinates model. The discretized equation is obtained by integrating the differential equation over the control volume and solid angle. By applying the Gauss' divergence theorem, the intensity derivative term is transformed to a surface integral over all surfaces of the volume. The idea of the upwind scheme can be used in solution that the marching direction depends on the main propagation direction of the radiation intensity.

The Discrete Transfer Radiative Model is principally based on the concept of solving radiation rays in an enclosure. The radiation rays are solved along the paths between the walls. The wall surfaces can be divided into many elements. For each surface element, the solid angle is preliminarily divided into a finite number of angles and the outgoing intensity is assumed to be constant within any given angle. The governing equation, having a form similar to Beer's law, is used to obtain the outgoing intensity immediately.

The Monte Carlo model is essentially a statistical method and it attains its name from many different statistical approaches. The model simulates a finite number of photon histories by use of a random number generator to randomly determine the

emission location and direction to produce probabilistic distributions for the traveling distance.

In summary, the P-1 model is the basic model that can produce accurate results for optically dense cases, however, for both dense and thin cases the other models may need to be used. The discrete ordinates method and the finite volume method are quite similar to each other and with the same order of accuracy. The discrete transfer radiative and the Monte Carlo methods are more time consuming but could have higher accuracy. For applications in tunnel fire safety, the discrete ordinates and the finite volume method are recommended to reduce the computation cost.

17.3.5.3 Heat Conduction

The general three-dimensional heat conduction equation for an anisotropic medium without an internal energy source can be expressed as:

$$\rho_s c_s \frac{\partial T_s}{\partial t} = \frac{\partial}{\partial x_i}(k_{ij} \frac{\partial T_s}{\partial x_j}) \; i, j = 1, 2, 3 \tag{17.70}$$

where k is the thermal conductivity (kW/(m K)) and T_s is the temperature inside a solid (K). Subscript s indicates solid, i and j correspond to different axis, for example, x axis (1), y axis (2) or z axis (3). Note that for an anisotropic medium, such as wood, the conductivity varies with the direction.

Generally the medium is isotropic, such as the tunnel walls. Therefore, the above equation can be simplified into:

$$\rho_s c_s \frac{\partial T_s}{\partial t} = k_s (\frac{\partial^2 T_s}{\partial x^2} + \frac{\partial^2 T_s}{\partial y^2} + \frac{\partial^2 T_s}{\partial z^2}) \tag{17.71}$$

with boundary condition at the wall, for example, x = 0:

$$-k_{s,x} \frac{\partial T_s}{\partial x}\Big|_{x=0} = \dot{q}''_{w,net} \tag{17.72}$$

The net heat flux at the wall accounts for both radiation and convective heat transfer. In most cases, the equation can be simplified into a one-dimensional problem with sufficient accuracy. For example, the tunnel wall can be assumed to be an infinite plate. This governing equation is an energy diffusion equation which can be easily solved.

17.4 Recommendations for CFD Users

17.4.1 Computation Domain and Boundary Conditions

A tunnel is usually a very long space. Tunnel height and width are very small in relation to the tunnel length. Simulation of the whole tunnel may be impossible but is also not necessary in practice. While doing CFD simulations, an appropriate computation domain needs to be determined together with appropriate boundary conditions.

The computational domain should consist of the fire section and a certain length of tunnel section where the boundary conditions can be appropriately set without inducing large errors.

For a tunnel where longitudinal ventilation is used to prevent backlayering, a limited length including the fire section is enough. A velocity or volume flow rate or mass flow rate boundary can be used at the upstream tunnel inlet, and pressure or mass flow boundary can be used for the downstream tunnel outlet. It is best if the upstream section is long enough to simulate the whole backlayering. In this scenario, the reason why the downstream outlet can be considered as a pressure boundary is that at a certain distance downstream of the fire, the vertical pressure gradient is small and close to a fixed pressure plane, that is, the smoke is not well stratified. By setting the outlet as a pressure boundary, small errors will be induced for the field close to the exit. Therefore, the simulation results in this region are not credible, which should be considered in determination of computation domain. From this point of view, the mass flow rate is a better boundary condition for the outlet of the domain, although, convergence problems could emerge due to the accumulation of computation errors.

For a metro station or a rescue station in a long tunnel, the ventilation system may have many vents and thus many boundary conditions need to be determined. Further, the cross section is much larger than a single tunnel which suggests that a shorter length has to be used while choosing the computation domain. In this scenario, the boundary conditions of the computation domain have to be considered appropriately. Note that the ventilation system works as a system, and it is generally unreasonable to set the boundaries as ambient. The general solution is to obtain the time dependent boundary conditions by simulating the fire ventilation system using a one-dimensional simulation. For a vent where only fresh air goes in or out, velocity, volume or mass flow rate can be used. For each vent where hot gases may flow into, a volume flow rate boundary should normally be used rather than mass flow rate, for example, a fan vent could be simulated using a volume flow rate boundary or a fan curve. Another solution could be to use pressure boundaries if appropriate pressure values can be estimated based on a one dimensional simulation.

17.4.2 Fire Source

Modeling of fire development in vehicles is a difficult task which should be avoided in any case where it is not necessary. Generally for an engineering application, a typical or worst scenario is firstly determined and then the design fire is proposed

for the specific scenario. The design fire proposed is used as input to the CFD modeling of tunnel fires. There are different methods developed for modeling fires, for example, combustion models and volumetric heat source method. The volumetric heat source method only simulates the heat output and ignores the combustion process and combustion products. Therefore, radiation and convection heat transfer which is of greatest importance in large tunnel fires cannot be reasonably modeled. In the following, only the combustion models are of interest and discussed.

The chemical formula for the fuel generally needs to be determined. A fire could involve different types of fuels. In these cases, the combined chemical formula for the fuels can be obtained by accounting for the fraction of each fuel type. In the gas phase combustion, one step reaction is mostly assumed although the combustion occurs through a large number of reactions.

Some key parameters for the fuel also need to be known, that is, heat of combustion, soot yield, carbon monoxide yield. Heat of combustion, that is, the amount of heat produced per kg of the fuel, affects the production of combustion products. The soot yield, that is, the amount of soot produced per kg of the fuel, is required for modeling of radiation and visibility. Similar to the soot yield, the CO yield represents the amount of CO produced per kg of the fuel and is required for estimation of tenability. For CFD modeling related to toxicity, the toxic gas production also needs to be accounted for in the fire source in a similar way. The heat of combustion and the yields of soot, CO, and toxic gases can be obtained from small-scale laboratory tests of similar combustion conditions. Note that the yields of soot and combustion products depend on the combustion conditions, and they could be much higher in underventilated enclosures at the stage of fully developed fires. More information on combustion products in under-ventilated fires can be found in Chap. 7. Generally the fire in a tunnel is well ventilated and data obtained from lab tests could be directly used as input.

17.4.3 Grid Size

Grid cell size is a key issue related to both computation time cost and accuracy. For fire modeling, the fire region attracts our special attention. Note that the flame properties are directly related to the fire characteristic diameter, which can be expressed as follows [26]:

$$\left[D^* = \left(\frac{\dot{Q}}{\rho_o c_p T_o \sqrt{g}} \right)^{2/5} \right] \tag{17.73}$$

where $\dot{Q}$ is HRR (kW) and D^* is the fire characteristic diameter (m). Note that the characteristic diameter D^* is directly related to the HRR. Li et al.'s work concluded that a cell size of $0.075D^*$ is a reasonable value for simulation of tunnel fires [27].

Note that a smaller fire corresponds to a smaller cell size based on the above analysis. In a model-scale fire, the grid size is much smaller than that in full scale. For a tunnel with a height of H, Eq. (1) can be transformed into:

$$\frac{D^*}{H} = \left(\frac{\dot{Q}}{\rho_0 c_p T_o g^{1/2} H^{5/2}}\right)^{2/5} = Q^{*2/5} \tag{17.74}$$

where H is the tunnel height, regarded as the characteristic length here.

This means that at the same dimensionless HRR (Q^*), the fire characteristic diameter is directly related to the tunnel height, that is, the reasonable mesh size is proportional to the tunnel height. This means that the ratio of reasonable mesh sizes between model- and full-scale equals the scale ratio. In other words, the mesh numbers required for model- and full-scale is about the same. Note that this conclusion is deduced based on a similar flow mode and the same dimensionless HRR.

Another requirement for cell size results from wall stress and related heat transfer. For laminar flows, the first grid cell near wall needs to fall into the viscous layer, that is, y^+ is less than 1 or slightly higher but not higher than 11.63. For turbulent flows, the first grid cell requires to fall into the log layer, that is, $11.63 < y^+ < 500$. This generally affects not only the flow field but also the temperature field near the wall.

17.4.4 Verification of Modeling

Due to the complexity of CFD modeling itself and the variety of application fields, verification of modeling is a necessity, especially for modeling with any new application. Either data from full-scale tests or model-scale tests related to the same phenomenon can be used for verification, based on which the general uncertainty of CFD modeling can be obtained for the specific scenario.

17.5 Limitations of CFD Modeling

The current state-of-the-art of CFD modeling technique has many limitations.

The key limitation for fire modeling is the inability to fully model pyrolysis. Firstly, the fuels normally have complicated geometry and the thickness could be incompatible with the grid size, which suggests that the fuel and the fluid field are at different scales. Secondly, the pyrolysis is such a complicated phenomenon that the present models seldom succeed in pyrolysis modeling even for a simple sample test. The state-of-the-art pyrolysis models lack credibility and should only be used for research purpose at present.

Modeling of combustion requires very fine meshes in order to simulate a large number of flamelets. However, to reduce the computation cost, quite coarse grids

and infinite rate mixture fraction combustion model are normally used. Further, the flammability limit is not well established for the coarse girds. The approximate combustion model cannot model the combustion products.

The limitation of pyrolysis modeling directly results in the limitation for modeling of fire suppression, given that surface cooling is the key mechanism of suppression of tunnel fires in most cases. Another reason for the limitation in modeling of fire suppression is also that the extinction criteria or the flammability limit under fire suppression are not well established.

Radiation is one key mechanism of heat transfer especially in the vicinity of a large tunnel fire. However, the accuracy of modeling of flame radiation strongly depends on the accuracy of modeling of flames. Modeling of radiation from smoke depends on the yields of soot and other combustion products which are obtained either from lab tests or estimation of the typical fuel.

Convection heat transfer is in reality the heat conduction between a surface and its neighboring gas. The direct solution of convection heat transfer is only possible using DNS with very fine grids. For RANS and LES, the process of convection heat transfer has to be modeled by semi-empirical equations which could result in large errors in some cases. Especially for modeling of tunnel fires, the walls could be very rough and its effect on heat transfer may be overlooked, for example, in FDS [1].

CFD modeling strongly depends on the performance of computer hardware which is clearly a bottleneck. Recently, parallel processing is widely used in CFD modeling as a novel technology to reduce the computation time. However, this reduces the accuracy of CFD modeling, and could easily cause stability problems. Therefore, caution should be exercised in its application.

These limitations need to be kept in mind, together with the uncertainty obtained from verification of modeling in the specific application field.

17.6 Summary

CFD modeling is a powerful tool to be used in engineering applications. The CFD users are required to not only efficiently use CFD tools, but also to understand the embedded mechanisms and limitations of the CFD modeling used. At present, CFD modeling is mainly used to simulate smoke movement arising from a design fire in order to investigate the performance of a ventilation system on smoke control in a tunnel fire, and to simulate the fire environment to obtain the available evacuation time. It should be kept in mind that modeling of pyrolysis of fuels and fire suppression is still a difficult challenge at present.

Although, there have been many general CFD tools available, CFD tools specifically developed for use in fire modeling are recommended to be used in tunnel fire safety design. Due to the complexity of CFD modeling itself and the variety of application fields, validation of modeling is always required. The computation domain needs to be chosen appropriately together with the boundary conditions and the cell sizes.

References

1. McGrattan K, Hostikka S, Floyd J, Baum HR, Rehm R, Mell W, McDermott R (2008) Fire Dynamics Simulator (Version 5), Technical Reference Guide: Volume 1: Mathematical Model. National Institute of Standards and Technology, Gaithersburg, Maryland, USA
2. Wang Y, Chatterjee P, de Ris JL (2011) Large eddy simulation of fire plumes. Proceedings of the Combustion Institute 33 (2):2473–2480
3. Cheong MK, Spearpoint MJ, Fleischmann CM (2009) Calibrating an FDS Simulation of Goods-vehicle Fire Growth in a Tunnel Using the Runehamar Experiment. Journal of Fire Protection Engineering 19 (3):177–196
4. Li Y.Z., Ingason H., Lönnermark A. Numerical simulation of Runehamar tunnel fire tests. In: 6th International Conference on Tunnel safety and Ventilation, Graz, Austria, 2012. pp 203–210
5. Ingason H, Lönnermark A (2005) Heat Release Rates from Heavy Goods Vehicle Trailers in Tunnels. Fire Safety Journal 40:646–668
6. Ingason H, Lönnermark A, Li YZ (2011) Runehamar Tunnel Fire Tests. SP Technicial Research Institute, SP Report 2011:55, Borås, Sweden
7. Yeoh GH, Yuen KK (2009) Computational Fluid Dynamics in Fire Engineering - Theory, Modelling and Practice. Elsevier, Burlington, USA
8. Roe PL (1986) Characteristic-Based Schemes for the Euler Equations. Annual Review of Fluid Mechanics 18:337–365
9. Leonard BP (1979) A stable and accurate convective modelling procedure based on quadratic upstream interpolation. Computer Methods in Applied Mechanics and Engineering 19:59–98
10. Harlow FH, Welch JE (1965) Numerical Calculation of Time-Dependent Viscous Incompressible Flow of Fluid with Free Surface. Phys Fluids 8:2182–2189
11. Amsden AA, Harlow FH (1970) The SMAC Method: A Numerical Technique for Calculating Incompressible Fluid Flows. Report LA-4370. Las Alamos Scientific Laboratory, Los Alamos, New Mexico
12. Hirt CW, Amsden AA, Cook JL (1997) An arbitrary lagrangian-eulerian computing method for all flow speeds. Journal of Computational Physics 135:203–216
13. Williams F.A. (1974) A unified view of fire suppression. Journal of Fire and Flammability 5:54–63
14. Williams F.A. (1974) Chemical kinetics of pyrolysis. In: Blackshear P.L. (ed) Heat Transfer in Fires. John Wiley & Sons, New York, pp 197–237
15. Novozhilov V (2001) Computational fluid dynamics modeling of compartment fires. Progress in Energy and Combustion Science 27:611–666
16. Atreya A (1983) Pyrolysis, ignition and fire spread on horizontal surfaces of wood. PhD thesis. Harvard University
17. Drysdale D (1999) An Introduction to Fire Dynamics. 2nd Edition edn. John Wiley & Sons, England
18. Prasad K., Li C., Kailasanath K., Ndubizu C., Ananth R., Tatem P.A. (1999) Numerical modelling of methanol liquid pool fires. Combustion Theory and Modelling 3:743–768
19. Yu H-Z, Lee JL, Kung H-C Suppression of Rack-Storage Fires by Water. In: Fire Safety Science – Proceedings of the fourth International Symposium, 1994. pp 901–912
20. Versteeg HK, Malalasekera W (1995) An Introduction to Computational Fluid Dynamics. Longman, England
21. Schlichting H (1979) Boundary-layer theory. 7th edn. McGraw-Hill, New York
22. Stephen BP (2000) Turbulent Flows. Cambridge University Press
23. Launder BE, B. SD (1974) The Numerical Computation of Turbulent Flows. Computer Methods in Applied Mechanics and Engineering 3:269–289
24. Lienhard IV JH, Lienhard V, John H. (2012) A heat transfer textbook , Phlogiston Press, Cambridge, Massachusetts

25. Kader BA (1981) Temperature and concentration profiles in fully turbulent boundary layers. International Journal of Heat and Mass Transfer 24:1541–1544
26. McGrattan K, Forney G (2004) Fire Dynamics Simulator (Version 4), User's Guide. National Institute of Standards and Technology, Gaithersburg, Maryland, USA
27. Li YZ, Lei B, Ingason H (2012) Scale modeling and numerical simulation of smoke control for rescue stations in long railway tunnels. Journal of Fire Protection Engineering 22 (2):101–131
28. Chan TS (1994) Measurements of water density and droplet size distributions of selected ESFR sprinklers. Journal of Fire Protection Engineering 6(2):79–87

Chapter 18
Scaling Technique

Abstract Physical scaling has been successfully applied throughout the development of fire safety science in the past several decades. It is a very powerful and cost-effective tool to obtain valuable information concerning, for example, fire characteristics, smoke movement, smoke control, fire development, and fire suppression. Typical scaling techniques that have been developed are summarized in this chapter to provide a theoretical benchmark and support for further development of more advanced scaling methods. Different scaling techniques are introduced although the focus is on the Froude scaling method which is the most common one used in fire safety science. Scaling of convective heat transfer, radiative heat transfer, and heat conduction is investigated as well as scaling of water sprays, response time of sprinklers, and combustible materials.

Keywords Scaling · Heat transfer · Water spray · Combustible material · Enclosure fire · Tunnel fire

18.1 Introduction

The physical scaling has been widely used in fire safety science community. Its application permeates nearly every aspect of fire research, from free plumes to fire suppression. Despite its introduction of simplification in various applications, the scaling technique has significantly improved our understanding of fire dynamics. Heskestad [1] reviewed scaling techniques, mainly pressure modeling and Froude modeling. These are the two main techniques that have been used. Quintiere [2] also reviewed the scaling applications in fire research with a focus on ceiling jets, burning rate, flame spread, and enclosure fires. Ingason [3] carried out numerous studies on fire development in rack-storage fires, both in large scale and model scale. The in-rack conditions were found to scale very well. Perricone et al. [4] investigated the thermal response of a steel tube covered by insulating materials using scaling principles. However, the scaling laws used for the thick insulating materials may not be accurate. Cross and Xin [5] examined the scaling of wood crib fires and found good agreement between different scales. Li and Hertzberg [6] conducted a scaling study of heat conduction and heat balance in a room fire. They carried out two series of

H. Ingason et al., *Tunnel Fire Dynamics,* DOI 10.1007/978-1-4939-2199-7_18

room fire tests in three different scales where the aim was to investigate the scaling of temperatures inside the walls. A good agreement between different scales was found.

Scaling of water-based fire suppression systems has also been conducted in open and enclosure fires. Heskestad [7, 8] carried out a series of gas and pool fire suppression tests to investigate the credibility of scaling the interaction of water sprays and flames, and obtained a simple correlation for extinguishment of gas and pool fires using water sprays. Quintiere et al.'s work [9] showed that the scaling of pool and gas fires worked well, although the results in rack-storage fires between model and full scale did not show a good correlation. Yu et al. [10–12] tested and investigated the scaling of suppression of gas fires and pool fires using water mist systems and obtained good agreement between model scale and full scale. In short, despite much work on scaling of water-based fire suppression systems, the phenomena in reality are not well understood.

In the field of tunnel fire safety, scaling techniques are widely used. The main reason promoting their applications is the high cost of full-scale tunnel tests. Note that even in model scales, the ratio of tunnel length to tunnel height should be great enough to scale a realistic tunnel fire. Fortunately the introduction of longitudinal flows allows us to slightly reduce the scaling ratio, compared to an enclosure fire. A large number of model scale tunnel fire tests have been carried out in the past two decades. Bettis et al. [13] carried out nine fire tests using scale models of vehicles in a model tunnel to mimic part of a train used to transport HGVs through the Channel tunnel. Oka and Atkinson [14] carried out a study of critical velocity in a model tunnel. Further, Wu and Bakar [15] carried out tests to investigate the influence of tunnel geometry on the critical velocity. Ingason and Li investigated the key parameters for large fires in model scale tunnels with longitudinal ventilation [16] and with point extraction ventilation [17]. Ingason [18] also carried out a series of 1:10 scale model railcar tunnel fire tests to investigate the effect of openings on the fire sizes. Vauquelin et al. [19] carried out a series of model scale experiments with a helium/nitrogen gas mixture in an isothermal test-rig to investigate the extraction capability and efficiency of a two-point extraction system. Li and Ingason [17] pointed out that the cold gas method used by Vauquelin et al. [19] results in experimental inaccuracy, and therefore is not recommended to use in tunnel fire tests. Li et al. [20–24] carried out several series of model scale tunnel fire tests to investigate the critical velocity [20], back-layering length [20], maximum ceiling gas temperature [21, 22], smoke control in cross-passages [23], and smoke control in rescue stations in long-railway tunnels [24]. Lönnermark et al. [25] carried out a 1:3 model-scale metro car fire tests in preparation for the full-scale fire tests in the Brunsberg tunnel [26].

Model-scale tunnel fire tests with water-based fire suppression have also been carried out. Ingason [27] tested the water spray system in tunnel fires using hollow cone nozzles and wood crib fires. Deluge system and water curtain system were tested. Li and Ingason [28, 29] investigated the automatic water spray system in tunnel fires using full cone nozzles and wood crib fires. Response times for individual sprinklers were modeled using a scaling theory.

18.2 Methods of Obtaining Scaling Correlations

There are two main approaches for obtaining scaling correlations: the controlling equation method, and the dimensional analysis. The controlling equation method introduces normalizing parameters and obtains nondimensional equations. The dimensionless groups are typically the coefficients of the differential terms. For the dimensional analysis method, all the key parameters relevant to the phenomenon need to be determined manually, and then the dimension of every identified parameter is changed to a combination of the basic physical dimensions. The dimensionless groups can thus be obtained by checking the dimensions of the identified physical parameters. The method could, for example, be a π theorem. There are some other methods that could be used. For example, some dimensionless groups could be directly obtained from some basic equations; but, this method is still the differential method.

In any case, the controlling equation method is the fundamental and typically best method, which will be used in the following. Nonetheless, good understanding of the phenomena is required to determine the key parameters that must be preserved.

18.3 Classification of Scaling Techniques

The scaling techniques applied in fire safety can be classified into three types: Froude scaling, pressure scaling, and analogy scaling.

18.3.1 Froude Scaling

Froude scaling indicates that the main preserved dimensionless group in the fire tests is the Froude number which characterizes the ratio of inertial force and buoyancy force. Note that all the smoke flows are driven by the buoyancy. This is the main reason why Froude scaling works by simply preserving the Froude number.

According to Froude scaling, the tests can be carried out in ambient environment. The Reynolds number is not preserved but the fluid mode should be kept the same to preserve the similarity in the fluid field. Further, many related dimensionless groups that are implicitly preserved, however, have been proved to be reasonably scaled.

18.3.2 Pressure Scaling

Pressure scaling can preserve both the Froude number and the Reynold number by adjusting the environmental pressure in the test bed. This also indicates the preservation of the Grashof number. Therefore, both the buoyancy force and the fluid

field can be scaled well. However, in reality the pressure scaling is very difficult to use since the pressure scales as 3/2 power of the length scale. This implies that the pressure needs to be adjusted to very high levels in model scale, for example, 32 atmospheres for a scaling ratio of 1:10, and 89 for a scaling ratio of 1:20. This limits its use in fire modeling. Further, the benefit of pressure scaling may be quite limited since in most cases the Reynold number is much less important compared to the Froude number.

18.3.3 Analog Scaling (Cold Gas, Saltwater)

The analog scaling method uses two fluids of different densities to model smoke movement in a fire scenario. These two fluids could be air and helium, or water and saturated salt water, and so on. This method simulates a fire using the density difference, rather than the temperature difference. To some extent, it is possible to obtain the required density using different mixing ratios. The analog scaling is in fact also a type of Froude scaling, although it is significantly different from traditional Froude scaling and is, therefore, classified as an independent method. The Froude number is also the main preserved dimensionless group. Further, turbulent flow conditions can be obtained much more easily due to the small viscosity for water.

However, this method has some defects. First, when using analog scaling, the fluid density must be determined based on a reference gas temperature in a specific fire, despite the fact that it is known that the gas temperature changes significantly with position in many fire scenarios. In other words, a realistic fire has no so-called generic or characteristic gas temperature or gas density. Despite this, the state-of-the-art is to use the estimated characteristic temperature in a given scenario and then to calculate the mass flow rate from the fire source based on conservation of the convective heat release rate (HRR). This method is only useful in a typical enclosure fire where the gas temperature can be estimated accurately. Second, the heat loss to the surroundings is ignored except in the vicinity of the fire source, that is, the heat loss is considered by using the convective HRR to build up the energy equation. Generally speaking, the energy dissipates only by mixing with the ambient fluid. However, it should be kept in mind that in a tunnel fire, the heat loss to the walls dominates the heat transfer process or the change of gas temperature along the tunnel. This suggests that the analog scaling method is not suitable for research into the temperature distribution along the tunnel. Third, the analog scaling method generally can only simulate small fires. The saturated salt water is around 1200 kg/m^3 under ambient conditions. Therefore, the maximum variance in density is around 20%. However, a gas temperature of 600 °C corresponds to a variance of 67% in density. That is to say, saltwater under ambient conditions can only simulate a fire with gas temperature of around 94 °C. Finally, extra gases or liquids with a certain momentum may be introduced into the fluid domain which could result in a large error.

18.4 General Froude Scaling

In this application, the controlling equation method is used to obtain the dimensionless groups. At first, we focus on scaling of the fluid field, and detailed scaling of heat transfer will be discussed in the following sections. For simplification, we only analyze the one-dimensional conservation equations of mass, momentum, and energy which can be written as follows:

Mass:

$$\frac{\partial \rho}{\partial t} + \frac{\partial (\rho u)}{\partial x} = \dot{m}''' \tag{18.1}$$

or in terms of individuals species (mass fraction Y):

$$\frac{\partial \rho Y_i}{\partial t} + \frac{\partial (\rho u Y_i)}{\partial x} = \frac{\partial}{\partial x}(\rho D_i \frac{\partial Y_i}{\partial x}) + \dot{m}_i''' \tag{18.2}$$

Momentum:

$$\frac{\partial (\rho u)}{\partial t} + \frac{\partial (\rho u u)}{\partial x} = \frac{\partial}{\partial x}(\frac{4}{3}\mu \frac{\partial u}{\partial x}) - \frac{\partial p}{\partial x} + (\rho_o - \rho) g_x \tag{18.3}$$

Energy:

$$\left[\frac{\partial (\rho c_p T)}{\partial t} + \frac{\partial (\rho u c_p T)}{\partial x} = \frac{\partial}{\partial x}(k \frac{\partial T}{\partial x}) + \dot{Q}''' - \dot{Q}'''_{loss} + \frac{4}{3}\mu (\frac{\partial u}{\partial x})^2 + \frac{\partial p}{\partial t} + u \frac{\partial p}{\partial x} \right] \tag{18.4}$$

State equation of gas:

$$p = \frac{\overline{R}}{M} \rho T \tag{18.5}$$

where ρ is the density (kg/m^3), t is the time (s), x is the axis (m), u are the velocity at x direction (m/s), D is the mass diffusivity (m^2/s), m is the mass (kg), Y is the species mass fraction (%), μ is the dynamic viscosity (kg/(m s)), p is the pressure (Pa), g is the gravitational acceleration (m/s^2), T is the gas temperature in Kelvin (K), k is the heat conductivity (kW/mK), c_p is the heat of capacity (specific heat at constant pressure, kJ/(kg K)), $\overline{R}$ is the universal gas constant (8.314 J/(mol K)), M is the molecular weight (kJ/kmol), and Q is the heat (kJ). Subscripts i is the ith species and *loss* indicates heat loss. Superscripts (·) indicates per unit time and ($'''$) per unit volume. Note that the pressure in the equations is the absolute pressure.

The characteristic length l (m), velocity u_o (m/s), time t_o (s), pressure p_r (Pa), ambient temperature T_o (K), and ambient density ρ_o (kg/m^3) are introduced as reference values to normalize the above equations giving:

Mass:

$$\pi_1 \frac{\partial \hat{\rho}}{\partial \hat{t}} + \frac{\partial(\hat{\rho}\hat{u})}{\partial \hat{x}} = \pi_2 \tag{18.6}$$

or in terms of individuals species (mass fraction Y_i):

$$\pi_1 \frac{\partial \hat{\rho} Y_i}{\partial \hat{t}} + \frac{\partial \hat{\rho}\hat{u} Y_i}{\partial \hat{x}} = \pi_3 \frac{\partial}{\partial \hat{x}}(\hat{\rho}\frac{\partial Y_i}{\partial \hat{x}}) + \pi_4 \tag{18.7}$$

Momentum:

$$\pi_1 \frac{\partial \hat{\rho}\hat{u}}{\partial \hat{t}} + \frac{\partial \hat{\rho}\hat{u}\hat{u}}{\partial \hat{x}} = \frac{4}{3}\pi_5 \frac{\partial^2 \hat{u}}{\partial \hat{x}^2} - \pi_6 \frac{\partial \hat{p}}{\partial \hat{x}} + \pi_7(1-\hat{\rho}) \tag{18.8}$$

Energy:

$$\pi_1 \frac{\partial \hat{\rho}\hat{T}}{\partial \hat{t}} + \frac{\partial \hat{\rho}\hat{u}\hat{T}}{\partial \hat{x}} = \pi_8 \frac{\partial^2 \hat{T}}{\partial \hat{x}^2} + \pi_9 - \pi_{10} + \pi_{11}\frac{4}{3}(\frac{\partial \hat{u}}{\partial \hat{x}})^2 + \pi_1\pi_{12}\frac{\partial \hat{p}}{\partial \hat{t}} + \pi_{12}\frac{\partial \hat{p}}{\partial \hat{x}} \tag{18.9}$$

In the above equations, the dimensionless variables, that is, the parameter divided by the corresponding reference value, are denoted by (^), for example, $\hat{\rho} = \rho / \rho_o$. Note that the convection terms are the primary terms that need to be preserved. Therefore, these are used as the basis while obtaining the dimensionless groups. Further, note that the pressure rise in a normal fire scenario is very small compared to the ambient pressure, and thus the state equation is always applicable and it needs no special attention.

The dimensionless groups obtained are listed below.

Mass:

$$\pi_1 = \frac{l}{u_o t_o}, \quad \pi_2 = \frac{\dot{m}''' l}{\rho_o u_o}, \quad \pi_3 = \frac{D_i}{u_o l}, \quad \pi_4 = \frac{\dot{m}_i''' l}{\rho_o u_o} \tag{18.10}$$

Momentum:

$$\pi_5 = \frac{\mu}{\rho_o u_o l}, \quad \pi_6 = \frac{p_r}{\rho_o {u_o}^2}, \quad \pi_7 = \frac{gl}{{u_o}^2} \tag{18.11}$$

Energy:

$$\begin{aligned} &\pi_8 = \frac{k}{\rho_o u_o c_p l}, \quad \pi_9 = \frac{\dot{Q}''' l}{\rho_o u_o c_p T_o}, \quad \pi_{10} = \frac{\dot{Q}'''_{loss} l}{\rho_o u_o c_p T_o}, \\ &\pi_{11} = \frac{\mu}{\rho_o c_p T_o l}, \quad \pi_{12} = \frac{p_r}{\rho_o c_p T_o} \end{aligned} \tag{18.12}$$

Note that:

$$\pi_7 = \frac{gl}{u_o^{\,2}} = \frac{1}{\mathrm{Fr}}, \qquad \frac{\pi_5}{\pi_3} = \mathrm{Sc}, \qquad \frac{\pi_5}{\pi_8} = \mathrm{Pr}, \qquad \pi_5 = \frac{1}{\mathrm{Re}} \tag{18.13}$$

where Re is the Reynolds number, Fr is the Froude number, Sc is the Schmidt number, and Pr is the Prandtl number. Now we check which terms could be preserved in the scaling. First we know for buoyancy driven flows, the Froude number, that is, π_7, has to be preserved. To preserve the transient characteristics of the key parameters, the time derivative term has to be preserved, that is, π_1. Therefore, we have:

$$u \propto t \propto l^{1/2} \tag{18.14}$$

This indicates that the velocity and time scales as 1/2 power of the length scale. In other words, if the geometrical scale ratio is L_M/L_F (model scale M and full scale F), the velocity and the time scale as $u_M/u_F = t_M/t_F = (L_M/L_F)^{1/2}$.

Further, the source terms, including mass source (π_2 and π_4) and heat source terms (π_9 and π_{10}), need to be preserved, especially the heat source terms. To preserve mass source terms, we have:

$$\dot{m} \propto \dot{m}_i \propto l^{5/2} \tag{18.15}$$

To preserve heat source terms, we have:

$$\dot{Q} \propto \dot{Q}_{loss} \propto l^{5/2} \tag{18.16}$$

By preserving the above terms, it can be concluded that the temperature should approximately be the same between different scales. Further, note that if different fuels are used, the mass and energy cannot be simultaneously scaled. The heat terms should always have higher priority in such cases.

Further we check each term in the three controlling equations. From the mass equation it can be known that the mass should be scaled very well. Even when the fuel mass is not scaled well, good agreement can still be found in different scales since the fuel mass is normally negligible in the smoke flow. For the species equation, the concentrations should be scaled well if the mass source is scaled correctly.

Note that by default the dynamic pressure is proportional to the second power of the velocity. In addition, from the momentum equation, it can be seen that the buoyancy forces have been scaled. Given that the viscous term is negligible compared to the buoyancy in most cases, the pressure term should be scaled as:

$$p_r \propto l \tag{18.17}$$

This indicates that the pressure rise is proportional to the length scale.

From the energy equation, it can be known that the heat source is scaled but not the diffusion terms and the pressure terms. However, this is much less important.

Further, note that the heat loss term could not be scaled very well, but the influence should be limited, especially close to the fire source since the majority of the heat is carried away by the convective flows. Therefore, the energy should be scaled well.

In short, all the key terms are scaled, including the time derivative terms. Therefore, the basic theory of Froude scaling works well.

By checking the theory for turbulent flows, we can have an interesting finding. Note that the viscous stress cannot be preserved for laminar flows as discussed above. However, for turbulence flows, we can easily find that all turbulent diffusion terms can be scaled well in both Reynolds-averaged Navier–Stokes (RANS) models and Large Eddy simulations (LES) models. This suggests that Froude scaling works better in turbulent flows. Therefore, in carrying out model scale tests we should try to have turbulent flows in mode scales.

Note that in enclosure fires or tunnel fires, heat transfer to the surrounding structures needs to be carefully considered which will be discussed in the following section.

18.5 Scaling of Heat Fluxes

Scaling of heat conduction, convective heat transfer, and radiative heat transfer are presented in the following. Finally, the scaling of heat balance in an enclosure is presented.

18.5.1 Scaling of Convective Heat Transfer

In an enclosure fire or a tunnel fire, the key pattern of the convective heat transfer is the forced heat transfer due to the movement of the hot gases in the upper layer and also the forced heat transfer in the lower layer due to the movement of fresh air through the openings. The main mechanism should, therefore, be forced convective heat transfer. The convective heat transfer to the walls, $\dot{Q}_{loss,c}$, can be expressed as:

$$\dot{Q}_{loss,c} = h_c A_w (T_g - T_w) \tag{18.18}$$

where h_c is the convective heat transfer coefficient (kW/(m^2 K)), A_w is the contact wall surface area (m^2), T_g is the gas temperature (K), and T_w is the wall temperature (K). This suggests that the convective heat flux should scale as 1/2 power of the length scale. In the following, we examine the actual scaling correlations for different flow modes on smooth and rough surfaces to check whether they follow this law.

For turbulent flows on smooth wall surfaces, the convective heat transfer coefficient h_c could be correlated with the Nusselt Number and the Prandtl number:

$$\mathrm{Nu} = \frac{h_c l}{k} = 0.037\,\mathrm{Re}^{4/5}\,\mathrm{Pr}^{1/3} \tag{18.19}$$

The above equations indicate that:

$$\dot{q}_c'' \propto h_c \propto l^{1/5} \tag{18.20}$$

For laminar flows on smooth surfaces, the convective heat transfer coefficient h_c can also be correlated with the Nusselt Number and the Prandtl number, which can be expressed as:

$$\mathrm{Nu} = \frac{h_c l}{k} = 0.66\,\mathrm{Re}^{1/2}\,\mathrm{Pr}^{1/3} \tag{18.21}$$

This means that:

$$\dot{q}_c'' \propto h_c \propto l^{-1/4} \tag{18.22}$$

For a heated wall at the lower layer in an enclosure fire, the convective heat transfer could be natural convection, and the Nusselt number could be expressed as:

$$\mathrm{Nu}_L = 0.678\,\mathrm{Ra}_L^{1/4}\left(\frac{\mathrm{Pr}}{\mathrm{Pr}+0.952}\right) \tag{18.23}$$

where the Rayleigh number, Ra_L, is defined as:

$$\mathrm{Ra}_L = \frac{g\beta\Delta T L^3}{\nu^2}\mathrm{Pr} \tag{18.24}$$

In the above equation, ν is the kinematic viscosity (m^2/s), β is the expansion coefficient (equivalent to $1/T$ for ideal gas in an isobaric process). From the above equation we also obtain the scaling coefficient of $-1/4$.

Note that some tunnel walls could be very rough, for example, rock tunnel walls. The expressions for the Nusselt number needs to be revised to account for the effect of wall roughness. Recall the Reynold-Colburn analogy:

$$St = \frac{h_c}{\rho c_p u} \approx \frac{1}{2} C_f \tag{18.25}$$

For turbulent flows on rough surfaces, the skin friction coefficient, C_f, mainly depends on the relative roughness, and approaches a constant at high Reynolds numbers for each relative roughness, ε/D. Therefore, if the relative roughness is kept as the same value in both scales and the flow mode is turbulent, the convective heat flux scales as:

$$h_c \propto u \propto l^{1/2} \tag{18.26}$$

This suggests that the convective heat flux can scale very well if the flow is turbulent and the relative roughness is kept as the same value in model scale. In reality, the requirement for the conservation of the relative roughness could be eased due to the fact that the friction coefficient is not so sensitive to the wall roughness. Generally for turbulent flows, the relative roughness for tunnel walls range from 0.1 to 1 %, corresponding to a skin friction coefficient, C_f, ranging from 0.08 to 0.16.

Based on the above analysis, it is known that the convective heat transfer can be scaled very well for turbulent flows in model tunnels with the same relative roughness. The convective heat transfer for laminar flows in model scales could be slightly overestimated.

18.5.2 Scaling of Radiative Heat Transfer

The scaling of radiative heat transfer on the wall surface, $\dot{q}''_{w,r}$ (kW/m^2), can be expressed as:

$$\dot{q}''_{w,r} = \varepsilon_w \int_{2\pi} I d\Omega - \varepsilon_w \sigma T_w^4 \tag{18.27}$$

where ε_w is emissivity of the wall surface, I is intensity of incident radiation (kW/(m^2 steradium)), Ω is solid angle, and σ is the Stefan-Boltzmann constant (5.67×10^{-11} kW/(m^2 K^4)).

Using the controlling equation method to normalize the above controlling equation, we can easily obtain the following scaling correlations:

$$\pi_{13} = \frac{\dot{q}''_{w,r}}{\varepsilon_w \sigma T_o^4}, \qquad \pi_{14} = \frac{I_o}{\sigma T_o^4} \tag{18.28}$$

Note that the dimensionless group π_{14} indicates the definition of radiation intensity. The other dimensionless group suggests the scaling of wall emissivity:

$$\varepsilon_w \propto l^{1/2} \tag{18.29}$$

Generally the emissivity of the walls is not scaled. This suggests that the radiation at the wall is normally overestimated in model scales, which tends to reduce the vertical temperature difference.

Now let us analyze the scaling of radiative heat transfer in a fluid element. The radiation transport equation (RTE) is:

$$\frac{dI}{dx} = -\kappa\left(I - \frac{\sigma T^4}{\pi}\right) \tag{18.30}$$

where κ is the absorption coefficient (1/m).

For a fluid element, the term in the energy equation related to heat loss by radiation can be written as:

$$\dot{Q}'''_{loss,r} = 4\kappa\sigma T^4 - \kappa\int_{4\pi} I d\Omega \tag{18.31}$$

where Ω is the solid angle (steradian). Using the controlling equation method we can easily obtain the following scaling correlations:

$$\pi_{15} = \kappa l, \qquad \pi_{16} = \frac{\dot{Q}'''_{loss,r}}{\kappa\sigma T_o^4} \tag{18.32}$$

These two dimensionless groups indicate:

$$\kappa \propto l^{-1}, \qquad \kappa \propto l^{-1/2} \tag{18.33}$$

In an enclosure fire or a tunnel fire, the soot normally dominates the absorption coefficient, and thus the absorption coefficient in different scales should be essentially the same, if the same fuels are used. Therefore the local absorption coefficient cannot be scaled well, and both the local absorbed heat and the outgoing radiation may be underestimated. Thus the overall effect is difficult to estimate.

However, note that this conclusion is drawn from the analysis of a fluid element. In fact, in enclosure fires, scaling of the global radiative heat transfer is more meaningful and of more practical use. From the global point of view, the radiative heat transfer from the flame and hot gases to the walls can be expressed in a similar way as the convective heat transfer, that is, as:

$$\dot{Q}_{loss,r} = h_r A_w (T_g - T_w) \tag{18.34}$$

For simplicity, the radiative heat transfer coefficient for the wall surfaces could be written as follows:

$$h_r = \varepsilon\sigma(T_g^2 + T_w^2)(T_g + T_w) \tag{18.35}$$

where the emissivity is:

$$\varepsilon = 1 - e^{-\kappa_m L_m}$$

In the above equations, h_r is the equivalent radiative heat transfer coefficient (kW/(m^2 K)), κ_m and L_m are the mean absorption coefficient (1/m) and mean beam length of the flame and smoke flow (m), respectively.

It is clear that the emissivity of the gas in model scale normally becomes smaller than in full scale, however, the emissivity strongly depends on the length scale and thus in reality is very difficult to estimate. Here we make a simple analysis of the optically thick and optically thin cases. In the optically thick case, the emissivity is close to unit. Therefore scaling of the global radiative heat flux is:

$$\dot{q}_r'' \propto l^0 \tag{18.36}$$

In the optically thin case, scaling of radiative heat flux could be:

$$\dot{q}_r'' \propto \kappa_m L_m \propto l^1 \tag{18.37}$$

Note that the radiative heat flux is the inverse of the radiative resistance R_r. At the beginning of an enclosure fire, the scenario is optically thin. However, after a period of time, the scenario could become optically thick. Therefore, the radiative heat flux could be scaled as l^a $(0<a<1)$. Note that the heat flux should scale as $l^{1/2}$. It could be expected that in the model scale, the radiative heat flux may be underestimated at the beginning of the fire and overestimated a short time after ignition. We can also try to ascertain the coefficient a in the optically thick case.

The absorption coefficient is mainly dependent on the soot yields and volumetric flow rate of the smoke. In other words, it depends on the fuel type, ventilation conditions, and specific geometry of the room and the burner. In model scales, if the fuels are the same as in full scale, it can be expected that the absorption coefficient is also the same as in full scale, given that the ventilation conditions and specific geometry are well scaled. Therefore, the scaling of radiative heat flux is mainly related to the mean beam length. In engineering applications, the global radiative heat flux could be calculated using a mean beam length, L_m, which could be estimated by:

$$L_m = 3.6\frac{V_b}{A_b} \tag{18.38}$$

where V_b is the volume of the hot gases (m^3) and A_b is its bounding area (m^2). The mean beam length in an enclosure fire is mainly related to the smoke depth. Therefore, it is a variable for different fire sizes. For large flames and sooty smoke, the emissivity always approaches one and the mean beam length has no influence on the radiation. However, for small fires, both the absorption coefficient and the smoke depth are small values, and thus the mean beam length could play an important role in the total emissivity.

We may choose different fuels in model scales to explicitly scale the radiative heat flux in enclosure fires. However, it should be kept in mind that the absorption coefficient is not only related to the fuel type and HRR, but also the length scale, the entrainment of the smoke flows, and the combustion conditions, for example, an under-ventilated fire produces much more soot. In realistic fires, the absorption coefficient could be a time-dependent variable during a fire. In any case, the scaling of radiation is difficult based on the above analysis. In reality, the fire scales the radiation itself as there is limited heat available to be lost by radiation. Therefore in a real fire, the temperature will decrease if the emissivity is too high in model scales. The radiation fraction in the total HRR in open fires and enclosure fires has been observed to be around 20–40 %. This mainly results from the self-adjustment of the heat radiation. Although the gas temperature could decrease in model scales,

the difference in gas temperature between different scales could still be insignificant since heat radiation is proportional to the fourth power of gas temperature. In short, the scaling of radiative heat transfer is still expected to be acceptable in model scales, as proved by Li and Hertzberg [6].

18.5.3 Scaling of Heat Conduction

18.5.3.1 Thermally Thick Materials

In most cases, heat conduction normal to a wall surface dominates heat conduction into the wall. Therefore, only the one-dimensional heat conduction equation for the material temperature is discussed here.

The wall materials can be classified into two categories: thermally thick materials and thermally thin materials. For a thermally thick material, there is always a temperature gradient inside the material, even after thermal penetration. This state is important when considering temperatures created by fires. For a thermally thin material, the temperatures inside the material are homogeneous. In fact, thermally thin materials are only special case of thermally thick materials. There is no clear distinction between these two types of "materials," but the definition will depend on the specific case that is investigated. Generally, metal objects and very thin materials and can be considered as thermally thin materials, and others are thermally thick materials.

For thermally thick materials, the controlling equation for heat conduction can be written as:

$$\rho_s c_s \frac{\partial T_s}{\partial t} = k_s \frac{\partial^2 T_s}{\partial z^2} \tag{18.39}$$

and the boundary condition at $z=0$ and $z=\delta_s$, can be expressed as:

$$k_s \frac{\partial T_s}{\partial z} = \dot{q}_c'' + \dot{q}_r'' \tag{18.40}$$

In the above equations, z is the depth below surface (m). Subscript s indicates solid, c and r are convective and radiative heat transfer, respectively.

In the following analysis, it is assumed that the convective and radiative heat fluxes at the surface scale as 1/2 power of the length scale.

By introducing the following normalizing parameters: reference time, t_o, reference temperature, T_o, and reference material thickness, δ_s, the above equations can be normalized:

$$\frac{\partial \hat{T}_s}{\partial \hat{t}} = \frac{k_s t_o}{\rho_s c_s \delta_s^2} \frac{\partial^2 \hat{T}_s}{\partial \hat{z}^2} \tag{18.41}$$

and

$$\frac{\partial \hat{T}_s}{\partial \hat{z}} = \frac{(\dot{q}_c'' + \dot{q}_r'')\delta_s}{k_s T_o} \tag{18.42}$$

yielding the dimensionless groups:

$$\pi_{17} = \frac{k_s t_o}{\rho_s c_s \delta_s^2} \tag{18.43}$$

and

$$\pi_{18} = \frac{(\dot{q}_c'' + \dot{q}_r'')\delta_s}{k_s T_o} \tag{18.44}$$

Note that as $\dot{q}_c'' \propto l^{1/2}$ and $\dot{q}_r'' \propto l^{1/2}$, the above two equations indicate that:

$$\frac{\rho_s c_s \delta_s^2}{k_s} \propto l^{1/2} \tag{18.45}$$

and

$$\frac{\delta_s}{k_s} \propto l^{-1/2} \tag{18.46}$$

Introducing (18.44) into (18.43) suggests:

$$k_s \rho_s c_s \propto l^{3/2} (\text{thermal inertia}) \tag{18.47}$$

and

$$\frac{k_s}{\delta_s} \propto l^{1/2} (\text{thickness}) \tag{18.48}$$

The wall materials and the noncombustible surface materials should be chosen according to the above two equations. Note that based on the scaling, the wall temperature at depth δ in the full scale generally corresponds to that at a different position in the model scale.

In the following, we simply check the scaling of heat conduction. At the beginning of an enclosure fire, that is, when the heat has not yet penetrated the walls, the conductive heat flux through wall surfaces can be written as:

$$\dot{q}_k'' = k_s \frac{dT_s}{dz} \propto \frac{k_s (T_w - T_o)}{\sqrt{k_s t / \rho_s c_s}} \tag{18.49}$$

This indicates that

$$\dot{q}_k'' \propto (k_s \rho_s c_s)^{1/2} l^{-1/4} \tag{18.50}$$

Note that as $k_s \rho_s c_s \propto l^{3/2}$, the above equation indicates:

$$\dot{q}_k'' \propto l^{1/2} \tag{18.51}$$

After a period when the thermal penetration occurs, the conductive heat flux through wall surfaces can be expressed as:

$$\dot{q}_k'' = \frac{k_s}{\delta_s}(T_w - T_{wb}) \tag{18.52}$$

Note that as $k_s / \delta_s \propto l^{3/2}$, the above equation also indicates the scaling law for the conduction heat flux.

Therefore, it is clear that the heat conduction in thermally thick materials can be scaled well if the proposed two dimensionless groups are preserved in model scale and the wall surface temperature scales well.

18.5.3.2 Thermally Thin Materials

For thermally thin materials, for example, thin wall materials or metal objects, the properties inside the materials can be assumed to be homogeneous, and the controlling equation can be simply expressed as:

$$\rho_s V_s c_s \frac{\partial T_s}{\partial t} = \dot{q}_{net}'' A_s \tag{18.53}$$

where V indicates volume (m^3) and A_s is surface area (m^2). The characteristic parameters are introduced to normalize the above equation to yield:

$$\frac{\partial \hat{T}_s}{\partial \hat{t}} = \frac{\dot{q}_{net}'' A_s t_o}{\rho_s V_s c_s T_o} \tag{18.54}$$

In this case we also assume that the convective and radiative heat fluxes are scaled well, that is, $\dot{q}_{net}'' \propto l^{1/2}$. Thus the above equation indicates the following relationship:

$$\rho_s V_s c_s \propto l^3 \tag{18.55}$$

This suggests that in order to scale the heat conduction in thermally thin materials, the same materials can be used, if the materials are geometrically scaled. In reality, scaling of the thermally thick materials also fulfills Eq. (18.55), assuming the temperatures inside the material are homogeneous or the conductivity is infinite.

Thus, as discussed previously, a thermally thin material is only a special case of a thermally thick material.

In summary, to scale the heat conduction inside thermally thick materials, Eqs. (18.45) and (18.46) need to be preserved while choosing the materials and the wall thicknesses. For thermally thin materials, the same materials can be used if the materials are geometrically scaled.

18.5.4 Scaling of Heat Balance in an Enclosure

Note that tunnels can be regarded as a special type of enclosures. The total heat released in an enclosure can be balanced by the heat loss by smoke flow exiting through openings, that is, doors and windows, $\dot{Q}_c$ (kW), and the heat loss by conduction into the walls, $\dot{Q}_k$ (kW), and the radiation through the openings, $\dot{Q}_r$ (kW), which can be expressed as follows:

$$\dot{Q} = \dot{Q}_c + \dot{Q}_k + \dot{Q}_r \tag{18.56}$$

18.5.4.1 Heat Loss by Convection Through Vents

The heat loss by convection through vents can be expressed as:

$$\dot{Q}_c = \dot{m}_g c_p (T_g - T_o) \tag{18.57}$$

where $\dot{m}_g$ is the smoke mass flow rate (kg/s) and T_g is the gas temperature (K).

In an enclosure fire, the mass flow rate of smoke flow through an opening normally can be written as:

$$\dot{m}_g \propto C_d A_o \sqrt{\Delta P} \tag{18.58}$$

where C_d is the flow coefficient (0.7 in most cases) and ΔP is the thermal pressure (Pa).

Assuming that the smoke layer can scale well and noting that the pressure difference scales as the length scale, the smoke mass flow rate through an opening should approximately scale as:

$$\dot{m}_g \propto l^{5/2} \tag{18.59}$$

For a flashover fire, which is probably ventilation controlled, the mass flow rate of the fresh air flowing into the enclosure should equal the smoke mass flow rate out of the opening, both of which can be approximately expressed as:

$$\dot{m}_a = \dot{m}_g = 0.5 A_o \sqrt{H} \propto l^{5/2} \tag{18.60}$$

where H is height of the opening (m), and $\dot{m}_a$ is the fresh air mass flow rate (kg/s).

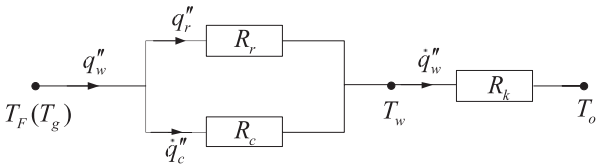

Fig. 18.1 Circuit analogy of heat loss to the walls in an enclosure fire

The heat loss by smoke flow out through the openings can be expressed as:

$$\dot{Q}_c \propto l^{5/2} \tag{18.61}$$

According to this, it is clear that the heat loss by smoke flow out through openings can scale well even for a flashover fire. In addition, it is known that a large amount of heat released in an enclosure fire is taken away by smoke flowing out of openings, which is normally called the convective HRR. The fraction of the convective HRR in the total HRR is normally in a range of 60–70 %. This is the main reason why the simplified Froude scaling can scale the fire scenario well even in model scales when the heat fluxes are implicitly scaled.

18.5.4.2 Heat Loss by Conduction into the Walls

According to the above analyses, the convective heat flux and the radiative heat flux cannot be scaled precisely as $l^{1/2}$. This definitely will affect the heat conduction inside the wall, since all the heat into the walls comes from the wall surfaces. To analyze the influence of convective and radiative heat transfer on the heat conduction in the walls, the circuit analogy of the heat loss to the walls in an enclosure fire is given, as shown in Fig. 18.1.

The total heat loss by conduction to the wall surfaces can be simply expressed as:

$$\dot{Q}_k = \dot{q}''_w A_w = h_t A_w (T_g - T_o) = A_w \frac{(T_g - T_o)}{R_t} = A_w \frac{(T_g - T_o)}{\overline{R} + R_k} \tag{18.62}$$

where the resistances are defined as:

$$R_k = \frac{1}{h_k}, \quad R_c = \frac{1}{h_c}, \quad R_r = \frac{1}{h_r}, \quad \overline{R} = \frac{R_r R_c}{R_r + R_c}$$

The conductive heat transfer coefficient, h_k (kW/m^{2}K), is defined in a similar manner as the convective heat transfer coefficient, h_c, and can easily be found for different boundary conditions. Note that $\dot{q}''_k$ is the heat flux into the wall surface, rather than heat flux deep into the wall, and the circuit analogy therefore is only a schematic description according to the relationship between the heat flux equations. Apparently, the conductive heat transfer coefficient varies with time for an unsteady state heat conduction problem.

Note that it is assumed that the radiative heat transfer is directly related to the flame or gas temperature and is proportional to the temperature difference, that is, has the same form as the convective heat transfer. However, the radiative heat transfer coefficient is not a constant except for a constant radiation temperature. The analogy is only used to clarify the interaction between different modes of heat transfer.

The above equation indicates that the all the heat resistances should be scaled as:

$$R \propto l^{-1/2} \tag{18.63}$$

Note that the lesser of R_r and R_c dominates the heat transfer to the wall surfaces. Quintiere [30] gave typical ranges for the heat transfer coefficients where $h_k \approx$ 10–30 W/(m^2 K), $h_r \approx$ 5–100 W/(m^2 K), and $h_c \approx$ 5–60 W/(m^2 K). For commonly used gypsum board, the conductive heat transfer coefficient is about 28 W/(m^2 K) in half an hour after ignition and 14 W/(m^2 K) in 1 h. We can also calculate the radiative heat transfer coefficient using Eq. (18.35). Assume that the emissivity equals 0.8 and the wall surfaces are bounded by hot gases, the radiative heat transfer coefficient is about 34 W/(m^2 K) for a gas temperature of 500 °C and 125 W/m^2·K for 1000 °C. It is clearly shown that after the gas temperature increases to about 500 °C radiation dominates the heat transfer to the wall surface. It can be expected that for a large enclosure fire, the conductive heat transfer dominates the total heat transfer from the hot gases to the surrounding walls for a long period. This means that if the heat conduction scales well, the total or overall heat transfer should also scale well in such cases. In our cases, the wall temperatures between the wall surface (T_g) and the backside (T_o) are the focus.

Note that the total heat transfer corresponds to the heat transfer from the flame and hot gases (T_g) to the penetration boundary inside the wall (T_o). However, the penetration boundary moves deeper into the wall as time goes by. Therefore, the effective thermal resistance of the wall is not constant but increases with time. For the wall temperatures at a position close to the wall surface (far away from the penetration boundary), the effective thermal resistance of the wall at the beginning of the fire cannot dominate the overall heat transfer from the hot gases to the wall, and thus the internal wall temperature does not scale very well. However, as the penetration depth increases with time, the thermal resistance becomes the dominant term in the overall heat transfer from hot gases to the internal walls. In such cases, the internal wall temperatures should scale well.

18.5.4.3 Heat Loss by Radiation Through the Vents

The heat loss by radiation through the vents could be estimated by:

$$\dot{Q}_r = \varepsilon \sigma A_o (T_g^4 - T_o^4) \tag{18.64}$$

For enclosures with small openings, the heat loss by radiation through vents can be neglected relative to other losses. However, for enclosures with large openings, the heat loss by radiation through vents should be taken into account.

The heat loss by radiation through vents scales as the radiation heat flux. Its effect on the entire heat balance mainly depends on vents area.

18.5.4.4 Global Heat Balance in an Enclosure Fire

Note that the main heat released from a fire is carried away by the smoke flows in an enclosure or a tunnel fire, which generally corresponds to 60–80 % of the total HRR. This part of the heat can be scaled well, even if the heat loss by conduction into the walls and radiation through openings are implicitly scaled. Therefore, heat flows in an enclosure fire can be scaled well. In reality, if the heat conduction is scaled as presented above, the global heat balance can be scaled better.

18.6 Scaling of Water Sprays

If water-based fire suppression systems are involved in model scale tests, additional equations need to be considered.

18.6.1 Single Droplet

At first, we analyze the equations for single water droplet.

The mass equation for a single water droplet can be expressed as [31]:

$$\frac{dm_l}{dt} = -A_l h_m \rho_l (Y_l - Y_g) \tag{18.65}$$

where

$$h_m = \frac{ShD_l}{d_l} \propto u_l^{1/2} d_l^{-1/2},$$

$$Y_l = \frac{X_l}{X_l(1 - M_a / M_l) + M_a / M_l},$$

$$X_l = \exp\left[\frac{L_v M_l}{R}\left(\frac{1}{T_b} - \frac{1}{T_l}\right)\right]$$

The momentum equation for a single water droplet is:

$$m_l \frac{d\boldsymbol{u}_l}{dt} = m_l \boldsymbol{g} - \frac{1}{8} C_d \rho_l \pi d_l^2 \left|\boldsymbol{u}_l - \boldsymbol{u}\right| (\boldsymbol{u}_l - \boldsymbol{u}) \tag{18.66}$$

where the drag coefficient, C_d, can be expressed as [32]:

$$C_d = B\,\mathrm{Re}^{-1/2} = B\left(\frac{\left|u_l - u\right| d}{v}\right)^{-1/2}$$

and

$$u_l = \frac{dx_l}{dt}$$

The energy equation for a single water droplet is:

$$m_l c_l \frac{dT_l}{dt} = h_l A_l (T_g - T_l) + h_s A_l (T_s - T_l) + \frac{dm_l}{dt}\left[c_p (T_{boil} - T_l) + L_{v,w}\right] + \dot{Q}_r \tag{18.67}$$

where

$$h_l = \frac{\mathrm{Nu}\,k}{d_l} \propto u^{1/2} d_l^{-1/2}$$

In the above equations, h_m is the mass transfer coefficient (m/s), h_l is the convective heat transfer coefficient between gas and a liquid droplet (kW/(m^2 K)), h_s is the convective heat transfer coefficient between a liquid droplet and a solid surface (kW/(m^2 K)), *Sh* is the Sherwood number, *D* is the mass diffusivity (m^2/s), *d* is the droplet diameter (m), Y_g is the vapor mass fraction, Y_l is the equilibrium vapor mass fraction, X_l is the equilibrium vapor volume fraction, $\boldsymbol{x}_l$ is the droplet trajectory (m), *B* is a constant, *c* is the heat capacity (kJ/(kg K)), C_d is the drag coefficient, A_l is exposed surface of the droplet (m^2), T_g is the gas temperature (K), u_l is the droplet velocity (m/s), *u* is the gas velocity (m/s), *k* is the conductivity of the gas (kW/(m K)), $\dot{Q}_r$ is the radiation absorbed by the droplet (kW), and $L_{v,\,w}$ is heat of vaporization of the water droplet (kJ/kg). Subscript *l* denotes the liquid, *b* the bulb, *boil* indicates the boiling state, *v* the vaporization, *s* is the solid surface, and *a* is air. Bold terms indicate vectors.

The characteristic parameters are introduced to normalize the above equations giving:

Mass:

$$\frac{d\hat{m}_l}{d\hat{t}} = -\pi_{19}(\hat{Y}_l - \hat{Y}_g) \tag{18.68}$$

Momentum:

$$\frac{d^2\hat{\boldsymbol{x}}_l}{d\hat{t}^2} = \pi_{20}\boldsymbol{g} - \pi_{21}\left|\pi_1\frac{d\hat{\boldsymbol{x}}_l}{d\hat{t}} - \hat{\boldsymbol{u}}\right|^{1/2}(\pi_1\frac{d\hat{\boldsymbol{x}}_l}{d\hat{t}} - \hat{\boldsymbol{u}}) \tag{18.69}$$

Energy:

$$\hat{m}_l\frac{d\hat{T}_l}{d\hat{t}} = \pi_{22}(\hat{T}_g - \hat{T}_l) + \pi_{23}(\hat{T}_s - \hat{T}_l) + (\pi_{24} + L_v)\frac{d\hat{m}_l}{d\hat{t}} - \hat{T}\frac{d\hat{m}_l}{d\hat{t}} + \pi_{25} \tag{18.70}$$

The dimensionless groups obtained are listed below:

$$\pi_{19} = \frac{h_m A\rho_l Y_o t_o}{m_o}, \quad \pi_{20} = \frac{t_o^2}{l}, \quad \pi_{21} = \frac{3B\rho v^{1/2}u_o^{3/2}t_o^2}{4\rho_l l d^{3/2}} \tag{18.71}$$

$$\pi_{22} = \frac{h_l A t_o}{m_{l,o}c_l}, \quad \pi_{23} = \frac{h_s A t_o}{m_{l,o}c_l}, \quad \pi_{24} = \frac{T_{boil}}{T_o}, \quad \pi_{25} = \frac{\dot{Q}_r t_o}{m_{l,o}c_l T_o} \tag{18.72}$$

Note that the dimensionless group π_1 also needs to be preserved, which also indicates that:

$$u_l \propto l^{1/2} \tag{18.73}$$

From dimensionless group π_{19} we have:

$$d_l \propto l^{1/2} \tag{18.74}$$

The correlation for the droplet diameter can also be obtained by preservation of dimensionless groups, π_{21}, π_{22}, or π_{23}. Also, note that π_{24} is always preserved. The preservation of the dimensionless group π_{25} will be discussed latter. Until now, all the dimensionless groups except π_{25} are preserved. If the radiation is insignificant, it can be expected that this scaling works very well.

18.6.2 Water Sprays

Now we consider water sprays as a whole. Note that the heat absorbed by the water spray is one of the heat loss terms for the hot gases and solid surfaces. Therefore, the water flow rate needs to be scaled as:

$$\dot{m}_l \propto l^{5/2} \tag{18.75}$$

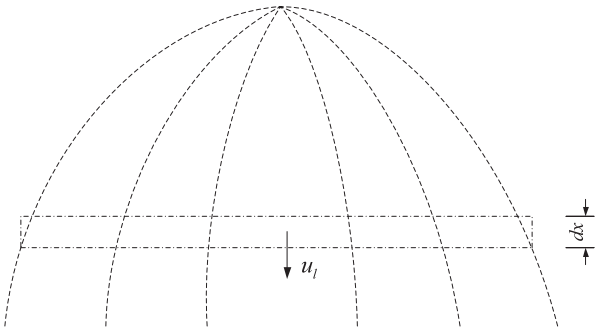

Fig. 18.2 A diagram of water sprays from one sprinkler

Further, note that initial velocity of the water spray is very important and thus needs to be scaled. Therefore, the diameter of the nozzle or sprinkler, d_n (m), needs to be geometrically scaled:

$$d_n \propto l \tag{18.76}$$

The other parameters, including the cone angle of the nozzle, spatial distribution of the water droplets, and droplet size distribution, also need to be accounted for.

Assuming that the sizes of the droplets are the same, we can estimate the total number of the droplets produced per second by the nozzle, N, as:

$$N \propto \dot{m}_l / d_l^3 \propto l \tag{18.77}$$

In the following we analyze the effect water sprays on the controlling equations for the gas flows. Figure 18.2 shows a diagram of water sprays from one sprinkler. An element with a volume of dV (m^3) and a depth of dx (m) covering the whole droplets is focused on. The average downward velocity of the droplets relative to the fluid is u (m/s), and the covered area is A (m^2). Therefore, we have:

$$dV = Adx, \quad dx = u_l dt \tag{18.78}$$

The sprays have influences on the controlling equations for the gas flows, and all the terms related to water sprays can be regarded as source terms in the controlling equations for gas flows.

Let us consider the fluid element, as shown in Fig. 18.2. It is assumed that the scaling of single water droplets works very well. Thus the source terms of the controlling equations for the fluid element due to the water sprays can be explored.

The mass source for the fluid element is:

$$\dot{m}'''_{l,tot} = \frac{N}{Au}\frac{dm_l}{dt} \propto l^{-1/2} \tag{18.79}$$

The momentum source for the fluid element is:

$$S_M = \frac{dP_l}{dx} = \frac{NdtC_d\rho_l \pi d_l^2 u_l^2}{8Adx} \propto \frac{NC_d d_l^2 u_l^2}{Au} \propto l^0 \tag{18.80}$$

The energy source for the fluid element is:

$$\dot{Q}'''_{loss} = \frac{Nm_l c_l}{Au}\frac{dT_l}{dt} \propto l^{-1/2} \tag{18.81}$$

Therefore, it can be concluded that the water sprays can be scaled well provided the single water droplet is scaled well.

18.6.3 Radiation Absorbed by Water Sprays

The absorption of radiation by water sprays is similar to the absorption of radiation by soot in the smoke flows. In a similar way, the transmittance for water sprays, τ_l, can be expressed as [7, 33]:

$$\tau_l \propto e^{-4f_v L/d_l} \tag{18.82}$$

where f_v is the volume fraction of water spray and L is the path length (m). This indicates the absorption coefficient of the water sprays scales as:

$$\kappa_l \propto f_v / d_l \propto l^{-1/2} \tag{18.83}$$

This correlates well with the obtained correlations for radiation. Heskestad [7] argues that the transmittance needs to be preserved. However, based on the above analysis, we know it should not be a constant in different scales.

As pointed out earlier, in enclosure or tunnel fires, scaling of the global radiative heat transfer is more meaningful and practical. From the global point of view, the radiative heat absorbed by the water sprays can be expressed as:

$$\dot{q}''_{r,tot} \propto \alpha_{l,tot}\sigma T^4 \tag{18.84}$$

where the absorptivity $\alpha_{l,\,tot}$:

$$\alpha_{l,tot} = 1 - e^{-\kappa_l L}$$

Note that the radiation emitted from water spray is ignored since it is much less important compared to the radiation absorbed. The above equation indicates that the absorptivity could become lower in model scales, which is reasonable according to the analysis of scaling of heat fluxes.

18.6.4 Droplet Diameter

Dombrowski et al. [34] found that the median droplet diameter is related to a Weber number, that is, the ratio of inertial forces to surface tension forces, and the correlation can be expressed as:

$$\frac{d_l}{d_n} \propto \mathrm{We}^{-1/3} \tag{18.85}$$

where the Weber number, We, is defined as:

$$\mathrm{We} = \frac{\rho_l u_n^2 d_n}{\sigma}$$

In the above equation, σ is the liquid surface tension (N/m) which can be considered as constant for a certain temperature, and u_n is the initial discharge velocity of the droplets (m/s). Therefore, the median droplet diameter produced by geometrically similar sprinkler scales as:

$$d_n \propto l^{1/3} \tag{18.86}$$

Comparing this with the previously obtained correlation shows a discrepancy for the scaling of droplet sizes. Heskestad [7] pointed out that the discrepancy may not be serious for scales varying within a moderate range.

18.6.5 Surface Cooling

According to the above analysis, water sprays are reasonably scaled before arriving at the fuel surfaces. Therefore, the mass flow rate of the water arriving at fuel surfaces, $\dot{m}_{w,s}$ (kg/s), approximately scale as:

$$\dot{m}_{w,s} \propto l^{5/2} \tag{18.87}$$

On the fuel surface, the water droplets absorb heat by evaporation to cool the fuel surface. An extinction due to surface cooling occurs when the net heat absorbed by a fuel surface decrease to a certain value, that is, the critical mass burning rate as defined by Tewarson [35] is obtained. The scaling of the heat gain and heat loss scales as:

$$\dot{m}_{w,s} L_{v,w} \approx \dot{m}_f L_{v,f} \propto l^{5/2} \tag{18.88}$$

where $\dot{m}_f$ is the fuel burning rate (kg/s) and L_v is the heat of vaporization (kJ/kg). Subscripts *w* and *f* indicate water and fuel, respectively.

This suggests that the surface cooling scales well. Note that the water sprays are also scaled well before arriving at the fuel surface. It can, therefore, be concluded that the scaling of fire suppression should be reasonably good.

18.6.6 Automatic Sprinkler

For scaling of automatic sprinklers, the response time of the bulb needs to be scaled, together with scaling of the water spray. The thermal response equation for the sprinklers can be expressed as follows [28, 29, 36–39]:

$$\frac{dT_b}{dt} = RTI^{-1}u^{1/2}(T_g - T_b) - C\cdot RTI^{-1}(T_b - T_m) - C_2\cdot RTI^{-1}X_w u \tag{18.89}$$

Where,

$$C = \frac{C'RTI}{m_b c_b}, \qquad \mathrm{RTI} = \tau u^{1/2}, \qquad \tau = \frac{m_b c_b}{h_b A_b}$$

In the above equation, RTI is the response time index ($m^{1/2}/s^{3/2}$), c is the heat of capacity (kJ/(kg K)), C is the C-Factor, C_2 is a factor accounting for the influence of upstream sprays, T_g is the gas temperature (K), T_b is the bulb temperature (K), T_m is the temperature of the sprinkler mount (close to ambient) (K), and X_w is the volume fraction of water droplets in the gas stream. Subscript b is bulb. Note that C_2 and C' are constants but C is not.

The characteristic parameters are introduced to normalize the above equation:

$$\frac{d\hat{T}_e}{d\hat{t}} = \pi_{26}(\hat{T}_g - \hat{T}_b) - \pi_{27}(\hat{T}_b - \hat{T}_m) - \pi_{28} \tag{18.90}$$

The dimensionless groups obtained are listed below:

$$\pi_{26} = \frac{u^{1/2}t_o}{\mathrm{RTI}} = \frac{h_b A_b t_o}{m_b c_b} = \frac{t_o}{\tau}, \qquad \pi_{27} = \frac{Ct_o}{\mathrm{RTI}}, \qquad \pi_{28} = \frac{C_2 u t_o X_w T_o^{-1}}{\mathrm{RTI}} \tag{18.91}$$

For sprinklers, the response time also needs to be scaled in model scales. Note that three dimensionless groups related to RTI have been obtained. To preserve π_{26}, RTI needs to be scaled as:

$$\mathrm{RTI} \propto l^{3/4} \tag{18.92}$$

To preserve π_{27}, RTI needs to be scaled as:

$$\mathrm{RTI} \propto l^{-1} \tag{18.93}$$

To preserve π_{28}, RTI needs to be scaled as:

$$\mathrm{RTI} \propto l^1 \tag{18.94}$$

Thus, comparing the three correlations shows a self-contradiction between them. Note that the ratios for π_{26} and π_{28} are close to each other, and the convective heat transfer dominates the heat balance of the element before its activation. Therefore, preservation of π_{28} is ignored. In short, RTI should be scaled as:

$$\mathrm{RTI} \propto l^{3/4} \tag{18.95}$$

It is normally impossible to obtain a very small automatic nozzle. Let us consider two methods to scale RTI. First, we can use a small cylinder with a specific material and diameter which fulfills the condition discussed later. Note that a typical sensing element can be seen as a circular cylinder. Due to the Reynolds Number being in a range of 40–4000, the convective heat transfer coefficient can be approximately expressed as:

$$h_c = \frac{kNu}{d_b} = \frac{k}{d_b} C_k \,\mathrm{Pr}^{1/3}\,\mathrm{Re}^{1/2} = C_k \,\mathrm{Pr}^{1/3}\,\frac{k}{d_b}\left(\frac{ud_b}{v}\right)^{1/2} \tag{18.96}$$

where C_k is a coefficient, d is the diameter (m), and subscript b indicates bulb. Therefore,

$$\mathrm{RTI} = \frac{m_b c_b u^{1/2}}{h_c A_b} = \frac{v^{1/2}}{4C_k \,\mathrm{Pr}^{1/3}\,k}\rho_b c_b d_b^{3/2} \tag{18.97}$$

This indicates that:

$$\rho_b c_b d_b^{3/2} \propto l^{3/4} \tag{18.98}$$

If a small cylinder can fulfill the above condition, the RTI of the element is scaled properly. The problem is that the element in model scale is generally so small that makes it impossible to produce it. The second way of scaling RTI is using a bulb with a small RTI.

18.7 Scaling of Combustible Materials

To scale the combustible materials, three basic parameters need to be preserved: geometry, HRR, and energy content. The coverage of the fuels needs to be scaled geometrically.

The HRR can be simply expressed as:

$$\dot{Q} = \dot{m}_f'' A_f \chi \Delta H_c \propto l^{5/2} \tag{18.99}$$

where $\dot{m}_f''$ is the fuel mass burning rate (kg/(m^2 s)), A_f is the fuel surface area (m^2), χ is the combustion efficiency, and ΔH_c is heat of combustion (kJ/kg).

The total energy can be estimated in the form:

$$E = m_f \chi \Delta H_c = \rho_f V_f \chi \Delta H_c \propto l^3 \tag{18.100}$$

where m_f is the fuel mass (kg) and V_f is the fuel volume (m^3).

Li et al. [40, 41] proposed a theoretical model of maximum HRRs in metro carriages which are correlated with the data from different scales of metro carriage fire tests very well. The results suggest that for scaling of the maximum HRR in a fully developed vehicle fire, the following correlation also needs to be fulfilled:

$$\frac{\Delta H_c}{L_{v,f}} \propto l^0 \tag{18.101}$$

where $L_{v,f}$ is heat of gasification of the fuel (kJ/kg).

Scaling of combustible materials is one of the most challenging tasks in physical scaling. The main problem is caused by the difficulty in choosing materials that fulfill all the requirements based on the scaling theory [40, 41]. At present, the main practical use of scaling of combustible materials is the scaling of wood crib fires.

18.8 An Example of Scaling Application in Fire Safety Engineering

Scaling applications in tunnel fires can be found in many chapters in this book, for example, gas temperature, tunnel fire ventilation, and flame length. On these specific topics, good agreement has been found between model- and large-scale tests. Therefore, they are not described further here.

The example presented here has been chosen to illustrate the scaling of internal wall temperatures in enclosure fires. Li and Hertzberg [6] proposed a method for scaling internal wall temperatures, based on which two series of enclosure fire tests were carried out in three different scales of enclosures: full scale (1:1), medium scale (1:2), and small scale (1:3.5). The method is depicted in Sect. 18.5.3. Figure 18.3 shows the comparison of the internal wall temperatures in full scale and medium scales of room fire tests with the fire source placed at the center of the room, and Fig. 18.4 shows the comparison of the internal wall temperature in full scale and small scales of the center fires. Ten percent corresponds to the location at

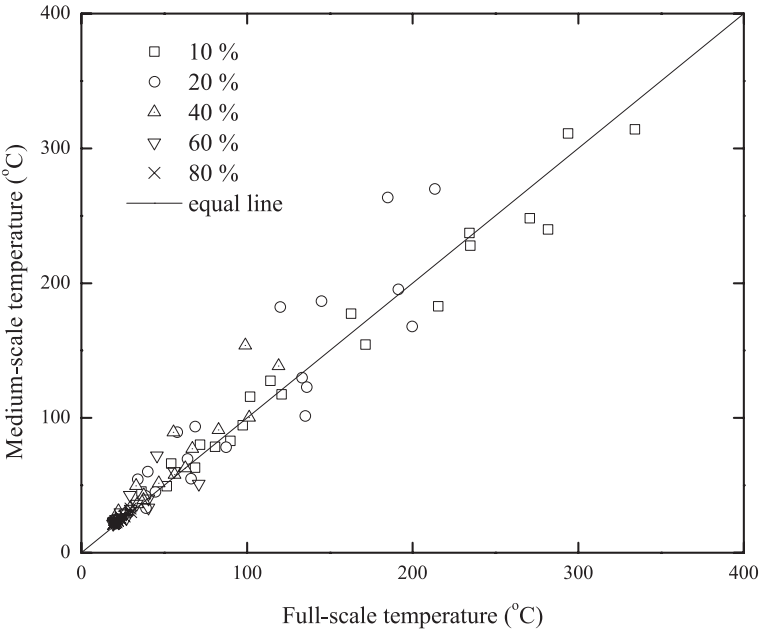

Fig. 18.3 Internal wall temperatures in full scale vs. medium scale [6]

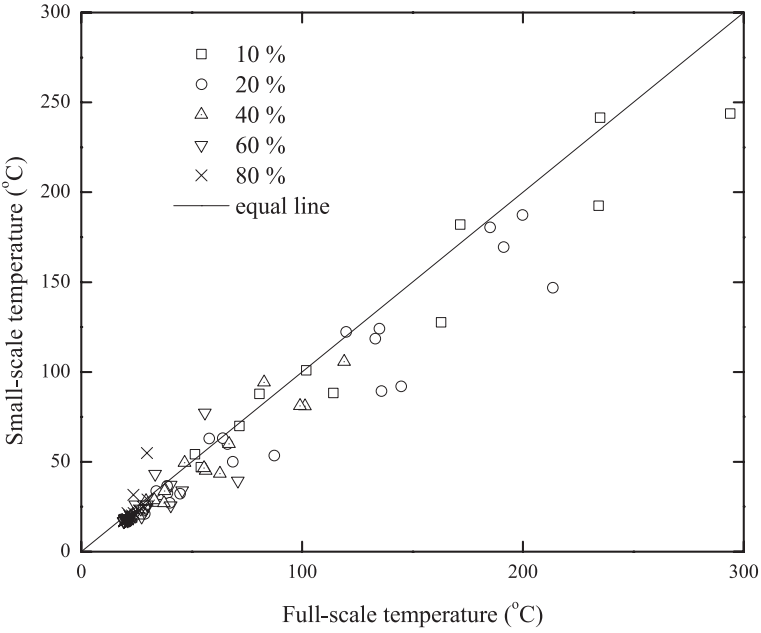

Fig. 18.4 Internal wall temperatures in full scale vs. small scale [6]

Table 18.1 A list of scaling correlations

Type of unit	Scaling
Heat release rate (HRR) (kW)	$\dot{Q}_M / \dot{Q}_F = (l_M / l_F)^{5/2}$
Velocity (m/s)	$V_M / V_F = (l_M / l_F)^{1/2}$
Time (s)	$t_M / t_F = (l_M / l_F)^{1/2}$
Energy content (kJ)	$E_M / E_F = (l_M / l_F)^3$
Mass (kg)[a]	$m_M / m_F = (l_M / l_F)^3$
Temperature (K)	$T_M / T_F = 1$
Gas concentration[a]	$Y_M / Y_F = 1$
Pressure (Pa)	$P_M / P_F = l_M / l_F$
Fuel mass burning rate (kg/(m^2 s))	$(\dot{m}''_f \Delta H_c)_M / (\dot{m}''_f \Delta H_c)_F = (l_M / l_F)^{1/2}$
Fuel density (kg/m^3)	$(\rho \Delta H_c)_M / (\rho \Delta H_c)_F = 1$
Fuel heat of pyrolysis	$(\Delta H_c / L_p)_M / (\Delta H_c / L_p)_F = 1$
Thermal inertia (kW$^2 \cdot$s$\cdot$m$^{-4} \cdot$K^{-2}))	$(k\rho c)_{s,M} / (k\rho c)_{s,F} \propto (l_M / l_F)^{3/2}$
Thickness (m)	$(k / \delta)_{s,M} / (k / \delta)_{s,F} \propto (l_M / l_F)^{1/2}$
Heat flux (kW/m^2)[b]	$\dot{q}''_M / \dot{q}''_F = (l_M / l_F)^{1/2}$
Water droplet size (mm)	$d_M / d_F = (l_M / l_F)^{1/2}$
Water density (mm/min)	$\dot{q}''_{w,M} / \dot{q}''_{w,F} = (l_M / l_F)^{1/2}$
Water flow rate (l/min)	$\dot{q}_{w,M} / \dot{q}_{w,F} = (l_M / l_F)^{5/2}$
Operating pressure (bar)	$P_M / P_F = l_M / l_F$
Response time index, RTI	$\mathrm{RTI}_M / \mathrm{RTI}_F = (l_M / l_F)^{3/4}$

M is model scale and *F* is full scale

[a] Assume $\Delta H_{c,F} = \Delta H_{c,M}$

[b] The scaling of the conductive and radiative heat flux could deviate from the scaling law. The scaling of conductive heat flux depends on the conductive and radiative heat flux. Details can be found in Sect. 18.5

ten percent of the wall thickness below the interior wall surface. Clearly, it shows that there is very good correlation between the full scale and the medium scale. Although the internal wall temperatures in the small scale is slightly lower at some positions, very good correlation can also be found between the full scale and the small scale. Most data lie close to the equal line.

18.9 Summary

Scaling has been successfully applied throughout the development of fire safety science in the past several decades. It is a very powerful and cost-effective tool to obtain valuable information on fire development and suppression, fire characteristics, smoke movement and smoke control, etc.

Scaling theory that has been developed is depicted in this chapter in detail for understanding its mechanism in support of further development of more advanced scaling methods. The focus is on the Froude scaling method which is the most common one used in fire safety science. Scaling of convective heat transfer, radiative heat transfer, and heat conduction is investigated as well as scaling of water sprays, response time of sprinklers, and combustible materials. A list of scaling correlations is given in Table 18.1.

Heat conduction can be scaled very well. Convective heat transfer can be scaled very well for turbulent flows in model tunnels with the same relative roughness. The convective heat transfer for laminar flows in model scales may be slightly overestimated.

Radiative heat flux may be a time-dependent variable during a fire, and emission and absorption of radiation by the walls in model scales are generally overestimated. However, radiation is scaled reasonably well by the fire itself. This could result in a slight difference in gas temperatures between scales.

It should always be kept in mind that the scaling techniques presented here can only produce scenarios similar to full scales in model scales, rather than accurate results. Despite this, the tested fires themselves are still realistic fires.

References

1. Heskestad G (1975) Physical Modeling of Fire. Journal of Fire & Flammability 6:253–273
2. Quintiere JG (1989) Scaling Applications in Fire Research. Fire Safety Journal 15:3–29
3. Ingason H In-Rack Fire Plumes. In: Fire Safety Science – Proceedings of the Fifth International Symposium, Melbourne, Australia, 3–7 March 1997. IAFSS, pp 333–344
4. Perricone J, Wang M, Quintiere J (2007) Scale Modeling of the Transient Thermal Response of Insulated Structural Frames Exposed to Fire. Fire Technology 44 (2):113–136
5. Croce PA, Xin Y (2005) Scale modeling of quasi-steady wood crib fires in enclosures. Fire Safety Journal Vol. 40:245–266

6. Li YZ, Hertzberg T (2013) Scaling of internal wall temperatures in enclosure fires. SP Report 2013:12. SP Technical Research Institute of Sweden, Borås, Sweden
7. Heskestad G (2002) Scaling the interaction of water sprays and flames. Fire Safety Journal 37:535–548
8. Heskestad G (2003) Extinction of gas and liquid pool fires with water spray. Fire Safety Journal 38:301–317
9. Quintiere J.G., Su G.Y., N. S (2007) Physical scaling for water mist fire suppression – a design application. International Journal on Engineering Performance-Based Fire Codes 9 (2):87–108
10. Yu H.Z., Zhou X.Y., Ditch B.D. Experimental validation of Froude-modeling-based physical scaling of water mist cooling of enclosure fires. In: 9th International Symposium on Fire Safety Science (Poster), Karlsruhe, Germany, 21–26 September 2008. IAFSS, pp 553–564
11. Jayaweera T.M., Yu H.Z. (2008) Scaling of fire cooling by water mist under low drop Reynolds number conditions. Fire Safety Journal 43:63–70
12. Yu H.Z. Physical scaling of water mist suppression of pool fires in enclosures. In, College Park, MD, 2011. 10th International Symposium on Fire Safety Science.
13. Bettis RJ, Jagger SF, Wu Y (1993) Interim Validation of Tunnel Fire Consequence Models: Summary of Phase 2 Tests. Health and Safety Executive, Buxton, Derbyshire, UK
14. Oka Y, Atkinson GT (1995) Control of Smoke Flow in Tunnel Fires. Fire Safety Journal 25:305–322
15. Wu Y, Bakar MZA (2000) Control of smoke flow in tunnel fires using longitudinal ventilation systems – a study of the critical velocity. Fire Safety Journal 35:363–390
16. Ingason H, Li YZ (2010) Model scale tunnel fire tests with longitudinal ventilation. Fire Safety Journal 45:371–384
17. Ingason H, Li YZ (2011) Model scale tunnel fire tests with point extraction ventilation. Journal of Fire Protection Engineering 21 (1):5–36
18. Ingason H (2007) Model Scale Railcar Fire Tests. Fire Safety Journal 42 (4):271–282
19. Vauquelin O, Telle D (2005) Definition and experimental evaluation of the smoke "confinement velocity" in tunnel fires. Fire Safety Journal 40:320–330
20. Li YZ, Lei B, Ingason H (2010) Study of critical velocity and backlayering length in longitudinally ventilated tunnel fires. Fire Safety Journal 45:361–370
21. Li YZ, Lei B, Ingason H (2011) The maximum temperature of buoyancy-driven smoke flow beneath the ceiling in tunnel fires. Fire Safety Journal 46 (4):204–210
22. Li YZ, Ingason H (2012) The maximum ceiling gas temperature in a large tunnel fire. Fire Safety Journal 48:38–48
23. Li YZ, Lei B, Ingason H (2013) Theoretical and Experimental Study of Critical Velocity for Smoke Control in a Tunnel Cross-Passage. Fire Technology 49 (2):435–449
24. Li YZ, Lei B, Ingason H (2012) Scale modeling and numerical simulation of smoke control for rescue stations in long railway tunnels. Journal of Fire Protection Engineering 22 (2):101–131
25. Lönnermark A, Lindström J, Li YZ (2011) Model-scale metro car fire tests. SP Report 2011:33. SP Technical research Institute of Sweden, Borås, Sweden
26. Lönnermark A, Lindström J, Li YZ, Claesson A, Kumm M, Ingason H (2012) Full-scale fire tests with a commuter train in a tunnel. SP Report 2012:05. SP Technical Research Institute of Sweden, Borås, Sweden
27. Ingason H (2008) Model scale tunnel tests with water spray. Fire Safety Journal 43 (7):512–528
28. Li YZ, Ingason H (2013) Model scale tunnel fire tests with automatic sprinkler. Fire Safety Journal 61:298–313
29. Li YZ, Ingason H (2011) Model scale tunnel fire tests - Automatic sprinklers SP Report 2011:31 SP Technical Research Institute of Sweden, Borås, Sweden
30. Quintiere JG Fire behaviour in building compartments. In: Proceedings of the Combustion Institutes, 2002. pp 181–193

31. Cheremisinoff N (1986) Encyclopedia of Fluid Mechanics, Volume 3: Gas-Liquid Flows. Gulf Publishing Company, Houston, Texas
32. Schlichting H (1968) Boundary-layer theory. 6th edn. McGraw-Hill, New York.
33. Dembele S, Wen JX, Sacadura JF (2000) Analysis of the two-flux model for predicting water spray transmittance in fire protection applications. Journal of Heat Transfer 122 (1):183–186
34. Dombrowski N., Wolfsohn DL. (1972) The atomization of water by swirl spray pressure nozzles. Trans Inst Chem Engrs 50:259–269
35. Tewarson A (2002) Generation of Heat and Chemical Compounds in Fires. In: DiNenno PJ, Drysdale D, Beyler CL et al. (eds) The SFPE Handbook of Fire Protection Engineering. Third edition edn. National Fire Protection Association, Quincy, MA, USA, pp 3–82 – 83–161
36. Heskestad G (1988) Quantification of thermal responsiveness of automatic sprinklers including conduction effects. Fire Safety Journal 14:113–125
37. Ruffino P., Di Marzo M. (2003) Temperature and Volumetric Fraction Measurements in a Hot Gas Laden with Water Droplets. Journal of Heat Transfer 125 (2):356–364
38. Ruffino P., Di Marzo M. (2002) The Effect of Evaporative Cooling on the Activation Time of Fire Sprinklers. Proceedings of the Seventh International Symposium on Fire Safety Science, pp. 481–492
39. Gavelli F., Ruffino P., Anderson G., Di Marzo M. (1999) Effect of Minute Water Droplets on a Simulated Sprinkler Link Thermal Response. NIST GCR 99-776. National Institute of Standards and Technology, Maryland
40. Li YZ, Ingason H, Lönnermark A (2014) Fire development in different scales of train carriages. In: 11th International Symposium on Fire Safety Science (IAFSS) New Zealand
41. Li YZ, Ingason H, Lönnermark A (2013) Correlations in different scales of metro carriage fire tests. SP Report 2013:13. SP Technical Research Institute of Sweden, Borås, Sweden